J Vol. 64 October, 1960 No. 10

THE JOURNAL OF PHYSICAL CHEMISTRY

(Registered in U. S. Patent Office)

CONTENTS

(Continued on inside cover)

THE JOURNAL OF PHYSICAL CHEMISTRY

(Registered in U. S. Patent Office)

Published monthly by the American Chemical Society at 20th and Northampton Sts., Easton, Pa.

Second-class mail privileges authorized at Easton, Pa. This publication is authorized to be mailed at the special rates of postage prescribed by Section 131.122.

The *Journal of Physical Chemistry* is devoted to the publication of selected symposia in the broad field of physical chemistry and to other contributed papers.

Manuscripts originating in the British Isles, Europe and Africa should be sent to F. C. Tompkins, The Faraday Society, 6 Gray's Inn Square, London W. C. 1, England.

Manuscripts originating elsewhere should be sent to W. Albert Noyes, Jr., Department of Chemistry, University of Rochester, Rochester 20, N. Y.

Correspondence regarding accepted copy, proofs and reprints should be directed to Assistant Editor, Allen D. Bliss, Department of Chemistry, Simmons College, 300 The Fenway, Boston 15, Mass.

Business Office: Alden H. Emery, Executive Secretary, American Chemical Society, 1155 Sixteenth St., N. W., Washington 6, D. C.

Advertising Office: Reinhold Publishing Corporation, 430 Park Avenue, New York 22, N. Y.

Subscription Rates (1960): members of American Chemical Society, $12.00 for 1 year; to non-members, $24.00 for 1 year. Postage to countries in the Pan American Union $0.80; Canada, $0.40; all other countries, $1.20. Single copies, current volume, $2.50; foreign postage, $0.15; Canadian postage $0.05; Pan-American Union, $0.05. Back volumes (Vol. 56–59) $25.00 per volume; (starting with Vol. 60) $30.00 per volume; foreign postage, per volume $1.20, Canadian, $0.15; Pan-American Union, $0.25. Single copies: back issues, $3.00; for current year, $2.50; postage, single copies: foreign, $0.15; Canadian, $0.05; Pan American Union, $0.05.

NOTES

COMMUNICATION TO THE EDITOR

THE JOURNAL OF
PHYSICAL CHEMISTRY

(Registered in U. S. Patent Office) (© Copyright, 1960, by the American Chemical Society)

VOLUME 64 OCTOBER 28, 1960 NUMBER 10

THE HEAT OF FORMATION OF THE HYPOCHLORITE ION[1]

BY J. E. MCDONALD,[2] J. P. KING[3] AND J. W. COBBLE

Department of Chemistry, Purdue University, Lafayette, Indiana

Received October 10, 1959

The heat of formation of the hypochlorite ion has been redetermined calorimetrically at 25° by measuring the heat of hydrolysis of chlorine in basic solutions. The value obtained was $\Delta H^0 = -26.2 \pm 0.1$ kcal./mole. Using this value in conjunction with that for the free energy of formation, $\Delta F^0 = -8.858$ kcal./mole, the entropy is calculated to be 8.6 ± 0.3 e.u.

Introduction

The hypochlorite ion has many advantages as a calorimetric oxidizing agent. It is reasonably stable and is a powerful and rapid oxidizing agent even in dilute solutions. As a 1:1 electrolyte, it has a heat of dilution which, although not known, will be small at reasonable concentrations. Easily prepared and standardized, hypochlorite can be used with transition metal halides[4] and oxides if these are oxidized to well-defined species in basic media, as well as with many other possible calorimetric reactions.

The direct calorimetric standardization of the hypochlorite ion, although reported at 18° by at least three separate investigators[5] in the older literature has not been listed in the most recent compilations.[6,7] Bichowsky and Rossini[5] had recommended $\Delta H_{18}^0 = -25.9$ kcal./mole. Correction to 25° by an estimated $\overline{C_{p_2}}^0$ value of −30 cal./mole/degree for $H^+ + ClO^-$, yields ΔH_{25}° of −26.1 kcal./mole. In view of this situation the heat of hydrolysis of chlorine in dilute sodium hydroxide solutions has been redetermined. The value so obtained is $\Delta H_{25}^\circ = -26.2 \pm 0.1$ kcal./mole. This value appears to be the only direct determination available at 25° and is only in fair agreement with the value of $\Delta H^\circ = -25.94$ kcal./mole determined from the temperature coefficients of certain chlorine equilibria which was recently reported.[8]

Experimental

Chemicals.—The chlorine gas used was Pennsalt tank C.P. grade. Purification was accomplished by passage of the gas through four distilled water washes followed by two concentrated sulfuric acid washes. The entire purification system was constructed of glass; where stopcocks were necessary, halocarbon grease was used.

After purification, the gas was passed into an evacuated line to which the glass sample bulbs were sealed. When the pressure of chlorine became approximately 725 mm., the sample bulbs were cooled in a salt–ice-bath and sealed. The bulbs were designed with a long, thin capillary tip at right angles to the vertical axis of the bulb. In this manner the tip of the bulb was broken first so that the basic solution from the calorimeter was forced slowly into the bulb as it reacted with the chlorine. After this initial reaction had taken place, the entire bulb was broken to ensure complete mixing of the contents.

The amount of hypochlorite so formed was determined iodometrically.[9] The absence of significant decomposition of the hypochlorite as a result of its disproportionation into chloride and chlorate was demonstrated by comparison of the iodometric thiosulfate end-points in both sulfuric and acetic acid.[10]

Sodium hydroxide solutions were prepared by dilution of a concentrated stock solution made from Mallinckrodt rea-

(1) This research was supported by the United States Air Force through the Air Force Office of Scientific Research of the Air Research and Development Command under Contract AF 18(600)-1525. Reproduction in whole or part is permitted for any purpose of the United States Government.

(2) Dow Chemical Fellow, 1959–1960.

(3) Some of this work is reported in the Ph.D. thesis of J. P. King, Purdue University, 1959.

(4) J. P. King and J. W. Cobble, *J. Am. Chem. Soc.*, **82**, 2111 (1960).

(5) As compiled in F. R. Bichowsky and F. D. Rossini, "Thermochemistry of the Chemical Substances," Reinhold Publ. Corp., New York, N. Y., 1936.

(6) "Selected Values of Chemical Thermodynamic Properties," U. S. Bureau of Standards, Washington, D. C., 1948.

(7) W. M. Latimer, "Oxidation-Reduction Potentials," 2nd Ed., Prentice-Hall Inc., New York, N. Y., 1952, p. 54.

(8) R. E. Connick and Yuan-tsan Chia, *J. Am. Chem. Soc.*, **81**, 1280 (1959).

(9) I. M. Kolthoff and E. B. Sandell, "Textbook of Quantitative Analysis," 3rd Ed., The Macmillan Co., New York, N. Y., 1952, p. 608.

(10) A. I. Vogel, "Textbook of Quantitative Inorganic Analysis," Longmans, London, 1957, p. 349.

gent grade pellets and distilled water. The presence of trace amounts of carbonate was not significant.

Apparatus.—The submarine calorimeter, hereafter designated laboratory calorimeter SMC-2, consists of a 300-ml. Dewar flask with a specially constructed ground glass stopper lid which has vertical tubes sealed through it to allow entrance of the stirrer, thermistor probe, heater, and glass ramrod for breaking the sample bulbs. The thermal modulus of the system has been estimated at 0.005°C./°C./min.

A thermistor temperature sensing element of 2000 ohms (Veco 32A24) is electrically located in one of the arms of a standard d.c. bridge. The second arm consists of three Helipot type potentiometers (linearity 0.1%) which are used to balance the bridge. The other two arms contain fixed, 2000 ohm, wire-wound resistances. An additional variable resistance in the variable arm allows the coarse balancing of the bridge prior to operation. A voltage of 1.5 volts is applied across the bridge. The bridge proper is located in a thermally insulated box, and the calorimeter apparatus is located in a temperature controlled room (±2°). The output of the bridge is amplified by a Hewlett-Packard, Model 425A, d.c. Amplifier, the output of which is used to drive a Leeds and Northrup 10 mv. recorder.

The sensitivity of the system is variable and determined by the level of amplification used. In this set of experiments a gain of approximately 100 was used. The thermal ranges of the bridge and amplifier corresponded to 2, 6 and 18 cal./mv., or approximately to 0.007, 0.021 and 0.06°, respectively, at 25° and using the above calorimeter.

Using the recorder as a null-point device, the variable resistances were used to rebalance the bridge continually during electrical or chemical runs. The effect of this procedure is an expansion of the recorder scale. The advantage in the use of such a process lies in the fact that errors in reading the millivolt change from the recorder chart are greatly reduced. In addition, the bridge always operates very near the balance point and any error resulting from the degree of unbalance is thereby eliminated.

The variable resistors are calibrated in terms of arbitrary units per millivolt. From this calibration, the total millivolt change which occurred can be calculated.

Calibration of the system is performed electrically through the use of a heater of known resistance and a constant current source (Sargent Coulometric Current Source, Model IV). The calorie is taken to be 4.184 absolute joules. The accuracy of the over-all system has been verified chemically by means of the heat of solution of potassium chloride. The reported value[6] at very low concentrations (4.164 kcal./mole) could be duplicated to within 0.18% (4.172 kcal./mole).

Procedure.—Sample bulbs containing between 5 and 10 cc. of chlorine were sealed to the end of the glass rod. The calorimeter was filled with a known volume of sodium hydroxide solution, assembled, and submerged in a thermostat whose temperature was controlled to ±0.005°. The system was then heated to within 0.5° of the equilibrium temperature and allowed to equilibrate for approximately one hour. The calorimeter was calibrated electrically before and after the chemical run, and the average heat capacity of both determinations was used for the calculations.

After the second electrical calibration, the calorimeter was opened and the number of milliequivalents of hypochlorite formed was determined. Separate experiments proved that the rate of decomposition of the hypochlorite under these conditions was negligible.

Experimental Results

The hydrolysis of chlorine in base can be assumed to be

$$Cl_2 + 2OH^- \rightleftharpoons ClO^- + Cl^- + H_2O \quad (1)$$

This stoichiometry was checked by comparison of the quantity of base used, corrected for the hydrolysis of the OCl^- at lower pH ranges, to the quantity of hypochlorite formed. In these experiments the hypochlorite concentration was determined iodometrically, while the hydroxide concentrations were determined potentiometrically with standard HCl. The heat of hydrolysis data obtained are summarized in Table I. The heat of reaction extrapolated to infinite dilution was $\Delta H_1^0 = -24.6 \pm 0.1$ kcal.

Table I

The Heat of Hydrolysis of Chlorine in Sodium Hydroxide Solutions at 25°

Run no.	NaOH concn., N	OCl^- formed, meq.	Heat evolved, cal.	$-\Delta H$, kcal./mole
VI	0.10	0.6316	7.9959	25.024
VII	.10	.6523	8.2789	25.386
VIII	.10	.6443	8.1991	25.454
X	.10	.4499	5.6226	24.996
		Av.	$-\Delta H = 25.22 \pm 0.12$[a]	
XII	0.048	0.3196	3.9340	24.616
XIII	.048	.3893	4.8551	24.942
XV	.050	.4091	5.0521	24.696
XVI	.050	.3105	3.8691	24.920
XVII	.050	.3047	3.8235	25.100
		Av.	$-\Delta H = 24.86 \pm 0.09$[a]	
XIV	0.025	0.3313	4.1031	24.772
(Extrapolated) 0			$-\Delta H = 24.6 \pm 0.1$[b]	

[a] Standard deviation. [b] Probable error.

Using auxiliary thermodynamic data,[6,7] the ΔH^0 of formation for OCl^- then is calculated to be -26.2 ± 0.1 kcal./mole. This value can be compared to that recently calculated from various chlorine equilibria of -25.94[8] kcal./mole. The reason for the small discrepancies between the two values is at present unknown; however, it is conceivable that they are the result of errors in the data on the temperature coefficients of the solubility of chlorine[11] which were used in the equilibrium calculations.

The entropy of the OCl^- may be calculated using the free energy, -8.858 kcal./mole, reported by Connick and Chia[8] and the present value for the enthalpy. The value so obtained is 8.6 ± 0.3 e.u.

(11) L. W. Winkler, *Mathematikai es Termeszettudomanyi Ertesito*, **25**, 86 (1907) Budapest.

THORIUM TARTRATE COMPLEXES BY POLARIMETRY[1]

BY LEONARD I. KATZIN AND ELSIE GULYAS

Argonne National Laboratory, Argonne, Illinois

Received October 26, 1959

It is shown that optical rotation changes can be used to follow the formation of complexes between tartrate and Th(IV). The greatest rotation change in acid solutions is given by a species with one tartrate per thorium, found at *p*H 3–3.5. Two tartrates per thorium on the average are required through the whole *p*H range to keep the thorium in solution. In the region of *p*H 3, resin column experiments indicate the dominant complexes to be neutral. Increases of *p*H introduce increasing proportions of negatively charged complex, probably basic. More alkaline solutions show marked slow changes of rotation, accompanied by changes of *p*H, which indicate probable release of H^+ by tartrate hydroxyl groups, which does not occur in alkaline tartrate solutions without thorium.

Rosenheim, Samter and Davidsohn[2] reported that thorium markedly altered the optical rotation of tartaric acid solutions. Darmois and Heng[3] investigated the system polarimetrically, using the method of continuous variations to follow the reaction of $Th(OH)_4$ (by the action of NaOH *in situ*) with tartaric acid, bitartrate and sodium tartrate. They concluded that there existed a stable 1:1 complex, which appeared in the reaction with tartaric acid, and that there was a less stable complex with two tartrates per thorium, which showed itself when bitartrate and sodium tartrate were used.

Investigation of a complexing system in which both cation and ligand are colorless, and direct measurements of free cation or ligand are not possible electrometrically, is rather difficult. Optical activity can serve as a spectrum to be followed, and is particularly apropos, when, as in this instance, the groups involved in coördination are directly linked to the center of asymmetry. We have therefore chosen to investigate this system polarimetrically with modern sensitive equipment, to demonstrate the potentialities of using the rotatory property and because the system is of interest to us. We have also controlled the *p*H, which had not been done in previous work.

Experimental

Polarimetric Measurements.—A Rudolph High Precision Polarimeter Model 80 was used, in conjunction with the Rudolph Model No. 95 spectroscope-monochromator and a tungsten lamp source. For each reading 10 settings of the instrument were made, the average deviation being ± 0.002–3°. Cell length was 102 mm. Room temperature variation in the range 21–27° had no apparent effect on the optical activities recorded.

The rotations of the solutions were read as soon as possible after final *p*H adjustment. Though this was usually only a few minutes after mixing, it was sometimes delayed while waiting for temporary turbidities (thorium tartrate or hydroxide) to clear. Solutions to be followed for a period of time (weeks or months) were returned to glass stoppered erlenmeyer flasks and sealed with Parafilm between readings. The *p*H was usually checked at each rotation reading. All measurements were made with light of 5461 Å. wave length. *p*H was measured with the Beckman Model G *p*H meter to a precision of about ±0.02 unit.

Adsorption Experiments.—Resin columns about 5 cm. high were set up in tubes 1 cm. in internal diameter, with a sintered glass plate as base. A ground semi-ball joint at the top of the tube enabled pressure to be applied when necessary to increase flow. For an anion column, Dowex 2-X10 (capacity, 3 meq./g.) and for the cation column, Dowex 50-X12 (5 meq./g.) were the resins used. The effective column volume was 3 to 4 ml.

Results

Preliminary Observations.—On mixing 0.2 formal solutions of tartaric acid and thorium chloride (or nitrate), precipitation occurs, and the acidity of the supernatant increases markedly, from the approximately *p*H 2 of the individual solutions. The acidity increases when even a small amount of thorium salt is added to the tartaric acid, and if the thorium is added to a 1:1 mole ratio, the *p*H of the supernate drops to 0.86 or less. Two preparations of precipitate from a 1:1 mixture, washed with 0.1 *N* HCl, and dried in air, showed on analysis 43.6% Th, carbon content of 11.0–12.4% (equivalent to about 1.3 tartrate groups per thorium), insignificant chloride, and 16–20% of hydroxyl groups and water of hydration (by Karl Fischer titration). The material is therefore mainly a hydrated basic tartrate, either disturbed in the washing procedure, or not yet at its equilibrium composition (both preparations were equilibrated about 10 days before separation from supernatant).

With mixtures containing 2.5 tartrates per thorium, homogeneous solution is preserved when the liquid phase *p*H is maintained at *p*H 2.5 or higher. In Fig. 1 are shown the rotations of solutions formed from mixtures of 2.5 volumes of 0.2000 *M* tartaric acid and 1 volume of 0.2000 *M* thorium nitrate, for the *p*H range 2.8–10.7. Temporary initial cloudiness sometimes was encountered. Solution *p*H's were adjusted with 5–10 *M* NaOH. Since some of the solutions at high *p*H showed rapid initial changes of rotation, Fig. 1 shows both initial readings, and rotations observed after the solutions had aged for two weeks. In the case of the more alkaline solutions, changes in rotation were usually accompanied by marked decreases in *p*H of solutions. In one experiment, a solution originally at *p*H 9.0 was followed with rotation readings on aliquots every day or two. At the time of each reading, the *p*H was readjusted to 9.0. The rotation increased faster than when the *p*H was not so readjusted, and after 27 days reached a value about 80° higher than for tartrate in the absence of thorium.

No quantitative measure of the stability of the tartrate complexes was obtained. Qualitatively, the normal precipitation of thorium was repressed even in very alkaline solutions, and fivefold to

(1) Based on work performed under the auspices of the U. S. Atomic Energy Commission. Presented in part at American Chemical Society meeting, New York City, Sept. 9–13, 1957.

(2) A. Rosenheim, V. Samter and J. Davidsohn, *Z. anorg. Chem.*, **35**, 424 (1903).

(3) E. Darmois and Y. K. Heng, *Compt. rend.*, **194**, 703 (1932).

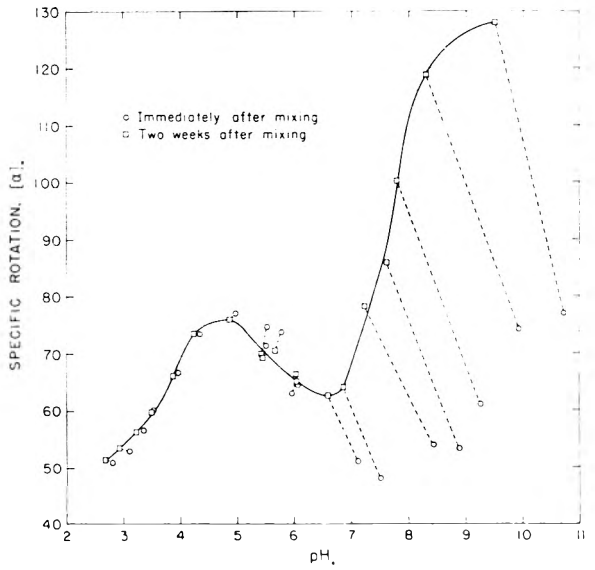

Fig. 1.—The variation of pH of the specific rotation of 2.5:1 mixtures of 0.2000 F sodium tartrate and 0.2000 F thorium nitrate; λ 5461 Å.

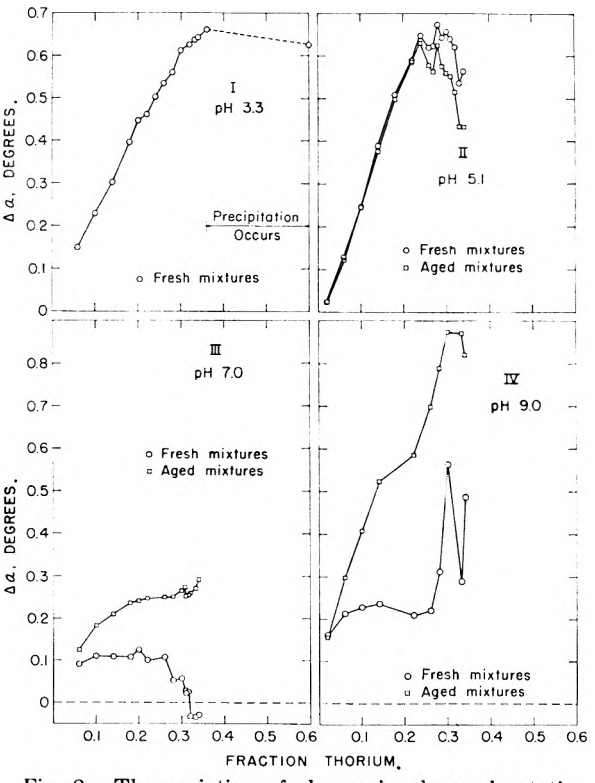

Fig. 2.—The variation of change in observed rotation, $\Delta\alpha$, with thorium content for tartrate–thorium mixtures at pH 3.3–3.4 (I), 5.1 (II), 7.0 (III), and 9.0 (IV) at λ 5461 Å.

twenty-fivefold dilutions of solutions often failed to show detectable specific rotation changes.

Rotation of Sodium Tartrate–Thorium Nitrate Mixtures at Constant pH as a Function of Composition.—A continuous variations[4,5] series of experiments was attempted to determine which of the possible thorium tartrate complexes might be contributing most to the alteration of rotation under various conditions. The systems at pH 3.3, 5.1, 7.0 and 9.0 were chosen for test, on the basis of the curve of Fig. 1. Solutions to be mixed were 0.2000 formal in tartrate and in thorium; an additional series with 0.1000 formal solutions was run at pH 9.0.

At pH 3.3–3.4 (Fig. 2), immediate precipitation is found in the composition range between thorium fractions 0.36 and 0.60, and the solution at fraction 0.60 deposited a gelatinous precipitate only a short time after measurement of its rotation. The data show, however, that the most important contribution to the rotation increase over that of tartrate in the absence of thorium[6] probably comes with a complex having a single tartrate per thorium, while a complex having two tartrates per thorium is apparently almost equally responsible. Since the concentration of the 1:1 complex is probably relatively low, with approximately 1.78 tartrates per thorium being required to maintain the solution homogeneous, the rotational effect of the 1:1 complex must be considerably the larger. In two weeks, the rotations showed no significant change.

At pH 5.1 several differences are seen. Most obviously, the rotation contribution attributable to a 1:1 complex, which was seen at pH 3.3, has been sharply curtailed. The equilibria seem to be attained rapidly so long as at least 3 tartrates per thorium are present, but at lower ratios slow reactions set in. It is not possible to say with certainty whether the peaking apparent at approximately 0.23 thorium fraction represents a 3:1 complex, or whether one still is dealing principally with the same 2:1 complex seen at pH 3.3, which is undergoing slow reactions, in the presence of lesser excesses of tartrate, to produce one or more species of the same or perhaps lower tartrate: thorium ratio, with a markedly lower specific rotation.

At pH 7.0, as expected from the results at constant tartrate ratio, the rotation change is much less than at lower pH values. Slow reactions are seen over the whole composition range, but this time the direction of alteration is different than at pH 5. The initial complex products are lower in rotation than the final and, in fact, in the range near 2:1 tartrate–thorium ratio, the initial rotations are perhaps less than for uncomplexed tartrate. The change of rotation with time, for these solutions, is accompanied by a decrease of pH, which approximates 0.30 unit for the solutions lower in thorium, and 0.40 for those with the higher thorium contents.

The mixtures which were originally at pH 9.0 showed marked change with time over the whole composition range. As some solutions had to be held for turbidities to clear before the initial rotations were read, the irregularities in the initial values around a thorium fraction of 0.3 are not meaningfully interpretable. After two weeks, it is seen that the major contribution to the altered rotation is from a complex with two tartrates per thorium, though indications can be seen for possible 3:1 and 4:1 complexes with different specific rotations.

(4) P. Job, *Ann. Chim.*, [10] **9**, 113 (1928).

(5) L. I. Katzin and E. Gebert, *J. Am. Chem. Soc.*, **72**, 5455 (1950).

(6) L. I. Katzin and Elsie Gulyas, This Journal, in press.

Ion Exchange Experiments.—Adsorption experiments were performed at *p*H 3, 5 and 7 to gain additional information on the nature of the thorium complex. First, using cation-exchange resin, the column was pre-equilibrated with sodium tartrate of the appropriate *p*H. One ml. of 0.2 formal solution with 2.5 equivalents of tartrate per thorium was placed on the resin, and elution was performed with solution similar to that used in pre-equilibration. The first milliliter of eluate was blank, for all three *p*H values, and in all three cases the total thorium added was eluted in 7–7.5 ml. (two column volumes). This was interpreted as showing the absence of positive charge on the complex.

Anion-exchange resin was used in both the tartrate form, and in the chloride form. At *p*H 3, with tartrate pretreatment and elution as above, thorium appears after a milliliter or so of negative solution, but then continues to elute through at least 4 column volumes, in contrast to the cation-exchange resin behavior. If the resin is in the chloride form, tartrate eluate contains thorium for 6 or 7 column volumes. This suggests that there is an anionic component among the thorium species, under these conditions, and this form competes for resin positions better with chloride than with tartrate. With tartrate-equilibrated resin and *p*H 5, the largest part of the thorium seems to be eluted in two column volumes, most of it in the first portion. Later washes with 4 *M* HCl eluted some small additional amounts of thorium. At *p*H 7, thorium elutes for one to 1.5 column volumes, and thereafter the eluate is negative. However, washing the resin with 4 *M* HCl now releases some two-thirds of the original thorium. There would therefore seem to be an indication either that the thorium is present in two different forms which interconvert very poorly even with excess tartrate eluant, or that there is some reaction with the resin.

Discussion

The fact that under quite acid conditions a basic tartrate of thorium precipitates, which contains less than two tartrates per thorium, while at *p*H 2.5 and higher one finds stable solution, with two or more tartrates per thorium, allows the conclusion that thorium probably complexes bitartrate so firmly that the weak-acid tendency of tartaric acid furnishes practically no hindrance to the reaction; the *p*H change shows that all but a small fraction of the tartaric acid must have been affected. The rather unusual hydrolysis of the thorium, in solutions of *p*H 1, suggests that this is related to solid state stability effects, and does not reflect correctly the balance of the species in solution.

At about *p*H 2.5, the *p*H at which precipitation ceases, tartaric acid is still over 60% associated, and only 1% is in the tartrate form.[6] It seems necessary to conclude, however, that the cessation of precipitation is due to the increasing dominance of the form with two tartrates per thorium over the form with a single tartrate (the latter still visible in the continuous variations experiment at *p*H 3.3), and that the complex with two tartrates involves the tartrate ion, and is therefore neutral. Further increase of *p*H, through *p*H 3.3 and up through 4.5 or so, throws the balance further so that no more 1:1 complex is to be found, as the ionization of the tartrate is further increased. Because of the mobility of the equilibrium at *p*H 3, indicated by the lack of slow rotation effects, the failure of the resin experiment to demonstrate positively charged complex is not definitive, though the absence of very strongly marked anionic complexes in the presence of excess tartrate may be more significant.

At *p*H 5, one sees the first signs of a slow reaction, at the lower tartrate–thorium ratios (3–2:1), and the implication that there is a second form of complex, with 2 tartrates per thorium, with a lower specific rotation. The ion-exchange results indicate that with the dominant, probably neutral, thorium species there exists a small fraction of negatively charged material, which is not readily converted to the neutral form, even with excess tartrate. At *p*H 7, this species seems to be the dominant one present. As one goes to more alkaline solutions still another species with two tartrates per thorium appears, formed by a rather slow reaction, and with a specific rotation higher than that of either of the others. Both sets of slow reactions release protons.

An acquisition of negative charge of the complexes may come about in several ways. In addition to the obvious one of adding more tartrate (*e.g.*, to $ThTart_3^{--}$), for which one does not anticipate a slow reaction, and which will not yield protons, one possible way is partial hydrolysis, to yield, for example, a $(Th(OH)Tart)_2^-$. In view of a known tendency for thorium to hydrolyze, this is a reasonable possibility for the *p*H 5–7 range. In view of the fact that the specific rotation of the tartrate in this form is lower than in the presumably unhydrolyzed form, there exists the possibility that the $(OH)^-$ group has entered the thorium coördination sphere by displacing one end of a tartrate group, so that only three carboxyls are attached to thorium, and one is waving free. This would give a basis for lowering the average specific rotation from that in which both ends of the tartrate are coördinated to thorium, introducing a strain which increases the rotation over that of free tartrate ion. Such a displacement reaction could account for the slow course of the reaction.

A third mechanism for increasing negative charge is appropriate to the more alkaline solutions, in which the highly rotating species is formed. This is release of protons by the hydroxyl groups of tartrate coördinated to thorium. If a tartrate has been held by both of its carboxyl groups, as would be the case in $ThTart_2$ or $Th(OH)Tart_2^-$, the thorium charge neutralization demands can now be satisfied by forming a 6-membered ring, as against the previous 7-membered ring, and the ionized carboxyl may now wave free. (Unionized hydroxyl groups may be coördinated in both cases.) Though it does not occur for uncomplexed tartrate, ionization of the tartrate hydroxyls in metal complexes has been postulated for many systems,[7] but in general the process has

been reported to proceed rather faster than with the thorium tartrate. The alteration of the tartrate rotation in response to this direct attack on one of the centers of optical activity needs no comment. The quantitative relation with alkalinity suggests a quantitative correlation with completeness of the transformation to the ionized form or forms.

Darmois and Heng[3] presented evidence for a 1:1 complex of tartrate and thorium in relatively acid solutions, but the lack of *p*H control greatly diminishes the significance of this evidence. Their data also show there must be another complex, probably with two tartrates per thorium, but again little more could be said. Bobtelsky and Graus[8] have also published a paper on thorium–tartrate complexes, which is based on "heterometric" (nephelometric) titrations. We can say little about this work other than that the authors did not seem to be aware that thorium tends to hydrolyze in all but reasonably acid solutions, and proceeded to mix solutions of very different *p*H values to obtain their results. Further, we do not see how the authors could have obtained the quantitative results reported, in view of the qualitative behavior we observed on adding thorium solutions to tartaric acid solutions and *vice versa*. At the least, their results must be highly dependent on the exact details of solution concentration, etc., and the interpretation correspondingly uncertain.

(7) *E.g.*, S. Kirschner, Abstracts of Papers, 129th Meeting, American Chemical Society, Dallas, Texas, April 8–13 (1956), p. 21-Q; M. E. Tsimbler, *Sbornik Statei Obshchei Khim., Akad. Nauk S.S.S.R.*, **1**, 330 (1953) (*C. A.*, **49**, 868d (1955)).

(8) M. Bobtelsky and B. Graus, *Bull. Res. Council Israel*, **3**, 82 (1953).

THE SORPTION OF WATER VAPOR ON DEHYDRATED GYPSUM

By R. I. Razouk, A. Sh. Salem and R. Sh. Mikhail

Chemistry Department, Faculty of Science, Ain Shams University, Abbassia, Cairo, Egypt, UAR

Received November 18, 1959

Sorption isotherms of water vapor on completely and partially dehydrated native and precipitated gypsum are similar. Quick uptake is noted at very low vapor pressures followed by an almost horizontal plateau in the isotherm until saturation pressure, when the uptake becomes a function of time. Sorption–desorption along the plateau is reversible, but hysteresis becomes pronounced when desorption is carried out from sorption values at saturation. The isotherm is then parallel to the sorption plateau but displaced to higher values depending on the time of exposure to saturation pressure. When dehydration of gypsum is conducted below 400°, the initial quick uptake of water corresponds to the formation of the hemihydrate. The dihydrate is formed after several days' exposure of the hemihydrate to saturated water vapor. But exposure for several days to water vapor at a pressure 3.5% short of saturation results in an uptake only slightly greater than corresponds to the formation of the hemihydrate, although raising the pressure to the saturation value induces further uptake to an amount exceeding that required to form the dihydrate. Dehydration above 500° renders the anhydrite incapable of forming the dihydrate, although the hemihydrate may still be formed. Sorption isotherms on partially dehydrated gypsum show a linear relation between the amount of formed hemihydrate and the percentage of decomposition when dehydration is at 150°. It is concluded that the transformation of the anhydrite into the hemihydrate in presence of water vapor is a quick process, whereas the transformation of the hemihydrate into the dihydrate is a slower process which takes place in presence of the saturated vapor of water, and which is more readily affected by the temperature of dehydration. Experiments on the rate of sorption of water vapor as well as infrared absorption spectra and X-ray analysis of various states of the system $CaSO_4$–H_2O confirm the above views.

Introduction

Extensive work has been done on the uptake of water vapor by dehydrated gypsum. Particular attention may be drawn to the work of Gaudefroy,[1] Kishimoto,[2] Linck and Jung,[3] Budnikov,[4] Hammond and Withrow,[5] Turtsev,[6] Gregg and Willing,[7] and Jury and Light.[8] But in spite of the immense literature on the subject, no comprehensive study of the isothermal uptake of water vapor by the anhydrite formed from gypsum by dehydration *in vacuo* has been undertaken. Moreover, the effect of partial dehydration on the isothermal uptake of water vapor has not yet been investigated. The present work includes a study of the equilibrium uptake of water vapor on partially and completely dehydrated gypsum, together with measurements of the rate of uptake at saturation vapor pressure of water. The infrared absorption spectra and X-ray diffraction patterns of different states of the calcium sulfate–water system have also been determined in order to throw more light on the mechanism of the uptake.

(1) C. Gaudefroy, *Compt. rend.*, **158**, 2006 (1914).

(2) K. Kishimoto, *J. Japan Ceram. Assoc.*, **357**, 201 (1922).

(3) G. Linck and H. Jung, *Z. anorg. allgem. Chem.*, **137**, 407 (1924).

(4) P. P. Budnikov, *Kolloid-Z.*, **46**, 95 (1928).

(5) W. A. Hammond and J. R. Withrow, *Ind. Eng. Chem.*, **25**, 633 (1933).

(6) A. A. Turtsev, *Bull. Akad. Sci., URSS, Geol.*, **4**, 180 (1939).

(7) S. J. Gregg and E. G. J. Willing, *J. Chem. Soc.*, 2916 (1951).

(8) S. H. Jury and W. Light, Jr., *Ind. Eng. Chem.*, **44**, 591 (1952).

Experimental

The uptake of water vapor was determined with the aid of a spring balance of the McBain–Bakr type,[9] the sensitivity of which was 0.045 mm./mg.

The infrared absorption spectra were determined with the aid of a Perkin–Elmer Infracord Spectrophotometer Model 137, using the Nujol mull technique.

The X-ray diffraction patterns were made in the Centre National de la Recherche Scientifique (Paris), using Debye–Scherrer technique with monochromatic Cu Kα radiation and curved crystal monochromator.

Crystalline gypsum (selenite) was kindly presented by Basic Dolomite Inc., Cleveland, Ohio. It was transparent and very pure with lamellae-like structure. Precipitated gypsum was a pure Schering–Kahlbaum preparation. Both the native and precipitated forms contained the stoichio-

(9) J. W. McBain and A. M. Bakr, *J. Am. Chem. Soc.*, **48**, 690 (1926).

metric amount of water according to the formula $CaSO_4 \cdot 2H_2O$.

Results and Discussion

I. Uptake of Water Vapor on Partially and Completely Dehydrated Gypsum. (i) **Sorption–Desorption Isotherms on Completely Dehydrated Gypsum.**—Naturally occurring gypsum (selenite), as well as precipitated gypsum, was dehydrated *in vacuo* at different temperatures, and the sorption isotherms of water vapor on the products of dehydration were determined. Desorption isotherms as well as resorption isotherms on the products obtained by outgassing at room temperature also were determined. In all cases the sorption-desorption-resorption isotherms are similar. The results of a typical complete set of isotherms on a specimen of calcium sulfate formed from precipitated gypsum by dehydration *in vacuo* at 150° are drawn graphically in Fig. 1. Water is taken up readily at the lowest pressures until the uptake reaches a value which corresponds very closely to the stoichiometric amount required to form the hemihydrate. In this region the isotherm is almost vertical. After taking this amount of water, the isotherm turns abruptly and runs along an almost horizontal straight line, so that the amount of water taken increases only very slightly as the vapor pressure is raised until saturation is attained, when the uptake increases appreciably with time of exposure (curve I). When desorption is carried out from a point on the plateau of the isotherm (say a, curve I), the desorption curve coincides with the almost horizontal sorption limb of the isotherm, so that sorption and desorption are reversible in this region, but the amount retained on evacuation at room temperature corresponds to the formation of the hemihydrate. Hysteresis becomes more pronounced when desorption is conducted from a point on the vertical limb of the isotherm which is obtained by exposing the material to saturation vapor pressure for variable intervals of time. The extent of hysteresis depends on the saturation uptake, being greater the higher is the uptake. Curves 2, 3, 4, 5 and 6 are the desorption isotherms obtained after exposing the sample to the saturated vapor of water for one day, two, four, seven and ten days, respectively. Curves II, III and IV, on the other hand, are resorption isotherms obtained when resorption is conducted after completing the desorption isotherms 3, 4 and 5, respectively. The system behaves in a similar manner on desorption following resorption. It is to be noted that the last desorption isotherm 6 gives a retained value somewhat higher than the value required for the formation of the dihydrate.

To test the effect of the time of contact of the sorbent with the saturated water vapor on the hysteresis, a specimen of gypsum was dehydrated at 150° and the isotherm was determined as usual up to saturation vapor pressure. A quick uptake was then effected by slightly cooling the container of the sorbent, when point b was obtained after one day's exposure, the amount taken up being very close to the amount taken up after five days' exposure to saturated vapor under ordinary conditions. The desorption isotherm starting from this point b is shown in curve 7 of Fig. 1, and it indicates that water which has been taken rapidly is readily given off on lowering the vapor pressure. In this case, the amount of retained water is just above the value required for the formation of the hemihydrate and very close to the amount obtained after one day's exposure (curve 1, Fig. 1).

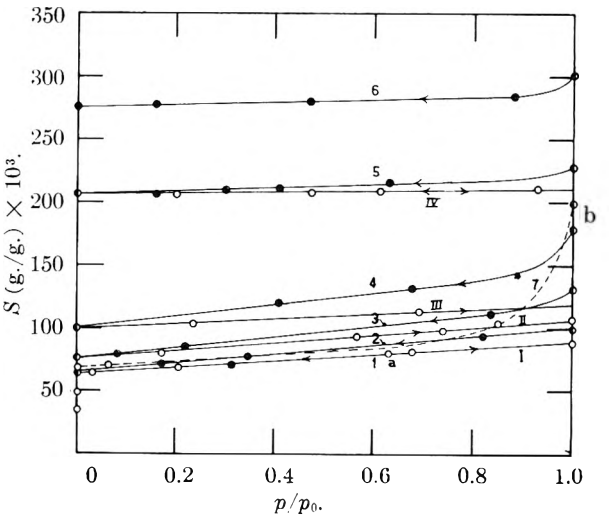

Fig. 1.—Sorption–desorption–resorption isotherms of water vapor on calcium sulfate prepared by the dehydration of precipitated gypsum at 150°. Isotherms at 30°: ○, sorption and resorption; ●, desorption. Curve I, sorption on original dehydrated gypsum; curve 1, desorption from point a; curves 2, 3, 4, 5 and 6, desorption isotherms obtained after exposing the system to the saturated vapor of water for one day, 2, 4, 7 and 10 days, respectively; curves II, III and IV, resorption isotherms obtained when the process is conducted after completing the desorption isotherms 3, 4 and 5, respectively.

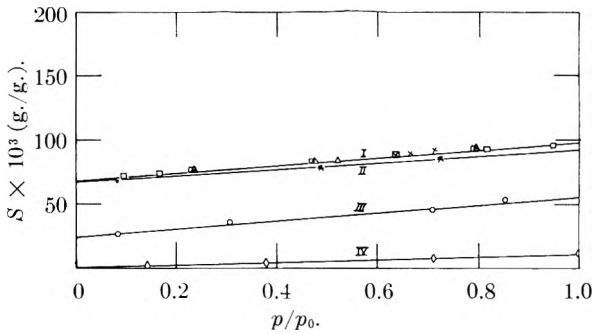

Fig. 2.—Effect of the temperature of dehydration of precipitated gypsum on the water isotherms: curve I, samples dehydrated at 100, 113, 150 and 200°; curve II, samples dehydrated at 90 and 300°; curve III, sample dehydrated at 400°; curve IV, sample dehydrated at 600°.

Similar results were obtained with native gypsum that had been dehydrated at the same temperature.

The results obtained in the present investigation resemble those obtained by Gregg and Willing[7] and Jury and Light[8] in so far as their isotherms are also square-shaped with the plateau corresponding to the formation of the hemihydrate, but in neither case were the measurements extended to saturation vapor pressure. Furthermore, their desorption isotherms which were carried out from points short of saturation lie always above the sorption isotherms. This may be accounted for by the different conditions of experimentation, especially

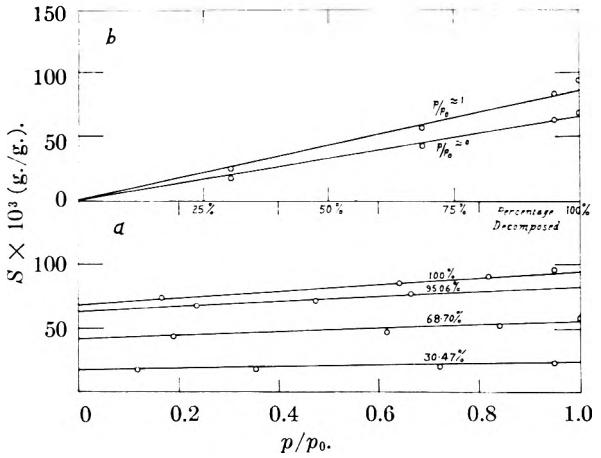

Fig. 3.—Sorption of water vapor on partially dehydrated gypsum prepared at 150°; isotherms at 35°.

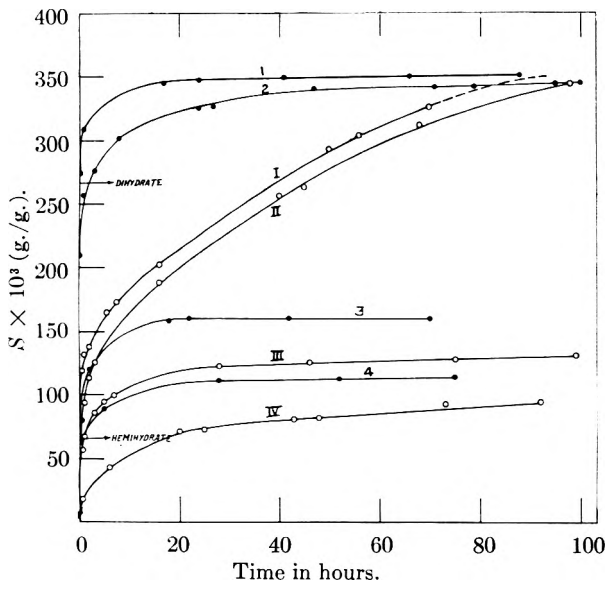

Fig. 4.—Effect of the temperature of dehydration of precipitated gypsum on the rate of hydration and rehydration of calcium sulfate when exposed to the saturated water vapor at 35°: curves I, II, III and IV, rate of hydration for samples dehydrated at 150, 400, 500 and 800°, respectively. Curves 1, 2, 3 and 4, rate of rehydration for samples originally dehydrated at 150, 400, 500 and 800°, respectively, and then hydrated and outgassed at room temperature.

with respect to the method of dehydration, being *in vacuo* in the present investigation, and in presence of air in the experiments of earlier authors.

(ii) **Effect of Temperature of Dehydration.**—The effect of the temperature of dehydration of native and precipitated gypsum on the water vapor isotherms has been studied also, and the results of experiments on the latter are shown in Fig. 2. When gypsum is dehydrated at temperatures lying between 100 and 200°, it gives rise to the same isotherms (curve I), while samples dehydrated at 90 and at 300° give a slightly lower isotherm (curve II). But in all cases, the water uptake at the lowest pressures corresponds to the formation of the hemihydrate. However, when dehydration is carried out at higher temperatures, the plateau falls progressively with rise of decomposition temperature (curves III and IV for products obtained by dehydration at 400 and 600°, respectively).

(iii) **Effect of Partial Dehydration.**—The effect of partial dehydration of gypsum on the sorption isotherm of water vapor was studied also in case of natural and precipitated forms. The specimen was dehydrated until a certain fraction was decomposed and the isotherm determined on the product. The results of a typical set of experiments is shown in Fig. 3a, which gives the sorption isotherms of water vapor on partially dehydrated precipitated gypsum having lost varying amounts of its water of crystallization. Figure 3b represents the relation between the water uptake at $p/p_0 \approx 0$ and at $p/p_0 \approx 1$ as a function of percentage decomposition.

Assuming that the amount of water taken up almost instantaneously at $p/p_0 \approx 0$, and which is retained on outgassing at room temperature, is an indication of the hemihydrate formation, it can be safely inferred from the direct proportionality between the water uptake and the percentage of decomposition that dehydration *in vacuo* leads directly to the formation of the anhydrite, and docs not proceed in two steps, namely, prior formation of the hemihydrate and then the anhydrite. This is in agreement with the idea which was originally presented by van't Hoff, Hinrichsen and Wegert,[10] and which has been supported by the work of several other authors,[11] that the dihydrate passes directly to the soluble anhydrite at the lower temperatures of dehydration. Experiments carried out in this Laboratory on the rate of dehydration of native and precipitated gypsum also confirm this view.[12]

II. Rate of Hydration of Dehydrated Gypsum from the Saturated Vapor Phase.—Throughout the course of the present investigation, it has been noticed that the time factor plays an important role in the process of water uptake at saturation vapor pressure, and hence a study of this effect undoubtedly would throw some light on the mechanism of the process. Experiments were, therefore, conducted in order to measure the rate of water uptake when calcium sulfate, formed from precipitated gypsum by dehydration *in vacuo* at 150, 400, 500 and 800°, was exposed to the saturated vapor of water at 35°. The uptake was followed even until it exceeded the amount required for the stoichiometric formation of the dihydrate, or else reached a constant limiting value. The product then was outgassed cautiously at room temperature for several hours, the retained amount determined, and finally the course of rehydration was followed again after exposing the system to saturation vapor pressure. The curves of the rate of uptake are parabolic in shape but tend to limiting values, and a rise of the dehydration temperature leads to a lowering of the rate of uptake.

The results of a typical series of experiments are shown in Fig. 4. Thus, when gypsum is dehydrated, for instance, at 150°, and then exposed to saturated vapor, it takes up water, in the first

(10) J. H. van't Hoff, W. Hinrichsen and F. Wegert, *Sitzber. Akad. Berlin*, 570 (1901).

(11) See *e.g.*, Ch. Mitsuki, *J. Ceram. Assoc. Japan*, **60**, 95 (1952).

(12) A. Sh. Salem, Ph.D. Thesis, Ain Shams University, 1959.

few minutes, more than is required to form the hemihydrate (curve I). The rate of uptake then decreases, but remains considerable, until the amount corresponding to the formation of the dihydrate is surpassed, then the curve tends to a limiting value. The amount of retained water obtained after outgassing at room temperature for 5 hours is slightly above that required to form the dihydrate. The rehydration curve (curve 1) is also parabolic and meets the hydration curve at the limiting water uptake.

The sample dehydrated at 400° reveals the same behavior (Fig. 4, curves II and 2), but the rate of hydration and the amount of water taken up at saturation are slightly less. However, the retained value is less than corresponds to the dihydrate, and the hydration and rehydration curves meet also at a value higher than what is required to form the dihydrate.

When dehydration is conducted at 500°, however, the behavior is different (Fig. 4, curve III). Thus after a region of quick uptake, lower in itself than the corresponding values for the products of dehydration at 150 and 400°, but still exceeding the amount required to form the hemihydrate, the curve tends to reach slowly a limiting value which is far less than what is required to form the dihydrate. The amount of retained water is again close to that which corresponds to the formation of the hemihydrate. The rehydration curve (Fig. 4, curve 3) is also parabolic but it tends to become parallel to the time axis.

A similar behavior is observed with gypsum dehydrated at 800° (Fig. 4, curve IV), but the hydration curve is still lower, and the uptake which corresponds to the formation of the hemihydrate is attained only after 12 hours. About half molecule of water per molecule of sulfate also is retained in this case. The rehydration curve (Fig. 4, curve 4) is, as usual, above that of hydration and almost parallel to it, as with the product prepared at 500°.

III. Infrared Absorption Spectra.—Infrared absorption spectra of gypsum, anhydrous calcium sulfate and some hydration products were determined and the results obtained are found to be similar in many respects to those of Miller and Wilkins.[13] The absorption spectra of typical systems are shown in Fig. 5. The important bands present in the spectrum of the dihydrate are those absorbing at 9.85 and 8.85 μ (characteristic for the sulfate radical,[14] together with those absorbing at 6.13, 5.9 and 2.82 μ (characteristic for the absorption of water).[15] The first two bands are associated with free or molecular water, while the band absorbing at 2.84 μ has been identified by Keller and Pickett[16] to be due to the presence of dimeric forms of hydroxyl groups.

The spectrum of "dead burnt" calcium sulfate prepared by dehydration at 800° lacks the bands characteristic for water, but those due to the sulfate group are not significantly altered.

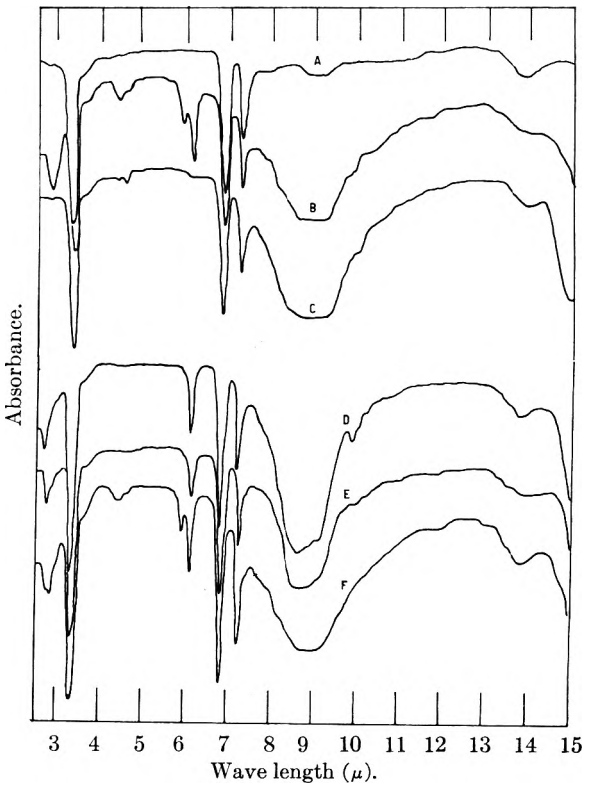

Fig. 5.—Infrared absorption spectra for the system $CaSO_4$–H_2O: A, Nujol spectrum; B, spectrum of dihydrate; C, spectrum of anhydrite prepared by dehydration at 800°; D, spectrum of the hemihydrate prepared by hydration at $p/p_0 = 0.2$; E, spectrum of a sample first dehydrated at 150° and then exposed to saturation vapor pressure of water for few hours; F, same as E but exposed to saturation pressure for 4 days.

The spectrum of the hemihydrate obtained at the plateau of the sorption isotherm of water vapor on calcium sulfate prepared by the dehydration of gypsum at 150°, shows only the band absorbing at 6.1 μ but not that absorbing at 5.9 μ, whereas the band absorbing at 2.84 μ is shifted to a shorter wave length at 2.7 μ. According to Keller and Pickett,[16] this band is due to the absorption of "unbound" or independent monomeric hydroxyl groups, and is thus expected to be present at the early stages of hydration. On exposing the hemihydrate to saturated water vapor, it was found that the band absorbing at 2.7 μ is shifted toward longer wave lengths, while all the bands characteristic of the dihydrate appear after exposure for four days, a period which is sufficient for the formation of the latter.

Another change was noticed also in the bands characteristic of the sulfate group. Thus whereas dehydration at 800° does not produce any pronounced alteration in the bands, the hemihydrate formed by the uptake of water by the product obtained by dehydration at 150° possesses a spectrum in which the band absorbing at 8.85 μ is resolved into a group of three bands absorbing at 8.7 μ (weak and broad), 9.1 μ (shoulder) and 9.9 μ (weak and broad). This behavior may be explained by assuming that in the hemihydrate the

(13) F. A. Miller and C. H. Wilkins, *Anal. Chem.*, **24**, 1253 (1952).

(14) L. J. Bellamy, "The Infrared Spectra of Complex Molecules," Methuen and Co., London, 1956, p. 284.

(15) R. M. Barrer, XVIth International Congress of Pure and Applied Chemistry, Lecture, pp. 113 *et seq.*

(16) W. D. Keller and E. E. Pickett, *Am. Mineral.*, **34**, 861 (1949).

sulfate vibration absorbing near 1100 cm.$^{-1}$ is triply degenerate as a result of changes in the crystal symmetry.[13] It is to be noted that Miller and Wilkins[13] obtained similar results with the product obtained by heating the dihydrate overnight at 170°, when the three bands were observed. It is probable that owing to the high reactivity of the anhydrite obtained under these conditions and to its pronounced tendency to combine with water vapor from the atmosphere, the absorption spectrum obtained by these authors is that of partially hydrated sulfate, and, in particular, that characteristic of the hemihydrate.

It may thus be inferred that the hemihydrate is readily formed through the vapor phase when the dehydration of gypsum is conducted at not very high temperatures, whereas the transformation of the hemihydrate into the dihydrate is a slow process and it takes place only in presence of saturated water vapor.

IV. X-Ray Analysis.—X-Ray diffraction patterns of the original precipitated dihydrate, of the products of dehydration at 150 and 600°, and of the hydrated sulfate obtained under varying conditions have been made. The results obtained with the parent dihydrate agree well with the established pattern of the gypsum lattice[17] which crystallizes in the monoclinic system. The *d*-distances for the three most intense lines having relative intensities of 100, 80 and 80 are found to be 7.65, 4.32 and 3.06 Å., respectively. Dehydration at 600° yields a product possessing the typical anhydrite lattice[17] belonging to the orthorhombic system. The *d*-distances for the strongest three lines having intensities 100, 40 and 30 are found to be 3.46, 2.84 and 2.32 Å., respectively. On the other hand, when complete dehydration is carried out at 150°, the product obtained yields a pattern which differs from that obtained with the product dehydrated at 600°, for it belongs to the hexagonal system characteristic of soluble anhydrite.[17] The *d*-distances of the lines having relative intensities 100, 80 and 80 are found to be 6.05, 3.00 and 2.78 Å., respectively. This soluble anhydrite combines readily with water vapor, since exposure to even very small relative vapor pressure leads to the appearance of the pattern of the hemihydrate which crystallizes also in the hexagonal system.[17] The *d*-distances for the most intense three lines in the pattern of the hemihydrate which have intensities 90, 90 and 100 are found to be 6.08, 3.00 and 2.79 Å., respectively. Furthermore, it has been observed that the hemihydrate pattern is always obtained when the soluble anhydrite is exposed to a wide range of relative humidities, up to the saturated vapor pressure of water, and repeated experiments have shown that in order to obtain once more the dihydrate pattern, exposure to the saturation pressure of water for several days is required.

General Discussion

It is a known fact that gypsum contains structural water, but the water molecules play a far more important role than in the perfect zeolites. The structure of gypsum may be described as a layer lattice in which the sheets of Ca^{++} and SO_4^{--} ions are so arranged that each cation is surrounded by six oxygen ions and by two water molecules. Each water molecule is linked to one Ca^{++} ion, to one O^{--} ion in its own sheet and to one O^{--} ion in a neighboring sheet, and it is these latter bonds only which bind the sheets together.[18]

When gypsum is dehydrated, it is probable that a pseudolattice is first formed, in which the Ca^{++} ions and the O^{--} ions still occupy the same positions which they held in the original lattice. But recrystallization to the stable anhydrite lattice soon sets in, presumably spreading outwards from nuclei of the new phase present in the parent one.

When dehydration is conducted at low temperatures, X-ray diffraction patterns indicate the formation of the soluble anhydrite. Exposure of the anhydrite so-prepared to water vapor even to very low pressures leads to the formation of the hemihydrate, as inferred by the stoichiometric uptake as well as by X-ray analysis and infrared absorption spectra. The ease of this transformation may be due to the fact that the two lattices of the soluble anhydrite and the hemihydrate belong to the same system, and even most of the planes of both crystals possess almost the same spacings. Indeed, the description by many authors of the hemihydrate as zeolitic in nature may be due to the high reactivity of the soluble anhydrite, which under the usual experimental conditions of measurement takes up water vapor and becomes converted partially into the hemihydrate.

The reactivity of the anhydrite, however, is greatly reduced if the dehydration is conducted at higher temperatures (above 400°), when the anhydrite formed crystallizes out into a different lattice possessing the pattern characteristic of the insoluble anhydrite. The latter is converted into the hemihydrate with much greater difficulty.

The hemihydrate takes up small quantities of water by adsorption forces when it is exposed to increasing vapor pressures of the latter, but there is strong evidence that no dihydrate is formed except after exposure to the saturated vapor of water for long periods. This view is further supported by the failure of calcium sulfate to form the dihydrate when it is exposed to vapor pressures which are slightly less than the saturation value. Thus in a typical experiment in which the soluble anhydrite was exposed during several days to a relative vapor pressure of 96.5% (obtained from an appropriate solution of sulfuric acid), the water uptake reached the limiting value of 0.1018 g. of water per g. of sulfate. On outgassing at room temperature, the amount retained was reduced to 0.0697 g. of water per g. of sulfate, which corresponds nearly to the hemihydrate formation. Moreover, when the system then was exposed to the saturated vapor of water, quick uptake was noticed and the amount ultimately taken up exceeded the value required for the formation of the dihydrate. This indicates that the transformation of the hemihydrate into the dihydrate becomes possible when the former is in contact with liquid water formed by saturation condensation. This is in

(17) ASTM Index for Crystallographic Data, Philadelphia, Pa.

(18) W. A. Wooster, *Z. Krystallogr.*, **94**, 375 (1949).

agreement with the results obtained by several authors from the study of the hydration of the hemihydrate from the liquid phase. Thus Birss and Thorvaldson,[19] and Cunningham, Dunham and Antes[20] found that the direct hydration of the hemihydrate without the solid passing into solution is improbable, and the dihydration is consistent with a "through solution" mechanism involving the passage of structural units of a solid hemihydrate through solution followed by crystallization, a process which requires some time to be achieved.

However, when the anhydrite is formed at higher temperatures, a process of sintering develops, leading to a decrease in the surface area and a diminution of the pore volume of the solid. The amount of water taken up by the new structure at saturation vapor pressure becomes much less than would correspond to the formation of the dihydrate, although the hemihydrate formation is not excluded.

It may thus be concluded that the hydration from the vapor phase of anhydrous calcium sulfate prepared *in vacuo* takes place in two steps: prior formation of the hemihydrate from the anhydrite by a quick process, followed by the transformation of the hemihydrate into the dihydrate. The latter process is much slower, and there is sufficient evidence that it takes place only in presence of the saturated vapor of water. Raising the temperature of dehydration affects the second phase transformation more than it affects the first.

The authors wish to thank Professor F. G. Baddar for his help in making the measurements of the infrared absorption spectra.

(19) F. W. Birss and J. Thorvaldson, *Can. J. Chem.*, **33**, 870 (1955).

(20) W. A. Cunningham, R. M. Dunham and L. L. Antes, *Ind. Eng. Chem.*, **44**, 2402 (1952).

FREE RADICAL LIFETIMES IN RADIATION-INDUCED REACTIONS. THE ADDITION OF *n*-BUTYL MERCAPTAN TO OCTENE-1

BY WILLIAM H. CLINGMAN, JR.

Research and Development Department, American Oil Company, Texas City, Texas

Received December 7, 1959

The free radical lifetime in the radiation-initiated reaction of *n*-butyl mercaptan and octene-1 has been measured by a modification of the rotating sector technique. The reactants were sealed in a circular glass tube, which was fastened to a plastic wheel and rotated past a β-radiation source. The radical lifetime could be determined from the variation of the yield with the rate of rotation of the wheel. The inhomogeneous absorption of the β-radiation in the sample and possible effects of reactant diffusion during an experiment were considered in the quantitative interpretation of the data. The experimental value of the lifetime was used to estimate the individual rate constants of the chain reaction. From a comparison of the results with data for similar systems, it was concluded that only part of the radicals produced by the radiation initiate the mercaptan–olefin reaction.

Recently, a radiation-induced reaction of mercaptans in hydrocarbon solutions was reported,[1] and there is evidence that with an olefin the reaction occurs by a free radical chain mechanism.[1,2] This reaction has been further investigated by us in an effort to increase the efficiency with which the radiation is utilized. During the course of this investigation, it was desired to determine the radical lifetime, and a new experimental technique based on the rotating sector method was devised for this purpose.

The radiation-induced reaction of *n*-butyl mercaptan with pentene-1[2] and the photoinitiated reaction[3-5] have been established as free radical chain processes with second-order chain ending. The radical lifetime in such processes can be determined by using intermittent radiation, which is provided by a rotating sector.[6] With high energy radiation, however, it is difficult to construct a sector which is opaque to the radiation. Hart and Matheson[7] attached the samples to be irradiated to the periphery of a wheel. As the wheel rotated, the samples underwent successive dark and irradiated periods. In our laboratory, the reactants were sealed in a circular glass tube, which was fastened to a plastic wheel and rotated past a radiation source.

The radical lifetime can be determined from the variation of the yield with the rate of rotation of the wheel, and the value of the lifetime can be used to estimate the reaction rate constants. In addition, the experimental method is analogous to using a flow system with recycle of the reactants. Thus, the effect of flow rate on reaction efficiency, which is important in commercial applications, has been determined from the same data used to measure the radical lifetimes.

Experimental

Apparatus.—The reactants were sealed under their own vapor pressure in a circular glass tube of about 13 cm. diameter. This was fastened to a plastic wheel and rotated past a Sr^{90}-Y^{90} source of β-radiation. With this system, each portion of the reactants is irradiated intermittently.

The source was a Tracerlab Medical Applicator with a strength of 400 millicuries. In order to protect laboratory personnel from the radiation, the irradiation tube and source

(1) T. D. Nevitt, W. A. Wilson and H. S. Seelig, *Ind. Eng. Chem.*, **51**, 311 (1959).

(2) A. Fontijn and J. W. T. Spinks, *Can. J. Chem.*, **35**, 1384, 1379, 1410 (1957).

(3) R. Back, *et al.*, *ibid.*, **32**, 1078 (1954).

(4) M. Onyszchuk and C. Sivertz, *ibid.*, **33**, 1034 (1955).

(5) C. Sivertz, THIS JOURNAL, **63**, 34 (1959).

(6) R. G. Dickenson, "Photochemistry of Gases," Noyes and Leighton, eds., Reinhold Publ. Corp., New York, N. Y., 1941, p. 200.

(7) E. J. Hart and M. S. Matheson, *Disc. Faraday Soc.*, No. 12 169 (1952).

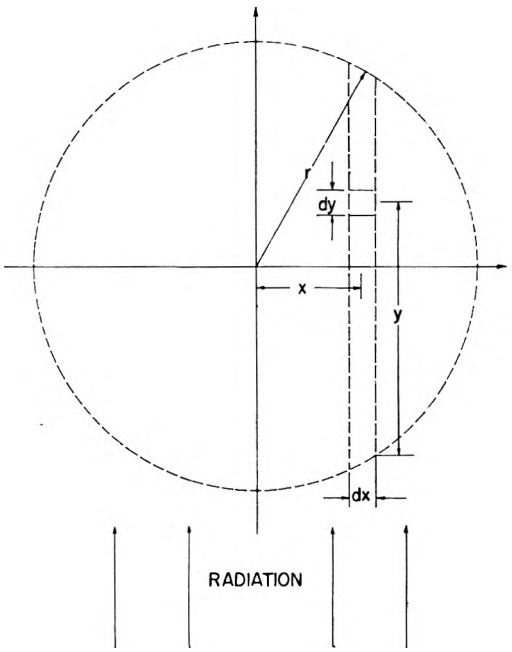

Fig. 1.—Geometric arrangement of radiation and sample.

were enclosed in a box constructed of one-half inch Plexiglas. Surrounding the active end of the applicator was a Plexiglas tube, which helped to collimate the β-radiation. From the diameter of the radiation beam, the ratio of the total cycle time to the radiation period was determined to be 25.1. The beam diameter was measured by allowing the radiation to darken the Pyrex irradiation tube while the latter was in a stationary position.

Materials.—The *n*-butyl mercaptan was distilled before use and an overhead fraction taken at 97.5–98.0°. The octene-1 was Phillips pure grade and was redistilled before use. Both reactants were dried over anhydrous sodium sulfate.

The water used in the dosimetry experiments was distilled from acidic potassium permanganate, then from alkaline permanganate, and finally redistilled to remove inorganic and organic impurities. This water was used to prepare the dosimeter solution, which was 10^{-3} *M* ferrous ammonium sulfate, 0.4 *M* sulfuric acid, and 10^{-3} *M* sodium chloride. Analytical reagent grade materials were used.

Procedure.—Solutions of *n*-butyl mercaptan in octene-1 (90 m*M*/l. of *n*-butyl mercaptan) were degassed by alternately freezing in liquid nitrogen, pumping to a pressure less than one micron, and melting. This procedure was repeated three times. The circular irradiation tube formed part of the degassing apparatus. The solution thus could be transferred to and sealed in the irradiation tube under its own vapor pressure. A sample also was taken for analysis in order to determine the initial mercaptan concentration. In sealing off the irradiation tube there is a possibility that impurities were introduced into the solution as a result of pyrolysis of the vapor. A comparison of the results with those obtained independently in another laboratory,[1] however, indicates that such impurities, if any, did not significantly affect the reaction rate.

The solution was irradiated for 16–24 hours. The reaction rate was determined by measuring the difference between the initial and final mercaptan concentrations. To improve the accuracy of the reaction rate determination, conversions between 25 and 75% were used. The decrease in mercaptan concentration during the course of the experiment was taken into account in the quantitative interpretation of the results.

The octene-1 solutions were analyzed for mercaptan by titrating with an isopropyl alcohol solution of silver nitrate. The end-point was determined potentiometrically using the procedure of Tamele and Ryland.[8]

(8) M. W. Tamele and L. B. Ryland, *Ind. Eng. Chem., Anal. Ed.*, **8**, 16 (1936).

Dosimetry.—The rate of energy absorption by the reactants was determined with a Fricke dosimeter.[9] The irradiation tube was filled with ferrous ammonium sulfate solution and rotated through the electron beam for a measured interval. The solutions were analyzed for ferrous ion both before and after irradiation by a colorimetric method. The complex of *o*-phenanthroline with ferrous ion was formed and the concentration of this complex determined by absorption at 515 μ. The method was calibrated using pure iron wire as a primary standard. The total energy absorption in water was then determined from the conversion of ferrous to ferric ion, assuming G = 15.6 molecules/100 e.v. for this reaction.

Since the β-radiation is attenuated as it passes through the sample, it was of interest to compute the energy absorption at the point where the radiation first enters the reaction tube. A cross section of this tube and its relation to the radiation beam are shown in Fig. 1. It is assumed that the beam of radiation is parallel and that the sample tube is a cylinder with its axis perpendicular to the radiation beam. Before entering the reactants, the β-rays from the Sr^{90}–Y^{90} source pass through the source cover (thickness = 100 mg./cm.²) and the glass wall of the irradation tube (thickness = 220 mg./cm.²). The combined thickness, 320 mg./cm.², is sufficient to absorb all the β-particles from Sr^{90} (maximum energy = 0.537 Mev.).[10] Thus, only the β-particles from Y^{90} (maximum energy = 2.18 Mev.) need be considered. The radiation absorption rate at distance y through the sample is $I_0e^{-\delta y}$ where δ is the absorption coefficient and I_0 is the absorption rate at $y = 0$.[10] The average rate of absorption $\bar{I}$ by a sample with this geometry and absorption law has been previously evaluated.[11] If r is the radius of the sample tube, then $\bar{I} = I_0J(\alpha)$, where $\alpha = 2\delta r$. Values of $J(\alpha)$ have been tabulated as a function of α.[11]

In the present experiments, the measured (Fricke dosimeter) value of $\bar{I}$ was 3.1×10^{19} e.v./l./hr. This is the average volume dose rate over the entire system when the sample is rotating. The values of r and δ were 0.3 and 6.2 cm.$^{-1}$, respectively. The latter was evaluated according to Loevinger.[10] Substituting these values in the above equation gives $I_0 = 2.7 \times 10^{16}$ e.v./l./sec. for water in the system. The corresponding dose rate for octene-1 is 2.0×10^{16} e.v./l./sec., due to the lower electron density of the octene-1. This is the time-average dose rate the reactants receive at $y = 0$.

Theory

The reactions (1) to (4) occur in the *n*-butyl mercaptan–olefin system[3–5]

(1) Radiation + Reactants → Free Radicals (X·)
(2) X· + *n*-BuSH → *n*-BuS· + XH
(3) *n*-BuS· + >C=CH$_2$ → >C—CH$_2$SBu
(4) 2X· → Termination

In reaction 1, radicals are produced by the radiation at the rate of $IG_R/100N$ expressed as mole/l./sec., where I is the dose rate in e.v./l./sec., G_R is the yield of radicals produced by the radiation in radicals per 100 e.v., and N is Avogadro's number. Radicals that are produced by the radiation but do not subsequently initiate the chain reaction are not included in G_R. Reactions 2 and 3 are chain-propagating reactions. In reaction 4, radicals are removed from the system by recombination or disproportionation. From literature data[4] on the *n*-butyl mercaptan–pentene-1 system, it is assumed that reaction 2 is the rate-determining propagation step at high olefin concentrations. Thus the radical in highest concentration is the mercapto-octenyl radical. This radical predominantly abstracts hydrogen from the mercaptan

(9) J. Saldick and A. O. Allen, *J. Chem. Phys.*, **22**, 438 (1954).

(10) R. Loevinger, *et al.*, "Radiation Dosimetry," G. J. Hine and G. L. Brownell, eds., Academic Press, Inc., New York, N. Y., 1956, pp. 704–716.

(11) W. H. Clingman, Jr., *J. Chem. Phys.*, **27**, 322 (1957).

rather than reacting further with the olefin.[4] It is the mercapto-octenyl radical which primarily enters into the termination reaction.

The variation in dose rate through the sample has been discussed above in the Experimental section. Referring to Fig. 1, the dose rate I is a function of y. Thus, the kinetics of the reaction will first be developed for constant y.

Consider the behavior of the reaction system at a fixed point of the circular irradiation tube as the latter passes through a complete cycle. At a time, $t = 0$, it will be assumed that the point is just entering the radiation beam. At $t = T_1$ the point leaves the radiation beam. At $t = T_2$, the cycle is complete and the point again enters the radiation. The behavior of the radical concentration [X·] during this cycle is given by the two differential equations shown, where k_4 is the rate constant for the termination reaction

$$d[X\cdot]/dt = (IG_R/100N) - 2k_4[X\cdot]^2 \quad 0 \leq t \leq T_1 \quad (1)$$

$$d[X\cdot]/dt = -2k_4[X\cdot]^2 \quad T_1 \leq t \leq T_2 \quad (2)$$

For steady-state operation, the following boundary condition must also be met

$$[X\cdot]_{t=0} = [X\cdot]_{t=T_2} \quad (3)$$

It is assumed that the rate of product formation is proportional to the radical concentration and the mercaptan concentration.[2] If k_2 equals the rate constant for reaction 2 and R equals the average reaction rate for a complete cycle of the irradiation tube, then

$$R = 1/T_2 \int_0^{T_2} k_2[n\text{-BuSH}][X\cdot]dt \quad (4)$$

At very fast rotation rates, the decay in radical concentration during the dark period will be negligible; and the concentration [X·] will be independent of time. The rate of radical production averaged over the entire cycle will be $(T_1IG_R/100NT_2)$. The lifetime λ which is to be measured is then defined by

$$[X\cdot] = \lambda(T_1IG_R/100NT_2) \quad (5)$$

The relationship between R, λ, T_1 and T_2 has been deduced by Dickenson.[6] If f equals the rotation rate of the irradiation tube in revolutions per second, R_∞ equals the limiting reaction rate as f increases, then

$$R/R_\infty = Q(f\lambda) \quad (6)$$

The functional form of $Q(f\lambda)$ depends only on T_2/T_1. The value of this latter quantity was 25.1 for the present apparatus. Using this value and the equations given by Dickenson,[6] Q was evaluated as a function of $(f\lambda)$.

Since the radiation intensity varies over the cross section of the irradiation tube, the lifetime and reaction rate will also vary. In addition, at finite diffusion rates for *n*-butyl mercaptan, the concentration of the latter will become a function of y as an experiment progresses. In order to calculate the observed reaction rate $\bar{R}$ it is necessary to integrate the rate, $R(y)$, over the cross section of the irradiation tube. Two cases will be considered: first, with a zero diffusion rate of *n*-butyl mercaptan in octene-1 and, second, with an infinite diffusion rate. As it turns out, the final results are nearly the same with either assumption.

Let

$c(y, t)$ = mercaptan concn. at time t after irradiation is begun and at a position y in the reaction tube

$\bar{c}(t)$ = av. mercaptan concn. at time t after irradiation is begun

Then

$$\bar{c}(t) = 1/\pi r^2 \int_S c(y, t)dx\,dy \quad (7)$$

where the integration is to be performed over the entire cross section of the irradiation tube.

$$\delta c/\delta t = -k_f(y)c \quad (8)$$

where k_f is a rate constant at rotation rate f

$$k_f(y) = k_\infty(y)Q[f\lambda(y)] \quad (9)$$

At fast rotation rates, the lifetime varies inversely with the square root of the radiation dose rate, and $k_\infty(y)$ varies directly with the square root of the dose rate.[2]

$$\therefore \lambda(y) = \lambda(0)e^{\delta y/2} = \lambda_0 e^{\delta y/2} \quad (10)$$

$$k_\infty(y) = k_\infty(0)e^{-\delta y/2}$$

First consider the case of zero diffusion rate. Integrating equation 8 with respect to t gives

$$c = c_0 \exp[-k_f(y)t] \quad (11)$$

where t is the reaction time and c_0 is the initial mercaptan concentration. c_0 is independent of y. The quantity $(\bar{c}(t)/(c_0)$ is the fraction of initial mercaptan that is unreacted at time t. It is this quantity which is measured directly in the experiments.

$$\bar{c}(t)/c_0 = (1/\pi r^2) \int_S \exp[-tk_\infty(0)e^{-\delta y/2} Q(f\lambda_0 e^{\delta y/2})\,dx\,dy \quad (12)$$

Next consider the case of an infinite diffusion rate. Then the concentration c is no longer dependent on y. Integration of equation 8 over the cross section of the reaction tube gives

$$d\bar{c}/dt = \bar{c}(t)(1/\pi r^2) \int_S -k_f(y)\,dx\,dy \quad (13)$$

$$= \bar{c}(t)(1/\pi^2) \int_S -k_\infty(0)e^{-\delta y/2}\, Q[f\lambda_0 e^{\delta y/2}]dx\,dy$$

Integration of the latter equation with respect to t then gives

$$\bar{c}(t)/c_0 = \exp\left\{-tk_\infty(0)(1/\pi r^2) \int_S e^{-\delta y/2} Q[f\lambda_0 e^{\delta y/2}]dx\,dy\right\} \quad (14)$$

The quantities $\bar{c}(t)/c_0$ and t are measured experimentally, and equations 12 and 14 give the relation between these quantities and the lifetime. By comparing experimental and theoretical values of $\bar{c}(t)/c_0$ at different rotation rates, both λ_0 and $k_\infty(0)$ can be determined.

Experimental Results

The rate constant, $k_\infty(0)$, was first evaluated using experimental data obtained at very fast rotation rates. As the rotation rate increases, the right-hand sides of equations 12 and 14 become independent of the lifetime, λ_0. At a reaction time of 17.5 hours, the limiting value of $\bar{c}(t)/c_0$ was 0.30 as the rotation rate increased. Using these

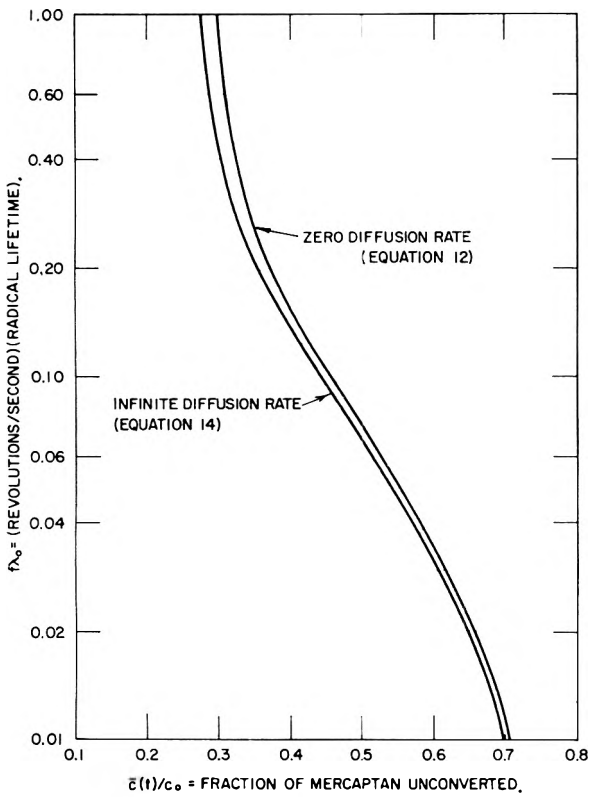

Fig. 2.—Predicted mercaptan conversion for zero and infinite diffusion rates; rate constant = $k_\infty(0) = 0.12$ hr.$^{-1}$; reaction time = 18 hr.

data, equations 12 and 14 were solved numerically for $k_\infty(0)$. The values obtained were 0.125 hr.$^{-1}$ for the case of a zero diffusion rate and 0.116 hr.$^{-1}$ for the case of an infinite diffusion rate. The slight difference between these values implies that the magnitude of the diffusion constant for *n*-butyl mercaptan in octene-1 has little effect on the experimental results. For $k_\infty(0)$ equal to 0.12 hr.$^{-1}$, a mercaptan concentration of 0.090 mole/l., and an average rate of energy absorption at $y = 0$ equal to 2.0×10^{16} e.v./l./sec., the G value for mercaptan conversion is 9.0×10^3. The G value for similar conditions that is predicted from the data of Nevitt, *et al.*,[1] is 5.3×10^3. The higher value obtained in the present study may have been due to a more efficient degassing of the reactants. It is known that oxygen inhibits the radiation-induced mercaptan-olefin reaction.[2]

That diffusion is unimportant in the present system can be further illustrated by comparing values calculated for $\bar{c}(t)/c_0$ by equations 12 and 14 at different rotation rates. In Fig. 2 are shown plots of $\bar{c}(t)/c_0$ *vs.* $(f\lambda_0)$ as calculated from both equations 12 and 14. In these calculations, $k_\infty(0)$ was given the value 0.12 hr.$^{-1}$ and the reaction time was assumed to be 18 hours. It can be seen that at any given value of $(f\lambda_0)$ the predicted mercaptan conversion is nearly independent of the diffusion constant for *n*-butyl mercaptan in octene-1. One would not expect this result to be general. With different values for the radiation absorption coefficient and apparatus dimensions, diffusion may become important.

In determining the lifetime from the experimental data, equation 14 was used. Let k_f equal $\{-\ln [c(t)/c_0]/t\}$. The quantity k_f can be determined directly from the experimental data and also calculated from equation 14. For an infinite diffusion rate, k_f is a function of $(f\lambda_0)$ alone and is independent of the reaction time. The value of the reaction rate averaged over the cross section of the irradiation tube is equal to $k_f c$. In Fig. 3, the theoretical curve is given for (k_f/k_∞) *vs.* $(f\lambda_0)$. This curve was calculated using equation 14. The experimental points also are shown in Fig. 3. The quantities (k_f/k_∞) and f were determined directly from experiment, while $(f\lambda_0)$ was calculated assuming that the lifetime λ_0 was 0.45 second. This value for the lifetime gave the best agreement between the experimental points and the theoretical curve.

The experimental results for a very fast rotation rate and $y = 0$ are summarized in Table I. The values for the lifetime and reaction rate may be used to determine the individual reaction rate constants. If G_M equals the G-value for mercaptan conversion and I_0 equals the time-average rate of energy absorption, then equations (15), (16) and (17) are valid at $y = 0$ and $f = \infty$

$$I_0 G_M = 100 N k_2 [c] [X\cdot]_\infty \quad (15)$$

$$[X\cdot]_\infty = \lambda_0 G_R I_0 / 100N \quad (16)$$

$$2k_4 [X\cdot]^2_\infty = G_R I_0 / 100N \quad (17)$$

TABLE I

SUMMARY OF EXPERIMENTAL RESULTS FOR ADDITION OF *n*-BUTYL MERCAPTAN TO OCTENE-1

Mercaptan conversion	$= G_M = 9.0 \times 10^3$ molecules/100 e.v.
Radiation absorption	$= I_0 = 2.0 \times 10^{16}$ e.v./l./sec.
Radical lifetime	$= \lambda = 0.45$ sec.
Mercaptan concn.	= 0.090 mole/l.

Equation 15 states that the rate of product formation is proportional to the mercaptan and radical concentrations; (16) that the radical concentration equals the radical formation rate times the lifetime; and (17) that the rate of disappearance of the radicals equals the rate of formation in the steady state. Using these three equations and the data in Table I, it can be deduced that $G_R k_2 = 2.2 \times 10^5$ (molecules/100 e.v.) (l./mole/sec.) and $G_R k_4 = 7.4 \times 10^9$ (molecules/100 e.v.)(l./mole/sec.).

Discussion

In order to determine completely the rate constants k_2 and k_4, it is necessary to know the radical yield G_R from the radiation. The value of G_R for *n*-heptane is 6.1, as determined using *n*-butyl mercaptan as a radical scavenger.[12] Assuming the same radical yield for octene-1 gives 3.6×10^4 and 1.2×10^9 l./mole/sec. for k_2 and k_4, respectively. These rate constants are compared in Table II with those given in the literature for similar systems.

The rate constants for the mercapto-octenyl radical are higher than those for the mercapto-styryl radical. This latter radical is resonance-stabilized, which probably accounts for its lower reactivity.[3] The mercapto-octenyl radical, how-

(12) R. H. Schuler, THIS JOURNAL, 62, 37 (1958).

ever, appears much less reactive than the mercapto-pentenyl radical. This latter result may in part be the result of assuming too high a value for G_R.

The G-value that is pertinent is actually the radiation yield of mercapto-octenyl radicals, since it is assumed that these are the predominant chain carriers.[4,5] Radicals that are produced by the radiation but do not eventually give mercapto-octenyl radicals should not be included in G_R. Olefins, as well as *n*-butyl mercaptan, can act as radical scavengers.[12] Thus, with octene-1 as a solvent, side reactions may occur in which some of the radiation-produced radicals are converted to stable products without forming mercapto-octenyl radicals.

TABLE II

COMPARISON OF REACTION RATE CONSTANTS

Radical	k_2 (l./mole/sec.)	k_4 (l./mole/sec.)	Ref.
Mercapto-styryl	2.6×10^3	5×10^8	3
Mercapto-octenyl	3.6×10^4	1.2×10^9	This work
Mercapto-pentenyl	1.4×10^{6a}	5×10^{10a}	4

[a] Estimated values.

In addition to estimating the rate constants, the experimental data may be used to predict the effect of flow rate on the mercaptan–olefin reaction. The radical lifetime in the above experiments was sufficiently long that flow rate had a marked effect on mercaptan conversion. This point is illustrated in Fig. 3, using the alternative coordinate system. The reaction rate is given as the G-value for mercaptan conversion; the rotation rate of the sample tube is expressed in terms of the linear flow rate of the reactants. The data illustrate the use of a flow system to increase the efficiency of a fixed source of radiation.

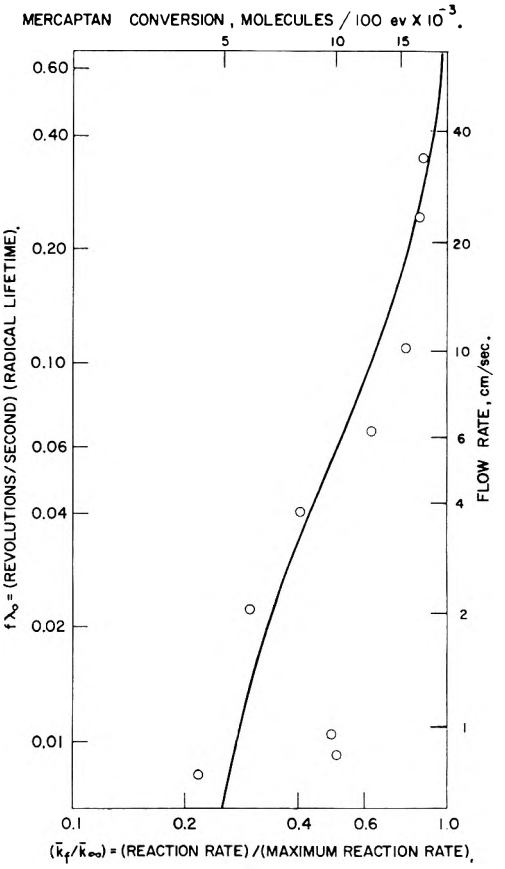

Fig. 3.—Comparison of theoretical and experimental relative reaction rates for *n*-butyl mercaptan–octene-1 system.

THE MASS SPECTRA OF DEUTERATED BIPHENYLS: MECHANISMS OF HYDROGEN AND CARBON LOSS PROCESSES[1]

BY J. G. BURR, J. M. SCARBOROUGH AND R. H. SHUDDE

Research Department of Atomics International, A Division of North American Aviation, Inc., Canoga Park, Cal.

Received January 25, 1960

The monoisotopic mass spectra of biphenyl (I), biphenyl-4,4′-d_2 (II), biphenyl-3,3′,5,5′-d_4 (III), biphenyl-2,2′,6,6′-d_4 (IV), biphenyl-2,2′,4,4′,6,6′-d_6 (V), biphenyl-2,2′,3,3′,5,5′,6,6′-d_8 (VI) and biphenyl-d_{10} (VII), corrected for the contributions of less deuterated contaminants, are presented. The discussion is concerned with (1) the question of chemical selectivity in bond breaking where a possible preference for breaking of the *para* C–H bonds is shown; (2) the nature and use of the secondary isotope effect in the loss of hydrogen and deuterium where this is defined in terms of normalized specific probabilities (Γ and Π factors); (3) the nature and significance of the primary isotope effect in the loss of hydrogen and deuterium from the molecule-ion; and (4) the factors governing the distribution of peaks within the peak groups corresponding to successive loss of carbon atoms and also some factors probably governing the relative size of these peak groups.

I. Introduction

Isotopic substitution of organic molecules has been used in mass spectrometry[2] both as a means for identifying the fragments observed and as a means for verifying one or another of the theories of ionization and the dissociation of ions.

Information thus gained about the identity of fragments formed has served to provide knowledge about the modes of decompositions of alcohols[3,4]

(1) Work performed under AEC Contract AT-(11-1)-GEN-8. This material was presented in part at the Boston Meeting of the American Chemical Society, April 5–10, 1959.

(2) F. H. Field and J. L. Franklin, "Electron Impact Phenomena," Academic Press, Inc., New York, N. Y., 1957, pp. 204–217 and Chap. V in general.

(3) (a) J. G. Burr, THIS JOURNAL, **61**, 1447 (1957); (b) W. H. McFadden, M. Louisbury and A. L. Wahrhaftig, *Can. J. Chem.*, **36**, 990 (1958).

(4) L. Friedman and J. Turkevich, *J. Am. Chem. Soc.*, **74**, 1666 (1952).

and the simpler straight chain alkanes.[5,6] Similar information has revealed the existence of extensive rearrangements consequent upon ionization of several alkylbenzenes.[7,8] In several cases information thus obtained has been correlated with data from the liquid and gas phase radiolyses of the same substances; evidence for the occurrence of similar dissociation processes in both the mass spectrometer and in the radiolyses was found.[9,10]

The isotope effect observed in the dissociation of labeled organic molecules has been used to examine several semi-empirical treatments of mass spectra. Dissociation of isotopically labeled diatomic molecules (such as hydrogen and nitrogen) has been explained successfully in terms of a Franck–Condon model,[2] but several effects in the dissociation of more complicated molecules seem more easily treated by the quasi-equilibrium theory of mass spectra.[2]

The easier loss of hydrogen from partially deuterated molecule-ions than from the completely protonated species, and the more difficult loss of deuterium, can be expressed in terms of normalized specific relative probabilities for hydrogen and deuterium loss—the Π and Γ factors[2] as calculated from the mass spectra of a series of deuterated methanes and ethylenes.[11–13]

However, the effects of isotopic substitution upon dissociation and rearrangement processes of molecule-ions have been carried out chiefly upon simple saturated and unsaturated aliphatic molecules. With the exception of the admirable work of Meyerson and Rylander on the mass spectra of alkylaromatic molecules,[7,8] little effort has been made to use this technique to study the mass spectra of aromatic molecules.

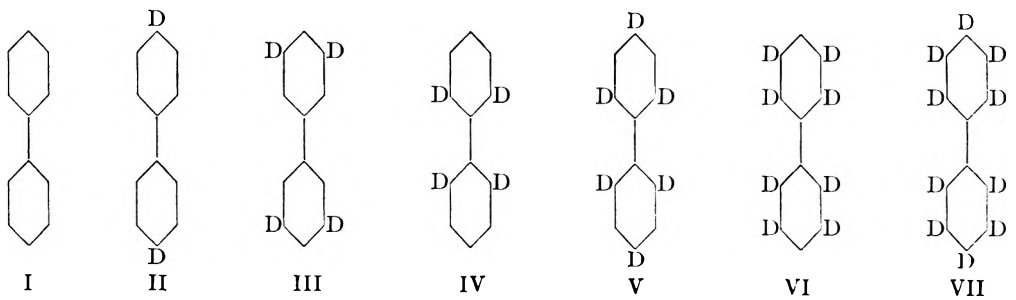

We are presenting in this paper information which has been gained by examining the mass patterns of the deuterated biphenyls, II–VII, together with the mass pattern of biphenyl itself, I. The preparation and purity of these materials has been reported elsewhere.[14] Our principal interest is in the radiation chemistry of these materials; some aspects of this are reported in an accompanying paper.[15] We hoped that an understanding of the molecule-ion dissociation processes would help us understand the radiation chemistry. This expectation has been fulfilled only in part.

Many of our reasons for choosing biphenyl as the object of our efforts are discussed in the other paper.[15] We should like here to point out that the *ortho*, *meta* and *para* positions of biphenyl are distinctly non-equivalent to substitution by ionic and free radical reagents; however the rate-determining step in these reactions is addition to the aromatic ring and the non-equivalence of the several positions in substitution appears to be principally an empirical function of the quantum chemistry of the ring carbon atoms rather than a function of the strengths of the carbon–hydrogen bonds at these several positions. It is not known whether these bonds do actually differ in strength,[16] and an *a priori* guess cannot be made as to whether these bonds should dissociate at different rates in the various molecules-ions generated in the mass spectrometer.

II. Experimental

The mass patterns reported here were obtained from samples of the pure deuterated biphenyls synthesized here[14] and of purified Eastman Kodak biphenyl. The samples were run in a modified Model 620 mass spectrometer, manufactured by Consolidated Electrodynamics Corporation at a nominal ionizing potential of 70 volts. A series of runs at nominal voltages from 9–70 volts was made from which it was determined that fragmentation did not occur below 12 volts. All purity determinations were made at 11 volts. The temperature of the sample inlet system was 250°, and the temperature in the ionizing region was also 250°.

III. Results

Monoisotopic partial mass patterns of the biphenyls (I–VII) are shown in Tables I through IV; the patterns have been broken into sections simply for convenience in reading.[17] Table V

(5) F. E. Condon, *J. Am. Chem. Soc.*, **73**, 4675 (1951).

(6) W. H. McFadden and A. L. Wahrhaftig, *ibid.*, **78**, 1572 (1956).

(7) P. N. Rylander, S. Meyerson and H. M. Grubb, *ibid.*, **79**, 842 (1957).

(8) S. Meyerson and P. N. Rylander, THIS JOURNAL, **62**, 2 (1958).

(9) J. G. Burr, *ibid.*, **61**, 1483 (1957).

(10) J. G. Burr, *J. Am. Chem. Soc.*, **79**, 751 (1957).

(11) V. H. Dibeler and F. L. Mohler, *J. Research Natl. Bur. Standards*, **45**, 441 (1950).

(12) V. H. Dibeler, F. L. Mohler and M. deHemptinne, *ibid.*, **53**, 107 (1954).

(13) F. L. Mohler, V. H. Dibeler and E. Quinn, *ibid.*, **61**, 171 (1958).

(14) R. I. Akawie, J. M. Scarborough and J. G. Burr, *J. Org. Chem.*, **24**, 946 (1959) reports the preparation of II, III, V, VII. The synthesis of IV and VI together with the catalytic deuteration of biphenyl will be reported in a forthcoming note (R. I. Akawie, *J. Org. Chem.*, in press).

(15) J. M. Scarborough and J. G. Burr, THIS JOURNAL, **64**, 1367 (1960).

(16) In forthcoming papers by R. H. Shudde and G. W. Lehman and by R. H. Shudde and J. M. Scarborough, on the vibrational modes of biphenyl it will be reported that the best fit between computed and experimental infrared spectra was obtained by using differing force constants for the C–H bonds in the *ortho*, *meta* and *para* positions; this, however, still does not provide useful information about the dissociation energies of these bonds.

(17) The complete raw and corrected patterns will be submitted to the American Petroleum Institute for publication in the Tables of Mass Spectral Data.

TABLE I

THE MONOISOTOPIC PATTERNS OF THE DEUTERATED BIPHENYLS (I–VII) PARENT REGION

m/e	$C_{12}H_{10}$ (I)	$C_{12}H_8D_2$ (II)	$C_{12}H_6D_4$ (III)	$C_{12}H_5D_4$ (IV)	$C_{12}H_4D_6$ (V)	$C_{12}H_2D_8$ (VI)	$C_{12}D_{10}$ (VII)
164							100.00
163							2.00
162						100.00	33.71
161						11.12	1.84
160					100.00	26.26	19.80
159					18.63	10.34	0.38
158			100.00	100.00	23.13	11.18	4.64
157			26.04	25.59	13.20	2.78	0.14
156		100.00	23.16	22.35	7.24	2.22	0.91
155		31.94	13.00	12.97	2.88	0.67	
154	100.00	24.65	5.31	5.50	1.28	0.29	
153	36.68	10.90	2.16	2.57	0.47		
152	26.83	3.78	0.66	0.89			
151	7.17	1.19	0.14	0.17			
150	2.19	0.20					
149	0.19						

TABLE II

Loss of 1 carbon

m/e	$C_{12}H_{10}$	II $C_{12}H_8D_2$	III $C_{12}H_6D_4$	IV $C_{12}H_5D_4$	Calc. $C_{12}H_6D_4$	V $C_{12}H_4D_6$	VII $C_{12}H_2D_8$	VII $C_{12}D_{10}$
146							0.09	1.74
145						0.02	1.10	
144				0.01		0.65	0.88	0.05
143			0.318	0.40	0.33	1.08	0.05	
142		0.01	1.16	1.31	.99	0.30		0.06
141		0.89	0.60	0.77	.59			
140		1.05	0.08	.14				
139	1.97	0.14		.02				
138	0.09							
137	0.05							

Loss of 2 carbons

136								4.13
135							1.58	
134						0.50	2.72	3.09
133						2.40	1.62	
132			1.34	1.70	1.32	2.31	1.57	2.13
131			3.05	3.44	2.66	1.80	1.36	
130		2.35	2.43	2.86	2.40	1.59	0.61	0.22
129	0.02	2.97	2.17	2.38	2.18	0.85	0.13	
128	3.96	2.49	1.30	1.55	1.59	0.20		
127	3.07	1.83	0.34	0.44				
126	2.90	0.41						
125	0.36							
124	0.01							

Loss of 3 carbons

122							0.225	6.10
121						0.15	3.51	
120						1.77	2.29	0.36
119			0.88	1.15	0.93	3.45	0.23	
118			3.57	4.30	2.80	1.00	0.20	0.68
117		2.21	1.93	2.17	1.68	0.34	0.44	
116		3.54	0.56	0.59	0.22	0.41		
115	5.92	0.55	.49	.52		0.18		
114	0.42	.60	.15	.19				
113	0.81	.13						

shows the sum probabilities for the various carbon loss processes (Molecule-ion peak = 100) and also shows the "total ionization" for each molecule. Various aspects of data presented in these Tables I–VI are treated separately below. The half-integral peaks (double ionization) for biphenyl are omitted for the sake of clarity (but see Section B, footnote, below). The peaks for doubly ionized biphenyl-d_{10} species occur at integral mass numbers only.

TABLE III

m/e	$C_{12}H_{10}$	II $C_{12}H_8D_2$	III $C_{12}H_6D_4$	IV $C_{12}H_6D_4$	Calc. $C_{12}H_6D_4$	V $C_{12}H_4D_6$	VI $C_{12}H_2D_8$	VII $C_{12}D_{10}$
Loss of 4 carbons								
110								
109								
108							0.33	3.89
107			0.18			0.35	2.84	
106			0.30	0.37	0.28	2.35	1.05	1.18
105		0.13	1.48	2.74	1.51	1.56	0.70	0.12
104		0.90	2.72	2.39	1.97	0.77	0.30	0.29
103	0.23	3.05	0.91	1.05	1.06	0.38		
102	3.87	0.99	0.47	0.51	0.34			
101	1.33	0.50						
100	0.35							0.60
99	0.61							
98	1.06							0.70
Loss of 5 carbons								
96								
95						0.39		
94			0.38	0.51		0.74	0.49	2.47
93		0.21	.75	.33		0.54	1.54	
92		.39	.57	.76	0.51	1.36	0.47	0.67
91	0.62	.33	1.52	1.65	1.10	0.75	.37	
90	0.02	1.54	0.90	0.97	0.83	.58	.74	1.35
89	2.16	0.92	0.88	0.99	.78	.80	.53	
88	0.70	1.04	1.11	1.13	.88	.72	.62	0.82
87	1.69	1.18	0.84	0.87	.28	.43		
86	1.16	0.79	0.43	0.47				0.27
85	0.34	0.24						

TABLE IV

m/e	$C_{12}H_{10}$	II $C_{12}H_8D_2$	III $C_{12}H_6D_4$	IV $C_{12}H_6D_4$	Calc. $C_{12}H_6D_4$	V $C_{12}H_4D_6$	VI $C_{12}H_2D_8$	VII $C_{12}D_{10}$
Loss of 6 carbons								
84								
83							1.50	
82						1.21	0.78	20.38
81			0.73	1.37	0.70	1.24	16.38	
80			1.98	2.07	3.98	14.93	5.56	40.19
79		1.87	15.21	16.02	11.60	12.25	21.71	
78	1.48	13.64	22.79	23.37	21.40	12.88	2.67	4.38
77	14.30	29.57	8.66	9.01	17.70	2.83	1.72	
76	41.76	20.40	3.55	4.32	6.00	2.71	2.73	3.77
75	5.82	3.20	3.14	3.69	2.72	1.83	0.92	
74	4.75	2.51	1.36	1.37	1.17	0.42	0.23	0.24
73	0.39		0.21	0.24				1.08
Loss of 7 carbons								
70							0.44	2.36
69						0.41	1.47	
68			0.48	0.715	0.47	1.06	1.03	22.99
67		0.23	1.00	1.27	2.60	3.55	11.74	
66		0.89	7.31	8.48	7.55	6.89	4.28	12.59
65	1.23	10.23	5.45	6.46	9.80	6.35	4.18	
64	15.89	6.09	6.85	7.27	7.55	2.89	2.02	3.15
63	13.67	4.48	2.71	3.21	3.36	1.44	0.69	
62	3.41	1.95	1.28	1.46	1.15	0.66	0.70	0.70
61	1.09	0.65	0.41	0.55	0.47			

A. Isotopic Purity.—Isotopic purity was determined from the relative peak heights of the parent peak and the adjacent isotopic impurity parent peaks at a nominal ionizing potential of 11 volts. The isotopic purities obtained in this way are recorded in the earlier paper.[14] However, use of the isotopic purity thus measured for biphenyl-d_{10} (95.1% with 4.7% biphenyl-d_9) did not result in

TABLE V

VALUES FOR GROUP[a] AND TOTAL IONIZATIONS[b]

Group by carbon loss	$C_{12}H_{10}$ (I)	$C_{12}H_8D_2$ (II)	$C_{12}H_6D_4$ (III)	$C_{12}H_6D_4$ (IV)	$C_{12}H_4D_6$ (V)	$C_{12}H_2D_8$ (VI)	$C_{12}D_{10}$ (VII)
Parent	173.23	172.71	170.69	169.86	166.88	164.77	163.64
1[a]	2.10	2.15	2.15	2.57	2.07	2.11	1.88
2	10.97	10.45	10.73	12.43	9.82	9.61	9.59
3	7.59	7.51	7.87	9.29	7.24	9.67	7.41
4	7.62	7.41	7.66	8.95	6.76	6.45	6.76
5	6.77	6.73	7.68	7.90	6.71	6.06	5.61
6	69.05	72.89	58.24	60.63	50.44	54.05	72.86
7	35.63	24.62	25.70	29.22	23.33	26.79	41.24
8	35.07	25.94	30.18	37.32	27.54	29.56	37.41
9	13.46	9.98	11.83	15.12	10.12	11.38	12.65
Σ	361.49	340.39	332.73	353.29	310.91	320.45	359.05

[a] By this we mean the group of peaks associated with the formation of an ion where 1,2,3,4 . . 9 carbon atoms have been lost from the biphenyl molecule-ion. [b] This is not precisely what is usually known as total ionization since we were unable to measure sensitivities for these samples; we know of no reason, however, why sensitivities should vary appreciably for any of these samples.

perimental peak heights corresponding to the loss of 1H, 2H, 3H or 4H from biphenyl were taken as the total probabilities for the loss of 1, 2, 3 or 4 particles from the deuterated compounds. These probabilities then were multiplied by the appropriate statistical factor to give contributions of the several processes to a given m/e. In making these calculations the isotope effect in the relative rates of H and D loss was neglected since this matter is better dealt with by the methods described below.

D. Γ and Π Factors.—The calculation of Γ and Π factors has been made according to the definitions[2]

$$\Gamma = \frac{\text{Specific probability of H loss from } C_{12}H_nD_{10-n}}{\text{Specific probability of H loss from } C_{12}H_{10}}$$

$$\Pi = \frac{\text{Specific probability of D loss from } C_{12}H_nD_{10-n}}{\text{Specific probability of H loss from } C_{12}H_{10}}$$

and the specific probabilities are defined in the following manner: the specific probability of H loss from $C_{12}H_nD_{10-n}$ is equal to relative peak height of peak corresponding to loss of one H from $C_{12}H_nD_{10-n}$ divided by n.

TABLE VI

SPECIFIC PROBABILITIES FOR HYDROGEN AND DEUTERIUM LOSS

Compound	Loss of H or D: Γ_1	Π_1	IE = Γ_1/Π_1	Loss of 2H + HD + 2D: Γ_2	Π_2	IE = Γ_2/Π_2
Biphenyl (I)	1.00	(0.47)[a]	(2.12)[a]	1.00	..	..
Biphenyl-d_2 (II)	1.10	.56	1.91	1.07	0.47	2.30
Biphenyl-d_4 (III) and (IV)	1.18	.66	1.80	1.09	.62	1.76
Biphenyl-d_6 (V)	1.29	.73	1.72	1.12	.67	1.68
Biphenyl-d_8 (VI)	1.51	.79	1.91	1.42	.64	2.22
Biphenyl-d_{10}	(1.48)[a]	.93	(1.59)[a]	(1.15)[a]	.74	(1.56)[a]

[a] Values obtained by extrapolation; *cf.* Fig. 1 as an example.

complete removal of the peak at $m/e = 163$ in the monoisotopic pattern. We can only assign this deviation to slight instrumental instabilities since we also noted that the $^{13}C/^{12}C$ ratio varied slightly as the ionizing voltage was reduced.

B. Preparation of Monoisotopic Patterns.—The observed mass spectrometer records were corrected for carbon-13 contributions and for contributions from the hydrogen impurity in the deuterium contaminant by a modification of the standard calculation.[18]

C. Calculated Patterns.—Calculated monoisotopic patterns of these materials that would represent the hydrogen (deuterium) loss processes and the carbon cleavage processes as purely statistical processes were prepared. These calculated patterns do not take into account any isotope effects; they are based on the isotopic composition of the materials and a statistical loss of hydrogen and deuterium. The calculated values for one of the substances, IV, appear in Tables II through IV; calculated values for other substances have a similar agreement with observation and have been omitted for the sake of compactness and clarity.

To obtain the calculated peak heights, the ex-

(18) *Cf.*, for example, G. P. Barnard "Modern Mass Spectrometry," the Institute of Physics, London, 1953, p. 201–202. The particular modification which we used is described in the report NAA-SR-MEMO-5125; our method was programmed in Fortran language for an IBM 709 computer and details of this program will be found in the NAA-SR-MEMO-5125 report. The $^{13}C/^{12}C$ ratio used was 0.1455 (the average value obtained from the low voltage patterns; the results were quite insensitive to the exact value of this ratio). The value of the H/D ratio used for each spectrum depended upon the size of the impurity peak in the low voltage patterns since our corrections for hydrogen content were confined to the hydrogen impurity in the substituent deuterium.

The only term in these expressions not directly available from the mass patterns is the probability for D loss. The value of this has been obtained by considering that the relative probability for the loss of one particle (H or D) from a molecule-ion is a linear function of the deuterium content of the molecule-ion. The peak height for the loss of one particle (RPH_1) is established unambiguously for biphenyl by the size of the peak at $m/e = 153$, and for biphenyl-d_{10} by the size of the peak at $m/e = 162$. The corresponding values for the partially deuterated biphenyls were obtained from the expression $RPH_1 = 36.68 - 0.0297N$ where N is the per cent. of deuterium in the molecule-ion. If the value of the RPH_h for the peak corresponding to loss of one H is subtracted from this computed value, the difference is then equal to the value of the RPH_d for loss of one D. The values thus computed can be reduced to the Γ and Π factors by application of the above definitions. The values thus obtained for the Γ and Π factors are listed in Table VI, and shown also on Fig. 1.

The specific probabilities for double particle loss of hydrogen (*i.e.*, 2H + $^1/_2$HD) and deuterium (*i.e.*, 2D + $^1/_2$HD) can be estimated by a similar but longer and more approximate procedure. The steps involved in determining the loss of 2H + HD + 2D from a particular molecule-ion are shown below

$$RPH_2 = 2H + HD + 2D = 26.83 - 0.070\,N$$

where N is the % deuterium in the molecule-ion.

RPH_h and RPH_d are obtained from the calculations of Γ and Π listed above. Finally if we represent the peak at m/e = (molecule-ion) − (one mass unit) as $P - 1$ and the peak at m/e = (molecule-ion) − (two mass units) as $P - 2$, etc., then

Loss of 2H = $(P - 2) - RPH_d$
Loss of HD = $(P - 3) - RPH_{3h}$
Loss of 2D = $RPH_2 - (2H + HD)$

RPH_{3h} was estimated by multiplying the value of this peak in biphenyl (at m/e = 151) by the fractional hydrogen content of the particular molecule-ion—probably the most approximate part of the calculations, but the least important since three particle loss from biphenyl is not a large contributor to the ionization in the parent ion region. The values for double particle hydrogen loss and double particle deuterium loss were normalized and made specific in the same way that this was accomplished for the single particle losses. The values for the factors and the isotope effects thus calculated are shown in Table VI, as Γ_2 and Π_2.

IV. Discussion

I. Preliminary Considerations.—For the purposes of the following discussion we are representing the dissociation processes of the biphenyl molecule-ion by a simplified diagram

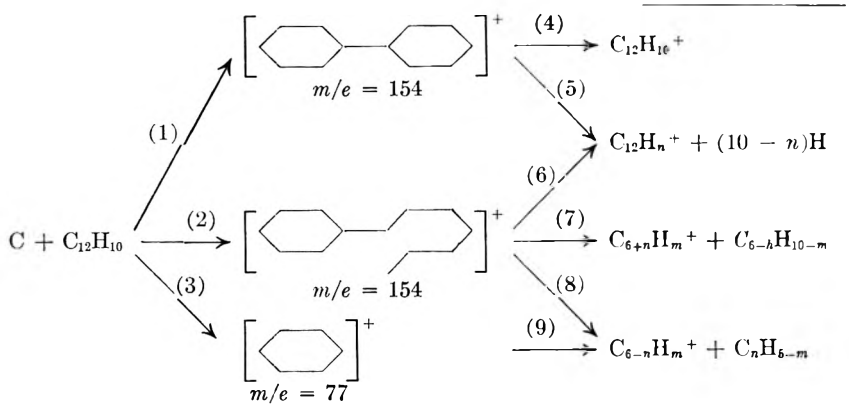

II. Hydrogen Loss Processes in the Molecule-ion Region.—The ions produced by rupture of carbon–hydrogen and carbon–deuterium bonds in the molecule appear in Table I. The molecule-ion whose dissociation produces this set of fragment ions has an undetermined structure; two of the most likely types of structure are shown on the preceding diagram (paths (1) and (2)).

The losses of H and D atoms from a partially deuterated biphenyl molecule-ion are subject to the possibility that not all of the carbon–hydrogen bonds in the molecule-ion are of the same strength and that the weaker ones may have a higher probability of rupture; this we shall define as chemical selectivity in bond rupture. The probability of carbon–hydrogen bond rupture is always higher than the probability of rupture of a similarly situated carbon–deuterium bond; we define this as a primary isotope effect. Existence of a secondary isotope effect appears in the observation that the probabilities of C–H bond rupture are higher in the deuterated molecule-ions than the probability of C–H rupture in the biphenyl molecule-ion.

Inspection of Table I shows that chemical selectivity is not obvious, if present. If the *ortho*, *meta* and *para* carbon–hydrogen bonds in biphenyl dissociate at different rates, these differences must be of the same order of magnitude as the isotope effects and thus be masked by the isotope effects. The situation cannot be untangled by use of *a priori* information since there is no *a priori* quantitative information about the strengths of the several carbon–hydrogen bonds, the effect of differences in bond strength upon rates of molecule-ion dissociation, or about the magnitude of the several isotope effects.

A. The Secondary Isotope Effect.—The question of chemical selectivity can only be answered if this effect can be untangled from the two isotope effects. We shall make use of the normalized specific rate factors defined above (Γ and Π factors) both for the purpose of disentangling isotope effects from chemical effects and also as a means for determining the magnitude and nature of the primary isotope effect. The manner in which we shall do this is qualitatively apparent from inspection of Fig. 1, the plot of Γ and Π factors as functions of the deuterium content of the molecule-ion.

It can be seen that each of these factors is a rather good linear function of the deuterium content, except that the Γ factor for biphenyl-d_8 (VI) is high, and the Π factor is low (these two are not necessarily independent variables; *cf.* Section III, D). This means that hydrogen is being lost abnormally easily from the 4,4′-position, and that deuterium is being lost with unusual difficulty from the other two sets of positions. One naturally then expects deuterium to be lost unusually easily from biphenyl-4,4′-d_2; the point for the Π factor of this molecule-ion does not appear to deviate from the line. The primary isotope effect should, however, reduce the deviation of this point from the line to about one-third or less of the deviation of the gamma point for VI from the line thus making the effect of selectivity in Π more difficult to detect.

Before it can be said that one of these points deviates from a normal relationship, it is necessary to establish the nature of the normal relationship. In Fig. 2 are shown the corresponding plots for the deuteriomethanes[11−13] and the deuterioethylenes.[11−13] It will be noted that in each case the

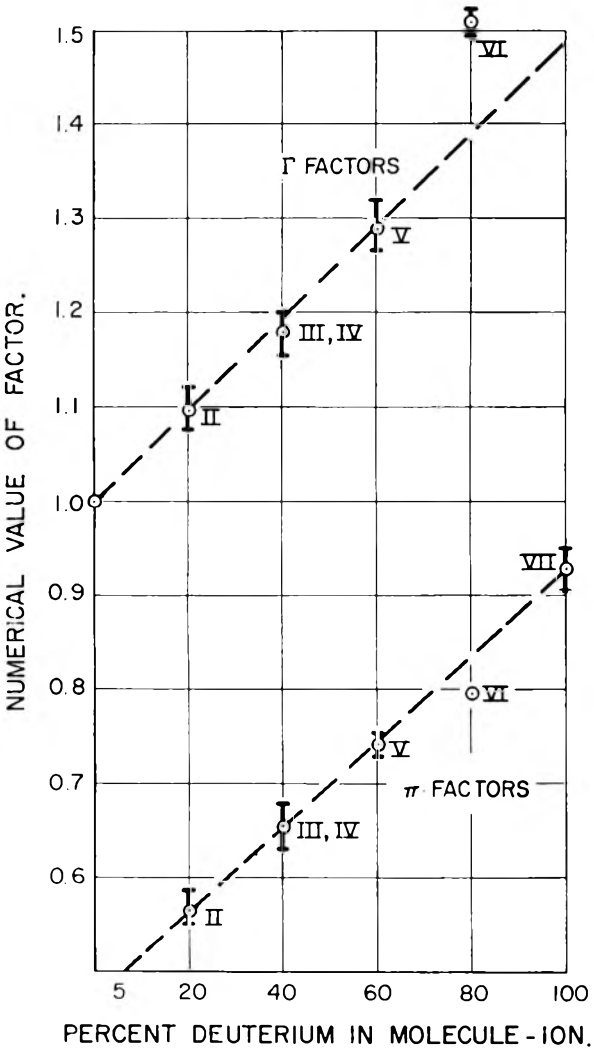

Fig. 1.—The Γ and Π functions calculated from the mass spectra of the deuterated biphenyls.

Γ and Π factors are smooth functions of the deuterium content of the molecule-ion; there is marked curvature to the methane plot and the ethylene plot appears to be linear although the data seem to distinguish between the two di-deuterioethylenes. The different Γ and Π factors for the two di-deuterioethylenes may possibly reflect an effect of the two different molecular structures. A rather more extreme example of such an effect is found in the mass spectra of the deuterated ethanols,[2] where the almost complete preference of single hydrogen loss from the $-CH_2-$ group is accurately reflected in the jagged function of the Γ and Π factors with deuterium content of the carbinols.

A view of the mathematical nature of these factors can be obtained from the quasi-equilibrium theory of mass spectra[19,2] where the rate constant for a particular dissociation process of the molecule-ion is expressed (for a collection of loosely coupled oscillators) as

$$K = \left[\frac{E - B - C - E_0}{E - C}\right]^{N-1} \frac{\prod_{i=1}^{N} \nu_i}{\prod_{j=1}^{N-1} \nu_j^{\ddagger}} \quad (1)$$

$$B = \frac{h\nu_{ch} - h\nu_{cd}}{\exp(h\nu_{ch} - h\nu_{cd}) - 1} \quad (2)$$

$$C = {}^1/_2(h\nu_{ch} - h\nu_{cd}) \quad (3)$$

where B (eq. 2) is the change in non-fixed energy of the systems which results from progressive substitution of C-D bonds for C-H bonds, and where

Table VII

Energy Levels, Electron Densities and Bond Orders

Biphenyl, $C_{12}H_{10}$

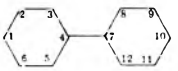

Energy levels: $\pm 2.2784\beta$; $\pm 1.8912\beta$; $\pm 1.3174\beta$; $\pm 1.0000\beta$; $\pm 0.7046\beta$. Calcd. excitation energy: $1.4092\beta \times 2.39 = 3.37$ e.v. Calcd. ionization potential: $0.705\beta \times 2.39 + 7.18 = 8.87$

Bond	Atom	Ground state	Excited state	Ion
1-2, 1-6, 9-10, 10-11	....	0.6601	0.5485	0.6043
2-3, 5-6, 8-9, 11-12	....	.6766	.7605	.7186
3-4, 4-5, 7-8, 7-12	....	.6188	.4087	.5137
4-7	....	.3697	.6161	.4929
.....	1, 10	1.0000	1.0000	.8415
.....	2, 6, 9, 11	1.0000	1.0000	.9803
.....	3, 5, 8, 12	1.0000	1.0000	.9105
.....	4, 7	1.0000	1.0000	.8768

Phenylhexatriene, $C_{12}H_{12}$,

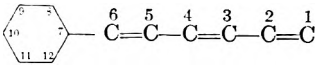

Energy levels: $\pm 2.1577\beta$; $\pm 1.7919\beta$; $\pm 1.4142\beta$; $\pm 1.0000\beta$; $\pm 1.0000\beta$; $\pm 0.3658\beta$. Calcd. excitation energy: $0.7316 \times 2.39 = 1.75$ e.v. Calcd. ionization potential: $0.3658 \times 2.39 + 7.18 = 8.05$ e.v.

Bond	Atom	Ground state	Excited state	Ion
1-2	....	0.8639	0.7000	0.7819
2-3	....	.4926	.6346	.5636
3-4	....	.7633	.4982	.6308
4-5	....	.5206	.7092	.6149
5-6	....	.7764	.5254	.6509
6-7	....	.4461	.5618	.5039
7-8, 7-12	....	.5954	.5309	.5632
8-9, 11-12	....	.6830	.7055	.6942
9-10, 10-11	....	.6550	.6309	.6429
....	1	1.0000	1.0000	.7759
....	2	1.0000	1.0000	.9700
....	3	1.0000	1.0000	.8318
....	4	1.0000	1.0000	.8956
....	5	1.0000	1.0000	.9148
....	6	1.0000	1.0000	.8152
....	7	1.0000	1.0000	.9819
....	8, 12	1.0000	1.0000	.9426
....	9, 11	1.0000	1.0000	.9978
....	10	1.0000	1.0000	.9341

C (eq. 3) is the difference in zero point energy between a C-H bond and a C-D bond (meaning of the other terms in the equations is the same as in the original references[19]).

Thus progressive substitution of C-D vibrations for C-H vibrations progressively increases the non-

(19) H. M. Rosenstock, A. L. Wahrhaftig and H. Eyring, Tech. Report. No. 11, June 25, 1952, Univ. of Utah, Inst. for Study of Rate Processes, Salt Lake City; H. M. Rosenstock, M. B. Wallenstein, A. L. Wahrhaftig and H. Eyring, *Proc. Nat. Acad. Sci. U. S.*, **38**, 667 (1952).

fixed energy of the whole molecule and thus progressively increases the rate constant for dissociation of any particular C–H or C–D bond[19]; on the other hand the rate constant for dissociation of a C–D bond is lower than the rate constant for a C–H bond in a given compound by an extent measured by the numerical value of C.[19] The numerical value of C is about three orders of magnitude greater than the numerical value of B. To the extent that this approximation is qualitatively valid, it can be seen that the specific normalized rate factors (Γ and Π) should be smooth monotonic functions of the deuterium content of the hydrocarbon.

The several bits of evidence thus accumulated above all strongly suggest that these factors should be smooth monotonic functions of the deuterium content of the molecule-ions—*as long as all of the C–H bonds in the molecule-ion dissociate at equivalent specific rates.* If some of the C–H bonds in a non-symmetrical molecule-ion dissociate more easily than others then it seems reasonable to expect that this chemical selectivity will be reflected in deviations of these factors from the monotonic relationship. From this point of view, we propose that the deviation (Fig. 1) of the specific rate factors for the biphenyl-d_8 (VI) may represent a distinct preference for the breaking of the C–H bonds in the *para* positions of biphenyl. We also suggest the general approach outlined above as a method for distinguishing isotope effects from chemical selectivity when these two effects are of the same order of magnitude.

If double particle loss processes are considered (*i.e.*, 2H + $^1/_2$HD, and 2D + $^1/_2$HD) the corresponding normalized specific loss factors (Γ_2 and Π_2; *cf.* Table VIII) these are found to be similar functions of the deuterium content of the molecule-ion.

B. The Primary Isotope Effect.—This effect is defined as the ratio of specific probability of hydrogen loss from the molecule-ion to the specific probability of deuterium loss; each of these specific rates has been shown above to be a sensitive function of the deuterium content of the molecule-ion so that it is necessary to specify further that each of these specific probabilities is measured in the same molecule-ion. Definition of the primary isotope effect as the ratio of Γ to Π factors takes into account the variation from molecule-ion to molecule-ion. Thus the primary isotope effect in the decomposition of biphenyl molecule-ion is not simply the ratio of probability of hydrogen loss from biphenyl molecule-ion to the probability of deuterium loss from biphenyl-d_{10} molecule-ion, 1.09; its value ranges from the ratio of hydrogen loss in biphenyl to the (extrapolated) deuterium loss from biphenyl, 2.12, to the ratio of (extrapolated) hydrogen loss from biphenyl-d_{10} to deuterium loss from biphenyl-d_{10}, 1.59. These values are collected in Table VIII.

It is interesting to compare these numbers with the primary deuterium isotope effect observed in the dissociation of some other molecule-ions. In the dissociation of H_2^+ and D_2^+ the isotope effect is 1.9.[2] The primary isotope effect in the dissociation of deuterated ethylene molecule-ions, measured by the ratio of Γ to Π factors, is 1.76[2]; whereas that for the deuterated methanes, measured similarly, is 3.00.[2] For monodeuterioethane, the ratio is 2.5.[2] The average value reported above for the biphenyls is 1.83.[20] These are very scanty data but we suggest that there may be one range of values for dissociation of unsaturated molecules, about 1.8–1.9; and another set of values for dissociation of saturated molecules-ions, about 2.5–3.0. It also seems suggestive to us that the isotope effect in the loss of two particles (*e.g.*, 2H + $^1/_2$HD) (see Table VI) has very nearly the same value as that for the loss of one particle. It is reported in the following paper[15] on the radiolysis of these deuterated biphenyls that the isotope effect in the formation of molecular hydrogen species is 3.0.

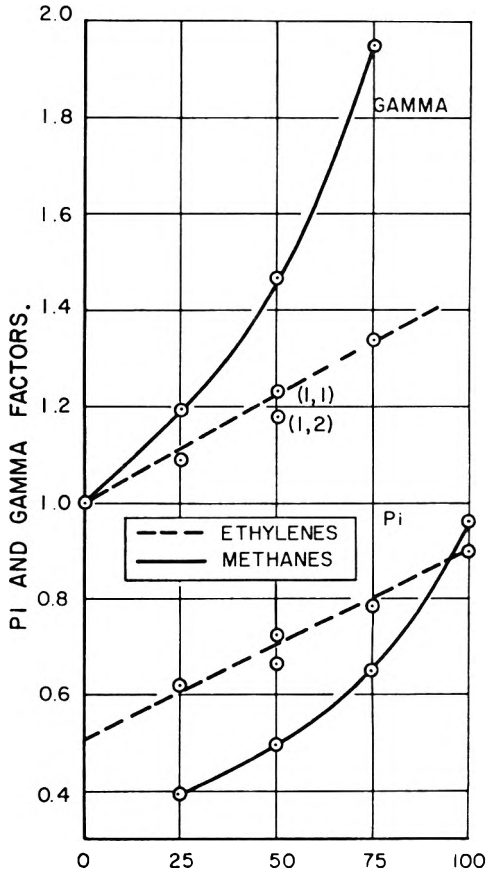

Fig. 2.—The Γ and Π functions calculated from the mass spectra of deuterated ethylenes and methanes.

III. Carbon–Carbon Bond Dissociations of the Biphenyl Molecule-ion.—Inspection of the mass spectra presented in Tables II–IV shows that dissociations of the biphenyl molecule-ions produce well defined groups of peaks corresponding to successive loss of carbon atoms from the molecule-ion; the distribution of peaks within each group is

(20) We do not have independent measurements of H loss and D loss from the biphenyl molecule-ions, and thus cannot be quite sure that the variation of the primary isotope effect with deuterium content of the molecule-ion is real or simply an artifact of the calculations. Under these circumstances it is more conservative to use an average value of the isotope effect rather than attach too much importance to the variation of the isotope effect. We think that this matter is worth further attention, however.

a measure of the probability of one or more hydrogen or deuterium atoms remaining or becoming associated with the lost group of carbon atoms. The spread and distribution of peaks within a group is observed to vary with the deuterium content of the original molecule-ion.

The distribution of peaks within each of the groups (for loss of 1–5 carbon atoms) can be reasonably well predicted by assuming that each carbon or group of carbons becomes associated with a quite random collection of H and D atoms (see Tables II–IV and the Section III, C); thus the partial selective deuteration of the original biphenyl molecule does not in this case provide us with information about the structure of the fragments resulting from dissociation of the molecule-ion, in contrast with the results obtained by application of this technique to other types of molecules (*cf.*, Section I). We can only assume that prior to separation of the carbon-containing fragments from the several molecule-ions, the C–H and C–D bonds have all become structurally equivalent. The poorer statistical predictability for the distribution of peaks for the groups of six or more lost carbon atoms probably is associated with substantial contributions of doubly ionized molecule-ions and fragment ions.[21]

A. Application of the Franck–Condon Principle.—We have calculated, by the simplest semi-empirical LCAO method,[22] the energy levels, the Π electron densities, and the bond orders for biphenyl, and an excited phenylhexatriene and for the ionized phenylhexatriene. Extension of the bond order definition to excited and ionized molecules is certainly open to serious theoretical objections, but calculation of excited molecule bond orders has been found qualitatively useful in several instances,[23] particularly in evaluating the effect of bond twisting upon the ultraviolet spectra of unsaturated molecules.[24] The results are shown in Table VII, for biphenyl and for 1-phenylhexatriene-1,3,6.

The effects of excitation and ionization upon the mobile bond orders are particularly interesting. From Table VII, the interannular bond which is the weakest bond in the ground state of biphenyl appears strengthened by excitation or ionization, whereas the four annular bonds adjacent to this bond are weakened by excitation or ionization. In the ion, these five bonds appear very nearly of the same strength. The bonds in the phenylhexatriene chain which are formally written as alternating single and double bonds do not seem so clearly distinguished from each other, as shown by the high double bond character of the formal single bonds. Excitation or ionization does not change this very much except that the chain bonds become even more nearly alike, and there is little difference between formal single or formal double bonds in the molecule-ion. The bond between the ring and the first chain carbon atom is about as strong as the other chain bonds.

If the mobile bond orders reported here are considered as the empirically equivalent equilibrium bond distances, then the changes of mobile bond orders with excitation or ionization are related to the probabilities that vertical excitation brings the bonds close to the left-hand turning point of the dissociation asymptote—*i.e.*, to the probabilities that vertical excitation or ionization is accompanied by dissociation. These calculations suggest, then, that scission of the biphenyl molecule-ion at the interannular bond (path 3) and ring opening at a given one of the bonds adjacent to the interannular bond (path 2) are energetically about equally probable. This inference is similar in principle to the application[25] of equivalent orbital theory to interpretation of the bond scission in the mass spectra of paraffins.

From this inference and from the higher probability that two C–C bonds will rupture successively rather than simultaneously, we conclude that a preliminary opening of one biphenyl ring precedes loss of carbon containing fragments. Deuterium and hydrogen have been observed to randomize along the chain very rapidly upon ionization of partially deuterated olefins[26] (and even in some cases upon ionization of deuterated aliphatic hydrocarbons[27]) so that preliminary ring opening in the biphenyl molecule-ion followed by rapid randomization of hydrogen and deuterium in the molecule-ion offers an explanation of the random deuterium content of the hydrogen associated with the carbon-containing fragments.

Additional evidence for this sequence of processes comes from comparison of Tables V and VII. It will be seen from Table V that the probability of loss for one carbon, two carbons, etc., are roughly the same, except for lower probability of one carbon loss. It will be seen from Table V that these probabilities are in good accord with the bond strengths in the phenylhexatriene molecule-ion even to the predicted much smaller probability of one carbon loss; we cannot easily make a similar comparison from the bond strengths in the intact biphenyl molecule-ion; the symmetry of this species makes the possible number of ways in which any fragmentation process can occur too large for any estimation.

B. Comparison of Total and Partial Ionization.—It will be noted from Table V that the "total ionizations" for biphenyl and biphenyl-d_{10} are nearly the same, but that the "total ionizations" for the partially deuterated biphenyls are less—and are progressively smaller with increasing deuterium content, in a fairly regular manner.

(21) Although we have not listed half-integral peaks in Tables IV and V for reasons of compactness and clarity, in biphenyl the following ratios of peak heights were observed: 77.5/155 = 0.13; 77/154 = 0.17; 76.5/153 = 0.19; 76/152 = 1.5. It seems probable that the peak at 77 is largely double ionization of $C_{11}H_{10}$, whereas the peak at 76 is a real fragmentation peak. Similar conclusions about the nature of the 77 peak have been reached by Hall and Elder, *J. Chem. Phys.*, **31**, 1420 (1959), from consideration of appearance potentials.

(22) B. Pullman and A. Pullman, "Les Theories Electroniques de la Chemie Organique," Masson et Cie., Paris, 1952.

(23) C. A. Coulson, "Valence," Clarendon Press, Oxford, 1952, p. 252.

(24) L. L. Ingraham, in "Steric Effects in Organic Chemistry," edited by M. S. Newman, John Wiley and Sons, Inc., New York, N. Y., 1956, p. 494.

(25) Ref. 2, pp. 171–172.

(26) W. A. Bryce and P. Kebarle, *Can. J. Chem.*, **34**, 1249 (1956).

(27) Ref. 2, p. 188.

We also note that this decrease in "total ionization" is owing to the decreased probability of the processes in which loss of six, seven and eight carbon atoms are lost. The probability of the other carbon loss processes appears to be closely similar in all of these molecules.

Acknowledgment.—We wish to acknowledge the invaluable assistance of R. A. Meyer who obtained all the spectra reported in this paper; we also wish to acknowledge many helpful conversations with D. E. McKenzie, J. P. Howe and H. Eyring in particular.

THE RADIOLYSIS OF DEUTERATED BIPHENYLS: MECHANISM OF HYDROGEN FORMATION[1]

BY J. G. BURR AND J. M. SCARBOROUGH

Research Department of Atomics International, A Division of North American Aviation, Inc., Canoga Park, Calif.

Received January 25, 1960

Certain general characteristics of the radiation chemistry of aromatic hydrocarbons are summarized. The values of G(hydrogen), G(H), G(D) and the $H_2/HD/D_2$ ratios observed in the radiolysis with cobalt-60 γ-rays of biphenyl, biphenyl-4,4′-d_2, biphenyl-2,2′,6,6′-d_4, biphenyl-3,3′,5,5′-d_4, biphenyl-2,2′,4,4′,6,6′-d_6, biphenyl-2,2′,3,3′,5,5′,6,6′-d_8 and biphenyl-d_{10} are reported. The formation of radiolytic hydrogen is insensitive to any difference between the *ortho*, *meta* and *para* positions of biphenyl (although it is sensitive to the 1.3 kcal./mole difference between C–H and C–D bonds) since the specific rates of H and D formation are insensitive to the location of deuterium on the hydrocarbon and the total hydrogen yield is a linear function of the deuterium content of the biphenyl. The isotope effect in the formation of radiolytic hydrogen and deuterium (3.00) is observed to be different from that observed in the loss of one or two hydrogen atoms (or deuterium atoms) in the dissociation of the corresponding molecule-ion in the mass spectrometer (1.8). It is shown that this same isotope effect of 3.00 and simple statistical considerations can be used successfully to account for the H_2, HD and D_2 ratios in the hydrogen from individual hydrocarbons. However, the H_2, HD and D_2 content of the hydrogen from a mixture of biphenyl and biphenyl-d_{10} cannot be so described, and is also observed to be unequilibrated. It is suggested from this that at least two processes are involved in the formation of radiolytic hydrogen from biphenyl.

I. Introduction

In this article we are reporting the results of using partial selective deuteration to obtain information about the mechanisms of hydrogen formation in the radiolysis of biphenyl. An accompanying paper[2] contains the results obtained by applying this same technique to study the mechanism of the molecule-ion dissociation processes of biphenyl in the mass spectrometer; we are reporting elsewhere on the radical scavenging ability of several types of aromatic substances.[3]

We have chosen biphenyl as the subject for this research because biphenyl is the simplest aromatic molecule which has sets of distinguishable carbon–hydrogen and carbon–carbon bonds and which still retains much of the structural and electronic simplicity of benzene. We did desire an aromatic molecule which possessed distinguishable sets of carbon–hydrogen bonds to enable the use of selective deuteration as an aid in investigating the mechanisms of hydrogen formation. This procedure has been found useful in examining the radiation chemistry of ethanol,[4] acetic acid,[5] choline chloride[6] and methanol.[7] With this aim in mind we have prepared a number of selectively deuterated biphenyls.[8]

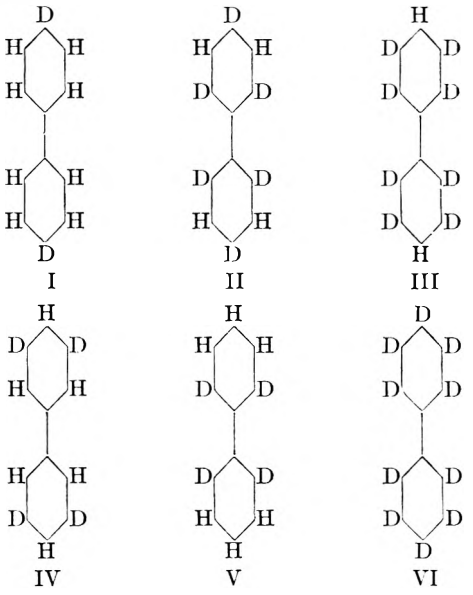

Degassed samples of these substances have been exposed to the ionizing γ-radiation from a 1500-curie cobalt-60 source. The yield of radiolytic hydrogen and its isotopic composition were de-

(1) Work performed under AEC Contract AT-(11-1)-Gen-8. This material was presented in part before the Boston Meeting of the American Chemical Society, April 5–10, 1959; and before the Congress of Nuclear Energy, Rome, Italy, June 15–19, 1959.

(2) J. G. Burr, J. M. Scarborough and R. H. Shudde, THIS JOURNAL, **64**, 1359 (1960).

(3) J. G. Burr and J. D. Strong, "The Radiolysis of Organic Solutions: III. Mixtures of Biphenyl with Propanol-2 and of Biphenyl with Benzophenone," Abstracts of the 137th Meeting of the American Chemical Society, p. 43-K, *J. Am. Chem. Soc.*, **81**, 775 (1959); J. G. Burr and J. D. Strong, THIS JOURNAL, **63**, 873 (1959).

(4) J. G. Burr, *ibid.*, **61**, 1477 (1957); *J. Am. Chem. Soc.*, **79**, 751 (1957).

(5) J. G. Burr, THIS JOURNAL, **61**, 1481 (1957).

(6) R. O. Lindblom and R. M. Lemmon, AEC Report UCRL-8204, p. 5, 1958.

(7) J. G. Burr, Abstracts of the 137th Meeting of the American Chemical Society, p. 43-K.

(8) The preparations of I, II, IV and VI are reported in an article by R. I. Akawie, J. M. Scarborough and J. G. Burr, *J. Org. Chem.*, **24**, 946 (1959). The preparations of III and V will be reported in a subsequent similar article together with some other aspects of deuterating aromatic hydrocarbons, *J. Org. Chem.*, in press.

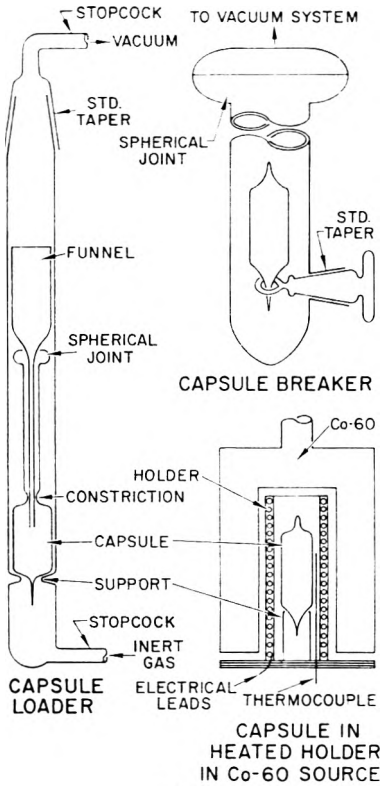

Fig. 1.

termined. The total dose of radiation was kept very low in order to minimize any possible dose dependency effects; under such conditions the quantities of hydrocarbon gases (which comprise only 2–3% of the gaseous products from biphenyl radiolysis) and the quantities of polymer were too low for measurement.

II. Experimental

(a) **Preparation.**—The synthesis of the deuterated biphenyls used in this investigation has been reported elsewhere.[8] Gas chromatography at two temperatures, infrared spectrophotometry and mass spectrometry of these materials indicated chemical purities greater than 99.5%. Small amounts of less deuterated materials were present but the isotopic purities ranged from 95.1 to 98.0 mole % of the species shown.[8]

(b) **Encapsulation and Capsule Opening.**—Capsules were prepared from 22 mm. Pyrex tubing, in a form shown in Fig. 1. These were filled in inert atmosphere with liquid biphenyl by means of the capsule loader shown in Fig. 1. The body lengths of the loaded capsules were about 75 mm. The filled capsules were attached to a vacuum system and degassed by conventional freeze–melt technique (the "freeze" portion of the cycle was to room temperature only since lower temperatures prevented effective degassing). The effectiveness of the degassing technique was measured by means of dummy runs (without irradiation); the amount of gas recovered from these runs was immeasurable in our gas buret system. Weight of sample was obtained from the weights of the empty capsule and the two parts of the filled, degassed and sealed ampule. The sample weights of the biphenyls were about ten grams in nearly all cases. The irradiated ampules were opened on a high vacuum line, using an ampule breaker of the design shown in Fig. 1.

The radiolysis gases were removed from the ampule with a Toepler pump through an ice-cooled trap and a liquid nitrogen-cooled trap, and were collected in a calibrated gas buret. During this pumping process the biphenyl was degassed by subliming it into the ice-cold trap. The volume of gas in the gas buret was determined by pressure and temperature measurements, and the composition of the gas was determined by mass spectrometry using a modified CEC Model 21-620 Mass Spectrometer.

(c) **Irradiation.**—All samples were irradiated with cobalt-60 gammas from a source of about 1500 curies in the shape of a hollow cylinder.[9] The source could be lowered around a heated capsule and holder, approximately 1 inch diameter by 4 inch height, as shown in Fig. 1. The dosage rate was determined by conventional ferrous sulfate dosimetry and measurement of hydrogen yield from benzene. Appropriate corrections for electron density were made for biphenyl samples. All samples were irradiated at 100 ± 5°. The dose rate was $1.4–1.5 \times 10^{18}$ e.v./ml. water-min.

Experiments with biphenyl-d_0 showed that G(hydrogen) was independent of dosage within the limits of error of these experiments since all values lie within the region of 0.00768 ± 0.0002 for dosages ranging from 1×10^{21} e.v./g. to 4×10^{21} e.v./g. Since dosages for most samples reported here were very similar, little error would be introduced unless there were a very large dose dependency.

Although the scanty existing data[10] for gas yields from biphenyl suggest that these are not very sensitive to temperature up to about 300°, the mechanisms for hydrogen formation which the work presented here has led us to propose (see below) require a sensitivity to temperature. It may very well be that some of the scatter of our data is caused by insufficiently precise control of the biphenyl temperature during the radiolysis.

III. Results

1. The 100 e.v. Yields of Hydrogen—$G(H_2, HD, D_2)$.—The observed yields of hydrogen (as $H_2 + HD + D_2$) are shown in Table I. These values were obtained by combining the experimental values of G(gas) with the experimental composition of the gas reported by mass spectrometry.

Our value for G(hydrogen) for biphenyl, 0.00768 ± 0.00019 (at a dose of 4.3×10^{21} e.v./g.) can be compared with the value of 0.0098 reported by Colichman and Gercke[10] at the considerably higher dose, 22.6×10^{21} e.v./g.; and the value of 0.0067 reported[11] for a dose of 1.9×10^{21} e.v./g. at 82°.

The variation of G(hydrogen)[12] with the deuterium content of the various biphenyls is shown in Fig. 2.

2. $G(H)$,[12] $G(D)$[12] and the Specific Rate Factors, γ and π.—The isotope effect in the formation of hydrogen and deuterium during these radiolyses has been determined by comparing the fractional hydrogen and deuterium contents of the radiolytic hydrogen with the fractional hydrogen and deuterium contents of the substrate hydrocarbon.

We have found it convenient to make this comparison in terms of specific hydrogen and specific deuterium yields which have been normalized to the same process in biphenyl. Our definitions are

$$\text{Specific hydrogen yield} = \frac{G(\text{H}) \text{ per C–H bond in hydrocarbon molecule}}{G(\text{H}) \text{ for biphenyl}/10} = \gamma$$

$$\text{Specific deuterium yield} = \frac{G(\text{D}) \text{ per C–D bond in hydrocarbon molecule}}{G(\text{H}) \text{ for biphenyl}/10} = \pi$$

(9) E. L. Colichman, P. J. Mallon and A. A. Jarrett, *Nucleonics*, **15**, No. 4, 115 (1957).

(10) E. L. Colichman and R. H. J. Gercke, *Nucleonics*, **14**, No. 7, 50 (1956).

(11) K. L. Hall and F. A. Elder, *J. Chem. Phys.*, **31**, 4120 (1959).

(12) We define G(hydrogen) as $G(H_2 + HD + D_2)$. $G(H)$ as $G(H_2 + {}^1/_2HD)$ and $G(D)$ as $G(D_2 + {}^1/_2HD)$.

TABLE I

PRODUCTS FROM RADIOLYSIS OF DEUTERATED BIPHENYLS

Substance	G(hydrogen)[a] × 10^2	No. of detns.	% H_2	% HD	% D_2	$G(H)_2$[a] × 10^3	$G(D)_2$[a] × 10^3	γ[d] (gamma)	π[d] (pi)	γ/π[c]
Biphenyl	7.68 ± 0.19	8	100	.....	.....	7.68	..	1.000	...	..
I	6.03 ± .28	3	83.8 ± 0.9	15.5 ± 1.0	0.77 ± 0.2	5.53	0.50	0.903	0.325	2.78
IV	5.79 ± .69	2	66.8	30.7 ± 2.2	2.56 ± 0.3	4.75	1.04	1.03	.338	3.05
V	6.03	1	69.8 ± 2.6	29.3	0.8	5.10	0.88	1.10	.296	3.72
II	4.30 ± .05	3	40.2 ± 3.0	45.7 ± 1.7	14.2 ± 1.3	2.72	1.58	0.89	.343	2.60
III	3.30	1	17.5	40.7	42.0	1.39	1.99	0.91	.342	2.80
VI	2.49 ± .31	3	3.6	5.9	90.5	0.16	2.34	(---)[b]	.31	
Biphenyl + VI 50/50 mixture	5.01 ± .12	2	60.3	27.6	12.2	3.71	1.30	0.97	.34	2.86
									Av.	2.97 ± 0.28

[a] G(hydrogen) = $G(H_2 + HD + D_2)$; $G(H) = G(H_2 + {}^1/_2HD)$; $G(D) = G(D_2 + {}^1/_2HD)$. [b] A value for this of 1.6 can be estimated very roughly since the 7% of H in the gas must have come from the approximate 1% of hydrogen in the biphenyl-d_{10} (although it is possible that some of the H_2 may have originated in water adsorbed on the ampule walls). [c] It should be noted that the ratio $G(H_2)/G(D_2)$ from biphenyl and biphenyl-d_{10} is 7.68 × 10^3/2.49 × 10^3 = 3.08. [d] Definition of these quantities will be found in section III-2 of the text.

These definitions are similar to the definitions[13] of γ and π factors which have been used elsewhere[2] to analyze the data obtained from the mass spectra of these biphenyls. As an example, we show computation of the specific hydrogen and specific deuterium yields for hydrogen obtained in the radiolysis of biphenyl-d_6 (II).

$$\gamma = \frac{2.70 \times 10^{-3} \times 10}{7.68 \times 10^{-3} \times 4} = 0.88$$

$$\pi = \frac{1.59 \times 10^{-3} \times 10}{7.68 \times 10^{-3} \times 6} = 0.34$$

The specific hydrogen yield for biphenyl is 1.00 by definition. It will be noted that the γ/π ratio is a measure of the apparent isotope effect for hydrogen formation relative to deuterium formation in the radiolysis of a particular hydrocarbon.

These definitions provide a simple means for comparing the radiolysis and molecule-ion dissociations of these deuterated biphenyls. Discussion of this comparison will be found in a later section of this paper. Compilation of the γ and π factors will be found in Table I, and the variation of these factors as a function of the deuterium content of the hydrocarbons is shown in Fig. 3.

3. Formation of H_2, HD and D_2.—The relative amounts of H_2, HD and D_2 are of interest because the H_2 is a hydrogen species which can be derived from the C–H bonds in the molecules; similarly the HD represents the result of *interaction* (by one or another mechanism, such as H and D atom abstraction) of the C–H and C–D bonds in the molecule or mixture of molecules; and finally the D_2 must be derived only from the C–D bonds in the molecules.

Measurements of this sort provide information about the degree of equilibration of these species. This may be evaluated by calculating the ratio $(HD)^2/(H_2)(D_2)$. If the species arise from equilibration of $H_2 + D_2$ or HD, then this ratio has the value at 25° of 3.25[14] (it will be shown later that when the hydrogen species arise randomly *via* the intermediacy of an organic molecule, the value of this constant seems to be 4.0). The values of this ratio for the gases evolved from the deuterated biphenyls are shown in Table II.

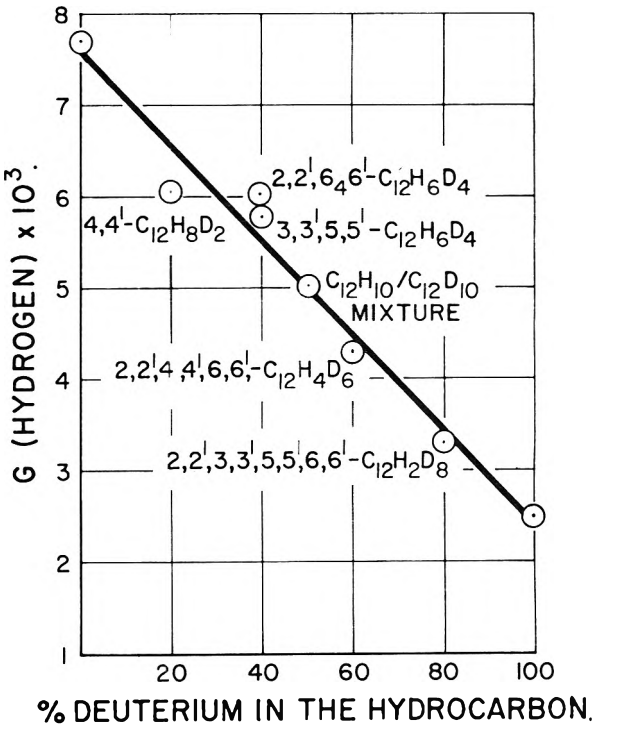

Fig. 2.

Ordinary probability theorems can be used to calculate the relative amounts of H_2, HD and D_2 to be expected in the hydrogen from each of the deuterated biphenyls if this formation is a purely random process. It is necessary to insert a weighting factor into these calculations for the comparison of calculation with experiment to be realistic.

Thus the relative probabilities of H_2, HD and D_2 formation correspond to the coefficients in the (normalized) binomial expansion of $(xNH + yMD)^2$, where N and M are the fractional abundances of C–H and C–D bonds in the molecule, and x/y is a weighting factor which can be considered to represent the isotope effect in the formation of H and D (as the molecular species H_2, HD

(13) F. H. Field and J. L. Franklin, "Electron Impact Phenomena," Academic Press, New York, N. Y., 1957, pp. 204–217.

(14) S. O. Thompson and P. G. Schaeffer, *J. Chem. Phys.*, **23**, 759 (1955); *cf.* also the original calculations by A. J. Gould W. Bleakney, and H. S. Taylor, *ibid.*, **2**, 362 (1934).

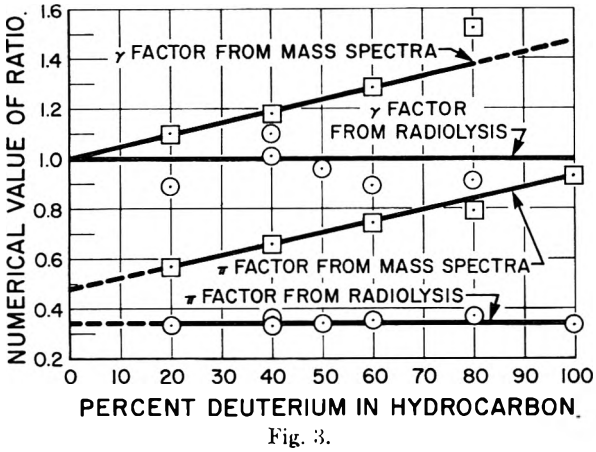

Fig. 3.

TABLE II

FORMATION OF H_2, HD AND D_2 IN THE RADIOLYSIS OF DEUTERATED BIPHENYLS

Substance	Species	(1.83 NH + MD)²	(3.0 NH + MD)²	Obsd.	K^a
Biphenyl-d_2 (I)	H_2	77.2	85.2	83.8	
	HD	21.1	14.2	15.5	3.72
	D_2	1.4	0.59	0.8	
Biphenyl-d_4 (IV)	H_2	53.7	67	66.8	5.52
(V)		53.7	67	69.8	(IV)
(IV)	HD	39.2	29.8	30.7	
(V)		39.2	29.8	29.3	15.4
(IV)	D_2	7.2	3.3	2.56	(V)
(V)		7.2	3.3	0.8	
Biphenyl-d_6 (II)	H_2	30.0	44.5	40.2	
	HD	49.3	44.5	45.7	3.67
	D_2	20.2	11.1	14.2	
Biphenyl-d_8 (III)	H_2	9.9	18.4	17.5	
	HD	43.1	49	40.7	2.25
	D_2	47.0	32.7	42.0	
Biphenyl–biphenyl-d_{10}	H_2	41.6	56.2	60.3	
	HD	45.5	37.5	27.6	1.04
50/50 Mixture	D_2	12.4	6.25	12.2	

[a] $K = (HD)^2/(H_2)(D_2)$.

and D_2). We use two values of x/y: 3.00 and 1.83. The results obtained by use of each of these values are shown in Table II.

TABLE III

THE ISOTOPE EFFECT IN THE LOSS OF H AND D FROM BIPHENYL AND DEUTERATED BIPHENYLS

Type of measurement	Value of isotope effect
1. $G(H_2)/G(D_2)$ from radiolysis of biphenyl and biphenyl-d_{10}	3.08
2. γ/π from radiolysis of deuterated biphenyls	2.97 ± 0.28
3. Γ/π from mass spectra of deuterated biphenyls[2]	(1.83)[a]

[a] Average value.

IV. Discussion

The radiation chemistry of aromatic hydrocarbons is distinguished by low product yields[15] (such as gases and "polymer"), and by the fact that the yield of polymer is about ten times the yield of hydrogen, whereas in the radiolysis of most saturated organic molecules the yield of hydrogen is two or three times the yield of polymer. It is also noteworthy that these materials are remarkably stable to ultraviolet light,[16] and that there is great predominance of the molecule-ion peak in the mass spectra.[2,13] The yield of radicals from aromatic hydrocarbons is about equal to the yield of "polymer."[17]

In the radiolysis of aromatic hydrocarbons some processes must be operative which, in a relative way, enhance the polymer yield and decrease the hydrogen yield. The formation of hydrogen in the radiolyses of saturated and aromatic substances may be discussed in terms of this set of elementary reactions.

$$RH \longrightarrow RH^* \quad (1a)$$

$$RH^* \longrightarrow R\cdot + H \quad (1b)$$

$$RH^* \longrightarrow R' + H_2 \quad (2)$$

$$RH^* + RH \longrightarrow R'' + H_2 \quad (3)$$

$$H + RH \longrightarrow H_2 + R\cdot \quad (4)$$

$$H + RH \longrightarrow RH_2\cdot \quad (5)$$

Reactions 1, 2 and 4 are sufficient in general to describe the formation of hydrogen in the radiolysis of saturated substances,[18,3] so that practically every molecule and atom of hydrogen which is formed in the dissociation process must necessarily appear in the product hydrogen. The effect which structural changes or isotopic substitution might have upon the dissociation processes must be reflected in the yield or composition of the product hydrogen.

On the other hand, aromatic hydrocarbons, and most of their derivatives, can be regarded as unsaturated substances to attack by hydrogen atoms and organic free radicals. It has been shown repeatedly that methyl radicals add readily to aromatic rings,[19] that hydrogen atoms can add readily to liquid[21] and gaseous aromatic hydrocarbons,[20] quite readily to solid olefins at liquid nitrogen temperature,[22] and that even phenyl radicals add readily to benzene at least at high temperatures in the gas phase.[21] The effect of dissolved aromatic hydrocarbons,[23] aromatic ketones,[24] and quinones[18] upon the radiolytic hy-

Swallow, *Chem. Revs.*, **56**, 471 (1956); B. M. Tolbert and R. M. Lemmon, A.E.C. Report UCRL-2704 (1954); J. G. Burr, Proceedings of the Second International Conference on the Peaceful Uses of Atomic Energy, Vol. 20, p. 187, Geneva, 1958; and the chapters on Radiation Chemistry in the several volumes of "The Annual Reviews of Physical Chemistry," Annual Reviews, Inc., Palo Alto, California.

(16) G. K. Rollefson and M. Burton, "Photochemistry," Prentice-Hall Book Co., New York, N. Y., 1939, Chap. VIII.

(17) A. Chapiro, THIS JOURNAL, **63**, 801 (1959), gives a summary of radical yields for benzene, toluene, xylene, ethylbenzene and styrene as measured by several different methods.

(18) G. E. Adams, J. H. Baxendale and R. D. Sedgwick, *ibid.*, **63**, 854 (1959).

(19) J. Smid and M. Szwarc, *J. Am. Chem. Soc.*, **78**, 3322 (1956), and earlier papers.

(20) P. E. M. Allen, H. W. Melville and J. C. Robb, *Proc. Roy. Soc. (London)*, **218**, 311 (1933); H. W. Melville and J. C. Robb, *ibid.*, **202**, 181 (1950).

(21) G. W. Taylor, *Can. J. Chem.*, **35**, 739 (1956).

(22) R. Klein and M. D. Scheer, THIS JOURNAL **62**, 1011 (1958).

(23) J. H. Baxendale, personal communication.

(24) J. G. Burr and J. D. Strong, THIS JOURNAL, **63**, 873 (1959).

drogen yield from several saturated substances has been shown to follow a simple kinetic scheme based upon a competition between hydrogen atom abstraction from the saturated substance and hydrogen atom addition to the aromatic substance (we do not wish to imply that we think that it is certain the effect of these additives is owing to addition scavenging, but that this is the most likely explanation at present).

It is thus apparent that the radiolysis of aromatic hydrocarbons differs from that of saturated substances at least to the extent that any hydrogen atoms arising in the dissociation step (1) might be removed not only by reaction 4 but also by reaction 5 and that more complicated radicals, such as phenyl, which also arise in the dissociation step might also be removed *via* a reaction similar to (5).

The high value of the radical yield measured for benzene, ranging from 0.8 to 3.1,[17,25] suggests that the dissociative split of aromatic hydrocarbons into radical pairs is an important process. The fate of the hydrogen atoms produced by the radical pair dissociation of the aromatic molecules is indicated clearly by several other studies. The yield of hydrogen in neutral, degassed aqueous benzene solutions has been observed to be 0.42,[26] equal to $G_w(H_2)$,[27] sensitive to *p*H or the presence of oxygen.[27] Phung and Burton cite this as evidence that the hydrogen atoms produced from radiolysis of water do not abstract (reaction 4) from benzene molecules under these conditions and this conclusion is reinforced by the observation of these same workers[24] that only a trace of HD is formed by the radiolysis of benzene-d_6 in water or the radiolysis of benzene in D_2O.

This evidence for the fate of water hydrogen atoms in the presence of benzene taken together with the low yield of hydrogen in the radiolysis of pure benzene suggests that hydrogen atoms produced in the benzene radiolysis disappear almost entirely by addition to surrounding benzene molecules. This concept is supported by the studies of Gordon, VanDyken and Doumani[28] who found that the yields of both hydrogen and biphenyl were low (0.044 and 0.090, respectively). The polymer, which was formed with a yield of about 0.90 (molecules of benzene appearing as polymer per 100 e.v. absorbed), consisted largely of hydrogenated biphenyls and terphenyls. These are the products which would be expected to be a consequence of the addition of hydrogen atoms to benzene, as suggested by the earlier observation of unsaturation in the polymer from irradiated benzene.[29]

Thus the evidence quoted here suggests that dissociation[30] into radicals is the predominant primary chemical process in the radiolysis of aromatic hydrocarbons; that the hydrogen atoms produced in this primary process are scavenged practically quantitatively[31] by addition to the surrounding aromatic hydrocarbon, and that other radicals produced in this primary process would also be extensively scavenged by a similar addition process.

However, hydrogen is produced in the radiolysis of benzene and in the radiolysis of biphenyl in yields which are about 10% of the radical yields or polymer yields; if the secondary reactions of hydrogen atoms are not important contributors to the formation of this hydrogen, then non-radical processes such as reaction 2 or reaction 3 must be the important contributors.

The hydrogen and deuterium obtained in the radiolysis of biphenyl and the deuterated biphenyls, I-VI, therefore must reflect characteristics of non-radical processes such as reactions 2 and 3. Products which would enable characterization of the radical reactions 1 and 5 would only be found among the monomer, dimer and other high boiling fractions of the radiolysis products. Other consequences of the non-radical processes 2 and 3 may possibly be found among the light hydrocarbon fractions of the radiolysis products, such as the acetylenes, which were obtained in too low a yield in this investigation to warrant examination.

1. The Yield of Hydrogen as a Function of Hydrocarbon Deuterium Content.—Selectivity in the formation of hydrogen during radiolysis of deuterated ethanols[4] was revealed in part by a non-linearity in the plot of G(hydrogen) *versus* deuterium content of the carbinol. A similar non-linearity has been observed in the radiolysis of deuterated methanols[7]; for the deuterated cholines,[6] the G(-M) value was a non-linear function of the deuterium content of the substance. It is apparent from inspection of Fig. 2 (and column 2, Table I) that the yield of hydrogen from the deuterated biphenyls is best considered as a linear function of the deuterium content of the biphenyl. The yield of hydrogen from the 50/50 mixture of biphenyl and biphenyl-d_{10} also falls accurately on this straight line.

Thus not only is the yield of hydrogen quite insensitive to the position of deuteration, but it is also insensitive to the manner of deuteration. The equation of the line in Fig. 2 can be presented as $G(\text{hydrogen}) = 7.68 \times 10^{-3} - (0.528 \times 10^{-3})N$, where N is the average number of deuterium atoms in the biphenyl, without regard to the position where the deuterium atoms are located on the biphenyl skeleton and, for a given N, without regard to the molecular species actually present.

It is thus apparent that the very real differences in reactivity among the *ortho*, *meta* and *para* posi-

(25) M. Burton and S. Lipsky, *ibid.*, **61**, 1461 (1957).

(26) P. V. Phung and M. Burton, *Radiation Research*, **7**, 199 (1957).

(27) T. J. Sworski, *J. Am. Chem. Soc.*, **76**, 4687 (1954).

(28) S. Gordon, A. R. VanDyken and T. F. Doumani, THIS JOURNAL, **62**, 20 (1958).

(29) W. N. Patrick and M. Burton, *J. Am. Chem. Soc.*, **76**, 2626 (1954).

(30) It is not meant by this statement to infer anything specific about the intimate mechanism of the radical formation: for example, it could occur *via* simple dissociation of excited or ionized molecules or *via* some much more complex process.

(31) For example, the G(scavengeable hydrogen atoms) in the Co-60 radiolysis of water is 3.70. All of these were scavenged by the concentration of benzene-d_6 used (ref. 25) since the observed $G(H_2)$ was 0.42. The G(HD) was observed to be 0.013. Thus (0.013/3.70) × 100, or 0.35% of the hydrogen atom reactions with this benzene were abstractive. If G(hydrogen atoms) from benzene is taken to be 0.4 (*i.e.*, one-half the radical yield), and 0.35% of these react with benzene *via* abstraction, then the G(hydrogen) produced by abstraction would be 0.0014 or about 2.5% of the observed total $G(H_2)$ from benzene, 0.040. We consider mechanistic contributions of this order of magnitude to be negligible.

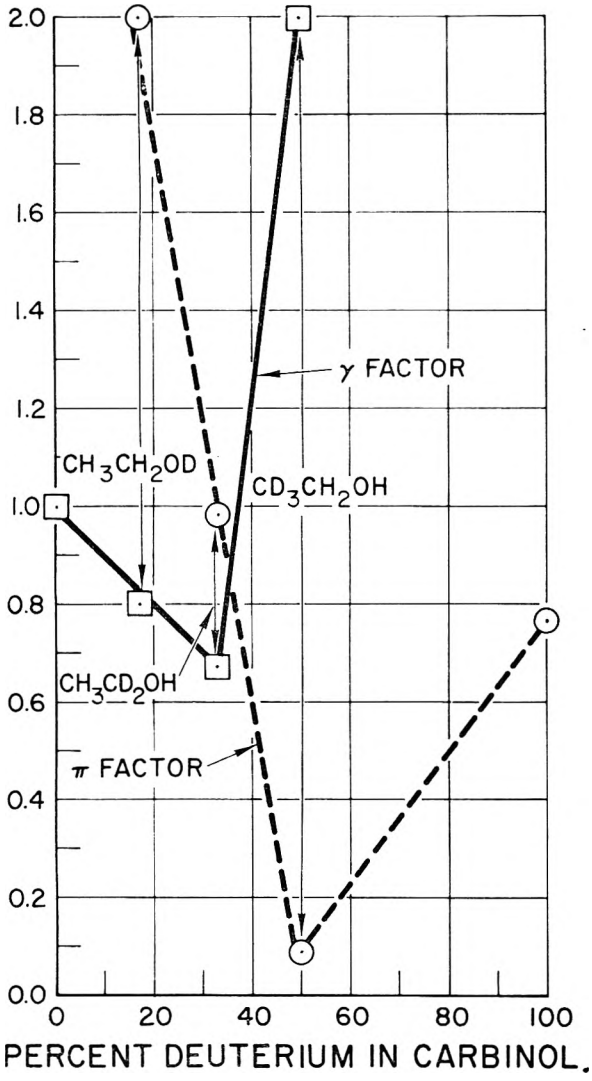

Fig. 4.

tions of biphenyl, which show up in ionic substitution reactions and in free radical substitution reactions of this molecule are not able to influence the over-all yield of hydrogen in this radiolysis.

2. **The Deuterium Content of the Hydrogen.**—It was observed in the earlier studies on saturated aliphatic substances that selectivity in the formation of hydrogen was evidenced not only in the variation of hydrogen yield with hydrocarbon deuterium content but was revealed also by consideration of the deuterium content of the radiolytic hydrogen.[4] The simple form of analysis usable for this problem when only the abstraction reactions of hydrogen atoms need be considered is obviously inapplicable to the radiolysis of biphenyl, since it appears that abstraction reactions are not important in the radiolysis of biphenyl.

We have found it convenient to represent the relative H and D content of the hydrogen from these biphenyls as $G(H)$ and $G(D)$, and the values of these quantities are found in Table I, columns 7 and 8. The values of $G(H)$ and $G(D)$ were made specific and normalized according to the definitions of γ and π factors given in the Results sections. The values of these functions are shown in Table I, columns 9 and 10. It will be noted on Fig. 3 that these functions seem, within experimental variation, quite insensitive to the deuterium content of the hydrocarbon, and again no evidence of position specificity appears in these normalized specific rates of hydrogen and deuterium formation.

Both hydrogen and deuterium are formed from these partially deuterated biphenyls at specific rates which do not depend upon the amount of deuterium present in the molecule—*i.e.*, the presence of deuterium in the biphenyl does not increase the specific rate of hydrogen formation or otherwise affect the breaking of carbon-hydrogen bonds.

If the data for the H and D content of the hydrogen produced in the radiolysis of the deuterated ethanols[4] are similarly reduced and plotted, as in Fig. 4—specificities in the dissociation of the C–H bonds in the ethanol molecule and in abstraction processes of the hydrogen and deuterium atoms are reflected very clearly in the variation of these γ and π factors with deuterium content of the carbinol. Thus in radiolyses where the formation of hydrogen may be reasonably considered to occur *via* simple dissociation into radicals followed by simple abstraction processes any position specificity is clearly revealed by this method for analyzing the data.

The insensitivity in biphenyl of the radiolytic specific hydrogen and deuterium yield factors (radiolytic γ and π factors) may be an artifact of the special nature of the liquid phase. The sensitivity of these yield factors in the dissociations of the molecule-ion to the deuterium content of the molecule-ion was assigned in the earlier paper[2] to the increased non-fixed energy content of the molecule-ion which is a demonstrable consequence of increasing the deuterium content. This effect can only influence the dissociation rates if the lifetimes of the molecule-ions are long enough for the excess energy to be distributed among all the possible degrees of freedom. This situation exists in the highly dilute gas phase of the mass spectrometer where the lifetime of the molecule-ion can be 10^7 normal vibrational periods or greater.

However, in the liquid phase this complete equilibration of absorbed ionizing energy may not be possible, since the collision frequency in the liquid is sufficiently high that all of the excess energy of the molecule-ion probably is removed within a few molecular vibration periods. Thus dissociation of a C–H bond in the energized molecule would not result from equilibration of energy but simply from excitation to a dissociative level of the potential energy curve for that bond in the energized molecule. The effect of increasing non-fixed energy with increasing deuterium content would never have a chance to influence the dissociation processes, and the liquid phase γ and π factors could be invariant with the deuterium content of the molecule.[32]

By either the measure of over-all hydrogen yield or by the measure of the specific hydrogen and

(32) However, since the excitation and ionization occur vertically, the Franck-Condon principle can be applied to explain why C–H bonds should still be broken faster than C–D bonds even in the liquid state—*cf.*, Field and Franklin, ref. 13, pp. 205 and 216.

deuterium yields, any difference among the bond strengths of the *ortho*, *meta* or *para* C–H bonds in biphenyl[33] apparently is not reflected in the rates of hydrogen formation from these deuterated biphenyls. Either there is no effective difference in the strengths of these bonds, or the difference is too slight to affect the radiolysis process (however, the radiolysis process is sensitive to the 1.3 kcal. difference between the C–H and the C–D bonds), or the mechanism is such that any differences in the bond strengths (*i.e.*, the structure of the molecule) would not be reflected in the radiolysis process—as an extreme example, the mechanism might be that of a completely random disengagement of hydrogen molecules from an essentially structureless transition state.

3. Consideration of the Isotope Effect.—In the first paper of this series[2] it was shown that the isotope effect observed in H and D loss from the deuterated biphenyl molecule-ions was a smooth function of the deuterium content of the molecule-ion with an average value of 1.83. It was suggested that this was a characteristic value for dissociation of single C–H and C–D bonds in the molecule-ions of unsaturated substances. It was also reported in that paper that the isotope effect, for the loss of two hydrogens from these molecule-ions, $(2H + {}^1/_2HD)/nH/(2D + {}^1/_2HD)/(10 - n)D$, was approximately the same as that for the loss of one hydrogen.

For the biphenyl radiolyses, we have two apparent measures of the isotope effect: (1) the ratio of the hydrogen yield from biphenyl to the deuterium yield from biphenyl-d_{10}; and (2) the calculated ratios of γ/π reported in Tables I and IV.

The numerical near-equality of these two isotope effects seems consistent with the conclusion reached above about the relative unimportance of the secondary reactions of hydrogen atoms as contributors to the formation of product hydrogen. It does not seem likely that the isotope effects for the secondary reactions of H and D atoms would all be equal to each other or be the same as the isotope effects in the dissociations of C–H and C–D bonds; the complex of possible reactions would be different for the substrates containing both C–H and C–D bonds than for the pure biphenyl and pure biphenyl-d_{10}. If the secondary reactions were important, it does not then seem likely that the ratios γ/π would be the same as the ratio $G(H_2)/G(D_2)$ for biphenyl and biphenyl-d_{10}, nor would the ratio γ/π be so nearly the same for all the partially deuterated substances.

4. Information to be Gained by Consideration of the H_2, HD and D_2 Content of the Radiolytic Hydrogen.—If the distribution of H_2, HD and D_2 to be expected from each of the deuterated biphenyls is computed statistically, it is then observed that the computed abundances do not agree at all with the observed abundances; this lack of agreement is not unexpected owing to the known existence of an isotope preference for the dissociation of C–H bonds. If the statistical computations are corrected by including a single weighting factor, then the entire set of computed abundances for the individual partially deuterated biphenyls can be brought into agreement with the observed abundances. The results are shown in Table II, columns 4 and 5; it is noteworthy that a single value of the factor, 3.00, suffices for the entire series.

Inspection of the data in Table II leads to two general conclusions. One of these is that the experimental data are in quite good agreement with statistical prediction if the radiolysis value of the isotope effect (3.00) is used—the value 1.83 from the mass spectra does not produce a satisfactory fit. This agreement is so good for the entire set of compounds (except for the biphenyl-d_8, where the data are from a single experiment) that it hardly can be fortuitous. The formation of hydrogen in these radiolyses is thus again shown to be a structurally random process, at least for H_2, HD, D_2; this conclusion is identical with the previous discussed lack of position selectivity in these processes. It also can be noted from this evidence for a structurally random process that the deviations from equilibrium suggested in the last column of Table II probably do not represent non-equilibrium situations of mechanistic importance.

The abundances of species in the hydrogen from the equimolar mixture of biphenyl and biphenyl-d_{10} are not in good agreement with the statistical expectation, nor are these species present in equilibrium amounts.[34] There is too much H_2 and D_2 and too little HD. A similar lack of equilibration of the hydrogen species has been observed in the hydrogen from an equimolar mixture of other unsaturated organics and their perdeutero-analogs,[35] such as benzene–benzene-d_6, toluene–toluene-d_8 and acetone–acetone-d_6.

Since any single random process which can be written for the production of hydrogen from biphenyl would produce from a mixture of biphenyl and biphenyl-d_{10} either an equilibrated mixture of hydrogen species or a mixture of pure H_2 and D_2, the mixture of hydrogen species actually obtained must result from the operation of at least two such reactions simultaneously.[36] If the arguments cited above are sufficient to allow exclusion of the reactions (1) + (4) as producers of

(33) In calculation of the potential function and assignment of the peaks in the infrared spectra of biphenyl and these deuterated biphenyls, the model adopted for the assignments and calculations required the use of different force constants for these *ortho*, *meta* and *para* C–H bonds. This work will be published shortly by R. H. Shudde, G. W. Lehman and J. M. Scarborough of this Laboratory.

(34) The value of K shown in Table II for the H_2, HD and D_2 from the equimolar biphenyl–biphenyl-d_{10} mixture, 1.04, is reduced even further if the data in Table I are corrected for the H_2 and HD which originate from the biphenyl-d_{10} component of the mixture. The value of K then becomes 0.85. This is a pronounced deviation from the expected equilibrium value range, 3.26–4.00, for a gas with such large amounts of each of the components (the K value for biphenyl-d_8, biphenyl-d_4 and biphenyl-d_{10} are much less reliable because the very small contents of D_2—in the first two cases—and H_2 in the last case make the value of K extremely sensitive to small errors in the analysis of the gas).

(35) J. G. Burr, "Proceedings of the Second United Nations International Conference on the Peaceful Uses of Atomic Energy," United Nations, Geneva, 1958, Vol. 20, p. 187.

(36) L. M. Dorfman, THIS JOURNAL, **60**, 826 (1956), considered that a similar deviation from equilibration of the hydrogen species produced in the radiolysis of ethane–ethane-d_6 mixture to result from the concurrent effect of two processes analogous to (2) and (1) + (4).

hydrogen,[37] then, of the reactions above, we must consider reactions 2 and 3. These reactions do fit the necessary conditions since reaction 2 should produce H_2 from biphenyl and D_2 from biphenyl-d_{10} but should not produce any HD. Several types of reactions are possible candidates for the reaction listed as (3)—namely, the reaction of biphenyl ions with biphenyl molecules, the reaction of excited biphenyl molecules with ground state biphenyl molecules, and the reactions of two excited biphenyl molecules with each other[38]—but it seems clear that any one or any mixture of these should produce an equilibrated mixture of H_2, HD and D_2 from an equimolar mixture of biphenyl and biphenyl-d_{10}.

If the hydrogen from radiolysis of biphenyl is thus accepted as arising from concurrent reactions 2 and 3, then the value of K reported in Table II corresponds to about equal contributions by each of these two processes. Other possible sources of the equilibration of the hydrogen species should be mentioned. Our data could be explained by reaction 2 alone together with some radiation-induced equilibration of the mixture of H_2 and D_2. We think that this is unlikely owing to the very low pressure of hydrogen in the gas phases, the very low concentration of hydrogen in the liquid phase, the low stopping power of gaseous hydrogen for γ-rays and the presence of organic chain terminators in the gas phase.[39] One also can consider a contribution of equilibrated hydrogen species from recombination of hydrogen and deuterium atoms from reaction 1 (possibly track recombination or recombination of "hot" hydrogen atoms) but we think that this is unlikely because of the very high concentration of scavenger molecules in this liquid biphenyl system.

(37) We have not considered "hot" hydrogen atoms as possible products of reaction 1 since these are species which, by definition, react with each other or with RH according to reaction 4 within the first collision or two. Under such conditions, the reactions of hot hydrogen atoms are difficult to distinguish experimentally from a reaction such as (3); we are willing to concede that among the types of reactions which (3) may include are those of "hot" hydrogen atoms.

(38) Ion-molecule reactions between benzene ions and benzene molecules have been shown to occur in the mass spectrometer (W. H. Hamill and R. Barker, personal communication) and the principal result of these probably is the formation of a dimer and hydrogen. Bimolecular combination in solution between excited phenanthrene and ground state phenanthrene molecules has been invoked to explain a delayed fluorescence (R. Williams, *J. Chem. Phys.*, **28**, 577 (1958)) and bimolecular combination of two excited molecules has been invoked to explain the lower efficiency of organic scintillators for alpha particles, and also to explain the effect of changing linear energy transfer upon the gas yields from polyphenyl hydrocarbons (Burns, Wild and Williams, Proceedings of the Second U.N. Conference, Vol. 29, p. 266 (1958)).

V. Conclusions

Consideration of the existing literature on the radiolysis and the radical scavenging ability of aromatic hydrocarbons suggests that the principal primary reaction in the radiolysis of liquid biphenyl probably is the dissociation of an energized (excited or ionized) biphenyl molecule into hydrogen atoms and biphenyl radicals. Substantially all of the hydrogen atoms are scavenged by addition to surrounding biphenyl molecules and do not contribute to the formation of product hydrogen; most of the biphenyl radicals are scavenged by a similar addition reaction. The probable result of both scavenging actions is the formation of polymer.

Data produced by the experiments described in this paper lead to the conclusion that at least two non-radical processes are involved in the formation of the product hydrogen. One of these processes is a unimolecular dissociation; the other is some sort of a bimolecular process. These two processes contribute about equally to the formation of product hydrogen. A not unexpected result of processes of these two types is that it is observed that the various types of carbon–hydrogen bonds in the biphenyl molecule all contribute in a structurally random fashion to the formation of the product hydrogen but that there is an isotope effect in the respective rates of hydrogen and deuterium formation.

Acknowledgment.—We wish here to acknowledge the assistance of R. A. Meyer who performed the mass spectrometer analyses, and of R. H. Shudde who advised on the statistical calculations. We also acknowledge many helpful conversations with D. E. McKenzie, J. P. Howe, Dean Henry Eyring and with many members of the Research Department Staff at Atomics International.

(39) J. G. Burr, *J. Chem. Phys.*, **25**, 587 (1956); Y. Yizuka, Y. Ouchi, K. Hirota and G. Kusumoto, *Nippon Kazuku Zasshi*, **78**, 129 (1957).

SPECIES INVOLVED IN THE ANION-EXCHANGE ABSORPTION OF QUADRIVALENT ACTINIDE NITRATES[1]

BY J. L. RYAN

Hanford Laboratories Operation, General Electric Company, Richland, Washington

Received January 26, 1960

The anion-exchange absorption of the quadrivalent actinides is compared with spectrophotometric and solubility data. The plutonium, neptunium and uranium species absorbing on anion exchangers from nitric acid and from calcium nitrate are $Pu(NO_3)_6^=$, $Np(NO_3)_6^=$ and $U(NO_3)_6^=$. The data indicate that in the case of thorium, $Th(NO_3)_5^=$ is absorbed. The presence of distinct maxima in the anion exchange distributions of the quadrivalent actinides in nitric is attributed to the formation of $HM(NO_3)_6^-$ and $H_2M(NO_3)_6$ at high acidity. The marked similarity between anion exchange of metal complexes and the solubility of quaternary amine salts of these complexes is pointed out.

Anion-exchange resins have long been known to show very high selectivities for certain of the metal complex ions. The distribution coefficients of many of the complexes requiring high ligand concentration for their formation are known to go through maxima as the concentration of the ligand acid is increased.[2-4] It is also known that in many systems the absorption of the metal complexes by the exchanger is much stronger when a metal salt of the ligand ion is used instead of the ligand acid.[3-6] The anion-exchange absorption of a metal complex by resin in the ligand anion form can be represented by the reactions

$$M^{+m} + nX^{-y} \rightleftharpoons MX_n^{-ny+m} \quad (1)$$

$$MX_n^{-ny+m} + \left(\frac{ny-m}{y}\right) X_{(r)}^{-y} \rightleftharpoons MX_{n(r)}^{-ny+m} + \left(\frac{ny-m}{y}\right) X^{-y} \quad (2)$$

$$MX_n^{-ny+m} + (ny-m)H^+ \rightleftharpoons H_{ny-m}MX_n \quad (3)$$

where the subscript (r) denotes resin phase and others are aqueous phase. Reactions 1 and 3 may occur stepwise, and X^{-y} might be any complexing anion including acid anions. Also an anion which is formed in an intermediate step of reaction 3 (complex acid anion) might absorb. Reaction 3 above has been either dismissed with only brief consideration or neglected entirely by most previous workers.[6-8] Recent papers[9,10] published while this work was being completed have proposed that formation of the free acid of the complex anion (reaction 3) is a factor affecting anion-exchange behavior. Attempts have been made to explain higher anion-exchange distributions in ligand salts than in ligand acids on the basis of different ligand activity in the resin phase in these media and on interaction of acid with the resin phase.[6,11] Attempts to explain maxima in anion-exchange distributions have been made only on the basis of absorption of neutral complexes[7] or on the basis of average zero charge for the metal species in solution at the maxima.[6,8,12]

The anion-exchange behavior of plutonium(IV) in nitric acid has been thoroughly studied[13] and several salts of the $Pu(NO_3)_6^=$ ion are known. The anion exchange behavior of Np(IV) and Th(IV) in nitrate media are qualitatively similar to that of Pu(IV). The purpose of this paper is to compare spectrophotometric and solubility data to the anion-exchange data for Pu(IV), Np(IV) and Th(IV) in nitrate media. By comparing both the spectrophotometric data and the solubility data, some insight into the relative significance of reactions 1 and 3 will be obtained.

Experimental

Preparation of Plutonium(IV) and Neptunium(VI) Stock Solutions.—The plutonium and neptunium used in this work were purified by anion exchange in nitric acid.[3,13,14] The Pu(IV) and Np(IV) anion-exchange products (*ca.* 40 g. M(IV)/l. in 0.6 *M* HNO_3) were acidified to about 2 *M* HNO_3 and evaporated to about 200 g. M./l. with a heat lamp. A small amount of nitrogen dioxide was passed through the plutonium solution to ensure (IV) valence, and the solutions were diluted with 15.7 *M* HNO_3 to produce stock solutions of 95 g. Pu(IV)/l. and 95 g. Np(VI)/l. in 13 *M* HNO_3. The neptunium stock solution was found spectrophotometrically to be Np(VI), and no attempt was made to adjust the valence in the stock solution. The purity of the plutonium was not determined, but previous experience would indicate that total impurities would be about 100 parts per million parts plutonium.[3,13] The neptunium was found by alpha energy analysis with a Frisch grid ionization chamber and 256 channel analyzer[15] to contain 0.011 weight % plutonium. Other impurities in the neptunium could be expected to be about 100 parts per million parts neptunium. The plutonium which consisted of a reactor produced isotopic mixture was used in the solubility and anion-exchange measurements within one month of the time of purification to minimize growth of Am^{241} from Pu^{241}. The neptunium was isotopically pure Np^{237} containing no

(1) This paper is based on work performed under Contract No. AT-(45-1)-1350 for the U. S. Atomic Energy Commission. Presented before the Northwest Regional Meeting of the American Chemical Society, Richland, Washington, June, 1960.

(2) K. A. Kraus and F. Nelson, "Proc. Intern. Conf. Peaceful Uses Atomic Energy, Geneva, 1955," Vol. VII, pp. 113, 131 (1956).

(3) J. L. Ryan and E. J. Wheelwright, *Ind. Eng. Chem.*, **51**, 60 (1958).

(4) J. Danon, *J. Am. Chem. Soc.*, **78**, 5953 (1956).

(5) K. A. Kraus, F. Nelson, F. B. Clough and R. C. Carlston, *ibid.*, **77**, 1391 (1955).

(6) K. A. Kraus and F. Nelson in Symposium on Ion Exchange and Chromatography in Analytical Chemistry (1956), Am. Soc. for Testing Materials. Special Technical Publication No. 195, 1958, p. 27.

(7) H. M. Newmann and N. C. Cook, *J. Am. Chem. Soc.*, **79**, 3026 (1957).

(8) K. A. Kraus and R. J. Raridon, in Oak Ridge National Laboratory Chemistry Division Annual Progress Report, ORNL-2584, Period ending June 20, 1958, pp. 62-63.

(9) J. K. Foreman, I. R. McGowan and T. D. Smith, *J. Chem. Soc.*, 738 (1959).

(10) Y. Marcus, THIS JOURNAL, **63**, 1000 (1959).

(11) K. A. Kraus and F. Nelson, *J. Am. Chem. Soc.*, **80**, 4154 (1958).

(12) S. Fronaeus, *Svensk, Kem. Tidskr.*, **65**, 1 (1953).

(13) J. L. Ryan and E. J. Wheelwright, Atomic Energy Commission Research and Development Report, HW-55983 (Hanford Laboratories), Jan. 2, 1959.

(14) J. L. Ryan, Atomic Energy Commission Research and Development Report, HW-59193 REV (Hanford Laboratories), Sept. 3, 1959.

(15) F. P. Brauer and R. E. Connally, Atomic Energy Commission Research and Development Report, HW-60974 (Hanford Laboratories), July 10, 1959.

alpha active impurities other than the plutonium previously mentioned.

Thorium Nitrate.—Thorium nitrate stock solutions were prepared from Baker and Adamson reagent grade $Th(NO_3)_4 \cdot 4H_2O$ and analyzed by the thoron colorimetric method.

Preparation of Tetraethylammonium Nitrate.—Tetraethylammonium nitrate was made by passing a solution of Eastman tetraethylammonium bromide through a water washed column of nitrate form Dowex 1, X-4 or Dowex 21 K (50 to 100 mesh). The nitrate was bromide free as determined by silver nitrate test. The solution was evaporated thermally until crystallization started and then was dried at 50° at 25 mm. pressure. A stock solution of 4.2 *M* tetraethylammonium nitrate was made up in water assuming the salt prepared in this manner contained no water of hydration. Tetrabutylammonium nitrate was prepared in a similar manner starting with Eastman tetrabutylammonium iodide dissolved in hot water. It was not evaporated to dryness but was used as a concentrated stock solution.

Plutonium Solubility Measurements.—Nitric acid and calcium nitrate were C.P. and reagent grade. To 8.6-ml. aliquots of nitric acid and calcium nitrate solutions were added 400 microliters of the Pu(IV) stock solution followed by 1,000 microliters of tetraethylammonium nitrate stock solution. This resulted in an initial concentration of 3.80 g. Pu/l. (0.016 *M*) and 0.4 *M* tetraethylammonium nitrate. Precipitation occurred immediately in all but one sample in which the solubility was not exceeded. Since a large constant excess of tetraethylammonium nitrate was used over the stoichiometric amount required for precipitation, a constant initial plutonium concentration was used, and precipitation of Pu was so complete, the final tetraethylammonium ion concentration can be considered constant (*ca.* 0.39 *M*).

The solutions were allowed to equilibrate with the precipitate at 25 ±1° with occasional agitation. Samples of the nitric acid supernates were filtered through medium porosity sintered glass filters after 24 hours and after 6 days and analyzed for total plutonium by α-counting and α-energy analysis. No change in total plutonium between one and six days was observed. Samples of the nitric acid supernates were suction filtered through fine porosity sintered glass filters 9 days after precipitation and analyzed within 5 hours after sampling for Pu(IV) by TTA (thenoyl trifluoroacetone) extraction and α-counting. The calcium nitrate solutions were sampled after 7 days equilibration in a similar manner except that due to the high density and high viscosity of these solutions and consequent poor settling of the precipitates, it was necessary to filter samples of them first through medium porosity sintered glass filters followed by fine porosity sintered glass. These samples were also analyzed for Pu(IV) by TTA extraction and α-counting immediately after sampling. It should be emphasized that analysis for Pu(IV) by TTA extraction was necessary even though the original plutonium stock had been carefully purified Pu(IV). Since only Pu(IV) precipitated, the ratio of the α-activity of Am^{241} and plutonium of other valence states (probably +6) to Pu(IV) α-activity in the supernates is much greater than in the stock solutions and is actually much greater than one in the samples of lower solubility. In the case of the lowest solubility values in calcium nitrate, the Am^{241} α-activity in the supernate was about 50 times that of Pu(IV). The Pu in other valence states was about equivalent in α-activity to the Am^{241}. Because of this, the accuracy of plutonium analysis increases from about ±25% for the lowest solubilities to about ±2% where Pu(IV) becomes the principal α-activity. The values reported for Pu(IV) are averages of two to six analyses per sample.

Nitric acid was determined in the nitric acid filtrates by titration with standard base. Calcium nitrate values were determined by analysis of the original stock solution, assuming that in the addition of the 0.4 ml. of plutonium stock solution and 1.0 ml. of tetraethylammonium nitrate to 8.6 ml. dilutions of this stock the volumes were additive. The calcium nitrate solutions all contained 0.5 *M* HNO_3 introduced in the Pu stock solution. This is sufficient to prevent Pu(IV) hydrolysis.

Neptunium and Thorium Solubility Measurements.—Measurements of the solubilities of the tetraethylammonium thorium(IV) and neptunium(IV) nitrate salts were carried out in the same manner as those for the plutonium compound. The neptunium solutions were made 0.05 *M* in ferrous sulfamate and 0.05 *M* in hydrazine to reduce Np(VI) to Np(IV) and to hold it reduced during the course of the experiment.

Neptunium in the nitric acid supernates was analyzed by total α-counting and α-energy analysis. The alpha per cent. neptunium on the counting plates ranged from 56% in some of the lower acid samples (where separation from the Pu present in the initial stock solution occurred through reduction to Pu(III)) to 96% at the higher acidities. Analysis of neptunium in the calcium nitrate filtrates was by adjustment of the sample to 4 *M* HNO_3, 0.05 *M* ferrous sulfamate, 0.05 *M* sulfamic acid and extraction of Np(IV) into trilaurylamine in xylene. Back extraction into water was followed by acidification with HCl, reduction with KI and extraction into TTA. The TTA extract was mounted and the neptunium was determined by total α-counting and α-energy analysis to check for separation from plutonium. The over-all yield was determined by use of Np^{239} tracer and γ-counting of the final plates. Thorium was determined in the thorium filtrates by the thoron colorimetric method. Unfortunately, this method was not capable of determining the low levels of thorium present in the high calcium nitrate systems.

Anion-exchange Distribution Measurements.—Distribution coefficients, K_D = mg. metal/g. resin/mg. metal/ml. soln., were obtained with Dowex 1, X-4 (50 to 100 mesh) resin vacuum dried in the nitrate form at 60°. Distribution measurements were carried out at 5% resin loading. The batch experiments were equilibrated at 25° 4 to 8 days for the nitric acid systems and three to four weeks for the calcium nitrate systems. Kinetic studies[13] indicate that this is sufficient time to reach equilibrium at these low loadings. The neptunium solutions contained the same reductant concentration as used in the solubility measurements. Analyses for solution constituents were by the same methods used in the solubility measurements with the same difficulty occurring in the analysis of low levels of Pu(IV) in the presence of appreciable quantities of Am^{241} and Pu(VI). Thorium K_D's in calcium nitrate were obtained only up to the limit of the thoron analytical method.

Preparation and Analysis of the Quaternary Ammonium Metal(IV) Nitrate Salts.—To a nitric acid solution plutonium and tetraethylammonium nitrate stock solution were added in several aliquots alternately with agitation until the final solution contained 7.8 *M* HNO_3 and approximately stoichiometric quantities (two moles of tetraethylammonium nitrate per mole plutonium) of the reactants. This technique was used to ensure that neither reactant was in large excess and to thus minimize carrying on the precipitate. The fine needle-like crystalline precipitate which formed immediately was allowed to digest at 25° for 24 hours and was then suction filtered on sintered glass and washed thoroughly with 7.5 *M* HNO_3. The compound was dried at atmospheric pressure at 25° for 9 days over solid NaOH which removed both water and HNO_3 and then 5 days over anhydrous $Mg(ClO_4)_2$.

The compound was found to be non-hygroscopic and easily weighable. Plutonium content was determined by dissolving in 1 *M* HCl and analyzing by controlled potential coulometry.[16] Carbon was determined by standard carbon train combustion method.

Anal. Calcd. for $[(C_2H_5)_4N]_2Pu(NO_3)_6$: Pu, 27.4, C, 22.0. Found: Pu, 27.3; C, 22.1, 22.9, 22.5, 17.2, 22.4, 16.2, 16.7.

The separate carbon analysis results are shown since it was felt that due to the nature of the method low results are more probable than high and that the three lower values probably are in error. Accurate carbon analysis of this compound is difficult because of the alpha hazards involved and because of the rapid decomposition of the organic radical by nitrate when heated.

Thorium(IV), cerium(IV) and neptunium(IV) tetraethylammonium salts were prepared and dried in the same manner as the plutonium salt. The thorium salt was analyzed by evaporating almost to dryness twice with concentrated HCl followed by neutralization with ammonium hydroxide, drying and ignition to ThO_2.

Anal. Calcd. for $[(C_2H_5)_4N]_2Th(NO_3)_6$: Th, 26.9. Found: Th, 27.0.

(16) F. A. Scott and R. M. Peekema, "Proc. Second Intern. Conf. Peaceful Uses Atomic Energy, Geneva, 1958," Vol. 28, p. 573 (1958).

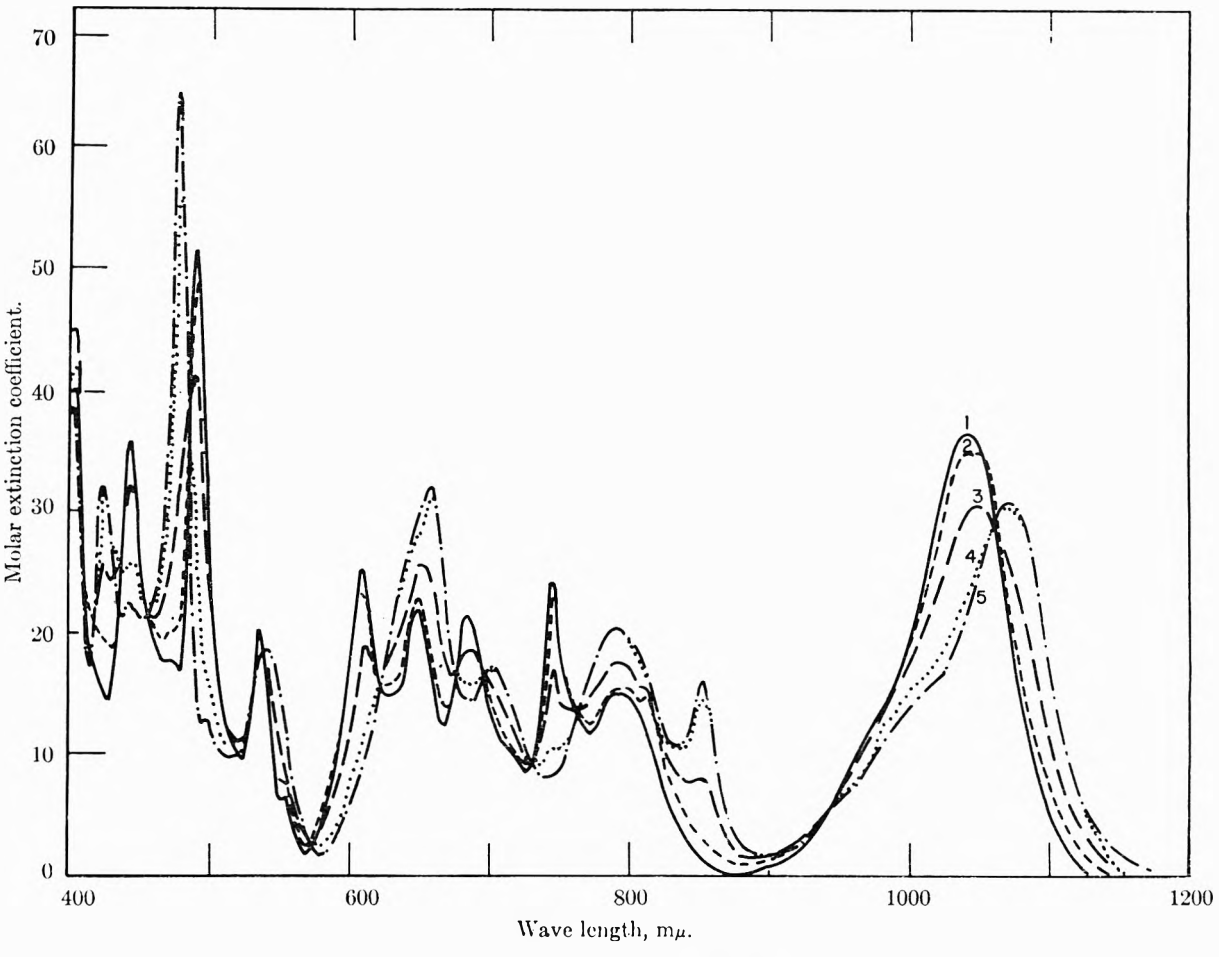

Fig. 1.—Absorption spectra of Pu(IV) in nitric acid: (1) 13.2, 14.0 and 15.5 *M* HNO_3; (2) 10.0 *M* HNO_3; (3) 8.0 *M* HNO_3; (4) 6.0 *M* HNO_3; (5) 5.0 *M* HNO_3.

The thorium and cerium compounds were found by X-ray diffraction to be isomorphous.

The neptunium compound was analyzed by dissolving a weighed amount in 1 *M* HNO_3 and determining Np by controlled potential coulometry.

Anal. Calcd. for $[(C_2H_5)_4N]_2Np(NO_3)_6$: Np, 27.3. Found: Np, 27.0

A tetrabutylammonium salt of Pu(IV) was prepared in similar manner and assumed by the method of preparation to be $[(C_4H_9)_4N]_2Pu(NO_3)_6$.

Spectrophotometric Studies.—Spectrophotometric measurements of solutions were made with a Cary Model 14 recording spectrophotometer using matched 2.00 cm. Corex cells. Aqueous Np(IV) spectra were obtained using 0.2 *M* semicarbazide, which is colorless over the wave length range of interest, as reductant for the initially hexavalent neptunium. Blanks were as nearly as possible the same composition as the solutions being examined. Non-aqueous solvents were all C.P., reagent, or U.S.P. grades and, with the exception of acetic anhydride, all were dried by shaking with CaO and filtering. No attempt to exclude moisture other than this drying of the solvent was made.

Absorption spectra of resins were obtained using matched 1.00 cm. silica cells. The resin with the desired metal absorbed was placed in the cell in the solution from which it was loaded. Due to the high K_D's involved at the low resin loadings used, the amount of the metal in the solution phase was negligible. The blank was resin treated identically except for the presence of the actinide of interest. The resins were allowed to settle for about 15 minutes in the cell to prevent changes in amount of resin in the light path during running of the spectra. The infrared source of the Cary Model 14 was used for these measurements at a slit width of 0.3–0.7 mm.

Results and Discussions

The compounds $(NH_4)_2Ce(NO_3)_6$, $(NH_4)_2Th(NO_3)_6$ and $(NH_4)_2Pu(NO_3)_6$ all have been prepared and have been found by X-ray analysis to be isomorphous,[17] and evidence has been presented that the hexanitratocerate salt is an ammonium salt of a nitrato complex and not simply a double salt of crystallization.[18] Several hexanitratoplutonium(IV) salts have been prepared and identified. These include the ammonium,[17] rubidium, cesium, thallous, pyridinium, quinolinium and potassium salts.[19] Electromigration studies have shown that in the range 4 to 8 *M* HNO_3 Pu(IV) changes from essentially completely cationic to predominantly anionic.[20] This conversion does not appear to be complete until at least 10 *M* HNO_3. From this and spectrophotometric studies, it has been proposed that the complex present at high

(17) J. C. Hindman in Metallurgcal Project Report CN-2088, Sept. 1, 1944, p. 6.

(18) G. F. Smith, V. R. Sullivan and G. Frank, *Ind. Eng. Chem., Anal. Ed.*, **8**, 449 (1936).

(19) H. H. Anderson, Atomic Energy Commission Research and Development Report, ANL-4064 (Argonne National Laboratories), Oct. 23, 1947.

(20) C. K. McLane, J. S. Dixon and J. C. Hindman, "The Transuranium Elements," Division IV, Vol. 14B, Paper 4.3, McGraw-Hill Book Co., Inc., New York, N. Y., 1949, p. 358.

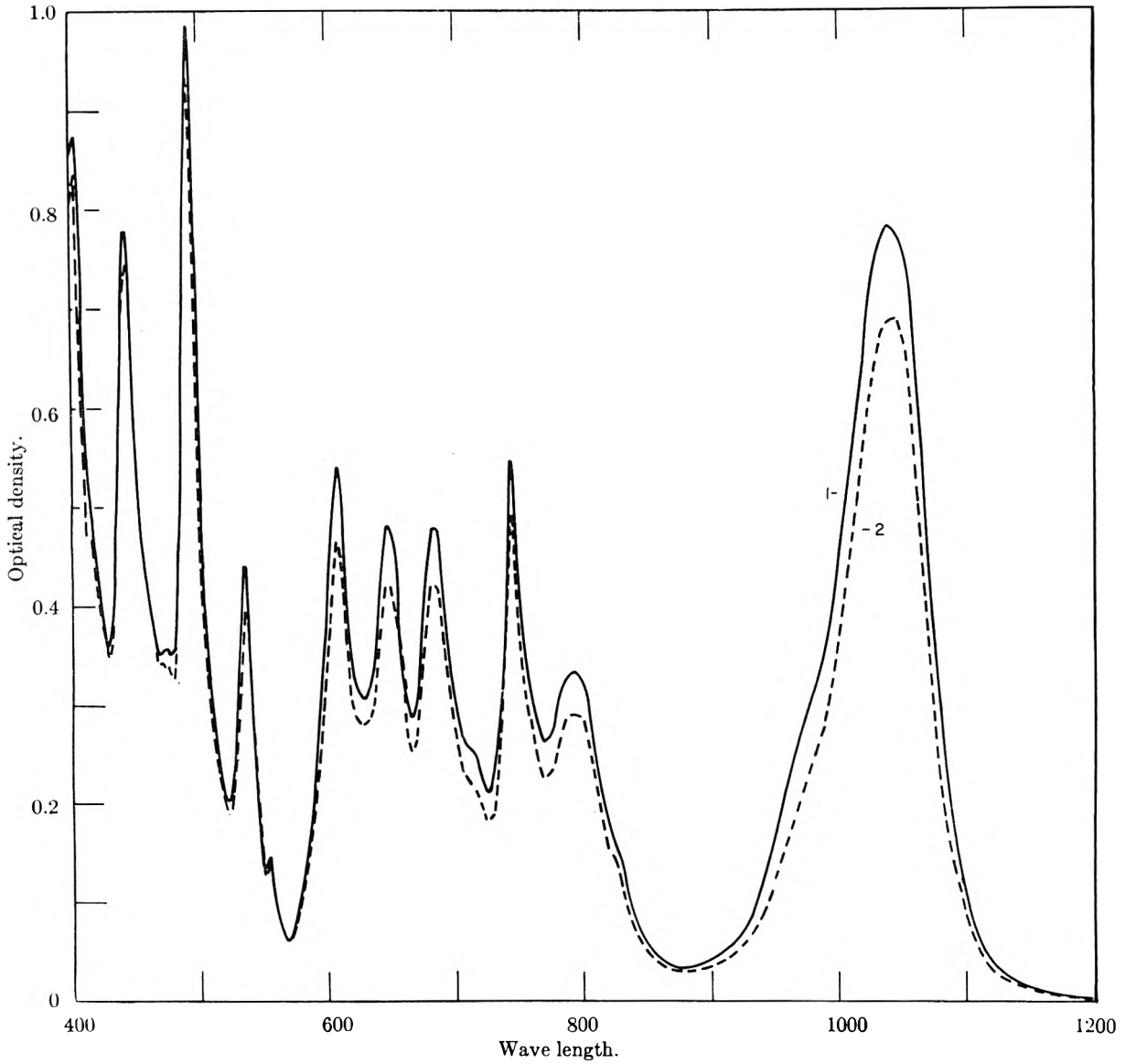

Fig. 2.—Absorption spectra of Pu(IV) hexanitrato complex: (1) Pu(IV) loaded on Dowex 1, X-1 (50 to 100 mesh) anion exchange resin from 4.0 M HNO_3; (2) 1.00×10^{-2} M $[(C_2H_5)_4N]_2Pu(NO_3)_6$ in acetonitrile (2.00 cm. cell).

nitric acid concentration is the hexanitrato species.[21] Anion-exchange studies with 1% cross-linked resin at varying Pu(IV) concentrations have shown that equilibrium resin capacity increases rapidly up to a certain Pu(IV) concentration above which it is almost constant.[13,22] This maximum capacity corresponds closely to the total exchange capacity for the $Pu(NO_3)_6^=$ ion.

The absorption spectra of Pu(IV) in 3 to 15.5 M HNO_3 solutions were examined at approximately one molar increments, and some of these spectra are shown in Fig. 1. Very little change in spectra was observed in 3 to 5 M HNO_3. From 5 to 10 M HNO_3, the spectra changed rapidly and above 13 M HNO_3, no further change occurred. The absorption spectra of $[(C_2H_5)_4N]_2Pu(NO_3)_6$ dissolved in acetone, acetic anhydride, acetonitrile and nitromethane and the tetrabutylammonium salt dissolved in methyl isobutyl ketone and nitromethane were essentially identical with that of Pu(IV) in >13 M HNO_3. The maximum variation observed in these spectra was up to about 5% difference in the relative molar extinctions of the absorption peaks in the various solutions. The positions of the absorption maxima were identical in all cases. The spectra of $[(C_2H_5)_4N]_2Pu(NO_3)_6$ in methanol and in ethanol were found to be markedly different from any of the aqueous nitric acid spectra, indicating reaction with the alcohol.

Because of the high α hazards involved with Pu and Np, it was not considered feasible to attempt to obtain the absorption spectra of the dry hexanitrato salts. Using U(IV) as a substitute, the absorption spectrum of $[(C_2H_5)_4N]_2U(NO_3)_6$ mulled in petrolatum was obtained. The spectrum was very similar to that of $[(C_2H_5)_4N]_2U(NO_3)_6$ in acetone and to U(IV) in 15.7 M HNO_3. The difference amounted to a change in the rela-

(21) J. C. Hindman, ref. 20, paper 4.5, p. 388.

(22) R. W. Durham and R. Mills, Atomic Energy of Canada Ltd., Research and Development Report CEI-62 (Chalk River Project), Sept. 29, 1953.

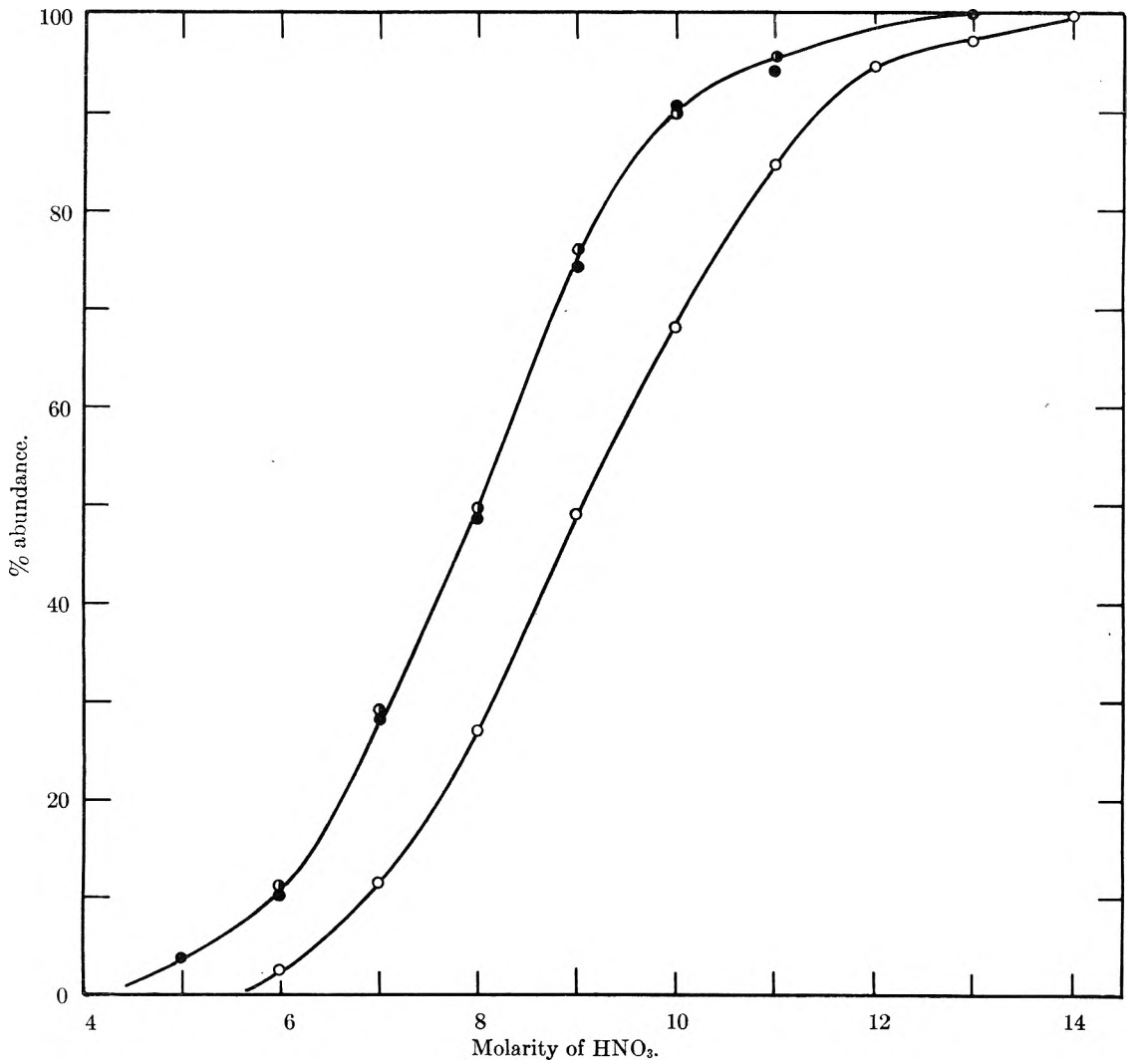

Fig. 3.—Abundance of Pu(IV) and Np(IV) hexanitrato complexes in nitric acid: ◑, Pu(IV) calculated at 609 mμ; ●, Pu(IV) calculated at 744 mμ; ○, Np(IV) calculated at 877 mμ.

tive intensity of some of the peaks and a wave length shift of up to 5 mμ in some of the absorption maxima coupled with some sharpening of the peaks. Addition of tetraethylammonium nitrate to acetone solutions of $[(C_2H_5)_4N]_2Pu(NO_3)_6$ produced no change in spectra. This and the comparison of the spectrum of the solid U(IV) salt to the spectrum of its acetone solution indicates that the spectra of the Pu(IV) salt in acetone, acetonitrile, acetic anhydride and nitromethane and of Pu(IV) in >13 *M* HNO_3 are the spectra of the pure hexanitrato complex.

The spectra of Pu(IV) loaded on Dowex 1, X-1 anion exchange resin were obtained with the resin loaded from and in contact with 4 *M* HNO_3, 8 *M* HNO_3 and 4 *M* $Ca(NO_3)_2$-0.2 *M* HNO_3. The spectra were identical in all three cases and were identical with that of $[(C_2H_5)_4N]_2Pu(NO_3)_6$ in the inert solvents and Pu(IV) in >13 *M* HNO_3. The spectra of Pu(IV) on Dowex 1, X-1 in 4 *M* HNO_3 and of $[(C_2H_5)_4N]_2$ $Pu(NO_3)_6$ in acetonitrile are compared in Fig. 2. This shows that the $Pu(NO_3)_6^=$ ion is the species absorbing on anion-exchange resins from both nitric acid and calcium nitrate solutions. The spectrum of U(IV) on Dowex 1, X-1 in 4 *M* HNO_3 was found to be identical with that of $[(C_2H_5)_4N]_2U(NO_3)_6$ in acetone.

About 10 isosbestic points in the absorption spectra of solutions of Pu(IV) in 4–15 *M* HNO_3 (see Fig. 1) indicate either that only two species are present in this range or that all the species in >4 *M* HNO_3 other than the hexanitrato complex have almost identical absorption spectra. Examination of Fig. 1 shows that the absorption peaks at 609 and at 744 mμ are due to the hexanitrato species and that lower species do not have absorption maxima at these wave lengths. Using these wave lengths, it is possible to calculate the amount of hexanitrato complex. Both the hexanitrato complex and lower species have peaks near 650 and 790 mμ which contribute to the total absorption at 609 and 744 mμ. The intensities of the 609 and 744 mμ absorption bands due to the hexanitrato species were determined by subtracting from the total optical density the contribution of the absorption peaks near 650 and 790 mμ, assuming the latter peaks to be symetrically shaped. The advantages of this technique are that no assumption as to whether more than one lower complex is formed is necessary, the molar extinction of

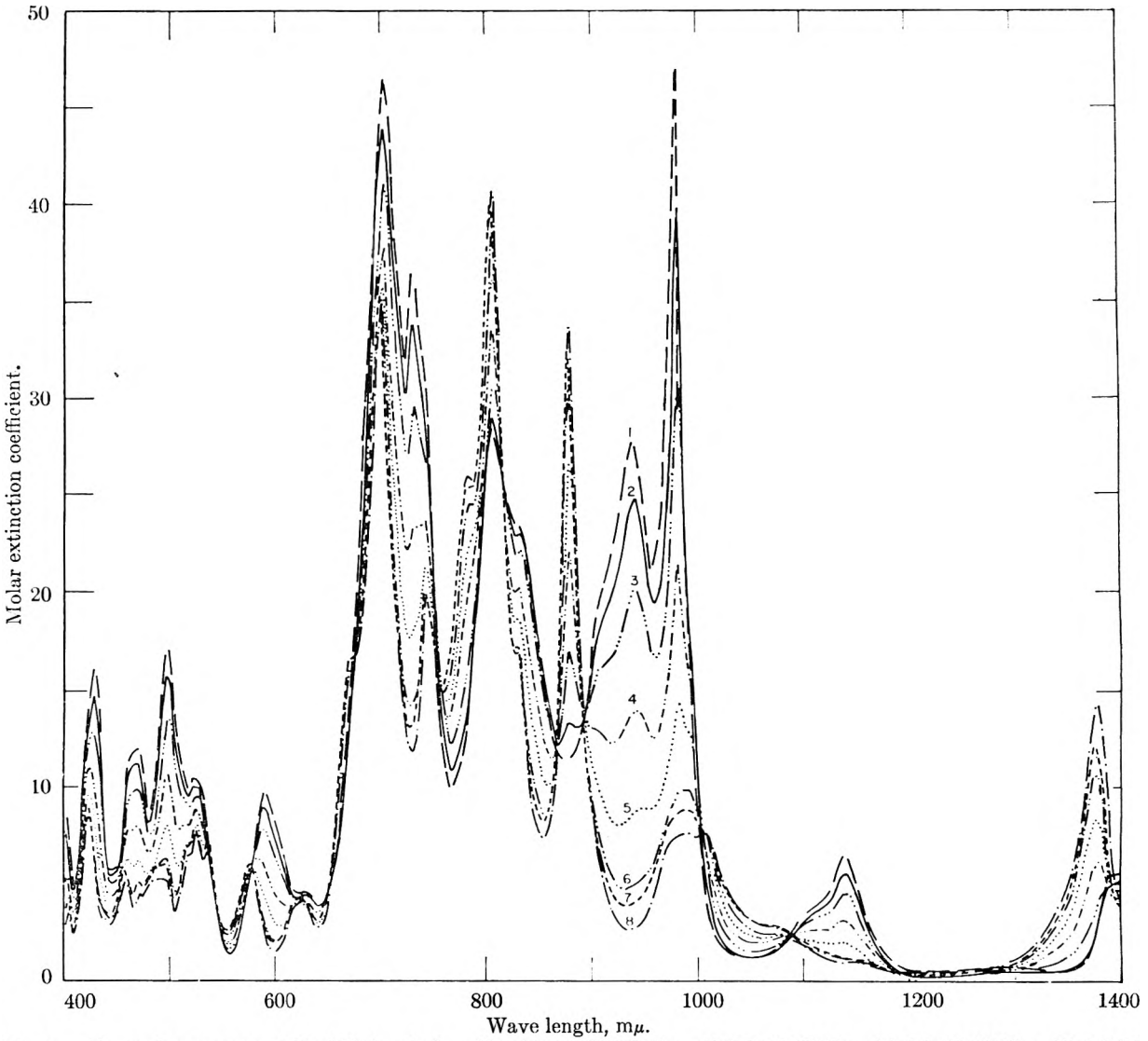

Fig. 4.—Absorption spectra of Np(IV) in nitric acid: (1) 6.0 *M* HNO_3; (2) 7.0 *M* HNO_3; (3) 8.0 *M* HNO_3; (4) 9.0 *M* HNO_3; (5) 10.0 *M* HNO_3; (6) 11.0 *M* HNO_3; (7) 12.0 *M* HNO_3; (8) 14.0, 15.0 and 15.5 *M* HNO_3.

the lower complex need not be determined, and the instrument balance with regard to the base line is critical only in the range where most of the Pu is present as the hexanitrato complex. The results so calculated at these two wave lengths are shown in Fig. 3. The amount of hexanitrato complex also was calculated by assuming that the total optical density at 609 and 744 mμ in 4 *M* HNO_3, where there is no evidence of hexanitrato complex, is that of the pure lower complex and that the optical density at these wave lengths in 13.2 *M* HNO_3 is due to the pure hexanitrato complex. The results obtained in this manner are practically identical with those obtained by the first method. The amount of Pu(IV) hexanitrato complex in 4.5 $Ca(NO_3)_2$–0.5 *M* HNO_3 (total 9.5 *M* nitrate) was 4%, in 5.75 *M* $Ca(NO_3)_2$–0.5 *M* HNO_3 (total 12 *M* nitrate) it was 26% and in 9 *M* $Ca(NO_3)_2$–0.25 *M* HNO_3 (total 18.2 *M* nitrate) it was 91%. This indicates that formation of the hexanitrato complex is much less pronounced in calcium nitrate than in nitric acid.

The absorption spectra of 6 to 15.5 *M* HNO^3 solutions of Np(IV) are shown in Fig. 4. The absorption spectra do not change above 14 *M* HNO_3. The absorption spectra of $[(C_2H_5)_4N]_2Np(NO_3)_6$ in acetone and acetonitrile and of Np(IV) on Dowex 1, X-1 in 8 *M* HNO_3 are identical with that in 14 *M* HNO_3 establishing the fact that $Np(NO_3)_6^=$ is the ion absorbed by the anion exchanger and that the spectrum in 14 *M* HNO_3 is the pure hexanitrato spectrum. The presence of many isosbestic points in the spectra of Fig. 4 indicates that all the spectra from 6–15.5 *M* HNO_3 are composed of a combination of only two basic spectra. Examination of Fig. 4 shows that the absorption peak at 877 mμ is due to the hexanitrato complex. Figure 5 shows the spectra in the region of the 877 mμ peak obtained at a slower scan rate. Since isosbestic points occur at 866 and 892 mμ, it is assumed that only two spectral entities are involved in this wave length range. The optical density at 877 mμ in 14–15.5 *M* HNO_3 was taken as that of the pure hexanitrato complex and that in 5 *M* HNO_3 as

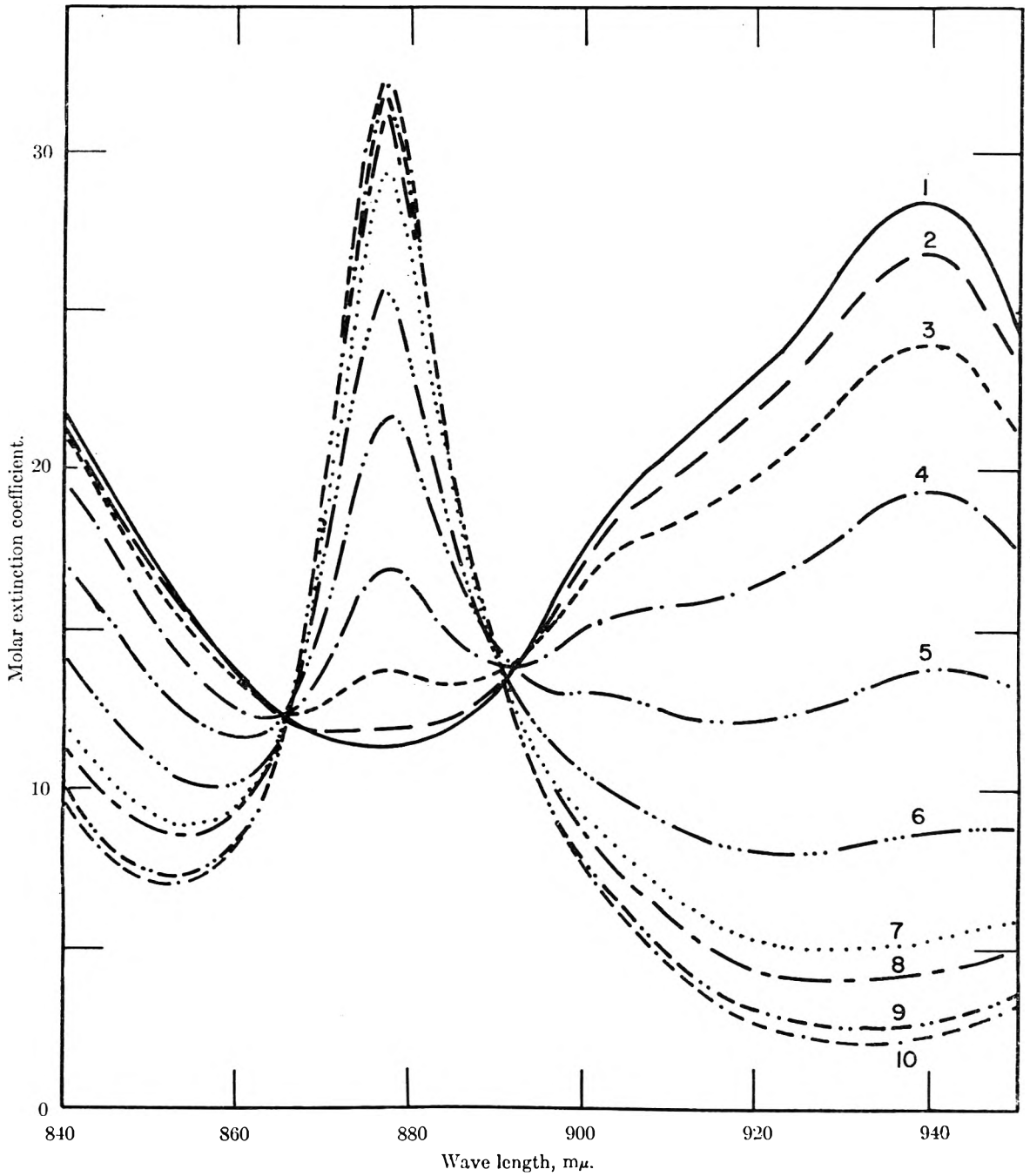

Fig. 5.—Absorption spectra of Np(IV) in nitric acid in region of 877 mμ peak: (1) 5.0 *M* HNO_3; (2) 6.0 *M* HNO_3; (3) 7.0 *M* HNO_3; (4) 8.0 *M* HNO_3; (5) 9.0 *M* HNO_3; (6) 10.0 *M* HNO_3; (7) 11.0 *M* HNO_3; (8) 12.0 *M* HNO_3; (9) 13.0 *M* HNO_3; (10) 14.0, 15.0 and 15.5 *M* HNO_3.

the optical density of the pure lower species. Figure 3 shows the percentages of Np(IV) hexanitrato complex so calculated.

The data of Fig. 3 show that Np(IV) has less tendency to form a hexanitrato complex in nitric acid than Pu(IV). If it is assumed, as was indicated by the spectrophotometric data, that in the acid range of interest only the hexanitrato complex and one other lower complex are present and that this lower complex is the same species in the case of Pu(IV) and Np(IV), the ratio of the constant for formation of the plutonium hexanitrato complex from the next lower complex to that of neptunium can be determined. The ratio of the formation constants under the above conditions is

$$K_{Pu}/K_{Np} = \frac{\text{hexanitrato Pu}}{\text{total Pu} - \text{hexanitrato Pu}} \Big/ \frac{\text{hexanitrato Np}}{\text{total Np} - \text{hexanitrato Np}}$$

This equation holds at any given acidity and nitrate concentration since all other terms in the formation constants are equal in the case of Np and Pu and cancel out. The values obtained in 6 to 11 *M* HNO_3 are given in Table I. The relative constancy of and lack of trend in the values ob-

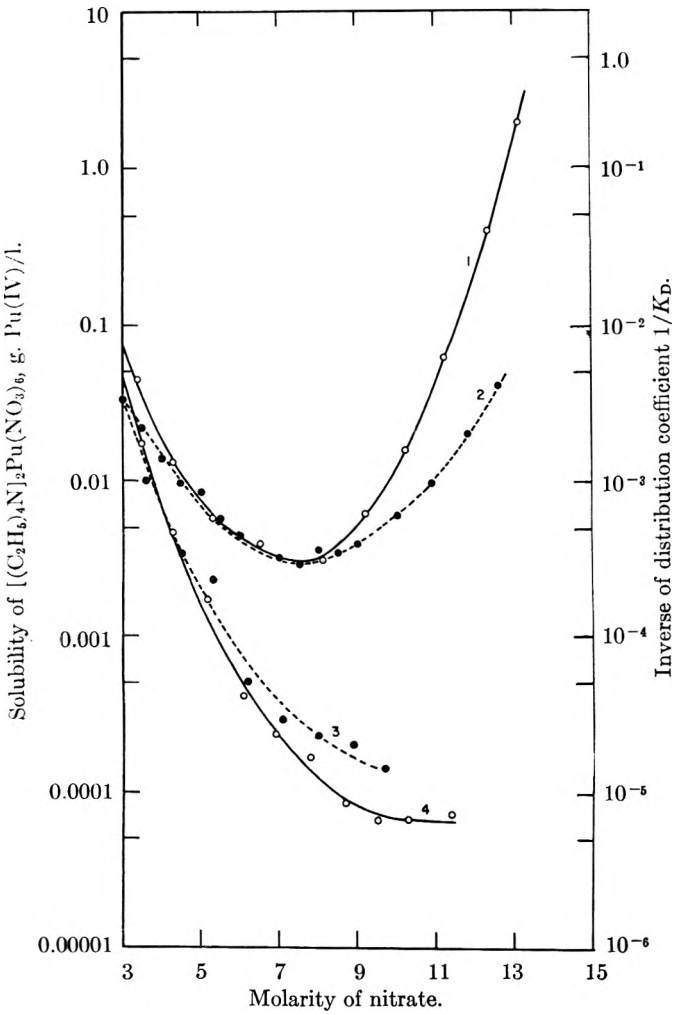

Fig. 6.—Comparison of anion-exchange behavior of Pu(IV) on Dowex 1, X-4 (50 to 100 mesh) with the solubility of $[(C_2H_5)_4N]_2Pu(NO_3)_6$ at constant 0.39 *M* $(C_2H_5)_4NNO_3$: (1) solubility in nitric acid; (2) anion exchange in nitric acid; (3) anion exchange in $Ca(NO_3)_2$, 0.5 *M* HNO_3; (4) solubility in $Ca(NO_3)_2$, 0.5 *M* HNO_3.

TABLE I

M HNO_3	6	7	8	9	10	11	Av. =
K_{Pu}/K_{Np}	3.79	2.99	2.62	3.15	4.16	3.44	3.4 ± 0.5

tained are further evidence of the validity of the assumption that only the hexanitrato and one lower complex exist in this acid range.

Of the known hexanitratoplutonium(IV) salts, thallous, ammonium and potassium salts are moderately soluble.[19] Cesium and rubidium nitrates are in themselves of relatively low solubility in concentrated nitrate solutions. The use of a quaternary ammonium ion as the precipitant in this work was based on three factors: (1) the desired solubility of the metal(IV) salt could be obtained, (2) the quaternary ammonium ions are salts of strong bases and the quaternary amines do not act as complexing agents in themselves, (3) the lower quaternary ammonium nitrates are quite soluble in concentrated solutions of nitric acid and calcium nitrate. The salts obtained with tetraethylammonium nitrate were found to have about the desired solubility for this work.

Figure 6 shows the solubility of the salt $[(C_2H_5)_4N]_2Pu(NO_3)_6$ as a function of total nitrate concentration in nitric acid and in calcium nitrate of constant 0.5 *M* HNO_3 and containing constant excess tetraethylammonium nitrate. Also shown are the anion-exchange data plotted as $1/K_D$. The corresponding solubility and anion-exchange data for neptunium(IV) and thorium(IV) are shown in Fig. 7 and 8, respectively.

Comparison of the spectrophotometric data with the data of Fig. 6 and 8 indicates that there is little correlation between the anion-exchange and spectrophotometric data. Thus, under conditions of equal amounts of the Pu(IV) hexanitrato complex in nitric acid and calcium nitrate (*i.e.*, 4% in 5 *M* HNO_3 and in 4.5 *M* $Ca(NO_3)_2$–0.5 *M* HNO_3) the distribution coefficient is a factor of 50 greater in calcium nitrate than in nitric acid. The maximum K_D for Pu(IV) is at 7.6–7.8 *M* HNO_3 and the maximum K_D for Np(IV) is at 7.7–7.9 *M* HNO_3, a difference of only 0.1 *M* HNO_3, whereas Fig. 3 shows that in this acidity range, equal amounts of the hexanitrato complex occur 1.0 *M* HNO_3 apart. The only apparent correlation is that the difference in the distribution coefficients for Np(IV) and for Pu(IV) in both nitric acid and $Ca(NO_3)_2$ is of roughly the same order of magnitude as the difference in their tendency to form hexanitrato complexes (see Fig. 3 and Table I). This is particularly true at the lower nitric acid concentrations and at all but the highest calcium nitrate concentrations. This indicates that the affinity of the resin for the $Pu(NO_3)_6^=$ and $Np(NO_3)_6^=$ ions is about the same and that the differences in K_D's are at least largely due to the difference in the two element's tendency to form hexanitrato complexes. It is unfortunate that similar spectrophotometric data cannot be obtained for thorium which shows much lower K_D's than Pu(IV) and Np(IV).

The solubility data of Figs. 6 to 8 show remarkable similarity to the anion-exchange data. The expression for the solubility product of $[(C_2H_5)_4N]_2M(NO_3)_6$ is

$$K_{s.p.} = A_{M(NO_3)_3^-} \cdot A^2_{(C_2H_5)_4N^+} \qquad (4)$$

Because the tetraethylammonium nitrate concentration was kept constant at a value much higher than the initial plutonium level, its concentration was not significantly changed by the precipitation. If it is assumed that at a constant 0.39 *M* $(C_2H_5)_4N^+$ the activity coefficient of $(C_2H_5)_4N^+$ is relatively constant, the activity of $M(NO_3)_6^=$ in solution in the presence of the precipitate will also be relatively constant. Although it is recognized that this assumption is not entirely correct, it is inconceivable that the activity coefficient of this ion could vary enough to produce the observed solubility differences between the nitric acid and calcium nitrate solutions. Thus, semiquantitatively the $Pu(NO_3)_6^=$, $Np(NO_3)_6^=$, or $Th(NO_3)_6^=$ activity is the same in the presence of the precipitate in each solution. Since the solubility measured is the concentration of all Pu(IV),

Np(IV) or Th(IV) species in solution, the solubility is a measure of the total Pu(IV), Np(IV) or Th(IV) species in equilibrium with a constant amount of $Pu(NO_3)_6^=$, $Np(NO_3)_6^=$ or $Th(NO_3)_6^=$, respectively. These equilibria with other species can be expressed by (5), (6) and (7) which are specific examples of the generalized reactions 1 and 3

$$M(NO_3)_n^{4-n} + (6 - n)NO_3^- \rightleftharpoons M(NO_3)_6 \quad (5)$$

where n = 0 to 5 and M is Pu, Np or Th

$$M(NO_3)_6^= + H^+ \rightleftharpoons HM(NO_3)_6^- \quad (6)$$

$$HM(NO_3)_6^- + H^+ \rightleftharpoons H_2M(NO_3)_6 \quad (7)$$

Reaction 5 may occur stepwise and reaction 6 and 7 may occur separately or almost simultaneously depending on the relative magnitude of the acid dissociation constants of the complex acids. Examination of the data of Fig. 6 indicates a minimum solubility of $[(C_2H_5)_4N]_2Pu(NO_3)_6$ at about 7.7 *M* HNO_3 indicating a maximum activity of $Pu(NO_3)_6^=$ at this acidity. In nitric acid reactions 6 and 7 decrease the activity of $Pu(NO_3)_6^=$ above 7.7 *M* HNO_3 despite the fact that hexanitrato complexing is not complete until much higher acidity. In calcium nitrate solutions, holding the acidity at a constant low value prevents reactions 6 and 7 from occurring to the degree they do in nitric acid. Continually decreasing solubility with no minimum solubility is observed since formation of $Pu(NO_3)_6^=$ *via* reaction 5 is the principal reaction with increasing nitrate. Similar considerations apply to Np(IV) and Th(IV) which show minimum solubilities at 7.6 and 7.8 *M* HNO_3, respectively, and which show much lower solubilities and again no minima in calcium nitrate solutions.

Reaction 3 can be expected to progress far to the right at high acidities if the complex acid is appreciably weaker than the ligand acid. This apparently occurs with the +4 actinide nitrates. Under these conditions the solubilities in nitric acid and calcium nitrate should diverge with increasing nitrate since in nitric acid hydrogen ion activity is increasing simultaneously. This is exactly what is observed. The solubility of $[(C_2H_5)_4N]_2Np(NO_3)_6$ is 2×10^4 times as great in nitric acid as in calcium nitrate at 11 *M* nitrate, whereas the solubilities are about equal below 4 *M* nitrate. The same effect is observed with Pu and Th.

The anion-exchange data in Fig. 6 to 8 are almost identical with the solubility data indicating that the distribution coefficient is proportional to the $M(NO_3)_6^=$ activity. Comparison of the anion exchange and solubility data shows that the resin behaves as a constant concentration of quaternary amine in solution. Thus, the maximum in the anion-exchange distribution in nitric acid corresponds to the minimum solubility of $[(C_2H_5)_4N]_2M(NO_3)_6$ and to the maximum activity of the $M(NO_3)_6^=$ ion. Kraus and Nelson[6] have shown that in hydrochloric acid the molal concentration of chloride in the water of the resin phase at high electrolyte concentration becomes equal to the molal concentration in the aqueous phase. This is not suprising in view of osmotic pressure considerations. It can be expected that in nitric acid also the molal concentration of nitrate in resin and solution will approach that in the aqueous phase at high concentrations. The reaction for the absorption of $M(NO_3)_6^=$ is

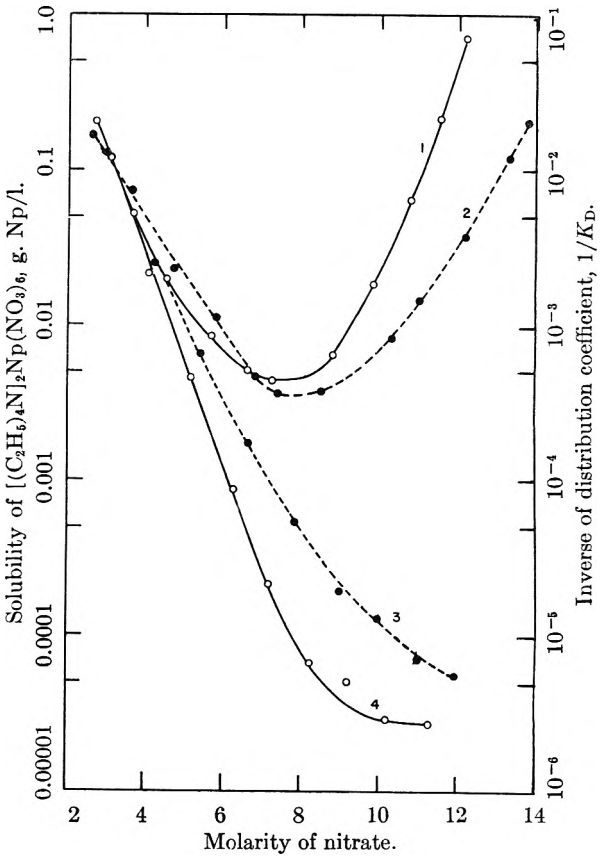

Fig. 7.—Comparison of anion-exchange behavior of Np(IV) on Dowex 1, X-4 (50 to 100 mesh) with the solubility of $[(C_2H_5)_4N]_2Np(NO_3)_6$ at constant 0.39 *M* $(C_2H_5)_4NNO_3$: (1) solubility in nitric acid; (2) anion exchange in nitric acid; (3) anion exchange in $Ca(NO_3)_2$, 0.5 *M* HNO_3; (4) solubility in $Ca(NO_3)_2$, 0.5 *M* HNO_3.

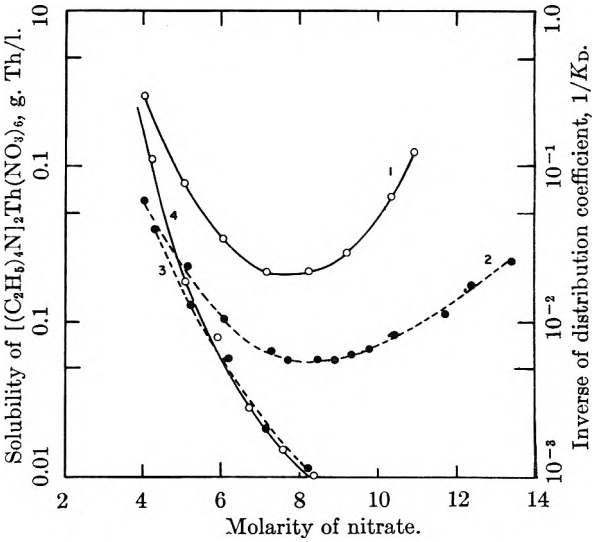

Fig. 8.—Comparison of anion-exchange behavior of Th(IV) on Dowex 1, X-4 (50 to 100 mesh) with the solubility of $[(C_2H_5)_4N]_2Th(NO_3)_6$ at constant 0.39 *M* $(C_2H_5)_4NNO_3$: (1) solubility in nitric acid; (2) anion exchange in nitric acid; (3) anion exchange in $Ca(NO_3)_2$, 0.5 *M* HNO_3; (4) solubility in $Ca(NO_3)_2$, 0.5 *M* HNO_3.

$$2NO_{3(r)}^{-} + M(NO_3)_6^{-}{}_{(aq.)} \rightleftharpoons M(NO_3)_6^{-}{}_{(r)} + 2NO_3^{-}{}_{(aq.)} \quad (8)$$

If the NO_3^- values cancel out at high electrolyte concentration as just discussed, the remaining part of reaction 8 is identical with the precipitation reaction at constant concentration of precipitant. In measuring values of K_D, where K_D is high, as is the case here except for the lower thorium K_D's, most of the initial metal loads into the resin and the resin loading is essentially constant. The activity of $M(NO_3)_6^-{}_{(r)}$ is nearly constant as is the activity of the $[(C_2H_5)_4N]_2M(NO_3)_6$ precipitates. K_D is thus a measure of the M(IV) species in equilibrium with a constant small amount of the $M(NO_3)_6^-$ ion. The solubility and K_D values are both measures of the initial amount of the free ion, $M(NO_3)_6^-$, in the solution and the variation of K_D with acid and nitrate concentration is explained by reactions 5, 6 and 7. The anion-exchange absorption of Pu(IV), Np(IV) and Th(IV) from nitric acid therefore is controlled by the generalized reactions 1, 2 and 3 with formation of un-ionized complex acid *via* reaction 3 being a major factor in acid solutions.

In order to show that the minimum in solubility of the tetraethylammonium salts in nitric acid was not a unique feature of the quaternary amines, the solubility of the cesium salt of hexanitratocerate was examined semiquantitatively and was found to also show a pronounced minimum solubility with increasing nitric acid. The Ce(IV) anion-exchange behavior in nitric acid is very similar to that of Th(IV) except that the K_D maximum occurs at about one molar lower acidity.[23]

These results emphasize the error involved in attempting to quantitatively correlate anion-exchange data with spectrophotometric measurements which are a measure of the total complexing of the central metal to the ligand and are not necessarily a measure of the free complex anion. Thus, spectrophotometric studies as carried out in this paper measure total hexanitrato complex which is made up of a variable proportion of $M(NO_3)_6^-$, $HM(NO_3)_6^-$ and $H_2M(NO_3)_6$. In the study of complex ions by anion exchange the formation of relatively weak complex acids must also be taken into consideration. The fact that strong absorption occurs in no way indicates that the complex anion is the principal species or that it ever contributes a significant percentage of the total metal concentration. This results from the fact that both reactions 1 and 3 may be driven far to the right by an extremely high equilibrium constant for reaction 2.

Aveston, *et al.*,[24] have shown that the affinity of anion-exchange resins for various anions can be explained on the basis of their polarizabilities and their shape. They have pointed out that when anions are very strongly absorbed strong interaction of the anion and the resin site results in ion pair formation and less ionic character to the resin. This results in loss of much of the hydration water from the resin and consequent resin shrinkage. Because of this, the activity of the strongly absorbed anion in the resin phase is probably much less than expected from its mole fraction in the resin alone. The polarizability and shape of anions is also a very important factor in the solubility of their salts. Insolubility tends to result when the anion is more readily polarized by the cation than is the solvent.[25] Thus, anions which are readily polarizable by the quaternary amine sites of anion-exchange resins and strongly absorbed might also be expected to form low solubility salts with similar large cations in the solution phase. This was found to be the case. Besides the nitrate salts discussed here, the following are precipitated by at least one of the first four tetra-*n*-alkyl amines: chloride; Co(II), U(VI), U(IV), Fe(III), Pu(IV), Zn(II), Cd(II), Zr(IV), Sn(IV), Nb(V) and Au(III): phosphate; UO_2^{++}: thiocyanate; Co(II): nitrates; U(VI) and Np(VI); neutral solution; MnO_4^- and $Cr_2O_7^=$. All of these were found to be of relatively low solubility in the solutions from which they are absorbed strongly by anion exchangers. The systems just mentioned were the only systems tried of those known to show high anion-exchange absorption. The Cd(II) chloride compound precipitated with tetrapropylammonium ion was found qualitatively to be much less soluble at 2 *M* HCl where the anion-exchange distribution is at a maximum than it is at 12 *M* HCl where the K_D is much lower.

The use of these low solubility salts to study anion exchange in the manner discussed here is thus apparent. The use of the solubility data of quaternary amine salts in studying formation of complexes is probably more reliable than the use of anion-exchange data for this purpose. This is because in the case of the anion exchanger, the concentration of the quaternary amine cation varies from one solution to another due to resin shrinkage. The concentration of the soluble quaternary amine can be held constant. Size and steric effects will affect solubility in a somewhat different manner than they affect anion exchange, and direct comparison of the relative anion-exchange behavior of different metal complexes *via* study of their solubility relationships probably is not possible. In order to study formation of anionic complexes by solubility studies and to correlate it to anion-exchange behavior, the insoluble compounds must be salts of the complex anion instead of addition compounds of crystallization. An example is the precipitation of a tan chloride of Ni(II) from hydrochloric acid and lithium chloride by Cs^+ whereas the complex absorbed on anion-exchange resin from concentrated lithium chloride is brilliant blue, and no anion-exchange absorption is observed in hydrochloric acid. In order to identify or compare the species absorbed in anion exchangers and the species present in precipitates spectrophotometric studies of the resin, of inert, high dielectric solvent solutions of the precipitates, and of mulls of the precipitates may be useful as discussed in this paper.

Kraus and Michelson[26] determined the solubility

(23) Private communication, F. P. Roberts, Hanford Laboratories.

(24) J. Aveston, D. A. Everest and R. A. Wells, *J. Chem. Soc.*, 231 (1958).

(25) T. Moeller, "Inorganic Chemistry," John Wiley and Sons, Inc., New York, N. Y., 1952, p. 343.

of tetramethylammonium and benzyltrimethylammonium chloroaurate in hydrochloric acid and lithium chloride and found that the solubilities of these were reminiscent of the anion-exchange behavior of gold in these media. Since their measurements are in an absence of a constant excess of the quaternary amine cation and both the cation and $AuCl_4^-$ concentration vary with chloride concentration in their solubility measurements the slopes of the solubility curves *vs.* chloride are less pronounced than the anion-exchange slopes. $AuCl_4^-$ is a stable complex and as such shows no maximum in anion-exchange distribution coefficient *vs.* hydrochloric acid concentration. The distribution coefficient (D) for Au(III) in hydrochloric acid decreases with increasing hydrochloric acid and increases slowly with increasing lithium chloride.[27] If the solubility data of ref. 26 are recalculated as a $K_{s.p.}$ (solubility squared) it becomes proportional to the $AuCl_4^-$ activity at constant amine concentration and agrees much more closely with the anion-exchange data for Au(III) in ref. 27. It appears that with Au(III) increasing hydrochloric acid promotes formation of chloroauric acid whereas increasing lithium chloride promotes increasing D and decreasing quaternary amine salt solubility through the effect of the highly hydrated lithium ion on the activity coefficient of water and thus on the chloroaurate ion (salting out effect). No maximum is observed in hydrochloric acid because formation of the $AuCl_4^-$ is complete at extremely low chloride concentration.

It is possible using generalized reactions 1, 2 and 3 to predict probable anion exchange distributions *vs.* ligand concentration data for ligand acid and ligand salt solutions. Consider first a very stable complex anion (high complexation constant) which is strongly absorbed by the anion resin (*i.e.*, $AuCl_4^-$, $PtCl_6^=$). If the ligand acid is stronger than the complex acid (likely the case in HCl, HNO_3, HBr, etc.) the distribution coefficient will decrease with increased ligand acid concentration due to reaction 3. In ligand salt solution at low concentration, the distribution coefficient will decrease due to common ion effect in reaction 2. At higher ligand salt concentration where resin invasion is significant the distribution coefficient will probably increase with such salts as those of Li, Ca, Al and other ions which are highly hydrated and change water activity markedly. With salts of NH_4^+ and similar cations less increase or actual decrease in distribution coefficient will be observed with increased ligand salt. Next consider complex anions of lower stability but strongly held by the resin (*i.e.*, $Pu(NO_3)_6^=$, $ZnCl_4^=$). Here if the complex acid is a relatively weak acid compared to the ligand acid a maximum in the distribution coefficient *vs.* ligand acid will result because of the combined effects of reactions 1 and 3. The position of the maximum will depend on the relative contributions of reactions 1 and 3. It must be pointed out that this maximum may be above the attainable ligand acid concentration if the complex formation constant is quite low or if the complex acid is moderately strong (probably the case with Zr, Hf, Pa, Nb, etc., in HCl). In ligand salts, complexes in this category will show markedly increasing distribution coefficients as the ligand salt is increased up to the point where complexation is complete, after which slower increase will probably be observed in salts such as those of Li, Ca, Al, etc., and probably decrease in salts of NH_4^+, etc. Third, consider complexes of high stability but more weakly absorbed by the resin (example Th sulfate[5]). Here the highest distribution will occur at low ligand concentrations and will decrease with both increasing ligand acid and ligand salt through common ion effect in reaction 2, but the decrease will be much more rapid in acid than in salt solution if the complex acid is weak. In the case of complexes of both low stability and low resin affinity, absorption will be slight at any ligand concentration. A further factor is introduced when the ligand acid is a polybasic acid such as sulfuric acid. Here increasing acid promotes bisulfate formation which may compete with the complex anion in the resin without contributing to its formation. Although the preceding division of complex anions into four general categories was made, it must be realized that such division does not in reality exist but instead only a continuous gradation of properties occurs. The relative stability of the complex, dissociation constant of the ligand acid, dissociation constant of the complex acid, affinity of the resin for the complex, and activity coefficient effects (salting effects) of the cations of ligand salts used must all be considered.

Acknowledgment.—The author expresses his appreciation to R. L. Braun who carried out the neptunium and thorium ion-exchange and solubility measurements and who measured many of the neptunium absorption spectra. The author also thanks the personnel of the Analytical Laboratories Operation who carried out most of the analyses.

(26) K. A. Kraus and D. C. Michelson, in Oak Ridge National Laboratory Chemistry Division Annual Progress Report, ORNL-2386, Period ending June 20, 1957, p. 104.

(27) K. A. Kraus, D. C. Michelson and F. Nelson, *J. Am. Chem. Soc.*, **81**, 3204 (1959).

METHANE–OXYGEN FLAME STRUCTURE. I. CHARACTERISTIC PROFILES IN A LOW-PRESSURE, LAMINAR, LEAN, PREMIXED METHANE–OXYGEN FLAME

BY R. M. FRISTROM, C. GRUNFELDER AND S. FAVIN

Applied Physics Laboratory, The Johns Hopkins University, Silver Spring, Maryland

Received February 18, 1960

The results of a study of the structure of a $^1/_{10}$ atmosphere laminar, lean, premixed methane–oxygen flame are presented in the form of profiles giving the local intensive properties as a function of distance through the flame front. Thirteen different profiles have been measured including local aerodynamics, temperature and composition. All species except atoms and radicals are included. These data allow comparisons among methods of measuring temperatures in flames; satisfactory agreement was found. The validity of describing this flame with a one-dimensional model has been tested by measuring the profiles both on the axis and off the axis. Since no significant trends were found in these results, it was concluded that a one-dimensional model provided a good quantitative description. The precision and sources of error in the measurements are discussed and the probable accuracy of the measurements is assessed. It was concluded that the results showed sufficient precision and spatial resolution to allow a quantitative interpretation of the results.

Introduction

The theory of flames has been sufficiently developed so that the important chemical and physical processes are well understood,[1] and experimental techniques have been developed for studying the detailed microstructure of laminar flames. These measurements allow the determination of local aerodynamics,[2] local temperature,[3] and local composition[4] at each point in the flame. Thus a quantitative interpretation of experimental flame structure should be possible.

As is frequently the case with new techniques, questions have been raised as to the validity of these experimental methods. These questions are difficult to answer directly since no accepted techniques are available for comparison, and the parameters required for a direct comparison with flame theory are either unavailable or of too low precision to be useful. This is true even in the case of the H_2–Br_2 system,[5] which is the best understood flame. In the case of the methane–oxygen flame, which is even more complex, theory offers no solution.

An earlier attempt was made to interpret experimental flame structure data quantitatively.[6] This study of the propane–air system was promising, but the results were not of sufficient precision to establish the techniques and interpretation beyond reasonable doubt. Therefore, the present system (Table I) was chosen as a proving ground for these techniques. This methane–oxygen flame was chosen because it is a simple chemical system. It has sufficient thickness so that spatial resolution is not a problem, and the velocities and temperatures fall in an experimentally convenient range. This paper deals with the reproducibility of experimental results and probable sources of error in measurements. Validity of the measurements will be discussed in paper II, where it will be shown using a one-dimensional model, that matter and energy are conserved at every point in the flame, as indeed must be the case if the data are valid and the interpretation correct. These tests are not trivial since they involve separate measurements of local flame aerodynamics, local temperature, local composition, their spatial derivatives, and a knowledge of the thermal conductivity of the mixture and the diffusion coefficients of each of the species over the entire temperature range covered by the flame. The chance of accidental agreement in such a complex interpretation without adjustable parameters seems remote.

Model for Flame Structure

The flame chosen for study had flat, axially symmetric geometry and approached in outward appearance the ideal one-dimensional flame usually discussed in theory.[1] All physically realizable flat flames are three-dimensional so that a one-dimensional model represents an abstraction, which greatly simplifies the problem. In such a flame, the local properties are assumed to vary only in the direction of flame propagation, the gradients along the other two directions being assumed negligible, and the aerodynamics is described by the equation ρv = constant. In real flames, lateral expansion of the gas occurs and the more general formula for one-dimensional flow in a duct of changing cross section must be used, namely, $\rho v a$ = constant. We will refer to this second type of flow as one-dimensional, reserving the term "ideal" one-dimensional to designate systems where ρv = constant. This modification of the general theory to include lateral expansion has been made by Westenberg,[6] and his formulation of Hirschfelder's flame equations will be used in the following paper II for the interpretation of our data. As previously pointed out, the criterion for a one-dimensional description is that the spatial derivatives of the intensive properties (temperature, composition, velocity) are small along the transverse coördinates X and Y compared with the derivatives along the coordinate of flame propagation Z. This was clearly the case for the present flame since no systematic

(1) J. O. Hirschfelder, C. F. Curtiss and R. B. Bird, "Molecular Theory of Gases and Liquids," John Wiley and Sons, Inc., New York, N. Y., 1954, p. 761.

(2) R. M. Fristrom, W. H. Avery, R. Prescott and A. Mattuck, *J. Chem. Phys.*, **22**, 106 (1954).

(3) R. Friedman, "Fourth Symposium on Combustion," Williams & Wilkins Co., Baltimore, Md., 1953, p. 259.

(4) R. M. Fristrom, R. Prescott and C. Grunfelder, *Combustion and Flame*, **1**, 102 (1957).

(5) E. S. Campbell and R. M. Fristrom, *Chem. Revs.*, **58**, 173 (1958).

(6) R. M. Fristrom and A. A. Westenberg, *Combustion and Flame*, **1**, 217 (1957).

TABLE I

INITIAL AND FINAL STATES OF METHANE–OXYGEN FLAME

	T, °K.	O_2	CH_4	A	N_2	CO_2	H_2O	CO	H_2	O	OH	H
Initial	350	0.9143	0.0785	0.0034	0.0008	0.0022	0.0006	0	0	0	0	0
Final												
Calcd.	2000	0.7498	0	0.0034	0.0008	0.0822	0.1569	0.0040	0.0002	0.00201	0.00528	0.00007
Exptl.		0.7603	0	0.0034	0.0008	0.0779	0.1559	0.0010	0.0005	.....	.....	.....
Pneum. probe	2015 ± 20											
Particle track	1930 ± 80											
Thermocouple cor.	1992 ± 10											

variation of the intensive properties was found with distance off axis (see Fig. IIIC and Table II and III). This finding was in agreement with other flame structure studies on Bunsen flame microstructure.[4,7–9] For quantitative study it is necessary that the flame diameter be large compared with the thickness of the reaction zone. This was the case except with respect to the slow secondary reaction of carbon monoxide where the problem is not serious since this region of the flame is not strongly coupled with the primary reaction and is not greatly influenced by gradients.[7] This reaction appears to be homogeneous and initiated by the primary reaction of methane.

TABLE II

EXPERIMENTAL PRECISION OF COMPOSITION DATA

Species	Mean deviations, % Run 1	Run 2	Run 3
O_2	1.92	1.01	0.374
CH_4	0.945	2.26	.100
CO_2	2.14	0.642	.075
H_2O	1.63	1.46	.208
CO	3.28	1.48	.454
OCH_2	2.07	1.41	.263
H_2	4.25	2.79	.254

Entries are mean deviations of normalized experimental data N_i (defined below) from the smoothed curves of Figs. 3A and 3B.

$$N_i(Z) = \frac{X_i(Z) - X_i(\text{initial})}{X_i(\text{final}) - X_i(\text{initial})} \text{ for } O_2,\ CH_4,\ CO_2,\ H_2O$$

$$N_i(Z) = \frac{X_i(Z)}{X_i(\text{max})} \text{ for CO, } OCH_2,\ H_2$$

This presentation of the data was necessary because of variations in purity of the O_2 from run to run.

TABLE III

EXPERIMENTAL PRECISION OF THERMOCOUPLE TEMPERATURE DATA

Run	Description	Mean deviation, %
1	0.0012 cm. coated (axial)	0.67
2	.0012 cm. uncoated (axial)	Max. temp. only
3	.0025 cm. coated (0.5 cm. off axis)	1.57
4	.0025 cm. coated (0.75 cm. off axis)	1.09
5	.0025 cm. uncoated (0.75 cm. off axis)	1.58

Necessary and Sufficient Profiles for the Description of a One-dimensional Flame.—A complete description of a one-dimensional flame consists of a family of profiles giving the intensive properties of the flame as a function of an independent coördinate. This description can take several different forms since the independent coördinate can be distance, time, temperature or composition.[9] Each of these coördinates requires a different choice of dependent variables. The systems are related and can be derived from one another. We will discuss the system used experimentally. Here, distance is the independent coördinate. The minimum number of variables or independent profiles required for the description is equal to the number of distinct chemical species plus one. In such a minimal description, the composition profiles used must be measurable in some absolute units (*e.g.*, mass per unit volume), and the remaining profile must describe the deviation from true one-dimensional behavior, *i.e.*, lateral expansion. In practice, compositions usually were measured in relative terms so a density or temperature profile had to be provided also. The remaining profile was expressed as the cross-sectional area expansion ratio of a stream tube in the flame front.

It was possible and desirable to measure more than the minimum number of profiles. We present twelve independently measured profiles; the minimum number is nine plus one for each radical species considered. Extra profiles provide a cross check on the experimental techniques and give a valuable confirmation of the validity of the temperature and aerodynamic measurements. The only information lacking from a complete description of this flame is the concentrations of the free radical and atomic species which cannot be determined using our present techniques. In principle, radical profiles might be derived from the comparison between the density measurements of the pneumatic probe and the measured composition of stable species, but present data are not precise enough to yield useful information. This lack of radical information is a common one in kinetic studies, but it is particularly unfortunate in flames since there is doubt[10] as to the validity of the steady-state approximation which is often used to avoid the problem. The measurement of free radical species has been attacked experimentally,[11–15] but some improvement in resolution will be necessary to apply the techniques to the rapid reaction zone of this flame. Meanwhile, the present in-

(7) R. M. Fristrom, *J. Chem. Phys.*, **24**, 888 (1956).

(8) R. M. Fristrom, W. H. Avery and C. Grunfelder, "Seventh Symposium on Combustion," Butterworth Scientific Publications, London, 1959, p. 304.

(9) R. M. Fristrom, Ch. 6 of "Experimental Methods of Studying Flames AGARDOGRAPH," edited by J. S. Surugue (to be published).

(10) E. S. Campbell, "Sixth Symposium on Combustion," Reinhold Publ. Corp., New York, N. Y., 1959, p. 213.

(11) A. S. Leah and N. Carpenter, "Fourth Symposium on Combustion," Williams & Wilkins Co., Baltimore, Md., 1953, p. 274.

(12) E. M. Bulewicz and T. M. Sugden, "Spectrochemica Acta IVth International Spectroscopic Colloquium," Amsterdam, Pergamon Press, New York. N. Y., 1956, p. 20.

(13) C. P. Fenimore and G. W. Jones, THIS JOURNAL, **62**, 693 1958).

(14) W. E. Kaskan, *Combustion & Flame*, **2**, 229 (1958).

(15) Th. Grewer and H. G. Wagner, *Z. physik Chem.*, **20**, 371 (1959).

formation provides a good initial basis for discussing the kinetics of flame processes.

Apparatus and Experimental Techniques

The techniques for making flame structure measurements are discussed in various places in the literature. Therefore the present discussion will outline them only briefly and indicate where more detailed information may be found.[2-4,7-9,18,19]

Materials.—The materials used in these studies were bottled gases, both for the flame and to calibrate the spectrometer. These gases were of the highest purity available and analyzed by us prior to use. Analyses of gases used in several runs are given in Table I. These analyses were obtained primarily through mass spectrometry, although several doubtful points were confirmed with gas chromatography. Changes in argon content of the oxygen from run to run are noticeable (they are within the manufacturers' specifications of 99.5%), but such minor variations should have no important effect on the flame system.

Burner System.—The flame chosen for this study was a flat, 1/10 atmosphere screen flame. It appeared as a flat luminous disc suspended above the burner. To maintain and stabilize such a flame at low pressure requires precise instrumentation. The apparatus consisted of a gas metering system, a burner, a low-pressure housing, and a pump.[16] The inlet flows were regulated to 0.1% by critical orifice flowmeter.[17] A modified Egerton burner of the screen-type was used. It was 3.2 cm. in diameter, and used a 100-mesh "lektromesh screen." This gave a uniform velocity profile (±1%). The burner housing was a 2" Pyrex pipe cross with a water-cooled chimney. The exhaust flow was led through a critical orifice so that pressure was maintained constant in the chamber (±0.1 mm.). The pressure was monitored by a Zimmerli-type absolute mercury manometer.

Distance Measurements.—The measurement of position in the flame was fundamental to these studies, and was accomplished by two different techniques. In the aerodynamic measurements, photographic methods were used and in the case of temperature and composition measurements, a precision cathetometer.

The camera is a New Vue Model VC3. It was used with a reversed Schneider Xenon 1:2 f2 lens at a magnification ratio of about 3.5 to 1. Cut film 4 × 5" of the contrast process Ortho-type was used and developed in D-19. Positions were read from these pictures by making a twelve-fold enlargement on contrast paper and measuring the enlargement directly, using a calibrated eyepiece mounted on a drafting machine. Positions could be read with the drafting machine to the nearest hundredth of an inch, corresponding to about 6μ in the flame. Short distances, such as those between adjacent images in the spot photographs, could be read to the nearest 0.003", corresponding to about 2 μ in the flame. Reproducibility of such measurements was 1% or 2μ, whichever was the larger figure.

The cathetometer used in these studies was an eighty power microscope with a long focal length and a crosshair eyepiece. This telescope was mounted to slide along a 3/4" diameter ground steel rod driven by a precision screw, which could be read directly in microns. With this system the position of a sharp-edged object easily could be read reproducibly to 5μ.

Flame Stability.—The first problem in making position measurements in flames is to determine whether the flame stays fixed in a space during the period of measurement. This means that a method for detecting small movements of the flame front is needed. To the eye this flame was completely stable, but previous experience[4,6] indicated that movement might still be a problem. The luminous zone of this flame could only be located to within 100μ, so a method of greater delicacy was required.

This was provided by placing a small (0.0025 cm. dia.) chromel–alumel thermocouple 0.01 cm. above the stabilizing screen. The temperature gradient here was steep (5×10^3 °K./cm.) so that a small movement of the flame front was reflected as a measurable temperature change in this thermocouple. With this system it was possible to detect movements as small as a micron. This includes both slow drifts and oscillations since flame vibrations result in quite noticeable fluctuations in the sensing galvanometer of the potentiometer. The frequency response of the galvanometer was limited to about ten cycles, but it was also possible to check for higher frequency oscillations using a low impedance amplifier and oscilloscope. The undisturbed methane flame showed no perceptible short period movements ($\delta Z < 2\ \mu$) and after a half hour warmup period, the drift was less than 1 μ per hour. Probes and thermocouples disturbed this reading in a reproducible manner. This was not expected since previous experience had been that small thermocouples and properly designed probes had no visible effect on the flame.[4] Detection of the effect was due to the increased sensitivity of the thermocouple monitor (±2 μ) over visual checks (±100 μ). Taken at face value, the maximum movement of the flame amounted to 50–100 μ (the limit of visibility), and between two adjacent positions, the shift amounted to no more than 2–3 μ. These displacements were so small that they have been neglected, although a correction could have been made using the observed temperature shift and the measured temperature profile in the region of the screen.

An interesting point, which is discussed elsewhere,[9] is that movements of the flame were detected which were a small fraction of the diameter of the thermocouple (*e.g.*, 1 μ movement could be detected by a 25-μ thermocouple). This was the case because the thermocouple reproducibly averaged the temperature over the region it occupied. It was this average that was read on the potentiometer and it changed reproducibly with minute shifts in position.

Reference Surfaces.—Having established that the flame was stable enough for precision measurements, the next problem was that of establishing a fixed reference surface or point as an origin for the measurements. There were several possible reference surfaces: The luminous zone of the flame, the surface of the burner screen, or the position of the monitoring thermocouple. The sharpest portion of the luminous zone was the inner edge, which could only be located to ±100 μ. Therefore, this surface was useful only as a cross check. The burner screen offered a fixed surface, but it was rather difficult to locate accurately. Therefore, these positions were measured with reference to the upper edge of the bead of the monitor thermocouple, which could be located to ±5 μ.

Relative Positions and Errors in Position Measurements.—Relative positions were determined either photographically or with a cathetometer. The photographic method is subject to a number of other limitations. These included resolution and distortion of the camera and the enlarger lenses, optical distortion due to inhomogeneities in the windows and density gradients in the flame, uneven shrinkage of the film and paper used, and possible deviation of scattered image from the center of gravity of a particle. These errors have been discussed in some detail,[2,18] and it was felt that photographic measurements could be made with a precision of about 2%, with a least count error of the order of 2–6 μ.

Cathetometer measurements used in thermocouple and probe traverses were subject to errors due to reading, the calibration of the precision screw, and optical distortion in the windows and flame gases. These sources of error amounted to only a few microns. The mounting was sufficiently free from vibration, and the adjustment of the tension was made so that hysteresis and mechanical reproducibility was ±2 μ. The cathetometer agreed with a standard laboratory ruled meter to within 5 μ in 10 cm. of travel.

Absolute Position.—To compare profiles obtained by different experimental techniques, it was necessary to rectify the coördinate systems to a common one. All of these coordinate systems had a common origin (the monitor thermocouple), but in general there was a displacement between the position of the "probe" and the region of the flame actually measured. In the case of particle measurements, this displacement was due to aerodynamic lag of the particles. In the case of the thermocouple, the displacement was due to its wake which distorted the flame slightly, so that the thermocouple measured a region slightly downstream of its

(16) R. M. Fristrom and S. D. Raezer, "Applied Physics Laboratory," The Johns Hopkins University, CM 919, August, 1957.

(17) J. Anderson and R. Friedman, *Rev. Sci. Instr.*, **20**, 61 (1949).

(18) R. M. Fristrom, R. Prescott, R. Neumann and W. H. Avery, "Fourth Symposium on Combustion," Williams & Wilkins Co., Baltimore, Md., 1953, p. 267.

(19) A. A. Westenberg, R. E. Walker and T. P. Fehlner (to be published).

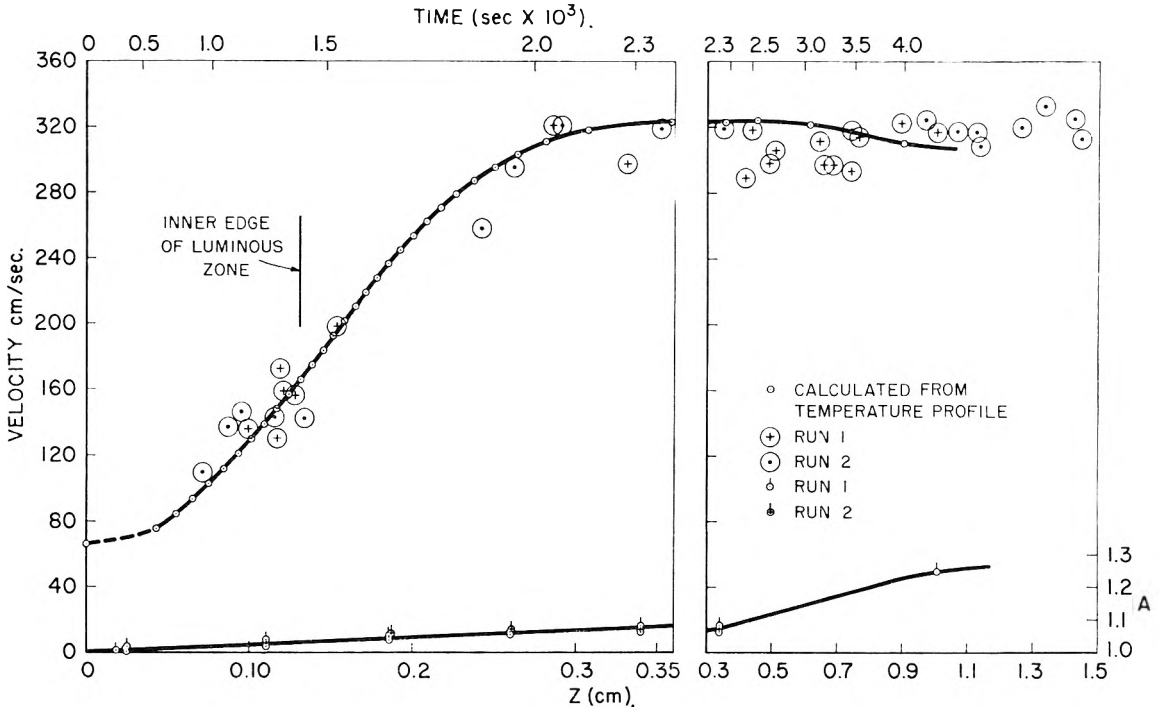

Fig. 1.—Aerodynamic profiles—velocity (cm./sec.) and area ratio as a function of distance (cm.) and time (sec.).

visual position. In the case of pneumatic probe and composition measurements, the probes withdrew a sample from a region slightly upstream of the measured position of the probe. These effects are understood qualitatively, and rough quantitative values can be assigned to the shifts of coördinate systems.[9] There was sufficient ambiguity in these corrections, however, so that an independent check was desirable. This was provided by comparing the temperature profiles which can be derived from these three types of measurements. They were aligned by superimposing the "knee" point of each of these curves. This allows a superposition of these measurements to about 100 μ. Closer alignments requires other criteria, which are discussed in paper II.

Spatial Resolution.—The spatial resolution which the several techniques allowed is an important factor since the interpretation of flame structure data depends upon spatial derivatives. This resolution was determined by the size of the instrument used; for thermocouple measurements, it was of the order of bead size; for microprobes, it was of the order of the orifice diameter; for particles, it was of the order of the space interval between successive images of the particle. Since the data may show reproducibility which is a small fraction of the instrument diameter, it is important to distinguish between positional reproducibility and spatial resolution. Positional reproducibility is an experimental quantity which indicates the least positional change which results in a reproducible variation. In these measurements, this least distance was of the order of 10 μ for each individual run. Resolution is an abstraction which refers to the "true" function being measured. Assuming that the experimental sensing element averages linearly over its sampling region, resolution was identified with the minimum distance over which a reproducible second derivative could be detected.

In these measurements, the resolution was believed to be 200 μ for the particle-track aerodynamic measurements, 100 μ for the thermocouple temperature traverses, and 100 μ for the microprobe sampling composition results.

Aerodynamic Measurements.—Because of lateral expansion, it was necessary to make direct measurements of the aerodynamics of the flame front. It was assumed that the flame obeyed the conservation equation $\rho v a$ = constant. Therefore, since temperature and average molecular weight were known, it was necessary to measure only a single aerodynamic parameter.

Actually, two parameters, velocity and stream tube area, were measured by introducing tracer particles of microscopic MgO dust into the incoming gas stream. These small particles (< 5 μ diameter) followed the accelerations in the gas stream with negligible lag.[2] These were illuminated at right angles to the direction of viewing and the images were recorded photographically. Illumination with zirconium flashbulbs gave streak pictures of particle paths which were measured to derive the area ratio. For velocity measurement, a double or multiple set of flashes of short duration were obtained from an electronic flash lamp and a repetitive pulser. Measurement of the resulting spots on the picture, combined with a knowledge of the time interval between flashes, allowed velocity to be calculated. It was possible to compare the directly measured velocity with that derived from the temperature measurements (Fig. 1). The agreement between the two sets of measurements was satisfactory. A detailed discussion of the techniques can be found in the literature.[2,18]

Sources of Error.—The direct errors in particle-track studies are those of position measurements on photographic film which have been discussed. Errors inherent in the method include inertial lag of the particles, drag due to the thermomechanical effects and gravity, and the asphericity of the particles. Questions involving the disturbance of the flame by the injected particles also must be answered. The average error of these measurements was 4%, or 20 cm./sec.

Temperature Measurements in Flame Fronts.—The temperature profile of this flame was measured with two instruments—a pneumatic probe and thermocouple. Temperatures could also have been derived from aerodynamic measurements,[2] but the results were of lower precision and resolution (see velocity curve, Fig. 1), so only the maximum temperature calculated from these measurements is presented (Table I).

Initial Temperature of the Flame.—The effective initial temperature of the gas in the burner is an important parameter since it and the initial composition define the enthalpy flux through the flame front. Although the gas originates at room temperature, it does not follow that this is the effective initial temperature of the flame, since the gas may either be preheated or precooled. Our burner was not externally cooled and was thermally isolated. The primary mechanism for energy transfer to the incoming gas is by convective heat transfer from the screen and burner which, in turn, receive energy by radiation from the chimney. Since the temperature of the burner and screen were lower (375°K.) than the temperature of the chimney which radiated onto it (1200°K.), the net effect considering the

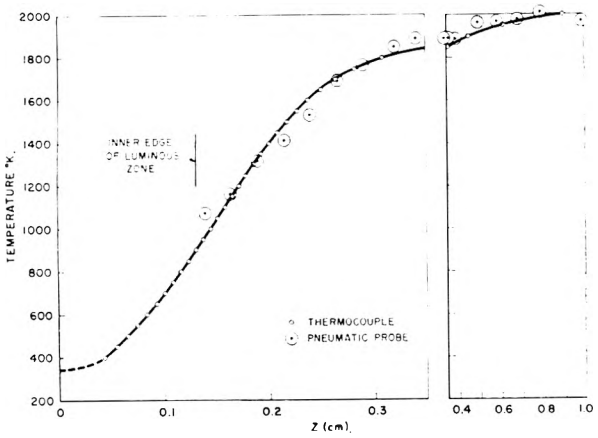

Fig. 2. Temperature profile—temperature (°K.) *vs.* distance (cm).

geometry of the situation was that of preheating and an increase in specific enthalpy of the flame gas. The calculation of the effective initial temperature is not straightforward even knowing the temperatures of the gas, screen and chimney, but a lower limit was set by the incoming gas temperature (300°K.) and the upper limit was set by the screen temperature (375°K.) Using the available information the best estimate of the effective initial temperature was 350 ±10°K. This value gives good agreement between the calculated adiabatic flame temperature and the values measured by several techniques.

Pneumatic Probe.—The pneumatic probe was a standard double orifice device[20] which was modified for this work to minimize flame disturbance and maximize spatial resolution. They were uncooled quartz microprobes similar to those used in composition sampling but of somewhat larger diameter (75 μ). The pressure measurements were made in the range around 1 cm. with a Zimmerli gage. Even with a minimum volume system, it was necessary also to use a large orifice in order to make measurements on a convenient time scale (5 min. per measurement).

The errors in the temperature measurements were dominated by those in pressure. Errors in determining second orifice temperature and in the calibration procedures were small. Spatial resolution with this probe was an important source of error due to the large size orifice necessary. The positional uncertainty was 0.0075 cm., while the uncertainty in temperature measurement was 1%.

There was good agreement between the measured maximum flame temperature (2015°K.) and the calculated adiabatic flame temperature (2000°K.).

Thermocouple.—Flame temperature profiles were most precisely measured by thermocouple traversing techniques (see Fig. 2).[3] In this work, the thermocouples were made from small Pt and Pt–10% Rh wires,[21] mounted on a micrometer traversing device, and the position of the bead determined with a precision cathetometer.

Three major problems were associated with these measurements. The first was catalytic reaction on the wire surface; the second was the problem of radiation losses from the thermocouple; and the third was the disturbance of the flame by the wake of the thermocouple.

In the case of the methane–oxygen flame, the problem of catalysis on the platinum surface was eliminated by "flame plating" the couple with silica.[22] This coating had the advantage of not only stopping catalysis but also inhibiting the evaporation of the platinum and prolonging thermocouple life in the flame. It had one principal disadvantage; it increased the size and emissivity of the thermocouple so that the effective emissivity had to be determined by calibration.

At temperatures above 1000°K., the radiation loss from these thermocouples was measurable. The laws governing this heat loss are well known.[23] For a long wire in a slow gas stream, it is proportional to the fourth power of temperature. The correction of thermocouple readings is straightforward[3] except for the evaluation of the emissivity–area constant. Emissivity is known with moderate precision for bright platinum but values given for the (SiO_2) coating[22] were not used because they depend somewhat on the conditions of deposition. The emissivity–area constant was determined by calibrating each thermocouple under conditions of use at the maximum temperature of the flame which was assumed to be the adiabatic value calculated thermodynamically. This is generally considered to be a good approximation. Its validity for our flame was substantiated by the agreement between the calculated value and temperatures measured by the pneumatic probe and particle track measurements (which do not involve the radiation correction) and the thermocouple measurements of run 2. This run employed a small, uncoated thermocouple, whose radiation correction was small (about 50°K.) and could be estimated with reasonable precision.

This procedure for estimating radiation corrections is self-consistent, and although corrections as high as 300°K. were necessary, the average deviation of the four runs from the average temperature curve given in Fig. 2 was 13°K.

The distortion of the flame due to the wake of the thermocouple was small, of the order of a few wire diameters. If the thermocouple wires are small compared with the flame front thickness, as was the case in these measurements, then to a first approximation this would result in a shift of the measured profile by a constant distance. The thermocouple would measure a temperature corresponding to a position slightly downstream of the measured position. Unfortunately, although this was a small absolute shift, it was not inappreciable compared with the measurements in the flame. The procedure for determining this shift was discussed in the section on position measurements. The assumption that the effect was primarily a simple shift rather than a distortion, was made reasonable by the agreement between the methods of temperature measurement and the general agreements between the temperature and composition curves.

The precision of these measurements was 13°K. (see Table III), and it was felt that the absolute accuracy was 25°K. These errors probably were dominated by positional reproducibility (0.001 cm.). However, errors due to change in rhodium content in the wire from the drawing process or preferential evaporation in the wire might account for as much as 10°K. error.

Composition Measurements in Flames.—The final piece of information necessary to describe the flame front is the profile of local concentrations. Composition measurements in this flame were obtained by sampling the flame gases with a quartz microprobe and analyzing them with a mass spectrometer (CEC-21-610 and CEC-21-620). These techniques have been given elsewhere[4,8,9] so the present discussion will cover, principally, improvements in the techniques.

Sampling was accomplished using a tapered quartz probe with an orifice tip. Careful control of the orifice shape was necessary to assure rapid decompression of the sample and quenching of the reaction. The techniques for accomplishing this have been given.[9] In the present work, the only difficulties encountered were in initial runs where the probe was found to be badly shaped and of too small diameter (~8 μ). These preliminary runs were discarded. All of the reported work was done with larger, carefully tapered probes whose diameters ranged from 15 to 40 μ.

Continuous flow sampling was found to be superior to the batch sampling techniques reported previously since adsorption problems, which are particularly serious for H_2O, were completely eliminated. By using a Teflon line inlet and a sapphire jewel inlet orifice to the spectrometer ionization chamber, the time taken for the flow system to reach equilibrium (±0.1%) was reduced to two minutes. This design eliminated metal surfaces and lubricants in the sampling system, and it was also possible to detect unstable species such as hydrogen peroxide and ozone. The sample was withdrawn at a pressure around 100 μ. The technique

(20) P. L. Blackshear, Jr., American Society of Mechanical Engineers paper No. 52-SA-38, April (1952).

(21) Two wire diameters were used, 0.002 and 0.001 cm. The beads were twice the wire diameter and the silica coating was 0.0003 cm. thick.

(22) W. E. Kaskan, "Sixth Symposium on Combustion," Reinhold Publ. Corp., New York, N. Y., 1957, p. 134.

(23) M. Jakob, "Heat Transfer," Vol. I, John Wiley and Sons, Inc., New York, N. Y., 1949, p. 23; Vol. II, p. 147.

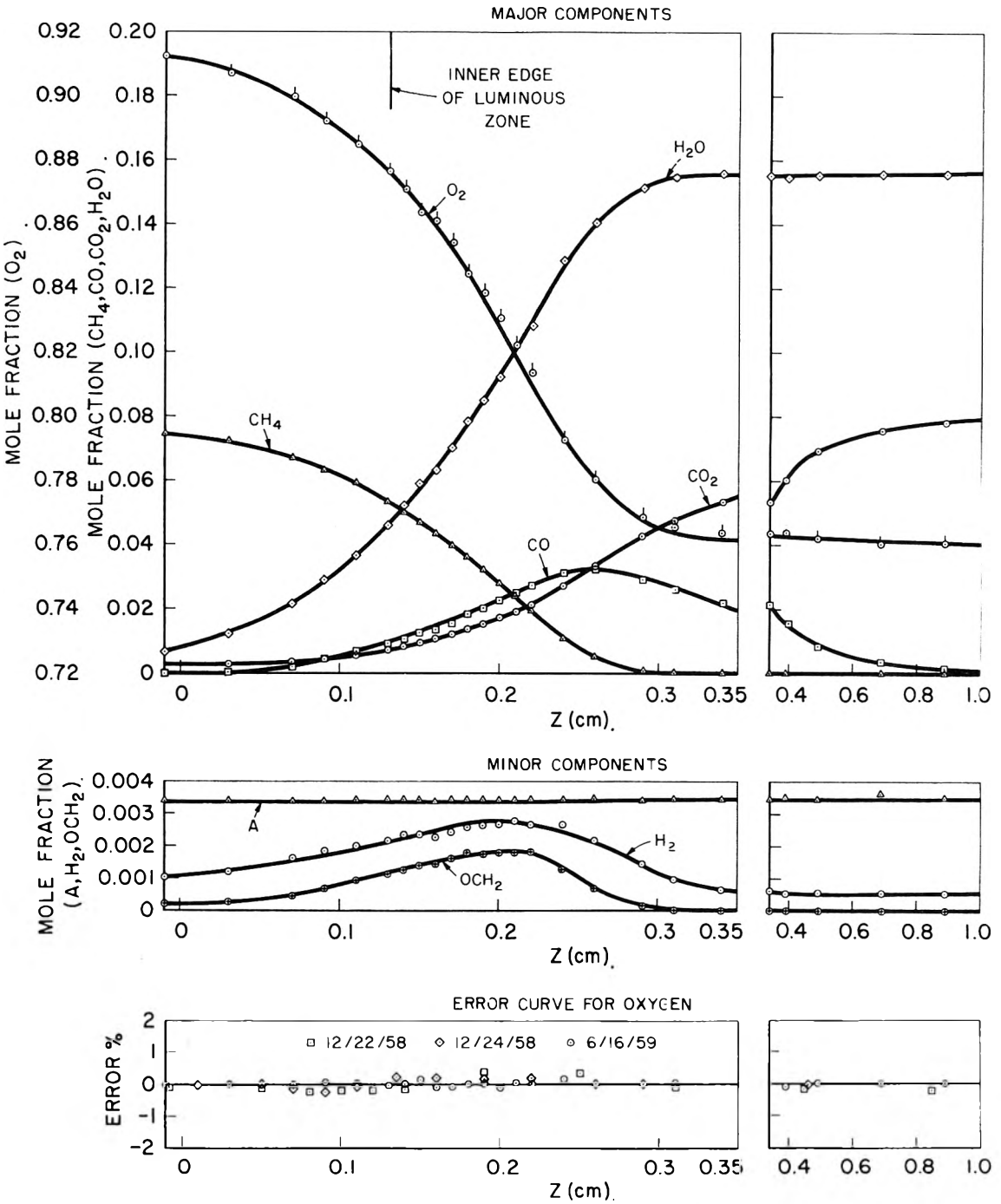

Fig. 3A.—Composition profiles—major species (CH_4, O_2, CO, CO_2, H_2O)—mole fraction *vs.* distance (cm); B—Composition profiles—minor species (A, H_2, OCH_2)—mole fraction *vs.* distance (cm). C—Error curve—oxygen per cent. deviation of three runs.

was to adjust the probe, measuring the position of the tip with the cathetometer. At this fixed position, a complete analysis of the stable constituents of the flame gases was made. To be certain that equilibrium had been attained and that the apparatus was functioning properly, the runs were duplicated (each peak was reported during a run, and two runs were made). If deviations greater than 0.5% of full-scale occurred, the run was repeated until successive runs agreed within this limit. Repetition was rarely necessary, and the average set of runs for a point could be obtained in 15–20 minutes. The three profiles taken on this system (each consisting of 25 complete analyses and their associated calibrations) were each completed during a single day. This was an important point in maintaining precision since calibrations of the mass spectrometer were found to drift several per cent. over a period of days. Over a single day, however, an analytical precision of better than 1% could be maintained by calibrating before and after the set of runs. Calibration of the instrument was accomplished by introducing gas samples at known pressures into the burner and recording the spectrometer output. Calibrations for water vapor and formaldehyde were less direct; here, a mixture of oxygen partially saturated with the vapor was passed through the burner. The total pressure was measured with the Zimmerli gage and the partial pressure of the oxygen was determined using a previous calibration and the partial pressure of the vapor deduced as the difference between the total pressure and the oxygen partial pressure. In the case of water, these calibrations could be compared with the results obtained in the high temperature equi-

librium region of the flame where the water concentration could be calculated. The two methods of determining the spectrometer sensitivity to water agreed to within 2%. The accuracy of the formaldehyde calibration was only 10–20%, but fortunately this is a quantitatively unimportant constituent. These measurements allowed the determination of local concentrations of all of the constituents of this flame except the reactive atoms and free radicals. It is presumed that these latter species do not represent a quantitatively important fraction of the species being measured. Analysis of our data from the standpoint of matter conservation substantiates this (see atom balance, paper II).

Sources of Error.—Reading errors and errors due to transient disturbances were not important since each run was repeated four times. The inherent stability and linearity of the instrument was a fraction of a per cent. for relative sensitivity over periods of 10–20 minutes. The reproducibility of analyses was 1%, with a least count better than 10-mole fraction. Errors in calibration were less than 2%, except in the case of formaldehyde where it was 20%. Positional errors (± 20 μ) are probably dominant in determining the reproducibility. Errors could occur because the sample measured was not representative of the concentration at the sampling point. Such deviations could stem from four sources: (1) biasing due to selective action of the probe, (2) non-linearities in averaging of the sample over the region of withdrawal, (3) adsorption of the sample in the transfer system and (4) inefficient quenching of the sample with resulting reaction in the probe. These questions have been discussed in some detail in the literature.[6,8,9] It is believed that these sources of error do not exceed 2%, provided the following conditions are met: The reaction rates have half lives exceeding ten microseconds, the radical concentrations do not exceed a fraction of a per cent., and a continuous flow Teflon-lined analytical system is used.

Data

With these techniques, it was possible to measure the important local properties in the flame front. This information was collected as a set of profiles which give these intensive properties as a function of distance (Z coördinate in the flame). These curves represent a complete description of this flame excluding only the composition of the free radical and atomic species. A number of duplicate runs were made since it was desirable to establish the applicability of a one-dimensional model to this system and to establish the reproducibility of the techniques. The bulk of the data makes it impractical to present them all directly. Therefore, the most reliable run of each type of data is presented directly and the other runs are given in the form of an error curve for oxygen composition and error tables for the other variables. The error curve and tables indicate the precision of the data and demonstrate the one-dimensional character of the flame since the off-axis runs show no significant trend.

Two types of aerodynamic information were obtained—the area ratio and velocity. Area ratio is the ratio of streamtube area at any point Z to the streamtube area at the coördinate origin (the screen). The values are recorded directly in Fig. 1 which gives the points measured on a number of streamtubes on two pictures. These data cover streamlines out as far as 1 cm. from the axis. The velocity measurements were taken from two pictures and cover the central region of the flame (± 1 cm.).

Temperature information was derived using both thermocouples and a pneumatic probe. Four separate complete runs were made on this flame using several different thermocouples. Thermocouple diameter, coating and positions of the measurement were varied in order to assess the effects of aerodynamic wake, radiation losses and deviations from one dimensionality. The curve of Fig. 2 is an average taken at every 50°K. interval from the experimental data interpolating linearly between adjacent points. Run number 2 was made with a small (0.0012 cm. dia.) uncoated couple so that the radiation correction could be estimated and the maximum temperature of the flame determined. The maximum value (1952°K.) when corrected for radiation was identical with the calculated adiabatic flame temperature (2005 ± 15°K. experimental *vs.* 2000°K. calculated).

The pneumatic probe data consist of a single run made with a probe similar in geometry but somewhat larger in size (75 μ) than those used in the composition studies. This study confirmed the presumption that the flame closely approached the calculated adiabatic temperature. It followed the same pattern as the thermocouple temperature but had somewhat lower precision and resolution. Because of interaction with the screen, data were taken only beyond 0.1 cm.

The composition data consist of three runs. The first run was made with a 30-μ probe on the axis. The 21–610 mass spectrometer was used for analysis of the gases. The second run was made with a 15-μ probe, with samples taken 1 cm. off axis. The 21–610 mass spectrometer was used for analysis. The third run was made with a 20-μ probe on axis using a 21–620 mass spectrometer. This last run was considered to provide the most reliable and complete data and is presented in Fig. 3 A, B. Data from the other runs are presented in the form of error curves of Fig. 3C and error Table II.

METHANE-OXYGEN FLAME STRUCTURE. II. CONSERVATION OF MATTER AND ENERGY IN THE ONE-TENTH ATMOSPHERE FLAME[1]

BY A. A. WESTENBERG AND R. M. FRISTROM

Applied Physics Laboratory, The Johns Hopkins University, Silver Spring, Maryland

Received February 18, 1960

The experimental data on temperature, composition and aerodynamic profiles through a flat, premixed CH_4–O_2 flame obtained by techniques described in paper I of this series are analyzed in terms of matter and energy conservation. The composition profiles for the seven stable species found in the flame are corrected for molecular diffusion, using diffusion coefficients measured in this Laboratory, and the resulting flux distributions are shown to give a satisfactory balance of carbon and hydrogen through the flame. The fluxes of enthalpy by means of convection, diffusion and conduction are given separately, and summed to show the degree to which energy conservation is fulfilled by the data. The various approximations used in the treatment are critically discussed, and it is shown that the general reliability of the results has been improved considerably over previous laminar flame structure analyses.

Introduction

The development of experimental techniques for the measurement of temperature, composition and aerodynamic profiles through laminar flame zones has been reported in earlier publications of a series from this Laboratory.[2,3] This work culminated in a set of data obtained in a stoichiometric, premixed, propane–air flame of conical geometry at 1/4 atm. pressure. Paper IV of that series[4] reported the analysis of these data in terms of material transport.

The experience gained up to that time pointed the way to various refinements and changes in the experimental techniques, and also to the desirability of studying a flame system which was chemically simpler insofar as the number of stable species present is concerned. The changes in technique were described in detail in paper I of the present series.[5] In brief summary, these included

(a) A flat-flame stabilized on a screen burner was used instead of the conical flame as in the previous work. This brought about some simplification in the geometrical handling of the data, and in the physical manipulation of the apparatus.

(b) The operating pressure was lower (0.1 instead of 0.25 atm.) which gave a thicker flame and hence eased the requirements on spatial resolution.

(c) Gas sampling and mass spectrometer analyses were done in a continuous flow system instead of batch-wise. This afforded much better precision, and circumvented wall adsorption difficulties. In particular, this system permitted good analyses for water to be realized.

(d) Temperature profiles were obtained with a fine, silica-coated Pt–Pt,10% Rh thermocouple rather than by particle-track photography (which was used only as a supplementary technique). Considerably better precision thus was attained.

(e) Improvements in controlling and monitoring the flow of gases to the burner were introduced which led to better flame stability. A monitoring thermocouple was mounted just downstream of the screen, which allowed the flame position to be monitored at all times.

The chemically simpler flame system finally decided on was a mixture of methane and oxygen. It was thought that this represented a reasonable compromise between chemical simplicity, ease of handling, and some degree of general interest as a common combustible mixture. As shown in reference 5, this flame contained five major stable species (methane, oxygen, carbon monoxide, carbon dioxide and water) and two minor ones (hydrogen and formaldehyde) for which analyses were made, which is considerably simpler than the twelve components found in the propane–air flame. No other species (other than impurities) at a concentration greater than 0.01% were found.

One other important improvement incorporated in this new work should be mentioned. This is that experimentally determined molecular diffusion coefficients were used in the data analysis to be described. In view of the pronounced—in some cases the predominant—effect of diffusion on the flux profiles of the various flame constituents, this is a decided gain in the reliability of this general approach to laminar flame studies, particularly in the derivation of chemical kinetic information from the data. In the previous work on propane–air flames it was necessary to use values of the molecular diffusion coefficients calculated from kinetic theory and empirical low temperature viscosity parameters, so that the reliability of the diffusion coefficients at flame temperatures was quite uncertain. Since then a new method of measuring diffusion coefficients up to moderately high temperatures (~1200°K.) has been developed in this Laboratory,[6–8] and used specifically to measure the pertinent coefficients for the methane–oxygen flame.[9]

The present paper describes the analysis of the data on the methane–oxygen flame from the viewpoint of the transfer of mass and energy. It is believed that the various changes and refinements noted above have contributed to making the analysis of this flame considerably more reliable than was possible before.

(1) Supported by the Bureau of Ordnance, U. S. Navy, under contract NOrd 7386.

(2) (a) R. M. Fristrom, W. H. Avery, R. Prescott and A. J. Mattuck, *J. Chem. Phys.*, **22**, 106 (1954); (b) R. M. Fristrom, *ibid.*, **24**, 888 (1956).

(3) R. M. Fristrom, R. Prescott and C. Grunfelder, *Combustion & Flame*, **1**, 102 (1957).

(4) R. M. Fristrom and A. A. Westenberg, *ibid.*, **1**, 217 (1957).

(5) R. M. Fristrom, C. Grunfelder and S. Favin, THIS JOURNAL, **64**, 1386 (1960).

(6) R. E. Walker and A. A. Westenberg, *J. Chem. Phys.*, **29**, 1139 (1958).

(7) R. E. Walker and A. A. Westenberg, *ibid.*, **29**, 1147 (1958).

(8) R. E. Walker and A. A. Westenberg, *ibid.*, **31**, 519 (1959).

(9) R. E. Walker and A. A. Westenberg, *ibid.*, **32**, 436 (1960).

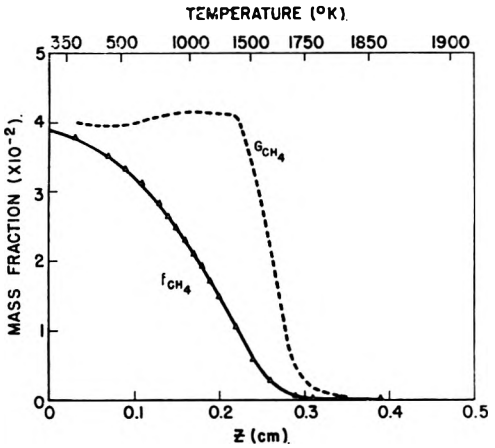

Fig. 1.—Concentration (f) and flux fraction (G) profiles of methane through flame zone.

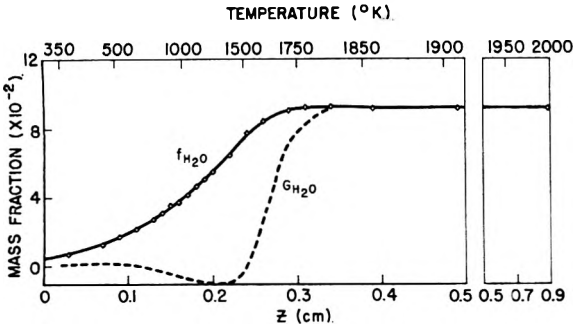

Fig. 2.—Concentration (f) and flux fraction (G) profiles of water through flame zone.

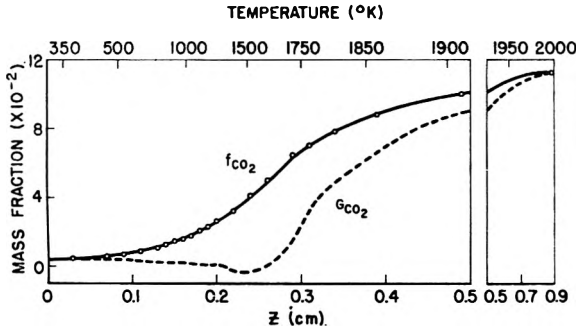

Fig. 3.—Concentration (f) and flux fraction (G) profiles of carbon dioxide through flame zone.

Preparation of the Data

As described in detail in paper I of this series,[5] the flame used in this study was flat, and held at a pressure of 7.60 cm. The initial mixture composition (mole fractions) aside from traces of impurities totaling less than 1% (argon, nitrogen, carbon dioxide and water) was

$$x_{CH_4} = 0.0785;\ x_{O_2} = 0.914$$

The data finally used in the subsequent analysis consisted of a set of concentration profiles for the stable species present, a thermocouple temperature profile, a streamtube area ratio profile, and a mass average gas velocity profile. The latter was obtained from a measurement of the final (hot boundary) gas velocity v_f by mans of particle-track photography and the temperature profile, making use of the continuity relation

$$\rho_f v_f a_f = \rho v a \qquad (1)$$

where ρ is density and a is the cross-sectional area of a streamtube, and the equation of state

$$\rho = P\bar{M}/RT \qquad (2)$$

where $\bar{M}$ is the mean molecular weight and the other symbols are conventional. Since the thermocouple temperature profile was much smoother and more reproducible than the particle-track velocity profile, it was felt that this procedure of deriving the velocity from the temperature by fitting at the measured point where the particle-track data were most reliable was preferable. Note that this is the reverse procedure to that used previously[4] where the temperature profile was derived from particle-track velocity measurements.

The problem then arises as to how best to superimpose, spatially, the temperature profile (as discussed above, the gas velocity and area ratio profiles were coupled to the temperature, and thus not independently variable) and the composition profiles determined by independent means. In paper I it was pointed out that the fact that temperature and composition are determined with different devices (thermocouple and sampling probe) leads to an uncertainty in referring both to a common spatial origin even though the positions of both are measured relative to a fixed point on the burner (the monitoring thermocouple). Since the pneumatic (sonic flow) probe temperature measurements were taken with a probe similar to that used in sampling, presumably a temperature read in this way would coincide automatically with the appropriate composition point. Thus the method used to determine the absolute origin was to superimpose the thermocouple and pneumatic probe temperature "knees," *i.e.*, the point of intersection of straight lines extrapolated from the hot gas region and the region of most rapid rise in the temperature profiles. The composition profile was then fixed relative to the thermocouple temperature profile. Additional discussion of this problem is included in the next section. The distance coördinate z was taken to be zero at the monitoring thermocouple just downstream of the screen.

Conservation of Matter

With the primary data on composition, temperature and mass average gas velocity available, the first step in the analysis was to take account of diffusion effects. The quantity G_i is the fraction of the total mass flow at any point in the flame which is due to chemical species i, and is given by

$$G_i = f_i(v + V_i)/v \qquad (3)$$

where f_i is the concentration expressed as mass fraction at any point and V_i is the diffusion velocity. It is a net flux variable which includes a positive contribution from diffusion if the concentration of i decreases downstream, or a negative contribution in the opposite case. As in the previous work,[4] the diffusion velocity V_i was calculated by assuming first, that each species i could be regarded as a trace component in the mixture and, second, since oxygen is present in large excess everywhere, each species i could be treated as being in a binary mixture with oxygen (see Appendix A). Under these conditions the approximate relation

$$V_i = -(D_i/x_i)(dx_i/dz) \quad (4)$$

may be used, where D_i is the binary diffusion coefficient with oxygen. (This also neglects the effect of thermal diffusion, a point which is discussed in Appendix B.) Equation 4 was used to compute the V_i for all the flame species (except oxygen, of course) at each point throughout the flame. The diffusion velocity for oxygen was then obtained from the required normalization condition (N_i is the

$$\sum_i N_i M_i V_i = 0 \quad (5)$$

molar density of species i, and M_i its molecular weight) which must be fulfilled in view of the definition of diffusion velocity (relative to the mass average gas velocity v).

The concentration gradients required in eq. 4 for each species were obtained by numerical differentiation of the smooth curves drawn through the experimental data, such as are shown as the solid curves in Fig. 1–7. The numerical process was supplemented by graphical differentiation at those portions of the curve where the slope changed rapidly. The internal consistency of the differentiations was checked using the requirement that $\sum_i (dx_i/dz) = 0$, since $\sum_i x_i = 1$.

The diffusion coefficients D_i used in eq. 4 were measured as a function of temperature in this Laboratory.[9] The point source technique used permitted measurement of the gas pairs CO_2–O_2 and H_2O–O_2 up to about 1100°K., while CO–O_2, H_2–O_2, and CH_4–O_2 were limited to slightly lower temperatures because of self-ignition. In all cases, however, the temperature range covered was enough to permit fitting the data to the appropriate kinetic theory formulas,[9] and reliable extrapolation to the highest temperatures needed in this flame (2000°K.). Diffusion coefficients for the CH_2O–O_2 pair were not measured. For this minor component, the necessary values were obtained from kinetic theory,[10] using the Lennard-Jones (6–12) potential and viscosity parameters. Since the latter are unavailable for formaldehyde, the values for methanol were used, this being a closely related molecule of similar size and mass. Table I lists the values of D_i *vs.* temperature. The underlined values were extrapolated using the Lennard-Jones (6–12) potential with parameters fitted to the lower temperature data.

Having all the diffusion velocities V_i at each 0.02 cm. interval throughout the flame, the mass flux fractions G_i were computed from eq. 3. These are shown as the broken curves in Fig. 1–7. The great importance of diffusion is obvious in all cases. It will be noted that some of the G_i curves (water, carbon dioxide, carbon monoxide and hydrogen) have regions of negative values, which would indicate a net upstream flux of these species. While there does not appear to be any *a priori* reason why this is not possible, the negative gradient dG_i/dz which exists upstream of these minima also implies that these species are undergoing a net disappearance due to chemical reaction.

(10) J. O. Hirschfelder, C. F. Curtiss and R. B. Bird, "Molecular Theory of Gases and Liquids," John Wiley and Sons, Inc., New York, N. Y., 1954.

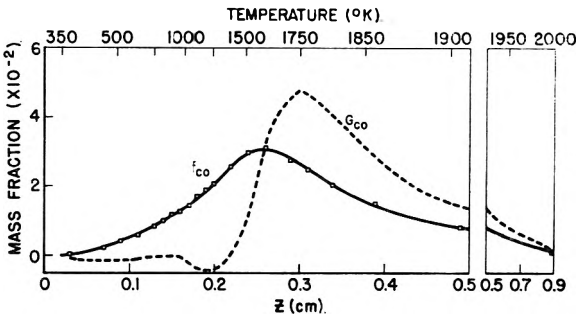

Fig. 4.—Concentration (f) and flux fraction (G) profiles of carbon monoxide through flame zone.

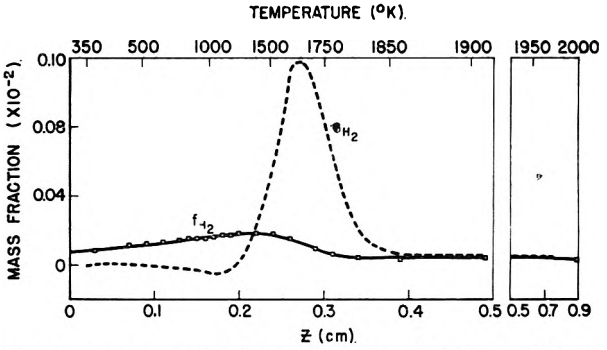

Fig. 5.—Concentration (f) and flux fraction (G) profiles of hydrogen through flame zone.

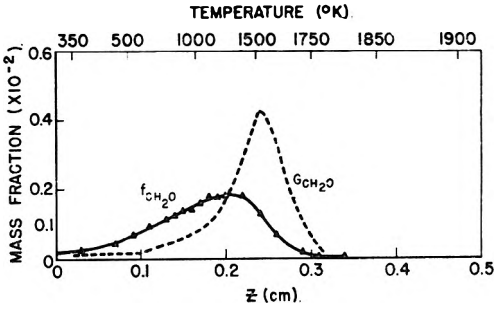

Fig. 6.—Concentration (f) and flux fraction (G) profiles of formaldehyde through flame zone.

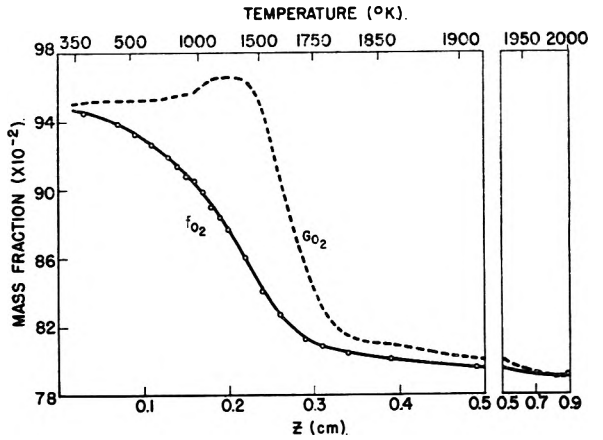

Fig. 7.—Concentration (f) and flux fraction (G) profiles of oxygen through flame zone.

Since it is difficult to see how this could happen, it seems likely that the negative G_i regions are not real and should be regarded as errors in the overall treatment. By the same token, the positive

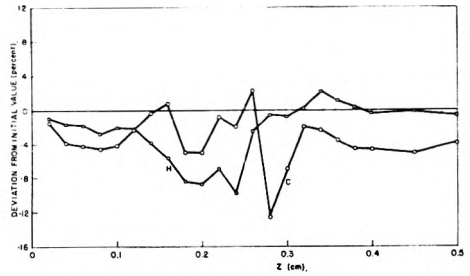

Fig. 8.—Conservation of carbon and hydrogen (atom balances) through flame zone.

maximum in the G_{O_2} probably is not real since it is a direct consequence of the negative G values for the other species, by the normalization procedure used to obtain the oxygen diffusion velocity.

TABLE I

BINARY DIFFUSION COEFFICIENTS AS FUNCTION OF TEMPERATURE

Underlined values are extrapolated; CH_2O–O_2 values computed from theory; pressure = 1 atm.

	D(cm.²/sec.)					
T, °K.	CH_4–O_2	CO_2–O_2	H_2O–O_2	H_2–O_2	CO–O_2	CH_2O–O_2
300	0.226	0.161	0.288	0.821	0.224	0.180
500	0.581	.419	0.692	2.09	.542	.422
700	1.05	.767	1.22	3.76	.956	.739
900	1.63	1.19	1.85	5.79	1.45	1.12
1100	2.29	1.68	2.58	8.14	2.03	1.57
1300	3.03	2.23	3.41	10.8	2.68	2.07
1500	3.86	2.84	4.32	13.7	3.40	2.63
1700	4.75	3.50	5.32	16.9	4.18	3.24
1900	5.72	4.21	6.40	20.3	5.03	3.91
2100	6.76	4.98	7.55	24.0	5.94	4.61

As in the previous propane–air flame,[4] it is important to examine the data in terms of conservation of atomic species. If n_i is the number of atoms of a particular element in a molecule of species i, it was shown that the relation

$$\sum_i n_i G_i / M_i = \text{constant} \qquad (6)$$

must hold throughout the flame, since atoms are neither created nor destroyed. In the methane–oxygen flame, carbon and hydrogen are the two elements whose conservation is to be examined, the oxygen being present in such excess in the form of O_2 that its constancy is practically assured. Results of applying eq. 6 for carbon and hydrogen to the G_i data given in Fig. 1–6 are shown in Fig. 8. The data are given as percentage deviation from the initial value of the summation, *i.e.*, the cold gas composition upstream of the screen. (Because of diffusion, the probe composition just downstream of the screen at $z = 0.03$ cm. is not quite equal to the true cold gas composition.) The balances are considered quite good, and are definitely better than those in the earlier propane–air work. The worst deviation is -12% for carbon and -9% for hydrogen, while in most of the flame the balances are considerably better (average deviations through the flame are about -3%). While the atom balance is not a very sensitive test of the sampling data and the diffusion corrections, the fact that it is reasonably good certainly indicates there are no large errors in the data as a whole.

Conservation of Energy

It is of interest next to examine the data in terms of energy considerations. Since the flame is an essentially constant pressure system, the convenient energy variable to use is the enthalpy. The energy continuity equation appropriate to a quasi-one-dimensional flow with area change such as is found in the flat flame must first be derived.

The basic energy equation for a steady-state system with no viscosity, radiation, or external forces may be written

$$\nabla \cdot (\rho \vec{v} \hat{H} + \vec{q}) = 0 \qquad (7)$$

where $\vec{v}$ is the mass average velocity vector, $\hat{H}$ is the specific enthalpy of the mixture, and $\vec{q}$ is the heat flux vector given by (ref. 10, p. 717)

$$\vec{q} = -\lambda \nabla T + \sum_i N_i H_i \vec{V}_i \qquad (8)$$

if the inverse thermal diffusion (Dufour) effect is neglected. λ is the mixture thermal conductivity, $\vec{V}_i$ is the diffusion velocity vector, and H_i the absolute molar enthalpy of species i. The enthalpy per unit mass $\hat{H}$ is related to the H_i by

$$\hat{H} = \sum_i x_i H_i / \sum_i x_i M_i \qquad (9)$$

Making use of the theorem (ref. 10, p. 815) which states that, if $\vec{F}$ is a vector which is tangent to the surface $f(x,y) = z$, then

$$\int (\nabla \cdot \vec{F}) \, dx \, dy = \frac{d}{dz} \int F_z \, dx \, dy$$

Equation 7 may be converted to

$$\int (\rho \hat{H} v + q) \, dx \, dy = \text{constant} \qquad (10)$$

where v and q are the z-components (*i.e.*, normal to the flame front) of their respective vectors. This may be written as

$$\rho v a \hat{H} + q a = \text{constant} \qquad (11)$$

the quantities ρ, v, $\hat{H}$ and q now representing suitably averaged values across the streamtube area a. Combining the z-component of eq. 8 with eq. 11, and using the quasi-one-dimensional over-all continuity relation in the form

$$\rho_0 v_0 = \rho v A \qquad (12)$$

where $A = a/a_0$ and the subscript "$_0$" refers to the cold boundary (*i.e.*, the screen), eq. 11 becomes finally

$$\rho_0 v_0 \hat{H} - A\lambda(dT/dz) + A \sum_i N_i H_i V_i = \rho_0 v_0 \hat{H}_0 \qquad (13)$$

assuming that gradients in temperature and composition are essentially zero at the screen.

This equation represents the enthalpy conservation through the flame zone in terms of the flux of enthalpy per unit of inlet area at the screen. The first term on the right side is the flux due to convection, the second is that due to conduction, and the third that due to diffusion. These terms were evaluated for the experimental methane–oxygen data. The specific enthalpy was obtained from eq. 9 using tabulated molar enthalpies from

standard sources.[11,12] The enthalpies for formaldehyde were obtained from the heat capacity data of Stevenson and Beach.[13] The thermal conductivity was taken to be that of pure oxygen, rather than attempting the exceedingly laborious computations for mixtures (for which all the necessary data are not available anyway). Because of the preponderance of oxygen, this approximation was adequate (see Appendix C). The thermal conductivity of oxygen has not been measured up to the temperatures required here, so it was calculated by a semi-empirical procedure: the translational (or monatomic) thermal conductivity λ_{mon} was obtained from the NBS tabulation[11] of viscosity (η) by means of the rigorous theoretical (first approximation) relation

$$\lambda_{mon} = (15/4)(R/M)(\eta)$$

The improved Eucken-type correction of Hirschfelder[14] then was applied, *i.e.*, to account for the

$$\lambda/\lambda_{mon} = 0.469 + 0.354\ (C_p/R - 1)$$

effect of internal degrees of freedom. The temperature gradient was obtained by numerical differentiation of the temperature profile, and the other quantities in eq. 13 were already available.

The various enthalpy fluxes are shown in Fig. 9. The conduction term is, of course, negative, since it always represents a flux of heat (positive enthalpy) upstream. The diffusion term would be expected to be positive relative to the inlet flux as it is, since the reactants of high enthalpy diffuse downstream and the products of low enthalpy diffuse upstream, both effects constituting a net positive enthalpy flux. (It seems unlikely that the effects of intermediates, which diffuse in both directions depending on which side of their maximum in concentration one considers, would alter this statement. They have enthalpies lower than the reactants and higher than the final products.) Whether the convection term, *i.e.*, the specific enthalpy profile, constitutes a positive or negative flux depends upon the relative magnitudes of the conduction and diffusion terms, as has been noted by Lewis and von Elbe.[15] These terms depend upon their respective transport coefficients. In the special case (the theoreticians' favorite) that all the binary diffusion coefficients are equal to each other and to the thermal diffusivity $\lambda/\rho\bar{c}$ (all Lewis numbers unity), the conduction and diffusion fluxes cancel and the convection flux is constant through the flame. This has been discussed recently by Hirschfelder.[16] In the data of Fig. 9, the convection term shows a small positive maximum, but the present authors attach no general significance to this. The sum of the three fluxes shown as the dotted curve would ideally be constant throughout the flame. The fact that the sum shows a maximum greater than the convection term itself indicates that the sign of the latter is not reliably established in this case.

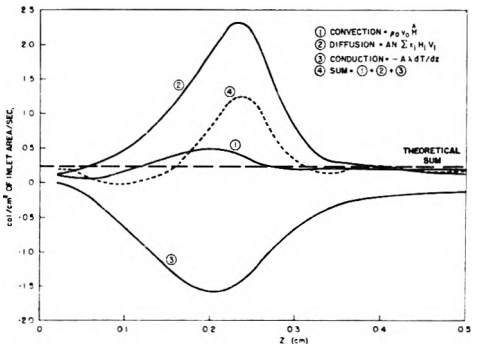

Fig. 9.—Conservation of energy (enthalpy balance) and enthalpy fluxes through flame zone.

With no absolute criterion or prior data to compare, it is difficult to say how good this energy balance result is. It might well be that the neglect of free radicals (which show up as stable products in the sampled gas, of course) is more serious from an energetic point of view than in the material balances. At any rate, the results given in Fig. 9 seem reasonable, and there are no gross violations of energy conservation. As noted in Appendix C, the actual mixture thermal conductivity is probably greater than the pure oxygen value assumed, and this would tend to made the total energy balance somewhat better.

Acknowledgment.—The authors are indebted to Mr. Stanley Favin for performing the numerical computations reported herein.

Appendices

A. Binary Mixture Approximation for Diffusion.—The use of rigorous, multicomponent diffusion coefficients in a mixture even as relatively simple as dealt with here is completely impractical, and (fortunately) not necessary either. For any species i present in small concentration in a mixture, it can be shown[17] that the effective diffusion coefficient of species i is closely approximated by

$$D_{i-mix} \cong \frac{1 - x_i M_i/\bar{M}}{\sum_{j \neq i} x_j/D_{ij}} \qquad (A1)$$

This relation has been verified experimentally.[18,19] If, in addition, one species k is present in such excess that all the other components may be regarded as traces, then the above simplifies still further to

$$D_{i-mix} = D_i \cong D_{ik} \qquad (A2)$$

which is the approximation used in eq. 4. This is certainly justified. In the flame considered here, in no case did the diffusion coefficient D_{i-O_2} differ from the D_{i-mix} calculated from eq. A1 by more than 3%, which is about the experimental error of the diffusion coefficient measurements.

B. Neglect of Thermal Diffusion.—For any trace component, the expression for the diffusion

(11) J. Hilsenrath, *et al.*, "Tables of Thermal Properties of Gases," NBS Circular 564, 1955.

(12) F. D. Rossini, *et al.*, "Selected Values of Physical and Thermodynamic Properties of Hydrocarbons and Related Compounds," American Petroleum Institute, Carnegie Press, Pittsburgh, 1953.

(13) D. P. Stevenson and J. Y. Beach, *J. Chem. Phys.*, **6**, 25 (1938).

(14) J. O. Hirschfelder, *ibid.*, **26** 274 (1957).

(15) B. Lewis and G. von Elbe, "Combustion, Flames and Explosions of Gases," Academic Press, New York, N. Y., 1951, p. 345.

(16) J. O. Hirschfelder, *Phys. Fluids*, **3**, 109 (1960).

(17) J. O. Hirschfelder and C. F. Curtiss, "Third Symposium on Combustion, Flame and Explosion Phenomena," Williams & Wilkins, Baltimore, Md., 1949, p. 124.

(18) D. Fairbanks and C. R. Wilke, *Ind. Eng. Chem.*, **42**, 471 (1950).

(19) N. deHaas, R. E. Walker and A. A. Westenberg, *J. Chem. Phys.*, **32**, 1314 (1960).

velocity including thermal diffusion may be written[10]

$$V_i \cong -\frac{D_i}{x_i}\left[\frac{dx_i}{dz} \pm \frac{k_T}{T}\frac{dT}{dz}\right] \qquad (B1)$$

where the positive sign holds if the trace i is heavier than the main component, and the negative sign if the trace is lighter. k_T is the thermal diffusion ratio given by

$$k_T \cong \pm D_i^T/NM_iD_i \qquad (B2)$$

D_i^T being the trace thermal diffusion coefficient, and N the total molar density. In most cases, D_i^T itself is positive if the trace is heavier and negative if it is lighter than (in our case) oxygen, so that k_T is generally positive. Therefore, the common situation is for a heavier trace species to thermally diffuse upstream and a lighter species downstream.

The thermal diffusion correction to the diffusion velocity was carried out for the case of H_2O, for which it probably would be as large as for any of the major species. The necessary thermal diffusion data were computed from our concentration diffusion coefficients and viscosities as outlined by Amdur and Mason.[20] At most, the thermal diffusion contribution to V_{H_2O} was about 10%. Thus, while the effect is not always as small as one would like, the error caused by its neglect is at worst probably no larger than others, and the simplification this neglect brings to an already complex analysis is most welcome.

C. Pure Oxygen Approximation for Thermal Conductivity.—The use of λ_{O_2} instead of the true mixture thermal conductivity was occasioned primarily (as with the other approximations) by the great simplification it afforded. The actual flame mixture was composed throughout of roughly 80% oxygen, with the remaining 20% mostly lighter components (except for CO_2) which might be expected to increase the thermal conductivity over that of pure oxygen. To get some idea of the error introduced here, an approximate calculation[21] was made of λ for a mixture composed of 85% oxygen and 15% water at 1500°K. This gave a value about 15% higher than the pure oxygen value. Such an increase in λ would improve the enthalpy balance of Fig. 9 somewhat.

(20) I. Amdur and E. A. Mason, *Phys. Fluids*, **1**, 370 (1958).
(21) R. S. Brokaw, *J. Chem. Phys.*, **29**, 391 (1958).

METAL COMPLEXING BY PHOSPHORUS COMPOUNDS. I. THE THERMODYNAMICS OF ASSOCIATION OF LINEAR POLYPHOSPHATES WITH CALCIUM[1]

BY R. R. IRANI AND C. F. CALLIS

Research Department, Inorganic Chemicals Division, Monsanto Chemical Company, St. Louis 66, Missouri

Received February 19, 1960

The stabilities of calcium complexes of the linear chain phosphates have been evaluated, from nephelometric titrations in the presence of an added precipitating agent, as a function of *p*H, temperature, ionic strength and length of the phosphate chain. At high *p*H values the number of phosphorus atoms that are in equilibrium with one calcium ion was evaluated and found to be 2, 3, 4, 4 and 5 for linear phosphates with average chain lengths of 2, 3, 6, 14 and 60, respectively. The free energy change at 25° accompanying the association of calcium with $P_2O_7^{-4}$, $HP_2O_7^{-3}$, $P_3O_{10}^{-5}$, $HP_3O_{10}^{-4}$ and $H_2P_3O_{10}^{-3}$ was found to be −7.6, −4.9, −9.5, −5.3 and −5.3 kcal., respectively. For the longer chain phosphates the corresponding free energy changes were found to be −10.2 ± 0.2 kcal. and independent of chain length. For $CaP_3O_{10}^{-3}$ and $CaP_2O_7^{-2}$ the enthalpies of association were found to be −3.2 and 4.6 kcal., respectively, whereas for the long chain phosphates the values were negligibly small. A large positive entropy change (21–46 e.u.) was found to accompany association in all cases. This positive entropy change is attributed to the release of waters of hydration upon association. The free energy, enthalpy and entropy of formation of aqueous pyrophosphate and tripolyphosphate anions are evaluated from published data.

Introduction

The ability of the polyphosphates to form soluble complexes with calcium ions has been known for about a century. Several investigators have reported evaluation of complexity constants. However, as indicated by Watters, *et al.*,[2] most of the evaluations were carried out in the presence of alkali metal ions that are well known to form complexes of their own with the polyphosphates.[3] A review[4] on this subject appeared as recently as 1958.

The purpose of this study is fourfold, namely (1) to check and extend by an independent method the results of Watters, *et al.*,[2] and thereby test the validity of both methods; (2) to investigate the effects of *p*H, total ionic strength and temperature on the stability constants in order to evaluate the thermodynamic formation constants and the related free energies, enthalpies and entropies of complex formation; (3) to investigate the effect of the chain length of the polyphosphates on the stability of their calcium complexes; and (4) to use the resulting thermodynamic quantities to test recent proposed theories[5–7] on entropy changes accompanying association reactions in solution.

(1) Presented before the Division of Inorganic Chemistry, 137th meeting of the American Chemical Society, Cleveland, Ohio, April, 1960.
(2) J. I. Watters and S. M. Lambert, *J. Am. Chem. Soc.*, **81**, 3201 (1959).
(3) U. P. Strauss and P. D. Ross, *ibid.*, **81**, 5295 (1959).
(4) J. R. Van Wazer and C. F. Callis, *Chem. Revs.*, **58**, 1011 (1958).
(5) E. L. King, *J. Chem. Educ.*, **30**, 71 (1953).
(6) J. W. Cobble, *J. Chem. Phys.*, **21**, 1446 (1353).
(7) W. J. Hamer, "The Structure of Electrolytic Solutions," John Wiley and Sons, Inc., New York, N. Y., 1959, Chapter 24 by J. M. Austin, R. A. Matheson and H. N. Parton.

Experimental

Chemicals.—Sodium tripolyphosphate hexahydrate was used as the source of tripolyphosphate ions. It was prepared by four repeated fractional crystallizations of commercial tripolyphosphate from aqueous solutions of ethyl alcohol. The final sample showed analysis to better than 99.7% $Na_5P_3O_{10}$, exhibiting the proper Na_2O/P_2O_5 ratio.[8,9] Mallinckrodt analytical reagent grade tetrasodium pyrophosphate decahydrate was used as the source of pyrophosphate anions and gave analysis to better than 99.5% $Na_4P_2O_7$, exhibiting the proper Na_2O/P_2O_5 ratio.[9] The three anhydrous long chain sodium polyphosphates that were investigated were randomly reorganized products, identified only by their Na_2O/P_2O_5 ratios.[10] The molar Na_2O/P_2O_5 ratios were found to be[11] 1.34, 1.15 and 1.033, indicating a distribution of chain lengths having an average[10] of 6, 14 and 60 phosphorus atoms per molecule, respectively.

Reagent grades of tetramethylammonium and tetraethylammonium bromides, chlorides and hydroxides were purchased from Eastman Kodak Co.

All the tetramethylammonium polyphosphates were prepared by ion exchanging the sodium salts with the hydrogen form of 100–200 mesh Dowex 50W-X2 and neutralizing the resulting acids immediately with tetramethylammonium hydroxide, as previously described.[12] The stock solutions were maintained at 25° and a *p*H of 12 to avoid hydrolytic degradation. The final phosphorus content of the stock solutions was checked[13] against the make-up concentrations and these values agreed within experimental error. The different stock solutions were found to contain 0.015–0.023 mole of phosphorus per 100 ml.

The tetramethylammonium iodate was prepared by neutralizing Fisher reagent grade iodic acid with tetramethylammonium hydroxide. The other chemicals were C.P. grade.

Equipment.—The nephelometric titrations were performed by recording the light transmittance of a solution containing the polyphosphate and precipitating anion as the calcium titrant was added in increments to an unstirred solution, followed by agitation. This cycle was repeated until the end-point was passed, as evidenced by persistence of a precipitate.

The housing and sensing elements of a Sargent–Malmstadt photometric titrator[14] were the basic elements in the set-up. The voltage output of the photoelectric cell was stepped down through a 0.5 megohm helipot and fed into a 0–100 MV Brown recorder with a 1 sec. response. The chart speed was usually 1 in./min. A 25-ml. automatic buret was fastened over the titrator and the input of a solenoid valve that regulates flow of titrant was hooked into one of the leads of a Flex-Pulse relay-timer, manufactured by Eagle Signal Corp., Moline, Ill. The other lead of the relay-timer was attached to the input of a 2000 r.p.m. stirring motor. The stirring cycle of the timer was 2 min., whereas the addition-of-titrant (Ca^{++} solution in this case) cycle varied from experiment to experiment, but ranged from 2–10 seconds. Capillary delivery tips of various diameters were inserted between the buret and the photometric titrator to further control the rate of titrant delivery. After repeated experimentation it was found that single titrant shots that were delivered by the above described process (0.15–0.9 cc.) did not vary by more than 0.02 cc., provided only the top 7 cc. of the buret was used, and this maximum volume never was exceeded. When more than 7 cc. was required, the titration was stopped and the buret refilled.

Procedure.—Aliquot volumes of the polyphosphate stock solution and the calcium-precipitating anion solution (either oxalic acid or tetramethylammonium iodate) were pipetted into a 400-ml. beaker, containing 150 ml. of distilled water.

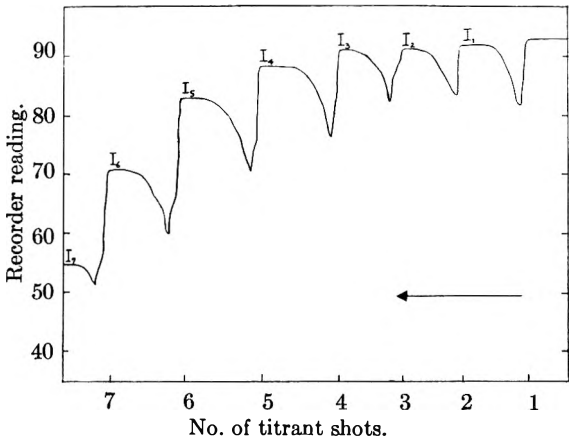

Fig. 1.—Typical recorder chart during nephelometric titration.

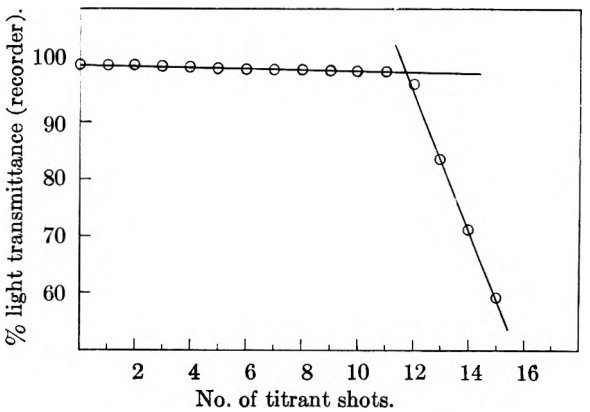

Fig. 2.—Typical determination of end-point.

The *p*H of the solution was adjusted to the desired value through the addition of either HCl or aqueous tetramethylammonium hydroxide. Additional water was put in so that the total solution volume was 250 cc. An appropriate weight of tetramethylammonium bromide[15] then was dissolved to give the desired ionic strength, namely, 0.1, 0.5 or 1.0. The *p*H was again checked at this point and was never found to have changed. It was assumed that the added tetramethylammonium bromide was completely ionized, and since only a small fraction of the ionic strength was due to the other cations and anions, the assumption of total ionization of the other salts is not important.

The beaker containing the solution then was placed in the titrator and the recorder and relay-timer switches were initiated. The shots of titrant solution were added periodically when the stirrer was off, causing high localized calcium ion concentrations that precipitated CaC_2O_4. If more than 2 min. of stirring were required for equilibration, smaller titrant shots were used. When the stirring cycles started, the precipitate dissolved in the excess polyphosphate. The cycles were automatically repeated until permanent and noticeable turbidity resulted which did not disappear upon more stirring. The total titrant volume and the number of shots then were read, and the volume per shot noted.

Meanwhile, the *p*H of the solution was controlled by periodic additions of tetramethylammonium hydroxide; this was not necessary for polyphosphate solutions with a *p*H over 10.5 due to buffering. The molarity of the calcium nitrate solutions was either 4.43×10^{-2} or 8.86×10^{-2} (from the solution make-up with $Ca(NO_3)_2 \cdot 4H_2O$) and checked to within 0.1% with disodium ethylenediaminetetraacetate titrations at a *p*H of 13 in the presence of calcon indica-

(8) O. Quimby, THIS JOURNAL, **58**, 603 (1954).

(9) J. R. Van Wazer, "Phosphorus and Its Compounds," Vol. I, Interscience Publ. Co., New York, N. Y., 1958.

(10) Ref. 9, Chapter 12.

(11) Kindly determined by Mr. A. B. Finley of Monsanto's Columbia, Tennessee plant.

(12) J. R. Van Wazer, E. J. Griffith and J. F. McCullough, *J. Am. Chem. Soc.*, **77**, 287 (1955).

(13) J. R. Van Wazer, E. J. Griffith and J. F. McCullough, *Anal. Chem.*, **26**, 1755 (1954).

(14) E. H. Sargent Co., Chicago, "Scientific Methods," Vol. 10, No. 2, Sect. 1, 1958.

(15) When tetramethylammonium chloride was used instead of the bromide, the same results were obtained, but the system came to equilibrium more slowly. Therefore, the bromide was used exclusively in all the experiments described here.

tor.[16] A fresh calcium solution was prepared every week, during which period no evidence of carbonate contamination was found.

Figure 1 is a reproduction of a typical recorder chart containing the continuous record of changes in the light intensity of 550 mμ filtered light across the beaker during a titration. The transmitted light intensities at the end of each cycle, the I_i values in Fig. 1, were plotted *vs.* the number of shots. Usually two intersecting lines resulted as illustrated in Fig. 2. The point of intersection of these two lines was taken as the point of incipient precipitation. The product of the number of shots at that point times the volume/shot is the total volume of calcium solution that can be held by the polyphosphates prior to calcium precipitation under the specific conditions.

To prove that the above described procedure did give equilibrium values, the equilibrium was approached many times from both sides. First, six to seven solutions with controlled alkaline *p*H values having various amounts of calcium but the same amounts of polyphosphate and precipitating anion were prepared and stirred with a magnetic stirrer for 1-2 weeks. In this time period no hydrolytic degradation is expected.[12] The end-point was then determined from light intensity measurements. Some mixtures originally clear became turbid with time. This supersaturation[17] is a serious source of error if sufficient equilibration time is not allowed and this probably accounts for some of the discrepancies found in the literature.

In the second procedure, excess calcium was added to form a precipitate. Various amounts of polyphosphate then were added and the solutions were stirred for one week. The end-point was again noted from light intensity measurements. In both procedures the results agreed within experimental error (0.2 cc.) with those from the rapid semi-automatic titration method developed and used in this work.

Since the semi-automatic titrations were performed in an airconditioned laboratory (25°) where temperature fluctuations are less than ±0.2° for an experiment duration, no special temperature control was used for the 25° runs. For the 37 and 50° experiments, the temperature was controlled to within ±0.2° by heating the solutions 2-3 times during titration. The repeatability of the results was not different at the three temperatures, and was found to be ±0.1 cc.

Precipitates and Solubility Products

The unwashed precipitates formed at the end of the nephelometric calcium titrations of oxalate–polyphosphate solutions were unequivocally proven to be $CaC_2O_4 \cdot H_2O$ from (1) X-ray measurements that showed an identical diffraction pattern to C.P. $CaC_2O_4 \cdot H_2O$, (2) wet chemical analyses for CaO[11] and oxalate, and (3) the fact that the P_2O_5 contents of the unwashed precipitates were less than 2% in all cases, the order of magnitude for adsorption. Washing the precipitate twice brought the P_2O_5 content down to 0.1-0.2%, while the CaO/oxalate ratio did not change.

The solubility product of CaC_2O_4 at the desired conditions was evaluated as follows. Half a gram of freshly prepared $CaC_2O_4 \cdot H_2O$ was shaken mechanically for several days at the desired temperature with 500 ml. of aqueous solutions made up to ionic strengths of 0.1 or 1.0 using tetramethylammonium hydroxide. The resulting saturated solutions were titrated with a 0.1 *N* $KMnO_4$ solution standardized with predried $Na_2C_2O_4$.

The solubility product of CaC_2O_4 at 25° was found to be 1.32×10^{-8} at 0.1 ionic strength; literature values at the same temperature and ionic strength are 1.26×10^{-8} and 1.96×10^{-8} in aqueous solutions of NaCl[18] and NH_4Cl,[19] respectively. The value at unit ionic strength and 25° was measured to be 7.80×10^{-8}, in good agreement with literature values of 7.39×10^{-8} and 8.75×10^{-8} in aqueous solutions of NaCl[18] and NH_4NO_3,[19] respectively. Similarly, the solubility product of CaC_2O_4 at 37° was measured and found to be 2.43×10^{-8} and 1.29×10^{-7} at ionic strengths of 0.1 and 1.0, respectively. At 50°, it was found to be 4.32×10^{-8} and 2.45×10^{-7} at ionic strengths of 0.1 and 1.0, respectively. Our data agreed well with those available in the literature[20] when compared under the same conditions. The plot of log solubility *vs.* $1/T$ gave straight lines at the different ionic strengths, and the lines were parallel.

From our measurements described above and from those of others at 37°[20] and different *p*H values, it is concluded that the solubility product of $CaC_2O_4 \cdot H_2O$ does not change with *p*H in the neutral or alkaline region. Also, changes in the solubility product of CaC_2O_4 due to the addition of foreign ions other than Ca^{++} or $C_2O_4^{=}$ are only dependent upon changes in the total ionic strength.

Equilibria and Treatment of Data

General.—The polyphosphates can be considered to be typical polyelectrolytes[21] consisting of a chain of alternate phosphorus and oxygen atoms that are held together by predominantly covalent bonding. Evidence for more than just simple electrostatic attraction holding the polyphosphate anions close to the "complexed" cations has been advanced and, hence, the sequestration data will be interpreted along the lines of "specific site binding."[22]

In general, the association reaction between a cation and a polyphosphate anion can be represented by equation (1), omitting the charges on the ions

$$M \cdot (H_2O)_a + P \cdot S(\theta) \cdot (H_2O)_b = M[S(\theta)]_P \cdot (H_2O)_c + (a + b - c)H_2O \quad (1)$$

where a, b and c are hydration numbers, θ is the number of phosphorus atoms per site, S, and P is the number of sites occupied by one cation. S may or may not have one or more hydrogens attached. The idea that linear polyelectrolytes are composed of individually independent sites has been suggested by Flory,[23] who envisioned the sites or segments as having elastic membranes separating them. The numerical values of P, b, c and θ presumably are dependent upon the chain length and hydrogen form of the polyphosphate, and may have different values for the same chain length molecule, being distributed around a certain mean value.

For each specific binding phenomenon, we may define a binding constant[3]

$$\beta_{M[S(\theta)]P} = \frac{[M]\,[S(\theta)]^P}{[M]\,[S(\theta)]_P} \quad (2)$$

In the special case of nephelometric titrations, if an end-point is chosen so that crystalline CaB_d just starts precipitating, then in addition to equation 2

$$K_{sp} = [Ca^{++}][B^{-2/d}]^d \quad (3)$$

where K_{sp} is the solubility product of CaB_d, and d can have the values of either one (divalent precipitating anion) or two (monovalent precipitating anion).

Pyrophosphate or Tripolyphosphate.—For the well-defined pyrophosphate or tripolyphosphate anions, not more than two hydrogen forms are needed to fit acid–base titration data. Therefore,

(16) C. A. Goetz and R. C. Smith, *Iowa State J. Sci.*, **34**, No. 1, 81 (1959).

(17) C. L. Mehltretter, B. H. Alexander and C. E. Rist, *Ind. Eng. Chem.*, **45**, 2782 (1953).

(18) W. H. McComas and W. Rieman, *J. Am. Chem. Soc.*, **64**, 2946 (1942).

(19) H. Shchyn and D. B. Pall, THIS JOURNAL, **44**, 166 (1940).

(20) W. F. Linke, "Solubilities," D. Van Nostrand Co., Inc., New York, N. Y., 1958, 4th Ed., Vol. I.

(21) C. F. Callis, J. R. Van Wazer and P. G. Arvan, *Chem. Revs.*, **54**, 777 (1954).

(22) U. P. Strauss, D. Woodside and P. Wineman, THIS JOURNAL, **61**, 1353 (1957).

(23) P. J. Flory, "Principles of Polymer Chemistry," Cornell University Press, Ithaca, N. Y., 1953, p. 630.

at any pH, three equations are sufficient to define the calcium–hydrogen–phosphate interaction, in the absence of other phosphate-complexing cations

$$\beta_{Ca[S(\theta)]^P} = \frac{[Ca^{++}][S(\theta)]^P}{\{Ca[S(\theta)]_P\}} \quad (4)$$

$$\beta_{Ca[HS_h(\theta)]^{P_h}} = \frac{[Ca^{++}][HS_h(\theta)]^{P_h}}{\{Ca[HS_h(\theta)]_{P_h}\}} \quad (4a)$$

$$\beta_{HS_h(\theta)} = \frac{[H^+][S(\theta)]}{[HS_h(\theta)]} \quad (5)$$

where the subscript h designates a site containing an additional hydrogen.

Average values of each of the parameters θ, P, P_h were computed from the experimental data as follows: Arbitrary values of P were first assigned, and then *ca.* 10 values of θ were computed by equating pairs of the expression for the apparent dissociation constant, each from a different experimental measurement. The best fit for various combinations of P and θ was judged from the constancy of the dissociation constant for the entire set of experiments.

As shown in the Results and Discussion section, the best fit to the experimental data for either pyrophosphate or tripolyphosphate was found for

$$S(\theta) = S_h(\theta) \quad (6)$$

$$P = P_h = 1 \quad (7)$$

Including the restrictions in equations 6 and 7, the material balances for calcium and phosphorus at the point of incipient precipitation are

$$\frac{yz}{A} = [Ca^{++}] + [CaS(\theta)] + [CaHS(\theta)] \quad (8)$$

$$\frac{10L}{\theta} = [S(\theta)] + [HS(\theta)] + [(CaS(\theta)] + [CaHS(\theta)] \quad (9)$$

where $10L/\theta$ is the molarity of sites, A the total volume of the solution in cc., and y is the number of cc. of a calcium solution of z molarity. The initial concentration of phosphates is L moles of *phosphorus* per 100 ml., and the concentration of the "B salt" (*e.g.*, tetramethylammonium oxalate) is s g./100 ml. In addition, the solubility product K_{sp} is related to the free calcium ion concentration and the molecular weight of the "B salt," M_s, by the expression

$$Ca^{++} = K_{sp}\left(\frac{M_s}{10s}\right)^d \quad (10)$$

where d is the same integer in equation 3.

The $[Ca^{++}]$ term in equation 8 is negligible compared to the other two terms, as will be seen from the magnitudes of $\beta_{CaS(\theta)}$ and $\beta_{CaHS(\theta)}$. If equations 5, 8 and 9 are combined then

$$[S(\theta)] = \frac{\left[\frac{10L}{\theta} - \frac{yz}{A}\right]}{[1 + (H^+)/\beta_{HS(\theta)}]} \quad (11)$$

and

$$[HS(\theta)] = \frac{\left[\frac{10L}{\theta} - \frac{yz}{A}\right]}{[1 + \beta_{HS(\theta)/(H^+)}]} \quad (12)$$

From equations 3, 4, 4a, 10, 11 and 12

$$[CaS(\theta)] = \left(\frac{M_s}{10s}\right)^d \frac{K_{sp}}{\beta_{CaS(\theta)}} \frac{\left[\frac{10L}{\theta} - \frac{yz}{A}\right]}{[1 + (H^+)/\beta_{HS(\theta)}]} \quad (13)$$

$$[CaHS(\theta)] = \left(\frac{M_s}{10s}\right)^d \frac{K_{sp}}{\beta_{CaHS(\theta)}} \frac{\left[\frac{10L}{\theta} - \frac{yz}{A}\right]}{[1 + \beta_{HS(\theta)/(H^+)}]} \quad (14)$$

and from equations 8, 13 and 14

$$\frac{10LA}{\theta yz} - 1 = \frac{\left(\frac{10s}{M_s}\right)^d}{K_{sp}\left\{\frac{1}{\beta_{CaS(\theta)}[1 + (H^+)/\beta_{HS(\theta)}]} + \frac{1}{\beta_{CaHS(\theta)}[1 + \beta_{HS(\theta)/(H^+)}]}\right\}} \quad (15)$$

If θ, K_{sp} and $\beta_{HS(\theta)}$ are known, then plots of the left-hand side of equation 15 *vs.* s^d at suitable pH values should give a straight line whose slope can be used to compute both $\beta_{CaS(\theta)}$ and $\beta_{CaHS(\theta)}$. When $\beta_{CaHS(\theta)} >> \beta_{CaS(\theta)}$, and the pH is such that $(H^+)/\beta_{HS(\theta)} << 1$, *e.g.*, $P_2O_7^{-4}$ at pH 12, then equation 15 becomes

$$\left(\frac{10LA}{\theta yz} - 1\right) = \frac{\left(\frac{10s}{M_s}\right)^d \beta_{CaS(\theta)}}{K_{sp}} \quad (16)$$

Mixture of Ligands.—It was shown above for tripolyphosphate or pyrophosphate that the best fit is obtained for the combination of one site occupied by the calcium. In a system of several noninteracting ligands and their hydrogen forms that bind calcium, the general expression of equation 15 is

$$y = \frac{10AK_{sp}}{z}\sum_{i=1}^{i=g}\frac{L_i\psi_i}{\theta_i\left[\left(\frac{10s}{M_s}\right)^d + K_{sp}\psi_i\right]} \quad (17)$$

L_i is the general value of L, g is the number of ligands present, and $S(\theta_i)$ is the site for any ligand, with θ_i being the average number of phosphorus atoms per calcium for that specific ligand. Also

$$\psi_i = \frac{1}{\beta_{CaS(\theta i)}[1 + (H^+)/\beta_{HS(\theta i)}]} + \frac{1}{\beta_{CaS(\theta i)}[1 + \beta_{HS(\theta i)/(H^+)}]} \quad (18)$$

Again if $\beta_{CaHS(\theta i)} >> \beta_{CaS(\theta i)}$, and $(H^+)/\beta_{HS(\theta i)} << 1$, then ψ_i becomes $1/\beta_{CaS(\theta i)}$, and the generalized version of equation 16 results

$$y = \frac{10AK_{sp}}{z}\sum_{i=1}^{i=g}\frac{L_i}{\theta_i\left[K_{sp} + \left(\frac{10s}{M_s}\right)^d \beta_{CaS(\theta i)}\right]} \quad (19)$$

Randomly reorganized linear polyphosphates[24] with $M_2O/P_2O_5 < 1.5$ are mixtures of higher homologs of pyrophosphate and tripolyphosphate. The interpretation of nephelometric data on the linear polyphosphates should therefore utilize equations 17 and 19. However, the value of θ_i for every single ligand cannot be evaluated. Therefore, it will be assumed that for any specific M_2O/P_2O_5 ratio in the longer-chain polyphosphate region, phosphorus atoms are equivalent in complexing calcium regardless of their position in the chain, or the size of the chain they belong to. With these necessary assumptions at this time, equation 16 becomes applicable. Obviously, if tetrapolyphosphate, pentapolyphosphate and the higher homologs

(24) J. R. Parks and J. R. Van Wazer, *J. Am. Chem. Soc.*, **79**, 4890 (1957).

TABLE I

SUMMARY OF DATA FOR THE Ca^{++}-H^{+}-$C_2O_4^{-}$-POLYPHOSPHATE SYSTEMS[a,b]

Temp., °C.	pH	Ionic strength	Moles of phosphorus per 100 ml. (L) × 10^4	Molarity of Ca soln. (z) × 10^2	Cc. of Ca soln. (y) to end-point for the following wt. % concn. (s) of ppt. agent 0.1	0.2	0.3	0.4	0.5
Phosphate with 2 phosphorus atoms per chain (pyrophosphate)									
25	12.0	0.1	4.98	8.86	2.30	1.27	0.93	0.69	..
		1.0	5.83	8.86	3.90	2.57	1.82	1.58	1.38
	8.0	0.1	5.81	4.43	0.40	0.22	..	..	..
		1.0	5.81	4.43	1.20	0.70	..	..	..
37	12.0	0.1	5.82	8.86	4.30	2.70	1.88	..	..
		1.0	5.82	8.86	3.30	2.34	1.62	..	..
50	12.0	0.1	5.82	8.86	4.92	..	2.99	..	..
		1.0	5.82	8.86	3.06	..	1.72	..	..
Phosphate with 3 phosphorus atoms per chain (tripolyphosphate)									
25	12.0	0.1	5.20	8.86	4.01	3.39	2.99	..	..
		1.0	5.20	8.86	3.35	2.67	2.14	1.85	1.64
	10.5	1.0	5.20	8.86	3.32	2.68	2.22	1.93	1.69
	9.0	1.0	5.20	8.86	3.06	..	..	..	..
	8.0	1.0	5.20	8.86	1.31	..	..	..	..
	7.5	0.1	7.15	4.43	2.54	1.46	0.99	..	..
		1.0	7.15	4.43	2.10	1.12	0.75	..	..
37	12.0	0.1	6.58	8.86	5.44	..	4.30	..	..
		1.0	6.58	8.86	4.55	..	3.20	..	..
50	12.0	0.1	6.58	8.86	5.73	..	4.82	..	..
		1.0	6.58	8.86	4.95	..	4.26	..	..
Phosphate with an av. of 6 phosphorus atoms per chain									
25	12.0	0.1	14.2	8.86	..	8.40	..	..	..
			7.1	8.86	..	4.30	..	..	..
		1.0	7.1	8.86	4.37	3.68	3.40	..	2.98
	7.0	0.1	7.1	8.86	3.18	2.87	2.76	..	..
		1.0	7.1	8.86	3.26	2.48	2.32	..	..
37	12.0	0.1	7.1	8.86	..	..	4.17	..	3.89
		1.0	7.1	8.86	..	..	3.89	..	3.25
50	12.0	0.1	7.1	8.86	..	..	4.72	..	4.34
		1.0	7.1	8.86	..	..	4.19	..	3.92
	7.0	0.1	7.1	8.86	..	..	2.73	..	2.43
		1.0	7.1	8.86	..	..	2.32	..	1.86
Phosphate with an av. of 14 phosphorus atoms per chain									
25	12.0	0.1	15.0	8.86	12.40	8.82	8.00	..	7.22
			7.6	8.86	5.95	4.34	4.21	3.98	3.78
		1.0	7.5	8.86	..	3.94	3.70	3.60	..
	7.0	0.1	7.5	8.86	..	3.88	3.68	..	..
		1.0	7.5	8.86	..	3.07	2.80	..	..
50	12.0	0.1	7.5	8.86	..	..	4.86	..	4.35
		1.0	7.5	8.86	..	..	4.25	..	3.95
Phosphate with an av. of 60 phosphorus atoms per chain									
25	12.0	0.1	8.8	8.86	..	4.47	4.32	..	..
		1.0	8.8	8.86	..	3.70	3.56	..	..
	7.0	0.1	8.8	8.86	..	4.12	4.01	..	..
		1.0	8.8	8.86	3.68	3.31	3.15	..	..
50	12.0	0.1	8.8	8.86	..	..	4.80	..	4.62
		1.0	8.8	8.86	..	..	4.31	..	4.15

[a] The total volume of solution (A) was always 250 cc., M_s = 134, d = 1. [b] The symbols have the same significance as in the text.

could be isolated and studied, then mixtures would be interpretable with equation 17.

Evaluation of θ.—In the series of experiments that were performed in this work, K_{sp} and $\beta_{HS(\theta)}$ were known, so that from the brief discussion following equation 15, it is clear that the knowledge of the value of θ is imperative if evaluation of the dissociation constants is desired. If one works at a fixed pH, temperature and ionic strength, then it is obvious from equation 15 that

$$\left(\frac{10LA}{\theta yz} - 1\right)/s^d$$

should be invariant. Therefore, by varying L, z and s, and solving the resultant simultaneous equations for θ, the number of phosphorus atoms per one calcium can be computed. As will be shown in the following section, the solution of up to 30 of these simultaneous equations gave values of θ that varied in any given system from ±0.2–0.6. This constancy is a proof of the internal consistency of the data.

In the treatment shown above we cannot ascertain whether a polymer of the $CaS(\theta)$ complex, *i.e.*, $[CaS(\theta)]_x$, was formed or not. Therefore, the calculated dissociation and related constants will only apply for the monomer formation, with similar values for possible polymers easily derivable from them.

Results and Discussion

The raw data for all of the phosphates are summarized in Table I. All the errors that are shown as (±) throughout this paper are the statistical 95% confidence limits.

Number of Sites Occupied by One Calcium (θ). Table II shows the data fitting which led to the conclusion that the best combination of P and θ is obtained for P equal to one. Obviously, a different choice of P gives wider variations in the calculated binding constants. Also, negative values of θ are meaningless. Therefore, in all of the computations discussed below, the number of sites occupied by one calcium will be taken as equal to one.

TABLE II

SITES OCCUPIED BY ONE CALCIUM

Phosphate	No. of sites per Ca (P)	Calcd. no. of phosphorus atoms per site (θ) Range	Average
Pyrophosphate	1	1.7 to 2.2	2.0
($P_2O_7^{-4}$)	2	−29 to + 5	..
	3	0 to ∞	..
Tripolyphosphate	1	2.7 to 3.3	3.1
($P_3O_{10}^{-5}$)	2	−7 to 0	..
	3	−5 to ∞	..

The Ca^{++}–H^+–$P_2O_7^{-4}$ System.—The data summarized in Table I offer some 25 sets of two simultaneous equations each, that were used to evaluate θ. The best value of θ was found to be two, indicating a (1:1) complex between Ca^{++} and either $P_2O_7^{-4}$ or $HP_2O_7^{-3}$. With this in mind and realizing that only one ionic species of the pyrophosphate anion exists at a pH 12, namely, $P_2O_7^{-4}$, equation 16 was utilized in conjunction with the data in Table I to obtain the dissociation constant of $CaP_2O_7^{-2}$ at 25, 37 and 50°, and ionic strengths of 0.1 and 1.0. The results are given in Table III.

The data in Table I at 25° and a pH of 8 were then utilized to evaluate the dissociation constant of $CaHP_2O_7^{-1}$ using equation 15 and the already evaluated dissociation constants of $CaP_2O_7^{-2}$ at the same temperature and ionic strength. The results are also given in Table III. From examining equation 15, it is obvious that $\beta_{HP_2O_7^{-3}}$ must be known before such computations could be carried out. At 25° and a unit ionic strength, the value of $p\beta_{HP_2O_7^{-3}}$ of 8.93, reported by Lambert and Watters,[25] was used. At 25° and ionic strength of 0.1, the value for $p\beta_{HP_2O_7^{-3}}$ of 9.26 was used; this was obtained by interpolating between the values at unit ionic strength (8.93) and infinite dilution (9.42).[2,26]

TABLE III

THE DISSOCIATION CONSTANTS OF $CaP_2O_7^{-2}$ AND $CaHP_2O_7^{-1}$

Complex	t, °C.	Ionic strength	Negative logarithm of dissociation constant This work	Ref. 2
$CaP_2O_7^{-2}$	25	0.1	5.39 ± 0.10	.....
		1.0	4.89 ± .10	4.95 ± 0.2
		2.0	.....	4.79 ± .3
	37	0.1	5.44 ± .11	.....
		1.0	4.63 ± .08	.....
	50	0.1	5.39 ± .10	.....
		1.0	4.31 ± .11	.....
$CaHP_2O_7^{-1}$	25	0.1	3.32 ± .2	.....
		1.0	2.22 ± .2	2.30 ± .2
		2.0	.....	2.40 ± .3

The calculated dissociation constants in Table III for $\beta_{CaP_2O_7^{-2}}$ and $\beta_{CaHP_2O_7^{-1}}$ agree very well with previously published values.[2] These constants also were used together with equation 15 to check several experiments at 25° and pH values between 8 and 11. The experimental results agreed well with the calculated ones.

The evaluation of $\beta_{CaHP_2O_7^{-1}}$ at temperatures higher than 25° was not possible because the value of $\beta_{HP_2O_7^{-3}}$ at these temperatures has not been determined yet. The experimental conditions in our nephelometric titrations were unfavorable for evaluating the dissociation constant of $CaH_2P_2O_7$.

The thermodynamic dissociation constants of $CaP_2O_7^{-2}$ at 25, 37 and 50° and of $CaHP_2O_7^{-1}$ at 25° are shown in Table VII and were evaluated by extrapolating the *apparent* dissociation constants at ionic strengths of 0.1, 1.0 and 2.0 to infinite dilution,[27] with the plot of $p\beta$ *vs.* the square root of the ionic strength giving a straight line.

The Ca^{++}–H^+–$P_3O_{10}^{-5}$ System.—The data given in Table I for tripolyphosphate were treated in exactly the same manner as the data for the Ca^{++}–H^+–$P_2O_7^{-4}$ system. It was found that $\theta = 3$, indicating (1:1) complex between Ca^{++} and either $P_3O_{10}^{-5}$ or $HP_3O_{10}^{-4}$. The apparent dissociation constants are shown in Table IV and the corresponding extrapolated thermodynamic constants in Table VII. In the calculations, the values for $\beta_{HP_3O_{10}^{-4}}$ at 25° and ionic strengths of 0.1 and 1.0 were taken at 1.86×10^{-9} and 1.55×10^{-9}, respectively.[28]

The data for tripolyphosphate in Table I at 25° and unit ionic strength are a proof that hydroxyl ions are absent from the $CaP_3O_{10}^{-3}$ complex since

(25) S. M. Lambert and J. I. Watters, *J. Am. Chem. Soc.*, **79**, 4262 (1957).

(26) H. S. Harned and B. B. Owen, "The Physical Chemistry of Electrolytic Solutions," Reinhold Publ. Corp., New York, N. Y., 1950, 2nd Ed., p. 188.

(27) A. E. Martell and M. Calvin, "Chemistry of the Metal Chelate Compounds," Prentice-Hall, Inc., New York, N. Y., 1952, p. 133.

(28) J. I. Watters, E. Dan Loughran and S. M. Lambert, *J. Am. Chem. Soc.*, **78**, 4855 (1956).

experiments at *p*H values of 10.5 and 12, where only the non-hydrogen bound $P_3O_{10}^{-5}$ exists, gave identical results. At the intermediate *p*H values of 8.0 and 9.0 where mixtures of $P_3O_{10}^{-5}$ and $HP_3O_{10}^{-4}$ co-exist, the calculated volumes of calcium solution to turbid end-point (y) from equation 15 were 1.31 and 3.06 cc., compared with the experimental values of 1.38 and 3.17, respectively, showing excellent consistency. These findings disprove the assumptions made by Wolhoff and Overbeek[29] in a recent article that a $Ca(OH)P_3O_{10}^{-4}$ complex is necessary to fit their data. They also ignored the existence of either $CaHP_3O_{10}^{-2}$ or $NaHP_3O_{10}^{-3}$, so that their computed dissociation constants are unrealistic and do not represent actual equilibria.

TABLE IV

THE DISSOCIATION CONSTANTS OF $CaP_3O_{10}^{-3}$, $CaHP_3O_{10}^{-2}$ AND $CaH_2P_3O_{10}^{-1}$

Complex	t, °C.	Ionic strength	Negative logarithm of dissociation constant: This work	Ref. 2
$CaP_3O_{10}^{-3}$	25	0.1	6.41 ± 0.04	.....
		1.0	5.36 ± .02	5.44 ± 0.2
		2.0	.....	5.29 ± .3
	37	0.1	6.33 ± .02	.....
		1.0	5.25 ± .10	.....
	50	0.1	6.27 ± .02	.....
			5.18 ± .12	.....
$CaHP_3O_{10}^{-2}$	25	0.1	3.78 ± .06	.....
		1.0	3.30 ± .16	3.01 ± .15
		2.0	.....	3.27 ± .3
$CaH_2P_3O_{10}^{-1}$	25	1.0	2.77 ± .4	.....

The stability of the $CaH_2P_3O_{10}^{-1}$ complex at unit ionic strength and 25° was evaluated by nephelometric titration in the presence of iodate as a precipitating anion. Iodate was chosen to be the calcium-precipitating anion because $Ca(IO_3)_2$ is not as insoluble as CaC_2O_4. Therefore, the $H_2P_3O_{10}^{-3}$ anion can compete favorably in tying up Ca^{++}; the use of $C_2O_4^{=}$ would make accurate measurements impossible since only a few drops of Ca^{++} are all that would be required to precipitate CaC_2O_4 in the presence of the relatively weak complexing $H_2P_3O_{10}^{-3}$ anion. At a *p*H of 6 and initial concentrations of HIO_3 of 3.9 and 5.0 wt. %, and moles of phosphorus per 100 ml. of 6.25×10^{-3} and 7.96×10^{-3}, 1.10 and 0.80 cc., respectively, of a 1.0 M calcium solution were required to bring the solution to a point of incipient precipitation. The solubility product of $Ca(IO_3)_2$ was taken as 2.4×10^{-5}, since its solubility in 1.0 M solutions of KCl, NaCl and LiCl is 0.0188, 0.0187 and 0.0172 mole/liter, respectively, at 25°.[20] Although the experiments were run at a *p*H of 6.0, where $HP_3O_{10}^{-4}$ and $H_2P_3O_{10}^{-3}$ co-exist, equation 15 together with the already determined values of $\beta_{CaHP_3O_{10}^{-2}}$ above and for $\beta_{H_2P_3O_{10}^{-3}}$ [28] of 1.48×10^{-6} were combined to give a value for $\beta_{CaH_2P_3O_{10}^{-1}}$ of 1.68×10^{-3} at unit ionic strength and 25°.

Evaluation of $\beta_{CaH_2P_3O_{10}^{-1}}$ at lower ionic strengths was hampered not only by the absence of solubility data for $Ca(IO_3)_2$ but also mainly because up to 0.8 N tetramethylammonium iodate was required to bring about precipitation of $Ca(IO_3)_2$ even when a 1 M calcium solution was employed as the titrant. The thermodynamic dissociation constant for $CaH_2P_3O_{10}^{-1}$ shown in Table VII was estimated by assuming that the negative logarithm of the dissociation constant at infinite dilution was 1.17 units higher than that at unit ionic strength. This 1.17 difference is attributable to the activity coefficient of the calcium ion and is the average of similar extrapolations for $\beta_{CaP_3O_{10}^{-3}}$, $\beta_{CaHP_3O_{10}^{-2}}$ and $\beta_{CaP_2O_7^{-2}}$, all of which did not differ much among one another. It is also significant to note that the stability constants of $CaHP_3O_{10}^{-2}$ and $CaH_2P_3O_{10}^{-1}$ are not significantly different from one another or from $CaHP_2O_7^{-1}$, suggesting that here electrostatic attraction is not the only factor in complex formation.

The Ca^{++}–$P_2O_7^{-4}$–$P_3O_{10}^{-5}$ System.—Since the Ca^{++}–$P_2O_7^{-4}$ and Ca^{++}–$P_3O_{10}^{-5}$ systems have been well defined, it is interesting to check if any interactions or mixed complexing exists between the $P_2O_7^{-4}$ and $P_3O_{10}^{-5}$ anions and Ca^{++}. Table V is a comparison of the experimental values of the volumes of calcium solution at nephelometric end-point with those computed from equation 19 for admixes of $P_2O_7^{-4}$ and $P_3O_{10}^{-5}$. For the conditions and restrictions listed in Table V, equation 19 reduces to

$$y = 9.68 \times 10^2(L_1' - 2.37L_2') \qquad (10)$$

where L_1' and L_2' are the molar concentrations of pyrophosphate and tripolyphosphate, respectively.

TABLE V

THE Ca^{++}–$P_2O_7^{-4}$–$P_3O_{10}^{-5}$–$C_2O_4^{-2}$ SYSTEM[a]

$P_2O_7^{-4}$, M	$P_3O_{10}^{-5}$, M	Cc. of 8.86×10^{-2} M calcium soln. (y) to end-point: Meas.	Calcd.[b]
2.96×10^{-3}	0.00×10^{-3}	3.02	2.87
2.37	.44	3.35	3.31
1.78	.88	3.70	3.74
1.18	1.32	4.08	4.15
0.59	1.77	4.50	4.62
0.00	2.17	4.90	4.95

[a] Conditions: *p*H 12, ionic strength = 0.1, A = 250, M_s = 134, $K_{sp} = 1.32 \times 10^{-8}$, s = 0.1. [b] Equation 20.

The agreement shown in Table V between the measured and calculated volumes confirms our previous assumption that no interaction exists between $P_2O_7^{-4}$ and $P_3O_{10}^{-5}$ in complexing Ca^{++}, and that the values of $\beta_{CaP_3O_{10}^{-3}}$ and $\beta_{CaP_2O_7^{-2}}$ are self-consistent. Examination of these data also show that the pyro content of tripolyphosphate or *vice versa* can be determined with the described experimental procedure with an accuracy of ±6%.

The Ca^{++}–H^+–Long Chain Polyphosphate System.—Table I is also a summary of the experimental results for the calcium complexing by three polyphosphate samples, with average chain lengths of 6, 14 and 60 phosphorus atoms. Even though the data should theoretically be interpretable with equation 19, the value of θ for every single chain length is unknown. Therefore, as previously discussed equation 16 will be used.

(29) J. A. Wolhoff and J. Th. G. Overbeek, *Rec. trav. chim.*, **78**, 757 (1959).

Solution of the appropriate simultaneous equations at *p*H 12 for θ (the average number of phosphorus atoms per site), reveals that for the polyphosphates with average chain lengths of 6, 14 and 60, θ is 4, 4 and 5, respectively. The corresponding values of θ at a *p*H 7 are 6, 4.5 and 5, respectively. Table VI is a tabulation of the calcium polyphosphate dissociation constants, whereas Table VII includes a summary of the corresponding thermodynamic constants. These variable θ values, all of which are larger than those for either pyrophosphate or tripolyphosphate, can be interpreted as follows.

TABLE VI

THE DISSOCIATION CONSTANTS OF CALCIUM POLYPHOSPHATE COMPLEXES

Temp., °C.	*p*H	Phosphorus atoms per site, θ	Neg. log. of dissociation constant at ionic strength of 0.1	1.0
Phosphate with an av. of 6 phosphorus atoms per chain				
25	12.0	4	6.80	5.78
37	12.0	4	6.71	5.72
50	12.0	4	6.76	5.70
25	7.0	6	6.90	6.13
50	7.0	6	6.39	5.29
Phosphate with an av. of 14 phosphorus atoms per chain				
25	12.0	4	6.77	5.80
50	12.0	4	6.67	5.61
25	7.0	4.5	6.75	5.72
Phosphate with an av. of 60 phosphorus atoms per chain				
25	12.0	5	6.99	5.80
50	12.0	5	7.03	5.88
25	7.0	5	6.80	5.55

First, we note that the stabilities of the calcium polyphosphate complexes with 4–6 phosphorus atoms per site are not appreciably greater than those of $CaP_3O_{10}^{-3}$, and neither are their thermodynamic formation constants given in the next section, so that it should not be assumed necessarily that the coördination number of the calcium is 4–6. It is suggested that what probably takes place is this. When the first fraction of calcium ions attach themselves to a polyphosphate chain, random spots are chosen and in between these random positions, there may be one phosphorus atom that by itself cannot complex calcium, or there may be one, two or more phosphorus atoms that are inaccessible to calcium due to steric hindrance caused by the coiling of the chain phosphate.[30] Therefore, it is reasonable to conclude that for very long chain polyphosphates some phosphorus atoms are being wasted at the high *p*H values, and that the most effective calcium complexing agents among the polyphosphates *per phosphorus atom* are the dimer and trimer. This statement does not apply in the neutral or acidic region because of the relatively larger proportion of H^+ which reacts with the ends of the chain (the fraction of phosphorus end groups decreases markedly with chain length).

At the *p*H of 7, for the relatively short polyphosphate chain length of 6, two more phosphorus atoms were required to complex calcium than at *p*H of 12. Interestingly enough, this percentage increase in not far off from the per cent. of end-group phosphorus, which at a *p*H of 7 would have one of their oxygens hydrogen-bound. For the longer polyphosphate chains, where the percentage of end groups is negligible, the number of phosphorus atoms per site was the same at *p*H values of 7 and 12.

The dissociation constant determined by Van Wazer and Campanella[31] for the calcium complex with a linear phosphate containing an average of 5 phosphorus atoms per chain and assuming a coordination number of four is slightly lower than the value determined in this work for a polyphosphate chain with an average of six phosphorus atoms.

The Changes in Thermodynamic Quantities Accompanying Formation of Calcium Polyphosphate Complexes.—Table VII is a compilation of the changes in free energy, enthalpy and entropy accompanying a reaction typified by equation 1 at 25°. These thermodynamic quantities were computed from the constants in Tables III, IV and VI, and the equilibrium relations

$$\Delta F^0 = RT \ln \beta_{CaS(\theta)} \quad (20)$$

$$\Delta H^0 = RT^2 \frac{d \ln \beta_{CaS(\theta)}}{dT} \quad (21)$$

$$\Delta S^0 = \frac{\Delta H^0 - \Delta F^0}{T} \quad (22)$$

where ΔF^0, ΔH^0, and ΔS^0 are the quantities accompanying the association reaction, whereas $\beta_{CaS(\theta)}$ refers to the dissociation reaction.

In association reactions the enthalpy change is related to the difference of the bond energies of the products and reactants, and in the case of reactions occurring in liquid media, due to the difference of solvation energies of the products and reactants.[5] For the long chain polyphosphates these differences in solvation energies are obviously small.

Examination of the typical association reaction shown in equation 1 might lead to the expectation that the entropy change should be negative since the calcium and polyphosphate combine in orderly arrangement. The observed significant increase in entropy, which contributed to the free energy decrease, is common to chelate formation,[32] but in the calcium polyphosphate complexes cannot be attributed to the formation of rings, as was proposed for metal chelates.[32] The entropy increase must be due then to the release of $(a + b - c)$ waters of hydration.

The free energy and entropy changes listed in Table VII are on a molal basis since the standard state for the ions was taken as the hypothetical one molal state while for the water the pure substance was chosen. Since the number of species exclusive of solvent decreased by one, magnitudes of ΔF^0 and ΔS^0 depend upon the concentration scale (standard state). The corresponding absolute values for ΔF^0 and ΔS^0 with the hypothetical mole fraction unity standard state can be computed from the values in Table VII by adding 2.4

(30) Ref. 9, Fig. 8-5.

(31) J. R. Van Wazer and D. A. Campanella, *J. Am. Chem. Soc.*, **72**, 655 (1950).

(32) Ref. 27, p. 150.

TABLE VII

CHANGES IN THERMODYNAMIC MOLAL QUANTITIES FOR CALCIUM POLYPHOSPHATE COMPLEXES

Temp., °C.	pH		Phosphorus atoms per site (θ)	Neg. log. of thermodynamic dissociation constant	$\Delta\bar{F}^0$, kcal.	$\Delta\bar{H}^0$, kcal.	$\Delta\bar{S}^0$, e.u.
		Phosphate with 2 phosphorus atoms per chain (pyrophosphate)					
25	10–12	$CaP_2O_7^{-2}$	2	5.60	− 7.6 + 0.3	4.6 ± 1.4	46 ± 5
37	10–12	$CaP_2O_7^{-2}$	2	5.75	− 8.2	.....	.....
50	10–12	$CaP_2O_7^{-2}$	2	5.86	− 8.7	.....	.....
25	Var.[a] ≃ 7	$CaHPO_2O_7^{-1}$	2	3.6	− 4.9	.....	.....
		Phosphate with 3 phosphorus atoms per chain (tripolyphosphate)					
25	10–12	$CaP_3O_{10}^{-3}$	3	6.90	− 9.5 ± 0.2	−3.2 ± 0.8	21 ± 3
37	10–12	$CaP_3O_{10}^{-3}$	3	6.80	− 9.7	.....	.....
50	10–12	$CaP_3O_{10}^{-3}$	3	6.72	−10.0	.....	.....
25	Var.[a] ≃ 7	$CaHP_3O_{10}^{-2}$	3	3.90	− 5.4	.....	.....
25	Var.[a] ≃ 5	$CaH_2P_3O_{10}^{-1}$	3	3.9	− 5.4	.....	.....
		Phosphate with an av. of 6 phosphorus atoms per chain					
25	10–12		4	7.28	−10.0 ± 0.3	−0.7 ± 3	31 ± 10
37	10–12		4	7.17	−10.2	.....	.....
50	10–12		4	7.24	−10.4	.....	.....
25	7		6	7.25	−10.0	.....	.....
50	7		6	6.90	− 9.5	.....	.....
		Phosphate with an av. of 14 phosphorus atoms per chain					
25	10–12		4	7.23	−10.3 ± 0.3	−1.2 ± 1.7	29 ± 7
50	10–12		4	7.16	−10.6	.....	.....
25	7		4.5	7.27	−10.0	.....	.....
		Phosphate with an av. of 60 phosphorus atoms per chain					
25	10–12		5	7.54	−10.4 ± 0.2	1 ± 3	38 ± 10
50	10–12		5	7.60	−11.2	.....	.....
25	7		5	7.35	−10.1 ± 0.2	.....	.....

[a] In aqueous solutions the free phosphate and hydrogen containing species always coexist in the presence of other ionic species. The *p*H values shown are where the maximum amount of the specified species is expected.

kcal. and subtracting 7.9 e.u., respectively, as was proposed by Adamson[33] and discussed by Williams[34] and King.[35]

The Thermodynamic Formation Constants of $CaP_2O_7^{-2}$ and $CaP_3O_{10}^{-3}$.—To evaluate the free energies, $\Delta\bar{F}^0$, enthalpies, $\Delta\bar{H}^0$, and standard entropies, $\bar{S}^0$, of *formation* for aq. $CaP_2O_7^{-2}$ and $CaP_3O_{10}^{-3}$ from the elements in their standard state, the knowledge of the same quantities for aq. $P_2O_7^{-4}$ and $P_3O_{10}^{-5}$ is imperative. For aq. $P_2O_7^{-4}$, consider the aqueous reaction

$$2H^+ + 2PO_4^{-3} \rightleftharpoons P_2O_7^{-4} + H_2O \qquad (23)$$

for which ΔF^0, ΔH^0 and ΔS^0 recently have been[36] found to be 3.1 kcal., 4.6 kcal. and 5.0 e.u., respectively. For aq. PO_4^{-3}, $\Delta\bar{F}^0$, $\Delta\bar{H}^0$ and $\bar{S}^0$ of *formation* are −306.9 kcal., −245.1 kcal. and −52 e.u., respectively,[37] while for water the corresponding quantities are −68.3 kcal., −56.9 kcal. and 16.7 e.u., respectively.[38] For aq. H^+, $\bar{S}^0$ is taken as the recent accepted value of −5.5 e.u.[39] When these quantities are combined with equation 23, $\Delta\bar{F}^0$, $\Delta\bar{H}^0$ and $\bar{S}^0$ for aq. $P_2O_7^{-2}$ are computed to be −430.4 kcal., −540.9 kcal. and −126.7 e.u. Latimer[37] reports only $\Delta\bar{H}^0$, giving a value of −543.1 kcal. for aq. $P_2O_7^{-4}$, in good agreement with our computed value.

For aq. $P_3O_{10}^{-5}$ consider the aqueous reaction

$$H_2O + P_3O_{10}^{-5} \rightleftharpoons P_2O_7^{-4} + PO_4^{-3} + 2H^+ \qquad (24)$$

whose ΔF^0, ΔH^0 and ΔS^0 are −3.1 kcal., −5 kcal. and −5 e.u., respectively,[12,36] if we make the assumption that the scission of a P–O–P bond from $P_3O_{10}^{-5}$ is the same energetically as that in $P_2O_7^{-4}$. These values combined with equation 24 and the thermodynamic quantities computed above yield for $\Delta\bar{F}^0$, $\Delta\bar{H}^0$ and $\bar{S}^0$ of aq. $P_3O_{10}^{-5}$ the values −615.7 kcal., −776.6 kcal. and −206.4 e.u., respectively.

Combining our computed $\Delta\bar{F}^0$,$\bar{H}^0$ Δ and $\bar{S}^0$ values for aq. $P_2O_7^{-4}$ and $P_3O_{10}^{-5}$ with the evaluated ΔF^0, ΔH^0 and ΔS^0 for the association reaction and $\Delta\bar{F}^0$, $\Delta\bar{H}^0$ and $\bar{S}^0$ for aq. Ca^{++},[40] yields for aq. $CaP_2O_7^{-2}$ the values of −570.2 kcal., −668.5 kcal and −93.9 e.u. for $\Delta\bar{F}^0$, $\Delta\bar{H}^0$ and $\bar{S}^0$, respectively. The corresponding formation quantities for aq. $CaP_3O_{10}^{-3}$ are −757.4 kcal., −912.1 kcal. and −198.6 e.u.

The computed $\bar{S}^0$ values for aq. $CaP_2O_7^{-2}$ and $CaP_3O_{10}^{-3}$ failed completely to fit the recent model proposed by Austin, *et al.*,[41] but gave interesting

(33) A. W. Adamson, *J. Am. Chem. Soc.*, **76**, 1578 (1954).
(34) R. J. P. Williams, THIS JOURNAL, **58**, 121 (1954).
(35) E. L. King, *ibid.*, **63**, 1070 (1959).
(36) C. D. Schmulbach, J. R. Van Wazer and R. R. Irani, *J. Am. Chem. Soc.*, **81**, 6347 (1959).
(37) W. M. Latimer, "Oxidation Potentials," Prentice-Hall, Inc., New York, N. Y., 1952, p. 106.
(38) Ref. 37, p. 39.
(39) R. W. Gurney, "Ionic Processes in Solution," McGraw-Hill Book Co., Inc., New York, N. Y., 1953, p. 175.
(40) Ref. 37, p. 318.
(41) Ref. 7, p. 376.

results when interpreted with the structural semi-empirical approach of Cobble.[6] For oxyions Cobble[42] proposes that $\bar{S}^0$ is represented by

$$\bar{S}^0 = 66 - \frac{81Zf}{(r_1 + r_2)} + \frac{3}{2} R \ln M + (a + b - c)\bar{S}^0_{H_2O} \quad (25)$$

$$\bar{S}^0 = \bar{S}^{0\prime} + (a + b - c)\bar{S}^0_{H_2O} \quad (26)$$

where f is a structural factor, Z and r_1 the charge and crystal radius of the anion, respectively, and M is its molecular weight. r_2 is the crystal radius of the metal cation. Equation 25 was used in combination with the $\bar{S}^0$ values for aq. $P_2O_7^{-4}$ and $P_3O_{10}^{-5}$ to calculate f, assuming $(a + b - c)$ to equal zero; f was found to be 1.48 and 2.28, respectively, not far off from Cobble's estimated values for tetrahedral ions. r_1 for $P_2O_7^{-4}$ and $P_3O_{10}^{-5}$ were taken as 2.3 and 3.2 Å., respectively.[36]

Equation 25 then was used to compute $\bar{S}^{0\prime}$ for aq. $CaP_2O_7^{-2}$ and $CaP_3O_{10}^{-3}$, using the same structural factors as those found above for the free anions and a value of 0.99 Å. for r_2 of Ca^{++}. $\bar{S}^{0\prime}$ for aq. $CaP_2O_7^{-2}$ and $CaP_3O_{10}^{-3}$ was found to be -128 and -221 e.u., respectively. From our computed values of S_0 and $\bar{S}^{0\prime}$, $(a + b - c)\bar{S}_{H_2O}$ for aq. $CaP_2O_7^{-2}$ and $CaP_3O_{10}^{-3}$ is found to be 24 and 23 e.u., respectively, indicating a release of about two water molecules. These water molecules probably are lost from the highly hydrated[43] Ca^{++} when it comes in close contact with the oxygens of the polyphosphate chain. For the association reaction producing aq. $CaP_3O_{10}^{-3}$ and the other polyphosphates, all the entropy change can be attributed to the freeing of the water molecules, whereas for aq. $CaP_2O_7^{-2}$ only half of the entropy change is attributed to changes in hydration. The deviation of $CaP_2O_7^{-2}$ from this picture must be the result of the unexpected endothermicity of its association reaction.

Naturally, if the value of $(a + b - c)$ is known with high certainty, then the free energy and enthalpy of complex formation should be corrected by subtracting $(a + b - c)\Delta\bar{F}_{H_2O}$ and $(a + b - c)\cdot\Delta\bar{H}_{H_2O}$, respectively.

Bjerrum Radii.—Bjerrum radii[44,45] have been used as a mathematical criterion for covalent bonding. For the $CaP_2O_7^{-2}$, $CaHP_2O_7^{-1}$, $CaP_3O_{10}^{-3}$, $CaHP_3O_{10}^{-2}$ and $CaH_2P_3O_{10}^{-1}$ complexes the calculated Bjerrum radii are 3.5, 3.8, 3.9, 5.2 and 6.5 Å., respectively. In agreement with previous calculations[4] these computed values of the distances of closest approach of calcium to the respective phosphate anions are significantly larger than those encountered in covalent bonding.[46]

Acknowledgments.—The authors wish to thank Mr. W. W. Morganthaler for making many of the measurements and Dr. John R. Van Wazer for many stimulating discussions.

(42) J. W. Cobble, *J. Chem. Phys.*, **21**, 1443 (1953).

(43) R. A. Robinson and R. H. Stokes, "Electrolyte Solutions," Academic Press, Inc., New York, N. Y., 1955, p. 247, 319, 320.

(44) J. Bjerrum, *Chem. Revs.*, **46**, 381 (1950).

(45) R. M. Fuoss, *Trans. Faraday Soc.*, **30**, 967 (1934).

(46) R. M. Fuoss, private communication.

INTERNUCLEAR DISTANCES IN HYDRIDES*

BY THOMAS R. P. GIBB, JR., AND DAVID P. SCHUMACHER

Contribution No. 259, Department of Chemistry, Tufts University, Medford 55, Massachusetts

Received January 28, 1960

Metal–hydrogen internuclear distances in substantially all the known binary metallic and saline hydrides may be rationalized equally well on the basis of an ionic model or on the basis of a model utilizing delocalized covalent bonding. In the former the anionic radius ($CN = 4$) of hydrogen is 1.29 Å., the cation radius is for the ion of maximum normal oxidation number. The internuclear distances in the Group I saline hydrides are shown to be increased by the anion-repulsion factor of Pauling. The covalent model is that suggested by Pauling for application to metals, and employs a single-bond radius of 0.37 Å. for hydrogen. Both models are applicable to saline as well as to metallic binary hydrides.

Introduction

As shown by Libowitz and Gibb[1] the metal–hydrogen internuclear distance in thirteen metallic hydrides of the Group IVA, lanthanide and actinide families is equal approximately to the sum of a constant H^- radius of 1.29 Å. (for coördination of less than six) and the radius of the cation of maximum normal oxidation number. In the present paper additional metallic hydrides and saline hydrides, *i.e.*, substantially all hydrides for which data are available, are also shown to obey this simple relationship provided suitable corrections for coördination are made. While "radii" of any sort must be viewed merely as useful aids without much fundamental significance, the prediction of internuclear distance is extremely useful in many ways. The only other rationalization of metal–hydrogen distances which appears accurate enough to be useful is that of Pauling[2] which has been applied to only three hydrides. An improved calculation based on Pauling's method is presented below.

Coördination Number Correction for the Hydride Anion.—Because of the dependence of coördination number corrections of ionic radii on the exponent $1/(n - 1)$[2a,3] where n is the Born repulsion exponent, it follows that for the hydride ion, where n is

* This research was supported by the United States Atomic Energy Commission.

(1) G. Libowitz and T. R. P. Gibb, Jr. THIS JOURNAL, **60**, 510 (1956).

(2) L. Pauling and F. J. Ewing, *J. Am. Chem. Soc.*, **70**, 1660 (1948); *cf.*, L. Pauling, *ibid.*, **69**, 542 (1947).

(2a) L. Pauling, "Nature of the Chemical Bond," (3rd Ed.), Cornell Univ. Press, Ithaca, N. Y., 1959.

(3) W. H. Zachariasen, *Z. Krist.*, **80**, 137 (1931); *cf.*, C. Kittel, "Introduction to Solid State Physics," John Wiley and Sons, Inc., New York, N. Y., 1957, p. 81.

TABLE I

INTERNUCLEAR DISTANCE (d_{MH}) AND CORRECTED SUM OF IONIC RADII. METALLIC HYDRIDES

Hydride	Cation radius and charge (CN = 6)	CM_{Cation}	Δ_{Cat}	CN_{H^-}	Δ_{H^-} (1.40 Å. for CN = 6)	Total CN corr.	d_{MH} calcd.	d_{MH} obsd.	Ref.
ScH_2	0.68[e] III	(8)	(0.08)	(4)	(−0.18)	(−0.10)	(1.98)	..	.....
YH_2	.88 III	(8)	(.08)	(4)	(− .18)	(.10)	(2.18)	..	.....
TiH	.80[f] II	6	0	6	0	0	2.20	2.20	17
TiH_2	.60[e] IV	8	0.08	4	−0.18	−0.10	1.90	1.92	7
ZrH	.92[e] II	6	0	6	0	0	2.32	2.39	17
ZrH_2	.77[e] IV	~8[a]	0.08	~4	−0.18	−0.10	2.07	2.07	7
HfH_2	.78[g] IV	~8	.08	~4	− .18	− .10	2.08	2.05	6, 7
$VH_{<1}$	.59[g] V	~4	− .11	~4	− .18	− .29	1.70	1.68	15
$NbH_{<1}$	.67[g] V	4	− .11	~4	− .18	− .29	1.78	1.72	7, 8
$TaH_{<1}$	.68[g] V	4	− .11	~4	− .18	− .29	1.79	1.74	7, 8, 9
CrH	.52[g] VI	4	− .11	4	− .18	− .29	1.63	1.67	7, 10
CuII	(.61 II)[c]	4	− .11	4	− .18	− .29	(1.72)	1.73	11, 12
$PdH_{<1}$	.65[g] IV	6	0	6	0	0	2.05	2.03	7, 13, 16
ThH_2	1.08[e] III	8	0.08	4	−0.18	−0.10	2.38	2.41	7
Th_4H_{15}	0.99[e] IV	~12	~ .19	~3.2[d]	− .26	− .07	~2.32	2.29	7
UH_3	0.93[e] IV[b]	12	.19	4	− .18	+ .01	2.34	2.32	7

[a] For less symmetrical structures the CN is approximate. The CN's for the group V metals are taken as 4 for an interpenetrating pair of bcc lattices. There is some uncertainty about the structure of these hydrides. [b] The choice of oxidation number IV is an exception to the general rule. It seems more likely that the central ion is U^{+6} and that ion-repulsion accounts for the large U-H distance. The tabular radius for U^{+6} is 0.86Å. [c] The cupric ion radius is not tabulated. The radius shown is an average for cupric halides and oxide. [d] 12(4/15). [e] Zachariasen, *cf.* ref. 3. [f] Goldschmidt, ref. 4. [g] Ahrens, *cf.* ref. 4.

small, the dependence of apparent radius on coordination number will be unusually large. Accordingly, we have chosen to apply a correction to the H^- radius of the same form used by Zachariasen[3] for cation radii but with an appropriate increase in the multiplier. The cation correction may be additive, when it has the form $\Delta = 0.6 \log (CN/6)$ where the 6 in the denominator adjusts the correction to zero for $CN = 6$, or the cation correction may be multiplicative as tabulated in reference 4, in which case it is arbitrarily adjusted to unity for $CN = 6$.

The resulting equation for internuclear distance is then given by either

$$d_{MH} = r_{M^+} + 0.6 \log(CN_M/6) + r_{H^-} + \log(CN_H/6)$$
$$= cr_{M^+} + c'r_{H^-}$$

where d_{MH} is the internuclear distance in the ionic substance, r_{M^+} is the tabular cation radius for $CN = 6$, r_{H^-} is a constant radius of H^- for $CN = 6$, c and c' are multiplicative corrections depending both on the Born exponent and on CN. The hydrogen anion radius r_{H^-} is taken as 1.40 Å. for $CN = 6$ and the value 1.29 Å. used previously is considered merely a rough average (for lower CN's).

The only novelty in these equations is the inclusion of a separate corrective term for H^-; for anions of $n = 7$–12 this correction is unnecessary. The two equations are substantially the same within the approximations customary in dealing with ionic radii.

The use of a single CN correction factor based on a mean Born exponent has better precedent, but the double correction cited above is convenient in that the well-known Zachariasen data may be used without change. Results are shown for metallic hydrides in Table I. Several dihydrides of more electronegative metals are included for comparison with Table III.

The sensitivity of the apparent H^- radius to CN is in line with what one might expect of a tenuous ion of low electron-density. This tenuosity and bulkiness (compared to covalent H) are strongly supported by the large internuclear distance and high refractive index in LiH, for example.

Ion-repulsion Correction of Internuclear Distance for Saline Monohydrides.—The Pauling expression for $F(\rho)$[2a] also includes the Born repulsion exponent and while very tedious to calculate it gives a rough relation of d_{MH} to the Born exponent and radius ratio. As the latter increases in the alkali metal group, the Born exponent also increases. Thus, $F(\rho)$ increases from 0.981 for LiH to 1.027 for CsH. The repulsive coefficient B[2a] is 0.0367 as evaluated from $F(\rho)$ for LiH. Data for the alkali metal hydrides are shown in Table II.

As noted by Pauling[2a] in the case of true salts of unsymmetrical valence type, *e.g.*, alkaline-earth metal fluorides, the observed metal–anion distances

(4) Landolt-Bornstein "Tabellen," Vol. 1, "Kristalle" Pt. 4, A. Eucken, Ed., Springer–Verlag, Berlin, 6th Ed., 1950, p. 523.

(5) (a) F. H. Ellinger, C. E. Holley, Jr., R. N. R. Mulford, W. C. Koehler and W. H. Zachariasen, THIS JOURNAL, **59**, 1226 (1955); (b) F. H. Ellinger, C. E. Holley, Jr., B. B. McInteer, D. Pavone, R. M. Potter, E. Staritzky and W. H. Zachariasen, *J. Am. Chem., Soc.*, **77**, 2647 (1955).

(6) S. S. Sidhu, L. Heaton and D. D. Zauberis, *Acta Cryst.*, **9**, 607 (1956).

(7) W. B. Pearson, "A Handbook of Lattice Spacings and Structures of Metals and Alloys," Pergamon Press, New York, N. Y., 1958.

(8) D. Knowles, IGR-R/C 190, March, 1957.

(9) B. Stalinski, *Bull. Acad. Polon. Sci.*, Cl. iii, **2**, 245 (1954).

(10) C. A. Snavely and D. A. Vaughn, *J. Am. Chem. Soc.*, **71**, 313 (1949).

(11) J. C. Warf and W. Feitknecht, *Helv. Chim. Acta*, **33**, 613 (1950).

(12) J. A. Goedkoop and A. F. Andresen, *Acta Cryst.*, **8**, 118 (1955).

(13) J. Worsham, W. K. Wilkinson and C. G. Shull, *J. Phys. Chem. Solids*, **3**, 303 (1957).

(14) J. C. Warf and W. L. Korst, *Acta Cryst.*, **9**, 452 (1956); *cf.*, also Ph.D. Thesis, W. L. Korst, Univ. Southern California (1956).

(15) M. J. Trzeciak, D. F. Dilthey and M. W. Mallett, BMI-1112 (1956).

(16) A. Maeland (unpub.) reports d_{MH} 2.03 Å. for limiting non-stoichiometric composition at room temperature.

are closely approximated by the sum of the uncorrected radii. This same behavior is shown by alkali-earth metal hydrides as evidenced by Table III. The poor agreement for MgH_2 is not more than one would expect to arise from the lack of similarity of the bonding in hydrides and fluorides. Magnesium hydride is crystallographically almost identical to MgF_2 where the anion (radius 1.33 Å.) is less easily deformed. The principal H–H distance in MgH_2 is 2.76 Å. which is close to twice the H^- radius (1.40 Å.) suggested herein. Excellent agreement is shown for most of the known di- and trihydrides with the exception of EuH_2, YbH_2 and Th_4H_{15} whose H^- positions are not known with certainty and in which the internuclear distances are therefore not final. The quadrivalent Ac ionic radius is not available.

TABLE II

SALINE MONOHYDRIDES

Hydride	Cation radius	Radius sum (r_H = 1.40 Å.)	Born exponent (av.)	$F(\rho)$	d_{MH} calcd.	d_{MH} obsd.[17]
LiH	0.68	2.08	5	0.981	2.04	2.04
NaH	0.98	2.38	6	0.992	2.36	2.44
KH	1.33	2.73	7	1.006	2.75	2.85
RbH	1.48	2.88	7.5	1.014	2.92	3.02
CsH	1.67	3.07	8.5	1.027	3.15	3.17

TABLE III

UNCORRECTED SUM OF TABULAR CATION RADII AND r_{MH} = 1.40 Å. FOR DIHYDRIDES AND TRIHYDRIDES OF ELEMENTS OF LOW ELECTRONEGATIVITY

Hydride	Tabular cation radius (charge)	Plus 1.40 Å.	d_{MH} obsd.	Ref. (d_{MH} obsd.)
MgH_2	0.65[c]	2.05	1.95	5(a)
CaH_2	0.94[c]	2.34	2.35(mean)	19
SrH_2	1.10[c]	2.50	2.53(mean)	19
BaH_2	1.29[c]	2.69	2.71(mean)	19
LaH_2	1.06[T]III[a]	2.46	2.45	5
CeH_2	1.03[T]III	2.43	2.43	7, 14
PrH_2	1.01[T]III	2.41	2.40	14
NdH_2	0.99[T]III	2.39	2.38	14
SmH_2	.96[T]III	2.36	2.33	1
EuH_2	.95[T]III	2.35	2.49(mean)	7, 14
GdH_2	.94[T]III	2.34	2.31	17
YbH_2	.86[T]III	2.26	2.35(mean)	7, 14
AcH_2	1.11[c]III	(2.51)	2.46	1
ThH_2	1.08[c]III	2.48	2.41	7
Th_4H_{15}	0.99[c]IV	2.39	2.29	7
PaH_3	.90[c]V	2.30	2.32	1
UH_3	.93[c]IV[b]	2.33	2.32	1
PuH_2	.90 IV	2.30	2.32	1
$PuH_{2.76}$	.90 IV	2.30	(2.31)	17

[a] [T]Templeton, *cf.* ref. 21. [b] Considered U^{VI} in ref. 1.

Discussion of the Ionic Model for Hydrides.—The data shown in Tables I–III indicate that the conventional treatment of internuclear distances in salts may be applied successfully to hydrides of the less electronegative metals. The only novelty is the choice of a saline model for the metallic or semi-metallic hydrides. The advantage of the saline model lies in the ease with which it may be adapted to the estimation of lattice-energies and the prediction of unknown hydride structures. Rationalization of known structures by Pauling's radius-ratio rules and detailed examination by means of crystal-field effects of small changes in internuclear distance with H-content become of interest in connection with this model.

In preparing the tables use was made of the compilations in references 7, 17 and 18. Most of the cited structures have been determined either by neutron diffraction or by analogy with closely similar substances so studied. Some question exists as to the structure of the Group V hydrides which is variously reported as NaCl-type, body-centered cubic, tetragonal and orthorhombic. A tetragonal distortion of the bcc structure was used for the calculations reported here. There is a progressive increase in *d*-spacings with increasing H-content for all three of the Group V metal–hydrogen systems, and the calculated values may therefore be in better agreement than appears from Table I. The very small M–H distances afford support for the marked effect of coördination number on the effective H-radius.

The three tables indicate that practically all hydrides may be treated as salts insofar as metal–hydrogen distances are concerned. Di- and trihydrides of those elements whose electronegativity is above about 1.2 on Pauling's scale, *e.g.*, Mg, Ti, Zr, Hf, etc., require coördination number corrections whereas such corrections are not required for the more salt-like metallic di- and tri-hydrides, *e.g.*, lanthanide and actinide hydrides, or the obviously saline hydrides such as CaH_2.

The H-positions in CaH_2, SrH_2 and BaH_2 are not known from neutron studies, but the original X-ray work[19] appears unequivocal. Note that in the case of ThH_2 and Th_4H_{15} different oxidation numbers for Th suggest themselves.

It is reasonable to suppose that the coördination number corrections for MH_2 and MH_3 structures are diminished by compensating errors, as mentioned above for CaH_2, etc. Actually, the *CN* correction for H appears too large here and somewhat better results are obtained if it is neglected, as in reference 1.

The Delocalized Covalent Bonding Model.—Pauling[2] has used the relation

$$r_1 = r_{cn} + 0.3 \log(v/CN)$$

to rationalize internuclear distances in metals. This relation was applied by Pauling to many metals, and to a few metallic hydrides using an r_1 for hydrogen of 0.28 Å. While giving good results in three cases (TiH_2, ZrH_2, PdH), it failed in the case of UH_3.

In obtaining the results shown in Table IV, the relation used is

$$d_{MH} = r_1 + 0.37 + 0.3 \log (CN_m CN_h / v_m)$$

where r_1 is the Pauling single-bond radius for the metal,[2] 0.37 is the single-bond radius of H (half the separation in H_2) and the subscripts m and h

(17) "Some Physical Properties of the Hydrides," UCRL 4519, R. E. Elson, H. C. Hornig and W. L. Jolly, *et al.*, Livermore, Calif., 1955.

(18) R. W. G. Wyckoff, "Crystal Structures," Interscience Publishers, Inc., New York, N. Y., 1948.

(19) E. Zintl and A. Harder, *Z. Elektrochem.*, **41**, 33 (1935).

(21) D. H. Templeton and C. H. Dauben, *J. Am. Chem. Soc.*, **76**, 5238 (1954).

refer to metal and hydrogen, respectively. The valence of H is assumed to be unity. The excellent agreement with observed d_{MH} is shown in the table.

It might be pointed out that both the delocalized bond and ionic models suffer from minor drawbacks. In the former, the appropriate valence of the metal is not always known in advance and this greatly diminishes the predictive value of the model.[20] In the ionic model one must accept the usual drawbacks of all spherical-ion models, namely, that the anions may sometimes interpenetrate, as in the classical instance of O^{2-} in rutile. Thus, in the ionic model of UH_3, if the H^- ions are not to penetrate one another, their radius must be approximately 0.86 Å. If the H^- radius is actually 1.29 Å. then they must interpenetrate by just $^1/_3$ of this radius, which seems high although H^- would be expected to be a "soft" and very tenuous ion. No such interpenetration occurs in the rutile analog, MgH_2, but it is observed in several metallic hydrides.

Both models suffer from a difficulty common to all expressions which rely quantitatively on coordination number. This term is only explicit in simple or highly symmetrical structures, and becomes somewhat arbitrary in distorted structures.

Conclusions.—The agreement of the ionic and delocalized covalent models with each other and with experimental metal–hydrogen distances, indicates that there is no sharp difference between saline and metallic hydrides. The ionic model provides a better rationalization of the metallic character of some hydrides (*i.e.*, when the normal cation oxidation number is in excess of the normal hydrogen–metal ratio) and interprets the consequent excess cationic charge in terms of generalized metallic bonding. Both models minimize the contribution of metal–metal interaction, in keeping with the observed properties of metallic hydrides, but the ionic model stresses the high electron density around H. This is in keeping with the considerable electron-affinity of H and the fundamental stability of the helium configuration.

(20) R. E. Rundle, *J. Am. Chem. Soc.*, **73**, 4172 (1951).

TABLE IV

INTERNUCLEAR DISTANCES BY THE PAULING EQUATION (REPRESENTATIVE EXAMPLES FROM FOUR GROUPS)

Hydride	*CN* of metal	Valence of metal	*CN* of hydrogen	d_{MH} calcd.	d_{MH} obsd.
KH	6	1	6	2.86	2.85
CaH_2	7	2	$3^1/_2$	2.43	2.35 (mean)
TiH_2	8	4	4	1.96	1.92
$VH_{\leq 1}$	4	5	4	1.69	1.68
$CrH_{<1}$	4	5.78	2	1.60	1.67
	4	2.90	2	1.67	1.67
CuH	4	5.44	4	1.78	1.73
RbH	6	1	6	3.00	3.02
SrH_2	7	2	$3^1/_2$	2.52	2.52 (mean)
ZrH_2	8	4	4	2.07	2.06
$NbH_{\sim 1}$	4	5	4	1.80	1.72[b]
$PdH_{\sim 1}$	6	2[a]	6	2.02	2.03
	6	6	6	1.88	2.03
CsH	6	1	6	3.19	3.19
BaH_2	7	2	$3^1/_2$	2.67	2.71 (mean)
LaH_2	8	3	4	2.37	2.45
HfH_2	8	4	4	2.08	2.05
$TaH_{<1}$	4	5	4	1.80	1.71[b]
YbH_2	8	2	4	2.43	2.35
ThH_2	8	4	4	2.29	2.41
	8	2[a]	4	2.38	2.41
Th_4H_{15}	12	4	3+	2.31	2.29
UH_3	12	6	4	2.07	2.32
	12	1.00[a]	4	2.29	2.32

[a] Indicates abnormal valence which must be assumed in order to obtain agreement with observed d_{MH} values. Some justification of these valences exists and will be discussed elsewhere. Poor agreement between d_{MH} calcd. and d_{MH} obsd. is encountered in the lanthanide and actinide hydrides, where the ionic model appears preferable. [b] d_{MH} is for hydride of less than stoichiometric composition, whereas that calculated is for MH. In the systems so marked the structure expands with increasing H-content.

Acknowledgments.—Mrs. Barbara M. Kearney carried out many of the computations and contributed materially to the study of the Group V metal hydrides. Mr. Arnulf J. Maeland assisted in the same manner and first observed the low valence of U in UH_3 (delocalized bonding model) which apparently is typical of lanthanide and actinide interstitials.

ABSORPTION SPECTRA OF NITRO COMPOUNDS. FURTHER SOLVENT PERTURBATIONS[1,2]

BY H. E. UNGNADE, E. D. LOUGHRAN AND L. W. KISSINGER

Los Alamos Scientific Laboratory, University of California, Los Alamos, New Mexico

Received February 29, 1960

Intensity measurements have been made in the 280 mμ region for nitromethane and 2,2-dinitropropane in primary, secondary and tertiary amines and other solvents. The observed intensity increases are believed to be due to an electron donor–acceptor interaction between solvent and solute. The magnitude of the effects in nitrogen-containing solvents parallels the basic strengths which would be predicted from inductive effects alone.

(1) This work was performed under the auspices of the U. S. Atomic Energy Commission.

(2) Presented in part before the thirty-fourth Annual Meeting of the Southwestern and Rocky Mountain Divisions of the American Association for the Advancement of Science and the New Mexico Academy of Science at Las Vegas, New Mexico, April 29, 1958.

Introduction

It has been demonstrated that the intensity of the 280 mμ band in mono- and dinitroparaffins is increased in dioxane, benzene and toluene compared

with inactive solvents such as cyclohexane, water and alcohols.[3-5] New measurements are now reported in amines, dimethylformamide and a series of solvent mixtures.

Experimental

The nitro compounds were purified by fractional distillation under reduced pressure. Nitromethane boiled at 48.0° (102 mm.), $n^{25}D$ 1.3813, and contained 99.2% of mononitro compounds (97.5% nitromethane) according to mass-spectrographic analysis. Primary and tertiary amines (excepting heptacosafluorotributylamine) were purified by refluxing for several days over sodium and fractionating the product from a 1.8 × 118 cm. packed column. With secondary amines, where this method led to considerable losses, it was found advantageous to reflux a mixture of amine and sodium hydroxide for several days and fractionate the product. The distillate often could be used directly. Subsequent refluxing with sodium involved only minor losses of secondary amines. The purification procedure was repeated when necessary until the transmittance in the ultraviolet region remained unchanged.

Pure liquid nitromethane, triethylamine and their binary mixtures were measured in a silica cell of 0.0016 cm. thickness against the same cell filled with ethanol in a Cary Model 14 spectrophotometer. All other determinations in the ultraviolet region were carried out in matched stoppered 1-cm. cells with a model DR Beckman spectrophotometer in 0.05–0.0001 *M* solutions. Carefully weighed amounts of nitro compounds were made up to 25 ml. with a given solvent or solvent mixture. A portion of this solution (5 ml.) was diluted to 25 ml. with the same solvent, etc., and the readings were made against the same solvent in the reference cell. Binary solvent mixtures were made up by weight. Within the absorbance range of 0.1–1.0 Beer's law was valid for all solutions. In anhydrous solutions of amines the absorption spectra of the nitro compounds remained unchanged for at least 6 hours at 21° after mixing.

Infrared absorption spectra were determined in solution in matched sealed cells of 0.1 mm. thickness against pure solvents with a Perkin–Elmer Model 21 spectrophotometer.

Results

The experimental results given in Figs. 1–7 and Table I represent ultraviolet absorption spectra of nitromethane, 2,2-dinitropropane and triethylamine in pure solvents and in binary or ternary mixtures consisting of known quantities of triethylamine and cyclohexane, or nitromethane and cyclohexane.

TABLE I

ULTRAVIOLET ABSORPTION OF NITRO COMPOUNDS

Solvent	Nitromethane λ_{max}, mμ	Nitromethane ϵ_{max}	Nitromethane ϵ_{320}	2,2-Dinitropropane λ_{max}, mμ	2,2-Dinitropropane ϵ_{max}	2,2-Dinitropropane ϵ_{270}
None	273	16.2	3.3	...[b]	...[b]	...[b]
$(C_4F_9)_3N$	274	10.4	1.8	278	38.8	7.4
Cyclohexane	278	17.6	3.7	280	55.0	13.8
CCl_4	277	20.2	4.1	280	53.5	13.0
Dioxane	272.5	22.7[a]	..[b]	(280)[c]	105	14.7
DMF[d]	(280)[e]	22.9	4.4	(280)[c]	162	18.0
Benzene	278	29.1[a]	4.8[a]	(280)[c]	174	19.2
n-$BuNH_2$	(280)[c]	33.3	5.8	(280)[c]	210	37.3
n-$HexNH_2$	(280)[c]	41.4	6.1	(280)[c]	207	37.6
n-Pr_2NH	(280)[c]	86.1	11.2	(280)[c]	306	99.0
n-Bu_2NH	(280)[c]	81.0	10.9	(280)[c]	273	90.2
Et_3N	(280)[c,e]	200	24.2	(280)[c,f]	485	246
n-Bu_3N	(280)[c]	180	24.6	...[b]	...[b]	...[b]

[a] From N. S. Bayliss, *et al.* (ref. 4). [b] Not determined. [c] No maximum. [d] Dimethylformamide. [e] In 0.01 *N* alcoholic potassium hydroxide ϵ_{280} 200 (S. Nagakura, Laboratory of Molecular Structure and Spectra, Physics Department, University of Chicago, Technical Report 1957–58, p. 49–60). [f] In 0.01 *N* sodium hydroxide in methanol λ_{max} 278 mμ (ϵ 54.7).

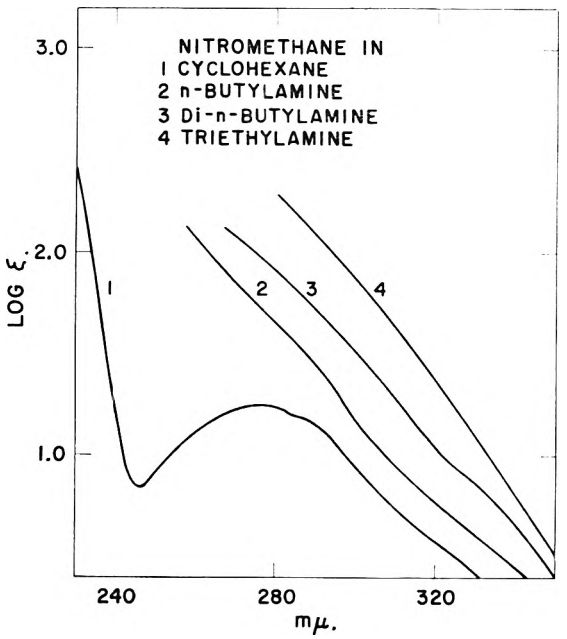

Fig. 1.—Ultraviolet absorption spectra of nitromethane in four solvents against the pure solvents in the reference cell.

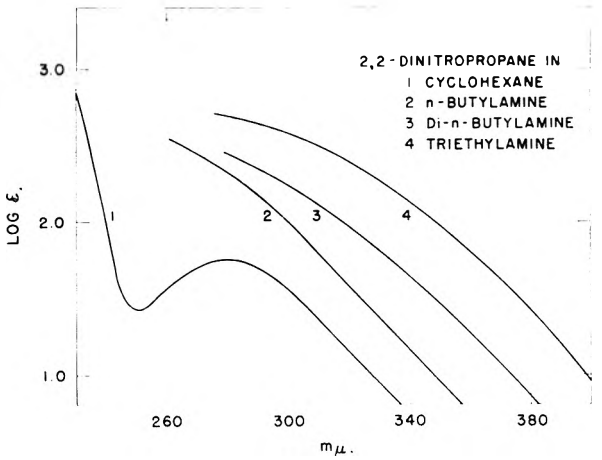

Fig. 2.—Ultraviolet absorption spectra of 2,2-dinitropropane in four solvents against the pure solvents in the reference cell.

Simple aliphatic amines as solvents give intensity increases for the nitro compounds in the 280 mμ region which are far stronger than those observed with aromatic hydrocarbon solvents and which are in the order prim. < sec. < tert. (Figs. 1 and 2). There are, however, only relatively small differences between amines of the same class (Table I). The molar absorptivities for nitromethane in triethylamine are so large that it is possible to study the effect of varying amounts of this amine in dilute cyclohexane solution (Fig. 3), or directly without solvents by measuring mixtures of amine and nitro compound in very thin cells (Fig. 6). In cyclohexane in very dilute solutions (0.003–0.007 *M*) nitromethane does not alter the absorption curve for triethylamine (Fig. 5), and triethylamine has no measurable effect on the spectrum of nitro-

(3) N. S. Bayliss and E. G. McRae, THIS JOURNAL, **58**, 1006 (1954).

(4) N. S. Bayliss and C. J. Brackenridge, *J. Am. Chem. Soc.*, **77**, 3959 (1955).

(5) H. E. Ungnade and L. W. Kissinger, *J. Org. Chem.*, **22**, 1088 (1957).

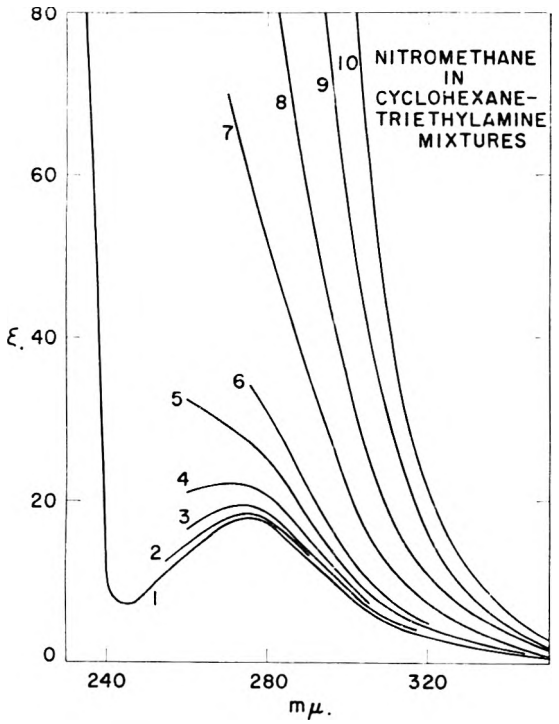

Fig. 3.—Ultraviolet absorption spectra of 0.034–0.039 *M* nitromethane in cyclohexane–triethylamine mixtures against the same solvent mixtures. Mole fraction of amine in cyclohexane: (1) 0, (2) 0.00225, (3) 0.00452, (4) 0.0103, (5) 0.0219, (6) 0.0435, (7) 0.111, (8) 0.285, (9) 0.612, (10) 1.0.

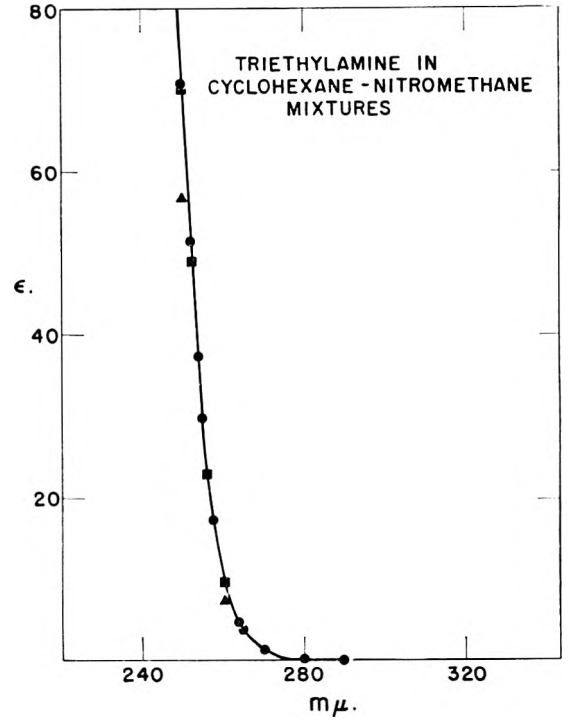

Fig. 5.—Ultraviolet absorption spectra of 0.004–0.008 *M* triethylamine in cyclohexane–nitromethane mixtures against the same solvent mixtures. Moles of nitromethane (per liter) are: ●, 0; ■, 0.003; ▲, 0.007.

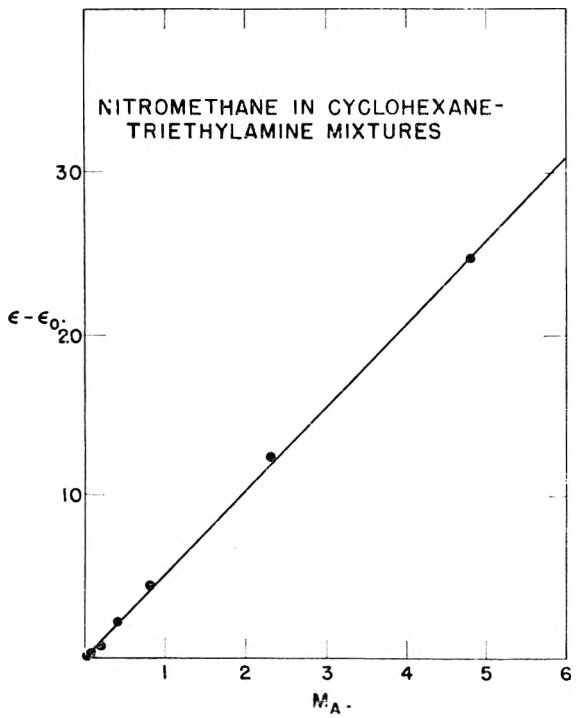

Fig. 4.—Molar absorptivities $\epsilon - \epsilon_0$ (observed absorptivities minus those in cyclohexane) at 280 mμ *vs.* number of moles of amine per liter (M_A) from ultraviolet absorption spectra shown in Fig. 3.

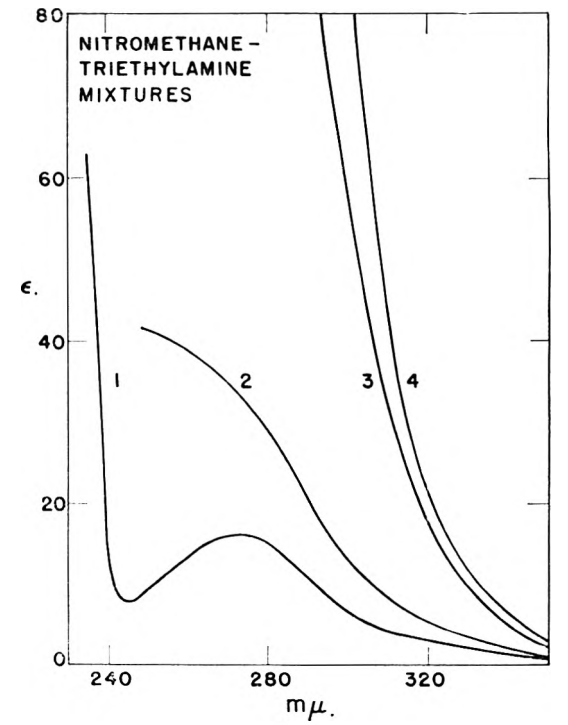

Fig. 6.—Ultraviolet absorption spectra of pure liquid nitromethane and nitromethane in triethylamine without additional solvent in a 0.0016-cm. cell against ethanol, corrected for the absorption of the pure liquid amine. Mole fraction of amine is: (1) 0; (2) 0.031; (3) 0.541; (4) 0.995.

methane. Mixtures of 0.0003, 0.003 and 0.05 *M* solutions of the two compounds of the type required for Job's continuous variations[6] showed no appreciable effect of the compounds upon one another (Fig. 7). Isosbestic points were observed at 260 mμ (A = 0.6 in 0.05 *M* solution) and near 210 mμ. The

(6) P. Job, *Ann. chim.*, [10] **9**, 113 (1928); W. C. Vosburgh and G. R. Cooper *J. Am. Chem. Soc.*, **63**, 437 (1941).

first measurable effect on the nitromethane spectrum occurs in a somewhat more concentrated solution (0.02 *M* amine and 0.039 *M* nitromethane) in cyclohexane (Fig. 3). Further increases in the amine concentration cause a corresponding intensity increase in the nitromethane absorption, both with and without solvent in the observable wave length range (Figs. 3 and 6). For cyclohexane solutions the plot of molar absorptivity *versus* moles per liter of triethylamine is linear and the line goes through the origin when the effective molar absorptivities $\epsilon - \epsilon_0$ (ϵ_0 = molar absorptivity in cyclohexane) are used (Fig. 4). The abnormal effect of the amine is therefore directly proportional to its concentration.

The absorption spectrum of nitromethane in dimethylformamide shows only a very slight increase in intensity (compared to cyclohexane), and the corresponding spectrum in heptacosafluorotributylamine shows none (Table I).

The infrared absorption spectra of the two nitro compounds have unchanged NO_2 stretching frequencies (Table II), except in primary amines where hydrogen bonding is believed to occur, the shift being of the order of magnitude observed in nitro compounds with intramolecular hydrogen bonds.[7]

TABLE II

NO_2 STRETCHING BANDS OF NITRO COMPOUNDS[a]

Compound	Solvent	as NO_2, μ	sym NO_2, μ
$MeNO_2$	None	6.40	7.27
	CCl_4	6.40	7.30
	$CHCl_3$	6.40	7.30
	n-$BuNH_2$	6.46	..[b]
	n-$HexNH_2$	6.43	..[b]
	n-Bu_2NH	6.40	..[b]
	n-Pr_2NH	6.40	..[b]
	i-Pr_2NH	6.40	..[b]
	Et_3N	6.40	..[b]
$Me_2C(NO_2)_2$	None	6.37	7.52
	CCl_4	6.36	7.55
	$CHCl_3$	6.36	7.55
	n-$BuNH_2$	6.40	7.55
	n-$HexNH_2$	6.37	7.54
	n-Bu_2NH	6.36	7.55
	n-Pr_2NH	6.35	7.53
	i-Pr_2NH	6.35	7.56
	Et_3N	6.35	7.56

[a] The concentration of nitro compound in the solutions was 2%. [b] This band could not be observed, as a result of solvent absorption.

Discussion

The experimental results indicate that amines, unlike alcohols, give abnormal spectra for the nitroparaffins examined, and that primary and secondary amines are less effective than tertiary amines. Primary amines, which evidently can form fairly strong hydrogen bonds with nitro compounds[7] (Table II), show only relatively small intensity increases (Table I). It appears that hydrogen bonds between nitro compounds and amines would tend to decrease the abnormal effect, if they do indeed play a part in this interaction,

(7) T. Urbanski, *Roczniki Chem.*, **31**, 37 (1957); *Tetrahedron*, **6**, 1 (1959); *Bull. acad. polon. sci., classe III*, **5**, 533 (1957).

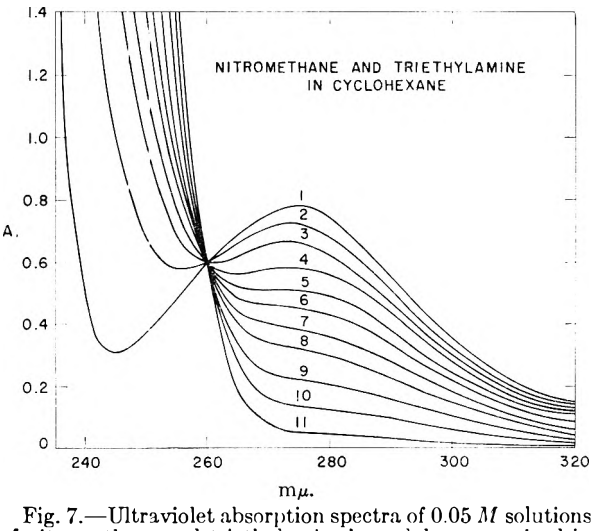

Fig. 7.—Ultraviolet absorption spectra of 0.05 *M* solutions of nitromethane and triethylamine in cyclohexane, mixed in the following proportions: 1, 100% NM; 2, 90% NM + 10% TEA; 3, 80% NM − 20% TEA; 4, 70% NM + 30% TEA; 5, 60% NM + 40% TEA; 6, 50% NM + 50% TEA; 7, 40% NM + 60% TEA; 8, 30% NM + 70% TEA; 9, 20% NM + 80% TEA 10, 10% NM + 90% TEA; 11, 100% TEA.

and therefore cannot explain the abnormal effect.

We have been unable to correlate the basic strength of the amines in water[8] or other physical properties of the amines, *e.g.*, dielectric constant or refractive index, with the observed changes.

Tautomerization to the aci-nitro form and salt formation are possible in nitromethane but not in 2,2-dinitropropane,[9] yet the ultraviolet absorption spectra of both compounds give substantially the same solvent effects with amines. Both changes should also cause a marked shift in the infrared absorption of nitromethane since the C=N group in salts of mononitroparaffins absorbs near 6.2 μ, but such a shift is not observed.

The infrared spectra of solutions of nitromethane and dinitropropane in secondary and tertiary amines exhibit bands identical in position and approximate intensity with those in normal solvents, *i.e.*, chloroform and carbon tetrachloride, and also with the bands observed in the pure nitro compounds. Since the formation of strong molecular complexes with $\pi \rightarrow \pi$ or $n \rightarrow \pi$ type charge transfer is generally accompanied by a shift of the asymmetric NO_2 stretching frequency or the appearance of a new band,[10] the existence of such complexes in these solutions is unlikely.

There is no appreciable chemical interaction between nitro compounds such as 2,2-dinitropropane and anhydrous amines at room temperature, inasmuch the nitro compound can be recovered unchanged after several hours.[11]

(8) H. K. Hall, *J. Am. Chem. Soc.*, **79**, 5441 (1957).

(9) Terminal dinitro compounds form salts with amines which have strong absorption bands near 380 mμ. Thus 1,1-dinitroethane in triethylamine containing 0.8% water absorbs at 375 mμ (ϵ 8730).

(10) R. D. Kross and V. A. Fassel, *J. Am. Chem. Soc.*, **79**, 38 (1957).

(11) In an attempt to study binary solvent pairs consisting of *n*-hexylamine and water, it was found that ultraviolet absorption spectra of such solutions of nitromethane change rapidly with time. A new maximum of high intensity appears at 306 mμ which is characteristic for methazonic acid [G. Kortüm, *Z. physik. Chem.*, **B43**, 271 (1939); *Z. Elektrochem.*, **47**, 55 (1941)]. The formation of this compound is

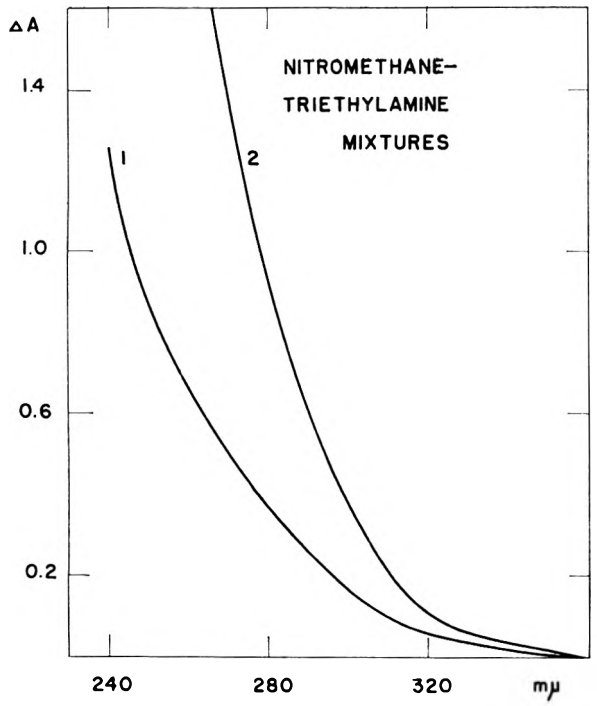

Fig. 8.—Observed absorbance minus absorbance of the pure liquid components *vs.* wave lengths: 1, 10.3737 g. of nitromethane and 0.5489 g. of triethylamine; 2, 2.8118 g. of nitromethane and 5.4963 g. of triethylamine, both in a 0.0016-cm. cell (*cf.* curves 2 and 3 in Fig. 6).

It was concluded therefore that amines exert a specific solvent effect upon the nitro compounds themselves. The high order of effectiveness of triethylamine made it likely that the nucleophilicity of the amine might be important, and indeed the effect of primary, secondary and tertiary amines is in the order of the inductive effects of the groups around the nitrogens.

In order to test this theory, amines with negative substituents, *viz.*, DMF (dimethylformamide) and heptacosafluorotributylamine have been examined in the same way. The spectrum of nitromethane in DMF shows only a slight increase in intensity, while its spectrum in heptacosafluorotributylamine has a normal maximum of decreased intensity. The solvent effect is therefore directly related to the electron density on the nitrogen of the amine. In view of this dependence on the absolute basic strengths of the amines the solvent effect is regarded as a donor–acceptor interaction. It must be weak because of the absence of measurable effects on the asymmetric stretching bands of the nitro compounds in tertiary amines and the lack of perturbations in dilute solutions. Definite complexes between nitromethane and triethylamine are not probable in view of the results of the modified Benesi–Hildebrand plot (Fig. 4) and an analysis of the measurements according to the method of Bayliss.[4] The data fit best the assumption that nitromethane has two nearest neighbor molecules and, for the possibility of a weak complex, that it has an association constant smaller than 1.

believed due to the presence of hydroxide ions and is analogous to its formation from nitromethane in aqueous ammonia [W. R. Dunstan and E. E. Goulding, *J. Chem. Soc.*, **77**, 1263 (1900)].

The identity of the observed perturbations has been examined with respect to the absorption bands of the component molecules.

The observed intensity increases occur at 260–400 mμ, coincidental with the low-intensity 280 mμ band of the nitro compound. (Regrettably the amine absorption prevents observations at shorter wave lengths.) If the effects are attributable only to the 280 mμ bands of the nitro compounds, they are unusual for their magnitude (ϵ in nitromethane is increased at least 10-fold in triethylamine).

Though the intensity increases could be due to an entirely new band which might happen to fall in the same region as the 280 mμ nitro transition, such bands usually are associated with strong charge-transfer complexes[12] for which there is little evidence in the present case.

Bayliss[4] has established that the solvent perturbation of the 280 mμ band of nitromethane in active solvents is accompanied by small shifts of the high intensity band (λ_{max} 198 mμ) to longer wave lengths. It is therefore possible that the observed curves are actually summation curves of an unchanged 280 mμ transition and a high-intensity transition which has undergone a red shift. Such a possibility, however, does not appear very likely in view of the required shift of nearly 80 mμ.

TABLE III

ULTRAVIOLET ABSORPTION OF LIQUID AMINES[a]

Amine	A_{250}[b]	A_{270}	A_{280}
$(C_4F_9)_3N$	0.24	0.14	0.08
n-$BuNH_2$	.50	.18	.13
n-$HexNH_2$	.58	.35	.09
n-Pr_2NH	..[c]	.62	.28
i-Pr_2NH	..[c]	.50	.23
n-BuEtNH	..[c]	.74	.28
n-Bu_2NH	..[c]	.65	.23
Et_3N	..[c]	..[c]	.65

[a] Determined for pure liquids without solvent. [b] Absorbance in 1 cm. cells against water. [c] Too large to measure.

Most of the experimental evidence favors the assumption that the observed curves consist of superimposed perturbed amine bands and 280 mμ nitro bands. Thus triethylamine shows fairly strong absorption at 250 mμ (Fig. 5), requiring a shift of only 30 mμ to account for intensity increases at 280 mμ, and the tail intensities from the amine absorptions fall roughly in the same order (Table III) as the observed solvent effects (Table I). The spectrum of the perturbation in nitromethane–triethylamine (corrected for the absorption of the components) (Fig. 8) even bears a superficial resemblance to the spectrum of the pure amine.

Experimental evidence has been discussed recently[13] which shows that acceptor excited states add little to the intensity of the absorption of a complex and that the most important contributions are due to the interaction of the donor excited states (in this case the amine excited states) with the

(12) W. Brackman, *Rec. trav. chim.*, **68**, 147 (1949); L. E. Orgel, *Quart. Rev.*, **8**, 440 (1954).

(13) J. N. Murrell, *J. Am. Chem. Soc.*, **81**, 5037 (1959).

complex state. It is also stated that this interaction can occur under conditions where no stable complex is formed, *i.e.*, it makes evidently little difference whether we deal with a weak complex or with contact-pairs.[14]

(14) L. E. Orgel and R. S. Mulliken, *ibid.*, **79**, 4839 (1957).

Acknowledgment.—The authors are indebted to Drs. L. C. Smith and R. S. Mulliken for a critical review of the manuscript and discussions of the intrepretation of the effects, and to one referee for pointing out the pertinence of reference 13 to this work.

THE RADIOLYSIS OF AQUEOUS CALCIUM BENZOATE AND BENZOIC ACID SOLUTIONS[1]

BY WILLIAM A. ARMSTRONG, BARBARA A. BLACK AND DOUGLAS W. GRANT

Defence Research Chemical Laboratories, Defence Research Board, Ottawa, Ontario, Canada

Received March 5, 1960

Fluorometric techniques were utilized to determine the yields of *o*-, *m*-, *p*-hydroxybenzoic acids and phenol formed, and the yield of benzoate ion (G_{-Bz}) consumed in irradiated aerated aqueous calcium benzoate solutions. For 6×10^{-4} *M* solutions irradiated with Co^{60} γ-rays, $G_{ortho} = 0.67$, $G_{meta} = 0.37$ and $G_{para} = 0.37$. Similar *o*:*m*:*p* ratios but slightly lower absolute yields were obtained at higher dose rates using 3 Mev. X-rays. For Co^{60} γ-irradiated calcium benzoate solutions G_{-Bz} is 2.05 (10^{-4} *M*) and G_{PhOH} is 0.05 (10^{-3} *M*). Initial hydrogen peroxide yields in Co^{60} γ-irradiated solutions are 2.55, 2.35 and 2.30 in 5×10^{-3} *M* calcium benzoate, 10^{-2} *M* benzoic acid and 5×10^{-4} *M* calcium benzoate solutions, respectively. Phenyl benzoate, biphenyl and 4-biphenylcarboxylic acid, if formed, are formed in small yield. For 10^{-3} *M* benzoic acid solutions (in 0.36 *M* H_2SO_4) irradiated with 300 kv. peak X-rays, G_{CO_2} is 0.68(aerated), 0.4(degassed) and G_{H_2} is 0.6(degassed). The results are discussed in terms of the free radical theory of radiation chemistry.

Introduction

In this Laboratory the radiation-induced conversion of the benzoate ion to the *o*-hydroxybenzoate ion in aqueous solution has been studied[2,3] for X- and γ-ray dosimetry. This paper describes the identification and the measurement of the yields of other products formed in the radiolysis. It seemed particularly desirable to determine accurately the yields of the *m*- and *p*-hydroxy acids in view of the conflicting results in the literature. For example, the *o*:*m*:*p* ratio was determined to be 5:2:10 by Loebl, Stein and Weiss[4] using 200 kv. X-rays and 9:5:4 by Downes[5] using Co^{60} γ-rays.

Experimental

Water from a commercial still was redistilled from alkaline $KMnO_4$ in an all Pyrex glass apparatus which incorporated a splash column. Calcium benzoate as the monohydrate (judged by wt. loss on heating) was prepared by mixing solutions of reagent grade calcium chloride and sodium benzoate, followed by repeated recrystallization of the calcium benzoate from aqueous solution. The *o*-, *m*- and *p*-hydroxybenzoic acids were reagent grade materials recrystallized from aqueous solution and dried. Benzoic acid was Hopkin and Williams P.V.S. grade. Cyclohexane was Brickman spectro-grade. All other materials were reagent grade and were used without further purification. The apparatus was cleaned using fresh chromic acid solutions and then repeated rinsings with doubly distilled water and, except for pipets and optical cells, a final steaming with steam freed from organic impurities.

Degassing of solutions where required was effected in a high vacuum system by means of a number of cycles of freezing with Dry Ice–acetone, pumping, melting and shaking. Where gas analyses were required in oxygenated solutions, oxygen (freed from CO_2) at a known pressure was introduced above the degassed solutions, which were allowed to equilibrate overnight prior to irradiation. Sample volumes varied from 3 to 10 ml., except where CO_2 and H_2 analyses were required, when they were 50 ml.

The *o*-hydroxybenzoic acid in an irradiated calcium benzoate solution was determined from the fluorescence of the unbuffered solution at 400 mμ which is excited by 295 mμ radiation.[2] The *meta* isomer was determined from the increase in the 400 mμ fluorescence (excited at 295 mμ) produced on adjusting the solution *p*H to 12.[6] The *para* isomer in the same solution was also determined at *p*H 12 from the fluorescence at 325 mμ excited by 285 mμ radiation. At the concentrations produced on irradiation the fluorescence intensity of a particular isomer was found to be unaffected by the presence of the other isomers. Consequently the concentration of an hydroxy acid in an irradiated sample could be derived from its fluorescence intensity relative to that of a single standard. All standard solutions of *o*-, *m*- and *p*-hydroxybenzoic acids were made up using doubly distilled water and contained the appropriate concentration of calcium benzoate. The hydroxy acid concentration of each standard was adjusted so that its fluorescence intensity was within a factor of two of the fluorescence intensity of the irradiated sample being analyzed. This was considered adequate on account of the linearity of the plots of concentration against intensity of fluorescence.

For benzoate ion analyses, use was made of the fact that in acid solution benzoic acid is weakly fluorescent. Since the intensity of fluorescence is a linear function of concentration below 10^{-5} *M*, the solutions were diluted by a factor of 25 prior to the fluorescence measurements at 315 mμ, which were carried out in 0.18 *M* H_2SO_4 with 235 mμ exciting radiation. Under these conditions there is negligible interference from the hydroxybenzoic acids and phenol present. The concentration of benzoate ion in an irradiated solution is given by

$$[Bz^-]_R = \frac{I_R - I_B}{I_0 - I_B} \times [Bz^-]_0$$

where $[Bz^-]_0$ is the concentration of benzoate ion in the unirradiated sample; and I_R, I_0 and I_B are the fluorescence intensities of the irradiated sample, unirradiated sample and solvent, respectively.

Standard aqueous phenol solutions were made up by dilution of a stock 10^{-2} *M* solution which had been standardized by the conventional bromine method.[7] Phenol analyses involved extraction of irradiated and unirradiated calcium benzoate solutions and standard aqueous phenol solutions with diethyl ether, followed by fluorescence measurements

(1) Issued as D.R.C.L. Report No. 316.

(2) W. A. Armstrong and D. W. Grant, *Nature*, **182**, 747 (1958).

(3) W. A. Armstrong and D. W. Grant, *Can. J. Chem.*, in press.

(4) H. Loebl, G. Stein and J. Weiss, *J. Chem. Soc.*, 405 (1951).

(5) A. M. Downes, *Australian J. Chem.*, **11**, 154 (1958).

(6) G. A. Thommes and E. Leininger, *Anal. Chem.*, **30**, 1361 (1958).

(7) "Scott's Standard Methods of Chemical Analysis," (N. H. Furman, Editor), D. Van Nostrand Co., Inc., New York, N. Y., 1939, Vol. 2, p. 2253.

Table I

Excitation (λ_A) and Fluorescence (λ_F) Bands of Possible Radiolytic Products from Aqueous Benzoate Solutions

Compound	λ_A, mμ	λ_F, mμ	Conditions for fluorescence Maximum	Minimum	Fluorescence relative to o-$HOC_6H_4COO^-$ at 400 mμ[a] λ_F[b]	
o-HOC_6H_4COOH (un-ionized)	305	435	Acid	Alkaline		
o-HOC_6H_4COOH (1st ionization)	295	400	Neutral	Acid	1.0	1.0
m-HOC_6H_4COOH	300	420	Alkaline	Neutral, acid		0.75
p-HOC_6H_4COOH	285	325	Alkaline	Neutral, acid		.08
2,3-$(HO)_2C_6H_3COOH$[c]	305	440	Neutral	Acid, alkaline		
2,4-$(HO)_2C_6H_3COOH$	290	390	Neutral	Acid, alkaline	0.25	.3
2,5-$(HO)_2C_6H_3COOH$	315	440	Neutral	Acid, alkaline	.18	1.1
2,6-$(HO)_2C_6H_3COOH$[c]	340–370	455	Alkaline	Acid, pH 14		
3,4-$(HO)_2C_6H_3COOH$[c]	300	370	Alkaline	Acid, pH 14		
C_6H_5OH	270 220	295	Acid	Alkaline		0.7 0.1
$C_6H_5C_6H_5$	250	310	Independent of acidity			1.0
4-$C_6H_5C_6H_4COOH$[d]	280	360	Acid	Alkaline	.21	12
4,4′-$HOOCC_6H_4C_6H_4COOH$[e,f] (dimethyl ester)	280					

[a] For unbuffered 10^{-6} M solutions with λ_A at 295 mμ. [b] For 10^{-6} M solutions at pH and λ_A for maximum fluorescence. [c] Data from American Instrument Co., Inc., Bulletin No. 2278 (1958). [d] Only biphenylcarboxylic acid available for testing. [e] Solvent alcohol; for others, water. [f] Data from B. Williamson and W. H. Rodebush, *J. Am. Chem. Soc.*, **63**, 3018 (1941).

at 295 with 220 mμ exciting radiation. However, it was found that hydrogen peroxide and hydroxybenzoic acids were present in the ether extracts in amounts sufficient to quench partially the phenol fluorescence. The required corrections were determined from measurements of the fluorescence of ether extracts of standard calcium benzoate–phenol solutions with and without added o-hydroxybenzoic acid and hydrogen peroxide. The amounts of o-hydroxybenzoic acid and hydrogen peroxide added were based on G-values of 1.5 ($G_{ortho} + G_{meta} + G_{para}$) and 2.5, respectively (see Table II).

Hydrogen peroxide in irradiated solutions was determined by the Ghormley method.[8] The molar extinction coefficient of the triiodide ion at 350 mμ was taken to be 2.54×10^4—mean of values quoted in references 8 and 9. The analytical method was found to yield the same results in the presence and absence of (10^{-2}–10^{-4}) M benzoic acid. The observed peroxide concentrations in irradiated solutions were unaffected by a ten-fold increase in their salicylic acid concentrations prior to analysis.

For gas analyses, irradiated solutions were degassed by means of a Toepler pump which delivered the gaseous mixture into a gas buret. Circulation of the gas around a trap, cooled with liquid N_2 to remove CO_2, was effected by raising and lowering the mercury in the Toepler pump. After pumping off the uncondensed gas the liquid N_2 refrigerant was replaced with a Dry Ice–acetone mixture, and the CO_2 liberated was transferred to the gas buret for measurement. The slight decrease in pressure, after ignition on a Pt filament, of the uncondensed gas from irradiated degassed solutions was presumed to derive from the presence of small amounts of O_2 in addition to H_2. The residual gas, assumed to be H_2, was corrected for the amount of H_2 consumed during ignition.

Optical measurements usually were made in 1 cm. quartz cells, but in the case of deaerated solutions the fluorescence measurements were taken directly in the cylindrical Pyrex irradiation vessels. Fluorescence and optical absorption measurements were made using a Bowman–Aminco spectrophotofluorometer and a Cary recording spectrophotometer, respectively.

These various radiations were employed: γ-rays from 2 curies of Cs^{137} and 200 curies of Co^{60}, X-rays from a 3 Mev. Van de Graaff generator and a 300 kv. Muller X-ray machine. All dose rates were determined using the Fricke dosimeter,[9,10] assuming $G_{Fe^{+++}}$ in 0.8 N H_2SO_4 to be 14.5 for unfiltered 300 kv. peak X-rays and 15.5 for all other radiations employed. The dose rates in water solutions were computed from those in 0.8 N H_2SO_4 using the appropriate density correction.

Results

After irradiation aerated unbuffered solutions of calcium benzoate and benzoic acid exhibited a fluorescence band at 400 mμ with an excitation band at 295 mμ. This fluorescence band disappeared on addition of acid (to pH < 1) and a new weak fluorescence band appeared at 435 mμ with its excitation band at 305 mμ. The wave lengths of these excitation and fluorescence bands are identical with those recorded for singly ionized and un-ionized o-hydroxybenzoic acid (Table I). On addition of alkali to irradiated solutions (to pH 12) the fluorescence at 400 mμ increased by about 40%, and a new band appeared at about 325 mμ excited by 285 mμ radiation. The increased fluorescence with an accompanying slight shift in the position of the peak wave length to 410 mμ is presumed to be due to the contribution from the *meta* isomer, while the new fluorescence band at 325 mμ is consistent with the presence of the *para* isomer (Table I).

The presence of the 2,3-, 2,4- and 2,5-dihydroxybenzoic acids would interfere with the analysis of the o-hydroxy acid, while the presence of the 3,4-dihydroxybenzoic acid would interfere with the analysis of the m-hydroxy acid (Table I). However, at the very low benzoate conversions produced (≯ 1%), the dihydroxy acids, presumably secondary products, would be expected to be present in much lower concentrations than the primary hydroxy acids. The results in Table I indicate that in the case of the 2,4- and 2,5-isomers the interference would be negligible provided their concentrations are at least an order of magnitude smaller than the concentration of the o-hydroxy acid. The presence of 2×10^{-5} M phenol was found to decrease the fluorescence of 2×10^{-5} M p-hydroxybenzoic acid at 325 mμ (λ_A at 285 mμ) by about 5% at pH 12. However, it will be shown later that phenol, a possible primary decarboxylation product, is formed in very small yield. Evidence will be presented also that biphenyl and the biphenylcarboxylic acids if produced are present in small yield.

(8) C. J. Hochanadel, This Journal, **56**, 587 (1952).

(9) A. O. Allen, C. J. Hochanadel, J. A. Ghormley and T. W. Davis, *ibid.*, **56**, 575 (1952).

(10) J. Weiss, A. O. Allen and H. A. Schwarz, *Proc. Int. Conf. Peaceful Uses of Atomic Energy*, **14**, 179 (1955).

TABLE II

G-YIELDS[a] OF RADIOLYTIC PRODUCTS

Benzoate, $M \times 10^4$	pH	Radiation	Dose, e.v./ml. $\times 10^{-16}$	Dose rate, e.v./ml./min. $\times 10^{-14}$	*G*-Yields $C_6H_4(OH)COO^-$ *o*-	*m*-	*p*-	H_2O_2	CO_2	H_2	PhOH	$-PhCOO^-$	% C balance
2.4[b,d]	6.0	Cs^{137} γ	7	2.65	0.61	0.37	0.37		0.61[i]		(0.05)	2.05[j]	99.5
2.4[b,d]	6.0	Cs^{137} γ	7	2.65	.59	.34	.35		.64[i]		(.05)	2.05[j]	96
12[b,d]	6.5	Co^{60} γ	7–25	43.8	.67[g]	.37[g]	.37[g]		.73[i]		(.05)	2.6[i] (2.3)[k]	84 (95)
12[b,d]	6.5	3 Mev. X	7–20	11,200	.59[g]	.36[g]	.36[g]						
12[b,d]	6.5	3 Mev. X	8–22	30,000	.53[g]	.35[g]	.35[g]						
2.4[b,e]	6.0	Cs^{137} γ	50	2.65	.070	.018	.22						
2.4[b,e]	6.0	Cs^{137} γ	50	2.65	.039[g]	.016	.18						
2.4[b,e]	6.0	Cs^{137} γ	50	2.65	.036	.024	.11						
100[c,d]	6.5	Co^{60} γ	36–190	900				2.3[5][h]					
100[b,d]	6.5	Co^{60} γ	36–180	900				2.5[5][h]					
10[b,d]	6.5	Co^{60} γ	36–180	900				2.3[0][h]					
10[c,f]	0.4	300 kv. peak	166–290	830					.68				
10[c,e]	.4	300 kv. peak	291	830					.43	0.62			
10[c,e]	.4	300 kv. peak	430	830					.40	0.55			
20[b,d]	6.5	Co^{60} γ	90–270	900							.05		

[a] Molecules/100 e.v. [b] Ca salt. [c] Benzoic acid. [d] Aerated. [e] Degassed. [f] pO_2 = 15 cm. [g] Slope of linear concn. *vs.* dose plot. [h] Initial slope of curve in Fig. 1. [i] Ref. 5. [j] Co^{60} dose rate = 9×10^{16} e.v./ml./min. [k] See discussion. [l] (o + m + p + PhOH + CO_2)/$-PhCOO^-$.

Removal of air prior to irradiation markedly reduces the *G*-yields (molecules/100 e.v.) of the hydroxybenzoic acids (Table II). However, the concentrations of the *ortho* isomer formed at a number of doses were not reproducible and in all experiments except one (Table II) extrapolation to zero dose resulted in a positive intercept on the vertical axis. These results can be explained on the basis of inadequate deoxygenation of the solutions. Apparently on deoxygenation the yield of the *p*-hydroxybenzoic acid is not reduced to the same extent as the yields of its isomers (Table II). However, it must be admitted that some doubt regarding the accuracy of the analyses in deoxygenated solutions exists, since the fluorescence bands of the biphenyldicarboxylic acids, presumably the major products, are unknown. It is noteworthy that for 1.2×10^{-3} *M* benzoate solutions there is a distinct decrease in the yields of all hydroxy acids with increasing dose rate (Table II).

For gaseous product studies benzoic acid was used rather than calcium benzoate, since solutions of the latter may contain some carbon dioxide fixed as carbonate ion. The solutions were irradiated with 300 kv. peak unfiltered X-radiation because fairly large doses, *i.e.*, (1–4) $\times 10^{18}$ e.v./ml., were required for accurate gas analysis, and a high intensity γ-source was not available at the time. As Downes[5] measured carbon dioxide yields in benzoate solutions over the *p*H range 4–9 it was decided to carry out the experiments in sulfuric acid solutions. A chromatographic analysis (a silica gel column at ambient temperature using He carrier gas) of the gas from irradiated oxygenated 10^{-3} *M* benzoic acid solutions in 0.36 *M* sulfuric acid revealed the presence of carbon dioxide, oxygen and hydrogen only. The amount of carbon dioxide in oxygenated solutions increases linearly with dose, and at two doses is significantly greater than that produced in degassed solutions (Table II).

Since hydrogen peroxide is known to be susceptible to decomposition by trace metal impurities it seemed desirable to compare the peroxide yields in calcium benzoate and benzoic acid solutions at the same *p*H. Prior to irradiation each benzoic acid solution was adjusted using sodium hydroxide to a *p*H of 6.5, *i.e.*, the *p*H of the calcium benzoate solutions. The *G*-yields of hydrogen peroxide decrease with increasing dose, the decrease being more pronounced at the lower benzoate ion concentration (Fig. 1). At a given dose the peroxide concentration in 10^{-2} *M* benzoic acid is always slightly lower than that in 5×10^{-3} *M* calcium benzoate (Fig. 1).

In order to obtain measurable changes in benzoate concentration at relatively low doses (thereby avoiding solution deoxygenation), dilute (10^{-4} *M*) calcium benzoate solutions were used in the determination of G_{-Bz}, the uptake yield of benzoate ion. The results indicate that G_{-Bz} is independent of dose up to about 20% conversion.

Phenol was identified in ether extracts of irradiated calcium benzoate solutions from its fluorescence at 295 mμ which was excited by 220 mμ and (260–280) mμ radiation. The position of the major excitation band 270 mμ could not be observed owing to the high intensity of scattered light. The phenol concentration increased linearly with dose for aerated 10^{-3} *M* calcium benzoate solutions irradiated with Co^{60} γ-rays.

On addition of alkali, irradiated aerated benzoate solutions were observed to turn yellow, the color change being characterized by the appearance of an absorption band at (365–370) mμ. In neutral solutions the band is at 355 mμ with a much reduced extinction, while in acid solutions (*p*H < 1) the band no longer exists. Although the yellow color can be restored by making the solution alkaline again, the band exhibits a slightly reduced extinction. This behavior is indicative of the presence of unstable acidic material. The shape of the plot of optical density against dose suggests that a primary product is responsible for the absorption. The material is not detectable in irradiated solutions of *o*-, *m*- and *p*-hydroxybenzoic acids. Since the optical density at 350 mμ of the unidentified product is approximately 2% of that exhibited by the triiodide ion in the hydrogen

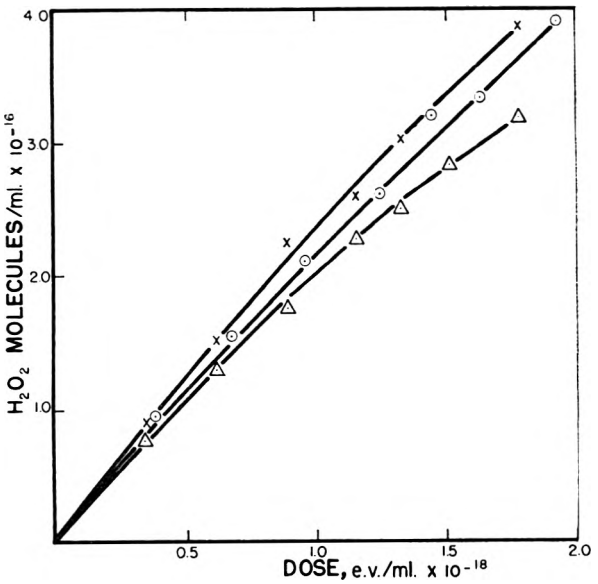

Fig. 1.—Formation of hydrogen peroxide in aerated benzoate solutions irradiated with Co^{60} γ-rays: ⊙, 10^{-2} M benzoic acid; ×, 5×10^{-3} M calcium benzoate; △, 5×10^{-4} M calcium benzoate; all points are the average of three determinations.

peroxide analyses, the peroxide yields recorded in Fig. 1 are probably about 2% high. The results in Table II have been corrected accordingly. Attempts to isolate enough material for identification were unsuccessful.

Ether extracts of irradiated calcium benzoate solutions which had been made strongly alkaline prior to extraction were refluxed for about 30 minutes and then neutralized with alcoholic acid. These extracts were found to exhibit fluorescence at 295 mμ (λ_A at 220 mμ) of about the same intensity as extracts which had been similarly treated but not refluxed. These results are taken as evidence that negligible amounts of phenyl esters are produced during irradiation.

One hundred ml. of aerated 10^{-3} M calcium benzoate was given a dose of about 2×10^{20} e.v. with Co^{60} γ-rays, made alkaline and extracted with 50 ml. of cyclohexane. An examination of the ultraviolet spectrum of the cyclohexane extract in a 10-cm. optical cell revealed broad absorption from 240 to 250 mμ with three weak absorption bands at 245, 250 and 261 mμ. From the optical density (0.22) and the extinction coefficient of diphenyl[11] at 250 mμ it was deduced that in the irradiated solution the yield of diphenyl G_{Ph_2}, if present, could not have exceeded a value of 0.01.

No fluorescence characteristic of 4-biphenylcarboxylic acid was detected in Co^{60} γ-irradiated (2.5×10^{18} e.v./ml.) aerated 10^{-3} M benzoic acid and calcium benzoate solutions, which after irradiation had been diluted by a factor of 20 to prevent fluorescence quenching (of the biphenyl acid) by benzoate, and acidified (pH < 1) to suppress salicylate ion fluorescence. Since a concentration of the biphenylcarboxylic acid as low as 2×10^{-9} M could be detected at the same pH and benzoate concentrations, it was deduced that the G-yield of this acid, if formed, is less than 0.001.

A fluorescence at (350–370) mμ excited by 280 mμ radiation was observed only in degassed benzoate solutions. This fluorescence may well be due to the presence of the biphenylcarboxylic acids, since they have absorption bands at 280 mμ (Table I).

Discussion

Since hydrogen peroxide at the concentrations produced in the radiolysis was found to exert no hydroxylating effect on aqueous benzoate ion solutions, it may be assumed that the formation of the hydroxybenzoic acids results from the action of free radicals. Possible reactions include

$$H_2O \rightsquigarrow H_2,\ H_2O_2,\ OHH \quad (1)$$

$$OH + C_6H_5COO^- \longrightarrow \cdot C_6H_4COO^- + H_2O \quad (2)$$

$$OH + \cdot C_6H_4COO^- \longrightarrow HOC_6H_4COO^- \quad (3)$$

$$H + O_2 \longrightarrow HO_2 \quad (4)$$

$$2HO_2 \longrightarrow H_2O_2 + O_2 \quad (5)$$

$$H + \cdot C_6H_4COO^- \longrightarrow C_6H_5COO^- \quad (6)$$

Reactions 4, 5 and 6 are included to explain the lower yields of the hydroxy acids in degassed solutions (Table II). The reaction scheme outlined is inadequate since it requires that in aerated solution the total yield of hydroxy acids does not exceed $G_{OH/2}$ or 1.0.[12] It is possible that in aerated solutions reaction 3 is replaced by

$$\cdot C_6H_4COO^- + O_2 \longrightarrow \cdot O_2C_6H_4COO^- \quad (7)$$

The subsequent reactions of the peroxy radical leading to the formation of the hydroxy acids are obscure. It has been suggested[13,14] that phenol formation in irradiated aerated benzene solutions involves a hydrolysis of the $C_6H_5O_2\cdot$ radical. Although such a step has been criticized[15] on the grounds of probable endothermicity, this question cannot be resolved without precise knowledge of the dissociation energies of the bonds involved.

Any mechanism for the radiolysis must explain the observed decrease in the yields of the hydroxy acids with increase in dose rate (Table II). The effect cannot be associated with a decreased hydroxyl radical yield due to overlap of tracks, since such effects are observed[16] only at dose rates higher by at least three orders of magnitude than the highest dose rate used. Furthermore, since the *initial* yield is dependent on dose rate, the effect cannot be attributed to oxygen depletion in the solutions irradiated at high dose rates. It is possible that at high dose rates some dimerization of the radical precursors of the hydroxy acids occurs even in the presence of oxygen, *viz.*

$$2 \cdot C_6H_4COO^- \longrightarrow {}^-OOCC_6H_4 \cdot C_6H_4COO^- \quad (8)$$

All the carbon dioxide evolved must come from the carboxyl group, since the value 0.68 determined for G_{CO_2} is in excellent agreement with the value 0.73 ± 0.03 reported by Downes[5] for Co^{60} γ-ir-

(11) R. A. Friedel and M. Orchin, "Ultraviolet Spectra of Aromatic Compounds," John Wiley and Sons, Inc., New York, N. Y., 1951, gives $\epsilon_{Ph_2} = 1.59 \times 10^4$ at 250 mμ in cyclohexane.

(12) C. J. Hochanadel and S. C. Lind, *Ann. Rev. Phys. Chem.*, **7** 83 (1956).

(13) T. J. Sworski, *Rad. Res.*, **1**, 231 (1954).

(14) P. V. Phung and M. Burton, *ibid.*, **7**, 199 (1957).

(15) N. Uri, "Progress in Radiobiology," J. S. Mitchell, B. E. Holmes and C. L. Smith, editors, Oliver and Boyd, Edinburgh, 1956, p. 99.

(16) H. C. Sutton and J. Rotblat, *Nature*, **180**, 1332 (1957).

radiated aerated solutions of [carboxy C^{14}] benzoic acid and its sodium salt. If the reasonable assumption is made that HO_2 does not abstract hydrogen atoms from the carboxyl group then there is evidence that hydrogen atoms do not participate in the decarboxylation process. If they did, then G_{CO_2} would depend on the relative concentrations of oxygen and benzoate ion, *i.e.*, in aerated solutions G_{CO_2} would be expected to increase with increasing benzoate ion concentration. Yet over the concentration range (5×10^{-4} -7×10^{-3}) M G_{CO_2} remains constant.[5] Furthermore, G_{CO_2} is *lower* in degassed solutions (Table II). The most probable reaction involving the carboxyl group is

$$OH + C_6H_5COO^- \longrightarrow OH^- + C_6H_5COO\cdot \quad (9)$$

However, there is abundant evidence to show that little carbon dioxide actually results from a direct decomposition of the benzyloxy radical

$$C_6H_5COO\cdot \longrightarrow C_6H_5\cdot + CO_2 \quad (10)$$

Since few phenyl radicals thus produced finish up as phenol or diphenyl, the possibility that they might react with the benzoate ion to form biphenylcarboxylic acids was considered. There is direct evidence that the 4-biphenylcarboxylic acid, if formed, is produced in negligible yield (results section). Furthermore, the presence of 10^{-4} M calcium benzoate was found to have no effect on the phenol yield from irradiated aerated 10^{-2} M benzene solutions. This result is taken as evidence that phenyl radicals react with oxygen at a very much faster rate than they react with benzoate ions. Therefore, the low phenol yield in aerated benzoate solutions might be attributed to a slow reaction 10, in accord with its high activation energy of 14 kcal./mole.[17]

From the chromatograms[5] of irradiated aerated solutions of [carboxy^{14} C] benzoic acid and [$^{14}C_7$] benzoic acid it appears that some decarboxylation products have low R_F values in 1-butanol saturated with 5 N ammonium hydroxide. A spectrophotometric analysis revealed that the species absorbing at 350–370 mμ would remain almost exclusively in an aqueous phase rather than in a 1-butanol–ammonia phase, indicating that the species would be found in the low R_F region of the chromatograms. The apparent absence of a chromatographic band with R_F of 0.93[18] in the butanol–ammonia solvent system is in accord with the low phenol yield found in the present investigation.

The yield of hydrogen gas from degassed benzoic acid solutions *i.e.*, $G_{H_2} \simeq 0.6$ (Table II) is in fair agreement with a reported[19] value of 0.45 ± 0.02 for the "molecular" hydrogen yield using 250 kv. X-rays. This result supports the view[14] that hydrogen atom abstraction by the hydrogen atoms is not important in the radiolysis of aromatic compounds in aqueous solution.

The curvature of the hydrogen peroxide concentration dose plots (Fig. 1) at high benzoate ion concentrations is probably due to a chain decomposition of peroxide with the O_2^- ion[20] as a chain propagator. The maximum initial peroxide yield expected on the basis of the "molecular" peroxide yield of 0.8[12] and the hydrogen atom yield of 2.75[12] would be about 2.2, indicating that peroxide is formed in reactions in addition to (1) and (5). Although the observed peroxide yields (Table II) appear to preclude a mechanism for the formation of the hydroxy acids involving hydrolysis of a peroxy radical, *viz.*

$$\cdot O_2C_6H_4COO^- + H_2O \longrightarrow HOC_6H_4COO^- + HO_2$$

the possibility that some hydrogen peroxide (or its precursor) is used up in reactions leading to decarboxylation cannot be overlooked.

Adopting Downes'[5] value of 0.64 for G_{CO_2} and assuming that the phenol yield does not change appreciably with benzoate ion concentration, good carbon balance is obtained between the yields of radiolytic products and benzoate ion consumed in 2×10^{-4} M solutions (Table II). Downes'[5] value of 1.8 for G_{-Bz} at this concentration is probably lower than the initial yield, since at the dose he used almost 60% of the benzoic acid is converted into products. At high benzoate ion concentrations the carbon balance based on Downes' value of 2.6 for G_{-Bz} is unsatisfactory (Table II). However, since G_{-Bz}[5], G_{CO_2}[5] and the yield of *o*-hydroxybenzoic acid[3] attain limiting values at a benzoate concentration of about 10^{-3} M, it seems reasonable to assume a similar concentration dependence for all these yields. On this basis, in 10^{-3} M solutions G_{-Bz} would be about 2.3, and a better carbon balance is obtained (Table II).

The 45:27:28 ratio for $G_o:G_m:G_p$ (average of yields in Table II) obtained in the present investigation is in fair agreement with the 9:5:4 ratio reported by Downes[5] for Co^{60} γ-irradiated aerated 1.15×10^{-3} M benzoic acid solutions. The agreement is particularly gratifying considering the widely different methods of analysis employed. Boyland and Sims[21] obtained a value of 2:1:1 for the ratio of $o:m:p$ yields in aqueous benzoic acid–hydrogen peroxide solutions irradiated with ultraviolet radiation. Bates and Uri[22] determined $o:m:p$ to be 2:2:1 in aqueous solutions of benzoic acid subjected to the action of hydroxyl radicals photochemically generated from the ferric ion-pair complex Fe^{3+} OH^-. The latter ratio indicates that the main factor determining the site of the nuclear attack by the hydroxyl radical is the number of available nuclear sites. However, in our opinion, their rather involved spectrophotometric analytical method is unlikely to furnish results of high accuracy. Thus $o:m:p$ ratios in aqueous benzoate solutions support the view[23] that aromatic substitution by free radicals occurs predominantly at the *ortho* position.

Acknowledgment.—The authors wish to thank Mr. F. A. Bury for help with experiments requiring the use of the Van de Graaff generator.

(17) J. C. Bevington and J. Toole, *J. Polymer Sci.*, **28**, 413 (1958).

(18) R. J. Block, E. L. Durrum and G. Zweig, "A Manual of Paper Chromatography and Paper Electrophoresis," Academic Press, Inc., New York, N. Y., 1958, p. 308.

(19) M. H. Back and N. Miller, *Nature*, **179**, 321 (1957).

(20) M. Ebert and J. W. Boag, *Disc. Faraday Soc.*, **12**, 189 (1952).

(21) E. Boyland and P. Sims, *J. Chem. Soc.*, 2966 (1953).

(22) H. G. C. Bates and N. Uri, *J. Am. Chem. Soc.*, **75**, 2754 (1953).

(23) For a recent review of homolytic aromatic substitution see D. R. Augood and G. H. Williams, *Chem. Revs.*, **57**, 123 (1957).

ULTRAVIOLET SPECTRA AND STRUCTURES OF 2,2′-BIPYRIDINE AND 2,2′,2″-TERPYRIDINE IN AQUEOUS SOLUTION[1]

BY KAZUO NAKAMOTO

Department of Chemistry, Clark University, Worcester, Mass.

Received March 10, 1960

The ultraviolet spectra of 2,2′-bipyridine and 2,2′,2″-terpyridine obtained at various *p*H values in aqueous solutions are compared with those of the metal-chelate compounds and with those of the ligands in organic solvents. It is found that, in basic solution as well as in organic solvents, the molecules are *trans* and *trans–trans* whereas, in acidic solutions, the *cis* and *cis–cis* forms predominate in 2,2′-bipyridine and 2,2′,2″-terpyridine, respectively. The *cis–trans* form is also found for 2,2′,2″-terpyridine at an intermediate *p*H. The existence of small twists along the central carbon–carbon bonds is suggested for these species. No positive evidence is found for intramolecular N^+—H · · · N hydrogen bonds in the protonated species.

Introduction

Although many studies have been made on the ultraviolet spectra and ionization constants of 2,2′-bipyridine and its derivatives, the configuration of the molecule in solution has not yet been reported. The following *trans* and *cis* forms are probable in 2,2′-bipyridine. The result of X-ray

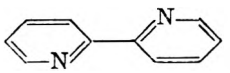

trans (Ia)

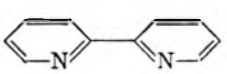

cis (Ib)

analysis[2] definitely indicates that the molecule has a *trans*-planar configuration in the crystalline state. It was also shown by the measurement of dipole moment that the molecule in solution is *trans* although small twisting around the central carbon–carbon bond was suggested.[3] The lack of information on the *cis* form may be due to the fact that the *trans* form is more stable.[4] Although the *cis* form has not yet been observed, the chelated-*cis* form undoubtedly exists in the metal chelate compounds of 2,2′-bipyridine.[5]

The following three configurations are probable in 2,2′,2″-terpyridine. As in the case of 2,2′-bipyridine, the *trans–trans* form (IIa) of minimum dipole moment is expected to be most stable. In the metal–chelate compounds, however, the molecule is planar *cis–cis* as is shown by the X-ray analysis on [Zn(trpy)Cl]Cl.[6]

The purpose of this work is to investigate the structures of the species predominant at various *p*H values in aqueous solutions mainly based on the ultraviolet spectra. Although the ultraviolet spectra of various isomers of phenylpyridines,[7,8] biphenylpyridines,[8] bipyridines[7] and phenanthrolines[7] have already been measured, no studies such as mentioned above have been attempted.

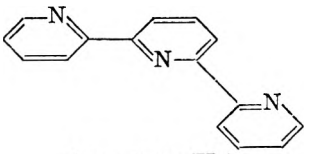

trans–trans (IIa)

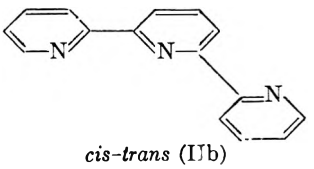

cis–trans (IIb)

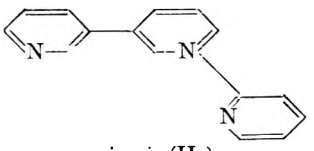

cis–cis (IIc)

Experimental

Materials.—2,2′-Bipyridine was purchased from Eastman Organic Chemicals, Rochester, N .Y., and was recrystallized from ethanol solution; colorless crystal, m.p. 70°. 2,2′,-2″-Terpyridine was purchased from G. F. Smith Chemical Co., Columbus, Ohio, and was recrystallized from ether solution; pale yellow crystal, m.p. 89°.

So far no complete descriptions of the hydrochlorides of these compounds are available in the literature. In order to determine the combining ratios between these bases and hydrochloric acid in the crystalline state, we have prepared the hydrochlorides and determined their chemical composition by analysis. Besides the above two bases, 1,10-phenanthroline hydrochloride was also prepared for comparison. All the hydrochlorides were prepared by saturating hydrogen chloride to ether solution of the base. They were dried for five days in a phosphorus pentoxide desiccator.

2,2′-Bipyridine Dihydrochloride: colorless crystal, m.p. 150∼155°. *Anal.* Calcd. for $C_{10}H_{10}Cl_2N_2$: C, 52.43; H, 4.40; N, 12.22; Cl, 30.95. Found: C, 52.64; H, 4.68; N, 12.20; Cl, 30.09.

1,10-Phenanthroline Monohydrochloride Monohydrate: colorless crystal, m.p. 175∼180°. *Anal.* Calcd. for $C_{12}H_{11}N_2ClO$: C, 61.42; H, 4.72; N, 11.93; Cl, 15.11. Found: C, 61.08; H, 4.74; N, 12.30; Cl, 15.15.

2,2′,2″-Terpyridine dihydrochloride monohydrate: pale yellow crystal m.p. 180∼185°. *Anal.* Calcd. for $C_{15}H_{15}N_3Cl_2O$: C, 55.57; H, 4.66; N, 12.96; Cl, 21.87. Found: C, 55.17; H, 4.83; N, 13.05; Cl, 21.90.

As to the hydrochloride of 2,2′,2″-terpyridine, Morgan and Burstall[9] previously reported the trihydrochloride of the composition $C_{15}H_{22}N_3Cl_3O_4$ (Cl, 25.8%), which is colorless and decomposes at 280∼285°. Thus their compound seems to be different from ours. Preparation was repeated several times by changing the conditions. However, we could not obtain the hydrochloride of such a high chlorine content as they found.

(1) This investigation was partly supported by a research grant, H-3246, from the National Heart Institute, Public Health Service.

(2) L. L. Merritt, Jr., and E. D. Schroeder, *Acta Cryst.*, **9**, 801 (1956).

(3) P. E. Fielding and R. J. W. LeFevre, *J. Chem. Soc.*, 1811 (1951); the twisting angle was estimated to be at most 28° based on the observed dipole moment, 0.9 *D*. This result is, however, difficult to understand since no sericus hydrogen repulsion is seen in the *trans*-planar form.

(4) G. H. Stewart and H. Eyring, *J. Chem. Educ.*, **35**, 550 (1958).

(5) H. J. Dothie, F. J. Llewellyn, W. Wardlaw and A. J. E. Welch *J. Chem. Soc.*, 426 (1939).

(6) D. E. C. Corbridge and E. G. Cox. *ibid.*, 594 (1956).

(7) P. Krumholz, *J. Am. Chem. Soc.*, **73**, 3487 (1951).

(8) A. E. Gillam, D. H. Hey and A. Lambert, *J. Chem. Soc.*, 364 (1941).

(9) G. Morgan and F. H. Burstall, *ibid.*, 1649 (1937).

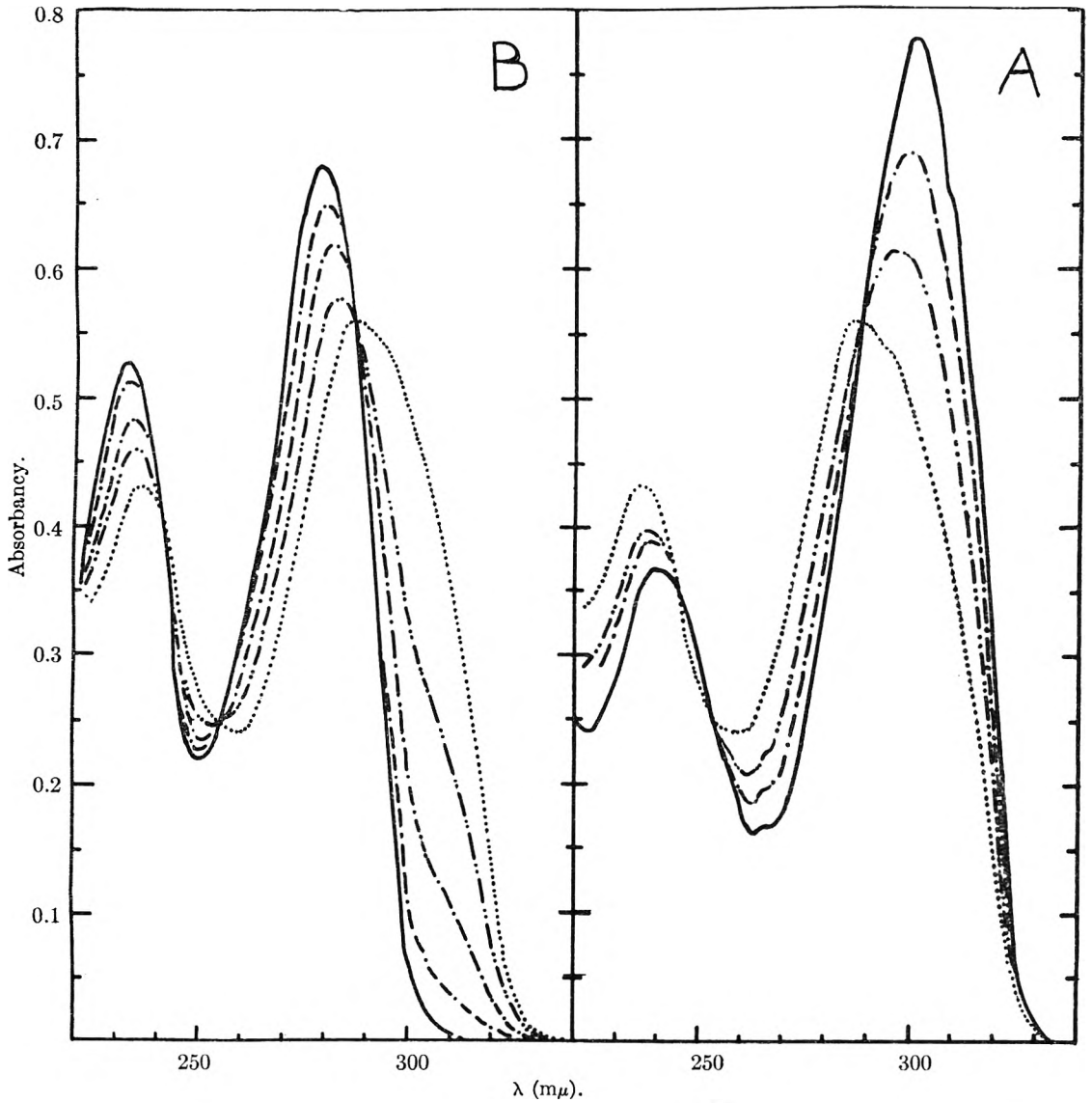

Fig. 1.—Absorption spectra of 2,2′-bipyridine in buffer solutions (5×10^{-5} mole/l.): A, in acidic solutions; —, *p*H 1.80; – ·—·, 3.63; —··—··, 4.02; ·····, 4.40. B, in neutral and basic solutions; ·····, 4.40; —··—··, 4.78: — ·– ·, 5.23; – —·— —·, 5.80: —, 9.15 ~ 12.05.

The metal chelate compounds of 2,2′-bipyridine and 2,2′,-2″-terpyridine were prepared according to the literature.[9]

Potentiometric Titration.—Approximately 2×10^{-3} mole/l. solution of terpyridine hydrochloride in 0.1 *M* KCl solution was titrated with 0.1 *N* NaOH solution. A sharp inflection was observed at 2 moles of base per mole of ligand.[10] *p*H measurements were made at 35° with a Beckman Model GS *p*H meter fitted with extension glass and calomel electrodes. The *p*H readings were calibrated with acetic acid buffer and with standard hydrochloric acid and sodium hydroxide solutions. Approximate *pK* values were estimated from the titration curve using Schwarzenbach and Ackermann's method.[11] The *pK* values of the first and second ionization were 2.59 and 4.16, respectively.

Spectral Measurements.—The ultraviolet spectra were measured at 20° with a Cary Model 14 spectrophotometer. A pair of 1 cm. quartz cells were used. With the exception of ethanol, organic solvents were of "spectro-grade" quality purchased from Eastman Organic Chemicals. The buffer solutions were: *p*H 0, 1 *N* HCl; 1.0~2.2, HCl + KCl; 3.6~5.4, CH_3COOH + CH_3COONa; 6.0~8.0, NaOH + KH_2PO_4; 8.9~11.4, $NaHCO_3$ + Na_2CO_3; 12.0~14.0 NaOH. The ionic strength was maintained approximately at 0.2 for most of the solutions. The infrared spectra were obtained by a Perkin–Elmer Model 21 infrared spectrophotometer equipped with a sodium chloride prism. The potassium bromide disk method was employed to obtain the spectra in the crystalline state.

(10) Same result was obtained by W. W. Brandt and J. P. Wright, THIS JOURNAL, **76**, 3082 (1954). However, they reported only the geometrical average value of pK_I and pK_{II} (7.1) for this compound.

(11) G. Schwarzenbach and H. Ackermann, *Helv. Chim. Acta*, **30**, 1798 (1947).

Results and Discussion

I. 2,2 -Bipyridine.—Figure 1 indicates the ultraviolet spectra of 2,2-bipyridine at *p*H values ranging between 1.8 and 12. In basic solution, two bands appear at 279 and 232 mμ. As is seen in Fig. 2, the spectrum in basic solution is very similar to those in organic solvents. Since the molecule is proved to be *trans* in organic solvents,[3] these two bands can be attributed to the characteristic absorption of the *trans* form.

In acidic solution, two bands are observed at 301 and 240 mμ. It was shown by Krumholz[6] and Westheimer and Benfey[12] that the mono-cation predominates in ordinary acidic medium (for

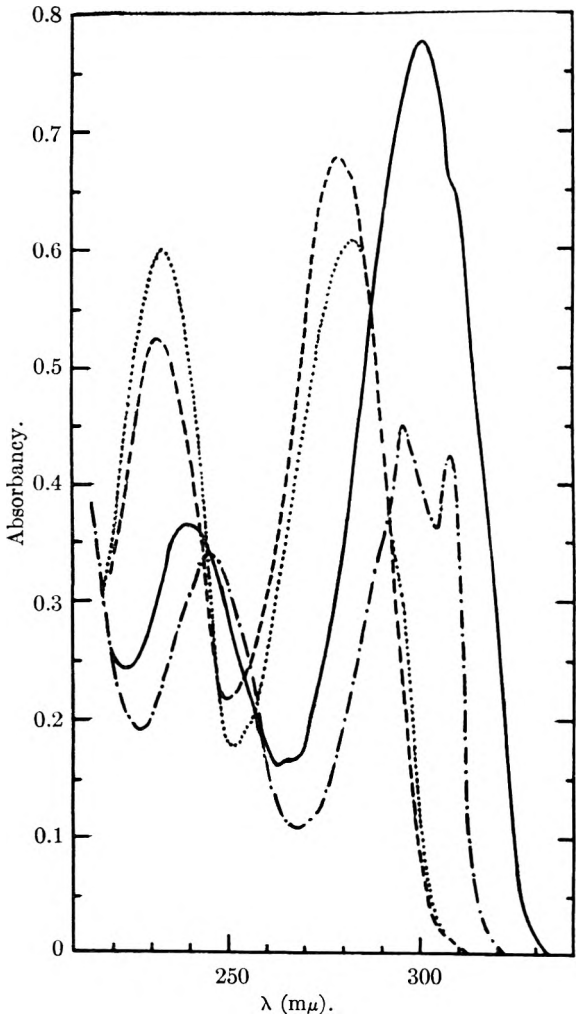

Fig. 2.—Comparison of the spectra in 2,2′-bipyridine: —, acidic solution (5×10^{-5} mole/l.); – – – –, basic solution (5×10^{-5} mole/l.); —·—, $[Ni(bipy)_3]Cl_2 \cdot 7H_2O$ (10^{-6} mole/l.); ·····, ethanol solution (6×10^{-5} mole/l.).

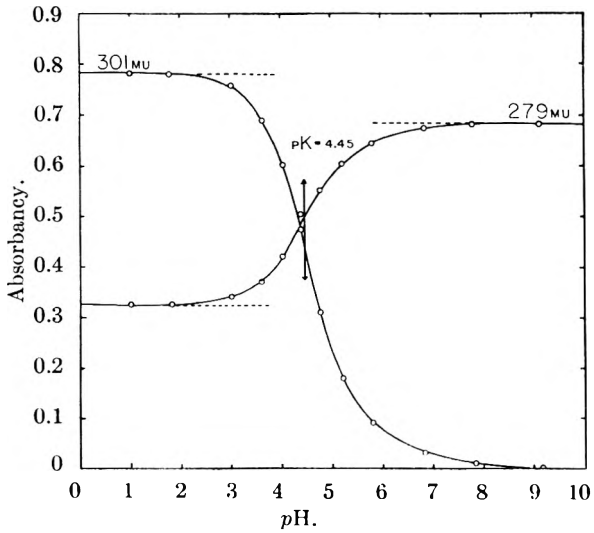

Fig. 3.—Absorbancy of 2,2′-bipyridine as a function of *p*H.

example, 1 *N* HCl). Therefore these two bands are reasonably attributed to the characteristic absorption of the mono-cation. As is seen in Fig. 2, the spectrum in acidic solution is similar to that of the metal chelate compounds such as $[Ni(bipy)_3]Cl_2$[13] except for the fact that the fine structure of the longer wave length band seen in the latter is blurred in the former.

The following two forms are probable for the mono-cation

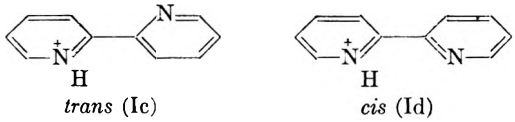

trans (Ic) *cis* (Id)

Both of these two forms are expected to be slightly twisted along the central carbon–carbon bond because of steric hindrance between two *ortho* hydrogens.[14] From the standpoint of electrostatic energy, Id is expected to be more stable than Ic because less negative nitrogen ($\gtrless N^+–H$) is more closely located to the more negative nitrogen ($\gtrless N$) in Id than in Ic. The similarity of the spectra between the mono-cation and the metal-chelate compounds also favors the *cis* form. Thus we conclude that the mono-cation is a slightly twisted *cis*.

The spectral change observed in Fig. 1 is then interpreted by the equilibrium between Id (301, 240 mμ) and Ia (279, 232 mμ). Hereafter these two bands observed in each species are called π_1 and π_2-bands, respectively, from the longer wave length. By plotting *p*H against the absorbancies of the π_1-bands (Fig. 3), the *pK* values for the equilibrium was estimated as 4.45. This value is in good accord with 4.44 obtained by potentiometric titration.[7]

As is seen above, 2,2′-bipyridine exhibits two bands in the ultraviolet region. This is an indication that a twist along the central bond is small, since it is shown both empirically[6] and theroretically[15] that, for a large twist, only one band usually is observed in this region. The splitting of the π_1-band in the metal chelate compounds was shown to be due to the vibrational fine structures.[16] If so, blurring of the fine structures in Id and Ia may imply that they are not completely planar.[17] In the metal chelate compounds, however, a perfect planarity is maintained because the resonance structures such as shown below stabilize the planar form.

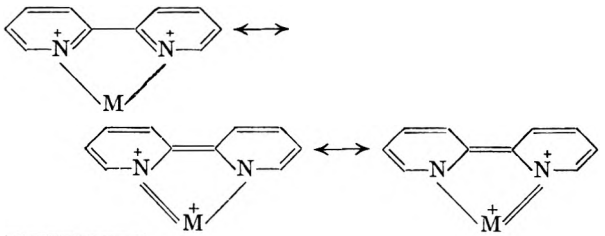

(12) F. H. Westheimer and O. T. Benfey, *J. Am. Chem. Soc.*, **78**, 5309 (1956).

(13) The bands at 308, 296 and 246 mμ observed in $[Ni(bipy)_3]Cl_2$ are undoubtedly due to the "ligand absorption" and not due to the metal.

(14) Because of hydrogen repulsion, biphenyl is twisted by 45° in the gaseous state and 20 ~ 26° in solution (see reference 15). The twisting angle in Ic and Id is expected to be somewhat smaller than that of biphenyl, since only two *ortho*-hydrogens are sterically hindered.

(15) H. Suzuki, *Bull. Chem. Soc. Japan*, **32**, 1340 (1959).

(16) K. Sone, P. Krumholz and H. Stammreich, *J. Am. Chem. Soc.*, **77**, 777 (1955).

(17) See, for example, M. S. Newman, "Steric Effects in Organic Chemistry," John Wiley and Sons, Inc., New York, N. Y., 1956, p. 500.

TABLE I

THE ULTRAVIOLET SPECTRA OF 2,2′-BIPYRIDINE IN VARIOUS SOLVENTS (mμ)

Compound	Solvent	π_1 Protonated or chelated *cis*	π_1 *trans*	π_2
2,2′-Bipyridine	Cyclohexane	.....	283(15.0)[a]	245(11.3)[a]
				237(12.1)[a]
	Chloroform	.....	284(14.5)[a]	245(9.9)[a]
				240(10.3)[a]
	Ethanol	.....	283(10.2)[a]	244(6.6)[a]
				237(7.7)[a]
	Water (*p*H 12)	.....	281(0.69)[a]	233(0.53)[b]
	Water (*p*H 1.8)	301(0.78)[b]	.....	239(0.37)[b]
$[Ni(bipy)_3]Cl_2 \cdot 7H_2O$	Water	308(42.6)[a]		
		296(45.2)[a]	.....	246(34.0)[a]

[a] The number denotes the molecular extinction coefficient ($\times 10^{-3}$). [b] The number indicates the absorbancy of 5×10^{-5} mole/l. solution in which two species are in equilibrium.

These structures are also responsible for the red-shift of the π_1-band of the metal chelate compounds relative to that of the ligand, although the degree of their contribution is slightly different from one metal to another.

Similar red-shift of the π_1-band of the cation (Id) relative to that of the base (Ia) can be explained by the following resonance contribution.

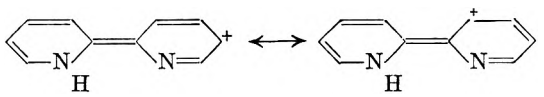

Thus the resonance caused by salt formation is responsible for the observed red-shift of the π_1-band. Although conversion of Ia into Id involves a change of configuration from *trans* to *cis*, this effect may be much smaller compared with the effect of salt formation or even act in the opposite direction to the effect of salt formation since *cis*-isomers usually absorb at shorter wave length than the *trans*-isomers.[18] The di-cation of 2,2′-bipyridine which exists only in extremely strong acid absorbs at 290 mμ.[12] From the viewpoint of charge distribution, a complete planar *trans* form is most favorable for the di-cation. Because of hydrogen repulsion, however, it may be slightly twisted. Since no resonance contributions such as

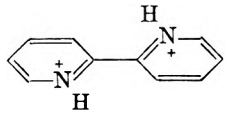

seen in the mono-cation are expected for the di-cation, the blue-shift of the π_1-band of the di-cation relative to that of the mono-cation is understood on this basis.

II. 2,2′,2″-Terpyridine.—Figure 4 indicates the ultraviolet spectra of 2,2′,2″-terpyridine at various *p*H values in buffer solutions. As is shown in Fig. 5, the spectrum of basic solution (*p*H 12) is very similar to those in organic solvents. Therefore, it is reasonable to conclude that the molecule is *trans–trans* (IIa) of minimum dipole moment in these solvents. Then the bands at 285 and 235 mμ are attributable to the π_1 and π_2-bands of IIa. It is noted that IIa does not show appreciable red-shift compared with *trans*-2,2′-bipyridine (Ia). This is due to the lack of resonance between the bipyridine portion of 2,2′,2″-terpyridine and the third pyridine attached to the *meta*-position of the former. The ultraviolet spectra of *meta*-polyphenyls show similar trends.[19]

Figure 5 indicates that the spectrum in acidic solution is similar to that of the metal chelate compounds such as [Zn(trpy)Cl]Cl in which the ligand is definitely *cis–cis* (IIc). The result of potentiometric titration clearly indicates that only two protons combine with one base. Furthermore no appreciable change of the spectrum was observed even in extremely strong acid (5 *M* H_2SO_4). Considering charge distribution together with the above mentioned observations, we conclude that the most probable structure for the di-cation is *cis–cis* shown below

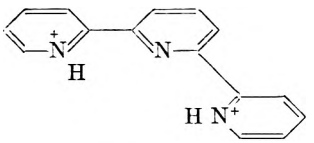

cis–cis (IId)

As is seen in Figs. 4 and 5, the spectra of acidic solution and the metal chelate compound exhibits three main bands at *ca.* 325, 285 and 230 mμ, although the fine structures in the latter are blurred in the former. The interval between 325 and 285 mμ bands is too large to assign them to the vibrational structures belonging to the same electronic transition. We have measured the ultraviolet spectra of the metal chelate compounds of 2,2′,2″-terpyridine with various metals. All of these compounds exhibit three bands around 340~320, 285~270 and 235~220 mμ although blurring of the satellite bands depends on the kind of the metal.[20] As stated before, the conjugation between pyridine rings is insulated in *meta*-polypyridines. Then the spectrum of IId can be interpreted based on the interaction between two bipyridines (300 mμ) both of which share the central pyridine ring. Thus the interval between 325 and 285 mμ band may indicate the magnitude of such a perturbation. In this sense, we call these two bands π_{1a} and π_{1b}, respectively. Other satellite bands clearly observed in the metal chelate compounds are assigned to their vibrational structures.

(18) For example, see: A. E. Gillam and E. S. Stern, "Electronic Absorption Spectroscopy," E. Arnold Publishers Ltd., London, 1954, p. 233.

(19) A. E. Gillam and D. H. Hey, *J. Chem. Soc.*, 1170 (1939).

(20) K. Nakamoto, unpublished.

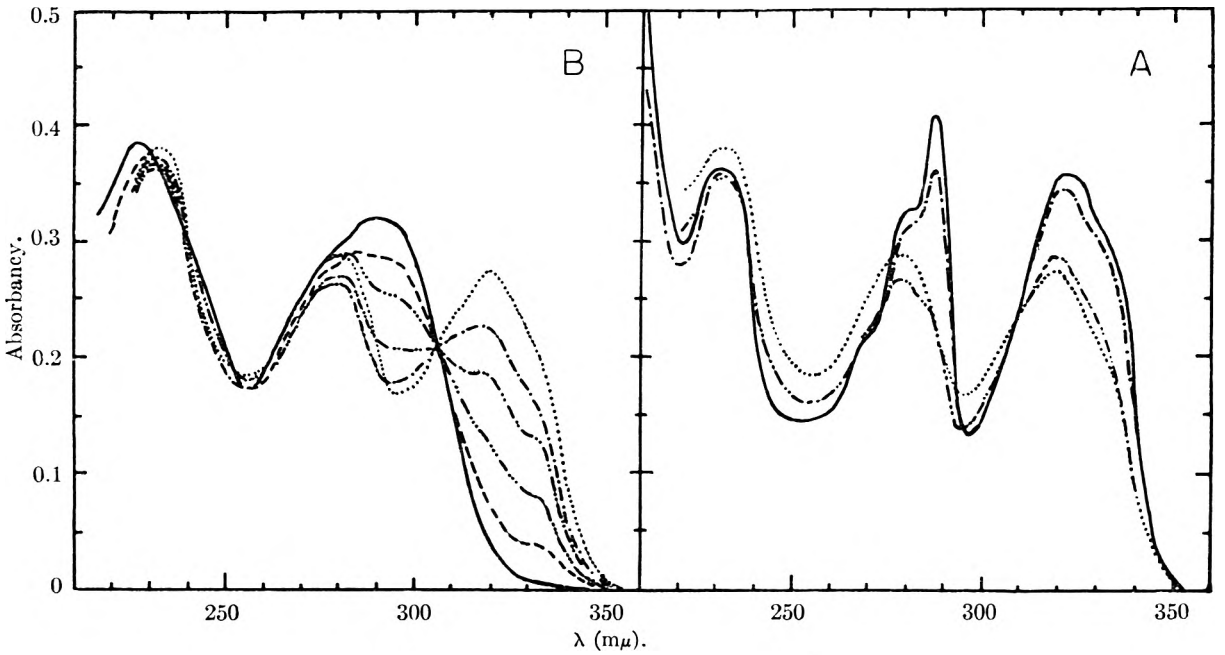

Fig. 4.—Absorption spectra of 2,2′,2″-terpyridine in buffer solutions (2×10^{-5} mole/l.): A, in acidic solutions: —, pH 1.80; — ·—·, 3.00; —··—··, 3.65; ·····, 4.05. B, in neutral and basic solutions; ·····, 4.05; —·—·, 4.40; —··—·· 4.87; —···—···, 5.25; — — — — —, 5.83; —, 12.0.

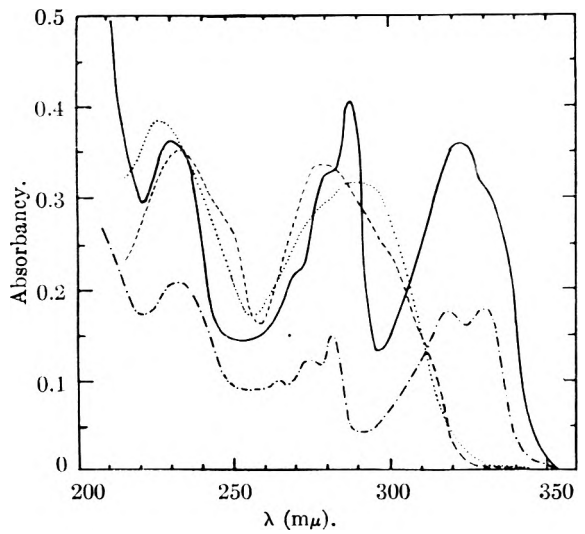

Fig. 5.—Comparison of the spectra in 2,2′,2″-terpyridine: —, acidic solution (2×10^{-5} mole/l.): ·····, basic solution (2×10^{-5} mole/l.): —·—·, [Zn(trpy)Cl]Cl (10^{-5} mole/l.); — — — —, ethanol solution (10^{-5} mole/l.).

The spectrum at an intermediate *p*H is different either from that of basic or acidic solution. As is seen in Fig. 4, three broad bands appear at 320, 279 and 232 mμ. The mono-cation is expected to be predominant at an intermediate *p*H. The following two *cis-trans* structures are most probable for the mono-cation. The *cis-cis* and *trans-trans* forms can be ruled out from consideration of charge distribution and spectra. Of these two, IIe is more favorable than IIf in explaining the process of protonation from the mono-cation to the di-cation (IId). Similar to the case of IId, the splitting of the π_1-band into 320 and 279 mμ band is interpreted as a perturbation between Ia and Id which share the central pyridine ring. Finally blurring of vibrational fine structures both in IId and IIe can be accounted for by a small twist around the central carbon–carbon bond.

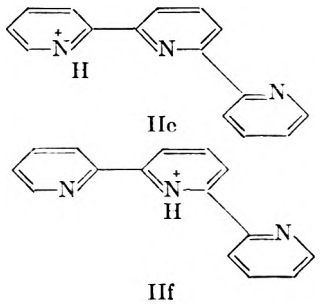

IIe

IIf

Thus the spectral change in Fig. 4 is interpreted by the equilibria between IId, IIe and IIa. It is rather difficult, however, to determine the individual ionization constants of the above two step dissociation from the spectroscopic data since overlapping of the bands of each species is serious.

Thus the individual ionization constants were determined from the analysis of the titration curve. The *pK* values were estimated to be 2.59 and 4.16, respectively. If the small difference between these two ionization constants is considered, the complex feature of the ultraviolet spectra at the intermediate *p*H range is reasonably understood.

III. Possibility for Intramolecular Hydrogen Bonding.—In the foregoing, we have concluded that the cations of 2,2′-bipyridine and 2,2′,2″-terpyridine have slightly twisted *cis* configurations. Intramolecular hydrogen bonded structures of these species such as shown below have advantages

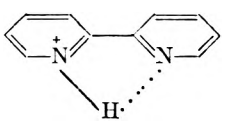

in the following facts. (1) The di-cation of 2,2′-

TABLE II

THE ULTRAVIOLET SPECTRA OF 2,2′,2″-TERPYRIDINE IN VARIOUS SOLVENTS (mμ)

Compound	Solvent	π_1 Protonated or chelated *cis–cis*	π_1 Protonated *cis–trans*	π_1 *trans–trans*	π_2
2,2′,2″-Terpyridine	Cyclohexane	.....	.....	278(18.8)[a]	235(20.4)[a]
	Chloroform	.....	.....	280(17.9)[a]	240(17.2)[a]
	Ethanol	.....	.....	279(18.6)[a]	234(19.4)[a]
	Water (*p*H 12)	.....	.....	290(0.32)[b]	227(0.39)[b]
	Water (*p*H 4)	.....	(A) 320(0.28)[b] (B) 279(0.29)[b]	.....	232(0.38)[b]
	Water (*p*H 1.8)	(A) 333(0.30)[b], 322(0.36)[b] (B) 288(0.41)[b], 280(0.33)[b], 270(0.22)[b]	.....	.....	231(0.36)[b]
[Zn(trypy)Cl]Cl	Water	(A) 331(17.3)[a], 318(17.2)[a] (B) 283(14.8)[a], 274(12.0)[a], 264(9.7)[a]	.....	.....	232(20.4)[a]

[a] The number denotes the molecular extinction coefficient ($\times 10^{-3}$). [b] The number indicates the absorbancy of 2×10^{-5} mole/l. solution in which three species are in equilibria.

bipyridine does not exist in ordinary acid, although the second proton is forced to combine with another nitrogen in extremely strong acid.[12] (2) The tri-cation of 2,2′,2″-terpyridine cannot be found either in the crystalline state or in strong acid. (3) Similarity of the spectra between the cations and the metal chelate compounds are well explained.

It should be noted, however, that (1) and (2) can be accounted for on the basis of unstable charge distribution caused by close location of ammonium nitrogens and (3) does not necessarily require the chelated structure. The estimated N···H distance from the reported structural data,[2] 2.60 Å., seems to be too long compared with that of other N···H distances so far reported.[21]

Also, similarity of the second ionization constants of various isomers of bipyridines[6] do not afford evidence for such a hydrogen-bonded structure. Westheimer and Benfey[12] arrived at the same conclusion by comparing the ratio of the first and second ionization constants in many di-basic acids.

(21) J. M. Robertson, "Organic Crystals and Molecules," Cornell University Press, Ithaca, N. Y., 1953, p. 245.

The infrared spectra of the hydrochlorides of pyridine, 2,2′-bipyridine and 2,2′,2″-terpyridine exhibit their N^+—H stretching bands at 2760, 2550 and 2680 cm.$^{-1}$, respectively, in the crystalline state. Although the bands are shifted to lower frequencies in the latter two compounds compared with the former, these shifts are not necessarily attributable to the effect of intramolecular hydrogen bonds since intermolecular hydrogen bonds of N^+—H···O and N^+—H···Cl^- types coexist in the crystalline state. Also an attempt has been made to study the proton magnetic resonance spectra of these compounds in solution, which was not successful, however, possibly because nuclear quadrupole relaxation of N^{14} smeared out the N^+—H proton signal. Thus no positive evidence was found for the N^+H···N hydrogen bonding.

It is hoped that more detailed studies on the structures of these compounds will be carried out in the near future.

Acknowledgment.—The author wishes to express his sincere thanks to Professor Arthur E. Martell for criticism of this manuscript.

MOLECULAR PROPERTIES OF SIX 4-*O*-METHYLGLUCURONOXYLANS[1]

BY D. A. I. GORING AND T. E. TIMELL

Pulp and Paper Research Institute of Canada and the Department of Chemistry, McGill University, Montreal, Canada

Received March 12, 1960

Six 4-*O*-methylglucuronoxylans have been isolated from various woody angiosperms in a maximum yield and with a minimum of depolymerization. Osmotic pressure measurements gave number-average degrees of polymerization ranging from 185 to 234. Light-scattering measurements were carried out with dimethyl sulfoxide solutions of the polysaccharides. Reliable results were obtained only after colloidal material had been eliminated by ultracentrifugation at 140,000 *g*, followed by ultracentrifugation at 35,000 *g* in light-scattering cells especially designed for removal of both sedimenting and floating debris. The weight-average degrees of polymerization obtained varied between 440 and 500. A comparison between degrees of polymerization and intrinsic viscosities indicated that the acidic side chains of the 4-*O*-methylglucuronoxylans increased the effective volume of the molecules in cupriethylenediamine but that this volume was only half of that of cellulose in the same solvent.

While the structural details of many of the xylans occurring in nature are now fairly well known,[2] little information is presently available concerning their molecular properties. It is evident from a recent review[3] that in the past many of the polysaccharides studied had been severely degraded during their isolation, especially when acid chlorite was used.[4,5] Low yield in the isolation often resulted in products hardly representative of the polysaccharide as it originally occurred in the living plant. In most cases, organic esters of the hemicelluloses have been investigated, many of them constituting only a portion of the original material because of the poor solubility properties of these derivatives. Lately, this difficulty has been partly overcome,[3] but so far only number-average molecular weights have been reported.

The present paper is concerned with the number- and weight-average molecular weights of some hardwood xylans as determined from osmotic pressure and light-scattering measurements, care being taken to avoid degradation in isolating the samples. Intrinsic viscosities were also measured from which an indication of the molecular configuration was obtained.

Four of the hemicelluloses were 4-*O*-methylglucuronoxylans containing a linear framework of (1 → 4)-linked β-D-xylopyranose residues, every tenth of which, on the average, carried a 4-*O*-methyl-α-D-glucuronic acid residue attached as a single side chain through C_2. These polysaccharides were obtained from the wood of white birch (*Betula papyrifera*),[5] yellow birch (*Betula lutea*)[6] and sugar maple (*Acer saccharum*),[7] as well as from the inner bark of white birch.[8] A fifth polysaccharide with the same constitution but with only 7 xylose residues per acid side chain was obtained from the wood of white elm (*Ulmus americana*).[9] An *O*-acetyl-4-*O*-methylglucuronoxylan containing one (1 → 2)-linked 4-*O*-methyl-α-D-glucuronic acid side chain and 3.6 *O*-acetyl groups per 10 xylose residues, was also isolated from the wood of white birch.[10]

The bark hemicellulose was obtained in almost quantitative yield by extraction of the bark with alkali after pretreatment with acid chlorite. The *O*-acetylated polysaccharide was isolated in a yield of 50% by extracting a chlorine holocellulose with dimethyl sulfoxide. The remaining hemicelluloses represented 70–80% of the amount present in the wood and were obtained by direct extraction with alkali of the latter.

A portion of each hemicellulose was converted to the fully substituted acetate derivative, a reaction which has been shown[11] to involve no depolymerization of the polysaccharide. The acetates were soluble in chloroform containing some ethanol, and osmotic pressure measurements were carred out in this mixed solvent. The osmometers used[12] contained large membranes, supported on both sides, thus making rapid and accurate measurements possible. Linear relationships between reduced osmotic pressure and concentration were observed throughout, and results obtained with different membranes and osmometers were in excellent agreement (Fig. 1). The number-average molecular weights obtained are given in Table I.

TABLE I

OSMOMETRY DATA

Polysaccharide	$(h/w)_{w\to 0}$	$\bar{M}_n \times 10^{-3}$
White birch	0.50	51
White birch, *O*-acetyl	.60	43
White birch, bark	.46	56
Yellow birch	.56	46
White elm	.56	46
Sugar maple	.50	51

The 4-*O*-methylglucuronoxylan from birch bark had evidently the highest molecular weight, the *O*-acetylated polysaccharide from birch wood the lowest. The high value observed for the bark xylan was rather surprising in view of the fact that this was the only hemicellulose which had been subjected to treatment with acid chlorite, a reagent known to degrade polysaccharides considerably.[4,13,14] It was also the only hemicellulose

(1) Paper presented at the Symposium on Wood Hemicelluloses before the Division of Cellulose Chemistry at the 136th Meeting of the American Chemical Society in Atlantic City, N. J., September, 1959.

(2) G. O. Aspinall, *Advances in Carbohydrate Chem.*, **14**, 429 (1959).

(3) C. P. J. Glaudemans and T. E. Timell, *Svensk Papperstidn.*, **61**, 1 (1958).

(4) C. P. J. Glaudemans and T. E. Timell, *ibid.*, **60**, 869 (1957).

(5) C. P. J. Glaudemans and T. E. Timell, *J. Am. Chem. Soc.*, **80**, 941, 1209 (1958).

(6) T. E. Timell, *ibid.*, **81**, 4989 (1959).

(7) T. E. Timell, *Can. J. Chem.*, **37**, 893 (1959).

(8) A. Jabbar Mian and T. E. Timell, *Tappi*, in press.

(9) J. K. Gillham and T. E. Timell, *Can. J. Chem.*, **36**, 410, 1467 (1958).

(10) T. E. Timell, *J. Am. Chem. Soc.*, **82**, 5211 (1960).

(11) J. O. Thompson, J. J. Becker and L. E. Wise, *Tappi*, **36**, 319 (1953).

(12) J. V. Stabin and E. H. Immergut, *J. Polymer Sci.*, **14**, 209 (1954).

isolated in an almost quantitative yield, a fact which appeared to preclude the possibility of a fractionation during its isolation.

Greater difficulties than usual were encountered in clarifying the chloroform–ethanol solutions for light scattering. Clarification by ultracentrifugation was ineffective because of the high density of the solvent and filtration through glass, paper or cellophane membranes of varying porosity resulted in fractionation of the polymers and loss of up to 50% of the hemicellulose acetates.

Better results were obtained with solutions of the polysaccharides themselves in dimethyl sulfoxide containing 2% of water. When dry, this solvent is extremely hygroscopic and the inclusion of the water was intended to obviate at least a part of this difficulty. Intrinsic viscosities measured in this solvent mixture and in dry dimethyl sulfoxide differed by less than 10%, indicating that the small quantity of water present had little effect on the configuration of the polymer in solution.

In preliminary experiments, the previously described striations[15] were very pronounced and rendered accurate measurements impossible. A modified Dandliker and Kraut[16] cell was therefore adopted, designed to eliminate both sedimenting and floating material (Fig. 2). These striations in the scattering light-beam were due to colloidal debris, as suggested by an experiment in which a 1% polymer solution was subjected to a preliminary ultracentrifugation for various lengths of time at 140,000 *g*, followed by ultracentrifugation at 35,000 *g* in the modified light-scattering cell. The results are summarized in Fig. 3. Both the dissymmetries (Z) and the reduced turbidities (τ/c) decreased markedly for the first three hours of high-speed ultracentrifugation after which they remained constant. In contrast, the decrease in concentration over the entire period was less than 2%. Obviously, a small portion of the polysaccharide was of colloidal dimensions. Whether this material was a non-xylan impurity or an aggregated xylan, its presence produced results which were not representative of the bulk of the polymer. A preliminary ultracentrifugation at 140,000 *g* for 3 hr. was therefore adopted as a standard procedure prior to the usual centrifugation at 35,000 *g* in the cell. Longer times were avoided because of the possibility of molecular fractionation of the polysaccharides.

Typical light-scattering data are given in Fig. 4. The variation of the dissymmetries with concentration exhibited no clear trend and a mean value was therefore adopted (Table II). The linear extrapolation to zero concentration applied for obtaining $(c/\tau)_{c=0}$ is also shown. The weight-average molecular weights ($\bar{M}_w$) in Table II were calculated from these values and from the refractive index increments (dn/dc) in the usual way. The values for dn/dc varied somewhat for the different polysaccharides, albeit with no apparent trend. A mean

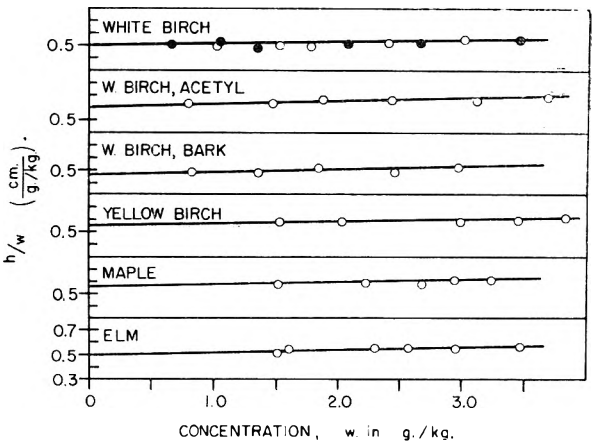

Fig. 1.—Osmometry data for six 4-*O*-methylglucuronoxylans.

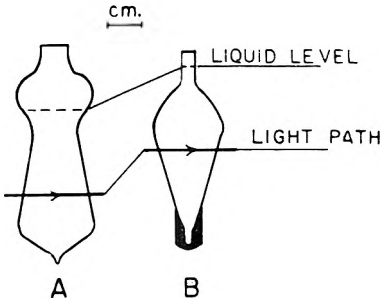

Fig. 2.—Light-scattering cells according to (A) Dandliker and Kraut and (B) present modification.

TABLE II

LIGHT-SCATTERING DATA

Polysaccharide	$(c/\tau)_{c=0}$	Z	$\bar{M}_w \times 10^{-}$
White birch	29.4	1.55	76
	29.4	1.63	
	34.3	1.28	
	24.4	1.48	
White birch, *O*-acetyl	24.4	1.08	78
Whit e birch, bark	27.0	1.06	70
Yellow birch	30.0	1.33	75
White elm	29.4	1.18	70

value was accordingly used throughout. As shown in Table II, the $\bar{M}_w$ values agree fairly well and are consistent with the number-average values ($\bar{M}_n$) in Table I.

Number- and weight-average degrees of polymerization are summarized in Table III, together with intrinsic viscosities determined in cupriethylenediamine and dimethyl sulfoxide containing 2% water. $\bar{P}_n$ and $\bar{P}_w$ represent the number of xylose residues in the linear framework of the polysaccharide, exclusive of the acid side chains. There is no great difference in the $\bar{P}_n$ and $\bar{P}_w$ values obtained for the various 4-*O*-methylglucuronoxylans. The ratio $\bar{P}_w/\bar{P}_n$ is 2.4 ± 0.2 which is near the value of 2 expected for a polymer with a Flory distribution.

The number-average degrees of polymerization found here are considerably higher than those reported by other investigators for 4-*O*-methylglucuroxylans from similar sources. In two cases[17,18] degradation undoubtedly occurred during the iso-

(13) T. E. Timell and E. C. Jahn, *Svensk Papperstidn.*, **54**, 831 (1951).

(14) J. D. Wethern, *Tappi*, **35**, 267 (1952).

(15) M. M. Huque, J. Jaworzyn and D. A. I. Goring, *J. Polymer Sci.*, **39**, 9 (1959).

(16) W. B. Dandliker and J. Kraut, *J. Am. Chem. Soc.*, **78**, 2380 (1956).

(17) E. Husemann, *J. prakt. Chem.*, **155**, 13 (1940).

(18) M. A. Millett and A. J. Stamm, THIS JOURNAL, **51**, 134 (1947).

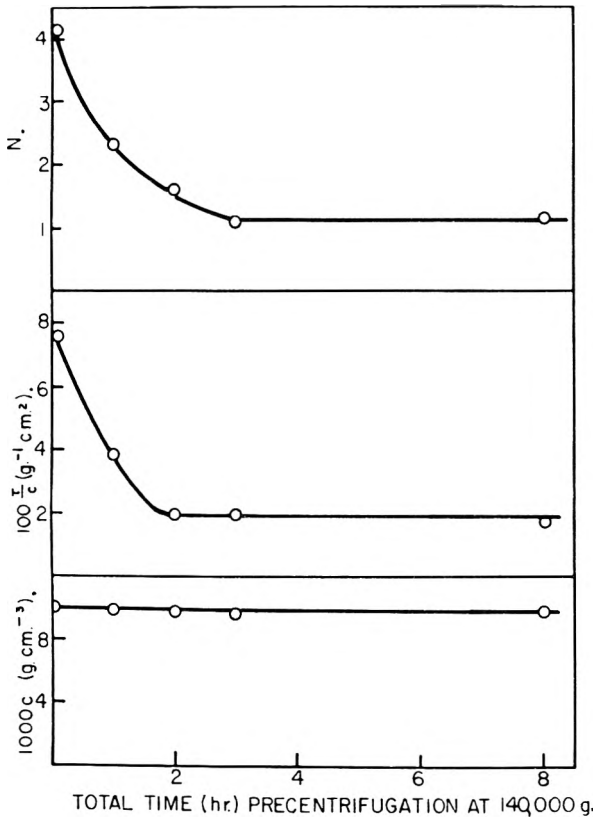

Fig. 3.—Effect of preliminary ultracentrifugation on dissymmetry (Z), reduced turbidity (τ/c), and concentration (c).

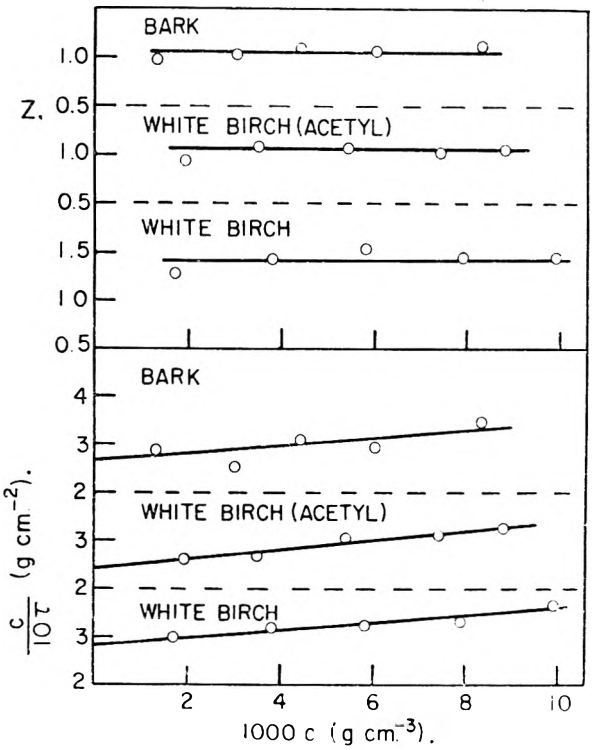

Fig. 4.—Light-scattering data for three 4-*O*-methylglucuronoxylans.

lation of the hemicelluloses. An aspen xylan[19] gave esters which were only partly soluble and it appears quite conceivable that the insoluble part had a higher average molecular weight than the soluble portion. The only previous attempt to determine the weight-average degree of polymerization of a xylan seems to be a light-scattering investigation of a hemicellulose from beech wood.[20] This 4-*O*-methylglucuronoxylan[21] was converted to a mixed acetate–benzoate derivative, the $\bar{P}_w$ of which was found to be 175 ± 10. This low value was probably due to several factors, including the degrading effect of the acid chlorite used for delignifying the wood, and the fact that fractionations were carried out for purification of the polysaccharide.

Light-scattering data recently obtained with nitrated, native celluloses from white birch wood[22] indicate a weight-average degree of polymerization for these polysaccharides of 9,000. Other hardwood celluloses appear to have approximately the same molecular weight.[23] When this value is compared with the $\bar{P}_w$ values found here for hardwood xylans, 450–500, the considerable difference in molecular size between these two wood components becomes evident.

The angular dependence of light-scattering has been used for evaluation of the configuration of the beech xylan referred to above.[20] It is clear, however, that the present dissymmetries were so near to unity and so markedly affected by small amounts of aggregates that this parameter cannot be used to elucidate the molecular shape. A somewhat more reliable indication of the configuration can be obtained by comparing the intrinsic viscosity with the degree of polymerization. If, as with cellulose in cupriethylenediamine,[24] the coefficient a in the Mark–Houwink equation

$$[\eta] = K\bar{M}^a$$

where $[\eta]$ denotes the intrinsic viscosity and K is a constant, is unity, the ratio $[\eta]/\bar{P}_n$ should be constant. Even if a departed somewhat from unity, this ratio would be almost constant in the present case because of the narrow range of molecular weights involved.

As is shown in Table III, the ratio of the intrinsic viscosity in dimethyl sulfoxide to the number-average degree of polymerization, $[\eta]_{DMS}/\bar{P}_n$, was virtually constant for the four 4-*O*-methylglucuronoxylans from wood. The larger ratio noted for the native, *O*-acetylated polysaccharide was probably due to the greater solvation of the *O*-acetyl groups by the dimethyl sulfoxide, which would cause the macromolecule to expand. Contrary to this, the ratio $[\eta]_{CED}/\bar{P}_n$ was somewhat variable, ranging from 3.59×10^{-3} to 6.00×10^{-3}. The 4-*O*-methylglucuronoxylans all carried acid side chains with carboxyl groups which would ionize in a solvent such as cupriethylenediamine. This would cause polyelectrolyte expansion which would cause an increase in the intrinsic viscosity over that expected for an uncharged chain. Thus, the exceptionally

(19) J. O. Thompson and L. E. Wise, *Tappi*, **35**, 331 (1952).

(20) M. Horio, R. Imamura and H. Inagaki, *ibid.*, **38**, 216 (1955).

(21) G. A. Adams, *Can. J. Chem.*, **35**, 556 (1957).

(22) D. A. I. Goring and T. E. Timell, *Svensk Papperstidn.*, in press.

(23) T. E. Timell, *ibid.*, **60**, 836 (1957).

(24) E. H. Immergut, B. G. Ranby and H. F. Mark, *Ind. Eng. Chem.*, **45**, 2483 (1953).

high value for the elm xylan is in accord with the higher acidity of this polysaccharide.[9] It is probable that in viscometric determinations of the molecular weight of 4-*O*-methylglucuronoxylans, dimethyl sulfoxide is a more suitable solvent than cupriethylenediamine.

TABLE III

DEGREES OF POLYMERIZATION AND INTRINSIC VISCOSITIES OF THE POLYSACCHARIDES

Polysaccharide	$\bar{P}_n$	$\bar{P}_w$	$[\eta]_{CED}$	$1000\,[\eta]_{CED}/\bar{P}_n$	$[\eta]_{DMS}$	$1000\,[\eta]_{DMS}/\bar{P}_n$
White birch	215	500	0.89	4.13	0.67	3.11
White birch, *O*-acetyl	180	470	.87	4.82	.98	5.44
White birch, bark	234	464	.84	3.59	..	..
Yellow birch	192	495	.93	4.84	.57	2.96
White elm	185	440	1.11	6.00	.56	3.02
Sugar maple	215	..	0.97	4.50	.65	3.02

The mean value of $[\eta]_{CED}/\bar{P}_n$ was 4.7×10^{-3}, which is considerably smaller than the value reported for cellulose[24] within this molecular range, 8.1×10^{-3}. Evidently, a 4-*O*-methylglucuronoxylan with the same number of residues in the main chain as the cellulose molecule will, nevertheless, occupy only one-half of the effective volume of the latter in cupriethylenediamine, and this in spite of the additional volume and polyelectrolyte expansion caused by the presence of the acid side chains. The xylose residue is of the same length as the glucose residue and both are probably present in the C 1 conformation in xylans and cellulose. The reason for this difference in hydrodynamic volume is therefore not clear at the present. Further physicochemical studies with fractions over a wide range of molecular weights should reveal additional configurational details.

Experimental

Isolation of the Hemicelluloses.—Extractive-free wood meal (800 g., 40–60 mesh) from a freshly cut specimen of white birch was extracted for 10 hr. in a nitrogen atmosphere with 24% (w./w.) potassium hydroxide (4 l.). After filtration through sintered glass and washing with water, the filtrate and washings (6 l.) were poured into ethanol (15 l.) and hydrochloric acid was added until a *p*H of 2.5 had been reached. The precipitate was recovered on the centrifuge and washed five times with three times its volume of 70% ethanol, followed by anhydrous ethanol and petroleum ether. The material was dried for a week *in vacuo* over potassium hydroxide to give a white, fluffy powder (176 g., 22% of the wood). The hemicellulose was ash-free and, on hydrolysis, gave only xylose and uronic acids on the paper chromatogram. The other 4-*O*-methylglucuronoxylans were isolated in a similar way.

The *O*-acetyl-4-*O*-methylglucuronoxylan was obtained from a white birch chlorine holocellulose[13] by exhaustive extraction with dimethyl sulfoxide[25] as described previously[10] (yield, 50%). The hemicellulose was ash-free and was easily soluble in water. Extractive-free inner bark of white birch was treated with hot water and hot aqueous ammonium oxalate for removal of pectic material, followed by treatment with acid chlorite as described elsewhere.[8] Extraction of the residue with aqueous potassium hydroxide gave a 4-*O*-methylglucuronoxylan containing only traces of glucose residues and representing almost all the xylose-yielding material in the bark. The yields obtained and the general properties of the polysaccharides are summarized in Table IV. All preparations were homogeneous on electrophoresis on glass fiber paper in a borate buffer.

TABLE IV

YIELD AND GENERAL PROPERTIES OF THE POLYSACCHARIDES

Polysaccharide	Wood, %	Obtained, %	Methoxyl, %	Uronic anhydr., %	Xylose per acid group	$[\alpha]_D$[a]
White birch	29	22	2.0	10.9	10	−83°
White birch, *O*-acetyl	33	17.5	2.1	9.8	10	−86°[b]
White birch, bark	30	28	2.2	9.9	10	−68°
Yellow birch	23	17.5	2.0	11.2	10	−81°
White elm	14	10	2.6	15.2	7	−70°
Sugar maple	17	13	2.1	12.0	10	−80°

[a] Specific rotation at 20° in 10% sodium hydroxide. [b] In water.

Acetylation of the Hemicelluloses.—Dry hemicellulose (2.0 g.) was dissolved or swollen in freshly redistilled and dry formamide (40 ml.).[26] After 24 hr., dry pyridine was added (80 ml.) and, with intervals of 12 hr., three portions of redistilled acetic anhydride (20 ml. each). The reaction mixture was shaken vigorously and soon settled to a transparent gel. After an additional 24 hr. at room temperature, the mixture was added with stirring to ice-water (3 l.) containing 2% hydrochloric acid. The product was washed with ice-water until neutral and then with ethanol and petroleum ether. After drying *in vacuo* at room temperature for 3 days, a hard, grayish powder was obtained (3.1 g.). Acetyl analyses[27] indicated complete substitution throughout. The acetates were soluble in chloroform only after addition of 10% (v./v.) of ethanol.

Osmotic Pressure Measurements.—The instrument used was the Stabin–Immergut[12] modification of the Zimm–Myerson osmometer.[28] The membranes were freshly prepared cellophane films which had never been allowed to dry.[29] Syringes with long needles were employed for filling the osmometers and mercury was used for closing the instruments completely during measurements. The osmotic height was measured with a cathetometer by the static method, equilibrium being established within 3–5 hr. The temperature was 30 ± 0.01°. No diffusion through the membranes was noticed. The solvent was a 9:1 (v./v.) mixture of reagent grade chloroform and anhydrous ethanol. Concentrations were determined by weight, thus eliminating the need for density measurements.

The osmotic height was determined at 5–6 different concentrations. In the case of the 4-O-methylglucuronoxylan from white birch wood, two series of measurements were made with different membranes and with different osmometers. The results obtained agreed closely (Fig. 1). Molecular weights were calculated from the general relationship.

$$\pi/c = RT/\bar{M}_n[1 + Bc]$$

where B is the second virial coefficient and the other symbols have their usual significance.

Linear extrapolation to zero concentration yielded the value $(h/w)_{w=0}$ where h was the osmotic height in cm. solution and w was the concentration in g./kg. solution.[30] Number-average molecular weights were obtained from the simplified relationship

$$\bar{M}_n = 25{,}700/(h/w)_{w=0}$$

The corresponding degree of polymerization, $\bar{P}_n$ (number of

(25) E. Hägglund, B. Lindberg and J. McPherson, *Acta Chem. Scand.*, **10**, 1160 (1956).

(26) J. F. Carson and W. D. Maclay, *J. Am. Chem. Soc.*, **68**, 1015 (1946); **70**, 293 (1948).

(27) L. B. Genung and E. C. Mallatt, *Ind. Eng. Chem., Anal. Ed.*, **13**, 369 (1941).

(28) B. H. Zimm and I. Myerson, *J. Am. Chem. Soc.*, **68**, 911 (1946).

(29) Provided by American Viscose Corporation through the courtesy of Dr. C. P. J. Glaudemans.

(30) P. M. Doty and H. M. Spurlin in E. Ott, H. M Spurlin and M. W. Grafflin, Editors, "Cellulose and Cellulose Derivatives," Interscience Publishers, New York, N. Y., 1955, pp. 1133–1163.

xylose residues in the main xylan chain), was calculated from the relationship $\bar{P}_n = \bar{M}_n(n/M_r)$, where n was the number of xylose residues per acid side chain and M_r was the molecular weight of the repeating unit of the polysaccharide.[31]

Viscosity Measurements.—The instrument used was a Craig–Henderson viscometer,[32] designed to eliminate effects of surface tension and to minimize kinetic energy corrections. Its capillary radius was 0.01778 cm., capillary length 18.59 cm., hydrostatic head 25.0 cm., and efflux volume 0.852 ml. The temperature was 30°. Samples of dry hemicellulose (225 mg.) were dissolved in M-cupriethylenediamine or in freshly distilled dimethyl sulfoxide containing 2% (v./v.) of water (15.0 ml.). For measurements, 10 ml. was used, and dilutions were made directly in the viscometer, the concentrations being varied from 1.5 to 0.2 g./dl. Reduced viscosities were plotted against concentrations according to Huggins[33] when linear relationships were obtained throughout. Extrapolation to zero concentration gave the intrinsic viscosity.

Light-scattering Measurements.—Light-scattering measurements were made with a Brice–Phoenix[34,35] photometer at a wave length of 5460 Å. The instrument was modified as described previously[36,37] to permit the use of light-scattering cells amenable to ultracentrifugation as described by Dandliker and Kraut.[38] Even in these cells, however, striations were observed in the light beam due to the presence of micellar debris, and a new type of cell was accordingly devised and used in all subsequent experiments (Fig. 2). The narrow tubings at the base and top of the new cell effectively captured all sedimenting or floating material.

The solvent was dimethyl sulfoxide, freshly redistilled *in vacuo*, and containing 2% of water (v./v.). A 1% solution of the polymer in this solvent was subjected to a preliminary ultracentrifugation at 140,000 *g* (40,000 r.p.m.) for 3 hr. in the No. 40 rotor of a Spinco Model L ultracentrifuge.[38] The clear solution was carefully decanted and transferred to the light-scattering cell which was floated with carbon tetrachloride–ethanol mixtures in the cups of a SW 25.1 swinging bucket rotor of the same ultracentrifuge. Centrifugation was at 35,000 *g* (20,000 r.p.m.) for 1 hr. The cells were transferred directly to the photometer and scattering intensities were measured at 45, 90 and 135° relative to the incident beam. The turbidity, τ, was calculated from the 90° scatter by means of a calibration factor determined with Ludox.[39,40] The refractive index correction of Carr and Zimm[41] was applied. The dissymmetry, Z, was calculated as the ratio of the intensities at 45 and 135°. Measurements were made at six different concentrations, c, ranging from zero to 0.01 g./ml. and solvent scatter was subtracted from that of the solution. Some polysaccharides, and especially the *O*-acetylated xylan, gave strongly fluorescent solutions. This difficulty was overcome as described in a previous publication.[42] The original concentration of the polymer was determined by adding a carefully measured aliquot to a 1:1 mixture of ethanol and ethyl acetate. The precipitate formed was collected on a sintered glass filter crucible (coarse), provided with a mat of acid-washed asbestos. After washing successively with ethanol and petroleum ether, the crucible with its content was dried at 60° *in vacuo* for 3 hr. and weighed. The reproducibility of this method was excellent.

Refractive index increments were measured in a Brice–Phoenix differential refractometer.[35] Both solutions and reference solvent had to be protected from osmospheric moisture to ensure reproducible results. In addition to the usual precautions, equal quantities of solution and solvent were carried through identical manipulations prior to measurements. Excellent agreement (±1.2%) was found between duplicate values of the increment on any one sample. The values obtained for the various fractions differed somewhat, however, and a mean value of 0.064 ± 0.006 was used.

The light-scattering data are summarized in Table II where $(c/\tau)_{c=0}$ values, dissymmetries (Z) and weight-average molecular weights ($\bar{M}_w$) are given. Molecular weights were calculated from the relationship

$$\bar{M}_w = \frac{3\lambda^4 N}{32\pi^3 n_0^2 (dn/dc)^2 (c/\tau)_{c=0}}$$

where λ is the wave length of the light, N is Avogadro's number and n_0 is the refractive index of the solvent. Dissymmetry corrections were applied. The rather high values for Z for the first two measurements with the 4-*O*-methylglucuronoxylan from white birch wood were probably due to a shorter time (2 hr.) of preliminary ultracentrifugation. The molecular weight of this polysaccharide was accordingly computed from the mean of the four c/τ values, corrected by a factor based on the two lower dissymmetries. The values obtained for the polysaccharide from sugar maple were not deemed reliable and have therefore not been included in Tables II and III.

Acknowledgment.—The authors wish to express their gratitude to Mr. W. L. Steyn, who carried out the osmotic pressure and light-scattering measurements. They are also thankful to Mr. J. Jaworzyn for valuable assistance.

(31) F. W. Barth and T. E. Timell, *J. Am. Chem. Soc.*, **80**, 6320 (1958).

(32) A. W. Craig and D. A. Henderson, *J. Polymer Sci.*, **19**, 215 (1956).

(33) M. L. Huggins, *J. Am. Chem. Soc.*, **64**, 2716 (1942).

(34) B. A. Brice, M. Halwer and R. Speiser, *J. Opt. Soc. Amer.*, **40**, 768 (1950).

(35) Manufactured by the Phoenix Precision Instrument Co., Philadelphia, Pa.

(36) M. M. Huque, D. A. I. Goring and S. G. Mason, *Can. J. Chem.*, **36**, 1952 (1958).

(37) M. M. Huque, J. Jaworzyn and D. A. I. Goring, *J. Polymer Sci.*, **39**, 9 (1959).

(38) Manufactured by Beckman Instruments, Inc., South Pasadena, California.

(39) A colloidal silica, manufactured by E. I. du Pont de Nemours and Co., Wilmington, Del.

(40) D. A. I. Goring, M. Senez, B. Melanson and M. M. Huque, *J. Colloid Sci.*, **12**, 412 (1957).

(41) C. I. Carr and B. H. Zimm *J. Chem. Phys.*, **18**, 1616 (1950).

(42) P. R. Gupta and D. A. I. Goring, *Can. J. Chem.*, **38**, 270 (1960).

THE PHOTOLYSIS OF METHYL MERCAPTAN[1]

BY T. INABA[2] AND B. DEB. DARWENT

Department of Chemistry, The Catholic University of America, Washington 17, D. C.

Received March 10, 1960

The effects of time, pressure and temperature on the photolysis of methyl mercaptan have been investigated. At low conversions hydrogen is the only important uncondensable gas. Methane arises from secondary reactions involving the product. Hydrogen results exclusively from the breaking of the S–H bond. The decomposition of CH_3S requires at least 30 kcal. mole^{-1}. The activation energy and "*P*" factor of the reaction $H + CH_3SH \rightarrow CH_4S + H_2$ are about 4.6 ± 0.1 kcal. mole^{-1} and 0.34, respectively.

Introduction

The photolysis of methyl mercaptan has been investigated by Skerrett and Thompson[3] who found that, on complete photolysis, the gaseous products consisted of H_2 (80%) and CH_4 (18%) and the condensable products were sulfur and dimethyl disulfide. The quantum yield for the disappearance of CH_3SH was about 1.7. They suggested that there may be two concurrent initial photochemical steps

$$CH_3SH + h\nu \longrightarrow CH_3S + H \quad (a)$$
$$\longrightarrow CH_4 + S \quad (d)$$

of which the former was the more prevalent and that the hydrogen atom disappeared by

$$H + CH_3SH \longrightarrow CH_3S + H_2 \quad (1)$$

The CH_3S radicals combined to form dimethyl disulfide.

Although the suggested mechanism is plausible, it is based on rather sketchy evidence. Thus, the experiments of Skerrett and Thompson were carried to extremely high conversion, with the consequence that, at least toward the end, there might have been serious complications from the photochemical or H atom reactions involving the products. There are strong indications[4] that the reaction

$$H + CH_3OH \longrightarrow H_2 + CH_2OH$$

is important in the photochemistry of methanol, so that the analogous reaction may have been expected with methyl mercaptan.

Accordingly, the photolysis of methyl mercaptan has been re-investigated, the conversion being restricted to less than 1%, to obtain further information concerning the nature of the initial photochemical and free radical reactions. Information concerning the rate constants of the elementary reactions has been obtained and an attempt was made to investigate the stability of the free radical intermediates.

Experimental

The methyl mercaptan (Mathieson Company, 99% pure) was subjected to thorough de-gassing, by trap-to-trap distillations *in vacuo*, and stored in flasks isolated by mercury cut-offs. Deuteromercaptan (CH_3SD) was prepared by repeated equilibration with 99.6% D_2O (Stuart Oxygen Company) and was shown by infrared[5] and mass spectrometry to be at least 95% pure. Ethylene was a research grade product (Philips Petroleum Company) and was thoroughly degassed before storage.

The apparatus was of the type usually used for gas-phase photochemical experiments. A medium pressure Hanovia quartz mercury lamp supplied the active light. Provision was make for mixing the gases thoroughly before photolysis. The temperature was controlled manually to ±2°. The volumes of the quartz cell and reaction system were approximately 200 and 300 cm.^{3}, respectively.

The gaseous products were separated, analyzed by hot CuO oxidation or mass spectrometrically, and measured by the use of standard techniques.

Results

The first set of experiments was done to investigate the effects of pressure, time and temperature on the rates of formation of H_2 and CH_4 when the conversion was restricted to less than 0.3%. The data (Table I) show that hydrogen was always the principal product. The formation of CH_4 varied rather erratically between 0 and 6% of the total uncondensable gas and did not change consistently with temperature, between 50 and 300° or with pressure. In other experiments at 50° and 54 mm. pressure, where the conversion was extended to 5.8%, methane became increasingly important; thus, at 0.61 and 5.8% conversion methane represented 7.5 and 12.8%, respectively, of the uncondensable gas. In later experiments, with CH_3SD, carried to still higher conversions, methane ac-

TABLE I

EFFECT OF TIME, PRESSURE AND TEMPERATURE ON THE PHOTOLYSIS OF CH_3SH

Reaction cell = 200 cm.^{3}; reaction volume = 300 cm.^{3}

Pressure,[b] mm.	Time, min.	Rates[a] H_2	Rates[a] CH_4	Pressure,[b] mm.	Time, min.	Rates[a] H_2	Rates[a] CH_4
(a) T = 50°				(b) T = 100°			
21	90	7.3	0.4	28	60	8.4	0.4
21	180	7.6	0.1	196	15	40.9	1.1
115	15	36.9	2.3	196	30	39.4	0.0
115	90	33.0	1.1				
209	15	43.7	2.3				
209	60	48.0	1.1				
(c) T = 200°							
35	60	13.6	0.3				
78	60	19.4	.4	(d) T = 300°			
78	30	18.2	.0	22	30	12.9	0.0
148	15	27.2	1.7	151	30	21.3	.0
148	30	27.7	0.9	24[c]	90	4.3	.0
79[c]	90	0.8	0.0	151[c]	90	12.9	.0

[a] Rates in cm.^{3} (N.T.P.) min.$^{-1}$ × 10^5. Rates of photochemical reactions were obtained by subtracting the thermal rate from the total rate. [b] Pressures—all corrected to 50°. [c] Denotes thermal reaction.

(1) This research was supported by a grant from the Petroleum Research Fund administered by the American Chemical Society. Grateful acknowledgment is hereby made to the donor of said fund.

(2) On leave from the University of Osaka, Japan.

(3) N. P. Skerrett and H. W. Thompson, *Trans. Faraday Soc.*, **37**, 81 (1951).

(4) M. K. Phibbs and B. deB. Darwent, *J. Chem. Phys.*, **18**, 495 (1950).

(5) We are grateful to Dr. E. D. Becker and Dr. N. E. Sharpless of the National Institutes of Health, Bethesda, Maryland, for the infrared analyses.

TABLE II

EFFECT OF ETHYLENE ON THE RATE OF FORMATION OF HYDROGEN[a]

p_1, mm.	p_2/p_1	R_a	R_p	k_2/k_1	p_1, mm.	p_2/p_1	R_a	R_p	k_2/k_1	p_1, mm.	p_2/p_1	R_a	R_p	k_2/k_1
	(a) T = 50°					(c) T = 220°					(b) T = 120°			
30	4.0	6.42	1.90	0.60	30	5.0	3.82	1.15	0.46	30	4.8	4.99	1.47	0.50
30	5.0	6.41	1.68	.57	45	5.0	5.56	1.73	.44	30	5.0	4.96	1.46	.48
45	5.0	9.10	2.33	.58	60	1.0	7.03	4.88	.44	30	5.0	4.82	1.37	.51
60	2.0	11.65	5.21	.61	60	3.0	6.46	2.64	.48	45	5.0	6.60	1.87	.51
60	3.0	11.01	3.91	.61	100	2.0	9.53	4.91	.47					Av. 0.50
60	4.0	10.20	3.08	.58	100	4.0	10.07	3.79	.41					
				Av. 0.59					Av. 0.45					

[a] Rates in cm.^{3} min.$^{-1}$ (N.T.P.) $\times$ 10^5.

counted for as much as 46% of the uncondensable gas. In those experiments, at pressure between 90 and 147 mm. and temperatures between 40 and 220°, the uncondensable gas was shown, by mass spectrometric analysis, to be entirely D_2 and CH_3D, no H_2 or HD was ever detected.

The effect of ethylene on the rate of formation of H_2 from CH_3SH was investigated at a variety of pressures and temperatures. The data (Table II) show clearly that the rate of formation of H_2 decreases with increase in the ratio C_2H_4/CH_3SH. Furthermore, if R_a and R_p are the rates of formation of H_2 in the absence and presence of C_2H_4, respectively, the ratio R_a/R_p is found to be a linear function of $[C_2H_4]/[CH_3SH]$ and to be independent of the total pressure at constant temperature. The presence of ethylene did not alter the rate of formation of methane, which was always very small.

Other experiments, with C_3F_6 in place of C_2H_4 show that C_3F_6 was also efficient in inhibiting the formation of H_2. However, the reproducibility of those experiments was very poor, and there are indications[3] that C_3F_6 changes slowly on storage, possibly by a polymerization or disproportionation type of process.

Discussion

The results of the present investigation indicate that hydrogen is the only uncondensable product when the conversion is kept small. Methane becomes of significance only when the extent of the conversion of mercaptan is large. Hence it is likely that CH_4 does not appear as a result of the photolysis of methyl mercaptan but comes from some process involving one of the stable products of the photolysis. Methane is not produced early in the photolysis even at 300°, where the thermal decomposition is becoming noticeable, and the rate of formation of hydrogen is essentially independent of temperature.

The results obtained with CH_3SD and the fact that olefins inhibit the production of hydrogen show clearly that the reactions

$$CH_3SH + h\nu \longrightarrow CH_3S + H \qquad (a)$$
$$H + CH_3SH \longrightarrow CH_3S + H_2 \qquad (1)$$

are the only important processes in the photolysis. The other possible processes

$$CH_3SH + h\nu \longrightarrow CH_2SH + H \qquad (b)$$
$$\longrightarrow CH_3 + HS \qquad (c)$$
$$\longrightarrow CH_4 + S \qquad (d)$$
$$H + CH_3SH \longrightarrow CH_2SH + H_2 \qquad (1')$$

do not occur to any appreciable extent.

The fact that, even at 300° where the thermal decomposition is noticeable, there is no increase in the rates of formation of either H_2 or CH_4 shows that the CH_3S radical possesses considerable thermal stability. The process

$$CH_3OCH_2 \longrightarrow CH_2O + CH_3$$

requires approximately 19 kcal. mole^{-1} and is easily detectable[6] at 150°. Hence, if we assume that at 300° CH_3S decomposed at 1/10th the rate of CH_3OCH_2 at 150° and that the frequency factors are the same, the activation energy for the thermal decomposition would be at least 30 kcal. mole^{-1}.

Some information concerning the rate and activation energy of reaction 1 has been obtained from the effect of ethylene on the rate of formation of H_2. The treatment of the data is similar to that used by Darwent and Roberts[7] for H_2S. Thus, in the presence of ethylene, the H atom has an alternative method of disappearing

$$H + C_2H_4 \longrightarrow C_2H_5 \qquad (2)$$

Provided the C_2H_5 disappears without generating H or H_2, or by reaction with H atoms, the following relationship holds

$$\frac{R_a}{R_p} - 1 = \frac{k_2}{k_1} \times \frac{p_2}{p_1}$$

where $p_1 = [CH_3SH]$ and $p_2 = [C_2H_4]$. Hence, by measuring R_a and R_p at known p_1 and p_2 we can calculate the ratio k_2/k_1. The above relationship requires R_a/R_p to be a linear function of p_2/p_1, and independent of the total pressure. The results show that those requirements have been met. In particular, the fact that the value of k_2/k_1 is not sensitive to changes in the total pressure is strong indication (a) that the H atom formed in reaction (a) does not possess energy significantly greater than the thermal equilibrium value or, if it does, it is nearly always deactivated by collision before it reacts, and (b) that the C_2H_5 formed in reaction 2 does not, under the conditions of the experiments, redissociate into C_2H_4 and H.

The effect of temperature on k_2/k_1 has been examined from an Arrhenius plot of the results of individual experiments. Although the points are rather scattered, the extreme values of $\Delta E = E_1 - E_2$ are 0.42 and 0.67 kcal. mole^{-1}. Adopting the average value of 0.54 $\pm$ 0.12 for ΔE and assuming

(3) W. J Ambs, unpublished results.

(6) R. A. Marcus, B. deB. Darwent and E. W. R. Steacie, *J. Chem. Phys.*, **16**, 987 (1948).

(7) B. deB. Darwent and R. Roberts, *Faraday Soc. Disc.*, **14**, 55 (1953).

$Z_1 = Z_2$, we find $P_2/P_1 = 0.26$. If we accept the previously[7] suggested values of $E_2 = 4.1$ kcal. mole^{-1} and $P_2 = 0.09$, we find $E_1 \approx 4.6$ kcal. and $P_1 = 0.34$. For the reaction of D with D_2S, the previously[7] derived values were $E = 5.0$ kcal. mole^{-1} and $P = 0.73$. The slightly lower activation energy and P factor for reaction 1 is not unexpected since substitution of H by CH_3 usually results in a lower dissociation energy of the remaining bond and also halves the intrinsic probability of the reaction.

THE KINETICS OF THE REACTIONS OF AROMATIC HYDROCARBONS IN SULFURIC ACID.[1] I. BENZENE

BY MARTIN KILPATRICK, MAX W. MEYER AND MARY L. KILPATRICK

The Department of Chemistry, Illinois Institute of Technology, Chicago, Ill.

Received March 18, 1960

The rate of sulfonation of benzene in sulfuric acid solution has been measured spectrophotometrically; the results obtained are in fair agreement with those of Gold and Satchell, obtained by an isotope-dilution technique. An empirical equation has been found which fits the experimental results and which can be interpreted in terms of the concentration of the molecular sulfuric acid present in mixtures of sulfuric acid and water, as determined by Young and co-workers using Raman spectra, and the activity of water in these mixtures, as determined by Giauque and co-workers.

In an attempt to unravel the kinetics of the Jacobsen reaction,[2] it became necessary to understand the kinetics of sulfonation of the four- and five-methylsubstituted benzenes. The range of concentration of sulfuric acid for pure sulfonation is limited for durene (1,2,4,5-methylbenzene), isodurene (1,2,3,5-methylbenzene) and pentamethylbenzene by desulfonation, isomerization and disproportionation reactions. To avoid complications, the first series of experiments was carried out with benzene.

The rate of reaction was determined by following the appearance with time of benzenesulfonic acid spectrophotometrically in the ultraviolet. A Cary Spectrophotometer Model 11 equipped with a program attachment was used. The reaction vessel was the absorption cell, and the general procedure was as follows.

Sulfuric acid of known concentration was cooled in a refrigerator below the temperature planned for the experiment, a drop of hydrocarbon added from a syringe to give a concentration of 1×10^{-4} mole per liter, and after shaking for five minutes the absorption cell was filled and placed in the thermostated compartment of the spectrophotometer. After allowing a suitable time for the establishment of thermal equilibrium, the recording spectrophotometer was started and the rate of formation of sulfonate determined at the absorption peak 272 mμ. The molar extinction coefficient for the benzenesulfonic acid is so much greater than that for benzene that no appreciable error is introduced by the presence of unreacted hydrocarbon. Experiments were carried out at 25 and 12.3° with temperature control of ±0.05° in most cases. As the reaction proved to be strictly first order in hydrocarbon, as shown by a typical run in Fig. 1, in most later experiments the Guggenheim[3] method of evaluating the velocity constant was used. The quoted rate constants have limits of error of ±5% (as compared with ±20% in the work of Gold and Satchell).

The equation

$$\frac{d[ArSO_3H]}{dt} = k_{obsd}[ArH] \qquad (1)$$

holds since there is a large constant excess of sulfuric acid and water in each experiment. That the reaction goes to completion with no residual hydrocarbon in equilibrium with the sulfonic acid has been shown by Gold and Satchell[4] at 25° and confirmed by us by showing that no desulfonation of benzenesulfonic acid occurs under our experimental conditions.

As shown in Fig. 2 a plot of log k_{obs} *vs.* sulfuric acid concentration is linear and gives a convenient interpolation equation. The agreement with the results of Gold and Satchell,[4] who used an isotopic dilution technique to follow the disappearance of benzene, is fair. The half-times are given on the right, and as benzene sulfonates too rapidly at 18 molar sulfuric acid for an accurate determination of the velocity constant, a few experiments were carried out with bromobenzene to test the linearity of the relation. Least squares treatment of the data for benzene at 25 and 12.3° gives the equations

$$\log(k_{obsd} \times 10^6) = -14.3685 + 1.133\,[H_2SO_4]_{st} \qquad (2)$$

$$\log(k_{obsd} \times 10^6) = -18.9574 + 1.380\,[H_2SO_4]_{st} \qquad (3)$$

where $[H_2SO_4]_{st}$ represents the stoichoimetric molarity of the acid.

In Fig. 2 the lines for the sulfonation of benzene at 25 and 12.3° are not parallel but show that the experimental (apparent) energy of activation decreases with increasing acid concentration. For example the calculated energy of activation at 15.7 M sulfuric acid is 21.8 kcal./mole and 12.0 kcal./mole at 17.0. This can only mean that we are dealing with elementary steps and intermediates involved in complex equilibria or steady states.

The problem is to find an empirical rate equation which fits the experimental data. A plot of log k_{obsd} *vs.* H_0 is linear with a slope of −2.2 while a

(1) Presented in part at the 134th Meeting of the American Chemical Society, Chicago, September 1958, before the Division of Physical Chemistry.

(2) O. Jacobsen, *Ber.*, **19**, 1209 (1886); **20**, 896 (1887).

(3) E. A. Guggenheim, *Phil. Mag.*, **1**, 538 (1926).

(4) V. Gold and D. P. N. Satchell, *J. Chem. Soc.*, 1635 (1956).

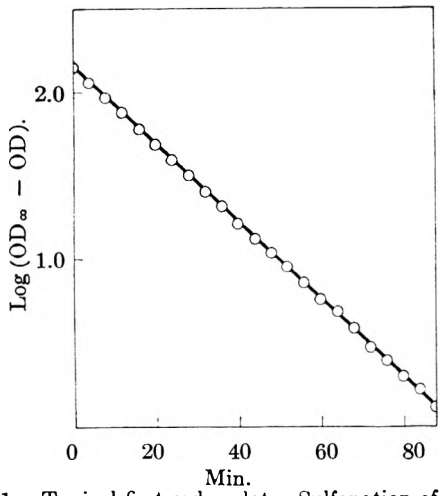

Fig. 1.—Typical first-order plot. Sulfonation of benzene in 16.90 M H_2SO_4 at 12.3°: 0.434 k_{obsd} = 231 × 10^{-4} min.$^{-1}$; $t_{1/2}$ = 13 min.

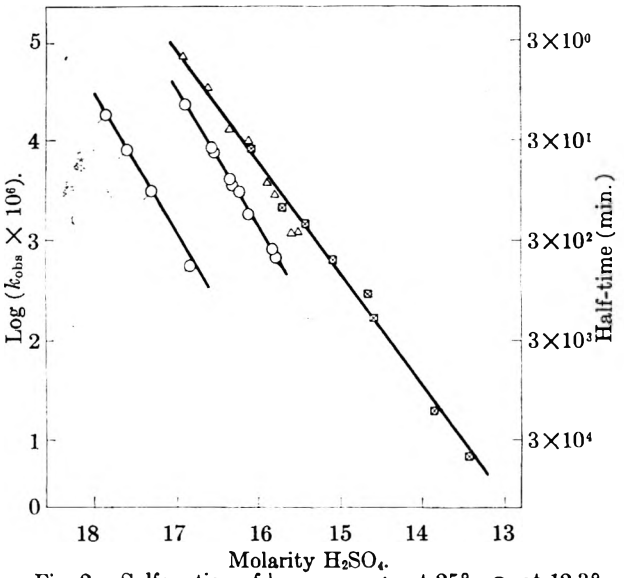

Fig. 2.—Sulfonation of benzene: △, at 25°; ○, at 12.3°; ⊠ Gold and Satchell's data at 25°; ⌀, bromobenzene at 12.3°.

plot of log k_{obsd} *vs.* the acidity function J_0[5] is not such a good straight line but gives a slope close to −1.0. Since a more rigid test is to plot log k_{obsd} +

$$J_0 = H_0 + \log a_{H_2O} \qquad (4)$$

H_0 *vs.* log a_{H_2O} using the recent values of Giauque and co-workers.[6] This plot does not give a linear relationship but the slope corresponding to the range 14–16 molar is −1.3 which may mean that water is not involved in the transition state of the rate-determining step. Brand,[7] studying the sulfonation of *p*-nitrotoluene and nitrobenzene in oleums containing up to 30% sulfur trioxide, used an acidity function to determine the relative concentration of the SO_3H^+ which he considered the sulfonating agent.

Sulfonation of methylbenzenes at 25° becomes noticeable above 12 molar sulfuric acid and this is where Young and his co-workers[8,9] begin to detect molecular sulfuric acid by Raman spectra. On the assumption that molecular sulfuric acid (or its reaction products) was involved in the sulfonation process it was found empirically that the over-all velocity constant for the sulfonation of benzene over the range of concentration studied may be written

$$\frac{d[\Sigma ArSO_3H]}{dt} = k \frac{[ArH][H_2SO_4]^2_{sp}}{a_{H_2O}} \qquad (5)$$

where the bracket $[H_2SO_4]_{sp}$ represents the species concentration of sulfuric acid obtained from the Raman spectral data of Young[8] by interpolation, and $\Sigma ArSO_3H$ represents total sulfonate.

Table I shows that at 25° equation 5 holds within the accuracy and limitations of the available Raman data. The data do not extend below a stoichiometric concentration of 15 M sulfuric acid and are not available at the temperature of the second set of kinetic data (12.3°) and the Raman data at 25° have been used. The values of a_{H_2O} are from Giauque and co-workers and have been converted to the molarity scale.[6] The values of the first-order velocity constant in Table I were calculated using decadic logarithms., *i.e.*, k_{obsd} is 0.4343 times the true constant.

Equation 5 indicates that the reaction is first order in hydrocarbon and second order in molecular sulfuric acid.

The self-ionization of pure sulfuric acid is represented by the equilibria

$$2H_2SO_4 \rightleftharpoons H_3SO_4^+ + HSO_4^- \qquad (6)$$

$$2H_2SO_4 \rightleftharpoons H_3O^+ + HS_2O_7^- \qquad (7)$$

which, however, become unimportant below 98–99% acid. Here the stable sulfate species, detected by Raman spectral measurements, are $SO_4^=$, HSO_4^- and H_2SO_4,[8] and a fourth recently reported[9] species $H_5SO_5^+$ which in the 80–100% range rises to a maximum concentration and then drops off to a negligible value in 100% acid.[10] The species $H_5SO_5^+$ (or H_3O^+ (H_2SO_4)) has also been reported by Wyatt.[11] It should be particularly noted that the species H_2SO_4 becomes detectable near 80% acid, *i.e.*, about where sulfonation sets in, and rises steeply thereafter to its maximum at 100%. On the oleum side, the Raman measurements[9] show $HS_2O_7^-$ and $H_2S_2O_7$ rising from undetectably low concentrations in 100% acid to a maximum (for Σ $H_2S_2O_7$) at *ca.* 50% oleum, and they show the species SO_3 as becoming detectable in *ca.* 30% oleum.

Using the species stable in aqueous sulfuric acid, no reaction scheme was found yielding a rate law in agreement with equation 5. If, however, as a working hypothesis $H_2S_2O_7$, or SO_3 or SO_3H^+, is assumed as an unstable intermediate in sulfonation in aqueous sulfuric acid, an equation of the form of (5) may be obtained. Thus for the scheme

(5) V. Gold and B. W. V. Hawes, *J. Chem. Soc.*, 2101 (1951).

(6) W. F. Giauque, E. W. Hornung, J. E. Kunzler and T. R. Rubin, *J. Am. Chem. Soc.*, **82**, 62 (1960).

(7) J. C. D. Brand, *J. Chem. Soc.*, 1004 (1950).

(8) T. F. Young, L. F. Maranville and H. M. Smith, "The Structure of Electrolyte Solutions," John Wiley and Sons, Inc., New York, N. Y., 1959, pp. 48–58.

(9) G. E. Walrafen, Dissertation, University of Chicago, June, 1959.

(10) T. F. Young, private communication.

(11) P. A. H. Wyatt, *Trans. Faraday Soc.*, **56**, 490 (1960).

$$\text{(i)}\quad 2H_2SO_4 \underset{2}{\overset{1}{\rightleftharpoons}} H_2S_2O_7 + H_2O$$

$$\text{(ii)}\quad ArH + H_2S_2O_7 \underset{4}{\overset{3}{\rightleftharpoons}} ArH{\cdot}H_2S_2O_7$$

$$\text{(iii)}\quad ArH{\cdot}H_2S_2O_7 \xrightarrow{5} \text{Products}$$

during the period of the stationary state the net rate, in the standard medium, is

$$\frac{d[\Sigma ArSO_3H]}{dt} = \frac{k_1k_3k_5[H_2SO_4]^2[ArH]}{k_3k_5[ArH] + [H_2O]\{k_2k_5 + k_2k_4\}}$$

and since k_3 would be expected to contain an exponential factor and k_2 none, or one close to unity, $k_3k_5[ArH] << k_2k_5[H_2O]$, and one has

$$\frac{d[\Sigma ArSO_3H]}{dt} = \frac{k_1k_3k_5}{k_2\{k_4 + k_5\}} \times \frac{[H_2SO_4]^2[ArH]}{[H_2O]}$$

With change in medium k_1/k_2 becomes $K_1 f^2_{H_2SO_4}/f_{H_2S_2O_7}f_{H_2O}$ where K_1 is the equilibrium constant for reaction (i), and if $f^2_{H_2SO_4}/f_{H_2S_2O_7}$ and the kinetic activity coefficient ratios for the other velocity coefficients are combined as F, one has

$$\frac{d[\Sigma ArSO_3H]}{dt} = \frac{K_1k_3k_5}{k_4 + k_5} \times \frac{[H_2SO_4]^2[ArH]}{a_{H_2O}} \times F$$

In the scheme just given, $H_2S_2O_7$ both sulfonates the aromatic and removes the dislodged proton. It is necessary, if SO_3 or SO_3H^+ is the sulfonating agent, to choose a proton-acceptor giving the observed rate law. Cowdrey and Davies,[12] in their study of the rate of sulfonation of nitrotoluene in 92–99% sulfuric acid, concluded that for each of the pairs

(a) SO_3 and H_2SO_4
(b) SO_3H^+ and HSO_4^-

the product of the concentrations of the sulfonating agent and the proton-acceptor depended on the same functions of medium concentration as did the rate of sulfonation. The same appears true here, and reaction schemes involving pair (a) or pair (b), and leading to an expression of the form of (5), are readily set up.

A more complex mechanism of sulfonation was proposed by Berglund-Larsson and Melander[13] to account for their results, in nitrobenzene as solvent, on the sulfonation of bromobenzene containing tracer amounts of bromobenzene-4-t by H_2SO_4–SO_3 mixtures. They found a weak isotope effect, and in explanation proposed a scheme involving two intermediates, one charged, one uncharged, formed from bromobenzene and the sulfonating agent SO_3H^+. Later experiments carried out by Berglund-Larsson[14] to determine the temperature dependence of the isotope effect strengthened belief in the complexity of the sulfonation process. Because of the rapidity of exchange, however, the use of isotopes does not appear helpful for studies on sulfonation in aqueous sulfuric acid; in 80% acid the hydrogen exchange is much faster than the sulfonation for benzene and toluene at 25°.[15] It therefore does not appear possible to correlate the mechanism of sulfonation of benzene in aqueous acid with the effect of the hydrogen isotopes present in substrate or solvent, as was done, for example, by Brand, Jarvie and Horning[16] in their recent study of sulfonation in oleum.

TABLE I

SULFONATION OF BENZENE

H_2SO_4 stoichiometric, moles/l.	0.434 $k_{obsd.}$ × 10^4, min.$^{-1}$	H_2SO_4, species moles/l.	a_{H_2O} × 10^5	$\frac{10^8\, k_{obsd.}\, a_{H_2O}}{[H_2SO_4]^2}$ species
		25°		
17.0	775	9.1	12.2	11
16.5	210	7.0	26.7	11
16.0	57.0	5.2	54.1	11
15.5	15.5	3.7	103	12
15.0	4.20	2.3	190	13
		12.3°		
16.90	22.9	8.6	14.4	4.5
16.58	82.8	7.3	23.8	3.7
16.54	72.9	7.2	25.2	3.5
16.35	39.9	6.4	33.3	3.2
16.33	37.4	6.3	34.2	3.2
16.32	36.2	6.3	34.7	3.2
16.24	28.1	6.0	38.9	3.0
16.12	19.2	5.6	45.9	2.8
15.84	7.89	4.7	65.3	2.4
15.79	6.73	4.5	71.6	2.4

Acknowledgment.—This research was supported in part by a grant from the Petroleum Research Fund administered by the American Chemical Society. Grateful acknowledgment is hereby made to the donors. Thanks are also due to the Simoniz Company for yearly grants to the department.

(12) W. A. Cowdrey and D. S. Davies, *J. Chem. Soc.*, 1871 (1949).
(13) U. Berglund-Larsson and L. Melander, *Arkiv för Kemi*, **6**, 219 (1953).
(14) U. Berglund-Larsson, *ibid.*, **10**, 549 (1957).
(15) L. Melander, private communication.
(16) J. C. D. Brand, A. W. P. Jarvie and W. C. Horning, *J. Chem. Soc.*, 3844 (1959).

RADIATION CHEMISTRY OF CYCLOPENTANE–CYCLOHEXANE MIXTURES[1]

By G. A. Muccini and Robert H. Schuler

Mellon Institute, Radiation Research Laboratories, Pittsburgh, Pennsylvania

Received March 21, 1960

Radiolysis of mixtures of cyclopentane and cyclohexane with γ-rays at 70,000 rads/hr. results in a greater yield of products derived from cyclopentane than would be expected from the fraction of this component in the system. This effect is attributed to a change in the identity of the intermediate radicals as a result of preferential abstraction of hydrogen from the cyclopentane. Studies of the primary radical yields by iodine scavenging methods and of the effect of intensity on the products from the mixed hydrocarbons confirm this explanation.

Previous investigations of the radiation chemistry of mixed hydrocarbons have focussed attention on the non-ideal behavior of systems where energy transfer between the various components is possible. Such non-ideality is particularly emphasized in the early work of Manion and Burton where the yields of gaseous products from benzene–cyclohexane solutions were found to be less than expected from the composition of the system.[2] The present work was undertaken in order to examine a system (cyclopentane–cyclohexane) in which the radiation chemical effect on each of the components present might well be expected to be proportional to their concentration. As is seen below, even when the inital chemical products do correspond to such an expectation, changes in the identity of the intermediate radicals due to purely chemical processes can result in a departure of the over-all behavior at low absorbed dose rates. As previously reported[3] approximate ideality returns at high dose rates where secondary chemical processes interfere less with the ultimate determination of the products.

Experimental

Phillips Research Grade hydrocarbons were used in all investigations. An olefinic impurity in the cyclohexane, which was detected by the brownish color of its iodine solution, was removed by passing the hydrocarbon through a silica gel adsorption column. Samples were outgassed and sealed before irradiation.

Irradiations were carried out for the most part at room temperature in a Brookhaven type cobalt-60 source at an absorbed dose rate of 70,000 rads/hr. Absolute yields have been calculated relative to the yield of the Fricke dosimeter [$G(Fe^{+++}) = 15.5$] with the assumption that energy absorption is proportional to the electron density of the irradiated sample. Certain additional irradiations were carried out at other dose rates where only the relative yields of products were measured. The total absorbed dose was approximately 3×10^{20} e.v./g. (5 megarads) except in experiments in which 0.003 *M* iodine was employed to measure the initial yield. In these scavenger studies the absorbed dose was limited to 6×10^{19} e.v./g. in order to maintain a significant iodine concentration throughout the irradiation.

After irradiation the samples were examined gas chromatographically with attention being focussed on the products in the C_{10} to C_{12} region. Fractionation was on a 250 cm. column of 25% silicone grease on firebrick and detection was by thermal conductivity methods. Typical chromatograms are shown in Fig. 1. The major products are cyclopentylcyclopentane, cyclopentylcyclohexane and cyclohexylcyclohexane. Small amounts of other products complicate the observed region to a certain extent but do not appear to alter the main conclusions drawn below. The sensitivity of the gas chromatographic apparatus was established with solutions containing known amounts of cyclopentyl and cyclohexyl iodides and of cyclopentylcyclopentane and cyclohexylcyclohexane. Since almost identical sensitivities were observed for the last two substances it was assumed that a mean calibration would hold for cyclopentcyclohexane. Only these three major products are considered below.

Results and Discussion

In the following discussion it is assumed that absorption of energy by each component of a mixture is proportional to the electron fraction present. This assumption is in turn based on the premise that the cross sections for the interactions of the ionizing electrons are independent of the nature of the bound electrons. Since radiation chemical effects are to a large extent ultimately produced by secondary and tertiary electrons having very low energies the above assumptions are obviously not generally valid. In particular these assumptions are not true for mixtures containing heavy atoms where the inner very energetically bound electrons contribute only slightly to the absorption. Mixtures of cyclopentane and cyclohexane however, provide an example where these assumptions must be very nearly valid. Since the empirical formulas of the components are the same, the average cross sections for electron–electron interactions must be identical (except for very slight differences due to chemical binding). Barring energy transfer between the components the initial chemical decomposition of each of the components should be proportional to the electron fraction present.

In Fig. 2 the yields are given for the various "dimer" products formed in the γ-ray experiments at 70,000 rads/hr. It is seen that the curves are skewed somewhat in favor of products derived from cyclopentane in spite of the fact that the yield of cyclopentylcyclopentane from pure cyclopentane is somewhat less than the corresponding yield from cyclohexane. This effect is readily seen in the upper chromatographic curve of Fig. 1, where for solutions 50 electron % in each component the ratio of yields of cyclopentylcyclopentane to cyclopentylcyclohexane to cyclohexylcyclohexane is 1.65:2.00:0.72. If each component were affected to the same extent a ratio of 1:2:1 would, of course, be expected. If the yield of "dimer" from the pure components represents the decomposition, then a ratio of 0.75:2.00:1.25 would be expected. It is seen that this latter ratio is nearly identical to the value of 0.70:2.04:1.26 observed at high intensities.[3] The favoring of products derived from cyclopentane is particularly obvious for solutions dilute in cyclo-

(1) Supported, in part, by the U. S. Atomic Energy Commission.

(2) J. Manion and M. Burton, This Journal, **56**, 560 (1952).

(3) R. H. Schuler and G. A. Muccini, *J. Am. Chem. Soc.*, **81**, 4115 (1959).

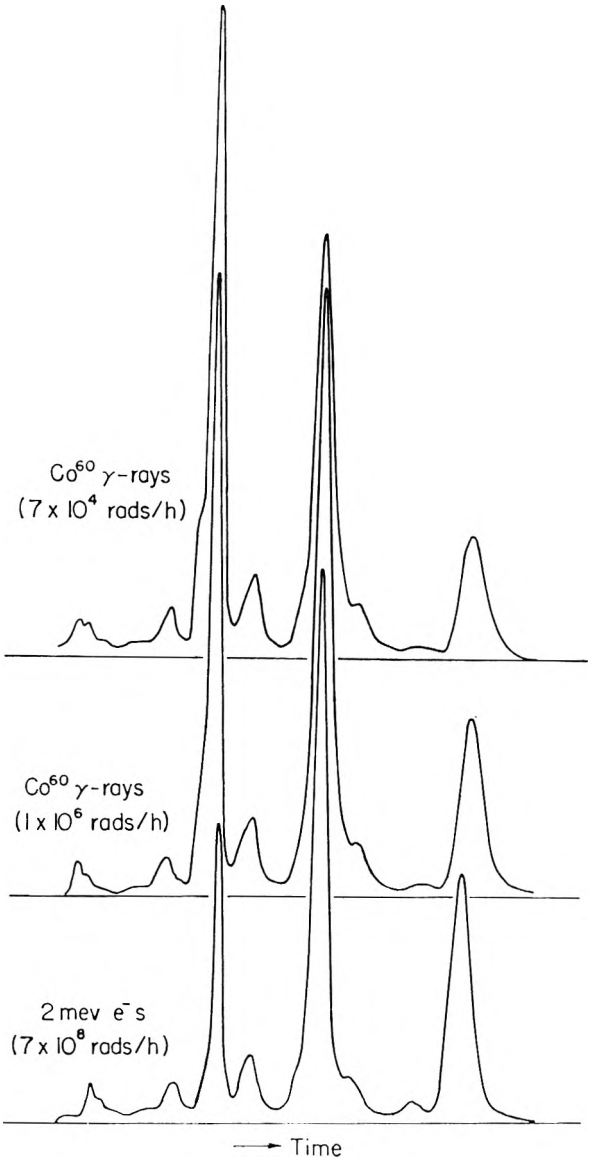

Fig. 1.—Gas chromatograms of products in the C_{10}–C_{12} region from cyclopentane–cyclohexane solutions irradiated at various intensities. Solutions are 50 electron % in each component.

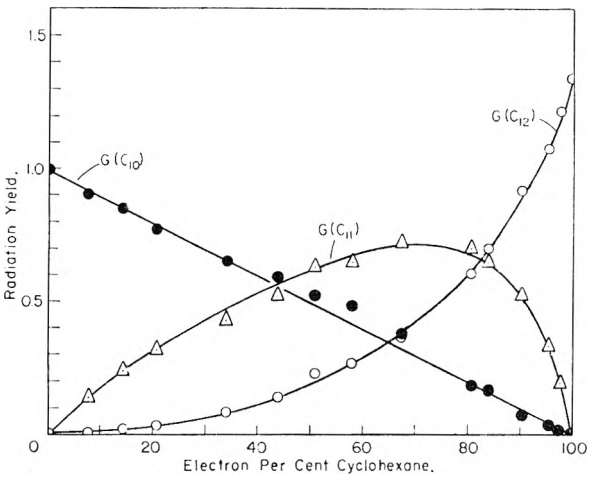

Fig. 2.—Yield of dimer products as a function of solution composition: ●, cyclopentylcyclopentane; △, cyclopentylcyclohexane; ○, cyclohexylcyclohexane.

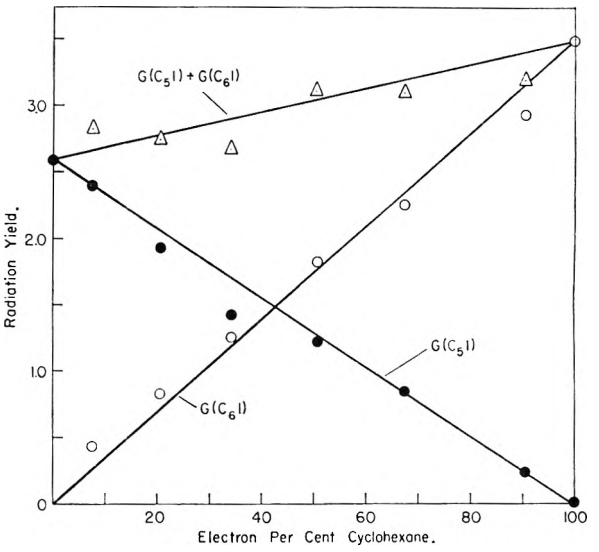

Fig. 3.—Iodide yields produced in the scavenging of cyclopentane–cyclohexane solutions with 0.003 *M* iodine: ●, cyclopentyl iodide; ○, cyclohexyl iodide; △, cyclopentyl iodide + cyclohexyl iodide.

pentane, *e.g.*, for solutions containing only 10% the total contribution of cyclopentane to the "dimer" products is 3.5 times the expected value.

These studies were extended by two types of experiments to determine if the above observations were a manifestation of the importance of physical processes such as transfer of energy from one component to the other or rather due to a purely chemical effect involving the preferential abstraction of hydrogen by the cyclohexyl radicals formed in the radiolysis, *i.e.*, $k_1 > k_2$ for the reactions

$$C_6H_{11}\cdot + C_5H_{10} \longrightarrow C_6H_{12} + C_5H_9\cdot \quad (1)$$

$$C_5H_9\cdot + C_6H_{12} \longrightarrow C_5H_{10} + C_6H_{11}\cdot \quad (2)$$

First the effect of intensity was examined and as previously reported[3] showed that the contribution of cyclopentane to the decomposition decreases significantly as the intensity increases. This is readily explained in terms of a decreased lifetime of the intermediate radicals due to the increased rate of the combination reaction

$$R\cdot + R\cdot' \longrightarrow RR' \quad (3)$$

relative to 1 and 2. If it is assumed that the bimolecular rate constant for reaction 3 is less than 10^{11} liter mole^{-1} sec.$^{-1}$ then it can be shown that for the intensities at which the present γ-ray experiments are carried out the lifetime of the intermediate radicals will be greater than 10 mseconds. Abstraction reactions which occur with reasonably low activation energies (less than 8 kcal./mole if we neglect steric and diffusion terms) should then effectively compete with 3. If, as was originally expected, the rate constants for reactions 1 and 2 were the same then no change in composition would result from the abstraction reactions. Apparently, however, abstraction of hydrogen from cyclopentane occurs somewhat more readily than from cyclohexane. Since these reactions probably recur a number of times before the ultimate determination of products it is necessary only that the rate con-

stants of 1 and 2 be very slightly different in order to explain the present observations. Change in the identity of radicals at the low intensities of most γ-ray experiments can be expected to be even more pronounced in cases where easily abstractable hydrogen atoms are present.

The change of product composition with intensity shows that chemical processes other than those of first order are involved. This rules out reactions of ions or excited species with solvent molecules as the sole source of these "dimer" products. Presumably these products result to a considerable extent from the combination of cyclopentyl and cyclohexyl radicals according to the competing reactions

$$C_5H_9\cdot + C_5H_9\cdot \longrightarrow C_{10}H_{18} \quad (4)$$
$$C_5H_9\cdot + C_6H_{11}\cdot \longrightarrow C_{11}H_{20} \quad (5)$$
$$C_6H_{11}\cdot + C_6H_{11}\cdot \longrightarrow C_{12}H_{22} \quad (6)$$

If combination is purely statistical, *i.e.*, $k_4:k_5:k_6 = 1:2:1$ then the product ratio $[C_{11}H_{20}]/[C_{10}H_{18}]^{1/2}[C_{12}H_{22}]^{1/2}$ should be equal to 2. A ratio between 1.8 and 1.9 was found for all the experiments of Fig. 2. This shows that differentiation does not occur as a result of a favored combination reaction, a possibility since a fraction of the radicals are lost in disproportionation processes. A slight tendency of this ratio to increase with intensity (to 2.2 at 7×10^8 rads/hr.) was observed and may be due to underlying reactions which produce "dimer" product by other processes.

The second type of experiment involved the use of iodine to scavenge the free radicals produced initially. Unfortunately because of the sensitivity limits presently imposed by chromatographic methods such studies must be carried out at relatively high iodine concentrations ($\sim$0.003 M) and are accordingly plagued by unresolved questions concerning the use of scavengers at these concentrations.[4] The results, however, appear to be in complete agreement with the conclusions reached above. It is seen in Fig. 3 that the yields found for the individual radicals in the scavenging experiments are directly proportional to the electron fraction of the parent material present. This is expected since secondary chemical processes should not interfere as they do in the absence of scavenger. Energy transfer between cyclopentane and cyclohexane apparently does not occur and we observe ideal behavior. This result also substantiates the assumptions on energy absorption made in the initial paragraph of the discussion.

(4) R. H. Schuler, THIS JOURNAL, **61**, 1472 (1957).

TABULATED FUNCTIONS FOR HETEROGENEOUS REACTION RATES: THE ATTACK OF VITREOUS SILICA BY HYDROFLUORIC ACID

BY AVROM A. BLUMBERG[1] AND STAVROS C. STAVRINOU[1]

Mellon Institute, Pittsburgh 13, Pennsylvania

Received March 21, 1960

The rate equation describing the reaction between a solid and liquid has been integrated in tabular form for the cases where the partial order with respect to the solute (liquid) reactant, $n = 1/2$, 1, $3/2$ and 2, and has also been integrated in functional form for $n = 1$. The reaction between powdered vitreous silica and aqueous hydrofluoric acid in strongly acidic media is very closely first order with respect to hydrofluoric acid concentration, and the order and rate constant obtained here agree with those calculated from the results of a different method.

Introduction

The reaction between hydrofluoric acid and silica was probably discovered by Scheele at the time he first prepared the acid in 1771.[2] Berzelius identified the products as silicon tetrafluoride and water,[3] and later the combination of the tetrafluoride with hydrofluoric acid to form the stable fluorosilicic acid was observed.[4] This last is a strong acid, comparable to sulfuric acid, and does not etch glass or attack silica.

Early studies on the rate of attack include the work of Gautier[5] who compared the degree of attack on glass, fused silica and two faces of crystalline quartz; of Lebrun[6] who measured the velocities of dissolution of quartz, along four different faces; and of Schwarz[7] who exposed, in turn, quartz, tridymite, cristobalite and amorphous (vitreous) silica to hydrofluoric acid and found the amount dissolved to increase in the order given. More recently, Palmer[8] found the rate of attack of "Vitreosil" to be related not to hydrofluoric acid concentration but to bifluoride concentration. At low ionic strength the rate increased with this property, too. Hydrogen ion had a catalytic effect.

Nevertheless, reaction has been observed using hydrogen fluoride gas[9] and in some aqueous systems of high acidity,[8] in neither case of which is there much bifluoride ion. It seems worthwhile to resolve this point by studying systems in which competing reactions are ruled out; and the present study, limiting the attacking species to hydrofluoric acid alone, was undertaken.

(1) Pittsburgh Plate Glass Company Research Project.

(2) A. B. Burg, "Fluorine Chemistry," Vol. I (J. H. Simons, Editor), Academic Press, Inc., New York, N. Y., 1950, p. 180.

(3) J. J. Berzelius, *Pogg. Ann.*, *I*, 169 (1824).

(4) N. V. Sidgwick, "The Chemical Elements and their Compounds," Vol. I, Oxford University Press, Oxford, England, 1950, p. 615.

(5) A. Gautier and P. Clausmann, *Compt. rend.*, **157**, 176 (1913).

(6) J. Lebrun, *Bull. Classe Sci. Acad. Roy. Belg.*, 953 (1913).

(7) R. Schwarz, *Z. anorg. Chem.*, **76**, 422 (1912).

(8) W. G. Palmer, *J. Chem. Soc.*, 1656 (1930).

(9) W. K. Van Hagen and E. F. Smith, *J. Am. Chem. Soc.*, **33**, 1504 (1911).

The equilibria of the hydrofluoric acid in water, described by

$$HF \longleftrightarrow H^+ + F^-,\ K_1\ (25°) = 7 \times 10^{-4}$$
$$HF + F^- \longleftrightarrow HF_2^-,\ K_2\ (25°) = 5$$

have been investigated by several workers and their values have been collected by Sidgwick.[10] At high acidity the first dissociation is suppressed, thus reducing the fluoride and bifluoride ion concentrations to negligibly low values. For example in a solution, one molal in each of hydrofluoric and hydrochloric acids, the bifluoride ion concentration is about 3.5×10^{-3} molal; and the fluoride ion is about 7×10^{-4} molal.

The work here does not involve hydrofluoric acid concentrations above two molal because there is evidence[11] that at higher concentrations hydrofluoric acid becomes a strong acid through the formation of polymers.

Experimentation

Hydrochloric acid was prepared from reagent grade stock and standardized against primary standard sodium carbonate, with methyl orange and carmine indigo mixed indicator, using a comparison standard buffered at *p*H 3.8. The precision was within two parts per thousand.

Hydrofluoric acid was prepared from reagent grade stock and standardized against sodium hydroxide solution (which, in turn, was standardized against the hydrochloric acid), using phenolphthalein indicator. Precision was within four parts per thousand.

Powdered vitreous silica was prepared by passing Corning fused silica 7940 lump cullet (analysis: less than 100 p.p.m. impurities) through a jaw crusher and a hammer mill and sifting to sort the powder in five ranges between 100 and 270 mesh. This was followed by repeated washing with aqua regia (to remove iron, as indicated by thiocyanate test) and repeated sedimentation along a four-foot column of water (to remove fines, as indicated by the Tyndall effect). Impurities, determined by emission spectroscopy, were less than 88 p.p.m. after this processing (*e.g.*, Al, 30 p.p.m.; Na, 20; Fe, 10; Cr, 9; Mg, 7; Ca, 4; also Cu, Li). Surface areas were determined by krypton adsorption.

Reagent grade ammonium chloride was used without further purification.

All reactions were carried out in polyethylene containers, suspended from a wrist-action shaker, and immersed in a thermostat bath at 32.1 ± 0.1°. Weighed samples of powdered silica were added to known amounts of reactant solution (maintained at the bath temperature) and shaken for suitable time intervals. The reactions were quenched by titration with ammonia water to the vicinity of *p*H 7. All quenchings were completed in about 30 seconds. Excess base was avoided to prevent alkaline hydrolysis of fluorosilicate[2] with re-formation of silica. The unreacted silica was collected on a platinum Gooch crucible, washed, dried overnight, ignited to volatilize any remaining ammonium fluoride, chloride or fluorosilicate, and then weighed to determine the mass of unreacted silica.

All solutions were prepared by weighing out the necessary amounts of stock solutions. Ionic strengths were adjusted by the addition of ammonium chloride, so that (HCl) + (NH_4Cl) = 4.00 molal, unless otherwise stated.

All runs involved about one g. of vitreous silica and solutions containing exactly 200 g. of water.

Treatment of Data.—The assumption was made that the solution of silica follows the rate law

$$dM/dt = -kS(HF)^n \qquad (1)$$

where M is the mass of the vitreous silica powder, S is its surface, and n is the appropriate exponent.

It has been pointed out[12] that in the case of heterogeneous reactions the order of a reaction determined by comparing initial rates of separate runs does not always agree with the order determined by following the progress of a reaction throughout a run. For this reason an expression was obtained to describe the amount of vitreous silica consumed as a function of time.

If the reaction between a solid (M) and a solute (L) is represented by the stoichiometric relationship

$$m\mathrm{M} + l\mathrm{L} \longrightarrow \text{products}$$

if M_0 and M are the mass of the solid at initial and any time, respectively, w is the formula weight of the solid, and L_0 and L the moles of solute reactant at initial and any time, then when $(M_0 - M)/w$ formula weights of solid are consumed, $L_0 - L$ moles of solute are also consumed, and

$$\frac{M_0 - M}{w} = \frac{m}{l}(L_0 - L)$$

or

$$L = L_0 - \frac{l}{mw} M_0 + \frac{l}{mw} M$$

Then (HF) = L/V, where V is the mass of the solvent.

The assumption is made that as the solid powder is consumed, the surface area varies as the two-thirds power of the remaining mass of solid

$$S = S_0 M^{2/3}/M_0^{2/3}$$

This is valid for isotropic solids with low surface-to-mass ratios; such solids, designated as pykna, have been discussed elsewhere[13] and the 2/3 power assumption confirmed. Also, since surface area is an extensive property, initially

$$S_0 = cM_0, \text{ and}$$
$$S = cM_0^{1/3}M^{2/3}$$

where, here, c has the dimensions cm.²/g. Introducing the last few expressions into equation 1

$$\frac{dM}{dt} = -kcM_0^{1/3}\left(\frac{l}{mw\bar{V}}\right)^n M^{2/3}(\Lambda + M)^n \qquad (2)$$

where

$$\Lambda = \frac{mw}{l} L_0 - M_0$$

is a measure of the excess of solute over solid reactant, expressed in grams of solid. Two cases may be distinguished, where Λ is or is not zero. In the former, equation 2, upon integration, becomes

$$M^{(1-3n)/3} - M_0^{(1-3n)/3} = \left(\frac{3n-1}{3}\right) kcM_0^{1/3}\left(\frac{l}{mw\bar{V}}\right)^n t \qquad (3)$$

In the latter case, where $z = (M/\Lambda)^{1/3}$, $z_0 = (M_0/\Lambda)^{1/3}$ equation 2 may be written

$$3\int_{z_0}^{z} \frac{dz}{(1+z^3)^n} = -kcM_0^{1/3}\left(\frac{l}{mw\bar{V}}\right)^n \Lambda^{n-1/3} t \qquad (4)$$

For the particular case $n = 1$, upon integration, this becomes

$$\left[\log \frac{z+1}{\sqrt{z^2 - z + 1}} + \sqrt{3}\arctan\frac{2z-1}{\sqrt{3}}\right]_{z_0}^{z} = -kcM_0^{1/3}\Lambda^{2/3}\left(\frac{l}{mw\bar{V}}\right) t \qquad (5)$$

It is more convenient to define

$$\varphi_n(0, a) \equiv 3\int_0^a \frac{dz}{(1+z^3)^n} \qquad (6)$$

where Λ, z, $M/\Lambda > 0$, and equation 4 becomes

$$\varphi_n\left(\frac{M_0}{\Lambda}, M/\Lambda\right) = \varphi_n(0, M/\Lambda) - \varphi_n(0, M_0/\Lambda) = -kcM_0^{1/3}\left(\frac{l}{mw\bar{V}}\right)^n \Lambda^{n-1/3} t \qquad (7)$$

The function $\varphi_n(0, a)$ has been computed for $n = 1/2$, 1,

(10) N. V. Sidgwick, "The Chemical Elements and their Compounds," Vol. II, Oxford University Press, Oxford, England, 1950, p. 1105.

(11) R. P. Bell, K. N. Bascombe and J. C. McCoubrey, *J. Chem. Soc.*, 1286 (1956).

(12) H. A. Taylor, *Ann. N. Y. Acad. Sci.*, **58**, 798 (1954).

(13) A. A. Blumberg, THIS JOURNAL, **63**, 1129 (1959).

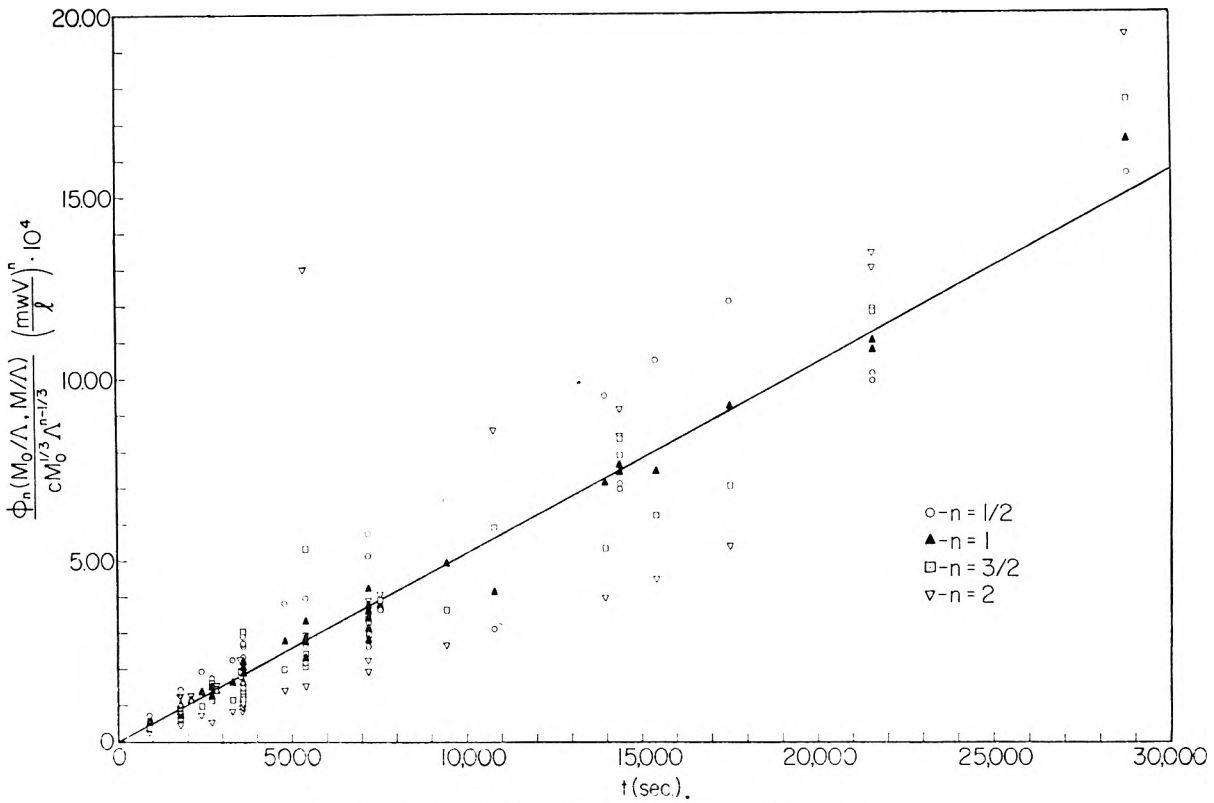

Fig. 1.—Determination of order of heterogeneous reaction.

$^3/_2$ and 2, for the argument $0.0001 \leq a \leq 2000$, and is presented in Table I.[14]

Where Λ, z, $M/\Lambda < 0$, as $t \to \infty$, $M \to -\Lambda = |\Lambda|$, M/Λ and $z \to -1$.

Thus

$$\varphi_n(-\infty, b) \equiv 3 \int_{-\infty}^{b} \frac{dz}{(1+z^3)^n}$$

and equation 4 may be rewritten

$$\varphi_n(M_0/\Lambda, M/\Lambda) = \varphi_n(-\infty, M/\Lambda) - \varphi_n(-\infty, M_0/\Lambda) = -kcM_0^{1/3}\left(\frac{l}{mwV}\right)^n \Lambda^{n-1/3}\, t \quad (8)$$

The function $\varphi_n(-\infty, b)$ for $n = {}^1/_2$, 1, $^3/_2$, 2 and $-1000 \leq b \leq -1.0005$ is given in Table II.[14]

From equation 7 or 8, for one particular $n = p$, the function

$$\frac{\varphi_n(M_0/\Lambda, M/\Lambda)}{cM_0^{1/3}\Lambda^{-n1/3}} \left(\frac{mwV}{l}\right)^n \quad (9)$$

should be linear with time. Also, the rate constant, k_p, for $n = p$, may be calculated for each set $\{M_0, M, \Lambda, V, c\}$, by dividing each function 9 by its corresponding time.

The general function 9 may be written as

$$\frac{\varphi_n(M_0/\Lambda, M/\Lambda)}{\varphi_p(M_0/\Lambda, M/\Lambda)} \left(\frac{mwV}{l\Lambda}\right)^{n-p} k_p t = A(n,p,\Lambda) \quad (10)$$

which is not in general linear in time for $n \neq p$. Further, it may not even be a monotonic function of time, for, if $i > j$, then

$$A(i,p\Lambda) < A(j,p,\Lambda) \text{ when } \Lambda > 1$$

and

$$A(i,p,\Lambda) \lesseqgtr A(j,p,\Lambda) \text{ when } \Lambda < 1 \quad (11)$$

(14) Tables I and II have been deposited as Document number 6310 with the ADI Auxiliary Publications Project, Photoduplication Service, Library of Congress, Washington 25, D. C. A copy may be secured by citing the Document number and by remitting $1.25 for photoprints, or $1.25 for 35 mm. microfilm. Advance payment is required. Make checks or money orders payable to: Chief, Photoduplication Service, Library of Congress.

Results

Table III lists the conditions and calculated results of forty-three runs, ranging in reaction time from 15 minutes to eight hours, with up to $^3/_4$ of the initially present silica dissolved. Initial hydrofluoric acid and hydrogen ion concentrations were $^1/_2$, 1 and 2 molal.

Columns 6–9 list calculated values, for $n = {}^1/_2$, 1, $^3/_2$ and 2, of the function 9. These are plotted against time in Fig. 1.

The best straight line (Fig. 1) is that for $n = 1$. The average of all the k_1 values from Table III is

$$k_1 = 5.212\ (\pm 0.402) \times 10^{-8} \frac{\text{g. SiO}_2}{\text{sec. cm.}^2\ \text{HF molality}}$$

With considerably more labor, the best straight line obtained by introducing the data to equation 5 has a slope

$$k_1 = 5.04\ (\pm 0.59) \times 10^{-8} \frac{\text{g. SiO}_2}{\text{sec. cm.}^2\ \text{HF molality}}$$

From Table III, the average k_1 for initial (HF) = 0.500, 1.000 and 2.00 molal are 4.99 ($\pm$ 0.97) $\times$ 10^{-8}, 5.13 ($\pm$ 0.32) $\times$ 10^{-8}, and

5.35 ($\pm$ 0.35) $\times$ 10^{-8} g. SiO_2/sec. cm.^{2} HF molal, respectively

The average k_1 for initial hydrogen ion concentration (H^+) = 0.50, 1.0 and 2.0 are 4.62 ($\pm$ 0.30) $\times$ 10^{-8}, 5.38 ($\pm$ 0.38) $\times$ 10^{-8}, and

5.46 ($\pm$ 0.25) $\times$ 10^{-8} g. SiO_2/sec. cm.^{2} HF molal, respectively

Table IV lists some runs where the initial (HCl) + (NH_4Cl) = 2.5 and 1.0 molal, in contrast to the conditions described in Table III where, initially, (HCl) + (NH_4Cl) = 4.0 molal.

TABLE III

C = 680 cm.²/g. SiO

Time t, sec.	Initial HF L_0, moles	Initial SiO_2 M_0, g.	Final SiO_2 M, g.	$A = \frac{mw}{l} L_0 - M_0$	$\frac{\varphi_n(M_0/A, M/A)}{cM_0^{1/2}A^{n-1/2}} \left(\frac{rwV}{l}\right)^n 10^4$ $n = 1/2$	1	3/2	2	Initial (H^+), m	k_1 g. SiO_2 cm.² sec. HF molality
3600	0.1000	0.9975	0.9274	0.0035	1.5	2.2	3.0	70	1.00	6.10×10^{-8}[a]
5400		.9896	.8933	.011	2.2	3.3	5.3	13	1.00	5.82[a]
7200		.9978	.9074	.0032	1.9	2.8	3.3	....	0.500	4.00[a]
10800		.9444	.8256	.057	3.1	4.1	5.9	8.6	0.500	4.05[a]
900	0.2000	1.0351	.9966	.966	0.536	0.529	0.527	0.525	2.00	5.88
1800		1.1213	1.0447	.880	1.010	1.014	1.014	1.024	2.00	5.64
1800		1.0335	0.9732	.968	0.839	0.829	0.824	0.822	0.500	4.61
1800		1.0553	.9879	.947	0.952	0.956	0.962	0.964	0.500	5.31
2100		0.9520	.8798	1.049	1.170	1.187	1.199	1.215	2.00	5.65
2700		1.0943	.9935	0.907	1.471	1.505	1.534	1.575	2.00	5.57
2820		1.1160	1.0136	.886	1.416	1.441	1.464	1.492	1.00	5.11
3540		1.0949	0.9710	.906	1.805	1.850	1.923	2.267	2.00	5.23
3600		1.1053	.9758	.896	1.858	1.901	1.944	1.989	2.00	5.28
3600		1.0383	.9259	.964	1.639	1.645	1.655	1.668	0.500	4.57
5400		1.1254	.9376	.876	2.697	2.753	2.832	2.920	2.00	5.14
5400		1.0259	.8735	.976	2.312	2.344	2.380	2.423	0.500	4.34
7200		1.1355	.8930	.866	3.487	3.603	3.727	3.852	1.00	5.00
7200		0.9400	.7466	1.062	2.649	3.418	3.506	3.597	1.00	4.75
7200		1.0148	.8181	0.987	3.127	3.209	3.294	3.800	0.500	4.46
7560		1.0955	.8533	.906	3.649	3.776	3.909	4.054	2.00	5.00
14400		1.5635	.9779	.438	6.97	7.63	8.36	9.19	1.00	5.29
14400		1.0659	.6529	.936	7.01	7.42	7.88	8.38	1.00	5.15
21600		1.1889	.6013	.813	10.11	10.75	11.80	13.02	1.00	4.98
21600		1.1544	.5624	.848	9.93	11.05	11.87	13.42	1.00	5.12
28800		1.0627	.4307	.939	15.64	16.52	17.68	19.40	1.00	5.74
900	0.4000	1.0760	1.0009	2.928	0.743	0.525	0.374	0.266	2.00	6.06
1800		1.1127	0.9663	2.891	1.447	1.035	.740	.618	2.00	5.75
1800		1.1547	1.0196	2.849	1.254	0.898	.639	.456	0.500	4.99
2400		1.0678	0.8811	2.936	1.948	1.391	.995	.711	1.00	5.80
2700		0.9881	.8294	3.016	1.792	1.281	1.136	.655	0.500	4.74
3300		1.1165	.8915	2.888	2.289	1.643	1.177	.844	0.500	4.98
3600		1.0659	.8176	2.938	2.712	1.985	1.454	1.064	2.00	5.51
3600		1.1618	.8931	2.842	2.676	1.927	1.387	1.000	2.00	5.35
3600		0.9446	.7091	3.059	2.911	2.095	1.505	1.094	1.00	5.82
3600		1.0375	.8242	2.967	2.364	1.700	1.221	0.879	0.500	4.72
4800		1.0172	.6940	2.988	3.834	2.774	2.005	1.452	1.00	5.78
5400		1.2789	.8607	2.725	3.976	2.895	2.107	1.535	2.00	5.36
7200		0.9635	.5684	3.040	5.149	3.732	2.716	1.973	2.00	5.18
7200		1.0996	.6109	2.904	5.739	4.215	2.965	2.258	1.00	5.85
9420		1.1301	.5647	2.874	6.692	4.926	3.628	2.674	2.00	5.23
13980		1.0947	.3894	2.909	9.561	7.132	5.319	3.971	1.00	5.10
15420		1.1649	.3707	2.839	10.50	7.476	6.218	4.472	1.00	4.85
17520		1.2597	.3280	2.744	12.12	9.238	7.049	5.386	1.00	5.27

[a] Calculated from equation 3.

TABLE IV

EFFECT OF IONIC STRENGTH[a]

Time t, sec.	Initial SiO_2 M_0, g.	Final SiO_2 M, g.	A	k_1 G. SiO_2 sec. cm.² HF molality
	(HCl) + (NH_4Cl) = 2.5 m			
1800	1.0324	0.9937	−0.032	6.0×10^{-8}
1800	0.9662	.9309	.034	6.5
3600	.9884	.9235	.012	5.4
3600	.9603	.8988	.040	5.6
5400	.9944	.8999	.006	5.9
5400	1.3371	1.2187	− .337	5.28
7200	1.0145	0.8938	− .014	5.3
7200	1.0055	0.8874	− .006	5.8
				$5.7(\pm 0.3) \times 10^{-8}$
	(HCl) + (NH_4Cl) = 1.0 m			
1800	1.0306	0.9932	−0.031	6.3
1800	1.0048	.9686	− .005	5.3
3600	1.0377	.9701	− .038	6.3
3600	1.1003	1.0277	− .100	6.4
5400	1.0196	0.9219	− .020	5.5
5400	0.9777	.8857	+ .022	5.5
7200	1.0212	.8968	− .021	5.6
				$5.8(\pm 0.4) \times 10^{-8}$

[a] L_0 = 0.1000 moles of HF; (H^+) = 1.00 molal, c = 680 cm.²/g. SiO_2; V = 0.2000 kg. of water.

From Tables III and IV, where initial (HF) = 0.500, initial (H^+) = 1.00 molal, the average rate constant where

(HCl) + (NH_4Cl) = 4.0 molal, $k_1 = 5.96 (\pm 0.14) \times 10^{-8}$
= 2.5 molal, $k_1 = 5.7 (\pm 0.3) \times 10^{-8}$
= 1.0 molal, $k_1 = 5.8 (\pm 0.4) \times 10^{-8}$

Discussion

The integrated form of a rate equation applicable to the heterogeneous reaction between a pyknic solid[13] (*i.e.*, where the surface varies as the $^2/_3$ power of the mass) and a solute is presented in tabular form for the cases where the partial order with respect to the solute is $n = {}^1/_2$, 1, $^3/_2$ and 2. The argument of the tabulated integrated equations depends on the initial and final masses of silica, M_0 and M, and the excess of solute over solid, Λ, expressed as grams of solid. This method is least sensitive for very low absolute values of Λ (*i.e.*, stoichiometric equivalence), but here the integrated rate equation has a simple form (equation 3).

By making equal use of all the experimental data, this method eliminates the errors and lower precision found in methods which extrapolate data back to initial rates of reaction.

The best description of the reaction between powdered vitreous silica and aqueous hydrofluoric acid (in strongly acidic media) is obtained when the partial order of the reaction with respect to hydrofluoric acid concentration is first order. It is possible that the dependence of reaction rate on hydrofluoric acid concentration involves a power somewhat greater than one, but more precise data would be needed to confirm this possibility.

Similarly, the rate constant may increase slightly with hydrogen ion concentration. No significant effect of ionic strength on the rate constant was observed.

By an entirely different procedure[13] the reaction was found to be first order, also; and at $t = 32.1°$, the rate constant obtained was

$$k_1 = 4.3 \times 10^{-8} \frac{\text{g. } SiO_2}{\text{sec. cm.}^2 \text{ HF molality}}$$

which agrees well with the results of this study.

Changing the amplitude of the wrist-action shaker did not cause any measurable difference in the rate of attack. So far it has not been possible to determine what role diffusion takes in the process. This will be discussed in a future paper.

Acknowledgment.—The authors thank Dr. Paul L. Smith of Carnegie Institute of Technology for computing Tables I and II.

DIELECTRIC ABSORPTION OF SOME INTRAMOLECULAR HYDROGEN BONDED PHENOLS IN SOLUTION

BY A. H. PRICE

The Edward Davies Chemical Laboratories, University College of Wales, Aberystwyth, Wales, United Kingdom

Received March 24, 1960

The dielectric absorption of picric acid, 2,6-dinitro-*p*-cresol and 2,6-dinitrophenol have been examined in benzene at different temperatures in the frequency range of 200 Mc/sec. to 8.5 Gc./sec. Only one absorption peak is observed in each system and the measured relaxation times are greater than those expected from the rotation of the simple solute molecules. 2,4,6-Tribromophenol was also measured and appears to act as a rigid structure.

Introduction

Meakins[1] has reported a dielectric absorption in solid substituted 2,6-dinitrophenols. This absorption is centered around 10 Mc./sec. at room temperature and arises from the transition of the phenolic –OH group from one hydrogen bonded position to another. Meakins further showed that the two positions were not equivalent, and accounted for this by assuming that the molecule is unsymmetrically placed with respect to its neighbors in the crystal lattice. Aihara and Davies[2] reported the dielectric absorption of some substituted 2,6-dinitrophenols in xylene solutions up to a frequency of 100 Mc./sec., and did not observed a maximum in the dielectric absorption at room temperatures. These authors concluded from the estimated relaxation times that the observed dielectric absorption arose from the rotation of the whole molecule, together with a contribution from the possible rotation of the phenolic –OH group. Davies and Meakins[3] have observed two such relaxation processes (below a frequency of 24 Gc./sec.) in decalin solutions of *e.g.*, 2,4,6-tri-*t*-butylphenol. The absorption at the lower frequency arose from the rotation of the whole molecule, and that at the higher frequency from the hindered rotation of the phenolic group.

The work described here is an extension to higher-frequencies and different temperatures of the investigations of Aihara and Davies on substituted 2,6-dinitrophenols, in an attempt to examine the large relaxation times observed by these authors.

Experimental

Apparatus.—The dielectric properties of the materials were measured in the frequency range of 200 Mc./sec. to 8.5 Gc./sec. using a General Radio Slotted line equipment between 200 Mc./sec. and 1 Gc./sec., and a Central Research Laboratory Dielectrometer at frequencies of 1, 3 and 8.5 Gc./sec. The experimental accuracy was such that, over the whole frequency range, the permittivity could be measured to an accuracy of $\pm$ 1% and the loss tangent (tan δ) to about $\pm$ 3% or at least to $\pm$ 0.1 $\times 10^{-3}$ (whichever was the greater). The apparatus, and methods used to calculate the results, have been described by Williams.[4]

Materials.—2, 6-Dinitro-*p*-cresol was prepared according

(1) R. J. Meakins, *Trans. Faraday Soc.*, **51**, 371 (1955).

(2) A. Aihara and Mansel Davies, *J. Colloid Sci.*, **11**, 671 (1956).

(3) Mansel Davies and R. J. Meakins, *J. Chem. Phys.*, **26**, 1584 (1957).

(4) (a) G. Williams, THIS JOURNAL, **63**, 534 (1959); (b) G. Williams, Ph.D. Thesis, University of Wales, 1959.

TABLE I

EXPERIMENTAL RESULTS FOR BENZENE SOLUTIONS

Solute	Molar concn., C	t, °C.	ϵ_0	$\epsilon_m'' \times 10^3$	β	$\tau_0 \times 10^{12}$, sec.	n_D	μD
Picric acid	0.203	35.0	2.36	27.6 ± 1.4	1.00	40 ± 2	1.4969	1.47
	.320	18.0	2.39	40.5 ± 2.0	0.84	50 ± 3		1.50
	.203	18.5	2.36	27.8 ± 1.4	.89	49 ± 3	1.5059	1.52
	.062	6.0	2.30	8.8 ± 0.4	.80	54 ± 5		1.62
2,6-Dinitro-*p*-cresol	.058	33.5	2.38	65.0 ± 3.3	1.00	32 ± 2	1.4932	4.20
	.118	17.5	2.57	124 ± 6	0.89	37 ± 2	1.5049	4.03
	.058	18.0	2.44	65.0 ± 3.4	.97	37 ± 2	1.5030	4.04
	.058	5.0	2.43	66.5 ± 3.3	.91	42 ± 2		4.22
2,6-Dinitrophenol	.291	19.0	2.82	241 ± 12	1.00	25 ± 2	1.5051	3.20
2,4,6-Tribromophenol	.323	18.5	2.40	42 ± 2	0.91	24 ± 2	1.5087	1.46

to the method of Dutton, *et al.*,[5] and the product (recrystallized from ligroin) melted at 83° (lit. 82°). Picric acid was recrystallized from water, 2,6-dinitrophenol and 2,4,6-tribromophenol recrystallized from alcohol. Their melting points agreed with the literature values.

Benzene was dried over calcium chloride. The middle fraction was collected on distillation from phosphorus pentoxide. It had an apparent dielectric loss tangent of about 0.1×10^{-3} over the frequency range measured. Allowance was made for this when deducing the solute loss tangent.

Results

Each system studied showed only one absorption peak, which was adequately defined by the Fuoss–Kirkwood equation[6] for dilute solutions. In

$$\frac{\epsilon_m''}{\epsilon''} = \cosh(\beta \ln f_m/f) \qquad (1)$$

this equation β represents the distribution factor, ϵ'' the loss factor at frequently f, and the subscript m refers to the values at maximum absorption. It is seen from this equation that if $\cosh^{-1} \epsilon_m''/\epsilon''$ is plotted against $\log f$ then a straight line should be obtained with a gradient of -2.303β and intercept of $\log f_m$ at $\cosh^{-1} \epsilon_m''/\epsilon'' = 0$. In cases where ϵ'' is not directly observed it may be found, by trial and error, as that value giving the best straight line for the graph of $\cosh^{-1} \epsilon_m''/\epsilon''$ against $\log f$. The mean relaxation time (τ_0) may then be easily calculated from the value of f_m ($\tau_0 = 1/2\pi f_m$) determined from the intercept of the graph.

The experimental results are summarized in Table I.

In this table ϵ_0 represents the static dielectric constant and n_D the refractive index of the solution, and μ the solute dipole moment in Debye (D) units.

The dipole moments were calculated using the equation[7]

$$\mu^2 = \frac{2\epsilon_m''}{\beta} \frac{6750kT}{(\epsilon_0 + 2)^2 N_A c \pi} \qquad (2)$$

where k, T, N_A and c are the Boltzmann constant, the absolute temperature, Avogadro's number and the molar concentration, respectively. Methods used to estimate dipole moments in solution usually involve determining the orientation polarization term from the differences between the dielectric constant and refractive index of the solutions and solvent. These differences are often small and do not allow for the contribution to the total polarization arising from the atomic polarization. If, however, one measures the maximum loss factor (and also the distribution parameter β), then the contribution from the orientation polarization to the permittivity of the system is given by[8]

$$(\epsilon_0 - \epsilon_\infty) = \frac{2\epsilon_m''}{\beta} \qquad (3)$$

where ϵ_0 is the permittivity of the system at very low frequencies, ϵ_∞ the permittivity on the high frequency side of the dispersion region where there is no contribution from the orientation polarization. ϵ_∞, therefore, includes contributions from the atomic polarization. Thus, when ϵ_0 is not known to better than ± 1%, the value of $(\epsilon_0 - n_D^2)$, (deduced using the refractive index data), is not as accurate as the value of $(\epsilon_0 - \epsilon_\infty)$ obtained from the experimentally determined loss factor maximum (the error in this determination is estimated as ±3%), and also the former term makes no allowance for the atomic polarization contributions. The dipole moments are thus best deduced using equation 2. In instances where multiple absorption peaks are observed, equation 2 may be used to determine the dipole moment contributing to each individual peak.[3]

Discussion

Aihara and Davies[2] estimated the relaxation times for picric acid, 2,6-dinitrophenol and 2,4,6-tribromophenol (assuming rigid molecules) on the basis of Perrin's equation

$$\tau = \frac{4\pi\eta}{kT}(abc)f \qquad (4)$$

where η is the viscosity for solute rotation in the solvent (*i.e.*, the microscopic viscosity), a, b and c are the semi-axes of the molecular rotational ellipsoid, and f a "form factor" which is a function of the ratios of the semi-axes of rotation (*i.e.*, b/a and c/a). This factor f has been evaluated by Budó, Fischer and Miyamoto.[9] The geometrical terms were established by measuring Courtauld's models of the molecules concerned. It was also assumed that the microscopic viscosity in a benzene solution was 0.23 times the macroscopic viscosity.[10] The estimated relaxation times (at 18°) are given in Table II,

(5) C. G. S. Dutton, T. I. Briggs, B. R. Brown and M. E. D. Hillman, *Canad. J. Chem.*, **31**, 685 (1953).

(6) R. M. Fuoss and J. G. Kirkwood, *J. Am. Chem. Soc.*, **63**, 385 (1941).

(7) (a) R. W. Sillars, *Proc. Roy. Soc. (London)*, **A169**, 66 (1939); (b) C. J. F. Böttcher, "Theory of Electric Polarization," Elsevier Publishing Co., Amsterdam, 1952, pp. 373, 377.

(8) Ref. 7b, p. 373.

(9) A. Budó, E. Fischer and S. Miyamoto, *Physik Z.*, **40**, 337 (1940).

(10) E. Fischer, *Z. Naturforsch.*, **4a**, 707 (1949).

together with the observed and the literature values of the dipole moments.

TABLE II

RELAXATION TIMES AND DIPOLE MOMENTS IN BENZENE AT 18°

Solute	Relaxation time $\tau \times 10^{12}$, sec. Obsd.	Calcd.	Dipole moments in Debye units Obsd.	Lit.
Picric acid	50	18	1.50	1.58[11]
2,6-Dinitro-*p*-cresol	37		4.12	
2,6-Dinitrophenol	25	15	3.20	
2,4,6-Tribromophenol	24	20	1.46	1.56[12]

On comparing the observed and calculated relaxation times it is seen that reasonable agreement is obtained for the 2,4,6-tribromophenol, showing that this molecule probably behaves as a rigid structure. The observed relaxation times for the nitrophenols are, however, very much larger than the calculated ones. This could arise from the existence in solution of the well known aromatic hydrocarbon complexes of picric acid, 2,6-dinitrophenol, etc.

The dipole moments deduced from the peak absorptions agree well with the literature values (determined in benzene) (see Table II). Due to the complexity of the dipole vectors in the region of the hydrogen bonded phenolic–OH group, the dipole moments of 2,6-dinitro-*p*-cresol and 2,6-dinitrophenol were calculated from the literature value of the picric acid dipole moment and the group moments listed by Smyth.[13] Thus the estimated dipole moments of 2,6-dinitro-*p*-cresol and of 2,6-dinitrophenol are 3.9 and 3.5 *D*, respectively. These agree with the observed values of 4.1 and 3.2 *D*. This agreement between the observed and the literature (or calculated) dipole moments again suggests that the dielectric absorption arises from the rotation of the whole molecule, effectively as a rigid structure, but they do not preclude the existence of a molecular complex in solution.

Application of the Eyring rate equation[14]

$$\tau = \frac{h}{kT} e^{\Delta G/RT} = \frac{h}{kT} e^{-\Delta S/R} e^{\Delta H/RT} \qquad (4)$$

(where h is Plank's constant, ΔG, ΔH and ΔS are the free energy, enthalpy and entropy changes in the dielectric process) to the picric acid and the 2,6-dinitro-*p*-cresol systems shows (see Table III) that both these systems have very similar activation energies, and, therefore, probably involve similar mechanisms for the dielectric absorption process, and are similarly solvated in solution.

TABLE III

MEAN THERMODYNAMICAL PARAMETERS

Solute	ΔG, kcal./mole	ΔH, kcal./mole	ΔS, e.u.
Picric acid	3.3	1.2	−7.2
2,6-Dinitro-*p*-cresol	3.1	1.1	−6.9

For a number of simple solutes in a low viscosity solvent Whiffen and Thompson[15] found that the enthalpy change during dielectric relaxation was about 1.5 kcal./mole, but that the entropy changes appeared to become more negative than the larger the solute molecule,[16] being, for example, −3.0 e.u. for chloroform in *n*-heptane and −5.1 e.u. for α-bromonaphthalene in the same solvent. On this basis the large negative entropy values found for picric acid and 2,6-dinitro-*p*-cresol could again indicate the presence of large (solvated?) polar molecules.

Acknowledgment.—The author wishes to thank the University of Wales for the award of an I.C.I. Fellowship.

(11) A. A. Maryott, *J. Research Natl. Bur. Standards*, **41**, 7 (1948).

(12) O. Hassel and E. Naeshagen, *Z. physik. Chem.*, **12B**, 79 (1931).

(13) C. P. Smyth, "Dieletric Behavior and Structure," McGraw-Hill Book Co., Inc., New York, N. Y., 1955, p. 253.

(14) H. Eyring, *J. Chem. Phys.*, **4**, 283 (1936).

(15) D. H. Whiffen and H. W. Thompson, *Disc. Faraday Soc.*, **42A**, 122 (1946).

(16) D. H. Whiffen, *ibid.*, **42A**, 164 (1946).

ELECTROMOTIVE FORCE MEASUREMENTS IN AQUEOUS SOLUTIONS AT ELEVATED TEMPERATURES. II. THERMODYNAMIC PROPERTIES OF HYDROCHLORIC ACID[1]

BY R. S. GREELEY,[2] WILLIAM T. SMITH, JR., M. H. LIETZKE AND R. W. STOUGHTON

Chemistry Division, Oak Ridge National Laboratory, Oak Ridge, Tennessee and the Department of Chemistry, University of Tennessee, Knoxville, Tennessee

Received March 28, 1960

The mean ionic activity coefficient, relative partial molal heat content, relative partial molal heat capacity, and osmotic coefficient of hydrochloric acid have been calculated from e.m.f. data for concentrations from 0.001 to 1.0 *m* at temperatures from 25 to 200° and in some cases to 275°. The extended Debye–Hückel equation was shown to represent the data about as well at temperatures to 275° as at room temperature.

Introduction

The thermodynamic properties of dilute aqueous hydrochloric acid solutions have been obtained from electromotive force measurements from 0 to 60° by Harned and Ehlers[3a] and from 0 to 95° by Bates and Bower.[3b] With the increasing use of aqueous solutions at higher temperatures, it was of interest to extend the measurements on hydrochloric acid to as high a temperature as possible. A previous communication[4] described the measurements of the electromotive force of the cell

$$\mathrm{Pt\text{-}H_2}(p)\,|\mathrm{HCl}(m)|\,\mathrm{AgCl\text{-}Ag}$$

and the evaluation of the standard potential of the silver–silver chloride electrode to 275°. The present paper presents the properties of hydrochloric acid derived from those measurements.

Experimental

The previous paper[4] gives the experimental details used to obtain all of the data presented here. A high speed digital computer was used to perform the involved calculations and least squares procedures.[5]

Calculations and Discussion

Mean Ionic Activity Coefficient of HCl.—As noted in the first paper in this series,[4] the mean ionic activity coefficient of hydrochloric acid was expressed using an extended form of the Debye–Hückel equation

$$\log \gamma\pm = -\frac{S\sqrt{\rho_0 I}}{1 + A\sqrt{\rho_0 I}} + Ext + BI + \ldots \quad (1)$$

where S = limiting slope, ρ_0 = density of water, I = ionic strength of solution, A = denominator coefficient = $50.29(DT)^{-1/2}\,\mathring{a}$, $\mathring{a}$ = ion size parameter, Ext = conversion from rational to practical scale plus extended terms of Gronwall, LaMer and Sandved,[6] B = linear term coefficient, and the . . . = higher terms if desired (*i.e.*, DI^2, etc.). At HCl concentrations from 0.005 to 0.1 *m* only the linear term BI (in addition to the first two terms on the right hand side) was included in equation 1 and the values of $\mathring{a}$ and B were determined at each temperature from the e.m.f. data for those solutions by varying $\mathring{a}$ until the standard error of fit was minimized for the least squares fit of

$$E^{0\prime\prime} = E^0 - \frac{4.606RT}{\mathfrak{F}} BI \quad (2)$$

Values of the mean ionic activity coefficient of hydrochloric acid (saturated with silver chloride) at concentrations from 0.001 to 0.1 *m* and at temperatures from 25 to 275° were calculated from equation 1 using these values of $\mathring{a}$ and B and are listed in Table I. The values of $\mathring{a}$ and B were given in the previous paper.[4] In these calculations the solubility of the AgCl was added to the molality of HCl to give the concentration of chloride ion, it being assumed that both electrolytes were completely dissociated. The AgCl solubility was known at various HCl concentrations as a function of temperature to 200° and ranged from 0.001 to 0.002 *m* at this temperature.[4,7]

The extended Debye–Hückel equation with the BI term was found to be applicable at all temperatures for the concentration range 0.005 to 0.1 *m* HCl. Straight lines were obtained for $E^{0\prime\prime}$ *vs.* I that were within the limits of experimental error (± 0.4 mv.) and which permitted extrapolation to infinite dilution. However, the value of the ion-size parameter, $\mathring{a}$, increased markedly with temperature becoming 11 Å. at 200° and 20 Å. at 275°.

In contrast, when fitting the data for the entire concentration range 0.005 to 1.0 *m* HCl at 25 to 200° and using either a BI term only or both $BI + DI^2$ terms in the extended Debye–Hückel equation and in equation 2, the minimum standard error of fit was obtained when $\mathring{a}$ was constant at 4 ± 1 Å. The standard errors of fit were slightly smaller if the quadratic term were included. At 225, 250 and 275° use of the D parameter was necessary and a value $\mathring{a}$ = 4 Å. gave the best fit of the data. Interestingly enough, Bates and Bower[3] found that $\mathring{a}$ increased from 4.3 to 6.0 in fitting their data at 25 and 60° over the concentration range 0.001 to 0.1 *m;* whereas Harned and Ehlers[3a] found $\mathring{a}$ increased only from 4.22 to 4.40 in going from 25 to 60° over the concentration range 0.1 to 1.0 *m*. Lietzke and

(1) This paper is based upon work performed for the United States Atomic Energy Commission at the Oak Ridge National Laboratory operated by Union Carbide Corporation.

(2) This paper is based in part on a thesis by R. S. Greeley presented to the Department of Chemistry of the University of Tennessee in partial fulfillment of the requirements for the Ph.D. degree, June, 1959.

(3) (a) H. S. Harned and R. W. Ehlers, *J. Am. Chem. Soc.*, **55**, 2179 (1933). (b) R. G. Bates and V. E. Bower, *J. Research Natl. Bur. Standards*, **53**, 283 (1954).

(4) R. S. Greeley, *et al.*, THIS JOURNAL, **64**, 652 (1960).

(5) M. H. Lietzke, "An ORACLE Code for Least Squares," Oak Ridge National Laboratory Publication ORNL CF-59-2-20, February 4, 1959.

(6) T. H. Gronwall, V. K. LaMer and K. Sandved, *Physik. Z.*, **29**, 358 (1928).

(7) R. J. Raridon, Ph.D. Thesis, Vanderbilt University, Nashville Tenn., 1958, p. 93.

Table I

Mean Ionic Activity Coefficient of Hydrochloric Acid, $\gamma\pm$

m	25°	60°	90°	125°	150°	175°	200°	225°	250°	275°
0.001	0.9655	0.963	0.960	0.955	0.949	0.939	0.925	0.904	0.87	0.85
.002	.9522	.949	.946	.940	.934	.926	.915	.898	.87	.85
.005	.9284	.924	.920	.912	.906	.898	.889	.875	.85	.84
.0075	.9149	.910	.905	.896	.889	.882	.862	.859	.84	.83
.01	.9044	.899	.893	.884	.876	.869	.860	.846	.82	.82
.02	.8754	.868	.861	.849	.840	.833	.824	.808	.78	.78
.025	.8650	.857	.849	.837	.826	.819	.810	.793	.76	.77
.05	.8310	.819	.807	.794	.779	.772	.760	.738	.69	.71
.075	.8109	.795	.780	.765	.746	.739	.724	.698	.63	.66
.1	.7972	.776	.758	.744	.720	.714	.694	.663	.58	.62
.2	.7632	.746	.722	.694	.670	.647	.618	.572	.49	.54
.5	.7540	.728	.692	.655	.621	.591	.554	(.572)	(.54)	(.53)
1.0	.8061	.762	.713	.653	.608	.560	.514			

Stoughton[8] also found that the A (and hence $\mathring{a}$) parameter for the Ag_2SO_4 activity coefficient and the HSO_4^- acid quotient in sulfate media were essentially temperature independent to over 200° for the ionic strength range 0.1 to 3.0.

On the other hand, differences in the value of $\mathring{a}$ are compensated to a certain extent by changes in the value of B so that, as was found here, the value of $\gamma\pm$ changes little whichever fit is chosen to represent the data. For instance, at 200° the value of $\gamma\pm$ at $m = 0.1$ for $\mathring{a} = 7$ and $B = -0.422$ was 0.694 and for $\mathring{a} = 4$ and $B = +0.0787$ was 0.675. This difference is only 2.8% which is essentially within the experimental error at that temperature.

Values of $\mathring{a}$, B and D were determined at each temperature using the e.m.f. data for solutions 0.005 to 1.0 m at 200° and 0.01 to 0.5 m at 225, 250 and 275°. From these values of $\gamma\pm$ for solutions 0.2, 0.5 and 1.0 were calculated using equation 1 and are listed in Table I. In Table II are listed the values of $\mathring{a}$, B, D, their standard errors and the standard errors of fit as determined above.

Table II

Values of $\mathring{a}$, B and D from Least Squares Fit of

$$E^{0\prime\prime} = E^0 - \frac{4.606RT}{\mathfrak{F}}(BI + DI^2)$$

Temp., °C.	$\mathring{a}$, Å.	B, m^{-1}	σ_B	D, m^{-2}	σ_D	σ_{fit}, mv.
25	4.3 ± 1	+0.130	0.0059	+0.0026	0.0060	0.25
60	4.3 ± 1	+ .124	.0091	− .0024	.0090	.38
90	4.3 ± 1	+ .101	.0073	+ .0056	.0072	.33
125	4.0 ± 1	+ .112	.0086	− .0134	.0085	.43
150	4.0 ± 1	+ .0960	.0080	− .0109	.0079	.45
175	4.0 ± 1	+ .0945	.0083	− .0245	.0081	.50
200	4.0 ± 1	+ .0787	.0150	− .0222	.0143	.81
225	4.0 ± 1	− .0840	.0230	+ .443	.0403	.46
250	4.0 ± 1	− .410	.139	+1.09	.236	3.09
275	4.0 ± 1	+ .129	.190	+0.169	.304	3.83

The logarithm of the activity coefficients for several of the concentrations listed in Table I were fitted over the temperature range 25 to 200° by the method of least squares to a quadratic function of the centrigrade temperature. The constants of these equations and the standard errors of fit are listed in Table III.

The values of $\gamma\pm$ and log $\gamma\pm$ decrease regularly with temperature at each molality from 25 to about 225°. In fact, the change with temperature of $\gamma\pm$ at 0.05 to 1.0 m is almost linear from 60 to 200°. Above 225° the activity coefficients decrease more rapidly and then between 250 and 275° they begin to increase for concentrations greater than 0.01 m. Since the main temperature-dependent factor in the expression for log $\gamma\pm$, at least at the lower concentrations, derives from the DT product term in the limiting slope, this behavior is understandable.

Table III

Constants of Quadratic Equations Expressing Log $\gamma\pm$ As A Function of Temperature

HCl concn., m	Constants[a] a	b	c	σfit
0.005	-3.165×10^{-2}	-1.854×10^{-5}	-3.870×10^{-7}	0.0001
.01	-4.202×10^{-2}	-5.125×10^{-5}	-3.287×10^{-7}	.0002
.02	-5.499×10^{-2}	-9.286×10^{-5}	-2.755×10^{-7}	.0005
.05	-7.558×10^{-2}	-1.765×10^{-4}	-2.143×10^{-7}	.0010
.075	-8.501×10^{-2}	-2.352×10^{-4}	-2.065×10^{-7}	.0015
.1	-9.136×10^{-2}	-2.914×10^{-4}	-2.076×10^{-7}	.0026
.2	-1.072×10^{-1}	-3.508×10^{-4}	-5.093×10^{-7}	.0031
.5	-1.084×10^{-1}	-4.636×10^{-4}	-9.543×10^{-7}	.0038
1.0	-7.682×10^{-2}	-6.007×10^{-4}	-1.874×10^{-6}	.0013

[a] Constants in the equation $\log \gamma \pm = a + bt + ct^2$.

Since, as was shown in the previous paper,[4] the e.m.f. data were in reasonable agreement with the data of Harned and Ehlers[3a] and of Bates and Bower[3b] at 25, 60 and 90°, the activity coefficients are also in agreement with their values. In order to obtain values of the activity coefficients at higher temperatures for comparison with this study, the extended equation of Harned and Ehlers[9] was solved at appropriate temperatures and concentrations. Agreement with values in Table I was within 1% at all concentrations to 200°.

The mean ionic activity coefficients of hydrochloric acid listed in Table I are stoichiometric activity coefficients based on the assumption that the HCl was saturated with AgCl and that both were completely ionized. Since complexes involving species such as $AgCl_2^-$ are known to exist in HCl solutions[10] and since some undissociated HCl may be present in solution at the higher temperatures and concentrations,[11] the activity coefficients of the actual species involved are not known.

(8) M. H. Lietzke and R. W. Stoughton, This Journal, **63**, 1183, 1186, 1188, 1190, 1984 (1959); **64**, 133 (1960).

(9) Equation 13 of ref. 3a was used with $\mathring{a} = 4.3$ Å. except B was set equal to 0.1390–0.00467 t, D was set equal to 0.0070–0.000032t, and the extended terms Z of Gronwall, *et al.*, were omitted.

(10) J. H. Jonte and D. S. Martin, Jr., *J. Am. Chem. Soc.*, **74**, 2052 (1952); M. H. Lietzke and R. W. Stoughton, *ibid.*, **79**, 2067 (1957).

(11) Roughly 0.2% of the total HCl in the system was present in the vapor space above 0.01 and 0.1 m HCl at 200 to 250°. See ref. 4.

Relative Partial Molal Heat Content and Heat Capacity.—The relative partial molal heat content $\bar{L}_2$ and heat capacity $\bar{J}_2$ are given by

$$\bar{L}_2 = -4.606RT^2 \left(\frac{\partial \log \gamma\pm}{\partial T}\right)_{m,P} \quad (3)$$

$$J_2 = \left(\frac{\partial \bar{L}_2}{\partial T}\right)_{m,P} = -9.212RT \left(\frac{\partial \log \gamma\pm}{\partial T}\right)_{m,P} - 4.606RT^2 \left(\frac{\partial^2 \log \gamma\pm}{\partial T^2}\right)_{m,P} \quad (4)$$

The change in the logarithm of the mean ionic activity coefficient of hydrochloric acid with temperature from 25 to 200° was determined by taking the first derivative of the quadratic equations the coefficients of which are given in Table III. The change of log $\gamma\pm$ with pressure was neglected. Then values of $\bar{L}_2$ were calculated by using equation 3 and these are listed in Table IV. Values of $\bar{J}_2$ calculated from the first and second derivatives of the quadratic equations, the coefficients of which are given in Table III are listed in Table V.

TABLE IV

VALUES OF THE RELATIVE PARTIAL MOLAL HEAT CONTENT OF HYDROCHLORIC ACID

Temp., °C.	$\bar{L}_2$ (cal.) 0.005 *m*	0.01 *m*	0.05 *m*	0.1 *m*	0.2 *m*	0.5 *m*	1.0 *m*
25	30.8	55.1	152	246	306	416	565
60	66.0	92.1	205	321	418	587	839
90	107	133	260	397	534	767	1130
125	167	193	334	498	693	1020	1550
150	221	246	395	580	825	1230	1900
175	283	306	462	669	972	1470	2310
200	355	374	537	767	1140	1730	2770

TABLE V

VALUES OF THE RELATIVE PARTIAL MOLAL HEAT CAPACITY OF HYDROCHLORIC ACID

Temp., °C.	$\bar{J}_2$ (cal./degree) 0.005 *m*	0.01 *m*	0.05 *m*	0.1 *m*	0.2 *m*	0.5 *m*	1.0 *m*
25	0.83	0.90	1.4	2.0	2.9	4.3	6.8
60	1.2	1.2	1.7	2.4	3.6	5.5	8.8
90	1.5	1.5	2.0	2.7	4.2	6.5	10.8
125	2.0	1.9	2.3	3.1	5.0	7.9	13.2
150	2.3	2.2	2.6	3.4	5.6	8.9	15.1
175	2.7	2.6	2.8	3.8	6.2	10.0	17.2
200	3.1	2.9	3.2	4.1	6.9	11.2	19.4

Reasonable agreement for the partial molal heat contents and heat capacities with the values of Harned and Ehlers[3a] and of Bates and Bower[3b] was obtained at 25, 60 and 90°. Since these quantities were obtained by fitting log $\gamma\pm$ over the range 25 to 200°, support is lent to the accuracy of the values at temperatures above 90°.

The partial molal heat content $\bar{L}_2$ and heat capacity $\bar{J}_2$ at each molality increase steadily with temperature. Harned and Owen[12] report that, since the $E°$ values and the e.m.f. values of Harned and Ehlers at each molality fit a quadratic function of the centigrade temperature, the relative partial molal heat capacity must vary with temperature directly with the difference between the coefficients of the quadratic terms, $c - c_0$.

(12) H. S. Harned and B. B. Owen, "The Physical Chemistry of Electrolytic Solutions," Third Edition, Reinhold Publ. Corp., New York, N. Y., 1958, p. 476.

$$J_2 = 46{,}120(c - c_0)T \text{ cal./degree} \quad (5)$$

Although the e.m.f. data of the present investigation could not be fitted to a quadratic within experimental error, the temperature variation of the e.m.f. being more complex, the approximate equation 5 and values of $c - c_0$ reported by Harned and Owen[11] were used to estimate $\bar{J}_2$ at 200°. Values of 1.7, 2.4, 4.8, 6.1, 7.4, 9.4 and 12.7 cal./deg. were obtained for 0.005, 0.01, 0.05, 0.1, 0.2, 0.5 and 1.0 *m*, respectively, which values may be compared with those in Table V. The agreement is satisfactory considering the approximations made. No attempt was made to estimate the first and second derivatives of log $\gamma\pm$ at temperatures above 200° since the data were less precise.

It is interesting that the $\bar{L}_2$ and $\bar{J}_2$ values at elevated temperatures when plotted as functions of the square root of I show deviations from the limiting slope on the high side at low concentrations and *vice versa* in a manner similar to that observed in dioxane–water mixtures[12] at comparable values of the dielectric constant. This behavior indicates that the dielectric constant or the DT product is perhaps more important than the exact nature or temperature (*per se*) of the solvent in causing such deviations.

Osmotic Coefficients.—The osmotic coefficient of a strong electrolyte is related to the activity coefficient by

$$\phi = 1 + \frac{1}{m}\int_0^m m \, \mathrm{d} \ln \gamma\pm \quad (6)$$

If the mean ionic activity coefficient of the electrolyte is expressed by the extended Debye–Hückel equation using both a linear and a quadratic term, equation 6 can be integrated[13] yielding

$$\phi = 1 - \frac{S}{A^3 I}\left[(1 + A\sqrt{I}) - 2\ln(1 + A\sqrt{I}) - \frac{1}{1 + A\sqrt{I}}\right] + \frac{B}{2}I + \frac{2D}{3}I^2 \quad (7)$$

The extended Debye–Hückel equation used in this derivation did not contain the term *Ext* shown in equation 1, since this term was small (being comparable to the experimental error) and since the extended equation with the adjustable parameters A, B (and D) in general fits activity coefficient data equally well without it.

In order to check equation 7, the A, B and D values of an extended Debye–Hückel equation were obtained by a non-linear least squares method from the activity coefficients of several of the alkali halides at 25° using the data listed by Robinson and Stokes[14] at 0.1 to 3.5 *m*. The osmotic coefficients of each alkali halide were then calculated by equation 7 using the derived A, B and D values. Conversely, the A, B and D values of equation 7 were obtained by a non-linear least squares method from the osmotic coefficients of the alkali halides at 25° listed by Robinson and Stokes,[13] and the activity coefficients then calculated from the extended Debye–Hückel equation. It was found that in each case, the calculated coefficients agreed with those listed to within about 0.003 of a unit. Further, the

(13) G. Scatchard, private communication.

(14) R. A. Robinson and R. H. Stokes, "Electrolyte Solutions," Academic Press, Inc., New York, N. Y., 1955, p. 468.

TABLE VI

VALUES OF THE OSMOTIC COEFFICIENTS OF HYDROCHLORIC ACID

m	25°	60°	90°	125°	200°	250°	275°
0.01	0.969	0.967	0.965	0.961	0.951	0.94	0.94
.05	.950	.946	.941	.933	.916	.88	.90
.1	.945	.939	.933	.923	.901	.85	.89
.2	.948	.941	.932	.920	.892	.84	.89
.5	.981	.970	.956	.939	.896	(1.0)	(.98)
1.0	1.05	1.03	1.02	.983	.912	(2.0)	(1.3)

calculated and listed values still showed close agreement when the calculations were extended to values of m below or above (to about $m = 4.5$) those used in evaluating the parameters.

Because equation 7 was found to hold so well for calculating osmotic coefficients of alkali halides from activity coefficient data at room temperature, it was felt worthwhile to use it for such calculations for HCl at various temperatures. The values of B and D used are those shown in Table II. The values of the osmotic coefficients of hydrochloric acid obtained are listed in Table VI. It is found that agreement between the osmotic coefficients determined at 25° and the values listed by Robinson and Stokes[13] is within 1% over the range 0.1 to 1.0 m.

The osmotic coefficients of HCl from 0.01 to 1.0 m regularly but slowly decrease with increasing temperature from 25 to 200°. As with the activity coefficients, the osmotic coefficients then decrease more sharply from 200 to 250° and finally increase again at 275°. At higher concentrations the osmotic coefficient values are much less precise since greater weight in equation 7 is put on the term containing D which is known with much less accuracy than A or B.

Acknowledgment.—The authors wish to express their sincere appreciation to Mr. Gerald North for taking much of the e.m.f. data, to Mrs. Laura Meers for helping with many of the calculations, and to Mr. Raymond Jensen for hand checking some of the computer calculations.

SOME TRANSPORT PROPERTIES OF AQUEOUS PENTAERYTHRITOL SOLUTIONS AT 25°

BY F. J. KELLY, REGINALD MILLS AND JEAN M. STOKES

School of Physical Sciences, Australian National University, Canberra, Australia, and the Physical Chemistry Department University of New England, Armidale, N.S.W. Australia

Received March 31, 1960

The following properties of aqueous pentaerythritol solutions are measured and discussed: viscosity and density, diffusion coefficient and self-diffusion coefficient, and the limiting conductance of sodium and potassium chlorides in the solution.

Introduction

The transport properties of the pentaerythritol molecule, $C(CH_2OH)_4$, are of interest because of its high symmetry. Being moderately soluble in water, it is suitable for comparison of properties of non-electrolytes with those of ions in solution. The studies now reported were undertaken to provide data needed in the interpretation of diffusion measurements in the ternary system sodium chloride-pentaerythritol–water, which are at present in progress.

Materials.—Pentaerythritol for all measurements except those of self-diffusion was prepared by repeated recrystallization of good commercial material; the measured properties were unaffected by the later recrystallizations, and a further check of purity is provided by the excellent agreement between the limiting mutual diffusion coefficient of this material and the limiting self-diffusion coefficient obtained with material purified in a different way. For the self-diffusion measurements (R.M.) the inert material was prepared by repeated vacuum sublimations of commercial pentaerythritol of 95–99% purity[1] (m.p. 256°) to give a purified product of m.p. 260–261°. Radioactive pentaerythritol labelled with ^{14}C was synthesized from ^{14}C-paraformaldehyde,[2] using the classical synthesis by condensation of paraformaldehyde with acetaldehyde in the presence of calcium hydroxide.[3] In order to keep the specific activity of the synthesized compound as high as practicable, the active starting material was diluted with about one gram of inactive paraformaldehyde. The other reactants were then added in the same proportions as in the above method. The product was purified by repeated crystallizations followed by vacuum sublimations, to give labelled pentaerythritol of m.p. 256°. Further purifications involving more recrystallizations would have resulted in considerable loss of active material. To check that the compound was sufficiently pure, some runs were made with a specimen melting at 252°. Within experimental error, there was no detectable difference in diffusion rate; it thus seems that any impurities present have a negligible effect.

Potassium and sodium chlorides used in the diaphragm-cell calibrations and the conductance measurements were of analytical reagent quality, dried at 400°. **Conductance water** at equilibrium with the atmosphere was used for all solutions; its specific conductance was $\sim 1 \times 10^{-6}$ ohm^{-1} cm.$^{-1}$.

All data in this paper refer to 25°.

(1) From Light & Co., Colnbrook, England.

(2) From the Radiochemical Centre, Amersham, England.

(3) H. Gilman and A. H. Blatt, "Organic Syntheses," Coll. Vol. 2nd Edition, John Wiley and Sons, Inc., New York, N. Y.

I. Self-diffusion of Pentaerythritol in Aqueous Solutions (R.M.).—These measurements were made with magnetically-stirred diaphragm-cells using the technique described by Stokes.[4] The cells were calibrated by the diffusion of 0.5 *N* potassium chloride into water using the accurately known integral diffusion coefficients,[5] the cell compartment concentrations being found by measurement of the conductance of suitably diluted samples using a Leeds and Northrup Jones conductance-bridge. For the self-diffusion measurements, a pentaerythritol solution containing a suitable proportion of the ^{14}C-labelled solute was diffused into an inert solution of the same total concentration.

The determination of tracer diffusion coefficients of ^{14}C-labelled species, when thin or infinitely thick solid sources are counted, usually involves error of the order of ±5%. This is mainly because of lack of sample reproducibility due to absorption differences. The use of liquid scintillation counting largely eliminates this problem and at the same time considerably enhances the sensitivity. In the procedure followed in this study, the scintillator solution consisted of 1,4-dioxane as solvent with these solutes: 50 g./l. of naphthalene, 4 g./l. of 2,5-diphenyloxazole and 0.1 g./l. of 1,4-di-2-(5-phenyloxazole)-benzene. Sample preparation was carried out as follows: From an automatic buret, 15-ml. aliquots of the dioxane-scintillator solution were admitted to counting bottles. Accurately measured 5-ml. aliquots of the aqueous compartment solutions were measured out with a siliconed pipet and added to the bottles and the liquid mixture was homogenized by agitation.

A Packard Tricarb Scintillation Spectrometer was employed for counting, using the standard technique, with the following additional precautions. Three to five samples from each compartment were prepared as above and the bottles left in the deep-freeze unit of the counter to equilibrate to temperature. The bottles were then counted in rotation with frequent standards to correct for counter fluctuations, and for a sufficient total number of counts to ensure low statistical error (~0.3%). As some differences in counting rate were observed for the same sample in different bottles, aliquots from top and bottom compartments were measured in the same bottle and a diffusion coefficient calculated in each case. As several samples were taken for each run, the reported value is the mean of the diffusion coefficients calculated in this way.

The self-diffusion coefficients of pentaerythritol in aqueous solution are listed in Table I below. The root-mean square error in these measurements had an average value of ±0.9%. Most of this error can be attributed to the radioactive analyses because calibration experiments using conductance analysis show that the diaphragm-cell can reproduce diffusion coefficients at least ±0.1%. As has been stated above, counting ^{14}C-labelled compounds in the solid state normally gives a precision of ±5%, so liquid scintillation counting is obviously a much superior technique.

TABLE I

SELF-DIFFUSION COEFFICIENTS OF PENTAERYTHRITOL IN AQUEOUS SOLUTION AT 25°

c, mole l.$^{-1}$	10^5D^*, cm.^{2} sec.$^{-1}$	c, mole l.$^{-1}$	10^5D^*, cm.^{2} sec.$^{-1}$
1.62×10^{-4}	0.754	0.1468	0.732
7.08×10^{-4}	.765	.2201	.711
0.0367	.751	.2936	.702
0.0734	.746	.3671	.670

II. Mutual Diffusion Measurements (FJK).—Diffusion coefficients in aqueous pentaerythritol solutions were measured by the Gouy interference method using an apparatus previously described.[6] The results are given in Table II. Here $\bar{c}$ denotes the mean concentration of the solution, Δc the concentration-difference across the free boundary, D the observed mutual diffusion coefficient, and j_m the refractive index difference across the boundary, expressed in wave lengths of the 5460.7 Å. mercury line for a light-path of 2.286 cm. through the cell.

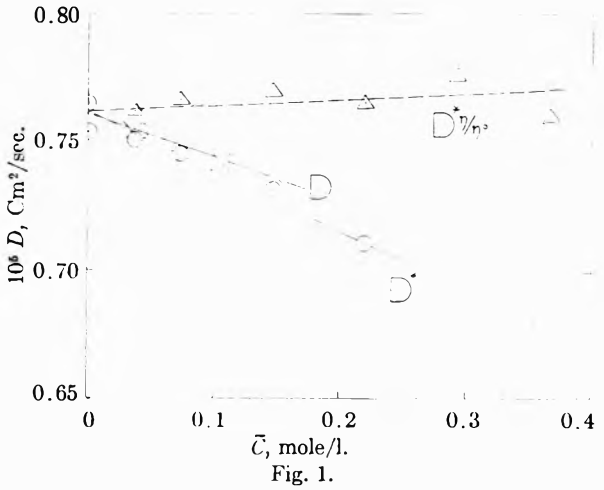

Fig. 1.

TABLE II

MUTUAL DIFFUSION COEFFICIENTS FOR THE SYSTEM PENTAERYTHRITOL–WATER AT 25°

$\bar{c}$, mole l.$^{-1}$	Δc, mole l.$^{-1}$	j_m	$D \times 10^5$, cm.^{2} sec.$^{-1}$
0.0350	0.0700	52.97	0.7542
		52.97	.7544
.0500	.1000	75.48	.7539
		75.50	.7539
.1050	.0900	67.90	.7425
.1498	.0996	75.40	.7370
		75.40	.7363

III. Viscosity and Density Measurements (JMS).—Viscosities were measured in an Ostwald viscometer, which was calibrated with water at 20, 25, 30, 35 and 40° using the data of Cragoe[7] as redetermined by Swindells, Coe and Godfrey.[8] Flow times were reproducible within 0.05%. This form of calibration made possible an accurate assessment of the kinetic energy correction for the pentaerythritol solutions, which had kinematic viscosities lying in the range covered by the calibrations. Densities were measured with a Sprengel pyknometer of ~20-ml. capacity and were reproducible to 1 or 2 in the fifth decimal place. Table III gives the densities, viscosities and apparent molar volumes.

TABLE III

DENSITIES, VISCOSITIES AND APPARENT MOLAR VOLUMES OF PENTAERYTHRITOL SOLUTIONS AT 25°

Wt. % PE	c, mole l.$^{-1}$	Density, g. m.$^{-1}$	ϕ_v, ml. mole^{-1}	η, cp.[a]
3	0.2214	1.00475	101.8	0.9599
5	0.3709	1.00995	101.7	1.0096

IV. Conductances of Electrolytes in Aqueous Pentaerythritol Solutions (JMS).—A stock solution containing 5% of pentaerythritol by weight was used as solvent. Dilute solutions of sodium and potassium chlorides in this solvent were made up and their conductances measured as described previously.[9] The ratio R of the equivalent conductance in the pentaerythritol solution to that at the same concentration in water was plotted against the salt concentration, giving a nearly horizontal linear extrapolation to limiting values $R_{NaCl} = 0.9064$ and $R_{KCl} = 0.9073$.

Discussion

Figure 1 shows the concentration-dependence of the self and mutual diffusion coefficients. Theory requires that these two quantities become identical

(4) R. H. Stokes, *J. Am. Chem. Soc.*, **72**, 763 (1950).

(5) R. H. Stokes, *ibid.*, **73**, 3527 (1951).

(6) J. R. Hall, B. F. Wishaw and R. H. Stokes, *ibid.*, **75**, 1556 (1953).

(7) C. S. Cragoe, cited in J. R. Coe, Jr., and T. B. Godfrey, *J. Appl. Phys.*, **15**, 625 (1944).

(8) J. F. Swindells, J. R. Coe, Jr., and T. B. Godfrey, *J. Research Natl. Bur. Standards*, **48**, 1 (1952).

(9) J. M. Stokes and R. H. Stokes, THIS JOURNAL, **60**, 217 (1956).

at zero concentration, and this is excellently confirmed by the data, which yield on extrapolation $D_0^* = 0.762 \times 10^{-5}$ cm.^{2}sec.$^{-1}$, $D_0 = 0.761 \times 10^{-5}$ cm.^{2}sec.$^{-1}$. The concentration dependence of the mutual diffusion coefficient requires for its interpretation a knowledge of the thermodynamic properties of the solution, which is not yet available, as well as a knowledge of the effect of solution viscosity on the mobility of both the pentaerythritol molecule and the water molecule.[10] For the self-diffusion coefficient, on the other hand, the thermodynamic properties are not required and the viscosity of the solution should be the only relevant factor. The simplest possible relation is $D^*\eta/\eta^0 =$ constant, which would be obeyed if the friction coefficient for the pentaerythritol molecule were directly proportional to the macroscopic viscosity, as for Stokes' law motion. The broken line in Fig. 1 indicates that this relation is not quite correct, though the departure from it is only slightly greater than the experimental uncertainty in the D^* values. The equation, $D^*\eta^{0.87} =$ constant, describes the results within experimental error, which suggests that the pentaerythritol molecule is not quite large enough to conform to Stokes' Law. For the motion of ions in pentaerythritol solutions, the viscosity effect is practically the same as that of the viscosity of a mannitol solution[11] and can be described by the relation

$$\Lambda^0\eta^p = \text{const.}$$

where the index p is 0.783 for NaCl and 0.773 for KCl, irrespective of whether the non-electrolyte is pentaerythritol or mannitol. The corresponding value of the index p for the motion of the pentaerythritol molecules among other pentaerythritol molecules is 0.87. The value of the index p appears from other work[11] to be determined mainly by the effective size of the moving particle, increasing from about 0.6 for very small particles to 1 for very large particles—the value unity being not quite attained even by the large ion $N(C_5H_{11})_4^+$. Thus the value of 0.87 for pentaerythritol seems to fit into the pattern already established for ions.

If we disregard the small departure of pentaerythritol from Stokes' law behavior, we may calculate an effective hydrodynamic radius for the pentaerythritol molecule from the self-diffusion data, obtaining

$$r = 3.23 \text{ Å.}$$

If we take the pentaerythritol molecule to be a sphere, as assumed in this calculation, its effective radius should also be calculable from its molar volume, which is seen from Table III to be 101.7 ml./mole in solution. This gives

$$r = 3.43 \text{ Å.}$$

The discrepancy of 6% may be attributed either to the inapplicability of Stokes' Law or to the imperfectly spherical shape.

Another estimate of the effective radius may be made from the viscosity-data[12]: the Einstein equation for the viscosity of a dilute solution of spherical particles in a continuum can be written:

$$\log \eta/\eta^0 = \frac{2.5\bar{V}c}{2.303}$$

where $\bar{V}$ is the hydrodynamically effective molar volume of the spheres at molar concentration c. The value of $\bar{V}$ required to fit the data of Table III is 136 ml./mole, which corresponds to a spherical molecule of radius

$$r = 3.78 \text{ Å.}$$

which is appreciably larger than the values from the diffusion coefficient and the apparent molar volume. Finally, a scale model of the molecule gives an average radius

$$r = 3.2 \text{ Å.}$$

Thus it appears that the diffusion coefficient of the pentaerythritol molecule in water is substantially in accord with classical hydrodynamics. We may compare its mobility with that of the tetraalkylammonium ions in water. The pentaerythritol molecule should be intermediate in size between the ions $N(CH_3)_4^+$ and $N(C_2H_5)_4^+$, which show deviations[13] from Stokes' Law of 70 and 40%, respectively, in marked contrast to the deviation of only 6% for pentaerythritol. This cannot be accounted for by assuming solvation of the ions, for the deviations are in the wrong sense, *i.e.*, the ions move *faster* than Stokes' Law requires. It seems rather to be another example of the effect noted by Müller and Stokes[14] who found that the monocitrate ion has a higher mobility than the citric acid molecule, and suggested that this was due to the effect of the ionic charge in breaking down the water structure in its vicinity. The viscosity of pentaerythritol solutions, on the other hand, is higher than would be estimated by Einstein's equation from the known molar volume. A similar situation exists with sucrose and glycerol solutions, and can be interpreted as due to solvation of these molecules which increases the effective size. In the case of pentaerythritol, this increase is 35 ml./mole, which corresponds to two molecules of "water of hydration." However, if this explanation is adopted we have to admit a deviation of 17% instead of 6% from Stokes' Law for the diffusion coefficient.

Acknowledgment.—F.J.K. wishes to thank the Australian Atomic Energy Commission for a scholarship during the tenure of which some of the work was done.

(10) G. S. Hartley and J. Crank, *Trans. Faraday Soc.*, **45**, 801 (1949).

(11) J. M. Stokes and R. H. Stokes, THIS JOURNAL, **62**, 497 (1958).

(12) *Cf.* R. A. Robinson and R. H. Stokes, "Electrolyte Solutions," 2nd Ed., Butterworths Scientific Publications–Academic Press, New York, N. Y., 1959, p. 305.

(13) Ref. 12, p. 125.

(14) G. T. A. Müller and R. H. Stokes, *Trans. Faraday Soc.*, **53**, 642 (1957).

STABILITY RELATIONS OF IRON OXIDES: PHASE EQUILIBRIA IN THE SYSTEM Fe_3O_4–Fe_2O_3 AT OXYGEN PRESSURES UP TO 45 ATMOSPHERES[1]

BY BERT PHILLIPS AND ARNULF MUAN

Contribution No. 59-50 from College of Mineral Industries, The Pennsylvania State University, University Park, Pennsylvania

Received March 31, 1960

Phase equilibrium data for the system Fe_3O_4–Fe_2O_3 have been obtained at oxygen pressures up to 45 atmospheres in the temperature range from 1194 to 1588°. The crystalline phases magnetite and hematite coexist in equilibrium with liquid and gas (oxygen pressure ~16 atmospheres) in a eutectic situation at 1566°. Magnetite contains oxygen in excess of the stoichiometric (Fe_3O_4) amount, up to a maximum of 40 weight % Fe_2O_3.

Introduction

Iron oxides have attracted a large amount of attention in earth sciences as well as in mineral technology and metallurgy for many decades. Added impetus to the interest in these oxides has been supplied recently by rapid advances in the fields of ferromagnetic and ferroelectric oxide materials.

The major contributions to knowledge of phase relations in the system Fe–O were made by Greig, Posnjak, Merwin and Sosman[2] and by Darken and Gurry.[3] Reviews of other investigations and comparisons of data obtained in these are given in the two above-mentioned papers. All these studies were restricted to parts of the system where the oxygen pressure is below one atmosphere. The present study was carried out at higher oxygen pressures and dealt specifically with determination of the eutectic between magnetite and hematite.

Experimental

General Procedure.—Phase relations were determined by the quenching technique. Mechanical mixtures of hematite and magnetite were sealed in 80 weight % platinum–20 weight % rhodium tubes and held for 15 to 30 minutes at selected temperatures until equilibrium was established among gas and condensed phases. The samples were then quenched rapidly to room temperature and the phases present determined by microscopic and X-ray techniques.

Starting Materials.—The mixtures used in the present investigation were prepared from hematite ("Baker Analyzed" 99.4 weight % Fe_2O_3) sintered in air at 1300°, and magnetite. The magnetite was prepared by heating a mixture of wüstite ("FeO") and hematite at 1420° in air for 16 hours. The product analyzed 25.6 weight % FeO, 74.4 weight % Fe_2O_3 (=82.3 weight % Fe_3O_4, 17.7 weight % Fe_2O_3). For checking purposes, additional mixtures were prepared from sintered hematite and wüstite. The results of equilibration runs on mixtures of identical composition prepared from different starting materials were in excellent agreement.

Furnaces and Temperature Control.—A vertical tube quench furnace with 80 weight % platinum–20 weight % rhodium alloy resistance winding was used in the experiments. Temperature constancy was maintained by a commercial electronic control instrument activated by a platinum–90 weight % platinum/10 weight % rhodium thermocouple whose junction was kept close to the hot spot of the furnace. Temperatures within the furnaces were measured before and after each run with another platinum–90 weight % platinum/10 weight % rhodium thermocouple calibrated frequently against melting points defined as follows: diopside ($CaMgSi_2O_6$), 1391.5°; pseudowollastonite ($CaSiO_3$), 1544°. Temperatures thus defined are on the Geophysical Laboratory Scale, which is almost identical to the 1948 International Scale up to approximately 1550°. Temperatures above 1550° have been converted to the 1948 International Scale.

Control of Oxygen Pressures.—High oxygen pressures were obtained in the present investigation by decomposition of one of the condensed phases (hematite) present. In most cases a simple sealed tube technique was used. Mechanical mixtures of sintered hematite and magnetite were funneled into 80 weight % platinum–20 weight % rhodium tubes which beforehand had been sealed at one end. The tubes, approximately 15 mm. long and with an inside diameter of 2.5 mm., were filled to approximately one-half of capacity. The upper, unfilled part was closed by squeezing the tube, and the sample-containing part was compressed as much as possible to keep free space in the tube at a minimum. The partially flattened tubes were then heated to a dull red for two to five seconds to remove adsorbed water from the sample and excess air from the tube before sealing the upper end of the tube in a hydrogen–oxygen flame. Chemical analysis was performed on two of the samples in order to check that no appreciable compositional change took place during the short heating before sealing of the tube. The removal of water and air from the sample was desirable in order to obtain a high ratio of oxygen to total gases in the closed tubes at the high temperatures of the subsequent equilibration runs. The oxygen pressure is controlled by temperature and composition of the sample enclosed. If other gases are present, the maximum oxygen pressure that the tubes will withstand before bursting (~18 atmospheres) will decrease, thus limiting appreciably the range over which the present technique may be used.

When the sealed tubes are heated in the quench furnace, some hematite is decomposed to provide the oxygen pressure of the gas phase corresponding to equilibrium with the condensed phases present. Because the density of the gas phase is very low in comparison with that of condensed phases, and because the volume of gas in the tube is small, the compositional changes of condensed phases caused by the decomposition is small under the experimental conditions used in the present investigation (~two weight % Fe_3O_4 as oxygen pressures up to 16 atmospheres are produced).

A slightly modified technique was used in a few runs in the present investigation in an attempt to extend the study to still higher oxygen pressures. The mixture of hematite and magnetite was placed in an 80 weight % platinum–20 weight % rhodium tube approximately 20 mm. long and with an inside diameter of approximately one mm. The tube was filled to three fourths of its capacity and treated in the same manner as just described until it had been sealed. This sealed tube was then dropped into another 80 weight % platinum–20 weight % rhodium tube approximately nine inches long and with an inside diameter of 2.5 mm. The bottom end of the latter tube had been sealed beforehand and the upper end was attached to a tank of nitrogen through a series of fittings and valves. Pressures up to approximately 27 atmospheres could be exerted in this outside tube while it was in a furnace at 1600° if the section of the outer tube kept at this temperature was reinforced by

(1) Paper based on parts of a dissertation submitted by the senior author (B.P.) in partial fulfillment of requirements for the degree of Doctor of Philosophy in Geochemistry at The Pennsylvania State University, June, 1959. At the time this work was done, the authors were graduate fellow in geochemistry and associate professor of metallurgy, respectively, The Pennsylvania State University. Bert Phillips is now senior scientist, Tem-Pres Research, Inc., State College, Pennsylvania.

(2) J. W. Greig, E. Posnjak, H. E. Merwin and R. B. Sosman, *Am. J. Sci.*, **30** (5th series), 239 (1935).

(3) L. S. Darken and R. W. Gurry, *J. Am. Chem. Soc.*, **67**, 1398 (1945); **68**, 798 (1946).

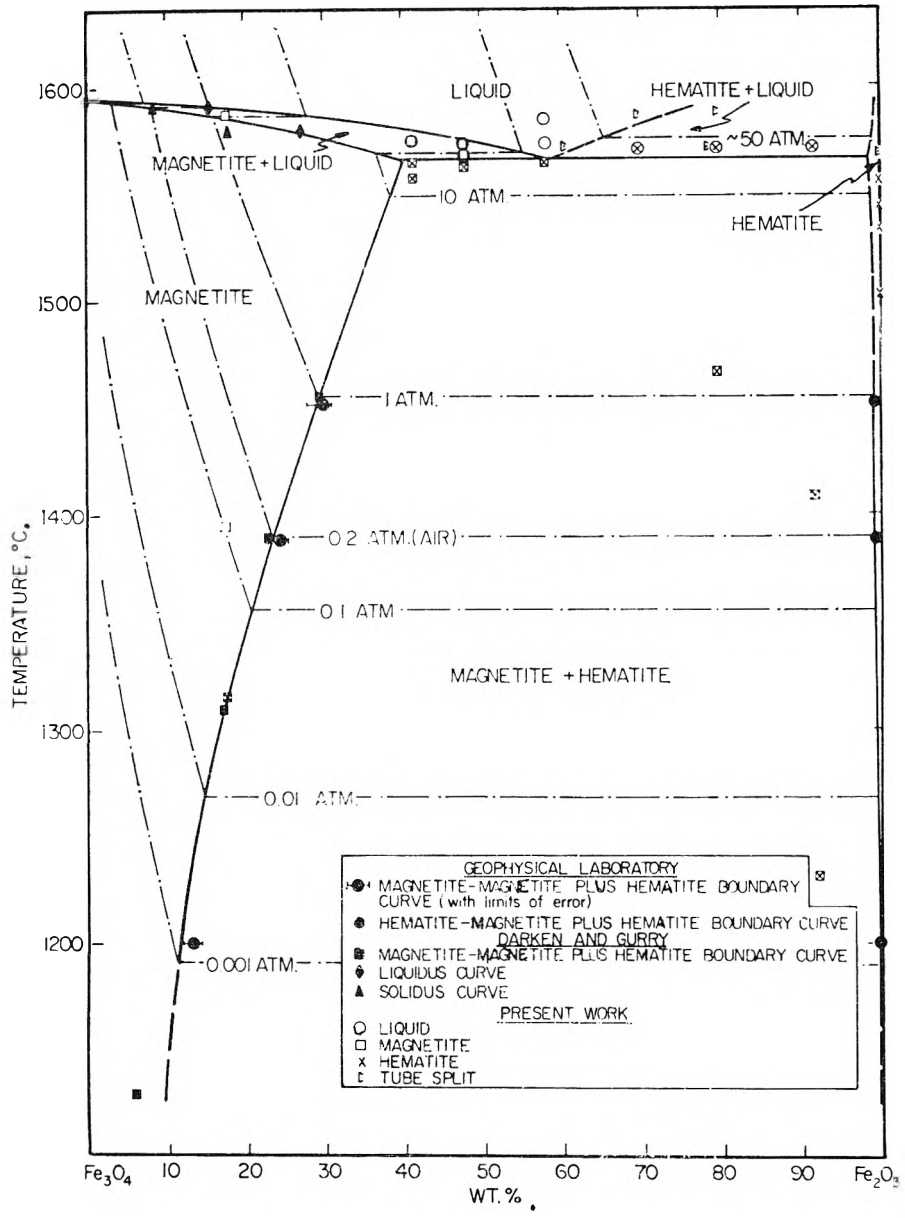

Fig. 1.—Diagram illustrating phase relations in the system Fe_3O_4–Fe_2O_3, based on data in the literature up to an oxygen pressure of one atmosphere and on data obtained in the present investigation up to approximately 45 atmospheres. Heavy solid and dash lines are boundary curves and lighter dash-dot lines are oxygen isobars. The various point symbols used are explained in the framed insert at the bottom of the diagram.

melting several layers of platinum–rhodium alloy onto its surface. In this way the inside tube could withstand internal pressures of up to approximately 45 atmospheres before bursting.

Results and Discussion

The equilibrium data obtained in the present investigation are presented in Table I. These data have been combined with those of Greig, *et al.*,[2] and of Darken and Gurry[3] to construct the phase diagram shown in Fig. 1. A eutectic is seen to exist at 1566°, with magnetite, hematite, liquid of composition 59 weight % Fe_2O_3, 41 weight % Fe_3O_4 and gas with oxygen partial pressure of approximately 16 atmospheres coexisting in equilibrium. The boundary of the hematite field above 1455° is sketched as a dash line forming a smooth continuation of the curve established by Greig, *et al.*,[2] at lower temperatures.

A rough estimate of the oxygen pressure of the gas phase present at the eutectic situation was arrived at by direct testing of the pressures which could be withheld by the tubes. Nitrogen gas supplied to the outer stage of the two-stage pressure device described in a previous section of this paper caused 2.5 mm. tubing (not reinforced) to fail at approximately 18 atmospheres at 1577°. By combining this observation with the observations of tube failures listed in Table I (and indicated in Fig. 1) it is inferred that the oxygen pressure at the eutectic situation is approximately 18 atmospheres. An independent check of this result is obtained by extrapolations to higher temperatures of the data of Darken and Gurry.[3] They determined experimentally oxygen pressures as a function of temperature at which hematite and magnetite coexist in equilibrium, covering the pressure range from $10^{-4.18}$ to one atmosphere and the temperature range from 1130 to 1455°. Their experimental data are plotted as solid dots on the diagram in Fig. 2, and a smooth curve is drawn to pass through these points as closely as possible. The intersection of the extension of this curve (dashed in Fig. 2)

TABLE I

SUMMARY OF DATA

Temp. of equilibration run, °C.	Phases present[a]	Compn. of mixture, weight % Fe_3O_4	Fe_2O_3
1588	Magn.	82.3	17.7
1394	Magn.		
1314	Magn. + hem.		
1575	Liq. + magn.	58.6	41.4
1566	Liq. + magn. + hem.		
1557	Magn. + hem.		
1194	Magn. + hem.		
1573	Liq. + magn.	52.1	47.9
1568	Liq. + magn.		
1564	Magn. + hem.		
1585	Liq.	42.0	58.0
1573	Liq.		
1565	Magn. + hem.		
1572	Tube split	39.5	60.5
1587	Tube split	30.3	69.7
1571	Tube split		
1571[b]	Liq. + hem.		
1588	Tube split	20.4	79.6
1573	Tube split		
1571[b]	Liq. + hem.		
1466	Magn. + hem.		
1571[b]	Liq. + hem.	8.1	91.9
1408	Magn. + hem.		
1231	Magn. + hem.		
1568	Tube split		99
1556	Hem.		
1543	Hem.		
1533	Hem.		
1502	Hem.		

[a] Abbreviations used have these meanings: magn. = crystals of magnetite; hem. = crystals of hematite; liq. = liquid. [b] The sealed tubes containing these samples were subjected to an external pressure of approximately 27 atmospheres.

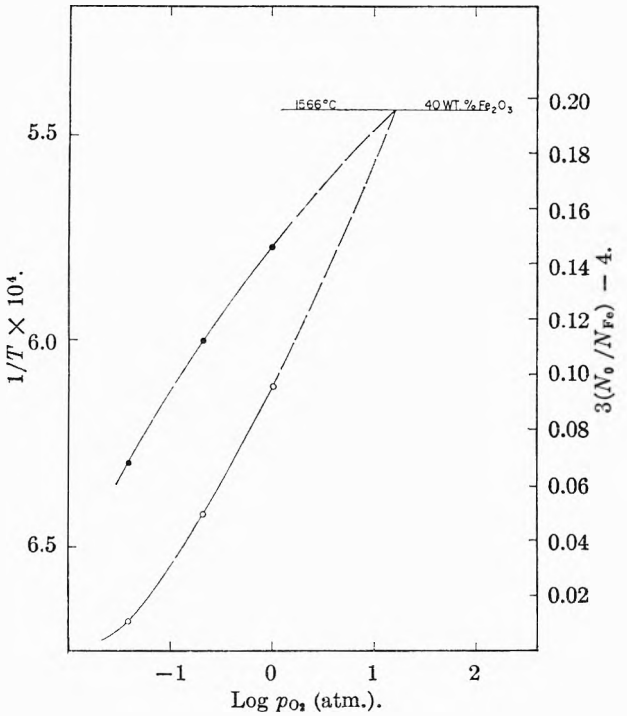

Fig. 2.—Extrapolations of data reported by Darken and Gurry[3] to estimate oxygen pressure of gas phase present in equilibrium at the eutectic in the system Fe_3O_4–Fe_2O_3. Solid dots represent experimentally determined oxygen pressures as a function of temperature for equilibrium coexistence of magnetite and hematite. Open circles represent compositions of magnetite as a function of oxygen pressure at 1566°. The straight, horizontal line represents composition of magnetite phase as well as temperature at eutectic situation, as explained in text.

with a straight line representing the eutectic temperature (1566°) defines the oxygen pressure of the gas phase at the eutectic. The value thus determined is approximately 16 atmospheres (log p_{O_2} = 1.2). Another extrapolation from a set of data obtained by Darken and Gurry[3b] is also shown in Fig. 2. Open circles represent compositions of magnetite at three different oxygen pressures at 1566°, and a smooth curve has been drawn to pass through these points. The scale for this curve (right-hand vertical axis) has been chosen such that the composition of magnetite (40 weight % Fe_2O_3) in equilibrium with hematite at 1566° (see Fig. 1) is represented by a point at the same height as the 1566° point on the left-hand temperature scale. Hence the two extrapolated (dash) curves must intersect at this common value on the vertical scale.

(4) A. Muan, *Am. J. Sci.*, **256**, 171 (1958).

ACTIVITIES IN AQUEOUS HYDROCHLORIC ACID MIXTURES WITH TRANSITION METAL CHLORIDES. II. MANGANESE(II) CHLORIDE AND COPPER(II) CHLORIDE[1]

BY T. E. MOORE, F. W. BURTCH AND C. E. MILLER

Department of Chemistry, Oklahoma State University, Stillwater, Oklahoma

Received April 6, 1960

The activity of each of the components in the systems $MnCl_2$–HCl–H_2O and $CuCl_2$–HCl–H_2O has been determined at 25° for three series of solutions at constant HCl molalities of 4.7, 7.0 and 9.0, respectively. The results are interpreted in terms of hydration and chlorocomplexing at high solute activities. Evidence for $CuCl_4^=$ is found. Water vapor pressure lowerings are closely additive for the manganese system, and a lower degree of hydration for $MnCl_2$ than for $NiCl_2$ in corresponding mixtures with HCl is indicated.

The first paper of this series reported the results of an investigation of the activities in the systems $CoCl_2$–HCl–H_2O and $NiCl_2$–HCl–H_2O at 30°.[2] The high values found for the salt and acid activities were correlated with the hydration parameters of the Stokes and Robinson hydration theory.[3] This paper presents an extension of the study to the systems $MnCl_2$–HCl–H_2O and $CuCl_2$–HCl–H_2O at 25° over a similar range of concentrations.

Experimental

Apparatus.—The apparatus was a modification[2] of that described by Bechtold and Newton[4] for the measurement of water vapor pressures by the gas transpiration technique. Rotating drum saturators were employed in all of the measurements of the $CuCl_2$ solutions.[5]

Procedure.—The operating procedure was essentially that described in the earlier paper.[2] Preliminary tests of the apparatus using H_2SO_4 standards (1–6 molal) showed agreement within ±0.1% between the measured water vapor pressures and hose adopted by Stokes[6] for isopiestic standards. Solutions of HCl (4.5–9 molal) were also investigated in the preliminary check of the apparatus. Water vapor pressures found using bubble saturators agree with those listed by Randall and Young[7] and Robinson and Stokes[8] to within ±0.2% but the values found using the drum saturators were uniformly slightly lower. Partial pressures of HCl measured with the drum saturators were also slightly lower than those obtained with the bubble saturators; the experimental pressures with both types of saturators, however, fall between those reported by Bates and Kirschman[9] and those listed by Zeisberg.[10] The results are considered to be in satisfactory agreement with the best literature values.

Materials.—C.P. or reagent grade chemicals were used throughout the investigation. The NaOH, $Mg(ClO_4)_2$ and asbestos in the absorbers were shown to be satisfactorily chloride-free.

Solutions.—Stock solutions of the desired molality and nearly saturated with the salt were prepared; subsequent dilutions with HCl of the same molality were by weight. Compositions were checked by analysis.

The solid phases in both the binary and ternary saturated solutions were found by analysis to be either $MnCl_2 \cdot 4H_2O$ or $CuCl_2 \cdot 2H_2O$.

Density Measurements.—Densities were measured with a 50-ml. pycnometer following standard procedures. The estimated accuracy is ±0.0002 density unit.

Calculation of Activities.—All activities are referred to standard states of ideal mean 1 molal binary solutions of the solutes. The data listed by Stokes[6] for the activity coefficients of $MnCl_2$ and $CuCl_2$ solutions were used to calculate the activities of the solid hydrates relative to the salts in the saturated solutions. Activities in the salt-saturated ternary mixtures were then calculated from the vapor pressures and the relative activities of the salt hydrates.[2] To obtain the salt activities over the experimental range of concentrations the H_2O and HCl activity values were fitted by empirical equations of the form

$$\log a = A + Bm + Cm^2 + Dm^3 + Em^4 \quad (1)$$

by the least squares procedure and the Gibbs–Duhem equation was integrated analytically. Table I gives the coefficients to be used with equation 1 while Table II gives the coefficients of the equations of the type

$$\log a = A + B \log m + Cm + Dm^2 + Em^3 \quad (2)$$

obtained by integration for the salt activity as a function of concentration.

Precision.—The H_2O vapor pressure measurements in the ternary systems were made with a precision of better than ±0.1% defined by

$$P = 1/n\Sigma\, \Delta p/p \times 100 \quad (3)$$

where n is the number of concentrations at which measurements were made in a series, and $\Delta p/p \times 100$ is the average percentage deviation from the mean pressure of two or more measurements at each concentration. The corresponding precision in the HCl vapor pressures is about ±0.2% for the $MnCl_2$ series and about ±0.4% for the $CuCl_2$ series, where the HCl pressures are smaller. Measurements were made in 0.2 molal steps over the salt-concentration range of from 0 to saturation in each series.

The standard error of estimate for each of the polynomials (eq. 1) is included in Table I. Unfortunately, the uncertainty in the values for the activity of $MnCl_2$ or $CuCl_2$ (a_3) calculated from the Gibbs–Duhem equation is inherently much greater than that in the directly measured values for water (a_1) or HCl (a_2). The uncertainty is estimated to be about 5% above 1 m, becoming larger below 1 m. The generally irreversible behavior of transition metal–metal ion electrodes precluded direct determination of the $MnCl_2$ or $CuCl_2$ activities by electromotive force measurements.

Discussion

A comparison of the osmotic coefficients of $NiCl_2$, $MnCl_2$ and $CuCl_2$ shows that they decrease in that order in binary solutions at the same concentration. This has been interpreted as indicating increasing ionic association.[6] It is also evident from Figs. 1–5 that after allowance is made for differences in temperature and HCl concentration, the same order is obtained for both the activities of the salts and their effect upon the activities

(1) This research was supported in part by the United States Air Force through the Air Force Office of Scientific Research of the Air Research and Development Command under Contract No. AF 18-(600)-478 and in part by the Office of Ordnance Research, United States Army, under Contract No. DA-23-072-ORD-1057.

(2) T. E. Moore, E. A. Gootman and P. C. Yates, *J. Am. Chem. Soc.*, **77**, 298 (1955).

(3) R. H. Stokes and R. A. Robinson, *ibid.*, **70**, 1870 (1948).

(4) M. F. Bechtold and R. F. Newton, *J. Am. Chem. Soc.*, **62**, 1390 (1940).

(5) H. A. Smith, R. L. Combs and J. M. Googin, THIS JOURNAL, **58**, 997 (1954).

(6) R. H. Stokes, *Trans. Faraday Soc.*, **44**, 295 (1948).

(7) M. Randall and L. E. Young, *J. Am. Chem. Soc.*, **50**, 989 (1928).

(8) R. A. Robinson and R. H. Stokes, *ibid.*, **71**, 612 (1949).

(9) S. J. Bates and H. D. Kirschman, *J. Am. Chem. Soc.*, **41**, 1991 (1919).

(10) F. C. Zeisberg, *Chem. Met. Eng.*, **32**, 326 (1925).

TABLE I

$MnCl_2$–HCl–H_2O SYSTEM AT 25°

HCl, m	Coefficients of equation 1					Range, m	Standard error of estimate[b]
	A	B	C	D	E		
			log a_1				
4.67	−0.1204	−0.05713	−0.0003321	0.0002766		0–3.59	0.0009
7.05	− .2237	− .07971	− .02552	− .01160	0.001805	0–2.67	.0012
9.01	− .3272	− .05994				0–1.4	.0004
9.01	− .3200	− .07115	.004023			1.4–2.28	.0011
			log a_2[a]				
4.67	1.9882	0.6182	−0.1107	0.02527	−0.003030	0–3.59	.0107
7.05	3.0014	.4962	− .1229	.04205	− .006907	0–2.67	.0049
9.01	3.7257	.3710	− .1103	.06586	− .01640	0–2.28	.0036
			$CuCl_2$–HCl–H_2O SYSTEM AT 25°				
			log a_1				
4.70	−0.1199	−0.03981	0.005258	−0.002309	0.000353	0–3.13	.0005
7.00	− .2238	− .02526	− .002515			0–2.31	.0007
9.00	− .3288	− .02379	− .002156			0–2.10	.0005
			log a_2[a]				
4.70	2.0157	0.3559	−0.08620	−0.02720	−0.003572	0–3.13	.0031
7.00	2.9662	.1907	− .008682			0–2.31	.0021
9.00	3.7091	.1164	− .002854			0–2.10	.0015

[a] $a_2 = 2.60 \times 10^3\ p$ (mm.). [b] Standard error of estimate: $\sqrt{\frac{\Sigma(Y - y)^2}{n - (N + 1)}}$ where Y = log a (experimental); y = log a (from equations); n = number of points; N = number of terms.

TABLE II

$MnCl_2$–HCl–H_2O SYSTEM AT 25°

HCl, m	Coefficients of equation 2					Range, m
	A	B	C	D	E	
4.67	1.571	0.655	1.071	−0.200	0.0189	0–3.59
7.05	3.963	2.134	−1.100	.521	− .0687	0–2.67
9.01	2.506	−0.038	1.988	− .890	.197	0–1.4
9.01	2.922	1.400	1.541	− .890	.197	1.4–2.28
			$CuCl_2$–HCl–H_2O SYSTEM AT 25°			
4.70	1.226	1.239	0.2260	0.00062	−0.003782	0–3.13
7.00	1.586	0.1558	.4007			0–2.31
9.00	1.941	0.6294	.2908			0–2.10

of HCl and H_2O in ternary mixtures. That chloro-complexing occurs in $CuCl_2$ solutions is well known[11]; however, the relative effects of $MnCl_2$ and $NiCl_2$ may be due in large part to differences in the hydration of the transition metal ions in the systems. The more intense electrostatic field of the smaller Ni^{++} and the stabilizing effect of the octahedral ligand field of the water molecules in the first hydration shell should favor the hydration of Ni^{++} relative to that of Mn^{++}.

A large amount of experimental data on activity coefficients has been successfully correlated in terms of long-range electrostatic and short-range ion–solvent interactions only.[3,12] An essential part of this "hydration theory" is the relationship of the *free* solvent mole-fraction x_1 to the solvent activity a_1 obtained by differentiation of equation 12 of ref. 12

$$\ln a_1 = \ln x_1 + B^{el} \qquad (4)$$

where B^{el}, the electrical contribution to the free solvent activity, is small,[13] and the primary effect of the electrical forces upon the solvent activity is included in the hydration parameter.[12] Equation 4 thus gives a basis for comparisons of the total hydration in mixtures without detailed knowledge of the division of the bound water among the solute species.

Assuming complete dissociation of both HCl and $NiCl_2$ or $MnCl_2$, $x_1 = N_1/(N_1 + 2m_2 + 3m_3)$, where N_1 is the number of moles of free water per 55.51 moles of total water.

Values of N_1 computed from eq. 4 for mixtures of $MnCl_2$ (molality m_3) and HCl (molality m_2) were used to find the number of moles of bound water b. Comparison of the values of b for the 4.7 m. HCl series of $MnCl_2$ and $NiCl_2$ shows that in the latter series there is a much greater degree of hydration of the solutes. If one makes the further assumption that the hydration number for HCl remains constant in each constant molality HCl series, the apparent hydration number h_3 for the salt is given by

(11) J. Bjerrum, G. Schwarzenbach and L. G. Sillen, "Stability Constants. Part II. Inorganic Ligands," The Chemical Society, 1958.

(12) E. Glueckauf, *Trans. Faraday Soc.*, **51**, 1235 (1955).

(13) R. H. Fowler and E. A. Guggenheim, "Statistical Thermodynamics," Cambridge University Press, 1939, p. 399.

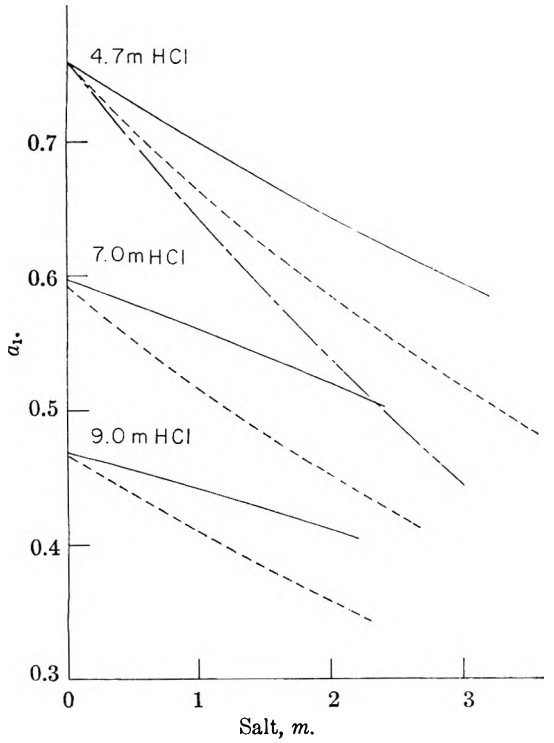

Fig. 1.—Water activity in mixtures of salts with constant molality HCl: —, $CuCl_2$ at 25°; — —, $MnCl_2$ at 25°; — — —, $NiCl_2$ at 30°.

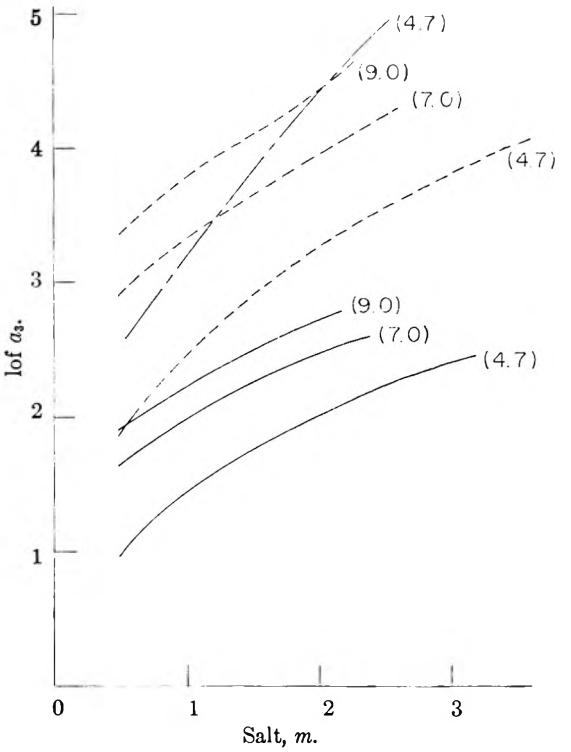

Fig. 3.—Activity of salts in mixtures with constant molality HCl: —, $CuCl_2$ at 25°, – – –, $MnCl_2$ at 25°; — — —, $NiCl_2$ at 30°.

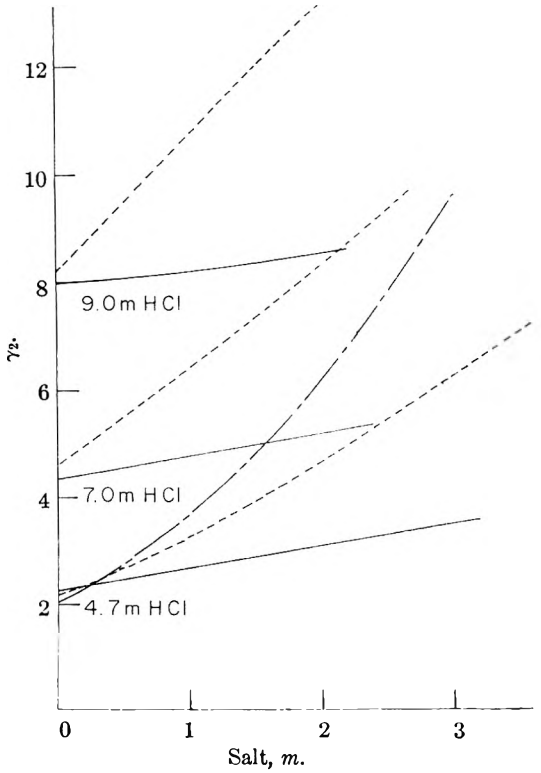

Fig. 2.—Activity coefficient of HCl in mixtures with salts: —, $CuCl_2$ at 25°; – – –, $MnCl_2$ at 25°; — — —, $NiCl_2$ at 30°.

$$b = h_3 m_3 + h_2^0 m_2 = 55.51 - N_1 \qquad (5)$$

where h_2^0 is the value of h_2 at $m_3 = 0$. One finds in this way that the hydration number for $NiCl_2$ in the 4.7 m series is about 2 moles H_2O/mole

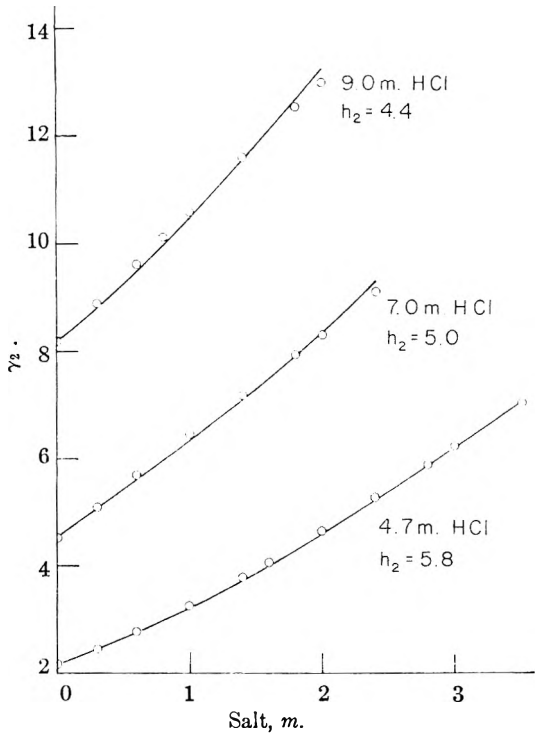

Fig. 4.—Activity coefficient of HCl in mixtues with $MnCl_2$ at 25°: lines, calculated; circles, experimental.

salt greater than that for $MnCl_2$ over the concentration range, the values decreasing with increasing salt concentration.

Since it is probable that water molecules primarily bound to H_3O^+ are strongly held owing to the charge distribution in this ion, the assumption

made in (5) together with values of N_1 make possible a calculation of the activity coefficient of HCl in the mixtures.[2]

$$\log \gamma_{\pm 2} = \frac{-h_2^0}{2} \log a_1 \frac{-0.509\sqrt{I}}{1 + 0.329a\sqrt{I}} - \log (N_1 + 2m_2 + 3m_3) + C \quad (6)$$

Here a is the usual distance parameter, arbitrarily taken to be 4.8 Å. for all pairs of ions, and I is the ionic strength.

The agreement between calculated and experimental values is shown in Fig. 4. Equations 4, 5 and 6 very satisfactorily account for the concentration dependence of the activity coefficient in the 4.7 *m* HCl series, and even in the two higher acid series where the experimental data do not fit the theoretical curves as closely, the average of the deviations between calculated and experimental values is of the order of 1.5%.

In the foregoing discussion the assumption has been that all of the solutes in the mixtures are completely dissociated. This is difficult to verify from experimental data on vapor pressures. However, a variety of evidence supports the conclusion that $CuCl_2$ forms a number of complexes with HCl, and since the fractional vapor pressure lowering $(1 - a_1)$ is determined to a first approximation (*cf.*, eq. 4) by the mole fraction of solvated ions, if one determines the vapor pressure lowering for a series of mixtures at constant chloride concentration, the curve showing the vapor pressure lowering as a function of the Cl/Cu mole ratio should change slope at a composition corresponding to one of the complexes. This of course assumes that only one complex predominates over the entire range of compositions. One sees from Fig. 5 that the two linear segments of the $\Delta p/p$ curve intersect at a Cu/Cl ratio of 0.25, corresponding to $CuCl_4^=$. In the same figure there is plotted (broken line) for comparison the number of ions expected if at Cl/Cu ratios greater than 4 all of the Cu^{++} ions are complexed and at ratios below 4 all Cl^- ions are complexed as $CuCl_4^=$ or $CuCuCl_4$. The ordinates have been arbitrarily scaled to emphasize the correlation. Also shown are the $\Delta p/p$ curves for $MnCl_2$ and $NiCl_2$, where there is no indication of a "break" point.

From the values of the formation constants of the chlorocomplexes of copper(II) given by Bjerrum[14] one calculates a value of K of about 10^{-5} for the formation of $CuCl_4^=$ from Cu^{++} and Cl_4^-, showing that $CuCl_4^=$ is a relatively weak complex. However, if tetrachlorocupric(II) acid is a strong electrolyte the expression for K is seen to be

$$K = \frac{a_{CuCl_4^=}}{a_{Cu^{++}} a_{Cl^-}^4} = \frac{a_{H_2CuCl_4}}{a_{CuCl_2} a_{HCl}^2} \quad (7)$$

and for the mixtures investigated the denominator may range from 10^4 to 10^{10}. Thus, in spite of the weakness of the 4:1 complex, it is probably the predominant one in the solutions.

Robinson and Stokes[15] have suggested the use of the isopiestic ratio as evidence for ion association in mixtures. They find, for example, that

(14) J. Bjerrum, *Kem. Maanedsblad.*, **26**, 24 (1945).

(15) R. A. Robinson and R. H. Stokes, *Trans. Faraday Soc.*, **41**, 752 (1945).

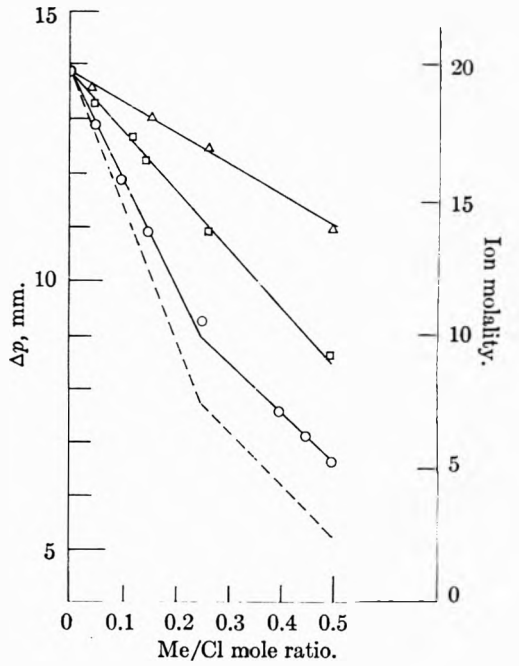

Fig. 5.—Vapor pressure lowering at constant chloride molality 10: ○, $CuCl_2$ + HCl; □, $MnCl_2$ + HCl; △, $NiCl_2$ + HCl. Broken line, calculated ion molality assuming tetrachlorocuprate formation.

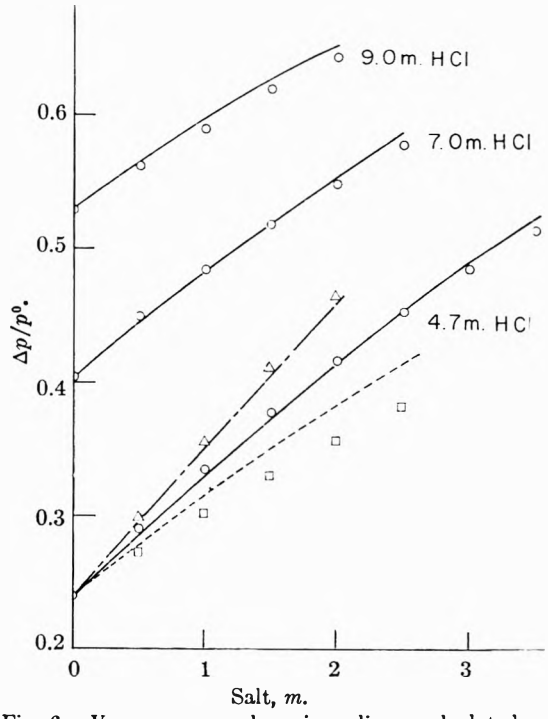

Fig. 6.—Vapor pressure lowering: lines, calculated; experimental: ○, $MnCl_2$ + HCl; △, $NiCl_2$ + HCl; □, $CuCl_2$ + HCl.

2:1 mixtures of KCl with $MnCl_2$, $NiCl_2$ or $CuCl_2$ at a concentration corresponding to a 1 *m* solution of the hypothetical compound K_2MCl_4 have isopiestic ratios of 3.75, 4.00 and 3.39, respectively, the ratio being defined by $R = m_{KCl}/m_{K_2MCl_4}$. According to equation 4, however, isopiestic solutions are those of the same free water mole fraction and hence the same hydrated solute particle fraction. Since the formation of a complex such

as $MCl_4^=$ would be expected to result in a simultaneous decrease in the number of solute particles and an increase in the number of free water molecules, the total number of both ions and molecules should not change greatly, and the isopiestic ratio should then give a reasonably good indication of complexing. Additivity of the vapor pressure lowerings for isopiestic binary and ternary solutions of dissociated electrolytes might also be expected, and it is easy to show that for additivity to hold the isopiestic concentrations of HCl and MCl_2 are related by

$$\frac{m_{2(13)}}{m_{2(1)}} + \frac{m_{3(12)}}{m_{3(1)}} = 1$$

where the numerators refer to the components in the mixtures and the denominators refer to solutions of the components isopiestic with the mixtures. This relation holds within 1% for the 4.7 *m* HCl series of both $NiCl_2$ and $MnCl_2$ over the entire range of concentrations for which data are available on the binary solutions. Equally close agreement is found for the higher acid series.

TABLE III

HYDRATION PARAMETERS

	h_2	h_3
4.67 *m* HCl + $MnCl_2$	5.8	5.5 (m_3 = 0.5) − 3.2 (m_3 = 3.0)
7.05 *m* HCl + $MnCl_2$	5.0	3.0 (m_3 = 0.5) − 2.0 (m_3 = 2.4)
9.01 *m* HCl + $MnCl_2$	4.4	2.0 (m_3 = 0.5) − 1.5 (m_3 = 2.0)

Robinson and Stokes have shown further that the vapor pressure lowerings are additive within a few per cent. for solutions of KCl with bivalent metal chlorides up to ionic strengths of 5 when the component lowerings have been corrected to the same ionic strength as the mixtures. While the extension of the ionic strength concept to values in excess of 10 for the solutions investigated may be questionable, equation 4 suggests that vapor pressure lowerings corrected to the same ionic molality might be more meaningful, and the calculated values of $\Delta p/p^0$ shown in Fig. 6 are on the latter basis. Agreement between calculated and experimental values for both $MnCl_2$ and $NiCl_2$ solutions is of the order of 1%, and the experimental lowerings for $CuCl_2$ solutions lie significantly below the values calculated assuming complete dissociation. Thus the degree of ionic association in the ternary mixtures does not appear to be greatly different from that of the component binary solutions at comparable concentrations, and the relative activities of the components in the different systems are easily accounted for by assuming smaller hydration for $MnCl_2$ than for $NiCl_2$ and a high degree of chlorocomplexing for Cu^{++} in solutions of high HCl activity.

Acknowledgment.—The authors are indebted to the Oklahoma State University Computing Center for assistance in programming the calculations.

INTERMOLECULAR EFFECTS IN SOLUTIONS OF METHYL ISOBUTYL KETONE IN ALCOHOLS AND FLUOROALCOHOLS[1,2]

BY HARTLEY C. ECKSTROM, JERRY E. BERGER AND LYLE R. DAWSON

Department of Chemistry, University of Kentucky, Lexington, Kentucky

Received April 6, 1960

The dielectric constants and the partial molar volumes were determined for mixtures of methyl isobutyl ketone and each of the six alcohols: $CF_3{\cdot}CH_2OH$, $HCF_2{\cdot}CF_2{\cdot}CH_2OH$, $HCF_2{\cdot}(CF_2)_3{\cdot}CH_2OH$, C_2H_5OH, n-C_3H_7OH and n-$C_5H_{11}OH$. Polarizations calculated from the Syrkin equation as a function of the concentration may be interpreted as showing that the ketone molecule has a greater ability to form hydrogen bonds with the polyfluoroalcohol molecules than with their corresponding hydrocarbon analogs. The partial molar volumes of the polyfluoroalcohol mixtures show positive deviations while those for the hydrocarbon alkanols remain constant throughout the entire concentration range.

Studies by Haszeldine[3] and Birchall and Haszeldine[4] of polyfluoroalcohols have shown that their ionization constants are many times greater than the ionization constants of their hydrocarbon analogs. The infrared spectra may be interpreted as revealing that hydrogen bonding in the polyfluoroalcohols is much reduced. These investigators believe that in the fluorine-substituted compounds the reduction in the basicity of the oxygen atom, reducing the strength of the hydrogen bond in which this oxygen acts as an electron donor, predominates over the effect created by the increase in acidity of the alcohol and hence the increase in the effective positive charge on the hydrogen atom. This latter effect should lead to an increase in the strength of the hydrogen bond in which the acidic hydrogen atom participates. Mukherjee and Grunwald[5] found that the system ethanol–2,2,2-trifluoroethanol was very non-ideal, and they interpreted the infrared spectra as showing the existence of mixed hydrogen bonds between the two alcohols.

It was the object of the present work to compare the dielectric constants of mixtures of methyl isobutyl ketone and each of the alcohols, $CF_3{\cdot}CH_2OH$, $HCF_2{\cdot}CF_2{\cdot}CH_2OH$, $HCF_2{\cdot}(CF_2)_3CH_2OH$ with mixtures of methyl isobutyl ketone and their corresponding hydrocarbon analogs. According to Syrkin[6] and to Osipov and Shelomov[7] the orien-

(1) Taken from a Ph.D. dissertation submitted by J. E. Berger.

(2) This work was supported in part by a research grant from the National Science Foundation.

(3) R. N. Haszeldine, *J. Chem. Soc.*, 1757 (1953).

(4) J. M. Birchall and R. N. Haszeldine, *ibid.*, 13 (1959).

(5) L. M. Mukherjee and E. Grunwald, THIS JOURNAL, **62**, 1311 (1958).

(6) V. K. Syrkin, *Comp. rend. Sci., U.R.S.S.*, **35**, 43 (1942).

(7) O. A. Osipov and I. K. Shelomov, *Zhur. Fiz. Khim.*, **30**, 608 (1956).

tation polarization of a mixture may be calculated from the equation[8]

$$P_i = \frac{\frac{D-1}{D+2}\frac{N_1M_1 + N_2M_2}{d_{12}} - N_1R_{D_1} - N_2R_{D_2}}{1 - \left(\frac{D-1}{D+2}\right)^2} = \frac{4N}{9kT}(N_1\mu_1^2 + N_2\mu_2^2)$$

If P_i exceeds a straight line relationship when P_i is plotted against mole fraction, the interpretation recognizes the existence of hydrogen bonding between components 1 and 2. If there are negative deviations, then there is dipole association, dipole–induced dipole interaction between components 1 and 2, or there is a decrease in hydrogen bonding between components 1 and 2 with dilution.

The present system using methyl isobutyl ketone was chosen because the alcohols are miscible with this ketone in all proportions. It was thought that the oxygen atom in the ketone molecule could participate readily in hydrogen bonding when a molecule containing a suitable hydrogen atom was available. It was thought further that differences in the results obtained with the six alcohols could be interpreted as being caused by differences in intermolecular hydrogen bonding of the alcohols. These mixtures could be interesting solvents for future studies of electrolytes where differences in the solvent intermolecular associative forces may play a role in the behavior of the solution.

Experimental

Materials.—The 2,2,2-trifluoroethanol was obtained from Pennsalt Chemical Corporation; 2,2,3,3-tetrafluoropropanol and 2,2,3,3,4,4,5,5-octafluoropentenol were obtained from the du Pont Company. These alcohols were dried for several days at room temperature over potassium carbonate and over magnesium sulfate. They were then fractionally distilled at atmospheric pressure.

Anhydrous ethanol was prepared by the method of Dawson and Golben.[9]

Normal propanol was dehydrated with the customary desiccants and fractionally distilled. The distillate was treated with activated alumina, after which the supernatant liquid was subjected to ternary azeotropic distillation using benzene as the third component to remove the last traces of water.

Normal pentanol was dried over activated alumina and then fractionally distilled at atmospheric pressure.

Methyl isobutyl ketone was dried over potassium carbonate and over magnesium sulfate, then fractionally distilled at atmospheric pressure.

Eastman White Label nitrobenzene was purified by a simple vacuum distillation using an efficient fractionating column.

Fisher Scientific Company Reagent Grade methanol was dried over magnesium sulfate and activated alumina; then it was fractionally distilled.

The physical constants obtained for these compounds are given in Table I.

Dielectric Constant Measurements.—All dielectric constants were measured with a General Radio Type 821-A Twin-T Impedance Measuring Circuit,[10] using a General Radio Type 1001-A Standard Signal Generator and a Hallicrafters Model S-40-A multiband receiver as a null detector. The temperature control, the experimental technique and principal aspects of the calibration and measuring procedures have been described in detail by Leader[11] in earlier work reported from this Laboratory. The cells employed were a modification of the type devised by Connor, Clark and Smyth.[12] Both cells were constructed of brass and were silver plated prior to use.

The standard media which were used to calibrate the dielectric constant cells were water, nitrobenzene, methanol, benzene and air. The values used for the dielectric constants of these liquids at 25° were 78.54, 34.82, 32.63 and 2.27, respectively.[13] All measurements were made at a frequency of ten megacycles; corrections applied for the residual impedances were those determined by Leader and Gormley at this frequency.[14]

Solutions were prepared on a weight basis and the necessary buoyancy corrections were applied. Each solution was

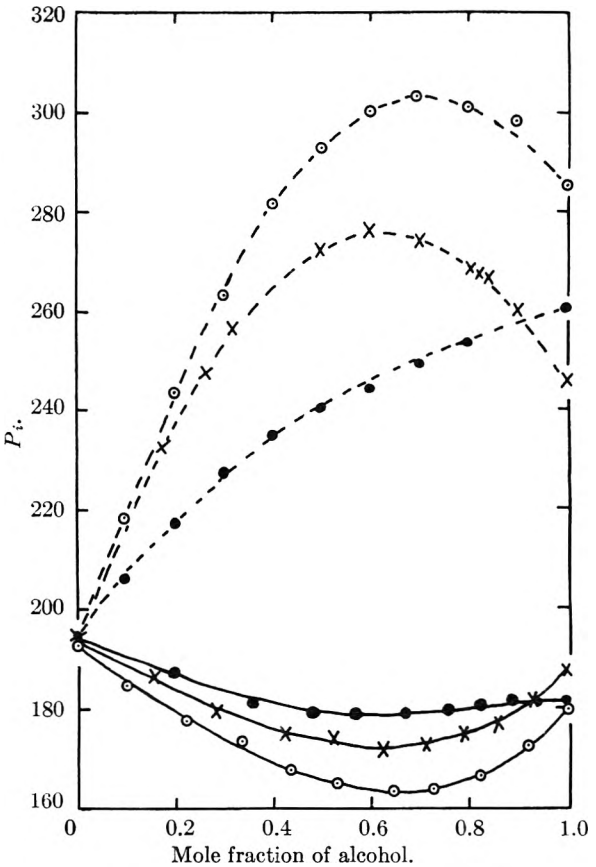

Fig. 1.—Syrkin orientation polarization *vs.* mole fraction of alcohol: ●—●, $CH_3{\cdot}CH_2OH$; X—X, $CH_3{\cdot}CH_2{\cdot}CH_2OH$; ○—○, $CH_3{\cdot}(CH_2)_3{\cdot}CH_2OH$; ●---●, $CF_3{\cdot}CH_2OH$; X---X, $HCF_2{\cdot}CF_2{\cdot}CH_2OH$; ○---○, $HCF_2{\cdot}(CF_2)_3{\cdot}CH_2OH$.

TABLE I

PHYSICAL CONSTANTS OF MATERIALS

	B.p., °C. (mm.)	Density (25°), g./ml.	Refractive index, 25°	Dielectric constant, 25°
$CF_3{\cdot}CH_2OH$	72.5 (738)	1.3820	1.291	26.67
$HCF_2{\cdot}CF_2{\cdot}CH_2OH$	105.5 (740)	1.4791	1.3196	21.03
$HCF_2{\cdot}(CF_2)_2{\cdot}CH_2OH$	139.5 (740)	1.6566	1.3169	15.67
C_2H_5OH	78 (740)	0.7860	1.3599	24.35
n-C_3H_7OH	97 (740)	.8012	1.3857	20.17
n-$C_5H_{11}OH$	137.5 (740)	.8107	1.4089	13.92
CH_3–CO–i-C_4H_9	114 (738)	.7961	1.3939	12.92

(8) P_i, ideal orientation polarization of the mixture; N_1, N_2, mole fractions; d_{12}, density of the mixture; D, dielectric constant; R_{D_1}, R_{D_2}, molar refraction using the sodium-D line. The other symbols have their usual meaning.

(9) L. R. Dawson and M. Golben, *J. Am. Chem. Soc.*, **74**, 4134 (1952).

(10) D. D. Sinclair, *Proc. Inst. Radio Eng.*, **28**, 310 (1940).

(11) G. R. Leader, *J. Am. Chem. Soc.*, **73**, 856 (1951).

(12) W. P. Connor, R. P. Clark and C. P. Smyth, *ibid.*, **64**, 1379 (1942).

(13) A. Maryott and E. Smith, National Bureau of Standards Circular Number 514, 1951.

(14) G. R. Leader and J. F. Gormley, *J. Am. Chem. Soc.*, **73**, 5731 (1951).

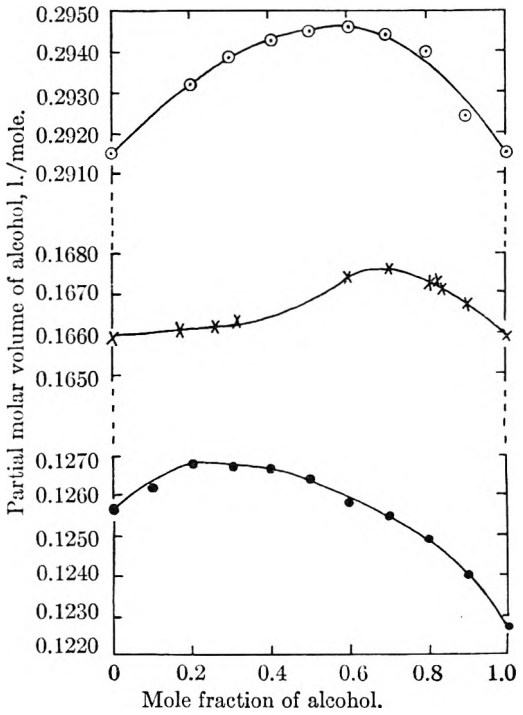

Fig. 2.—Partial molar volumes of alcohols *vs.* mole fraction of alcohol: -●-, $CF_3 \cdot CH_2OH$; -×-, $HCF_2 \cdot CF_2 \cdot CH_2OH$; -⊙-, $HCF_2 \cdot (CF_2)_3 \cdot CH_2OH$.

measured several times in each of two cells. The values listed in the tables represent mean values obtained from several measuring procedures. Individual measurements did not differ by more than 0.1 dielectric unit. Temperatures were measured with calibrated thermometers and were maintained at 25.00 ± 0.05°.

Density Determinations.—Densities were measured using conventional Reischauer specific gravity bottles. Excess liquid was introduced into the bottles and allowed to reach a constant temperature at 25.00 ± 0.05°. The level of the liquid was adjusted to the desired level using a fine capillary pipet. Any adhering liquid was removed from the exposed interior surfaces of the bottle by means of a fine capillary connected to an aspirator. The volumes of the bottles were determined by repetitive determinations using freshly prepared distilled water; these calibrations agreed to 1 part in 25,000.

Refractive Index Determination.—These measurements were obtained with a Spencer refractomer using white light. The instrument was designed to yield values using white light which approximate the sodium-D line value.

Results

The experimental values for the dielectric constant, density and refractive index as a function of the mole fraction for the six alcohol–methyl isobutyl ketone systems have been filed with the American Documentation Institute.[15]

The calculated Syrkin polarizations are plotted as a function of the mole fraction of the respective alcohol in Fig. 1. These polarizations were calculated from the equation given earlier in this paper.

The partial molar volumes of the given alcohol are plotted as a function of the mole fraction of the alcohol in Fig. 2. Those for the systems ethanol–, 1-propanol– and 1-pentanol–methyl isobutyl ketone are constant within experimental error at 0.0579, 0.0755 and 0.1107 l./mole, respectively.

Discussion

It has been known for some time that fluorine-containing compounds have some unexpected properties. The surface tensions of fluorocarbons are among the lowest recorded[16]; derivatives of fluorocarbons also exhibit this characteristic to a lesser degree. Parchors and boiling points are also abnormally low for fluorocarbons derivatives. In many organic compounds, the introduction of several fluorine substituents results in a marked decrease in boiling point. These various unusual properties have been attributed to a decrease in attractive forces between molecules of the fluorine containing compounds.

In the case of the alcohols, as mentioned earlier, the substitution of fluorine for hydrogen apparently has reduced the intermolecular hydrogen bonding to produce a less associative type of liquid. The differences in the characteristics of the polyfluoroalcohols when contrasted with their corresponding hydrocarbon analogs are apparent from the figures. The hydrocarbon alkanols in methyl isobutyl ketone show no apparent abnormal volume effect, their partial molar volumes remaining constant throughout the entire concentration range while each fluoroalcohol exhibits an expansion when mixed with the ketone. These polyfluoroalcohols show positive deviations in the Syrkin polarizations while their hydrocarbon analogs have negative deviations.

To interpret these results, one may consider the two competing factors: each alcohol is capable of intermolecular hydrogen bonding in the pure state and each alcohol is capable of participating in hydrogen bonding with the carbonyl oxygen of the ketone in the mixtures. It might be argued that the ketone molecule has a greater ability to form hydrogen bonds with the polyfluoroalcohol molecules than do the polyfluoroalcohol molecules with one another. In mixtures of the hydrocarbon alcohols and the ketone, factors are less favorable for alcohol–ketone association. However, in the latter cases, the negative deviations may be attributed to dipole–dipole interaction between the ketone and the alcohol or to a decrease in the intermolecular hydrogen bonding between the alcohol molecules.

From Fig. 1 it would appear that the formation of hydrogen bonds between the polyfluoroalcohols and ketone molecules is relatively less important in the case of 2,2,2-trifluoroethanol than for the other two fluoroalcohols. These differences may be due to the acidic ω-H in the latter cases since, presumably, this hydrogen can also hydrogen bond with the ketone. However, the deviation from ideality as manifested by the change in the partial molar volumes, as given in Fig. 2 would appear to be approximately the same for the three fluoroalcohols. It would appear also from Fig. 2 that by the addition of the ketone there is a degradation of the "well-ordered" structural aggregates of the fluoroalcohol to a more random struc-

(15) These data have been deposited as Document Number 6311 with the ADI Auxiliary Publications Project, Photoduplication Service, Library of Congress. A copy may be obtained by citing the document number and remitting $1.25 for a photoprint or $1.25 for 35 mm. microfilm in advance by check or money order payable to: Chief, Photoduplication Service, Library of Congress.

(16) R. Filler, *J. Am. Chem. Soc.*, **75**, 3016 (1953); R. Filler, *et al.*, *Ind. Eng. Chem.*, **46**, 544 (1954).

ture which utilizes the volume less economically. It is apparent that whatever the effect of adding ketone to the fluoroalcohols may be, it is not present in the case of the hydrocarbon alkanols since they exhibit no change in partial molar volume with concentration.[17]

(17) The Reviewer pointed out that part of the partial molar volume change of fluoroalcohols with ketones may be due to the interaction of the perfluoroalkyl chain with the alkyl groups of the ketone rather than to hydrogen bonding. The mixing of hydrocarbons with fluorocarbons is accompanied by large positive volume changes (up to 5% increase).

METAL-POLYELECTROLYTE COMPLEXES. VII. THE POLY-N-VINYLIMIDAZOLE SILVER(I) COMPLEX AND THE IMIDAZOLE-SILVER(I) COMPLEX

By Daniel H. Gold[1] and Harry P. Gregor

Department of Chemistry of the Polytechnic Institute of Brooklyn, Brooklyn, New York

Received April 6, 1960

A study of the binding of silver by imidazole and polyvinylimidazole in 1 *M* potassium nitrate showed two-fold coördination. Formation constants for the two steps with imidazole were: $\log k_1 = 3.11$; $\log k_2 = 3.73$. These values are almost the same as corresponding ones for ammonia. The polymer bound silver somewhat more strongly ($\log k_1k_2 = 8.00$), with the second step being much stronger than the first. Also, with the polymer, binding was found to occur at much lower *p*H levels, as compared with the monomer.

Previous papers in this series have reported on the binding of metallic cations by polyacids.[2] The binding of copper(II) by poly-N-vinylimidazole has also been studied,[3] and showed that the polybase bound Cu(II) ions strongly with small spreading factors between the stepwise formation constants. The present paper is concerned with potentiometric studies of the formation of complexes of silver(I) with imidazole and polymeric imidazole. Both studies were conducted in 1 *M* potassium nitrate solution.

Experimental

Materials.—The poly-N-vinylimidazole (PVI) used was the same as that employed before[3,4]; it was essentially of high purity. Imidazole (m.p. 90°, lit. 90°) was obtained from Eastman Kodak Co. and used without further purification after drying. Solutions of imidazole were prepared by weight; their titer was determined potentiometrically.

Analytical grade silver(I) nitrate was heated for 24 hours at 175° and then fused at 220° to remove occluded water. The salt was pulverized, redried and used directly to prepare standard stock solutions by weight. All operations involving the silver ion were performed at low light levels.

Titrations.—Hydrogen ion activity was measured with a Beckman Model G *p*H meter with external electrodes. The reference electrode was immersed in a saturated potassium nitrate solution and a potassium nitrate–agar bridge was used to complete the circuit. It was assumed that the junction potential thus introduced was constant during all titrations.

All PVI–Ag titrations were made in the stepwise manner previously described[3] at 25.0° using dark containers. It was found that equilibrium was always obtained within 24 hours. All imidazole–Ag titrations were made at 24.98° in a dark cell.

The titration of 0.01 *M* imidazole in 1 *M* potassium nitrate and several concentrations of silver is shown in Fig. 1. Similar titrations of 0.01 *M* PVI are shown in Fig. 2. The binding of imidazole and PVI by silver ions is apparent from the decrease in *p*H at all degrees of neutralization in both cases.

Calculation of Equilibrium Constants.—The use of potentiometric titration to calculate formation constants between a metallic ion and a ligand has been described in detail by Bjerrum.[5] Essentially, the total concentration of the metallic ion in solution is kept constant while the available ligand concentration is varied, as by the addition of base. The average number of ligands bound per metal ion present in all forms, $\bar{n}$, is expressed as a function of the free ligand concentration, A, to give the formation curve of the system. The formation curve makes it possible to determine the stepwise formation constants either directly by reading off the values of pA at half integral values of n if the constants are sufficiently separated or by an iterative procedure if they are not separated. Sullivan and Hindman[6] have reviewed some of the mathematical techniques associated with Bjerrum's method.

In order to calculate the imidazole–Ag and PVI–Ag formation constants it is necessary to know $\bar{n}$ as a function of the free ligand concentration. For simplification, the method employed to calculate the monomeric formation curve will be presented first; the modifications required to calculate the polymeric formation curve will be developed subsequently.

By definition, $\bar{n}$ in the former case is given by the relation

$$\bar{n} = \frac{[I_t] - [I] - [IH^+]}{[Ag_t]} \qquad (1)$$

where $[I_t]$ is the total molar concentration of imidazole, $[I]$ for free imidazole, $[IH^+]$ for the imidazolium ion and $[Ag_t]$ for the total silver ion concentration.

It is readily shown from material balance, including

$$[I_t] = [IH^+] + [I] + \sum_{i=1}^{N} i[AgI_i^+] \qquad (2)$$

and the electroneutrality requirement that

$$[IH^+] = [I_t](1 - \alpha) - [H^+] + [OH^-] \qquad (3)$$

where α is the degree of neutralization. The concentration of hydroxide ions was generally small in our experiments in comparison to the other terms in equation 3. In calculating the hydrogen ion concentration, the mean activity coefficient of the supporting electrolyte was taken.

Assuming that the dissociation constant of the acid (K_a) remains unaltered in the presence of a coördinating metal, the

(1) This work is abstracted from the Dissertation of Daniel H. Gold, submitted in partial fulfillment of the requirements for the degree of Doctor of Philosophy in Chemistry at the Polytechnic Institute of Brooklyn, June, 1957.

(2) H. P. Gregor, L. B. Luttinger and E. M. Loebl, This Journal, **59**, 34, 366, 559, 990 (1955).

(3) D. H. Gold and H. P. Gregor, *ibid.*, **64**, 1464 (1960).

(4) H. P. Gregor and D. H. Gold, *Z. physik. Chem., Neue Folge*, **15**, 93 (1958).

(5) J. Bjerrum, "Metal Ammine Formation in Aqueous Solution," P. Haas and Son, Copenhagen 1941.

(6) J. C. Sullivan and J. C. Hindman, *J. Am. Chem. Soc.*, **74**, 6091 (1952).

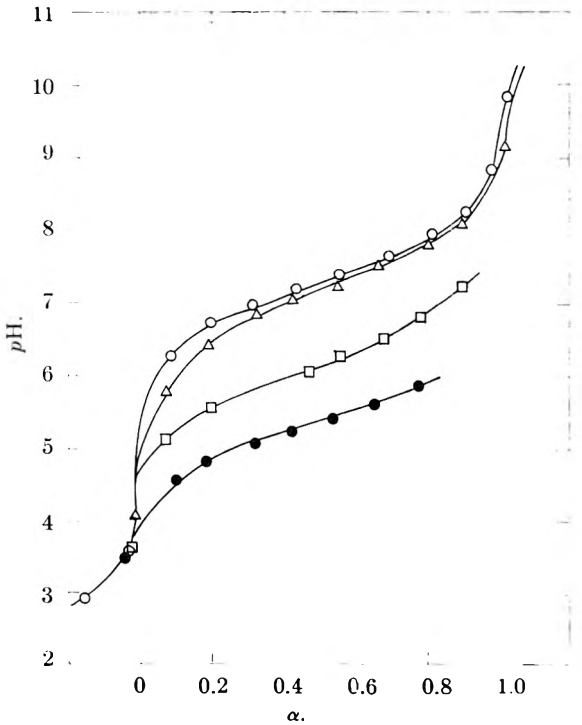

Fig. 1.—Titration of 0.01 M imidazole with base in the presence of 1 M potassium nitrate and silver nitrate at the following molar concentrations: zero (0); 5×10^{-4} (△); 5×10^{-3} (□); 5×10^{-2} (○).

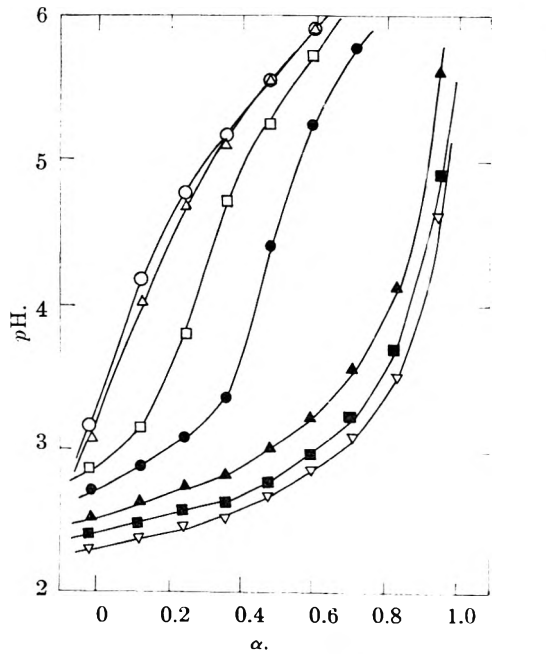

Fig. 2.—Titration of 0.01 M polyvinylimidazole with base in the presence of 1 M potassium nitrate and silver nitrate at the following molar concentrations: zero (0); 2×10^{-4} (△); 1×10^{-3} (□); 2×10^{-3} (○); 6×10^{-3} (▲); 2×10^{-2} (■); 6×10^{-2} (▽).

concentration of free imidazole is found from the expression

$$p[\mathrm{I}] = pK_a - p\mathrm{H} + p[\mathrm{IH}^+] \qquad (4)$$

Equation 1 can now be solved to yield $\bar{n}$.

Calculation of polymeric complexation constants proceeds along lines similar to the above. Thus $\bar{n}$ is given as

$$\bar{n} = \frac{[\mathrm{PVI_t}] - [\mathrm{PVI}] - [\mathrm{PVIH}^+]}{[\mathrm{Ag_t}]} \qquad (5)$$

where the terms have the same significance as before with concentrations of the polymer expressed in base moles per liter. Also, as before, from material balance and the electroneutrality requirement it can be shown that

$$[\mathrm{PVIH}^+] = [\mathrm{PVI_t}](1 - \alpha) - [\mathrm{H}^+] + [\mathrm{OH}^-] \qquad (6)$$

In the case of a polyacid (or polybase) the acid dissociation expression does not remain unaltered in the presence of a coördinating metal since the "constant" is a function of the degree of chain charging. It was shown empirically[2,4,7] that over a wide range of α the titration of PVI could be expressed as

$$K_a = \frac{[\mathrm{H}^+][\mathrm{PVI}]}{[\mathrm{PVIH}^+]}\left(\frac{1}{Z}\right)^{n-1} \qquad (7)$$

where Z is the ratio of charged to uncharged groups on the polymer chain; n is the Henderson–Hasselbach slope in the absence of added metal. In the presence of silver ions, the above expression becomes

$$K_a = \frac{[\mathrm{H}^+][\mathrm{PVI}]}{[\mathrm{PVIH}^+]} \times \left(\frac{[\mathrm{PVI}]}{[\mathrm{PVIH}^+] + \sum_{i=1}^{N} \mathrm{Ag(PVI)}_i^+}\right)^{n-1} \qquad (8)$$

The numerical solution of equation 8 requires information as to the species of complex present. As will be seen later, the principal coördination number N is two for the silver–imidazole complex, with the second formation constant greater than the first, thus indicating the predominant species to be the 2:1 complex. Bjerrum also found that $N = 2$ for the silver–ammonia complex.[5] Accordingly, it was assumed that the 2:1 complex was the predominant species in the polymeric system. Since in equation 8 the complexation does not in itself alter the dissociation relation of the acid, we can write

$$K_{av} = \frac{[\mathrm{H}^+][\mathrm{PVI}]}{[\mathrm{PVIH}^+]}\left(\frac{[\mathrm{PVI}]}{[\mathrm{PVIH}^+] + {}^1/_2(\alpha[\mathrm{PVI_t}] - [\mathrm{PVI}] + [\mathrm{H}^+] - [\mathrm{OH}^-])}\right)^{n-1} \qquad (9)$$

Equation 9 can now be solved for [PVI] by an iterative procedure, and $\bar{n}$ obtained as a function of p [PVI].

As will be shown later, the assumption of $N = 2$ leads to a maximum coördination number of 2; however, if $N = 1$ were the assumed value, the plot of $\bar{n}$ *vs.* p[PVI] still showed a maximum coördination number of 2, for the plot is not strongly affected by the choice of N.

Results and Discussion

The calculated formation curve for the imidazole–silver system is shown in Fig. 3. Three different concentrations of silver were employed, with all of the points corresponding to different metal ion concentrations falling on the same line. The formation curve extrapolates to a maximum of 2 imidazoles bound by one silver, but it is possible that more may be bound at higher concentrations of free imidazole. The consecutive formation constants k_1 and k_2 for the reactions

$$\mathrm{Ag}^+ + \mathrm{I} = \mathrm{AgI}^+$$
$$\mathrm{AgI}^+ + \mathrm{I} = \mathrm{AgI_2}^+$$

were calculated in the manner described by Bjerrum. The results are given in Table I. Their estimated accuracy is of the order of ±0.05.

The consecutive association constants of imidazole and silver are roughly similar to those of ammonia and silver, as is shown in Table I together with the formation constants of several other metals with imidazole and ammonia. It is seen that $k_2 >$

(7) R. Speiser, C. H. Hills and E. R. Eddy, THIS JOURNAL, **49**, 334 (1945).

TABLE I

COÖRDINATION OF IMIDAZOLE AND AMMONIA

System	Ionic strength	Temp., °C.	log k_1	log k_2	k_1/k_2
Ag^+–Im	1.0	25	3.11	3.73	0.240
Ag^+–NH_3[a]	0.5	30	3.24	3.81	0.269
Cd^{++}–Im[b]	0.15	25	2.80	2.10	5.01
Cd^{++}–NH_3[a]	0	30	2.51	1.96	3.55
Zn^{++}–Im[c]	0.16	24	2.58	2.39	1.55
Zn^{++}–NH_3[a]	0	30	2.18	2.25	0.852
Cu^{++}–Im[c]	0.16	23	4.36	3.57	6.17
Cu^{++}–NH_3[a]	0	30	3.99	3.34	4.47

[a] Ref. 5. [b] C. Tanford and M. L. Wagner, *J. Am. Chem. Soc.* 75, 434 (1953). [c] J. T. Edsall, G. Felsenfeld, D. S. Goodman and F. R. N. Gurd, *ibid.*, 76, 3054 (1954).

k_1 for the imidazole–silver system as for the ammonia–silver system. However, unlike the other systems shown in Table I, the formation constants of imidazole with silver are slightly smaller than those of ammonia with silver. No reason for this difference is known. It is also interesting to observe that in all cases the imidazole–metal ion association constants are similar to the ammonia–metal ion association constants. These results indicate that the binding site of the imidazole ring is the pyrrole-type nitrogen rather than the pyridine-type nitrogen. A comparison of the association constants of imidazole and 1-methylimidazole with copper(II) led Li, White and Doody[8] to the opposite conclusion.

The calculated formation curve for the association of PVI with silver ions is also shown in Fig. 3. Points corresponding to 5 different concentrations of silver ions fall on the same curve, thus confirming the validity of the approach used. The over-all association constant taken from the formation curve at $\bar{n} = 1$ is $\log K_2 = 8.00$; the value of the displacement constant for the reaction

$$2PVIH^+ + Ag^+ = Ag(PVI)_2^+ + 2H^+$$

is $\log B_2 = -2.17$.

A comparison of the formation curves of imidazole–Ag and PVI–Ag shows that for both systems the coördination number is 2 under the experimental conditions employed. The slope of the PVI–Ag formation curve is considerably greater than the slope of the imidazole–Ag formation curve, an effect that was also found with PAA–Cu(II)[2] and PVI–Cu(II)[3] associations. Because of the very low spreading factor between the successive polymeric formation constants, only the over-all constant is considered meaningful. The over-all imidazole–Ag formation constant ($\log K_2 = 6.84$) is about one order of magnitude weaker than the over-all PVI–Ag formation constant ($\log K_2 = 8.00$). Part of this difference can be attributed to the differences in the slopes of the Bjerrum plots; presumably, the second association step with the polymer is enhanced by the high, local concentration of available ligands once the silver ion enters the polyelectrolyte coil. Accordingly, in view of these facts and the difficulty in assigning exact values for the activities of ions in polyelectrolyte systems, it seems safe to assume that the first step in the coördination of both imidazole and PVI by the silver ion are essentially the same.

(8) N. C. Li, J. M. White and E. Doody, *J. Am. Chem. Soc.*, **76**, 6219 (1954).

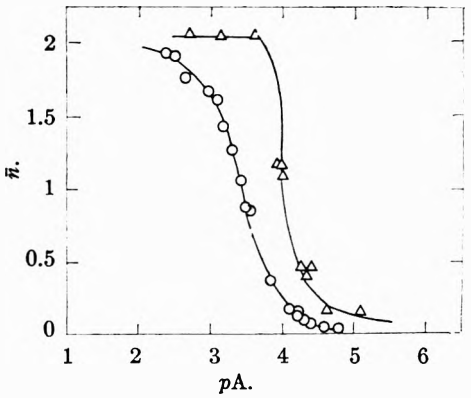

Fig. 3.—Formation curves for imidazole–silver (○) and polyvinylimidazole–silver (△) complexes in 1 *M* potassium nitrate. The base molar concentration of complexing agent was 0.01 *M*. The abscissa is $pA = p[PVI]$.

Since the binding of silver to PVI acts to charge the polymer chain, going from zero to plus one for each Ag^+ ion bound, it might be expected that binding would be *weaker* with the polymer than with the monomer, at least for the first step. However, the silver ion exhibits a low activity coefficient in 1 *M* potassium nitrate solutions ($\gamma_\pm = 0.43$), indicating an appreciable extent of association. When the silver ion is present on the polymer chain as a complex, an even greater extent of association would occur and the effective charge on the polymer would be quite low. Also, the high concentration of neutral salt tends to shield the chain.

A much stronger displacement reaction occurs with the polymer than with the monomer; the log B_2 values are -2.17 and -6.96, respectively. The five orders of magnitude in their difference reflects the experimentally observed fact that binding occurs at a much lower *p*H with the polymer than with the monomer (see Figs. 1 and 2).

Acknowledgment.—This investigation was supported in part by the Public Health Service Research Grant RG-2934 from the division of General Medical Sciences, Public Health Service.

METAL–POLYELECTROLYTE COMPLEXES. VIII. THE POLY-N-VINYLIMIDAZOLE–COPPER(II) COMPLEX

BY DANIEL H. GOLD[1] AND HARRY P. GREGOR

Department of Chemistry of the Polytechnic Institute of Brooklyn, Brooklyn, New York

Received April 6, 1960

Spectrophotometric studies of the poly-N-vinylimidazole–Cu(II) system showed that the complexes formed had an absorption maximum in the 550–650 mμ region with the peak shifting to shorter wave lengths as the ratio of metal ion to polymer was increased. Continuous variation analysis showed a preferred coördination number of four. Potentiometric titrations of the polybase in the presence of the metal were performed. The method of Bjerrum, modified for polyelectrolyte behavior, was used to calculate over-all formation constants for the reaction $Cu^{++} + 4I = CuI_4^{++}$, in the presence of 0, 0.1 and 1.0 *M* salt at 0.01 and 0.1 *M* polymer concentrations. These values were dependent upon salt and polymer concentrations and were comparable to those for the reaction of imidazole and copper under like conditions. Constants for the displacement reaction $Cu^{++} + 4IH^+ = CuI_4^{-+} + 4H^+$ were found to be nearly insensitive to the presence of salt and were considerably stronger than those with imidazole.

The imidazole group is found in many proteins and its complexes with metallic ions have been studied by potentiometric titration,[2–4] polarography[5] and spectrophotometry.[4] In general, it was found that the binding constant for the reaction of a metal ion with the imidazole group was of the same order of magnitude whether the imidazole was free or part of a protein structure.[3,4,6] Previous papers in this series have reported on the binding of metallic ions by polyacrylic and polymethacrylic acids and have shown that significantly stronger metal ion–carboxylate binding constants are obtained when the carboxylic acid is part of a polymer than when it is free.[7] It was of interest to investigate the binding of metallic ions by poly-N-vinylimidazole in order to provide a firmer basis for evaluating the binding power of the imidazole group in more complex structures. This contribution details an investigation of the binding of copper(II) by poly-N-vinylimidazole (PVI) as studied by potentiometric titration and spectrophotometry. Another communication[8] will treat the binding of silver(I) by this polybase.

Experimental

Methods and Materials.—The poly-N-vinylimidazole (PVI) used was the same as that described earlier.[9,10] This polymer was essentially of high purity, being polymerized from the 1-vinylimidazole monomer to yield

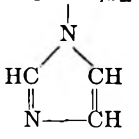

It was water soluble at all degrees of neutralization at concentration up to 0.4 *M* (base moles) in water; at concentration as high as 0.1 *M* it was not salted out by 1 *M* solutions of alkali metal chlorides and nitrates. Imidazole (I) was obtained from Eastman Kodak Co. (m.p. 90°, lit. 90°) and was used without further purification after drying at 60° and 10 mm. for several days. Stock solutions were prepared by weight and the titer checked potentiometrically with standard acid.

Copper(II) nitrate (hereafter Cu) solution was prepared from an analytical grade reagent, with about 10% nitric acid added to prevent hydrolysis. The amount of acid added was determined potentiometrically and taken into consideration in calculting degrees of neutralization. The titer of the Cu solution was determined both iodometrically[11] and electrolytically; both procedures agreed to within 0.3%.

All complexometric titrations were carried out by starting with a PVI solution to which an amount of nitric acid in excess of that required for neutralization had been added; where used, the Cu–nitric acid solution was added and then the titration performed with standard CO_2-free sodium hydroxide. Because gels formed in the presence of Cu, stepwise titrations similar to those described by Gregor, *et al.*,[7] were employed. Solutions were prepared in polyethylene containers and equilibrated for 24 hours at 25° between measurements, within which period of time a constant *p*H was attained. This stepwise procedure gave the same results as continuous titrations in those experiments where no gel phase was observed.

Hydrogen ion activities were determined with a Beckman Model G *p*H meter in the manner described previously.[10] When a neutral electrolyte was present, a sleeve-type saturated calomel electrode was employed; when no neutral salt was present a fiber tip electrode was used, which allowed a total salt contamination amounting to less than 10^{-6} *M*.

The point of incipient precipitation of copper(II) hydroxide was determined by titrating solutions of Cu in the different salt concentrations used and in the absence of PVI, employing the stepwise procedure and observing the first appearance of turbidity. This point was in the *p*H range 4.5 to 5.0; no data obtained above this *p*H level were used in subsequent calculations.

Absorption spectra measurements were made with a Beckman Model DU spectrophotometer against water blanks; 10 cm. quartz face cells were used. A preliminary study using 1 cm. cells was facilitated by the use of an automatic recorder. All quantitative measurements were taken manually.

Spectrophotometric Analysis.—Preliminary absorption spectra measurements with PVI showed a peak at 310 mμ. As Cu was added the absorbancy (log I^0/I) at this wave length increased with little shift in the peak while a new maximum appeared at 550–650 mμ. As Cu was further increased, the absorbancy at the longer wave lengths increased with the peak shifting to shorter wave lengths. The absorbancy of Cu, PVI and mixtures of the two are shown in Fig. 1 over the region where the PVI–Cu complex had an absorptivity considerably greater than either of the reactants.

(1) Taken in part from the Dissertation of Daniel H. Gold, submitted in partial fulfillment of the requirements for the degree of Doctor of Philosophy in Chemistry at the Polytechnic Institute of Brooklyn, June, 1957.

(2) F. R. N. Gurd, J. T. Edsall, G. Felsenfeld and D. S. Goodman, *Federation Proc.*, **11**, 224 (1952).

(3) C. Tanford and M. L. Wagner, *J. Am. Chem. Soc.*, **76**, 434 (1953).

(4) J. T. Edsall, G. Felsenfeld, D. S. Goodman and F. R. N. Gurd, *ibid.*, **76**, 3054 (1954).

(5) N. C. Li, J. M. White and E. Doody, *ibid.*, **76**, 6219 (1954).

(6) F. R. N. Gurd and D. S. Goodman, *ibid.*, **74**, 670 (1952).

(7) H. P. Gregor, with L. B. Luttinger and E. M. Loebl, THIS JOURNAL, **59**, 34, 366, 559, 990 (1955).

(8) D. H. Gold and H. P. Gregor, *ibid.*, **64**, 1461 (1960).

(9) H. P. Gregor and D. H. Gold, *ibid.*, **61**, 1347 (1957).

(10) D. H. Gold and H. P. Gregor, *Z. physik. Chem., Neue Folge*, **15**, 93 (1958).

(11) I. M. Koltboff and E. B. Sandell, "Textbook of Quantitative Inorganic Analysis," The Macmillan Co., New York, N. Y., 1947.

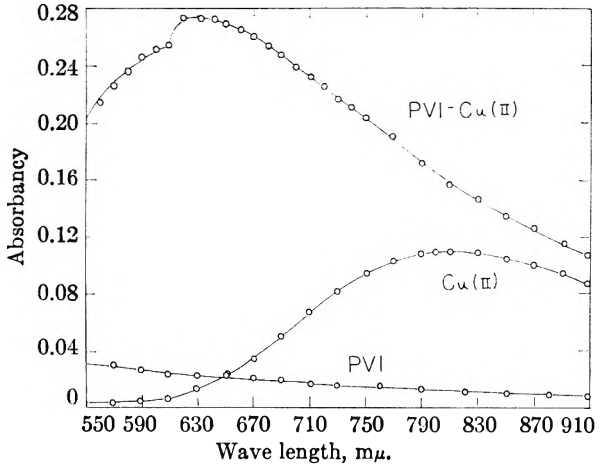

Fig. 1.—Absorbancy as a function of wave length at *p*H 4.20 for 9.86×10^{-4} *M* copper(II) nitrate, 1.8×10^{-3} *M* polyvinylimidazole and a solution 1.6×10^{-3} *M* in polyvinylimidazole and 3.94×10^{-4} *M* in copper(II) nitrate.

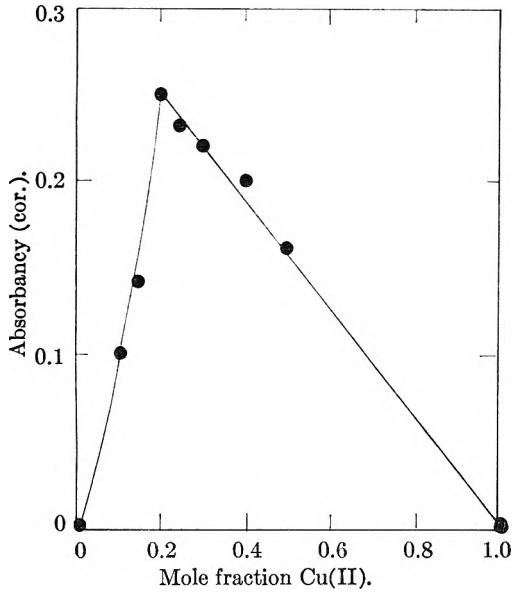

Fig. 2.—Continuous variations analysis of the poyvinylimidazole–Cu(II) complex measured at 620 mμ and *p*H 4.20 using a 0.002 *M* total solution concentration.

The method of Job[12] can be used to detect the predominant complex species present. Solutions were prepared of varying ligand to metal ion ratios, keeping the total concentration constant at 0.002 *M*. Absorbancy measurements were made at wave lengths where the complex absorbed strongly compared to either of the reactants. The solution absorbancy was corrected for reactant absorbancy assuming no reaction had occurred and assuming Beer's law. Figure 2 shows a sharp maximum when the Cu(II) mole fraction is 0.2 indicating that the predominant species formed under these experimental conditions was a complex of four imidazole groups with one cupric ion. Assuming complete reaction, the molar absorptivity $(1/bc) \log I^0/I$ of the complex was 63 l. mole^{-1} cm.$^{-1}$ at 620 mμ. Other measurements performed at higher total concentrations also led to a sharp maximum at a mole fraction of 0.2.

Edsall, *et al.*,[4] studied the imidazole–Cu system spectrophotometrically in the visible region and found that as the ratio of imidazole to Cu was increased the molar absorptivity increased and the absorption maximum shifted to lower wave lengths. Also, while the ultraviolet absorption of imidazole was virtually negligible above 240 mμ, Cu–I complexes showed marked absorption between 240 and 290 mμ. Here, as the ratio of imidazole to Cu was increased the absorptivity increased and the absorption maximum shifted toward longer wave lengths. Fourfold coördination of Cu with imidazole was found; the molar absorptivity of the CuI_4^{++} complex was estimated as 53 ± 2 l. mole^{-1} cm.$^{-1}$ at 590 mμ. In general, these results are similar to those obtained for the Cu–PVI complexes.

(12) P. Job *Ann. chim.*, [10] 9, 113 (1928); [11] 6, 97 (1936).

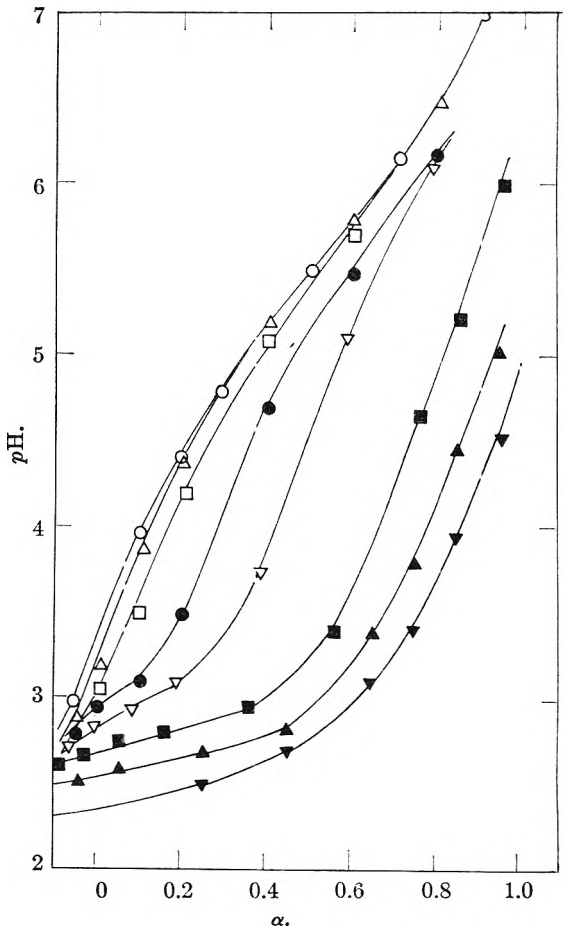

Fig. 3.—Titration of 0.01 *M* polyvinylimidazole in 1 *M* sodium nitrate. Copper(II) nitrate concentrations in millimoles liter^{-1} are: 0 (○); 0.0493 (△); 0.198 (□); 0.493 (●); 0.986 (▽); 2.96 (■); 9.86 (▲); 29.6 (▼).

Potentiometric Titrations.—Figure 3 shows titration data for 0.01 *M* PVI in the presence of 1 *M* sodium nitrate and several concentrations of Cu(II) varying from 5×10^{-5} to 3×10^{-2} *M*. In each case the polybase was overneutralized by a small excess of nitric acid and then titrated with standard base. Comparable titrations were performed in the presence of 0.0 and 0.1 *M* neutral salt and at a PVI concentration of 0.1 *M*. As the coördinating metal ion concentration was increased it was observed that the titration curves were displaced downward, typical with complex-forming systems. The decrease in *p*H at a given degree of neutralization, or the larger amount of base required to reach the same *p*H, are measures of the hydrogen ions displaced by the metal; approximate formation constants sometimes are calculated directly from these displacements.

When neutral salt is added to a polybase, the so-called shielding effect makes it stronger as a base and weaker as an acid, as discussed previously.[10] Figure 4 shows titration curves of 0.01 *M* PVI solutions carried out in the presence of no salt, in 1 *M* sodium nitrate and in the absence and presence of 0.000986 *M* copper. Data for additional titrations, those of 0.01 *M* imidazole in 1 *M* sodium nitrate in the absence and presence of 0.000986 *M* copper are also given in Fig. 4.

Calculation of Equilibrium Constants

Formation constants were calculated in the manner introduced by Bjerrum,[13] as modified for the

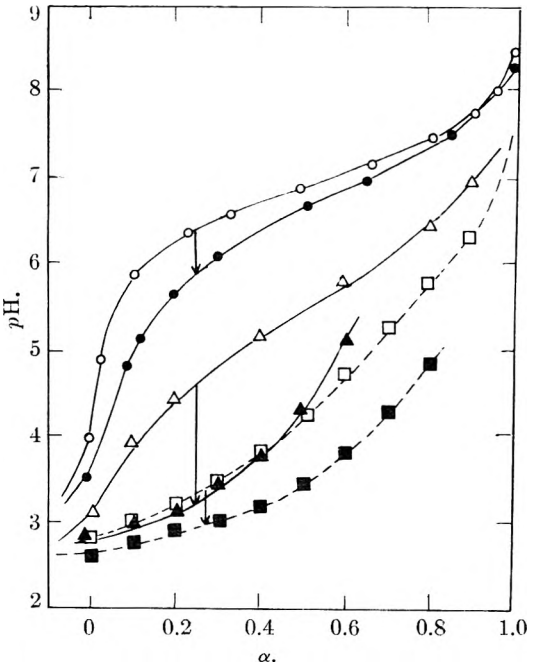

Fig. 4.—Titration of 0.01 *M* imidazole in the presence of 1 *M* sodium nitrate (○) and with 0.986 × 10^{-3} copper(II) nitrate (●). Comparable titrations of 0.01 *M* polyvinylimidazole in no salt (□) and with the same concentration of copper (■) and also in the presence of 1 *M* sodium nitrate (▲) and with copper (■).

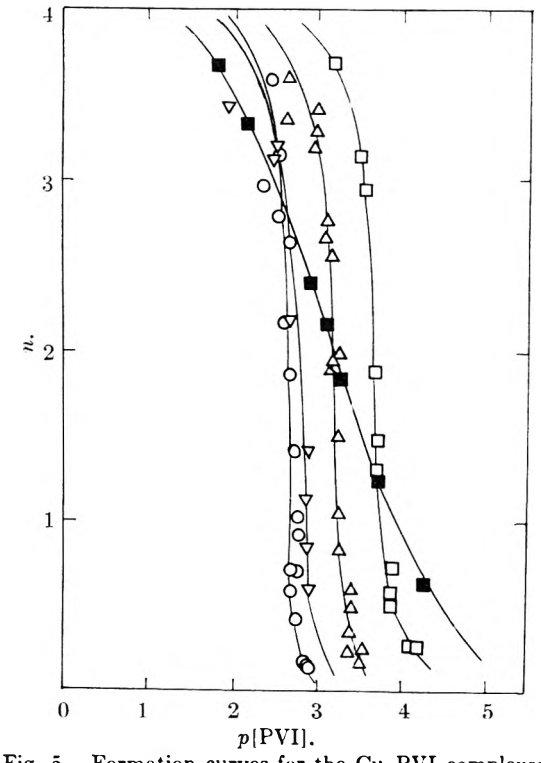

Fig. 5.—Formation curves for the Cu–PVI complexes in 0.01 *M* polyvinylimidazole in the presence of no salt (○), 0.1 *M* sodium nitrate (△) and 1 M sodium nitrate (□). Curve for the Cu–imidazole complexes[4] are shown (■). Curve for 0.1 *M* polyvinylimidazole in 1 *M* sodium nitrate is shown (▽).

(13) J. Bjerrum, "Metal Ammine Formation in Aqueous Solutions," P. Haas and Son, Copenhagen, 1941.

binding of metals by polyelectrolytes by Gregor, *et al.*,[7] the method will only be summarized herein. In Bjerrum's method, the average number of ligands bound per metal ion, $\bar{n}$, is determined as a function of the free ligand concentration to give the formation function of the system. For the imidazole–copper(II) system $\bar{n}$ is expressed as

$$\bar{n} = \frac{[I_t] - [I] - [IH^+]}{[Cu_t^{++}]}$$

where $[I_t]$ is the total base molar concentration of imidazole, $[I]$ and $[IH^+]$ the concentration of imidazole and imidazolium groups, respectively, and $[Cu_t^{++}]$ the total copper(II) concentration.

From material balance equations and the electroneutrality requirement it can easily be shown that the imidazolium ion concentration is given by measurable quantities.[8] For a polybase, the relation between $[PVIH^+]$, $[PVI]$ and $[H^+]$ in the absence of a coördinating metal is given by the modified Henderson–Hasselbach expression.[8]

Since spectrophotometric analysis had shown that the predominant complex species was $Cu(PVI)_4^{++}$, it was assumed that other possible species were present in negligible amounts only. The final expression here is identical with equation 9 of the previous paper,[8] because in the complex the ratio of charge to number of ligands was the same (1:2).

The hydroxyl ion concentration was generally negligible in these experiments compared to the other terms in the final expression and was neglected. Although it has been established experimentally that activity coefficients of counterions (at low ionic strengths) are depressed considerably below corresponding values in simple electrolytic solutions, for lack of a better approximation it was assumed that the hydrogen ion activity coefficient was the same as the mean activity coefficient of the supporting 1–1 electrolyte; $\gamma^{\pm}_{H^+}$ was taken as unity in the absence of salt, 0.76 in 0.1 *M* sodium nitrate and 0.55 in 1 *M* sodium nitrate.[14] The final expression may then be solved for the only unknown, $[PVI]$ through an iterative procedure and hence $\bar{n}$ obtained.

Results and Discussion

The formation curves for 0.01 *M* PVI–Cu in the absence of salt, 0.1 and 1 *M* sodium nitrate are shown in Fig. 5. This figure also shows the formation curve of 0.1 *M* PVI–Cu in 1 *M* sodium nitrate. For comparison, the formation curve of imidazole–Cu at 23° at ionic strength 0.16 determined by Edsall, *et al.*,[4] is shown. The PVI–Cu formation curves would appear to extrapolate to a maximum coördination number $N = 4$. If two- or sixfold PVI–Cu coördination were assumed in the calculation of $\bar{n}$ and $p(PVI)$, the formation curves still approached coördination number four; these polymeric formation curve plots tend to indicate the maximum value of $\bar{n}$ even if the assumed value of the maximum coördination number is incorrect. The job plot indication that $N = 4$ is more definitive.

All the PVI–Cu formation curves were constructed from titration data with, in most cases, five different copper ion concentrations. The gen-

(14) R. A. Robinson, *J. Am. Chem. Soc.*, **57**, 1165 (1935).

eral validity of the approach used is confirmed by the presence of points corresponding to copper ion concentrations ranging from 5×10^{-5} to 3×10^{-2} M on the same line.

The steep slopes evinced by the PVI–Cu formation curves indicate spreading factors of less than unity[13] between the stepwise formation constants. This effect appears to be quite general with polymeric complexing systems; once the coördinating metal ion is attached to one group on the polyelectrolyte coil the high, local concentration of available ligands triggers the completion of binding and make the apparent successive formation constants larger than the first.

Formation and displacement constants for the association of copper with PVI under several experimental conditions are summarized in Table I. For comparison, constants for copper with imidazole, 1-methylimidazole and serum albumin imidazole are also given. The formation constants are expressed in two ways: K_4 refers to the chelation reaction, $Cu^{++} + 4I = Cu(I)_4^{++}$; B_4 refers to the displacement reaction, $Cu^{++} + 4IH^+ = Cu(I)_4^{++} + 4H^+$. The K constant characterizes the formation process itself while the B constant is more descriptive of the actual extent of complex formation, particularly at lower pH levels.

With the Cu–PVI formation process, Table I and Fig. 5 show that as the ionic strength increases, the value of K_4 increases also. This effect appears to be analogous to our usual experience with chelate acids where K increases as the acidity of the acid decreases, for the strength of the acid $PVIH^+$ does decrease with the ionic strength.[10] However, since the chemical nature of the acid is not being altered, it is seen that the effect here is primarily one of electrostatic shielding. This formation process is accompanied by a successive charging of the polymer chain. As each successive mole of Cu(II) binds to four imidazole groups on the chain, the charge on the latter is increased by +2. The standard free energy change for any of these processes may be written

$$\Delta F^0 = \Delta H^0 - T\Delta S^0 - \Delta F_e$$

where ΔF_e refers to the electrical work which is positive (by convention) for processes which involve electrostatic attraction and negative for those which involve repulsion. It has been shown previously[7] that ΔH^0 is nearly the same for the binding of metals by polymeric and monomeric ligands. With polyacrylic acid–Cu(II) and glutaric acid–Cu(II) binding, the entropy change would similarly be expected to be nearly the same because the metal chelate rings differ only by the two side chains (with polyacrylic acid), and the addition of side chains to ligands does not make for profound differences in formation constants. Accordingly, for the carboxyl–Cu(II) system the *difference* in the magnitude of the electrical free energy terms for polymeric and monomeric binding is $\Delta F_{e\ \text{polymer}} - \Delta F_{e\ \text{monomer}} = RT \ln 10^6$ in the absence of salt; in concentrated (2 M) salt solutions the difference would be $RT \ln 10^4$.[7]

TABLE I

FORMATION CONSTANTS OF COPPER(II) WITH IMIDAZOLE-CONTAINING LIGANDS AT 25°

Ligand	Ionic strength	log K_4	log B_4
PVI, 0.01 M	0	10.64	− 6.40
PVI, 0.01 M	0.10	12.76	− 7.12
PVI, 0.01 M	1.0	14.72	− 7.08
PVI, 0.1 M	1.0	11.00	−10.96
Imidazole[a]	0.16	12.72	−15.72
Imidazole[b]	.15	12.6	−15.84
1-Methylimidazole[b]	.03	12.86	−15.94
Serum albumin imidazole[c]	.15	∼14.8	∼(− 9.60[d])

[a] Extrapolated from data of Edsall, *et al.*,[4] [b] From Li, *et al.*[5] [c] C. Tanford, *J. Am. Chem. Soc.*, 74, 211 (1952). [d] Value of $pK_a = 6.10$ for serum albumin imidazole from C. Tanford, *ibid.*, 72, 441 (1950).

In the case of the PVI–Cu complexes, one would similarly expect that the ΔH^0 terms are equal. Fourfold coördination along the same polymer chain is indicated here because the spreading factors are so small. This would give rise to considerable steric hindrance, but would not make for a large difference in the corresponding ΔS^0 values when comparing imidazole and PVI binding. Accordingly, the difference in the ΔF_e terms here is equal to $-RT \ln 10^2$ at low ionic strengths and $+RT \ln 10^2$ at high levels, referring to the fourfold coördination process.

A true basis for comparing the intrinsic binding process is to be found in the use of the first coördination constant k_1. With polymers the high, localized concentration of ligands in the coil makes k_2, k_3 and k_4 larger than k_1, so that K_4 (equal to $k_1k_2k_3k_4$) becomes considerably larger than K_4 for the process with monomeric ligands. With imidazole, $\log k_1 = 4.3$, while for PVI the value is $\log k_1 = 3.9$ in 1 M salt and $\log k_1 = 2.8$ in the absence of salt. Here it is seen that the *intrinsic* binding of imidazole with copper is the strongest, that the first imidazole group on PVI which binds copper even in the presence of concentrated salt is weaker, and that in the absence of salt where higher chain potentials must be overcome, polymeric binding is even weaker.

In the case of displacement reactions where the chain potential is lowered from +4 to +2, B_4 is nearly independent of ionic strength at constant polybase concentrations. The displacement constant is much larger with the polymeric reaction, and it is interesting to note that only serum albumin imidazole is comparable with the polymer in this respect.

Acknowledgment.—This investigation was supported in part by the Public Health Service Research Grant RG-2934 from the division of General Medical Sciences, Public Health Service.

SOME SOLIDUS TEMPERATURES IN SEVERAL METAL-CARBON SYSTEMS

BY M. R. NADLER AND CHARLES P. KEMPTER

Los Alamos Scientific Laboratory, University of California, Los Alamos, New Mexico

Received April 4, 1960

Minimum eutectic temperatures were determined for systems involving carbon and some refractory metals. These solidus temperatures for the systems C–, Ta, Os, W, Re, Nb, Ir, Mo, Ru, 50Ir-50Rh, Pt, Rh and Pd are 2902, 2732, 2732, 2486, 2328, 2296, 2210, 1942, 1932, 1736, 1694 and 1504°, respectively. For the Nb–C system, the Nb_2C peritectic and the NbC–C eutectic are located at 3080 and 3220°, respectively. For the Ta–C system, the Ta_2C peritectic and the TaC–C eutectic are located at 3500 and 3710°, respectively. The melting points of Mo_2C, WC and NbC are 2410, 2720 and 3480°, respectively.

Introduction

Measurement of temperatures above 1500° in carbon atmospheres is very difficult in situations where optical methods cannot be employed. Thermocouples using combinations of refractory metal wires, carbides and graphite have been most recently reviewed by Thielke and Shepard,[1] and are being further developed. The absolute maximum operating limits of such thermocouples are fixed by certain eutectic, peritectic and compound melting temperatures of the thermoelements in combination with carbon. Another method has been used in this Laboratory for determination of the maximum temperature which *was obtained* in short-time high-temperature situations. In this method, small pieces of refractory metals are placed in contact with graphite at the point of desired measurement. Indications that a liquid phase had formed with a particular metal is evidence that the lowest eutectic temperature had been exceeded in that metal–carbon system.

This investigation involved the determination of minimum (eutectic) solidus temperatures in various metal–graphite systems, and of some eutectic, peritectic, and compound melting temperatures in carbide systems. Materials of interest included all of the platinum group metals, molybdenum, tungsten, niobium, tantalum, rhenium and the carbides of molybdenum, tungsten, niobium and tantalum. These include all metals melting in excess of 2000°.

Of the six Group VIII noble metals, a carbon–metal solidus has been determined only for platinum. Using rigorous experimental techniques, Collier, Harrison and Taylor[2] found a platinum–carbon eutectic at 2007 ± 3°K. (1734 ± 3°) corresponding to approximately 1.2% carbon. (In this article, all carbon percentages are given in weight per cent.) Hughes[3] has reported an M–C solidus temperature of 2480° (at 1.3% carbon) for rhenium (Group VII). For the Mo–C system, Takei[4] reported a Mo–Mo_2C eutectic at approximately 2200° and 4% carbon. Sykes, Van Horn and Tucker[5] found this solidus point at 2200 ± 25° and approximately 1.8% carbon. For the W–C system, Ruff and Wunsch[6] found the first eutectic (W–W_2C) at 2690° and approximately 1.4% carbon. Sykes,[7] however, reported this eutectic to be at 2475° and approximately 1.5% carbon.

A phase diagram for the Nb–C system was first published by Pochon, McKinsey, Perkins and Foreng,[8] who reported the Nb–Nb_2C eutectic at 2335 ± 20° and 1.5% carbon and the Nb_2C peritectic at 3265 ± 20°. Elliott[9] reported the Nb–Nb_2C eutectic at 2230° and 1.50% carbon and the NbC–C eutectic at 3250°.[2] Storms and Krikorian[10] located the Nb–Nb_2C eutectic at 2335 ± 20°, the Nb_2C peritectic at 3090 ± 50°, and the melting point of $NbC_{0.86}$ at 3500 ± 75°. A phase diagram for the Ta–C system was first published by Ellinger,[11] who found the Ta–Ta_2C eutectic at 2800° and 0.6% carbon, the Ta_2C peritectic at 3400°, and the TaC–C eutectic at 3300° and ~10% carbon. Pochon and co-workers,[8] however, placed the Ta–Ta_2C eutectic at 0.8% carbon. No solidus temperatures have been reported for an NbC–C eutectic.

The melting points of Mo_2C, WC, NbC, TaC and Ta_2C have been most recently reviewed by Hansen.[12] The various reported values are Mo_2C: 2405, 2230–2330, 2690 ± 50°; WC: 2650 ± 50°, 2780, 2880, 2870, 2600 and 2630°; NbC: 3700–3800°, 3500 ± 125°; TaC: 3730–3830°, 3880 ± 150°, 3540°; and Ta_2C: ~3400°. The melting points of Nb_2C, NbC and Ta_2C reported too late for inclusion in Hansen's review are discussed above. The M_2C type carbides listed do not exhibit true melting points since they first show the appearance of liquid at a peritectic point.

Experimental

The experimental work was divided into two phases: (1) determination of the minimum solidus temperatures in metal–graphite systems, and (2) determination of eutectic, peritectic and compound melting temperatures in carbide systems.

For the metal–graphite systems, wires were obtained for all of the metals except ruthenium and osmium, which

(1) N. R. Thielke and R. L. Shepard, "High Temperature Thermocouples Based on Carbon and its Modifications," High Temperature Thermometry Seminar, Oak Ridge National Laboratory, October, 1959.

(2) L. J. Collier, T. H. Harrison and W. G. A. Taylor, *Trans. Faraday Soc.*, **30**, 581 (1934).

(3) J. E. Hughes, *J. Less-Common Metals*, **1**, 377 (1959).

(4) T. Takei, *Science Repts. Tohoku Univ.*, **17**, 939 (1928).

(5) W. P. Sykes, K. R. Van Horn and C. M. Tucker, *Trans. AIME*, **117**, 173 (1935).

(6) O. Ruff and R. Wunsch, *Z. anorg. Chem.*, **85**, 292 (1914).

(7) W. P. Sykes, *Trans. ASST*, **18**, 968 (1930).

(8) M. L. Pochon, C. R. McKinsey, R. A. Perkins and W. D. Forgeng, "The Solubility of Carbon and Structure of Carbide Phases in Tantalum and Columbium," Union Carbide Corporation Report, August 29, 1958.

(9) R. P. Elliott, U. S. At. Energy Comm. Report ARF 2120-4, May 6, 1959.

(10) E. K. Storms and N. H. Krikorian, THIS JOURNAL, **64**, 1471 (1960).

(11) F. H. Ellinger, *Trans. ASM*, **31**, 89 (1943).

(12) M. Hansen, "Constitution of Binary Alloys," McGraw-Hill Book Co., New York, N. Y., 1958.

TABLE I

SIZES AND SOURCES OF METALS USED

	Wire diameter, inches	Source
Palladium	0.039	Johnson, Matthey and Co., Ltd.
Rhodium	.020	Bram Metallurgical-Chemical Co.
Platinum	.025	Unknown
Iridium–50 Rhodium	.010	Engelhard Industries, Inc.
Ruthenium	.062[a]	Varlacoid Chemical Co.
Molybdenum	.080	Unknown
Iridium	.010	Engelhard Industries, Inc.
Niobium	.062	Fansteel Metallurgical Corp.
Rhenium	.062	Chase Brass and Copper Co.
Tungsten	.080	Unknown
Osmium	.062[a]	J. A. Samuel and Co., Inc.
Tantalum	.060	Unknown

[a] 0.062" diameter pellets pressed from metal powder. Wire not available from ruthenium or osmium.

were not commercially available in wire form. These two metals were obtained in powder form and cold-pressed into 1/16" diameter pellets in a steel die. Table I gives the sizes and sources of the metals used. Those metals known to carbide (*i.e.*, molybdenum, tungsten, niobium and tantalum) were used in large enough diameters to ensure a metal-rich system during the few minutes required to reach the testing temperatures.

Results of spectrographic analysis of the metals are given in Table II. The iridium–rhodium alloy wire analyzed 50.0 weight % rhodium.

A piece approximately 1/8" long of a metal to be tested was placed in an axial off-center hole drilled in a cylinder of spectro grade graphite 5/16" in diameter by 3/8" high. The hole was 1/4" deep and not more than 0.002" larger in diameter than the particular piece of metal to be contained. The graphite cylinder fitted snugly into a graphite crucible with lid, which was positioned inside a cylindrical graphite susceptor. A split graphite radiation shield 3/4" o.d. by 1-5/8" high with slotted lid separated the susceptor from a water-cooled copper concentrator. Temperatures were read optically through a 1/32" diameter hole in the crucible lid into a 1/16" diameter hole drilled 1/4" deep in the center of the spectro graphite cylinder. Temperature measurements were made with a Leeds and Northrup optical pyrometer which had been checked against an NBS-calibrated pyrometer. Corrections for the window and prism were made to 2000° using an NBS-calibrated standard lamp, and to 2850° by simultaneously observing an induction-heated tantalum carbide target directly with the NBS-

TABLE II

SPECTROGRAPHIC ANALYSIS RESULTS (IN P.P.M. BY WEIGHT[a])

	Pd	Rh	Pt	Ir-50Rh	Ru	Mo	Ir	Nb	Re	W	Os	Ta
Li	ND	ND	ND	ND	ND	<10	ND	<3	<10	<10	ND	<1
Be	ND	ND	ND	ND	ND	<10	ND	<1	<10	<3	ND	<2
B	ND	10–100	ND	ND	ND	<10	ND	<1	<10	<10	<10	<10
Na	ND	ND	ND	ND	10–100	<20	ND	<3	<10	<30	<10	<10
Mg	<1	<10	<10	<10	10–100	<10	<10	<1	<10	<3	<10	<1
Al	ND	<10	<10	10–100	<10	<10	<10	<10	<10	<30	10–100	<10
Si	<1	ND	ND	10–100	<10	<10	ND	10	100	<50	10–100	10
K	ND	ND	ND	ND	<10	<100	ND	<30	<10	50	10–100	..
Ca	2	<10	ND	<10	<10	<10	ND	<5	<10	30	<10	<1
Ti	ND	ND	ND	ND	ND	<100	ND	<10	<10	<30	ND	<5
V	ND	ND	ND	ND	ND	<30	ND	<50	<50	<30	ND	<20
Cr	ND	ND	ND	10–100	ND	<50	ND	<10	<10	<10	ND	<10
Mn	ND	ND	ND	ND	ND	<10	ND	<3	<10	<10	<10	<3
Fe	ND	10–100	ND	10–100	10–100	200	10–100	300	<10	30	10–100	15
Co	ND	ND	ND	ND	ND	<50	ND	<10	<10	<30	ND	<20
Ni	ND	<10	ND	10–100	ND	100	ND	<10	<10	<10	ND	<10
Zn	ND	ND	ND	ND	ND	<100	ND	<300	<100	<100	ND	<100
Sr	ND	ND	ND	ND	ND	<30	ND	<30	<10	<30	ND	<20
Zr	ND	..	..	ND	ND	<100	..	3000	<100	<30	ND	<30
Nb	ND	..	..	..	ND	..	.	Major	10	100	..	300
Mo	ND	ND	ND	ND	ND	Major	ND	<100	50	100	ND	<30
Ru	ND	ND	ND	10–100	Major	..	ND	..	..	..	ND	..
Rh	ND	Major	10–100	Major	10–100	..	10–100	..	..	..	ND	..
Cu	1	<10	<10	10–100	<10	<10	<10	<10	<10	<3	<10	<2
Pd	Major	10–100	10–100	ND	10–100	..	10–100	..	..	..	10–100	..
Ag	2	ND	ND	<10	ND	<10	ND	<1	..	<3	<10	<5
Cd	ND	ND	ND	..	ND	<30	ND	..	<10	..	ND	..
Sn	ND	ND	ND	<10	ND	<10	ND	<50	<10	<10	ND	<30
Ba	ND	ND	ND	ND	ND	<20	ND	<10	<10	<10	<10	<10
Ta	ND	..	..	ND	..	<300	..	<500	<100	<100	..	Major
W	ND	..	..	ND	..	1000	..	<1000	<100	Major	..	<100
Re	ND	..	..	..	..	..	..	..	Major	..	..	..
Os	ND	ND	ND	ND	ND	..	ND	..	..	..	Major	..
Ir	ND	100–1000	ND	Major	ND	..	Major	..	..	..	10–100	..
Pt	ND	10–100	Major	10–100	10–100	..	10–100	..	..	..	10–100	..
Au	ND	10–100	ND	10–100	ND	..	ND	..	..	..	10–100	..
Pb	ND	..	..	ND	..	<10	..	..	<10	..	ND	<30
Bi	ND	..	..	ND	..	<100	..	..	<10	..	ND	<10

[a] Analysis based on sample as received, except as follows: Mo, W, Nb and Ta analyses based on samples as MoO_3, WO_3, Nb_2O_5 and Ta_2O_5, respectively.

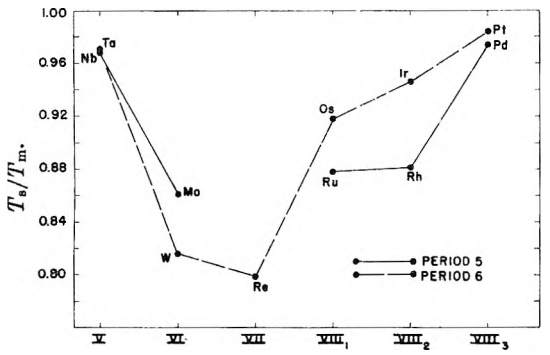

Fig. 1.—Ratio of minimum metal–carbon solidus temperature, °K., to metal melting point, °K., *vs.* group of the periodic table.

calibrated pyrometer and through the window and prism with the pyrometer used in the experiments.

The "black-body assembly" containing a metal sample was inductively heated in one atmosphere of helium with a Lepel 20 kilowatt radio-frequency induction heater. The test temperature was reached in from two to five minutes, and the sample was held at the test temperature for five minutes. Upon cooling, the metal was examined visually for evidence of liquid formation. The heating cycle was then repeated with a new piece of the same metal at a somewhat lower or higher temperature, depending on whether liquid had formed or not. Continuation of this procedure finally bracketted the lowest metal–graphite solidus temperature for the given conditions.

For the eutectic, peritectic and compound melting temperature determinations, briquettes were made using powders of spectro grade graphite, Fansteel niobium, niobium monocarbide, tantalum monocarbide, dimolybdenum carbide and tungsten monocarbide, and Kennametal tantalum. Spectrographic and chemical analyses of these materials (excepting spectro graphite) are given in Tables III and IV. The spectrographic analyses are based on the materials as Nb_2O_5, Ta_2O_5, MoO_3 and WO_3; elements not listed were present at the 50 p.p.m. level or less.

TABLE III

SPECTROGRAPHIC ANALYSIS RESULTS (IN P.P.M. BY WEIGHT)

	Nb	NbC	Ta	TaC	Mo_2C	WC
Major	Nb	Nb	Ta	Ta	Mo	W
3000	Zr					
<3000					Zr	Ta
<2000						Nb
1000	Ti					
<1000	Ta,W	W				
900				Nb		
< 500		Ta				
< 300	Zn	Zr,Zn				Zr
200	Fe		Nb			Fe
< 200						Mo,Zn
150			Fe	Fe,W		
100	Cr	Fe		Si	Fe	
< 100	Mo	Mo	W,Zn	Zn	K,Ti,Zn,Bi	V

TABLE IV

CHEMICAL ANALYSIS RESULTS

Material	M, %	Tot. C, %	Free C, %	% M + % tot. C
NbC	88.4	11.2	0.2	99.6
TaC	93.8	6.2	.1	100.0
Mo_2C	94.07	5.93	.04	100.00
WC	93.81	6.19	.03	100.00

The niobium and tantalum powders were mixed with appropriate amounts of spectro graphite to give the approximate eutectic or peritectic (solid) compositions, and cold-pressed without binder into cylinders $^5/_8$" in diameter by $^1/_4$"–$^3/_8$" high. The carbide powders were similarly compacted without binder. Each cylinder was inductively heated in one atmosphere of helium, the brightness temperature being read optically in holes 0.040" in diameter by $^1/_8$" deep drilled in the top of the cylinders. As previously described, the pyrometer was checked against an NBS-calibrated pyrometer, and corrections for window and prism were made using a tantalum carbide heated source. The temperature of each briquet was slowly raised until some melting was observed in the sight hole. This temperature was taken as the appropriate eutectic, peritectic or compound melting temperature.

Results and Discussion

The minimum (eutectic) solidus temperatures of metals in contact with graphite are given in Table V. Table VI lists the eutectic, peritectic and compound melting temperatures. The plus-or-minus deviations given in Table VI include possible errors in reproducibility of reading the pyrometer, uncertainties in the NBS-calibrated lamp and pyrometer, and constancy of temperature control during heating of the specimens. The temperature deviations in Table V include the possible errors outlined for Table VI plus the deviation from the arithmetic mean between the temperature where solid and that where liquid formed.

TABLE V

MINIMUM SOLIDUS TEMPERATURES FOR M–C SYSTEMS

	t_m, metal melting temp.[13] (°C.)	t_s, metal–carbon solidus temp., °C.	T_s/T_m, °K./°K.
Pd	1552	1504 ± 16	0.974
Rh	1960	1694 ± 17	.881
Pt	1769	1736 ± 13	.984
Ir-50 Rh	..	1932 ± 17	...
Ru	2250	1942 ± 16	.878
Mo	2610	2210 ± 14	.861
Ir	2442	2296 ± 16	.946
Nb	2415	2328 ± 17	.968
Re	3180	2486 ± 18	.799
W	3410	2732 ± 22	.816
Os	3000	2732 ± 22	.918
Ta	2996	2902 ± 30	.971

TABLE VI

EUTECTIC, PERITECTIC AND COMPOUND MELTING TEMPERATURES

Composition		Melting temp., °C.
Nb + graphite	Nb–Nb_2C eutectic	2328 ± 17
Nb + 7.0[a] C	Nb_2C–NbC peritectic	3080 ± 35
Nb + 11.0[a] C	NbC–C eutectic	3220 ± 40
Ta + graphite	Ta–Ta_2C eutectic	2902 ± 30
Ta + 4.0[a] C	Ta_2C–TaC peritectic	3500 ± 50
Ta + 8.0[a] C	TaC–C eutectic	3710 ± 50
NbC	NbC m.p.	3480 ± 50
TaC	TaC m.p.	>3550
Mo_2C	Mo_2C m.p.	2410 ± 15
WC	WC m.p.	2720 ± 20

[a] Weight per cent.

Formation of a liquid was easily determined by visual inspection for each of the metal samples heated in contact with carbon. In the case of molybdenum and tungsten, in which the metal-rich eutectic temperatures may be relatively close to a succeeding eutectic or peritectic (Mo_2C–MoC peritectic or W_2C–WC eutectic)[12] metallographic examination after heating of pieces treated almost

(13) (a) R. I. Jaffee, "Refractory Metals," International Symposium on High Temperature Technology, Asilomar, California, October, 1959. (b) Anon., *Platinum Metals Rev.*, **1**, 61 (1957).

identically to the test samples showed that free molybdenum and tungsten were indeed present after the first visible melting.

The periodic variation of the minimum solidus temperature may be seen in Fig. 1, where the ratio T_s/T_m from Table V is plotted as a function of the group of the periodic table. Group VII exhibits a minimum.

A chemical analysis of the NbC melting point cylinder gave a empirical formula of $NbC_{0.862}$, with free carbon not detectable.

Acknowledgments.—The authors thank Dr. E. VanKooten and Mr. G. C. Heasley for the chemical analyses, Messrs. O. R. Simi and J. A. Mariner for the spectrographic analyses, and Mr. C. G. Hoffman for the metallographic examinations.

THE NIOBIUM–NIOBIUM CARBIDE SYSTEM[1]

BY E. K. STORMS AND N. H. KRIKORIAN

University of California, Los Alamos Scientific Laboratory, Los Alamos, New Mexico

Received April 8, 1960

The solid portion of the Nb–NbC phase diagram has been determined. The following characteristic temperatures were measured: a eutectic temperature between $NbC_{0.08}$ and $NbC_{0.39}$ of 2335 ± 20°, a peritectic temperature between $NbC_{0.52}$ and $NbC_{0.56}$ of 3090 ± 50° and a melting point maximum at about $NbC_{0.86}$ of 3500 ± 75°. Congruent vaporization *in vacuo* takes place at a composition near $NbC_{0.71}$ at 2800°. Below 2000° Nb_2C has a very narrow range of homogeneity. Lattice parameters for the Nb_2C phase in equilibrium at the phase boundary were found to be $a_0 = 3.128 \pm 0.001$ A., $c_0 = 4.972 \pm 0.001$ Å. when NbC was present and $a_0 = 3.126 \pm 0.001$, $c_0 = 4.965 \pm 0.001$ when the Nb phase was detected. In both cases $c/a = 1.59$. The narrowness of the homogeneity range seems to preclude the possibility of obtaining a reliable relationship between composition and lattice parameter in this region.

Introduction

Three solid phases are known in the Nb-NbC system. They are the body-centered cubic, solid-solution of niobium metal and carbon, the hexagonal compound Nb_2C, and the face-centered cubic compound NbC. The relationship between these phases has been determined at several temperatures by previous workers.[2-6] This is by no means a complete list of references but represents only the most important and most recent papers. The work of Pochon, *et al.*,[5] should be consulted for a complete tabulation of earlier references. It is the purpose of this paper to present as complete a phase diagram as possible above 1500° based on these references and the results to follow.

Experimental

Niobium powder[7] and AUC graphite, both 325 mesh, were used as starting materials. Purity was shown by chemical analysis to be as high as 99.24% for the niobium and 99.4% for the carbon. In addition, a spectroscopic analysis was obtained for the niobium metal. The results are shown in Table I.

A weighed quantity (7 g. total) of the powders was dry mixed by tumbling in a glass container. Plugs measuring $^3/_8$ by $^3/_4$ inch were then pressed, without binder, in a steel die. After sintering at 1800° for about 5 minutes, a 0.060 by $^3/_8$ inch hole was drilled in the top to give black body conditions for pyrometric temperature measurement. Larger samples and samples high in carbon, which could not be pressed successfully, were sintered in a graphite crucible until compacted.

TABLE I

SPECTROSCOPIC ANALYSIS OF NIOBIUM METAL[a]

Element		Element	
Li	<3	Be	<1
B	<1	Na	<3
Mg	1	Al	<10
Si	<10	K	<30
Ca	10	Ti	<50
V	<50	Cr	<10
Mn	3	Fe	100
Co	<10	Ni	10
Cu	10	Zn	<300
Sr	<30	Zr	<300
Mo	<100	Ag	<1
Sn	<50	Ba	<10
Ta	<500	W	<1000
Pb	<30	Bi	50

[a] Values are based on sample after conversion to Nb_2O_5 and reported in parts per million.

Heating was done in an induction-field using an eddy-current concentrator. By this device, the samples could be heated without a crucible, thereby greatly reducing contact with foreign materials and lowering the power needed to obtain the high temperatures. After the pressure had been reduced to less than 10^{-3} mm., the temperature was slowly raised to the appropriate value and held for 30 minutes to 265 hours. During most of the heating the pressure was below 10^{-5} mm. and as low as 3×10^{-7} mm. during the long heatings. After heating, the plugs cooled by radiation, dropping to 900° in about one minute.

Melting points were determined by slowly raising the temperature until the hole filled with liquid. Ordinarily this occurred over a 10° temperature interval. Melting points below 2700° were determined *in vacuo;* at higher temperatures the samples were melted under an atmosphere of argon to prevent composition shifts caused by sublimation. The melting points are shown in Fig. 1; the temperature uncertainty is placed at the starting composition. This composition is projected horizontally to the final composition. This loss of carbon is caused by the reaction with free and combined oxygen and nitrogen in the starting materials.

After heating, the plugs were pulverized to 325 mesh, an X-ray powder pattern was made, and the rest was analyzed separately for niobium, combined carbon and free carbon.[8]

(1) This work done under the auspices of the Atomic Energy Commission.

(2) G. Brauer, H. Renner and J. Wernet, *Z. anorg. allgem. Chem.*, **277**, 249 (1954).

(3) G. Brauer and R. Lesser, *Z. Metallkunde*, **50**, 8 (1959).

(4) E. K. Storms and N. H. Krikorian, THIS JOURNAL, **63**, 1747 (1959).

(5) M. L. Pochon, C. R. McKinsey, R. A. Perkins and W. D. Forgeng, Metallurgical Society Conference, Vol. 2, "Reactive Metals," pp. 327, Interscience Publishers, New York, N. Y., 1959.

(6) R. P. Elliott, Armour Research Foundation Report, ARF-2120-4 (1959).

(7) Fansteel Metallurgical Corporation, North Chicago, Illinois.

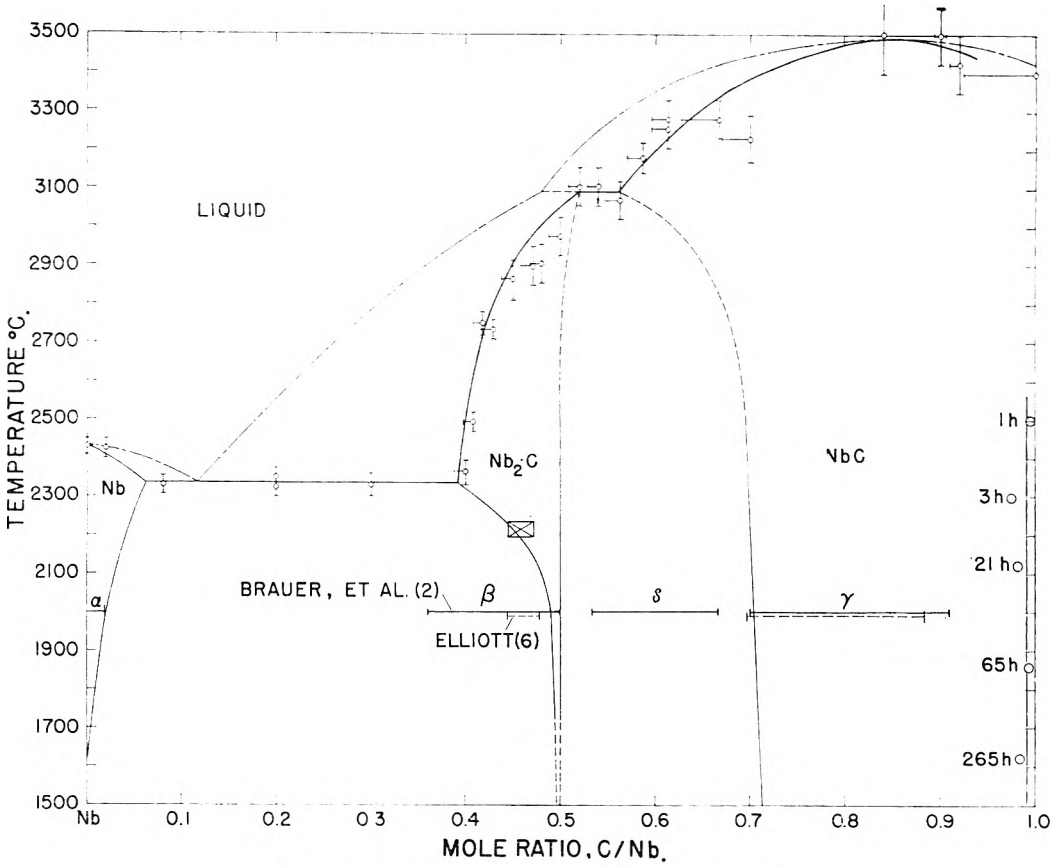

Fig. 1.—Niobium–niobium carbide phase diagram.

Several samples were also analyzed for oxygen and nitrogen. The analytical values were ordinarily accurate to better than 1%. The X-ray patterns were made in a 114.6 mm. Debye–Scherrer camera using nickel filtered, copper radiation. An exposure time of 16 hours allowed detection of NbC and Nb_2C in concentrations as low as 1 mole in 30.

Temperature measurements were made with a Pyro optical pyrometer that had been compared with a standard pyrometer. The standard was calibrated at the National Bureau of Standards and at the Argonne National Laboratory. In addition, several samples of rhodium metal (1966°), niobium (2430°), tantalum (2996°) and tungsten (3410°) were melted and the temperatures observed with the optical system used in this work. Each of these metals was better than 99% pure. Above 2300° corrections to the observed temperatures were based primarily on these melting points.

Results and Discussion

Phase Diagram.—Figure 1 shows the phase diagram of the Nb–NbC system. There are three solid, single-phase regions; a solid solution of carbon in niobium on the left (α-phase), Nb_2C near the center (β), and the NbC extending from about $NbC_{0.70}$ to $NbC_{0.99}$ on the right (γ). Each of these regions will be discussed separately. In addition, the liquidus boundary has been sketched in for the sake of clarity.

α-Phase.—According to Brauer and Lesser[3] the limit of carbon solubility in niobium lies at $NbC_{0.02}$, at 2000°, and is independent of temperature down to 1450°. A much more complete study by Elliott,[6] using metallographic techniques, detected a decrease in carbon solubility as the temperature was decreased. The line on the diagram is based on his results.

β-Phase.—Between the α-phase and the β-phase region there is a eutectic reaction at 2335 ± 20°. This temperature has been reported by Pochon, *et al.*,[5] at 2335 ± 20° and by Nadler and Kempter[9] at 2328 ± 17°. From $NbC_{0.39}$ the melting point curve rises to a peritectic temperature of 3090 ± 50°. Nadler and Kempter[9] melted a sample having an initial composition of $NbC_{0.58}$ at 3080°. This is excellent agreement. However, Pochon, *et al.*,[5] obtained 3265° for what they thought was the peritectic temperature. Because the composition of their melted material was not given, it is not possible to resolve this difference.

The region of single phase Nb_2C lies between the solidus and $NbC_{0.50}$. Near the peritectic temperature, carbon begins to dissolve, and the phase boundary moves to an upper limit of $NbC_{0.52}$. Below the eutectic temperature the single phase region becomes increasingly narrow. This is in direct conflict with the work of Brauer[3] who reported a range between $NbC_{0.36}$ and $NbC_{0.50}$ at 2000° and the results of Elliott who found a smaller range but one that was displaced from $NbC_{0.50}$. A summary of the samples heated in this region is found in Table II. The X-ray presence of niobium was seen in samples as high as $NbC_{0.495}$. No free carbon was found in any of these samples. From this and the results ob-

(8) O. H. Kriege, "The Analysis of Refractory Borides, Carbides, Nitrides and Silicides," Los Alamos Scientific Laboratory Report, LA-2306 (1959).

(9) M. R. Nadler and C. P. Kempter, THIS JOURNAL, **64**, 1468 (1960).

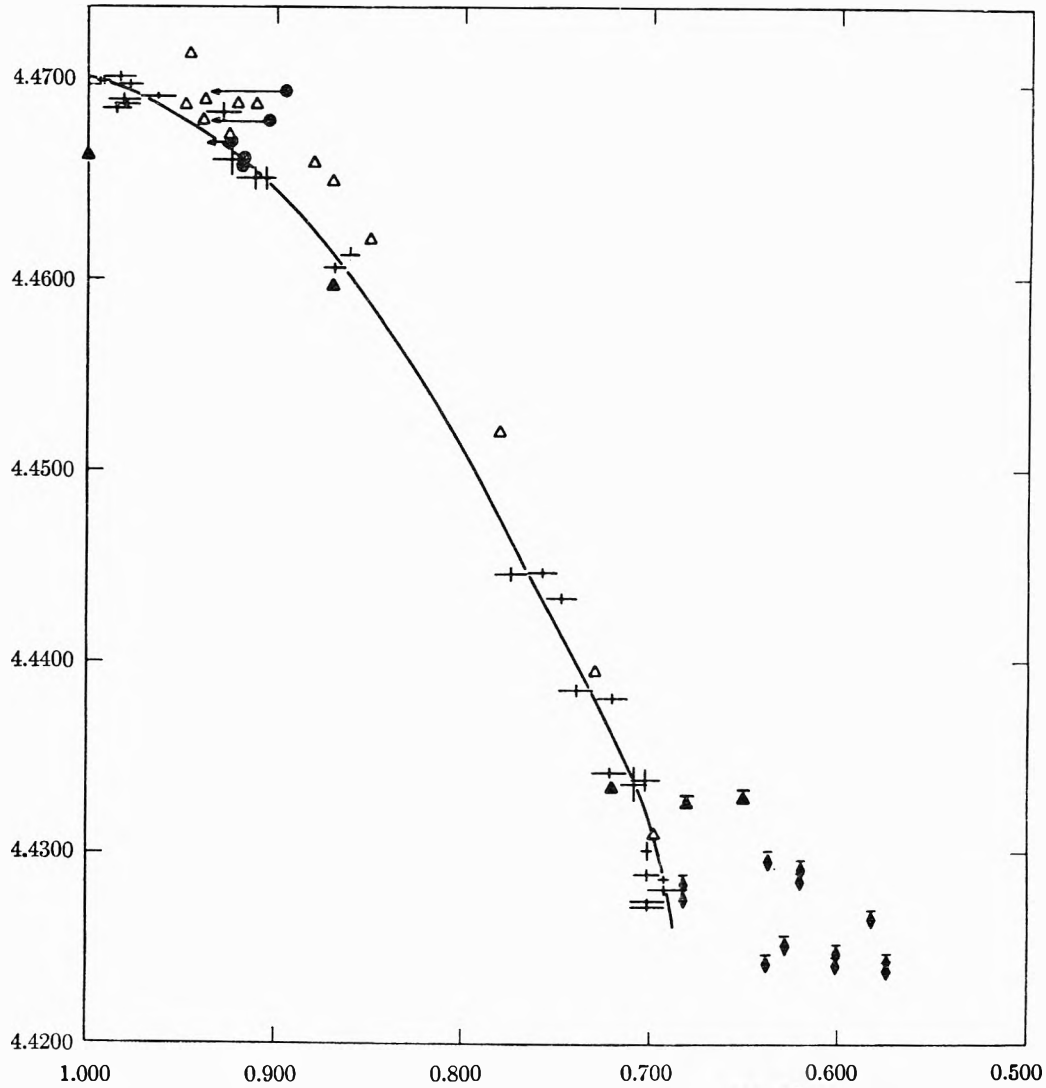

Fig. 2.—Variation of NbC lattice parameter with composition: + one phase, ◆ two phase } Storms and Krikorian[4] ▲ one phase, ▲ two phase } Brauer[2] △ one phase Brauer [3] ● This work, Table V.

tained during the reaction rate studies, to be discussed later, it is felt that all of these samples were at chemical equilibrium. Therefore, the presence of niobium was not due to unreacted starting material.

Samples between $NbC_{0.39}$ and $NbC_{0.50}$ when heated above 2335°, surprisingly contained niobium upon cooling. This suggested that niobium was precipitating during cooling and therefore the heat accompanying this reaction might be seen with a thermal arrest apparatus.[10] This device was operated by focusing the light from the sample on a photomultiplier tube which was connected to the y-axis of a time-sweep oscilloscope. Abrupt changes in the smoothly changing slope of the display trace, as the sample cooled, indicated a heat effect and, with proper calibration, gave the temperature at which the reaction took place. In this case a sample of $NbC_{0.47}$ was allowed to cool from about 2350°. Each time, a small break in the cooling curve was observed between 2195 and 2235°. It might be added that the precipitation of Nb was much faster than its dissolution upon reheating. A rectangle, in Fig. 2, defines the uncertainty in temperature and composition associated with this measurement. Although the measurement did not define the exact position of the phase boundary, it nevertheless shows that the boundary is not consistent with Brauer's data. Furthermore, if one does draw the phase boundary to include Brauer's data, one finds that a basic thermodynamic restriction is violated. The extrapolation of the phase boundary must extend into the two phase reigon, in this case, the liquid + Nb_2C region.

Between $NbC_{0.50}$ and $NbC_{0.7}$ there exists a two phase region consisting of NbC and Nb_2C. Recently Brauer[3] reported an additional phase (ζ) based on one very weak line at $\theta = 19.70°$, analogous to a similar phase he reported in the tantalum carbide system.[11] After this phase failed

(10) George N. Rupert, "An Apparatus for Observing Phase Transitions of Incandescent Material," to be published.

(11) R. Lesser and G. Brauer, *Z. Metallkunde*, **49**, 622 (1958).

TABLE II

SUMMARY OF SAMPLES CONTAINING Nb_2C

Compn.	C/Nb	Temp., °C	Heating time, hr.	a_0, Å.	c_0, Å.
Nb_2C + Nb	0.400	2285	3.0		
	.407	2200	1.0		
	.416	2300	6.0		
	.439	2450	0.5	3.126 ± 0.001	4.965 ± 0.001
	.442	2350	0.5		
	.443	1965	2.0		
	.451	2305	1.0	3.126 ± 0.001	4.965 ± 0.001
	.454	1925	2.0		
	.460	1750	44.0		
	.467	1630	55.0	3.127 ± 0.001	4.967 ± 0.001
	.471	1810	8.5	3.128 ± 0.002	4.965 ± 0.002
	.473	2200	1.2		
	.486	2100	2.0		
	.487	1730	50.0		
	.495	1800	29.0	3.125 ± 0.001	4.965 ± 0.001
	.34	2000		3.120	4.957 Brauer[2]
Single phase (?)	.49	1600–1700		3.119	4.959[3]
	.445	2000		3.1153	4.9540 Elliott[6]
	.35	1200		3.11	4.94 Pochon, *et al.*[7]
Nb_2C + NbC	.569	1730		3.1280 ± 0.0002	4.9722 ± 0.0003
	.645	2175		3.1270 ± 0.0007	4.9710 ± 0.0005
	.53	2000		3.128	4.974 Brauer[2]
	.65	1600–1700		3.125	4.963[3]
	.479	2000		3.1194	4.9663 Elliott[6]

TABLE III

HEATING SCHEDULE FOR SAMPLE MADE WITH LAMPBLACK

Operation	Composition	a_0, Å.	c_0, A.
Sintered at 1620° for 45 min. Outgassed at 2075° for 7 min. Heated at 2400° for 20 min. Analyzed	$NbC_{0.56}$ (no free carbon)	3.1297 ± 0.0004	4.9697 ± 0.0007
Heated in graphite crucible for:			
4 hr. at 1455°		3.1287 ± 0.0002	4.9730 ± 0.0003
5 hr. at 1455°		3.1286 ± 0.0003	4.9731 ± 0.0003
5 hr. at 2050°		3.1272 ± 0.0003	4.9713 ± 0.0005
8 hr. at 1730°			
Sample crushed to 325 mesh. Analyzed	$NbC_{0.57}$ (oxygen = 0.1%)	3.1280 ± 0.0002	4.9722 ± 0.0003

to appear in samples made with graphite, a better duplication of Brauer's work was undertaken using lampblack. The heating schedule for this sample is shown in Table III. As indicated, X-ray patterns were taken of the sample after various heating times. Although these were clear, well resolved patterns, no line was seen at or near $\theta = 19.70°$. Elliott[6] also was unable to find this phase.

γ-Phase.—The phase boundary for NbC has been defined by Brauer in two papers,[2,3] by Elliott[6] and by the authors in a previous paper.[4] Between 1600 and 2400° the boundary moves from $NbC_{0.71}$ to $NbC_{0.70}$. Above 2400° the exact position is in doubt because of rapid equilibrium between the phases as the material cools. A helium quench was not effective above 2600°. Below 2400°, normal cooling was able to quench in the NbC composition existing at the heating temperature.

The melting point rises from the peritectic temperature and reaches a maximum at a temperature of 3500 ± 75° at a composition of about $NbC_{0.86}$. Nadler and Kempter[9] found a melting point of 3480° ± 50° at $NbC_{0.86}$. Beyond the maximum, the solidus drops to meet the NbC–C eutectic at about 3250°. However, it still is not known for certain whether this point lies in the left or right of stoichiometric NbC. This flat, displaced maximum in melting point indicates, among other things, that NbC is highly dissociated in the melt.[12]

The NbC–C phase boundary, according to Brauer[3] lies at $NbC_{0.91}$ near 2000°. In this work, out of six samples heated at 2500° (see Table VII), one was above $NbC_{0.99}$. Apparently equilibrium between NbC and graphite is slow and difficult to obtain. This is consistent with the reaction rate studies which will be discussed later. To further locate the boundary, samples of the same starting composition were heated for various times at four temperatures. The point at 2300° represents the starting material (87.02% Nb, 12.98% total carbon, 2.00% free carbon and <100 p.p.m. nitrogen). Each point at lower temperatures was obtained by heating a graphite crucible containing a small amount of this material in a high vacuum (10^{-7} mm.). Because free carbon was present, at equilibrium the composition of the NbC phase will lie on the phase boundary. Chemical analy-

(12) J. Zernike, "Chemical Phase Theory," N. V. Uitgevers-Maatschappij AE. E. Kluwer, Deventer, 1955, pp. 228–230.

sis was used to determine the combined carbon to niobium ratio to an accuracy of 1%. Thus, provided equilibrium was obtained, the phase boundary has been located with the same precision. Otherwise the line drawn represents a lower limit.

Vapor Phase.—A preliminary study was made to determine the gross composition of the vapor by observing the change in composition of the solid during heating. Sintering causes samples to lose carbon by reaction with absorbed oxygen and oxides and, to a lesser extent, with nitrogen and nitrides. Additional heating at higher temperatures produces a material loss by evaporation.

A congruent composition of $NbC_{0.71}$ was found at 2800° by heating samples having a composition both above and below this value. Location of the congruent composition at lower temperatures was not undertaken although samples as far removed as $NbC_{0.48}$ lost niobium preferentially when heated between 2300 and 2400°.

Reaction Rate.—Very short or unreported heating times used by other investigators and the need to know the time to reach equilibrium made a study of the reaction rates in this system desirable. Many variables such as particle size distribution, completeness of mixing and compacting pressure, each having some unknown influence on the reaction rate, have not been investigated. Nevertheless it was hoped that relative reaction rates could be obtained.

A plug of $NbC_{0.8}$ was heated at 1550° for various lengths of time. After each heating a little material was scraped from the hole and X-rayed. A line density measurement was made of the following lines on each film: the Nb (110), the NbC (111), the Nb_2C (101) and the C (002). These values, the ratio Nb_2C/NbC and the a_0 value for the NbC phase in several samples are shown in Table IV. From the table, one can see the rapid disappearance of the niobium line and the more gradual fading of the carbon line even though carbon is a poorer reflector of X-rays. In fact, after 855 minutes the sample still contained 0.92% free carbon. It is clear from this that the niobium metal is being eliminated much faster than the graphite. Furthermore, the ratio Nb_2C/NbC starts high and slowly decreases. During the heating most of the NbC is in equilibrium with the Nb_2C rather than with carbon as shown by the value of the lattice constant.

From these crude observations some conclusions can be drawn. Upon heating a mixture of powdered niobium metal and graphite, a series of reactions takes place starting with the diffusion of carbon into the niobium. This reaction rapidly converts most of the niobium metal to Nb_2C. Simultaneously, if sufficient carbon is present, the Nb_2C is slowly converted to NbC. The diffusion of carbon from graphite into the surrounding layer of NbC is slower than the diffusion of carbon through the NbC. Once in the NbC lattice, carbon rapidly diffuses to the Nb_2C and reacts. As an example of the time scale involved, a sample of $NbC_{0.74}$ will require longer than 38 hours at 1800° to react completely. At lower carbon content and at higher temperatures the time is proportionately shorter. Lampblack appears to react more rapidly than graphite although quantitative information is lacking.

TABLE IV

REACTION RATE STUDIES

Time, min.	Relative intensity (002) C	(110) Nb	(111) NbC	(101) Nb_2C	Nb_2C/NbC	NbC, a_0(Å.)
15	9	18.5	12	29	2.4	
60	2.5	4.5	23.5	37	1.6	
75	0	?	33	41.5	1.3	
90	2.5	1	15.5	26	1.7	
135	1	0	16.5	25.5	1.5	
165	1	0	16	25	1.6	
291	0	0	30	30	1.0	4.4336
361	0	0	30	24.5	0.82	4.4338
483	0	0	30	21	.70	4.4339
663	0	0	33	22	.67	
855	0	0	29	16	.55	4.435

Final composition = $NbC_{0.70}$, 0.92% free carbon

Lattice Constants of Nb_2C.—The disagreement with Brauer in the β-phase region prompted a more complete study than was anticipated. In addition to the thermal arrest measurements already described, and the usual X-ray phase identification, an effort was made to determine the variation of Nb_2C lattice parameters with composition. It is this measurement that gave the greatest support to Brauer's conclusion and, therefore, should be examined most carefully.

Lattice constants were calculated for samples listed in Table II by applying the modified method of Cohen[13,14] to the back reflection lines using an I.B.M. 704. Standard deviations based on this method of extrapolation are shown. The indexing checked closely with that reported by Brauer.[2] And, when NbC is the second phase, the lattice constants agree reasonably well. However, when Nb is present the difference becomes marked. The earlier work of Brauer and the results of Elliott[6] and Pochon, *et al.*,[5] are included for comparison.

If the samples lying between $NbC_{0.400}$ and $NbC_{0.495}$ are indeed single phase, as Brauer's data would suggest, then the Nb_2C lattice parameters should increase as the carbon content increases. The value for a_0, because of the very limited change over the range of interest, allows no conclusion to be made. However, the c_0 value, which changes by 0.007 Å. over the homogeneity range, shows no variation up to $NbC_{0.495}$. This adds additional evidence that these samples contained some niobium as the second phase.

The inability of Brauer to see the presence of Nb at low concentrations can probably be explained if one realizes that the strongest line of Nb (110) is very close to the strongest line of Nb_2C (101). With a small diameter camera, as Brauer used, it is unlikely that these two lines would be resolved until the concentration of niobium had reached the value claimed to be the edge of the phase boundary.

Effect of Oxygen and Nitrogen.—It is very im-

(13) M. U. Cohen, *Rev. Sci. Instr.*, **6**, 68 (1935); *Z. Krystallogr.*, **94A**, 288 (1936); **94A**, 306 (1936).

(14) J. B. Hess, *Acta Cryst.*, **4**, 209 (1951).

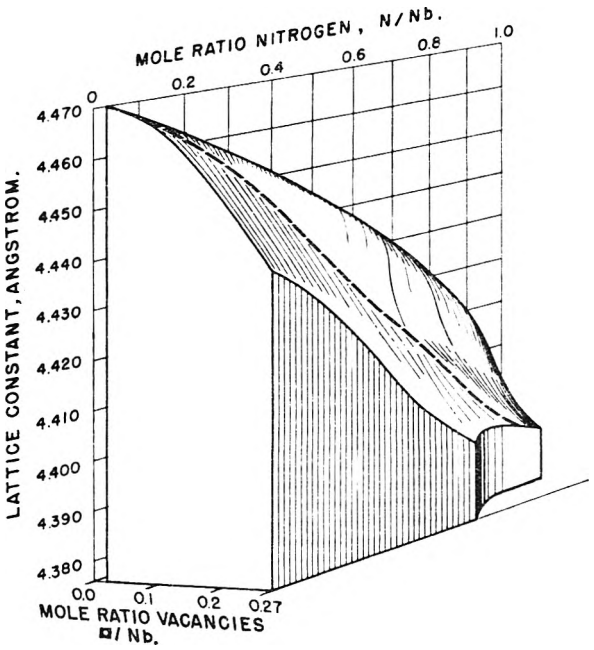

Fig. 3.—Lattice parameter *vs.* composition in the system NbN–NbC.

portant, when dealing with materials like niobium carbide to specify the amounts of oxygen or nitrogen present. Either of these impurities will change the lattice parameter if dissolved or, at least, make the sample appear richer in the metal. Thus, the various solid phase boundaries would appear to be shifted to the left from their true positions. For example, a sample having an analyzed composition of $NbC_{0.900}$, which contains 0.2 weight % nitrogen would actually be $NbC_{0.914}$, the amount of niobium combined with nitrogen as NbN being subtracted. With this in mind, it became necessary to determine how rapidly oxygen and nitrogen would be eliminated from niobium carbide by heating and, to a limited extent, what effect the remaining impurity would have. This is also an important corollary to earlier work by the authors on the variation of NbC lattice parameter with composition.[4]

Two experiments were made and the results are listed in Tables V and VI. In the first, separate samples of commercial grade NbC (Fansteel) were subjected to various heating times and temperatures in an effort to produce samples containing a smaller and smaller amount of impurity. The powder was contained in a graphite crucible during the heating. Apparently heating at 1900° for 20 minutes is sufficient to drive off most of the oxygen and nitrogen contained in a previously reacted sample. In Fig. 2 a comparison is made between the lattice parameter curve previously reported[4] and the values for these impure materials. The arrow from each point indicates the magnitude of the nitrogen correction. It is impossible to correct for oxygen since the form of the oxide is unknown. Two conclusions can be drawn: oxygen and nitrogen can be readily eliminated from NbC at the expense of free and combined carbon, and samples still containing these impurities will lie to the right of the published curve.

TABLE V

HEATING OF IMPURE NbC

Temp., °C.	Time, min.	Uncor. combined C to Nb ratio	Wt. % impurities: Free carbon	Oxygen	Nitrogen	a_0, Å.
No heating		0.895	0.33	0.28	0.66	4.4697
1300	5	.903	.06	.15	.54	4.4681
1650	10	.924	.00	.075	.17	4.4670
1900	20	.918	.00	.052	.05	4.4658
2200	120	.917	.00	.017	.00	4.4661

TABLE VI

HEATING OF CONTAMINATED NbC

Starting compn.	Nb = 87.81 wt. %	
	C = 9.25	
	N = 2.36	
	O = 0.58	a_0 = 4.469
	100.00	
Heated for 1 hr. at 1450°		a_0 = 4.468 + extra lines
Heated slowly to 1920° and continued for 30 min.		a_0 = 4.446 + extra lines
Final compn.	Nb = 90.53	
	C = 9.02	
	N = 0.30	
	O = 0.02	
	99.87	
Uncor. compn.	$NbC_{0.77}$	
Cor. compn.	$NbC_{0.79}$ assuming all nitrogen as $NbN_{1.00}$	

Table VI shows the results of the second experiment. Here, nitrogen and oxygen were added as NbN and Nb_2O_5 to pure NbC. Again the amount of nitrogen was reduced by a factor of ten and the oxygen essentially eliminated by heating *in vacuo* at 1920° for about 30 minutes. Based on the change in lattice parameter, heating at 1450° for 1 hour, apparently had very little effect.

It is not known how rapidly these impurities would be eliminated in the region near Nb_2C. The impurity would, however, have the same effect on the analyzed composition as described above.

The effect of nitrogen in the NbC system has recently been reported by Brauer and Lesser.[15] Figure 3 shows a line drawing of a model constructed by plotting their data as the ratios C/Nb, N/Nb and vacancies/Nb on the ternary axes and the lattice parameter on the vertical axis. The lattice parameter curve for pure NbC is based on Fig. 2. The surface thus created shows that dissolved nitrogen causes a lowering of the lattice parameter but in a manner dependent on the number of vacancies in the lattice. A small amount of nitrogen will cause a smaller decrease in a_0 at $NbC_{0.9}$ than would be produced if it were dissolved in $NbC_{0.7}$, for example.

In addition, this figure makes it clear that a study of lattice parameter in any binary system in which the starting materials have a range of homogeneity is not unique unless the amount of vacancy is specified. For example, Duwez and Odell[16] give the variation in a_0 for several binary systems including NbC–NbN. Based on the lattice parameter given, their NbC was nearly stoichiometric (4.470 Å. = $NbC_{0.99}$), but the NbN apparently contained a large number of vacancies (4.379 Å. ≅

(15) G. Brauer and R. Lesser, *Z. Metallkunde*, **50**, 487 (1959).
(16) P. Duwez and F. Odell, *J. Electrochem. Soc.*, **97**, 299 (1950).

$NbN_{0.81}$). As a result their data shows a slight positive deviation from linearity and cuts across the surface as indicated by the solid line. Had $NbC_{0.86}$ and $NbN_{0.86}$ been used, a nearly linear change in lattice parameter would have been obtained. Furthermore, by choosing the appropriate starting materials any number of odd shaped curves can be produced. Thus when making such studies it is extremely important to specify not only the purity but also how far removed the starting materials are from being stoichiometric.

Summary.—The Nb–NbC system contains the important features: (1) a eutectic temperature of 2335 ± 20° between $NbC_{0.06}$ (0.80 wt.%C) and $NbC_{0.39}$ (4.80 wt. % C); (2) a peritectic temperature of 3080 ± 50° between $NbC_{0.60}$ (6.30 wt. % C) and $NbC_{0.56}$ (6.75 wt.% C); (3) a melting point maximum at $NbC_{0.86}$ (10.00 wt.% C) of 3500 ± 75°; (4) a range of homogeneity of Nb_2C between $NbC_{0.495}$ (6.00 wt.% C) and $NbC_{0.500}$ (6.07 wt.% C) below 2000°. It should be recalled that, because of the techniques used, this region could be narrower than this; (5) a range of homogeneity of NbC between $NbC_{0.71}$ (8.41 wt.% C) and $NbC_{0.99}$ (11.35 wt.% C) below 2000°; (6) a composition of congruent vaporization near $NbC_{0.71}$ below 2800°.

TABLE VII

SAMPLES HEATED AT 2500° CONTAINING FREE CARBON

Heating time, min.	Combined carbon to Nb ratio	a_0, Å.
30	0 96	4.4705
60	97	4.4703
60	97	4.4703
60	.98	4.4699
90	.98	4.4692
60	.994	4.4702

Acknowledgment.—We gratefully acknowledge the advice and support of Dr. Melvin G. Bowman during the course of this work and the alert comments of Dr. James M. Leitnaker. We also wish to thank Dr. Paul W. Gilles, University of Kansas, for the use of his standard pyrometer and for several helpful discussions. Thanks are due Mr. C. G. Heasly for the analyses and Mrs. Mary Jane Jorgensen and Mr. Bobby Lee for reading the many X-ray diffraction patterns.

THE HEAT OF FORMATION OF POTASSIUM FLUOROBORATE

BY JAMES L. BILLS AND F. ALBERT COTTON

Department of Chemistry, Massachusetts Institute of Technology, Cambridge, Mass.

Received April 8, 1960

The enthalpy of formation of crystalline potassium fluoroborate has been determined from several measured enthalpies of reaction at 25°. The value obtained, −451.6 ± 0.6 kcal./mole, differs by ~19 kcal./mole from the previously tabulated value which had been calculated from experimental data of uncertain reliability. The new value is in satisfactory accord with other thermodynamic data for fluoroborate species, whereas the older value was not. The enthalpies of several reactions involving BF_4^- have been recalculated.

Introduction

In 1927, de Boer and van Liempt[1] measured the dissociation pressure of KBF_4 between 510 and 830°. This temperature range includes the melting point (530°) of KBF_4, but no break is visible in a plot of log p *vs.* $1/T$ of their data. The slope of the line has been used to evaluate ΔH^0 for the reaction

$$KBF_4(c) = KF(c) + BF_3(g)$$

and the heat of formation of KBF_4 at 25° has been calculated therefrom by several authors as −424 kcal./mole[2] and −433 kcal./mole.[3]

Thomsen,[4] long ago, measured the heat of the reaction of H_3BO_3(aq) with various quantities of HF(aq). His data, previously used in an estimate of ΔH_f^0 (BF_4^-, aq),[5] are now believed to indicate partial formation of BF_3OH^- (aq) under the conditions used. More recently, Ryss and co-workers have measured the thermodynamic changes in the step-wise hydrolyses of BF_4^-(aq).[6-8] They report, for the reaction

$$BF_4^-(aq) + H_2O(l) = BF_3OH^-(aq) + HF(aq)$$

ΔH^0 = 3.2 kcal./mole and ΔF^0 = 3.6 kcal./mole. The latter value has been confirmed by Wamser,[9] who reports $K_{eq} = 2.3 \times 10^{-3}$. Ryss and El'kenbard[10] have determined the heat of solution of KBF_3OH(c) in water and $NaOH \cdot 200H_2O$. From these data, a value of −373.7 has been calculated for ΔH_f^0 (BF_4^-, aq).[3]

A rough estimate of 22 kcal./mole[2] for the heat of solution of KBF_4(c) from existing solubility data[1] indicates that neither of the values mentioned above for ΔH_f^0(KBF_4, c) is consistent with the value of − 373.7 kcal./mole for ΔH_f^0(BF_4^-, aq), for

(1) J. H. de Boer and J. A. M. van Liempt, *Rec. trav. chim.*, **46**, 124 (1927).

(2) A. P. Altshuller, *J. Am. Chem. Soc.*, **77**, 6187 (1955).

(3) W. H. Evans, D. D. Wagman and E. J. Prosen, Nat. Bur. Standards Report No. 4943, 1956.

(4) J. Thomsen, "Thermochemische Untersuchungen," Vol. I, Verlag J. A. Barth, Leipzig, 1882, p. 231.

(5) F. D. Rossini, *et al.*, Circular 500, U. S. National Bureau of Standards, Washington, D. C., 1952.

(6) I. G. Ryss and M. M. Slutskaya, *Doklady Akad. Nauk, S.S.S.R.*, **57**, 689 (947).

(7) I. G. Ryss, M. M. Slutskaya and S. D. Palevskaya, *Zhur. Fiz. Khim.*, **22**, 1322 (1948).

(8) I. G. Ryss and M. M. Slutskaya, *Compt. rend. acad. sci. U.R.S.S.*, **52**, 417 (1946).

(9) C. A. Wamser, *J. Am. Chem. Soc.*, **70**, 1209 (1948).

(10) I. G. Ryss and A. G. El'kenbard, *Doklady Akad. Nauk, S.S.S.R.*, **91**, 865 (1953).

$$\Delta H_f^0(K^+,aq) + \Delta H_f^0(BF_4^-,aq) - \Delta H_f^0(KBF_4,c)$$
$$\simeq -60.0 - 373.7 + 433 = -0.7 \text{ kcal./mole, or}$$
$$-60.0 - 373.7 + 424 = -9.7 \text{ kcal./mole}$$

Instead, a value of $\Delta H_f^0(KBF_4, c)$ of near 456 kcal./mole would be required for consistency. This observation, coupled with the belief that a large error might be quite possible in the determination of the enthalpy of the dissociation of $KBF_4(c)$ by the method used, lead us to make an independent determination of $\Delta H_f^0(KBF_4, c)$ by a simple calorimetric method which might be expected to afford a more accurate value.

Method and Results

In the present investigation the enthalpy changes were determined for the following changes in state

$$[KNO_3 + 16.2HNO_3 + 54HF + 925Aq](l) + H_3BO_3(c) =$$
(Solution I) (1)
$$[KBF_4 + 17.2HNO_3 + 50HF + 3H_2O + 925Aq](l) \Delta H_1$$
(Solution II)

$$[17.2HNO_3 + 50HF + 925Aq](l) + KBF_4(c) =$$
(Solution III)
$$[KBF_4 + 17.2HNO_3 + 50HF + 925Aq](l) \Delta H_2 \quad (2)$$
(Solution IV)

$$[KNO_3 + 16.2HNO_3 + 54HF + 925Aq](l) + HNO_3 \cdot 92Aq$$
(Solution I)
$$(l) =$$
$$(KNO_3 + 17.2HNO_3 + 54HF + 1017Aq](l) \Delta H_3 \quad (3)$$
(Solution V)

$$[17.2HNO_3 + 50HF + 925Aq](l) + 4HF \cdot 23Aq)(l) +$$
(Solution III)
$$KNO_3(c) =$$
$$[KNO_3 + 17.2HNO_3 + 54HF + 1017Aq](l) \Delta H_4 \quad (4)$$
(Solution V)

These reactions combine to give

$$H_3BO_3(c) + 4(HF \cdot 23Aq) + KNO_3(c) = KBF_4(c) + HNO_3 \cdot 92Aq(l) + 3H_2O$$
$$\Delta H_1 - \Delta H_2 - \Delta H_3 + \Delta H_4$$

Hence

$$\Delta H_f^0(KBF_4,c) = \Delta H_1 - \Delta H_2 - \Delta H_3 + \Delta H_4 + \Delta H_f^0(H_3BO_3,c) + 4\Delta H_f^0(HF \cdot 23Aq,l) + \Delta H_f^0(KNO_3,c) - \Delta H_f^0(HNO_3 \cdot 92Aq,l) - 3\Delta H_f^0(H_2O,l)$$

Solutions II and IV are identical except for the three moles of water formed in reaction 1, which proceeds stepwise

$$H_3BO_3 + 3HF = HBF_3OH + 2H_2O \text{ (rapid)}$$
$$HBF_3OH + HF = H^+ + BF_4^- + H_2O \text{ (slow)}$$

The second step is slow, but the reaction is acid catalyzed.[11] Hence the solutions were formulated to contain 1.03 M HNO_3 at completion of the reaction. In reactions 1 and 2 a large excess of HF is present, sufficient, considering the hydrolysis constant of Wamser,[9] to keep the ratio $(BF_3OH^-)/(BF_4^-)$ less than 0.001.

We have obtained the values for the enthalpies of the four reactions

$$\Delta H_1 = -14.06 \pm 0.15$$
$$\Delta H_2 = +11.90 \pm 0.20$$
$$\Delta H_3 = -0.20 \pm 0.08$$
$$\Delta H_4 = +6.50 \pm 0.13$$

These results together with the auxiliary data

$$\Delta H_f^0(H_3BO_3,c) = -262.16^3$$
$$4\Delta H_f^0(HF \cdot 23Aq,l) = -306.55^5$$
$$\Delta H_f^0(KNO_3,c) = -117.76^5$$
$$\Delta H_f^0(HNO_3 \cdot 92Aq,l) = -49.23^5$$
$$3\Delta H_f^0(H_2O,l) = -204.95^5$$

lead to

$$\Delta H_f^0(KBF_4,c) = -451.6 \pm 0.6 \text{ kcal./mole}$$

taking no account of uncertainties in the auxiliary data.

Altschuler[2] has estimated the lattice energy of KBF_4, that is, the enthalpy of the reaction

$$KBF_4(c) = K^+(g) + BF_4^-(g)$$

to be 152 ± 10 kcal./mole. Using 123 kcal./mole for $\Delta H_f^0(K^+,g)$ and −452 kcal./mole for $\Delta H_f^0(KBF_4,c)$, we calculate $\Delta H_f^0(BF_4^-,g)$ to be −423 kcal./mole.

For the reaction

$$BF_3(g) + F^-(g) = Br_4^-(g)$$

we calculate $\Delta H^0 = -92 \pm \sim 10$ kcal./mole, using for $\Delta H_f^0(BF_3, g, -267$ kcal./mole and for $\Delta H_f^0(F^-, g), -64$ kcal./mole.[12]

Experimental

Apparatus.—Two separate calorimeter systems, A and B, were used in these investigations. Each consisted of a Dewar flask fitted with a bakelite cover, a Beckmann thermometer, and a heating coil. Each was coated with paraffin wax to protect it from the hydrofluoric acid.

A.—An electrically driven propeller-type stirrer was used in the first setup. The resistance of the heating coil was 6.217 ohms. The current was drawn from a 115 volt d.c. line and was reduced by passage through a rheostat to about 1.5 amp. The potential drop across a standard resistor (r = 0.508 ohm), connected in series with the heating coil, was recorded periodically during the heating period.

B.—A magnetic stirrer was used in the second arrangement. The Teflon-coated magnetic stirrer bar tended to scrape the wax off the bottom of the Dewar flask, so a small polyethylene plate, on which the stirrer bar could spin freely, was fastened to the wax on the bottom of the flask. The annoying tendency of the stirrer bar to stall in the middle of a run was eliminated by attaching a large horse-shoe magnet to the drive shaft of the motor. Besides being a stronger magnet than the rod magnet ordinarily used, the horseshoe magnet could be extended up beyond the exhaust tip of the Dewar flask, allowing closer approach to the stirrer bar. This apparatus contained a heating element of 1.245 ohm resistance. A direct current power supply capable of delivering 0–5 amp. with $\lesssim 0.1\%$ root mean square voltage ripple provided the calibration current. The current was read directly from a Weston ammeter with scales reading 0–2.5 and 0–5 amp., calibrated to ± 0.25%.

Reactions 1 and 2 were determined with both calorimeters; reactions 3 and 4 were determined only with calorimeter B. For use in reactions 3 and 4, a two-ounce polyethylene bottle with a small hole in the bottom was attached to a five inch length of one-half inch (outside diameter) polyethylene tubing. This assembly was used to contain the smaller amount of solution before reaction.

Reagents.—Solution I (approximately 0.97 M in HNO_3, 3.24 in HF, and 0.06 in KNO_3) was prepared by diluting 121 ml. of concentrated HNO_3, 268 g. of 48.8% HF, and 12.13 g. of KNO_3 to two liters in a polyethylene bottle. Solution II (approximately 1.03 M in HNO_3 and 3.00 M in HF) was prepared by diluting 125 ml. of concentrated HNO_3 and 246 g. of 48.8% HF to two liters in a polyethylene bottle. The $KBF_4(c)$ was prepared according to the method of "Inorganic Syntheses" for high purity.[13] A freshly prepared solution gave no precipitate with saturated lead chloride solution. All chemicals used were reagent grade.

(11) C. A. Wamser, *J. Am. Chem. Soc.*, **77**, 6187 (1955).

(12) J. G. Stamper and R. F. Barrow, *Trans. Faraday Soc.*, **54**, 1592 (1958).

(13) P. A. van der Meulen and H. L. Van Mater, "Inorganic Syntheses," Vol. I, McGraw-Hill Book Co., New York, N. Y., 1939, p. 24.

Procedure Reaction (1).—Five hundred ml. of solution I was placed in the Dewar flask. The temperature was adjusted to slightly below 25° and was recorded at 30-second intervals during the run. The slow steady rise in temperature due to the heat of stirring was recorded for a few minutes. Then 0.03 mole of H_3BO_3 was funneled into the solution. After a few minutes the steady temperature rise caused by the stirrer was again observed and recorded. The heater was turned on for a few minutes and either the potential drop across the standard resistor (calorimeter A) or the current flowing in the circuit (calorimeter B) was recorded periodically. A final record was made of the heat of stirring before the run was terminated.

Reaction (2).—The procedure of reaction 1 was carried out with KBF_4(c) and 500 ml. of solution II.

Reaction (3).—The small hole in the polyethylene bottle was sealed with halocarbon stopcock grease and 45 ml. of 0.60 *M* HNO_3 (HNO_3·93Aq) was poured down the tubing into the bottle. The bottle was lowered into 450 ml. of solution I. Temperature readings were again taken at 30-second intervals. After temperature equilibrium had been established the HNO_3 solution was expelled with compressed air. Calibration was effected as before.

Reaction (4).—The procedure of reaction 3 was carried out with 45 ml. 2.4 *M* HF·(HF·23Aq) and 450 ml. of solution II. Just before expelling the HF solution, 0.027 mole KNO_3(c) was funneled into solution II.

Calibration.—As a check on the accuracy of the apparatus, heat of solution measurements were made with KNO_3 and KCl. Three determinations of the heat of solution of KNO_3 to give KNO_3·400Aq yielded a ΔH of 8.325 ± 0.025 kcal./mole to be compared with the value of 8.308 kcal./mole reported[14] and four determinations, two with each calorimeter, of the heat of solution of KCl to give KCl·200 Aq, gave 4.201 ± 0.004 kcal./mole to be compared with the accepted[5] value of 4.201 kcal./mole.

Data.—For convenience in tabulation, the individual ΔH values are listed here. The average values are given with an uncertainty interval of twice the standard deviation of the mean plus an estimated uncertainty of 0.5%.

Calculations.—Initial temperatures were 23–25°, and no reduction to 25° was made. Time *vs.* temperature plots were prepared of the reaction and heating periods. The straight lines obtained before and after the reaction (the slope being a measure of the heat of stirring) were extrapolated to the time of mixing. The straight lines at the beginning and end of the heating period were extrapolated to the middle of the heating period. The temperature changes were read directly from the graphs. The details of the calculations differed with calorimeters A and B.

A.—The individual values of the potential drop E (in volts) were squared and a plot of E^2 *vs.* time was prepared. The area under the curve was determined graphically, yielding directly the value of E^2t (in volt² sec.). The heat of reaction in kcal./mole was calculated with the formula

$$-\frac{6.217\,E^2M\Delta T}{4184(0.508)^2W\Delta T'} = \Delta H(\text{kcal./mole})$$

where 6.217 is the resistance of the heater in ohms, ΔT is the temperature increase of the system during the reaction (in °C.), 4184 is the number of joules per kcal., 0.508 is the standard resistor resistance (in ohms), $\Delta T'$ is the temperature rise produced by the heater, W is the weight of solid used (in g) and M its molecular weight.

B.—The individual current values recorded periodically during the heating period were averaged. The formula used in calculating ΔH is

$$-\frac{i^2(1.245)tM\Delta T}{4184W\Delta T'} = \Delta H\ (\text{kcal./mole})$$

where i is the average current (in amp.), 1.245 is the heater resistance (in ohms), t is the time of the heating period (in seconds), and the other symbols are the same as in A. For reactions 3 and 4, W/M was taken to be 0.027.

A. Reaction 1

Detn.	E^2t, v. sec.	$\Delta T'$ calibn., °C.	ΔT reacn., °C.	W, g.	ΔH, kcal./mole
1	222.0	2.164	0.718	1.857	−14.12
2	177.5	1.677	.732	1.855	−14.03
3	175.8	1.727	.714	1.836	−14.09
4	175.9	1.740	.719	1.860	−13.91
5	176.2	1.709	.703	1.855	−13.92
6	175.9	1.716	.709	1.854	−13.95
	i, amp. t, sec.				
7	4.54 149.4	1.683	0.783	1.857	−14.20
8	4.54 151.3	1.712	.780	1.848	−14.15
9	4.54 149.3	1.688	.782	1.845	−14.14

$\Delta H_{av} = -14.06 \pm 0.15$

B. Reaction 2

1	178.9	1.768	−0.612	3.768	11.90
2	186.2	1.857	− .612	3.714	12.08
3	173.6	1.720	− .614	3.776	11.87
4	176.6	1.734	− .612	3.776	11.97
5	181.3	1.774	− .625	3.759	12.32
6	173.6	1.706	− .619	3.768	12.12
7	172.2	1.710	− .626	3.778	12.22
	i, amp. t, sec.				
8	4.59 151.5	1.745	−0.643	3.778	11.67
9	4.54 150.6	1.711	− .642	3.774	11.55
10	4.58 150.5	1.731	− .656	3.768	11.88
11	4.59 150.1	1.754	− .649	3.775	11.61
12	4.57 151.5	1.729	− .650	3.772	11.81
13	4.56 151.5	1.719	− .648	3.783	11.76

$\Delta H_{av.} = 11.90 \pm 0.20$

C. Reaction 3

1	2.36	450.0	1.339	0.012	−0.25
2	4.58	180.0	2.029	.006	− .12
3	4.55	150.5	1.676	.012	− .25
4	4.59	151.1	1.711	.008	− .16

$\Delta H_{av.} = -0.20 \pm 0.10$

D. Reaction 4

1	4.16	150.1	1.380	−0.315	6.53
2	4.66	150.5	1.742	− .308	6.37
3	4.63	149.5	1.735	− .322	6.56
4	4.69	149.6	1.772	− .320	6.55

Acknowledgment.—We are grateful to the Office of Ordnance Research for financial support under Contract No. DA-19-020-ORD-4919.

(14) E. Lange and J. Monheim, *Z. physik. Chem.*, *A***150**, 349 (1930).

VIBRATIONAL SPECTRA AND STRUCTURE OF MONOMERIC CYANAMIDE AND DEUTERIO-CYANAMIDE[1]

BY G. D. WAGNER, JR., AND E. L. WAGNER

Department of Chemistry, Washington State University, Pullman, Washington

Received April 9, 1960

The infrared spectra of sublimed films of cyanamide and deuterocyanamide have been obtained at low temperature in the region from 4000 to 400 cm.$^{-1}$. Under these conditions the monomeric forms of the compounds are apparently obtained. Satisfactory vibrational assignments for the monomeric molecules in the solid state can be made on the basis of the amide nitrile models, $H_2NC{\equiv}N$, which are consistent with the X-ray data where the actual crystal site symmetries are indicated to be C_1 but nearly C_s. No evidence is found for any exceptionally strong binding in the NCN group of the monomeric compounds nor is there any indication of a need for assuming planarity of the H_2N-group.

Introduction

Cyanamide is a relatively simple molecular substance that has been studied by a number of different methods in attempts to elucidate its molecular configuration. The Raman spectra of cyanamide in the solid and liquid states as well as in aqueous solution,[2] dipole moment studies in dioxane solution in comparison with diisopropyl cyanamide and diisopropyl carbodiimide,[3] molar magnetic susceptibility measurements,[4] the comparison of the experimentally determined refractivity with the calculated values for the different models,[5] and nuclear magnetic resonance measurements,[6] all have been interpreted as indicating that cyanamide molecules must exist as the amide nitrile form, $H_2NC{\equiv}N$, and that little if any of the carbodiimide tautomer, $HN{=}C{=}NH$, exists.

On the other hand, it has been suggested that the chemical properties of cyanamide indicate that there is good reason for regarding it as a substance in tautomeric equilibrium between the amide and the diimide forms.[7] Other chemical evidence has led to the conclusion that although tautomerism may exist between $H_2NC{\equiv}N$ and $H_2NN{\equiv}C$, the predominant form in dilute aqueous solution is the nitrile, and the isonitrile only becomes appreciable in acidic or strongly alkaline solutions, disappearing completely in the melted state.[8] In addition, the ultraviolet spectrum of cyanamide vapor has been analyzed and explained on the basis of the carbodiimide model alone.[9]

Recently, after our own work was completed, an extensive study of the infrared spectra of ordinary cyanamide as the molten liquid, the solidified melt, and in solutions of CH_3Cl and CH_3CN have been reported.[10] Here it was concluded that the structure of cyanamide is essentially all of the amide form, $H_2NC{\equiv}N$, but that there is considerable double bond character in the NC bond leading to exceptionally strong bonding in the NCN group and that the H_2N-group is then necessarily nearly planar. These latter conclusions were based mainly on the fact than an absorption band was found in the 1600 cm.$^{-1}$ region which only could be associated with an N=C group since it did not shift out of the region on deuteration.

All of these studies have been complicated by the fact that, even at room temperature, cyanamide readily polymerizes to the dimer dicyandiamide, $(H_2N)_2C{:}NC{:}N$. At higher temperatures this polymerization can take place with explosive violence and polymers of higher molecular weight may also form. The most common of these is melamine, $C_3N_3(NH_2)_3$. Ordinary cyanamide at room temperature apparently consists of a mixture of the monomer and polymers in a relatively constant ratio that gives a melting point, 42°, nearly 6° below that of cyanamide freshly sublimed at low temperature.

Our own infrared spectral studies, undertaken to resolve this structural problem while avoiding as much as possible the complications due to polymer formation, were carried out mainly on thin sublimed films of cyanamide and deutero-cyanamide at 25, −78 and −190° in the region from 4000 to 400 cm.$^{-1}$. Partial spectra were also obtained on these compounds as mulls, in pressed pellets of KBr, as the liquids, in solutions, and as the vapor.

Our solid state results can be interpreted satisfactorily on the basis of the amide nitrile model, $H_2NC{\equiv}N$. We find no evidence of any exceptionally strong binding as indicated by an unusually high N–C stretching frequency. Only the ordinary delocalization of other conjugated H_2N-systems is evident in the $N{-}C{\equiv}N$ group so that there is really no need for assuming complete planarity of the H_2N-group. The interpretation of the spectra on the basis of monomeric $H_2NC{\equiv}N$ molecules with actual crystal site symmetries of C_1 but nearly C_s is consistent with the X-ray crystal structure data, and the assignment of frequencies made for the monomer is consistent with those made in other related molecules.

Experimental Methods and Results

Commercial cyanamide[11] and cyanamide prepared from an aqueous solution of calcium cyanamide and sulfuric acid[12] were used as the starting materials in these investigations. These products had melting ranges of 40–42°. However,

(1) Based in part on the M.S. thesis work of George D. Wagner, Jr., at the State College of Washington, 1953, and reported at the Pacific N. W. Regional ACS meeting, June, 1953.

(2) L. Kahovec and K. W. F. Kohlrausch, *Z. physik. Chem.*, B37, 421 (1937); 188 (1944).

(3) W. C. Schneider, *J. Am. Chem. Soc.*, **72**, 761 (1950).

(4) J. Ploquin and C. Vergneac-Souvray, *Compt. rend.*, **234**, 97 (1952).

(5) E. Colson, *J. Chem. Soc.*, **111**, 554 (1917).

(6) W. G. Moulton and R. A. Kromhout, *J. Chem. Phys.*, **25**, 34 (1956).

(7) L. Hunter and H. A. Rees, *J. Chem. Soc.*, 617 (1945)

(8) Y. Otagiri, *J. Chem. Soc., Japan*, **70**, 263 (1949).

(9) S. Imanishi and T. Tachi, *ibid.*, **63**, 492 (1942).

(10) M. Davies and W. J. Jones, *Trans. Faraday Soc.*, **54**, 1454 (1958).

(11) Eastman Organic Chemicals, Distillation Products Industries, Rochester 3, N. Y.

(12) *Inorganic Syntheses*, **3**, 41 (1950).

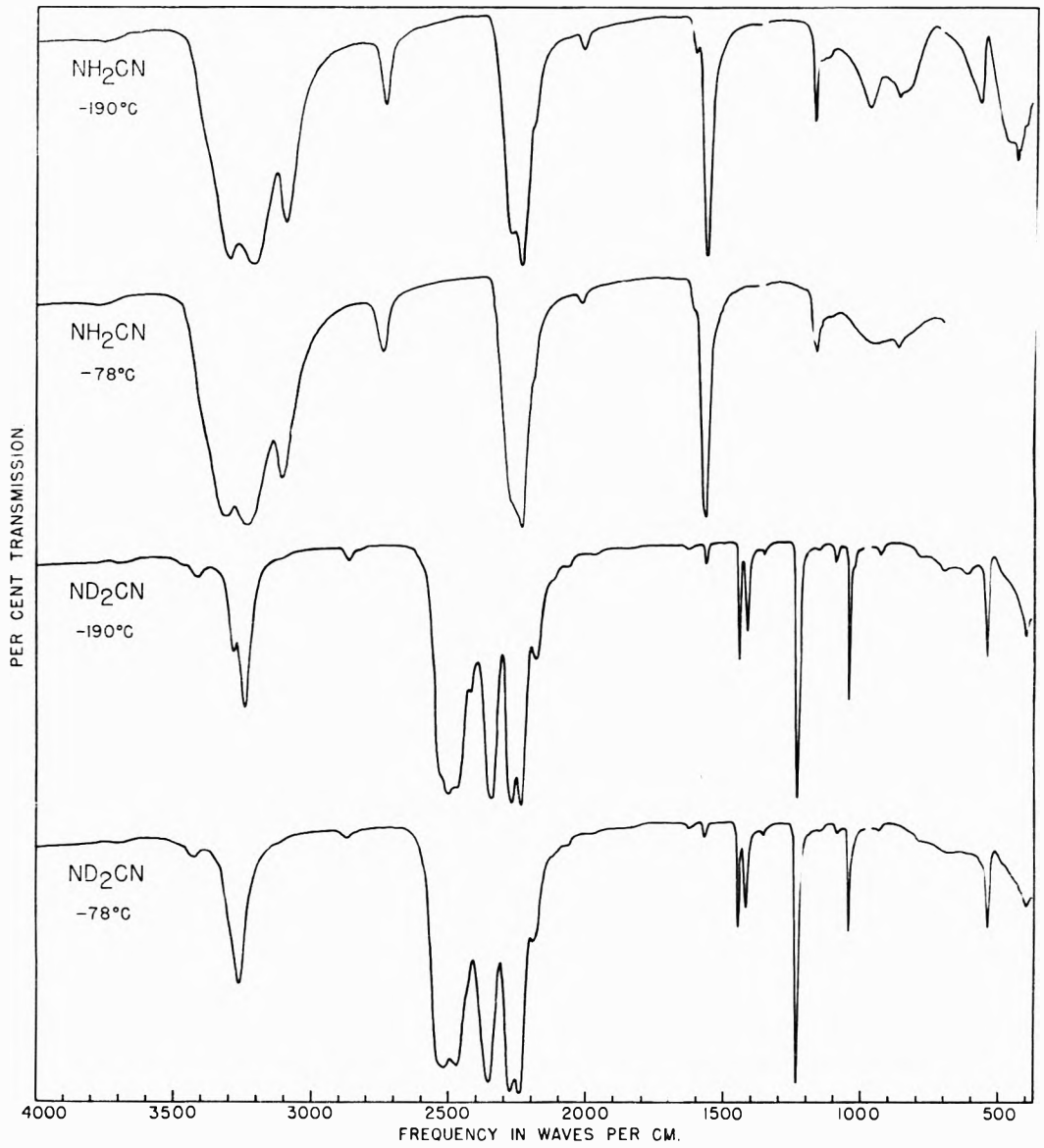

Fig. 1.—Infrared spectra of sublimed films of monomeric cyanamide and deutero-cyanamide at low temperature.

the freshly sublimed material from these products had a melting range of 47–48°. The melting point of the pure monomeric compound has been reported to be 48°.[3] Our melting points were obtained on samples sublimed in a vacuum directly into capillary melting point tubes which were immediately immersed into different temperature baths until melting occurred. On standing at room temperature, even the sublimed material reverted to a 42° melting point product.

Deutero-cyanamide was prepared from the purified cyanamide by successive exchanges with D_2O (99.75%). The exchange water was removed after each exchange without heating by vacuum evaporation. The sublimed product from this treatment could not be made to contain more than 80–85% of the theoretical amount of deuterium even though in all steps of the process, including recording the spectrum, the sample was kept in a closed system. This in itself is further evidence that room temperature cyanamide does not consist of a single species.

The thin films of cyanamide and deutero-cyanamide were prepared by direct sublimation in a vacuum onto the cooled rock salt or KBr plates of a low temperature infrared transmission cell[13] modified in such a way that the vapors could be introduced directly onto the sample plate from the side of the glass tee. Most of the crystalline films studied were condensed from the vapor at −78°. Lower or higher temperature film spectra were taken on films formed at −78°, and then cooled on down to −190° or warmed to the appropriate temperature. Films formed directly at −190° gave spectra in which the bands were all broad and unresolved but otherwise very similar to those formed at −78°. These lower temperature spectra are more characteristic of supercooled glasses or disordered phases than they are of the crystalline solids. In all cases the films were formed slowly and the samples were not heated during sublimation. The spectra of the sublimed films did not change significantly with time as long as they were kept cold.

Partial spectra of cyanamide were also obtained in pressed pellets of KBr, in Nujol and perfluorokerosene mulls, in solutions of acetone, dioxane and chloroform, and as the liquid. Spectra of cyanamide vapors at 80-90° were not inconsistent with the sublimed film spectra. The spectra of aged cyanamide as solid, liquid, or in solution at and above room temperature were very similar to one another but quite different from the low temperature solid film spectra and the spectra of freshly purified samples at room temperature. Spectra were also obtained for dicyanamide and melamine under the same conditions for comparison with those of cyanamide.

All of the spectra were taken on a Perkin-Elmer Model 21 Infrared Spectrometer recording directly in per cent. transmission *vs.* waves per cm. using both NaCl and KBr optics.

(13) E. L. Wagner and D. F. Hornig, *J. Chem. Phys.*, **18**, 296 (1950).

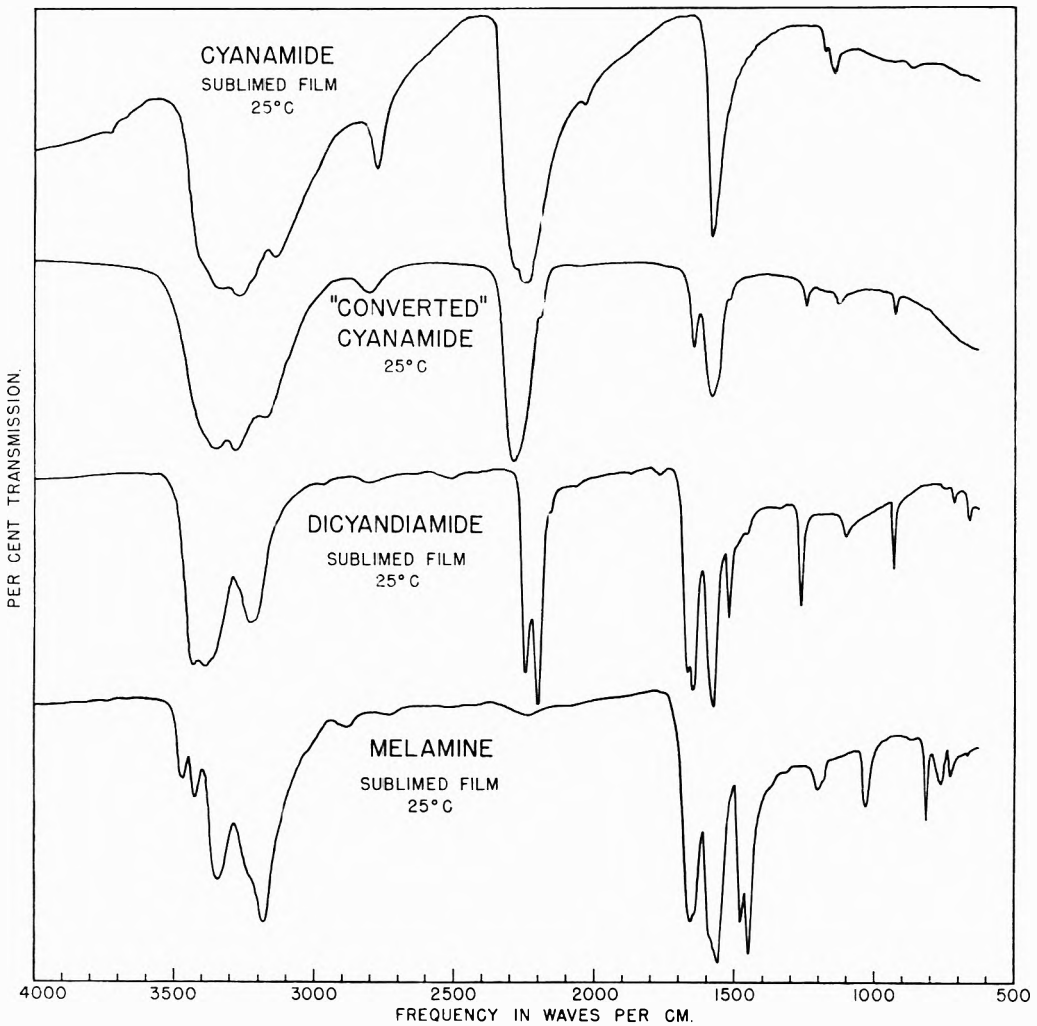

Fig. 2.—Infrared spectra of sublimed films of cyanamide and the polymerized cyanamides at room temperature.

The spectra obtained on representative sublimed films of cyanamide and deutero-cyanamide at −78 and −190° in the region from 4000 to 400 cm.$^{-1}$ are shown in Fig. 1. The corresponding peak frequencies of the −190° spectrum corrected for frequency errors in the spectrometer and the relative band areas are given in Table I. Figure 2 shows the room temperature spectra of sublimed films of cyanamide (freshly prepared and aged), dicyandiamide and melamine. When cyanamide was freshly sublimed into powdered KBr, pellets quickly made in a dry atmosphere, and spectra run as a function of time, the results for the 1600 cm.$^{-1}$ region shown in Fig. 3 were obtained.

The spectra shown in Figs. 1 to 3 clearly indicate that sublimed cyanamide partially converts to other products on standing at room temperature and that the true spectrum of monomeric cyanamide probably is obtained only on freshly sublimed or otherwise freshly purified material. Spectra of sublimed films warmed to room temperature also convert to those obtained directly from melted cyanamide, but on recooling to −190° the original spectra do not reappear so that the differences between the low and high temperature spectra are very likely not due to the occurrence of any kind of transition.

A comparison of the low temperature spectra of monomeric cyanamide and deutero-cyanamide in the 1600 cm.$^{-1}$ region, shows that the single strong band at 1567 cm.$^{-1}$ associable with the monomer completely shifts out of the region on deuteration and cannot therefore be assigned to the C=N double bond stretching mode. In addition, our spectra of dimethyl and diethyl cyanamide, both as liquids and as solid films condensed from the vapor at low temperature, show no equivalent absorption bands in the 1600 cm.$^{-1}$ region.

TABLE I

VIBRATIONAL ASSIGNMENTS FOR H_2NCN AND D_2NCN AT −190°

Corr. peak frequencies, cm.$^{-1}$ H_2NCN	D_2NCN	Isotope ratio	Assignment
3300 (70)	2505 (89)	0.758	ν_7(a″) antisym. NH_2 stretch
3215 (100)	2480 (100)	.772	ν_1(a′) sym. NH_2 stretch
3096 (53)	2348 (84)	.758	$2\nu_3$(A′)
2733 (7)	2188 (15)	.802	$(\nu_3 + \nu_4)$(A′)
2280	2275		$2\nu_4$(A′)
[2260][a] (46)	[2257][a] (90)	.997	ν_2(a′) antisym. NCN stretch
2240	2238		$2\nu_4$(A′)
2013 (2)	1630 (2)	.810	$(\nu_3 + \nu_9)$(A′)
	1460		
	1420		DNH bends
1610	1380	.858	
1567 (18)	1233 (15)		ν_3(a′) NHN scissor bend
	[1180][a]	.753	
	[1100][a]	.940	
1170 1140 (4)	1047 (6)		ν_4(a′) sym. NCN stretch
959 (8)	698 (8)	.729	ν_8(a″) NH_2 twist
866 (6)	629 (7)	.726	ν_5(a′) NH_2 rock
574 (7)	541 (8)	.942	ν_6(a′) NCN in-plane bend
440 (21)	405 (20)	.92	ν_9(a″) NCN out-of-plane bend

[a] Estimated unperturbed frequencies.

Other than the usual sharpening and better resolution of the bands at the lower temperatures, the only temperature effect noted not associated with the polymerization process,

is the change in the relative intensities of the two bands at 1170 and 1140 cm.$^{-1}$ in the spectrum of monomeric cyanamide. At low temperature the 1170 cm.$^{-1}$ band is favored while at room temperature and in the vapor the 1140 cm.$^{-1}$ band is more intense.

Discussion

The models considered for the interpretation of the spectrum of monomeric cyanamide in the solid state are the amide nitrile, $H_2NC{\equiv}N$, the amide isonitrile, $H_2NN{\equiv}C$, and the *gauche*-carbodiimide, $HN{=}C{=}NH$. The nitrile and isonitrile models would be of symmetry C_s unless the molecules were completely planar where the symmetries would be C_{2v}. The *gauche*-carbodiimide model would be of symmetry C_2. All of these models would have nine fundamental modes of motion, all infrared and Raman active. For the amide models, two of the modes could be classified as NH_2 stretching vibrations, one as the HNH scissor bend, one a $C{\equiv}N$ or $N{\equiv}C$ stretch, one an N–C or N–N stretch, one an NH_2 rock, one an NH_2 twist (wag) or in-plane rock, and two as NCN or NNC bending modes. The vibrational spectra of these two models should differ because of the differences in the $NC{\equiv}N$ and $NN{\equiv}C$ group frequencies. The modes of motion for the carbodiimide model would include two NH stretches, two HNC bends, a symmetric NCN stretch, an antisymmetric NCN stretch, two NCN bends, and a torsional motion about the NCN axis. The *cis*- and *trans*-carbodiimide models are not very likely possibilities on the basis of valence theory considerations.

X-Ray studies on cyanamide show it to be orthorhombic, belonging to the space group V_h^{15}-Pbca with 8 molecules per unit cell.[14] According to Halford's tables,[15] this means that the site symmetry of cyanamide molecules in the crystal must be either C_i or C_1. Since the site symmetry C_i is sufficient to guarantee that the exclusion rule between infrared and Raman spectra should hold and since the observed spectra are apparently not mutually exclusive, we conclude that the actual site symmetries are C_1 and not C_i. Thus, in principle, all fundamentals, overtones, and combination bands can appear in both the infrared and Raman spectra and any decision as to the molecular species present in the crystal must be based on arguments other than the simple enumeration of the fundamental bands observed in the spectrum. Furthermore, since there are 8 molecules in each unit cell, intermolecular coupling may cause each of the 9 fundamental modes to be split into 3 infrared active components and 4 different Raman active components. Thus one could expect 27 fundamental components in the infrared spectrum and 36 fundamental components in the Raman spectrum of the crystal. In addition, one might also expect translational and rotational components of the cyanamide molecules as units to appear in the spectrum both as fundamentals and as overtone and combination bands.

The distinction between the spectra of the amide and the diimide models of crystalline cyanamide should be found in the differences between the $NC{\equiv}N$ (or $NN{\equiv}C$) and the $N{=}C{=}N$ skeletal

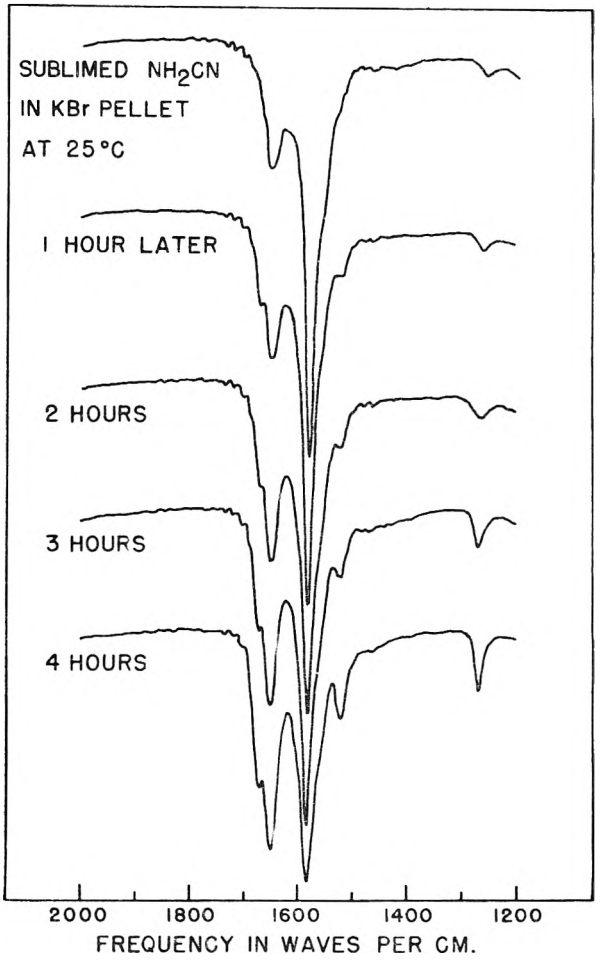

Fig. 3.—Growth of the dimer bands of sublimed cyanamide at room temperature in the 1600 cm.$^{-1}$ region.

frequencies and between the NH_2 and the two NH group frequencies. Actually, the values of the fundamental mode frequencies and the force constants of the $NC{\equiv}N$ and the $N{=}C{=}N$ groups are undoubtedly very similar (*e.g.*, methylacetylene and allene). The high frequency stretching vibrations of both groups should occur at about 2200 cm.$^{-1}$, the low frequency stretching vibrations at about 1200 cm.$^{-1}$, and the bending modes at about 500 cm.$^{-1}$. Appropriate bands for both groups are found in the low temperature cyanamide spectrum at 2280–2240, 1170 and 574–432 cm.$^{-1}$. Thus it may not be possible to differentiate between the amide and the diimide models on the basis of the heavy-atom frequencies alone, although in the cyanamide ion, NCN^{--} as in CaNCN, where the bonding is apparently equivalent in the two CN bonds,[16] the high frequency asymmetric stretch has shifted down to 2070 cm.$^{-1}$ and the symmetric stretch is not observed. If in cyanamide the two CN bonds approach equivalence, one would also expect the higher frequency mode to shift to lower values and the intensity of the symmetric stretching band to be much smaller.

The modes of motion involving hydrogen atoms in the amide model are the two NH_2 stretches, the HNH bend, the NH_2 rock, and the NH_2 twist

(14) C. L. Christ, *Acta Cryst.*, **4**, 77 (1951).
(15) R. S. Halford, *J. Chem. Phys.*, **14**, 8 (1946).
(16) M. A. Bredig, *J. Am. Chem. Soc.*, **64**, 1730 (1942).

(wag) or in-plane rock. Those in the diimide form are the two —NH stretches, the two HNC bends, and the torsional mode. Although the NH stretching mode in imines apparently occurs at about the same frequency as in amines,[17] the peak separation of the two bands in the diimide is very likely somewhat less than for the amines. The HNH bending mode of the NH_2 group occurs at a frequency somewhat higher than the two HNC bending vibrations. For example, in solid HN_3 the corresponding bending mode occurs in the 1200 cm.$^{-1}$ region[18] while the HNH bends in solids always seem to occur with frequencies near 1600 cm.$^{-1}$. The rocking and twisting modes of the NH_2 group would have no counterparts in the carbodiimide structures and the torsional mode in the carbodiimide would have no counterpart in the amide structures. Thus, although one probably cannot clearly distinguish between the amide and the diimide models on the basis of the heavy atom frequencies, one should be able to do so from the vibrational modes involving the hydrogen atoms.

A comparison of the spectrum of monomeric cyanamide with that of the corresponding deutero-cyanamide readily distinguishes the bands to be associated with the hydrogen atom motions. These apparently occur at frequencies of 3300, 3215, 3096, 2733, 1567, 959 and 866 cm.$^{-1}$. Two of these bands are in the overtone-combination band region, so that there are at least five bands which probably can be associated with fundamental modes involving hydrogen atoms. This, together with the general nature of the spectrum in comparison with the spectra of related compounds observed under analogous conditions[19] leads us to the conclusion that the cyanamide molecules in sublimed films at low temperature exist in the amide form rather than in the diimide form.

The distinction between the spectra of the nitrile and the isonitrile forms of cyanamide will necessarily lie in the differences in the skeletal frequencies of the NC≡N and the NN≡C groups. In all states of aggregation the frequency of the isonitrile stretching vibration has generally been found to occur about 100 cm.$^{-1}$ lower than that in the corresponding nitrile, *i.e.*, in the range 2120–2180 cm.$^{-1}$ rather than in the 2220–2280 cm.$^{-1}$ range. For example, in the solid state at −190° we have found the C≡N stretching frequency in $CH_3C{\equiv}N$ at 2270 cm.$^{-1}$ and the N≡C stretching frequency in $CH_3N{\equiv}C$ at 2170 cm.$^{-1}$. Also the low frequency stretching mode of NN≡C corresponding essentially to the N–N stretch should occur at a frequency below 1000 cm.$^{-1}$ rather than at 1170 cm.$^{-1}$.

We thus conclude that in the solid at low temperatures, monomeric cyanamide molecules exist in the amide nitrile form, $H_2NC{\equiv}N$. Our assignments of the bands in the observed spectra of cyanamide and deutero-cyanamide at −190° are given in Table I on the basis of this model with symmetry close to that of C_s sitting on sites of symmetry C_1 in the crystal. The assignments of these bands are based mainly on their observed isotope shifts and on their relationships to the frequencies of corresponding modes in related compounds. The assignments for the two NH_2 stretching modes, for the C≡N stretch, for the HNH scissor bend, and for the two NCN bends are probably the more certain because of the comparable band intensities, shapes, and isotope shifts in comparison with those of equivalent modes in related molecules.

The bond orders of cyanamide have been calculated by the LCAO MO method taking into account the effect of the formal charges acquired by the atoms using the "self-consistent" method of Nagakura.[20] Assuming that the lone pair electrons of the amino nitrogen were initially present both in the pure $2p_z$ and in the hybrid sp^3 orbitals, the final "self-consistent" Coulomb integrals (α) and exchange integrals (β) used are shown in Table II. In view of the observed frequencies related to the N–C and C≡N bonds and the observed dipole moment (4.52 *D.*), the calculated bond orders and dipole moment obtained by assuming the lone pair electrons are initially present in sp^3 hybrid orbitals are no less reasonable than when present in the pure $2p_z$ orbitals (Table II), so that there is no reason for assuming planarity of the amino group.

TABLE II

MOLECULAR ORBITAL PARAMETERS AND CALCULATED RESULTS

Parameter	Amino nitrogen lone-pair electrons present in: Pure $2p_z$ orbital	Hybrid sp^3 orbital
In plane of 3-atom bond:		
α (–N–)	$\alpha + 0.9329\,\beta$	$\alpha + 0.9107\,\beta$
α (C)	$\alpha + .1081\,\beta$	$\alpha + .1116\,\beta$
α (≡N)	$\alpha - .5990\,\beta$	$\alpha + .6177\,\beta$
β (N–C)	$0.8281\,\beta$	$0.7071\,\beta$
β (C≡N)	$1.1709\,\beta$	$1.1658\,\beta$
In perpendicular plane:		
α (≡N)	$\alpha + 0.6901\,\beta$	$\alpha + 0.6901\,\beta$
α (C)	$\alpha + .1299\,\beta$	$\alpha + .1299\,\beta$
β (C≡N)	$1.1452\,\beta$	$1.1452\,\beta$
Total bond orders:		
N(N–C)	1.4974	1.4470
N(C≡N)	2.8161	2.8434
π-Dipole moment	4.95 D	4.50 D

There is one other feature in the spectrum of cyanamide in need of comment. This is the distinct doubling of the 2280–2240 cm.$^{-1}$ band associated with the C≡N stretching mode. A doubling of this band apparently occurs in the spectra of several other cyanide compounds also. In cyanamide the lower frequency component is favored while in the deutero-cyanamide it is the higher frequency component which is more intense. Although the two components of the band are better resolved at the lower temperatures, there does not appear to be any significant change in their relative

(17) L. J. Bellamy, "The Infrared Spectra of Complex Molecules," Methuen and Company, Ltd., London, 1954, Chap. 14.

(18) D. A. Dows and G. C. Pimentel, *J. Chem. Phys.*, **23**, 1258 (1955).

(19) R. E. Nightingale and E. L. Wagner, *J. Chem. Phys.*, **22**, 203 (1954); A. M. Vuagnat and E. L. Wagner, *ibid.*, **26**, 77 (1957).

(20) S. Nagakura, *Bull. Chem. Soc., Japan*, **25**, 164 (1960).

intensities as the temperature is lowered. Since the other bands in the spectrum apparently are not split in this manner, it does not appear that the doubling of the C≡N stretching band is attributable to the presence of tautomers such as the isonitrile form. Fermi resonance between the C≡N stretching mode and the combination band of the C–N stretch and the NH_2 deformation, which has been used to account for the similar splitting in CH_3CN,[21] does not seem to be a likely explanation of the doubling here since the doubling occurs in the deutero-compound. A Fermi interaction with the overtone of the C–N stretch is a likely possibility if one assumes that the overtone frequency is slightly above the C≡N frequency in cyanamide and slightly below it in deutero-cyanamide This also would require that the observed C–N frequency in D_2NCN be lower than the unperturbed C–N frequency due to interaction with the ND_2 bending mode.[22] The frequencies of the unperterturbed modes have been estimated from a simple first-order perturbation calculation[13] and the results are included in Table I. One is tempted to attribute unknown splittings of this kind to "crystal effects" since these do often occur, but in this case an indication of the splitting still exists in the liquid and solution spectra so that crystal effects are probably not the cause of the splitting. Apparently many of the cyanamide derivatives with at least one hydrogen atom left on the amino nitrogen show this same splitting, *i.e.*, NaHNCH, $Ca(HNCH)_2$, etc., while those without hydrogens do not appear to show it, *i.e.*, CaNCN, R_2NCN (R = methyl, ethyl, allyl, etc.). It may be, therefore, that the splitting is in some way associated with the H or D atoms present.

(21) P. Venkateswarlu, *J. Chem. Phys.*, **19**, 293 (1951).

(22) T. A. Scott, Jr., and E. L. Wagner, *ibid.*, **30**, 465 (1959).

THE DIPOLE MOMENT OF UREA

BY W. R. GILKERSON AND K. K. SRIVASTAVA

Department of Chemistry of the University of South Carolina, Columbia, South Carolina

Received April 9, 1960

The dielectric constants of solutions of chlorobenzene, nitrobenzene and *o*-dinitrobenzene in polar solvents have been measured. Using Onsager's equation, the dipole moments of the solutes have been calculated and compared with those obtained from measurements in non-polar solvents. The method is then applied to the determination of the moment for urea in 20 weight % water–acetone and in pure water. The moment in the former is 6.25 debyes, and in the latter is 4.2 debyes.

There have recently[1] been reports of the application of Onsager's[2] equation relating the dielectric constant to the dipole moment to solutions of polar solutes in polar solvents. It is of interest to see if one can obtain reliable dipole moment values for solutes in such systems. There are a number of compounds which have high melting points and are difficultly soluble in non-polar solvents, so that their dipole moments remain in doubt. Further a number of polar solutes, while being soluble, indicate dimerization or other complex formation in non-polar solvents.

The values of the dipole moment of urea reported in the literature[3–5] have varied from 4.4 to 8.6 debyes. Early measurements by Furth[6] seemed to place urea in the same class as glycine, as having a "large" dipole moment since both caused a large increase in the dielectric constant of water solutions. However, in the case of urea Furth observed an initial decrease, followed by the increase mentioned above.

We report here the results of measurements of the dielectric constants of solutions of chlorobenzene in benzene and in 25 mole % *o*-dichlorobenzene–benzene, of nitrobenzene in chlorobenzene, 50, 75 and 100 mole % *o*-dichlorobenzene–benzene mixtures, of *o*-dinitrobenzene in benzene, 50 and 100 mole % *o*-dichlorobenzene–benzene and in nitrobenzene and of urea in 20 weight % water–acetone and in water, all at 25°.

(1) T. Gaumann, *Helv. Chim. Acta*, **41**, 1956 (1958).

(2) L. Onsager, *J. Am. Chem. Soc.*, **58**, 1486 (1936).

(3) C. Beguin and T. Gaumann, *Helv. Chim. Acta*, **41**, 1971 (1958).

(4) W. D. Kumler and G. M. Fohlen, *J. Am. Chem. Soc.*, **64**, 1944 (1942).

(5) E. Bergmann and A. Weizmann, *Trans. Faraday Soc.*, **34**, 783 (1938).

(6) R. Furth, *Ann. Physik*, **70**, 63 (1923).

Experimental

Chemicals.—All the organic liquids except acetone were Matheson, Coleman and Bell reagent grade. Acetone was from stock. All were passed through a 35 × 2 cm. column packed with Alcoa activated alumina, grade F-20. Benzene was recrystallized and distilled from sodium ribbon. Nitrobenzene was recrystallized twice. Chlorobenzene, *o*-dichlorobenzene (abbreviated DCB hereafter) and acetone were distilled, middle cuts being taken. *o*-Dinitrobenzene (Aldrich Chemical Co.) was used without further purification; m.p. 116.5–116.8°. Urea (J. T. Baker analyzed, C.P.) was used without further purification.

TABLE I

PHYSICAL CONSTANTS OF SOLVENTS AT 25°

No.	Solvent	Density, g./ml.	Dielectric constant
1	Benzene	0.8737[a]	2.275[b]
2	25 mole % DCB–benzene	0.998	4.16
3	50 mole % DCB–benzene	1.111	6.02
4	75 mole % DCB–benzene	1.211	7.94
5	DCB	1.300[c]	10.06[c]
6	Chlorobenzene	1.101[a]	5.63[a]
7	Nitrobenzene	1.198[e]	34.69[e]
8	20 wt. % water–acetone	0.8448	29.6[d]
9	Water	0.9971	78.54[b]

[a] J. Timmermans, "Physico-chemical Constants of Pure Organic Compounds," Elsevier Press, New York, N. Y., 1950. [b] J. Wyman, *Phys. Rev.*, **35**, 623 (1930). [c] P. H. Flaherty and K. H. Stern, *J. Am. Chem. Soc.*, 80, 1034 (1958). [d] G. Akerlöf, *Ibid.*, 54, 4125 (1932). [e] H. Sadek and R. M. Fuoss, *J. Am. Chem. Soc.*, 76, 5905 (1954).

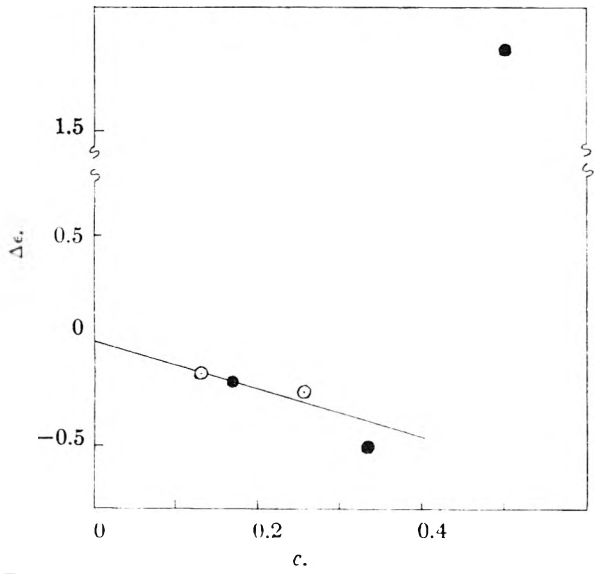

Fig. 1.—$\Delta\epsilon$ *vs.* molar concentration of urea in water: ○, this work at 25°; ●, ref. 6 at 20°.

Physical Constants.—The densities and dielectric constants of the benzene–DCB solvent mixtures were determined and appear in Table I together with the literature values for the pure solvents and for the water–acetone mixture. The dielectric constants of the benzene–DCB mixtures were measured at 100Kc using a General Radio Type 716-C capacitance bridge, equipped with a Type 716-P4 Guard Circuit. The dielectric cell was similar in design to that of Sadek and Fuoss.[7]

Solution Measurements.—These were carried out using a Sargent Model V Oscillometer (5Mc) and accompanying cell and range extender. The cell was thermostated at 25°. The cell was equivalent to two capacitors in series; a glass section having a capacity C_g 133.5 pf., and a solution section having an air capacity C_x^0 of 5.94 pf. These values were determined by separate measurements on the General Radio bridge. The calculations will be discussed below. The solvent mixtures and solutions were all made up by weight.

Results

The oscillometer yielded only scale readings, S, directly. This is related to the capacity of the cell sections by the equation

$$S = KC_gC_x/(C_g + C_x) \qquad (1)$$

where $C_x = C_x^0\epsilon$, ϵ is the dielectric constant of the solution and K is the proportionality constant. This equation can be arranged to give the dielectric constant

$$\epsilon = S/(KC_x^0 - SC_x^0/C_g) \qquad (2)$$

The value of KC_x^0 was determined for each solution by the equation

$$KC_x^0 = S_0(1 + C_x^0\epsilon_0/C_g)/\epsilon_0 \qquad (3)$$

where S_0 is the scale reading with pure solvent present alone.

The dielectric constants calculated from equation 2 were plotted *vs.* molar concentration of solute, C_1, and the slopes of the resulting straight lines are given in Table II. The plot for urea in water did not give a straight line and is shown in Fig. 1. The dipole moments of the solutes were calculated using a modification of Onsager's equation.[2] The latter may be written as

$$\epsilon - 1 = 4\pi \sum_i N_i \left[\frac{\mu_i^2}{9kT}\frac{(\epsilon_{\infty i} + 2)^2\epsilon(2\epsilon + 1)}{(2\epsilon + \epsilon_{\infty i})^2} + a_i^3\frac{\epsilon(\epsilon_{\infty i} - 1)}{(2\epsilon + \epsilon_{\infty i})}\right] \qquad (4)$$

where N_i is the number of molecules of type i per cc., $\epsilon_{\infty i}$ is the infinite frequency dielectric constant of the ith component, μ_i is the gas phase dipole moment of type i, and a_i is the radius of the hypothetical spherical molecule containing the point dipole μ_i.

Expressing the N_i in terms of the C_i, moles per liter of component i, then we have

$$\epsilon - 1 = \sum_i (A_i\mu_i^2 + B_i)C_i \qquad (5)$$

where

$$A_i = 4\pi N_a(\epsilon_{\infty i} + 2)^2\epsilon(2\epsilon + 1)/9000\,kT(2\epsilon + \epsilon_{\infty i})^2$$

and

$$B_i = 3V_i\epsilon(\epsilon_{\infty i} - 1)/(2\epsilon + \epsilon_{\infty i})$$

N_a is Avogadro's number, and V_i is the molar volume of pure i. We deal at most with three components. Subscript 1 will designate the polar solute, while 2 and 3 designate the two possible solvent components. We assume the solutions to be ideal. Then in terms of the solute concentration

$$C_2 = C_2^0(1 - V_1C_1) \text{ and } C_3 = C_3^0(1 - V_1C_1)$$

where the superscript zero designates the concentrations of the solvent components in pure solvent. Taking the derivative of ϵ with respect to C_1 and solving for μ_1^2, we obtain

$$\mu_1^2 = F(d\epsilon/dc_1)/A_1 + (A_2\mu_2^2C_2^0V_1 + A_3\mu_3^2C_3^0V_1 + B_2C_2^0V_1 + B_3C_3^0V_1 - B_1)/A_1 \qquad (6)$$

where

$$F = 1 - \sum_i \left\{A_i'\mu_i^2\left[\frac{2\epsilon(2\epsilon_{\infty i} - 1) + \epsilon_{\infty i}}{(2\epsilon + \epsilon_{\infty i})^3}\right] + \frac{B_i\epsilon_{\infty i}}{\epsilon(2\epsilon + \epsilon_{\infty i})}\right\} C_i;$$

$$A_i' = \frac{A_i(2\epsilon + \epsilon_{\infty i})^2}{\epsilon(2\epsilon + 1)}$$

Since the slope is taken in the limit as C_1 approaches zero, then the A_i, B_i and F are calculated using the dielectric constant of pure solvent for ϵ. The values of $\epsilon_{\infty i}$ are taken to be the square of the refractive index (Na-D line) of the pure liquids at 25°. The value for *o*-dinitrobenzene was calculated from atomic refractions.[8] The value for urea was calculated from the molar refraction of 13 cc. given by Gaumann.[1] The values of the dipole moments of the solvent molecules used in equation 6 were calculated by applying equation 5 to the pure liquids. The value of V_1, 0.061 l., for urea was determined from density data.[9] The value of V_1 for *o*-dinitrobenzene was calculated from density data in benzene solution.[11]

The concentration ranges used, the slopes $d\epsilon/dC_1$, and the dipole moments calculated using equation 6 are shown in Table II.

Discussion

The moments of the substituted benzenes are comparable with those obtained previously in

(7) H. Sadek and R. M. Fuoss, *J. Am. Chem. Soc.*, **76**, 5905 (1954).

(8) Auwers and Eisenlohr, *Ber.*, **43**, 806 (1910).

(9) F. T. Gucker, F. W. Gage and C. E. Moser, *J. Am. Chem. Soc.*, **60**, 2582 (1938).

TABLE II

DIELECTRIC INCREMENTS AND DIPOLE MOMENTS OF CHLOROBENZENE, NITROBENZENE, *o*-DINITROBENZENE AND UREA IN POLAR SOLVENTS AT 25°

Compound	Solvent[a]	Concn. range × 10, *M*	Slope $d\epsilon/dC_1$	Dipole moment, debyes
Chlorobenzene	1	0.5–2.0	0.292	1.51
	2	2.3–4.3	0.195	1.50
Nitrobenzene	1[b]			3.98
	6	0.8–5.3	2.29	3.82
	3	0.5–4.7	2.19	3.77
	4	1.1–8.2	1.74	3.59
	5	1.2–7.1	1.26	3.39
o-Dinitro-	1	0.22–0.88	5.38	6.31
benzene	3	.61– .99	8.37	6.52
	5	.28– .91	8.00	6.51
	7	.47–1.2	7.05	6.87
Urea	8	.23–0.85	5.60	6.25
	9	1.3–2.5	−1.12	4.20

[a] See corresponding number in Table I. [b] Reference 10.

benzene solution.[10] The decrease of the nitrobenzene moment with increasing dielectric constant of solvent is to be compared to the increase in the case of *o*-dinitrobenzene. The similarity in size and shape of the two molecules would seem to rule out any "shape effect" as an explanation for this behavior. Further, a 10% error in ϵ_∞ for *o*-dinitrobenzene could only give rise to a 6% error in the dipole moment in benzene, the most extreme case. One might also expect that a failure in the assumption of ideal solutions would operate in the same direction for these two compounds.

The moment for *o*-dinitrobenzene in benzene is slightly higher than the previously reported[11] value of 6.05 debyes. Smyth[9] has calculated on the basis of the solution moment for nitrobenzene, that if there is no "*ortho*" effect operating in the case of *o*-dinitrobenzene, its moment should be 6.9 debyes.

From the results for chlorobenzene, nitrobenzene and *o*-dinitrobenzene we conclude that, association effects aside, the calculation of moments of polar solutes in polar solvents is as feasible as the calculation of the moments from dielectric constants of pure liquids.[12]

Proceeding to the case of urea, the moment found in water compares favorably with those observed by Gaumann in acetone (4.38 debyes) and ethanol (4.51 debyes). The latter author gives a value of 5.68 debyes for the moment in water, but does not give the experimental data from which he made the calculation, nor does he refer to another source. It can be seen in Fig. 1 that the slope one obtains depends greatly on the concentration range one is working in. This is probably the source of the discrepancy. The higher value found in the case of the water–acetone solvent we believe to be due to failure of the assumption of a continuum in such a mixed solvent. If association with water were going to occur it would be favored by a lower dielectric constant.

Let us now estimate the moment for urea assuming the group moments of Smyth[13] to be applicable. The group moment for ketone or aldehyde (aliphatic) is given as 2.7 debyes. That for the $-NH_2$ group is 1.2. Further, the angle the $-NH_2$ moment makes with the C–N bond is 100°. It is assumed that the hydrogens are pointing away from the oxygen. Using the O–C–N bond angle is 120°, we calculate that the resulting moment is 4.5 debyes. Gaumann[3] estimated a value of 3.4 using bond moments. If one assumes the amino moment to make an angle of 140° with the C–N bond, which is characteristic of aromatic amines, then one obtains a moment of 3.1 debyes, in closer agreement with the bond-moment value. It might be concluded from this that there is no apparent aromaticity in urea, with respect to its dipole moment.

We wish to ackhowledge support of this work in part by contract with the Office of Ordnance Research, U. S. Army.

(10) C. P. Smyth, "Dielectric Behavior and Structure," McGraw-Hill Book Co., New York, N. Y., 1955, pp. 314 and 332.

(11) J. W. Williams and C. H. Schwingel, *J. Am. Chem. Soc.*, **50**, 362 (1928).

(12) C. J. F. Boettcher, *Physica*, **6**, 59 (1939).

(13) C. P. Smyth, "Physical Methods of Organic Chemistry," A. Weissberger, editor, Interscience Publishers, Inc., New York, N. Y., 2nd edition, 1949, Vol. I, Pt. II, Chap. XXIV.

THE CONDUCTANCE OF HEXAFLUOARSENIC ACID AND ITS LITHIUM, SODIUM AND POTASSIUM SALTS IN WATER AT 25°

BY GORDON ATKINSON AND CALVIN J. HALLADA

Department of Chemistry, the University of Michigan, Ann Arbor, Michigan

Received April 11, 1960

The conductances of $HAsF_6$, $LiAsF_6$, $NaAsF_6$ and $KAsF_6$ have been measured in water at 25°. The concentration range covered was 10^{-4} to 10^{-2} *M*; and the data were analyzed using the extended Fuoss-Onsager theory. Three of the salts have anabatic phoreograms only the $KAsF_6$ data approaching the limiting tangent from the bottom. The K_A calculated for the $KAsF_6$ is 1.76. The solution "*a*" values are larger than the crystallographic ones by approximately 1.5 Å. A comparison is made with the literature data on $NaClO_4$ and KNO_3.

Introduction

In recent years, there has been a continuous search for ion-interfering anions, that is, anions useful in electrolytes both for stability constant and solution thermodynamics studies. In the first case, the electrolyte is such that it can be added to change the ionic strength of the solution without complexing the cation or anion under investigation.

In the second case, an anion is needed whose salts are completely dissociated in aqueous solution; allowing the present theories of solutions to be more thoroughly examined regarding range of validity.

This anion must be inert toward hydrolysis and stable toward oxidation and reduction. It should have a charge of one, and ideally, have low polarizability and spherical symmetry. The salts of the anion with various cations should be easily prepared, soluble, stable and readily analyzed. Of late, this search has become more important since it has been observed that the anions commonly used, NO_3^- and ClO_4^- complex with certain metal ions. This information has cast serious doubt on much work.

In this paper, one solution property, the conductance, of the AsF_6^- ion is examined. The chemistry of this interesting ion was greatly clarified by Dess and Parry[1] when they showed that many of the properties of this ion reported in the literature (*e.g.*, ease of hydrolysis), were really those of the AsF_5OH^- ion. The AsF_6^- ion, when prepared, was very inert toward hydrolysis, and seemed to satisfy most of the criteria listed about for a non-interfering anion. Therefore, this investigation was undertaken to compare the dissociation of $HAsF_6$ and three of its salts to the equivalent NO_3^- and ClO_4^- salts, and the application of the extended conductance theory to these electrolytes.

Experimental

A quantity of very pure $KAsF_6$ prepared by the method of Dess and Parry,[1] was obtained from Professor Parry and used both for the K^+ salt measurements and the preparation of the other materials. The Li^+ and Na^+ salts and the acid were obtained by cation-exchange techniques with Dowex-50 resin. The most sensitive qualitative tests on the three salts and the acid showed no evidence of cationic or the common anionic impurities. A separate preparation of the Na^+ salt was carried out by reacting a portion of the acid with an equivalent amount of carbonate-free NaOH. All the salts were recrystallized twice from conductivity water and dried *in vacuo* over P_2O_5 in an Aberhalden pistol at 110°. They are all anhydrous. The salts were stored in a vacuum desiccator even though they are not hygroscopic in nature. Karl Fischer analyses of the salts using a dead-stop end-point technique showed no measurable water content (H_2O < 0.01%).

The acid has not yet been obtained in anhydrous form, but is a definite hexahydrate when dried at 25° over P_2O_5 for six hours. Analyses of the salts were done by an ion-exchange technique, converting a given weight of the salts to $HAsF_6$ by cation exchange (Dowex-50 resin) and titrating the acid with standard NaOH. Periodic checks of the analytical technique using repurified KCl showed that the accuracy of the method was 0.1% and the precision better than 0.05%. Although the AsF_6^- ion can reportedly[2] be quantitatively analyzed by precipitation with tetraphenylarsonium chloride, the precipitate is very difficult to handle and precision greater than 0.5% was not obtained. Analyses of K^+ by precipitation with sodium tetraphenylboron gave results within 0.08% of those obtained by ion exchange.

Two to four stock solutions were made of each substance at different times using two different salt preparations for each electrolyte. The concentration of these solutions varied from approximately 0.1 to 0.005 *N*. Stock solutions were made both by dissolving a weighed amount of salt in a weighed amount of conductance water and by dissolving a weighed amount of salt and diluting to volume in recalibrated volumetric ware. Densities of all solutions were determined at 25° to $\pm 5 \times 10^{-5}$ g./ml. by pycnometric measurement. As an additional check on the stock concentrations aliquots were analyzed by the ion-exchange technique described earlier. In no case did the concentrations determined by the two methods differ by more than 0.05%. A further check on the methods of solution preparation and analysis is afforded by the precision of the conductance data itself. Although at least two different salt preparations and three different stock solutions are represented in the data for a given salt, the average deviation of the Λ values from the theoretical curve is $\pm$ 0.02 mho.

The bridge arrangement consisted of a General Radio low-distortion, variable frequency oscillator, a Leeds and Northrup Jones Bridge, a battery powered pre-amplifier (with variable gain up to 120 times the input signal), and a DuMont 304H oscilloscope for null detection. A constant temperature bath, filled with mineral oil, provided a temperature control of 25.000 $\pm$ 0.005°. The Jones Bridge and constant temperature bath were placed on a large copper sheet to obtain a good ground.

A flask-type cell; a 1 liter erlenmeyer flask with a side arm containing smooth platinum electrodes, was used as the conductance cell. The cell constant was determined, using the Jones and Bradshaw KCl standards, as a function of frequency and the measured specific conductance. All measurements were extrapolated to infinite frequency to avoid polarization effects. The cell constant changed linearly with specific conductance over the concentration range measured; the decrease of k from 10^{-4} to 10^{-2} M being about 0.03%. The precision of the calibration data leads us to a calculated precision of the cell constant at a given specific conductance of 0.01%. The infinite frequency, zero conductance cell constant for the cell used is 0.26350.

The solutions of $HAsF_6$ and its salts were made up in the conductance cell by a weight dilution method. Conductance water was weighed into the cell which was then placed in the constant temperature bath until temperature equilibrium was attained and the resistance remained constant. Four to seven successive weighed amounts of stock solution were added, each time allowing the solution to equilibrate and reach a state of constant resistance. The resistance R was measured at one, two, four and ten thousand cycles per second, and a plot of resistance *vs.* $\omega^{-1/2}$ (ω = frequency in cycles/sec.) was extrapolated to infinite frequency. At least three runs were made with every stock solution. The concentration range was 1×10^{-2} to 1×10^{-4} equivalents per liter.

The advantages of preparing the measured solutions in the cell from stock solutions are twofold. It is possible to find the conductance of a material at 20 or more concentrations with relative ease. At the same time, the conductance of the solvent is found before each set of measurements, allowing a better solvent correction to be applied to the measured conductance than is available when using several solutions whose solvent conductances can vary from time to time. This is important for the very dilute salt solution where the conductance of the solvent contributes considerably to the measured conductance.

Table I gives some of the actual experimental results. Although no solvent correction is applied to the acid conductances, it nonetheless is imperative to keep a close check on the solvent, ensuring that its conductance is very low. It was not found possible to calculate a solvent correction for the acid runs to a high enough precision to make it worthwhile.

Calculations

The Shedlovsky Relationship.[3]—

$$\Lambda^{0\prime} \equiv \frac{\Lambda + \beta\sqrt{c}}{1 - \alpha\sqrt{c}} = \Lambda^0 + Bc \qquad (1)$$

where

Λ = equivalent conductance

c = concn. in moles per liter

α, β = constants from the Onsager theory,[4] dependent on charge, electrolyte type, solvent and temperature was used to find an initial Λ^0, extrapolating the $\Lambda^{0\prime}$ *vs.* c plot to infinite dilution.

(1) H. M. Dess and R. W. Parry, *J. Am. Chem. Soc.*, **79**, 1589 (1957).

(2) H. M. Dess, R. W. Parry and G. L. Vidale, *ibid.*, **78**, 5730 (1956).

(3) T. Shedlovsky, *ibid.*, **54**, 1405 (1932).

(4) L. Onsager, *Physik. Z.*, **28**, 277 (1927).

TABLE I

HAsF$_6$		LiAsF$_6$		NaSsF$_6$		KAsF$_6$	
10^4c	Λ	10^4c	Λ	10^4c	Λ	10^4c	Λ
3.4129	401.24	1.0560	93.87	0.8600	105.67	1.6862	128.20
8.7125	399.82	2.8355	93.46	1.4277	105.48	3.0154	127.78
22.131	397.20	7.3060	92.75	3.2306	104.95	5.9543	127.06
31.962	395.72	10.461	93.38	5.9423	104.47	7.8329	126.79
37.372	395.14	13.879	91.99	12.369	103.61	13.101	126.03
48.989	394.33	22.594	91.26	22.978	102.69	18.001	125.42
56.693	393.59	32.064	90.69	38.865	101.69	26.877	124.55
73.451	392.63	45.419	89.94	49.232	101.16	41.354	123.39
104.76	390.71	57.789	89.47	63.063	100.52	62.985	122.03
		80.273	88.82	75.938	100.00	72.009	121.51
		109.14	87.81	103.78	99.12	105.99	119.68

This Λ^0 was used to find the limiting equation[4]

$$\Lambda = \Lambda^0 - Sc^{1/2} \qquad (2)$$

where

$$S = \alpha\Lambda^0 + \beta \qquad (3)$$

Comparison of the limiting law plots with the phoreograms (Fig. 1) showed that all the substances were strong electrolytes. As can be seen from the figure, the experimental points approach the limiting law from above for all the substances except $KAsF_6$, whose points fall only slightly below the limiting law.

The form of the extended theory used then was that of completely dissociated electrolytes[5,6]

$$\Lambda = \Lambda^0 - Sc^{1/2} + Ec \log c + Jc \qquad (4)$$

where

$$S = \alpha\Lambda^0 + \beta \qquad (5)$$

$$E = E_1\Lambda^0 - E_2 \qquad (6)$$

$$E_1 = \frac{6.7747 \times 10^{12}}{D^3T^3} \qquad (7)$$

$$E_2 = \frac{0.9977 \times 10^8}{\eta D^2T^2} \qquad (8)$$

$$J = \sigma_1\Lambda^0 + \sigma_2 \qquad (9)$$

an explicit function of "a," the distance of approach of ions.

$$J = 0.4583\Lambda^0\,[h(b) + \ln \mathring{a} - 0.2052] + 13.79 + 18.15\mathring{a} - 17.66\,(\ln \mathring{a} - 0.0956)$$

for 1:1 electrolytes in water at 25°.

The data can be fitted to this equation by the method outlined by Fuoss and Accascina.[6]

The Λ° found from the Shedlovsky function is used to compute S and E. The quantity.

$$\Lambda' = \Lambda + Sc^{1/2} - Ec \log c \qquad (10)$$
$$= \Lambda^0 + Jc$$

is then evaluated. When Λ' is plotted against c, a straight line with intercept Λ^0 and slope J should be obtained if the extended theory used is valid. Figure 2 shows that Λ' is indeed a nearly linear function of c, although the values of Λ' at the higher concentrations of $NaAsF_6$ and $LiAsF_6$ seem to bend slightly below the best straight line drawn through the lower concentration range. The slopes indicated in Fig. 2 are the average slopes and the intercepts those from a least squares treatment of the data. In all cases, the Λ^0 obtained from this function was only slightly higher than that obtained from the Shedlovsky function, the average difference for the three salts being ±0.02 mho. The value of "a" was determined by interpolation, using a series of "a" values giving J values in the vicinity of J from the slope of Λ' *vs.* c.

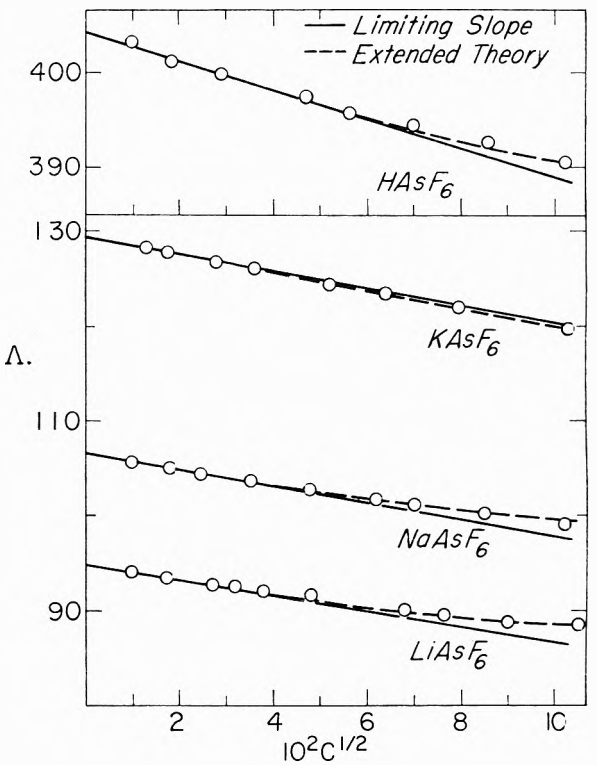

Fig. 1.

Table II gives the values of Λ^0 for each substance and values of λ_-^0 estimated by using the values of λ_+^0 given by Harned and Owen.[7] A few words on the differences between these λ_-^0 values seem in order. The λ_-^0 from the acid data cannot be weighted very heavily since no solvent correction could be made. The values obtained from the Li^+ and Na^+ salts are in good agreement but the value from K^+ salt (associated) is lower than the over-all data precision would lead you to expect. A definitive reason for this must await transference number data so that λ_-^0 can be calculated from $T_0\,\Lambda^0$ or, at least, further work on other 1–1 salts containing AsF_6^-. However, one possible

(5) R. M. Fuoss and L. Onsager, THIS JOURNAL, **61**, 668 (1957).

(6) R. M. Fuoss and F. Accascina, "Electrolytic Conductance," Interscience Publishers, Inc., New York, N. Y., 1959, Chapter 15.

(7) H. S. Harned and B. B. Owen, "The Physical Chemistry of Electrolytic Solutions," 3rd Edition, Reinhold Publ. Corp., New York, N. Y., 1957, pp. 239.

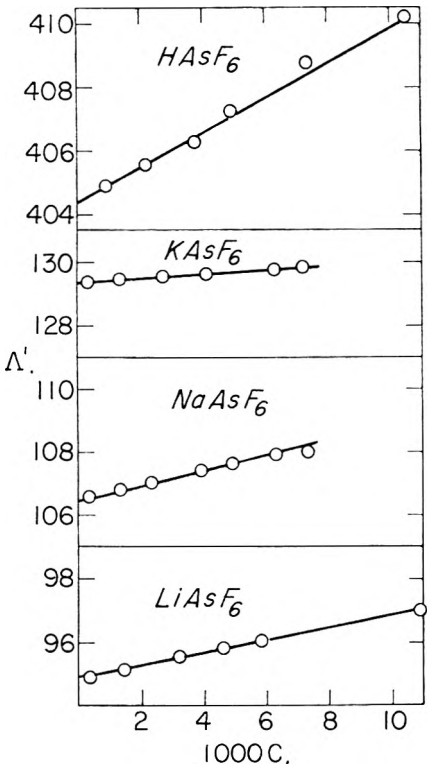

Fig. 2.

reason suggests itself. An associated salt will tend to give a lower Λ^0 than a completely dissociated electrolyte. This is because the increase in slope near the C = 0 point predicted by the extended theory will be masked by the association constant in the linear C term. This yields the straight line phoreograms found for slightly associated salts like KNO_3, $KClO_4$ and $KAsF_6$. This lower Λ^0 then would give a low λ_-^0 when combined with a λ_+^0 found from a completely dissociated salt. However, this is *ex post facto* reasoning and the real answer must await further experimental data. The table also contains the J and "a" values of each substance, and the value a^- for AsF_6^- obtained by subtracting the crystallographic radii[8] for the cations from "a", *i.e.*, assuming that "a" is the crystallographic distance of cation from anion.[6]

TABLE II

	Λ^0	λ_-^0(est.)	J	$\dot{a}$	$\dot{a}_{AsF_6^-}$
$HAsF_6$	404.4	54.6	544	3.80	3.80
$LiAsF_6$	94.87	56.21	203	4.44	3.84
$NaAsF_6$	106.46	56.35	243	4.93	3.98
$KAsF_6$	129.37	55.85			
(Unassociated)			66	1.35	..
(Associated			294	5.20	3.87 (est.)

Figure 1 shows how well the extended theory equation, with the value obtained for each parameter substituted, fits the experimental points. Both the phoreogram (in Fig. 1) and the J value (in Fig. 2 and Table II) for the $KAsF_6$ indicate that it is not as completely dissociated as the acid and other salts. This means that the slope of the Λ' *vs.* c plot is not J but actually $(J - K_A\Lambda^0)$.[6]

When the average "a" of the other three substances is used with the crystal radius of K^+, the value J = 294 is obtained; indicated in Table II by $KAsF_6$ associated. The K_A thus obtained is 1.76.

The value of K_A can also be determined by the method of Davies[9] assuming that both $LiAsF_6$ and $NaAsF_6$ are normal, completely dissociated hexafluoroarsenate salts. The values of K_A determined using both $NaAsF_6$ and $LiAsF_6$ as the normal salts at a concentration of 0.01 are identical, K_A = 1.56.

As mentioned, it has been assumed that the distance parameter[6] "a" is the crystallographic distance of cation from anion. Although Fuoss and Accascina find that the a's determined by the method outlined are almost identical to the crystallographic distances for KCl, KBr and KI, such is not the case for the hexafluoroarsenates. The structure of $KAsF_6$ has been determined by Roof[10] and by Ibens.[11] The As–K distance found is 3.62 Å., compared to the calculated "a" value of 5.20 Å. Some difference is to be expected from the fact that AsF_6^- is not as spherically symmetric as a monatomic anion. But, how much of this difference is attributable to that and how much to other factors is a question remaining to be answered.

It is planned to investigate the Rb^+, Cs^+ and Ag^+ salts of this interesting anion. From Dess' work, it is known that the Cs^+ salt is quite a bit less soluble than the K^+ salt. We might then expect the Rb^+ and Cs^+ salts to exhibit even more association than $KAsF_6$. The Ag^+ salt, which is very soluble, might give some indication of the effect of cation polarizability on association. It is intriguing that in the solubility trends and solution data obtained so far, the AsF_6^- is similar to the ClO_4^- ion. Another investigation of value would be the study of the rather similar BF_4^- anion.

The extended theory was also applied to the data available on KNO_3[12] and $NaClO_4$[13] whose phoreograms compare closely to those of $KAsF_6$ and $NaAsF_6$. The KNO_3 data yield an "a" value of 1.14 when the slope of the Λ' *vs.* C plot is assumed to be J. Since KNO_3 is not completely dissociated, however, the slope should really be taken as $(J - K_A\Lambda^0)$. When K_A = 0.63 is used[14] the value obtained for "a" is 2.27 Å. as compared to a K–N distance of 3.20 Å. in the crystal.[15] The $NaClO_4$ data yield an "a" value of 3.46 Å. as compared to the Na–Cl distance of 3.53 Å. in the $NaClO_4$ crystal.[16]

In conclusion it would seem that $NaAsF_6$ and $NaClO_4$ are both superior to KNO_3 as "inert electrolytes" if their behavior as pure electrolytes is taken as the criterion. However, more data is needed on the interaction of the AsF_6^- anion with polyvalent cations before a stronger case can be presented.

(8) L. Pauling, "The Nature of the Chemical Bond," Cornell University Press, Ithaca, N. Y., 1940, Chapter X, p. 343.

(9) C. Davies, *Trans. Faraday Soc.*, **23**, 351 (1927).

(10) R. B. Roof, *Acta Cryst.*, **8**, 739 (1955).

(11) J. A. Ibens, *ibid.*, **9**, 967 (1956).

(12) T. Shedlovsky, *J. Am. Chem. Soc.*, **54**, 1411 (1932).

(13) J. H. Jones, *ibid.*, **67**, 855 (1945).

(14) Reference 7, pp. 205.

(15) R. W. Wyckoff, "Crystal Structures," Vol. II, Interscience Publ., New York, N. Y., 1957, Chapt. VII.

(16) (a) Ref. 15, Chapt. VIII; (b) J. Donnay and W. Nowacki, "Crystal Data," The Geological Society of America, 1954.

Acknowledgments.—The authors here wish to express their thanks to Professor R. W. Parry for the loan of the conductance apparatus used in this work and for his gift of the $KAsF_6$.

KINETICS OF THE REACTION BETWEEN PLUTONIUM(IV) AND TIN(II)[1]

BY S. W. RABIDEAU

University of California, Los Alamos Scientific Laboratory, Los Alamos, New Mexico

Received April 14, 1960

In the reaction between Pu(IV) and Sn(II), it has been found that parallel paths are involved in the rate-determining steps and that four and five chloride ions participate in the formation of the activated complexes. The rate law can be written as $-d[Sn(II)]/dt = k_1[Pu^{+4}][Sn^{+2}][Cl^-]^4 + k_2[Pu^{+4}][Sn^{+2}][Cl^-]^5$; at 25° the values of the specific rate constants k_1 and k_2 are 720 M^{-5} sec.$^{-1}$ and 1636 M^{-6} sec.$^{-1}$, respectively. At 25° for the process, $Pu^{+4} + Sn^{+2} + 4Cl^- = (Pu{\cdot}Cl_4{\cdot}Sn)^{+2}$, $\Delta H^* = 26.9$ kcal./mole and $\Delta S^* = 44.7$ e.u. For the parallel reaction at 25°, $Pu^{+4} + Sn^{+2} + 5Cl^- = (Pu{\cdot}Cl_5{\cdot}Sn)^{+1}$, $\Delta H^* = 24.1$ kcal./mole and $\Delta S^* = 37.0$ e.u. These reactions have been found to be hydrogen ion independent over the range of acidity studied. The positive correlation between the charge and the entropy of the activated complex has been extended to include charge types of +1 and +2.

Introduction

Studies of the kinetics of various oxidation–reduction reactions involving plutonium[2] have been made not only to better understand the chemistry of this element of four oxidation states, but also to seek possible relationships between reaction parameters and the thermodynamic quantities for the activation process.

In this paper the kinetics of the reaction between Pu(IV) and Sn(II) in chloride and in chloride–perchlorate media has been studied by spectrophotometric means. The entropies of the activated complexes in this reaction correspond to charge types not previously tabulated[3] and additional support is given to a positive correlation between the entropy and the charge of the activated complex. Experimentally it is found that the reduction of Pu(IV) by Sn(II) proceeds very slowly in a perchlorate medium in the absence of appreciable quantities of chloride ion. Also in perchlorate solution, the formation of insoluble products and polymeric tin species[4] introduce additional experimental complications. At the Sn(II) and Sn(IV) concentrations used in this work (*ca.* 10^{-3} M), no turbidities were observed when the solutions were examined with a strong narrow beam of light and no insoluble products were formed when chloride ion was present in the solutions. Conformity to second-order reaction kinetics was observed in the Pu(IV)–Sn(II) reaction to within 90% or greater extent of completion. The large increase in the rate of reaction between Pu(IV) and Sn(II) in the presence of chloride ion indicates the latter's involvement in the activated complex. Thus, it appears that the reaction between Pu(IV) and Sn(II) in chloride solutions proceeds through the interaction of the chloro-complexed forms of the metal ions.

Experimental

Materials.—Water used in this study was redistilled from an alkaline permanganate solution in an all-Pyrex glass apparatus. Periodic conductivity checks were made to monitor the purity of the water. A stock solution of 6 M hydrochloric acid was prepared by the dilution of Baker and Adamson reagent grade hydrochloric acid. The acid was standardized by weight against Baker Analyzed grade mercuric oxide with the use of calibrated volumetric apparatus. A 0.02 N stock solution of stannous chloride was prepared from Baker and Adamson reagent grade crystalline $SnCl_2{\cdot}2H_2O$. This salt was dissolved in 2.000 M hydrochloric acid and placed in a vessel equipped with stopcocks and standard taper joints so that a slow stream of helium could be swept over the surface while a pipetted volume was removed. This inert atmosphere also was maintained in storage. Mallinckrodt 70% perchloric acid was standardized by weight against mercuric oxide. Sodium chloride was the C.P. product recrystallized from a saturated solution by salting out with concentrated hydrochloric acid. This salt was filtered, washed, ground and heated in a muffle furnace at 600°.

Plutonium(IV) solutions were prepared from a selected lot of high-purity metal. The mechanically-brushed plutonium metal was dissolved in 6 M hydrochloric acid which was cooled to 0° to moderate the rate of dissolution. The final acid and chloride ion concentrations were computed from the weights of the standardized reagents together with the measured solution densities. Consideration was given to the amount of acid consumed in the solution of the metal and in the oxidation of Pu(III) by the dichromate.

Analyses.—The Pu(IV) solution concentration was followed during a kinetic experiment through the absorption at 4694 Å. which was measured with the Cary Model 14 recording spectrophotometer. The molar extinction coefficients of Pu(III), Pu(IV) and Cr(III) were determined under the conditions of temperature and solution environment which closely corresponded to those used in the rate determinations. At 4694 Å., the contributions of Sn(II) and Sn(IV) to the measured optical densities were considered to be negligibly small.

In the analyses of Sn(II), a pipetted volume of stannous chloride stock solution was added to a measured excess of Pu(IV). From the change in the optical density at 4694 Å., before and after the addition of the Sn(II), with consideration given to the volume change, the concentration of Sn(II) in the stock solutions was computed. The solutions were allowed to stand from 30 to 60 min., which corresponded to t_∞, before recording the optical density differences. Also, a correction was made for the additional Pu(III) formed by the reduction of Pu(IV). The effectiveness of the storage vessel with the helium atmosphere was demonstrated by the fact that over a period of a week the titer of the Sn(II) remained essentially unchanged.

Apparatus and Procedure.—The equipment and technique used in the kinetic experiments did not significantly differ from those used in previous work at this Laboratory.[2] It has been found that with practice, the time required for the mixing of the solutions and the placement of the mixing cell in the water-bath with the Cary spectrophotometer cell compartment could be shortened so that usable data were

(1) This work was done under the auspices of the U. S. Atomic Energy Commission.

(2) For example, see S. W. Rabideau and R. J. Kline, THIS JOURNAL, **63**, 1502 (1959); **64**, 193 (1960).

(3) T. W. Newton and S. W. Rabideau, *ibid.*, **63**, 365 (1959).

(4) J. S. Johnson and K. A. Kraus, *ibid.*, **63**, 440 (1959).

obtained within 15 seconds of the start of the kinetic run. It is to be noted than an uncertainty is associated with the "time zero" point because of the finite time required for the mixing process and the variability of this operation from one run to another (see discussion below).

Calculations.—The values of the specific rate constants for the reaction between Pu(IV) and Sn(II) together with the associated standard deviations of these quantities were obtained by the method of least squares with the use of an IBM-704 computer and a program prepared for this purpose. The program was designed to evaluate the specific rate constants for second-order reactions from input data which consisted of optical densities at a specified wave length as a function of time, initial reactant and product concentrations together with their molar extinction coefficients at this wave length, the cell length and the stoichiometric reaction coefficients.

If the kinetic reaction under study is represented by the equation $aA + bB = pP + qQ$, and the rate law is written as $-d[A]/dt = k[A][B]$, then for the case I in which $0.98 \leqslant a(B_0)/b(A_0) \leqslant 1.02$, the relationship between D, the optical density at any time t and the specific rate constant k is given by the expression

$$D = D_0 - E(\bar{A}_0)\{(\bar{A}_0)kt/[(\bar{A}_0)kt + (a/b)]\}$$
$$E = (L/A)(a\epsilon_A + b\epsilon_B - p\epsilon_P - q\epsilon_Q)$$

where

L = path length in cm.; ϵ's = molar extinction coefficients

$$(A_0) = [b(A_0) - a(B_0)]/2b$$

The zero subscripts refer to initial concentrations in moles per liter.

For an alternate case II, in which $0.85 \geqslant a(B_0)/b(A_0) \geqslant 1.15$, the relationship between the optical density and the specific rate constant is

$$D = \left\{[E(A_0) - D_0]\frac{(B_0)}{(A_0)}e^{[(B_0)-b(A_0)/a]kt} - E(B_0) + \frac{bD_0}{a}\right\} \Big/ \left\{\frac{b}{a} - \frac{(B_0)}{(A_0)}e^{[(B_0)-b(A_0)/a]kt}\right\}$$

For those kinetic experiments in which the ratio $a(B_0)/b(A_0)$ was between the limits specified for case I and II, the specific rate constant was determined by both these methods.

The quantity minimized in this least squares treatment of the spectrophotometric data was in each instance the sum of the differences, $(D_{obsd.} - D_{calcd.})$.[2] Inasmuch as it appears that the measurements of the optical densities are subject to a constant error of about ± 0.002 optical density units, irrespective of the actual value between zero and 1.5, no weighting factors were introduced in the computations.

The requirement that $x = 0$ when $t = 0$, where x corresponds to the number of moles/liter of A reacted, was not imposed upon the system because of the uncertainty in the time corresponding to a "true zero." Instead, values of $\pm\Delta t$ were programmatically computed for each experiment. In most instances the time error was about ± 0 to 2 seconds. The uncertainty in the zero time arises from the difficulty of knowing when to start the electric clock because of the finite time required for the mixing process.

Computer methods were also used in the evaluation of the specific rate constants for the parallel paths in which the $(Cl^-)^4$ and $(Cl^-)^5$ terms are involved, namely, k_1 and k_2, respectively. Least squares slopes and intercepts were obtained at 10, 20 and 30° with the use of an analytical expression of the form, $k''/(Cl^-)^4 = k_1 + k_2(Cl^-)$, where k'' is the rate constant k corrected for the chloride complexing of Pu(IV) and Sn(II). Similarly, least squares methods were used in the evaluation of the energies of activation for the parallel paths.

Where uncertainties in the results have been given, it is to be understood that these correspond to standard deviations. In quantities which have been computed from estimated values of equilibrium quotients, uncertainties in the final results have been omitted.

Results

Stoichiometry.—Pipetted volumes of a stannous chloride stock solution were added to a measured excess of a standard potassium dichromate solution. After the reaction was considered to have reached completion, a weight aliquot of a Pu(III) stock solution of a size that was more than sufficient to consume the remaining dichromate was added. The concentration of Pu(IV) produced was measured spectrophotometrically. Thus, it was possible to calculate the concentration of Sn(II) in the stock solution. From changes in the optical density of a Pu(IV) solution of known concentration upon the addition of a known volume of the standardized Sn(II), it was concluded that within the limit of experimental error, approximately 1%, the stoichiometry can be represented by the equation

$$2Pu(IV) + Sn(II) = 2Pu(III) + Sn(IV) \quad (1)$$

In work which confirmed the existence of the trivalent oxidation state of plutonium, Hindman, *et al.*,[5] also concluded that the stoichiometry of this reaction was as shown in equation 1. No indication of a measurable slowness in the Pu(IV)–Sn(II) reaction was reported in this earlier work.

The Pu(IV) and Sn(II) Dependencies.—On the basis of linear plots of the integrated second-order rate law expression, $\log \{[Pu(IV)_0]/[Sn(II)_0] \cdot ([Sn(II)_0 - x]/[Pu(IV_0) - 2x)\}$ *versus* time, to an extent of completion 90% or greater, it was concluded that the applicability of the second-order law was confirmed. Further, essentially identical values of the specific rate constants were obtained in experiments in which the Pu(IV) and Sn(II) were present in equivalent quantities and in cases in which the Sn(II) was present in nearly a fourfold excess. Thus, it is considered that the reaction is first order in the Pu(IV) and in the Sn(II) concentrations.

Rate Expressions.—It has been found experimentally that the data for the reaction between Pu(IV) and Sn(II) at constant chloride ion concentration can be represented by the rate law

$$-d[Sn(II)]/dt = k[Pu(IV)][Sn(II)] \quad (2)$$

or

$$dx/dt = k(a - 2x)(b - x) \quad (3)$$

where k is the apparent rate constant and the quantities x and $2x$ are equal to the decrease in the concentrations of Sn(II) and Pu(IV), respectively, and use of the substitutions $a = [Pu(IV)_0]$ and $b = [Sn(II)_0]$ has been made. The zero subscripts refer to initial concentrations. Upon integration of equation 3, the usual second-order equation which is obtained is

$$1/(2b - a) \ln [(a/b)(b - x)/(a - 2x)] = kt \quad (4)$$

The values of the apparent rate constant k were obtained by computer methods as described in the Experimental section of this paper. It is to be emphasized that k as written in equations 2 and 4 contains a functional dependence upon the chloride ion concentration.

Acidity Dependence.—Experiments were made to determine the influence of the hydrogen ion concentration upon the rate of the reaction between Pu(VI) and Sn(II) in chloride media. The acidity was varied while the ionic strength and the total chloride ion concentrations were maintained

(5) J. C. Hindman, K. A. Kraus, J. J. Howland, Jr., and B. B. Cunningham, paper 3.2, "Transuranium Elements," Div. IV, Vol. 14B, 1949, p. 121.

at two in these kinetic runs at 24.8° by the use of appropriate quantities of standardized solutions of hydrochloric acid and sodium chloride. As shown in Table I, it appears that the Pu(IV)-Sn(II) reaction is independent of the acidity in solutions of constant chloride ion concentration, at least over the range of acidities examined in this work.

TABLE I

INFLUENCE OF ACIDITY UPON THE Pu(IV)-Sn(II) REACTION IN TWO MOLAR CHLORIDE MEDIA AT 24.8°

$[H^+]$, M	$[Na^+]$, M	k, M^{-1} sec.$^{-1}$
2.000	0	16.70 ± 0.15
1.688	0.312	16.76 ± .10
1.376	.624	17.09 ± .15
1.064	.936	17.83 ± .25
0.756	1.244	16.61 ± .12
0.445	1.555	16.30 ± .14

Search for Back Reaction.—If the oxidation of Sn(II) by Pu(IV) is considered to proceed in one-electron steps, the equations can be written as

$$Pu(IV) + Sn(II) \underset{k'}{\overset{k}{\rightleftharpoons}} Pu(III) + Sn(III) \quad (5)$$

$$Pu(IV) + Sn(III) \underset{k_0'}{\overset{k_0}{\rightleftharpoons}} Pu(III) + Sn(IV) \quad (6)$$

although no direct evidence has been obtained to support the existence of Sn(III). However, equations 5 and 6 are in concordance with the experimental facts that the stoichiometry requires the reduction of two moles of Pu(IV) for each Sn(II) that is oxidized and that the forward reaction is first order in Pu(IV) and in Sn(II). In the oxidation of Fe(II) by Tl(III), Ashurst and Higginson[6] observed an inhibition of the reaction by Fe(III). The initial Pu(III) and Pu(IV) concentrations used in the kinetic experiments were usually in the vicinity of 1×10^{-4} and 2×10^{-3} M, respectively. In the search for a back reaction, the initial concentration of Pu(III) was increased ten-fold while the initial Pu(IV) and Sn(II) concentrations were essentially unaltered. The specific rate constants obtained at 24.8° under these conditions were indistinguishable from those given in Table I. The rate law, with consideration of both the forward and the reverse reactions in equation 5 and 6 and with the assumption that $-d[Sn(III)]/dt = 0$, becomes

$$-d[Sn(II)]/dt = \{kk_0[Pu(IV)]^2[Sn(II)] - k'k_0'[Pu(III)]^2[Sn(IV)]\}/\{k_0[Pu(IV)] + k'[Pu(III)]\} \quad (7)$$

The specific rate constant k' must be small in comparison with k_0, otherwise an effect on the experimentally observed apparent rate constant would have been found with the increased concentration of Pu(III). If k' is very small, the rate expression in equation 7 would reduce to equation 2. Further, the product $k'k_0'$ must be small in comparison with kk_0 in order that the stoichiometry be as represented in equation 1. No direct conclusions can be drawn from these experiments about the magnitude of k_0' itself.

(6) K. G. Ashurst and W. C. E. Higginson, *J. Chem. Soc.*, Part III, 3044 (1953).

Chloride Ion Dependence.—To obtain the chloride ion concentration dependence in the rate law, equation 2, it is first necessary to consider the extent to which these ions are complexed by chloride ion. Uncomplexed stannous ion, Sn^{++}, is related to the total bivalent tin, Sn(II), by the relation

$$[Sn^{++}] = [Sn(II)]/(1 + \beta_1[Cl^-] + \beta_2[Cl^-]^2 + \beta_3[Cl^-]^3) \quad (8)$$

where the successive equilibrium quotients are defined by

$$\beta_n = [SnCl_n^{+2-n}]/[Sn^{++}][Cl^-]^n \quad (9)$$

Similarly for plutonium

$$[Pu^{++++}] = [Pu(IV)]/(1 + \beta'_1[Cl^-] + \beta'_2[Cl^-]^2) \quad (10)$$

and

$$\beta_n' = [PuCl_n^{+4-n}]/[Pu^{++++}][Cl^-]^n \quad (11)$$

The thermodynamic quantities associated with the equilibria defined by β_1, β_2, and β_3 have been measured in solutions of ionic strength 3.0 with the use of electromotive force methods employing concentration cells.[7] Earlier work concerning the measurement of these quotients at 25° in solutions of ionic strength two[8] was recalculated[7] in terms of a maximum of three chlorides attached to the tin(II). As a part of the present paper, the electromotive force measurements of Duke and Courtney[8] as a function of the chloride ion concentration were re-examined. The equation which relates the cell e.m.f., E, to the successive equilibrium quotients at 25° is

$$E = 0.0128 \ln (1 + \beta_1[Cl^-] + \beta_2[Cl^-]^2 + \beta_3[Cl^-]^3 + \dots) \quad (12)$$

With the use of the IBM-704 and a program[9] designed to minimize the sum of the differences, $(E_{obsd} - E_{calcd})^2$, it was found that the data were adequately represented by three formation quotients. This conclusion is also in agreement with an earlier,[7] presumably graphical recalculation. The least squares values of the formation quotients together with their standard deviations were found to be: $\beta_1 = 11.4 \pm 0.3$, $\beta_2 = 52.8 \pm 1.8$, and $\beta_3 = 32.5 \pm 2.4$. Inasmuch as ΔH usually does not change rapidly with ionic strength, the values of ΔH for the successive chloro-complexes of Sn(II) at $\mu = 3.0$[7] were considered to be applicable also to solutions at $\mu = 2.0$.[10]

From electromotive force measurements of the Pu(III)-Pu(IV) couple in mixed perchloric-hydrochloric acid solutions, values of β_1' and β_2' have been obtained at 25°.[10] Inasmuch as no direct measurements of the values of ΔH for the equilibria associated with β_1' and β_2' are available, an estimate of +3 kcal./mole and +4 kcal./mole, respectively, was made for these quantities. The

(7) C. E. Vanderzee and D. W. Rhodes, *J. Am. Chem. Soc.*, **74**, 3552 (1952).

(8) F. R. Duke and W. G. Courtney, *Iowa State J. Sci.*, **24**, 397 (1950).

(9) R. H. Moore and R. K. Zeigler, "The Solution of the General Least Squares Problem with Special Reference to High-Speed Computers," LA-2367, 1960.

(10) S. W. Rabideau, L. B. Asprey, T. K. Keenan and T. W. Newton, "Recent Advances in the Basic Chemistry of Plutonium, Americium and Curium," Paper P/2247, Proc. Intern. Conf. Peaceful Uses Atomic Energy, Geneva, Vol. 28, 1959, p. 361.

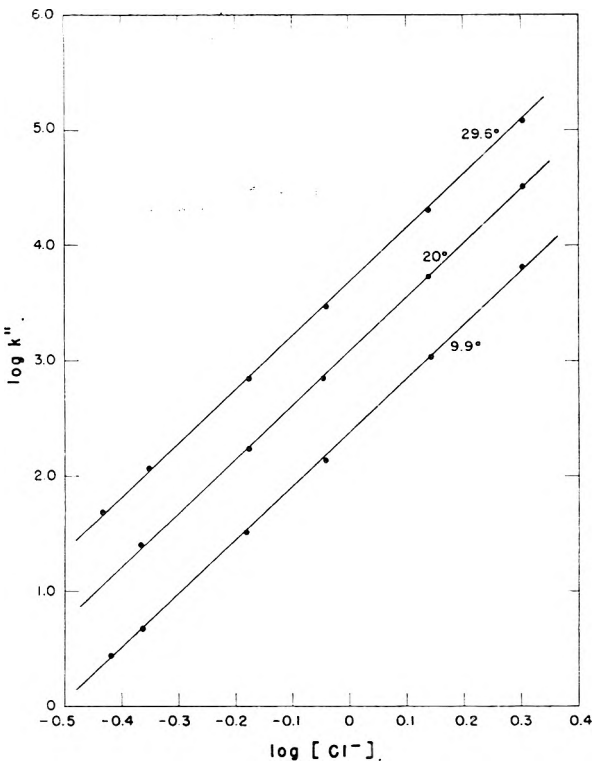

Fig. 1.—Chloride ion concentration dependence of specific rate constant for Pu(IV)-Sn(II) reaction as a function of temperature.

estimate was made on the basis of comparisons of heats for the formation of the hydroxy and chloro-complexes for ions of high charge types. A summary of the chloride complexing quotients used in this work is given in Table II.

TABLE II

TEMPERATURE VARIATION OF EQUILIBRIUM QUOTIENTS FOR CHLORIDE COMPLEXES OF Sn(II) AND Pu(IV), $\mu = 2.0$

Temp., °C.	β_1	β_2	β_3	β_1'	β_2'
9.9	9.0	39.5	19.6	1.05	0.47
20.0	10.6	48.0	27.6	1.26	.60
29.6	12.2	57.2	37.6	1.50	.75

The relationship between the observed specific rate constant k as found by equation 2 and k'', the rate constant corrected for the chloride complexing of Sn(II) and Pu(IV), is

$$k'' = k(1 + \beta_1[Cl^-] + \beta_2[Cl^-]^2 + \beta_3[Cl^-]^3)(1 + \beta_1'[Cl^-] + \beta_2'[Cl^-]^2) \quad (13)$$

A series of Pu(IV)-Sn(II) kinetic experiments were performed at 9.9, 20.0 and 29.6° in solutions of varied chloride ion concentration at a constant acidity of two molar. The solutions were prepared by the combination of appropriate quantities of standardized perchloric and hydrochloric acid solutions. The hydrolysis of Pu(IV) and Sn(II) has been considered to be negligibly small under the conditions of these experiments. Although k'' includes the correction of k for the chloride complexing of Pu(IV) and Sn(II) according to equation 13, it is to be noted that k'' still bears functional relationship to the chloride ion concentration. As shown in Fig. 1, straight lines with slopes of 4.68 were found at all three temperatures in plots of log k'' *vs.* log [Cl^-]. Since in these plots the influence of the chloride ion complexing of the metal ions has been removed, it is possible to rewrite equation 2 in the form

$$-d[Sn(II)]/dt = k''[Pu^{++++}][Sn^{++}] \quad (14)$$

$$= k_1[Pu^{++++}][Sn^{++}][Cl^-]^4 + k_2[Pu^{++++}][Sn^{++}][Cl^-]^5 \quad (15)$$

where

$$k'' = k_1[Cl^-]^4 + k_2[Cl^-]^5 \quad (16)$$

Thus it appears, as indicated by equation 15, that the reaction between Pu(IV) and Sn(II) proceeds through parallel paths in which the fourth and the fifth powers of the chloride ion concentration are involved. The values of the specific rate constants, k_1 and k_2, were evaluated with least squares computer methods as indicated in the experimental section of this paper from linear plots of $k''/[Cl^-]^4$ *vs.* [Cl^-]. In Table III are given the values of k_1 and k_2 as functions of temperature. Inasmuch as standard deviations were not assigned to the values of ΔH for the successive formation quotients for the chlorocomplexes of Sn(II),[7] and since an estimate was used for the temperature coefficients of β_1' and β_2', statistical uncertainties have not been assigned to the values of k_1 and k_2.

TABLE III

TEMPERATURE DEPENDENCE OF SPECIFIC RATE CONSTANTS

Temp., °C.	k_1, M^{-5} sec.$^{-1}$	k_2, M^{-6} sec.$^{-1}$
9.9	59.7	171
20.0	332	850
29.6	1503	3093

As an indication of the degree to which equation 16 reproduces the experimental data over a five-fold range in the chloride ion concentration with the k_1 and k_2 values of Table III at 9.9°, a comparison is presented in Table IV. The k_{expt}'' results were calculated with the use of equation 13 and the k_{calcd}'' values were obtained with the use of equation 16.

TABLE IV

COMPARISON OF EXPERIMENTAL AND CALCULATED VALUES OF k'' AT 9.9°

[Cl^-], M	k_{expt}, M^{-1} sec.$^{-1}$	k_{expt}'', M^{-1} sec.$^{-1}$	k_{calcd}'', M^{-1} sec.$^{-1}$
2.000	3.91 ± 0.02	6500	6427
1.383	2.26 ± .01	1067	1084
0.906	1.036 ± .007	136	144
.658	0.581 ± .003	32.6	32.3
.432	0.216 ± .001	4.61	4.65
.381	0.166 ± .001	2.75	2.63

Thermodynamic Activation Quantities.—From the temperature dependence of the specific rate constants, k_1 and k_2, as shown in Table III, least squares slopes of plots of ln k_1 and ln k_2 *vs.* $1/T$ were found by computer methods. Statistical weights were not assigned for the reasons stated previously. From absolute reaction rate theory,[11] thermodynamic quantities for the activation processes at 25° were computed. Equations 17 and 18 are the reactions for the activation steps and the calcu-

(11) S. Glasstone, K. Laidler and H. Eyring, "The Theory of Rate Processes," McGraw-Hill Book Co., New York, N. Y., 1941, p. 417.

lated heats and entropies for these processes are given.

	ΔH^*, kcal./mole	ΔS^*, e.u.	
$Pu^{++++} + Sn^{++} + 4Cl^- = (Pu{\cdot}Cl_4{\cdot}Sn)^{++}$	26.9	44.7	(17)
$Pu^{++++} + Sn^{++} + 5Cl^- = (Pu{\cdot}Cl_5{\cdot}Sn)^{+}$	24.1	37.0	(18)

In a recent review paper,[3] entropies of activated complexes of various charge types have been calculated from ΔS^* and from the individual ionic entropies involved. Values of +13.2 and −5.9 e.u. for Cl^- and Sn^{++}, respectively, were obtained from Latimer.[12] A value of −85 e.u. was used for Pu^{++++} as given by Katz and Seaborg.[13] Computed values of the activated complexes in equations 17 and 18 were found to be +6.6 and 12.1 e.u., respectively. As shown in Fig. 2, there appears to be a definite correlation between the charge and the entropy of the activated complex over the range of charge types between +1 and +6. The values for the +3, +4, +5 and +6 activated complexes shown in Fig. 2 indicate the range of results found for several different reactions reported previously.[3] Since the current work represents the first recorded results for the +1 and +2 charge types, an estimate of the uncertainty associated with these quantities has been indicated.

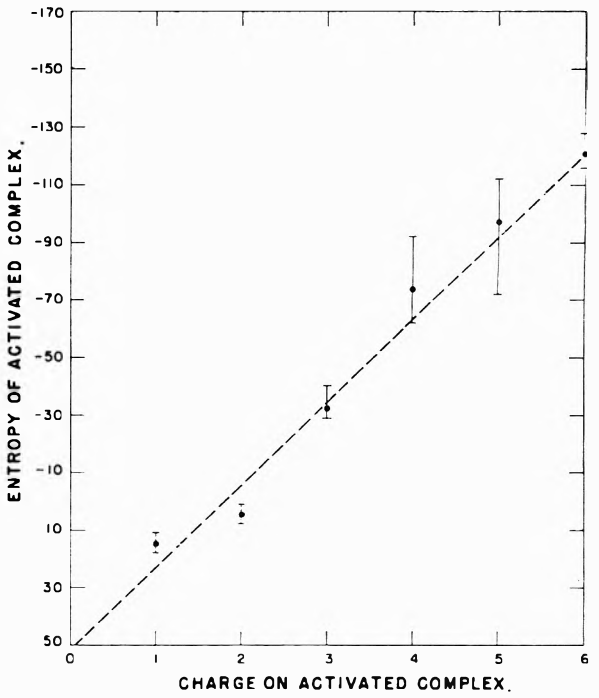

Fig. 2.—Charge–entropy relationships for activated complexes as derived from ΔS^* for various oxidation–reduction reactions.

Discussion

It has been observed in several instances that in the reduction of Pu(IV) in perchlorate solution with various metal ions, *e.g.*, V(III),[14] U(IV),[15] Ti(III),[16] etc., the mechanism of the reaction appeared to involve one or more hydrolyzed species in the rate-determining step. In the disproportionation of Pu(IV) in perchloric acid solution, the predominant path involves an inverse third power of the hydrogen ion concentration.[17,18] A similar hydrogen ion concentration dependence was observed in hydrochloric acid solution, but the rate of disproportionation is greatly enhanced in chloride media.[17,19] Apparently the chloride ions, like the hydroxyl ions, participate in the electron transfer process. Similarly, in the present study, the rate of reduction of Pu(IV) is very greatly influenced by the presence of chloride ions. The hydrogen ion concentration independence of the reaction indicates that in this instance the mechanism by which the reduction occurs does not involve the hydrolyzed species of the ions. However, if the acidity were to be lowered to about 0.1 *M*, and the proper corrections could be applied for the hydrolysis of the ions in this medium, it would be surprising if an inverse hydrogen ion concentration dependence were not observed.

The high power of the chloride ion dependence in the Pu(IV)–Sn(II) reaction seems to indicate that the tin(II) species involved in the reduction process is the chloride complex, possibly $SnCl_3^-$. Thus, mechanistic reactions which are consistent with the experimental data, but are not unique, can be written as

$$PuCl^{+3} + SnCl_3^- \xrightarrow{k_a} PuCl^{+2} + SnCl_3 \quad (19)$$

$$PuCl_2^{+2} + SnCl_3^- \xrightarrow{k_b} PuCl_2^{+} + SnCl_3 \quad (20)$$

$$PuCl^{+3} + SnCl_3 \xrightarrow{\text{fast}} PuCl^{+2} + SnCl_3^{+} \quad (21)$$

However, no direct evidence has been obtained to indicate the existence of Sn(III) in these reactions.

An interaction absorption between Sn(II) and Sn(IV)[20] and between Sn(II) and U(VI)[21] has been observed in strong hydrochloric acid solutions. In the present work, at 4694 Å., no enhancement of the Pu(IV) molar extinction coefficients was observed in the presence of Sn(II). Extrapolated optical densities to zero time corresponded closely to those calculated on the basis of the contributions of the Pu(III), Pu(IV) and Cr(III) present.

In Table I it is seen that the influence of the substitution of Na^+ for H^+ over a rather wide range has little effect upon the values of the specific rate constants. Under these conditions of ionic environment, the ionic strength principle holds well for this reaction.

With the possibility in mind of obtaining additional thermodynamic information for activated

(12) W. M. Latimer, "Oxidation Potentials," 2nd Edition, Prentice–Hall, Inc., New York, N. Y., 1952.

(13) J. J. Katz and G. T. Seaborg, "The Chemistry of the Actinide Elements," Methuen and Co., Ltd., London, 1957 (also John Wiley and Sons, Inc., New York, N. Y.), p. 294.

(14) S. W. Rabideau and R. J. Kline, *J. Inorg. Nucl. Chem.*, June, (1960).

(15) T. W. Newton, THIS JOURNAL, **63**, 1493 (1959).

(16) S. W. Rabideau and R. J. Kline, *ibid.*, **64**, 193 (1960).

(17) R. E. Connick and W. H. McVey, *J. Am. Chem. Soc.*, **75**, 474 (1953).

(18) S. W. Rabideau, *ibid.*, **75**, 798 (1953).

(19) S. W. Rabideau and H. D. Cowan, *ibid.*, **77**, 6145 (1955).

(20) C. I. Browne, R. P. Craig and N. Davidson, *ibid.*, **73**, 1946 (1951).

(21) R. L. Moore, *ibid.*, **77**, 1504 (1955).

complexes, it appears that the reduction of Pu(VI) by Sn(II) may offer an opportunity to obtain the entropy of an activated complex with a zero or negative charge.

Acknowledgments.—The author wishes to express his appreciation to Mr. R. H. Moore for the preparation of the IBM-704 program used in the evaluation of the specific rate constants and for helpful discussions on problems of statistical interest. Also, helpful discussions with Drs. J. F. Lemons, C. E. Holley, Jr., and T. W. Newton concerning this research are gratefully acknowledged.

THE REACTION OF OZONE WITH METHANE

BY FREDERICK J. DILLEMUTH, S.J., DUANE R. SKIDMORE, S.J. AND CLARENCE C. SCHUBERT, S.J.

Department of Chemistry, Fordham University, New York 58, New York

Received April 14, 1960

The reaction of ozone with methane was studied in temperature controlled, infrared, gas cells. Infrared analysis showed the major reaction products to be carbon monoxide, carbon dioxide, formic acid and water vapor. It was found that the reaction was substantially independent of Pyrex and sodium chloride surfaces. The activation energy calculated on the basis of the equation $-d[O_3]/dt = k[O_3][CH_4]$ was found to be 15.3 kcal./mole with oxygen as the ozone diluent. The pre-exponential term was 1.6×10^{11} cc. mole^{-1} sec.$^{-1}$. When oxygen was excluded from the reaction mixture of methane and ozone, a value for the activation energy of 13.9 kcal. was found and a pre-exponential term 1.4×10^{10} cc. mole^{-1} sec.$^{-1}$, a value regarded as being not significantly different. The low activation energy found for this reaction is taken as a strong indication that the reaction mechanism does not include a prior decomposition of ozone followed by an attack of oxygen atoms on methane. It was found that there is an approximate equivalence of gram atoms of oxygen fixed in products and moles of ozone consumed.

I. Introduction

In 1898, Otto[1] first studied the reaction of methane and ozone both at room temperature and at 100°, observing the formation of aldehyde. Blair and Wheeler,[2] repeating the same experiment at 100°, noted that 53% of the ozone present had reacted with methane after two minutes. No carbon monoxide was detectable. The effect of surface on the reaction was little, if any, serving only to destroy some of the ozone. Briner and Carceller,[3] reporting the action of ozone in the slow combustion of propane and butane, postulate a chain mechanism in which the chain initiating step is hydrogen abstraction by a molecule of ozone

$$RCH_3 + O_3 \longrightarrow RCH + H_2O + O_2 \qquad (I)$$

Schubert and Pease,[4] in their studies on the oxidation of the lower paraffin hydrocarbons, found that the reaction of methane with ozonized oxygen occurred with an activation energy of 14,900 cal./mole. To explain this relatively low activation energy, it was postulated that the reaction might occur between the hydrocarbon and an ozone molecule in a triplet low-lying excited electronic state. More recently, Kleimenov, *et al.*,[5] using a flow system, reinvestigated the methane–ozonized oxygen reaction. Because oxygenated products appeared only at and above the temperature at which ozone was found to decompose, these investigators concluded that the oxidation of methane and other hydrocarbons is primarily effected by an atomic mechanism, *viz.*

$$O_3 \longrightarrow O_2 + O \qquad (II)$$

$$RH + O \longrightarrow R\cdot + \cdot OH \text{ etc.} \qquad (III)$$

Reported here are the results of studies concerning the reaction of ozone with methane, both in the presence and in the absence of added oxygen.

II. Experimental

Tank oxygen (Ohio Chemical and Surgical Company, U.S.P.) was dried over calcium chloride and silica gel. It was next ozonized in a Siemens-type ozonizer, the effluent ozone–oxygen mixture being *ca.* 3 mole % in ozone. Ozone–oxygen mixtures of concentrations higher than 3 mole % in ozone, were prepared according to a method outlined by Cook.[6] The ozone–oxygen mixture was allowed to pass through a silica gel column cooled to −78° with a slurry of acetone and carbon dioxide snow. At this temperature, ozone adsorbed on the silica gel, while oxygen passed through the column unabsorbed to any significant extent. The effluent oxygen, after a washing with 2% potassium iodide solution in order to destroy any unadsorbed ozone, was allowed to escape into the atmosphere. The concentrated ozone was adsorbed as a wide purple band on the silica gel column. When required for use, concentrated ozone was desorbed from the silica gel at room temperature in a stream of dried oxygen or nitrogen.

Methane (Matheson Co., C.P.) was purified from traces of carbon dioxide by passing the gas through moist potassium hydroxide pellets and dried over calcium chloride. Methane and the enriched ozone were mixed in a capillary mixer and allowed to fill a previously evacuated ten cm. infrared gas absorption cell until the total pressure was one atmosphere. All gases were metered by calibrated flow meters.

The oxidations were followed by an infrared spectrophotometric method of analysis,[4] using a Perkin-Elmer Model 21 double beam spectrophotometer. The infrared absorbance of the various reactants and products was noted at specific intervals during the course of the reaction. The ozone absorbance was measured at 1055 cm.$^{-1}$, carbon monoxide at 2183 cm.$^{-1}$, carbon dioxide at 2344 cm.$^{-1}$ and formic acid at 1740 cm.$^{-1}$. Concentrations of reactants and products were calculated by comparison with calibration curves constructed from reference spectra run on pure compounds at various known partial pressures, under conditions as similar as possible to those obtaining during the oxidations. Methane concentrations could not be determined spectrophotometrically. Initial methane concentrations were obtained from initial flow rates.

(1) M. M. Otto, *Ann. chim. phys.*, [VII] **13**, 109 (1898).

(2) E. W. Blair and T. S. Wheeler, *J. Soc. Chem. Ind. (London)*, **41**, 303 (1922).

(3) E. Briner and J. Carceller, *Helv. Chim. Acta*, **18**, 973 (1935).

(4) C. C. Schubert, S. J. and R. N. Pease, *J. Am. Chem. Soc.*, **78**, 2044 (1956).

(5) N. A. Kleimenov, I. N. Antonova, A. M. Markevich and A. B. Nabaldian, *Zhur. Fiz. Khim.*, *XXX*, 794 (1956).

(6) G. A. Cook, A. D. Kiffer, C. V. Klumpp, A. H. Malik and L. A. Spence, "Separation of Ozone from Oxygen by a Sorption Process," Tonawanda Research Laboratory, Linde Air Products Company, Tonawanda, New York.

The ten-cm. infrared cells, constructed of Pyrex glass, were fitted with sodium chloride windows. They were equipped with a water jacket for temperature control to within ± 0.25°. In double beam operation, the reference cell was filled up to one atmosphere pressure with either dried oxygen or nitrogen, depending on whichever gas had been used to desorb the ozone from the silica gel. All stopcocks were lubricated with an ozone-resistant Halocarbon grease. Time zero was recorded from the moment when the reaction cell was brought up to temperature. Preliminary experiments showed that any reaction at room temperature which occurred in the brief time elapsing between filling the cells and the moment when the desired temperature was reached, was negligible.

III. Experimental Results

(a) **Products of the Ozone–Methane Reaction.**—The infrared absorption spectra of the products of the reaction showed principally, carbon monoxide, carbon dioxide, formic acid and water vapor. Although a slight amount of unreacted ozone could still be observed when the reaction was essentially complete, its concentration was usually of the order of 0.1 mmole/l., and product absorptions interfered to such an extent that any quantitative estimate of ozone concentration beyond this point was unreliable. Infrared bands characteristic of higher paraffin hydrocarbons, arising, presumably, from the reaction $R\cdot + \cdot R' \rightarrow RR'$, were not observed; neither was the presence of such compounds considered likely.[7] Formaldehyde was not detected in any of the infrared spectra, though trace amounts were probably present. Figure 1 shows a representative run conducted with ozonized oxygen at 66.6°.

In the whole series of runs, the hydrocarbon concentration was, on the average, 2.91×10^{-2} mole/l., while the ozone mixture was held at approximately 1.55×10^{-2} mole/l. In this manner a gas mixture rich in hydrocarbon was always assured. This experimental condition was forcibly suggested by a severe explosion which shattered one of the gas absorption cells in a preliminary investigation. It was observed that in all cases the concentration of carbon monoxide produced was roughly 1.5–2 times as great as that of the carbon dioxide. Formic acid appeared in all of the runs, but its concentration in no case exceeded 1.2×10^{-4} mole/l. Conceivably, in the runs at lower temperatures, some of the acid condensed on the cell walls and thus escaped detection.

Product yields, determined by infrared analysis for several runs, both when oxygen was added and when it was excluded from the reaction mixture, are given in Table I. It is not felt that the results are too significantly different in both cases.

The calculated values for the amounts of water produced are based on the assumption that two moles of water are produced for every mole of carbon appearing in products. Since the infrared spectra showed no hydrogen-containing oxidation products other than water, except in trace amounts, this would appear to be a reasonable approach toward a product balance.

The ratio of gram atoms of oxygen fixed in product to moles of ozone decomposed was calculated on the basis of sixteen independent runs. In eight of these oxygen was used as the ozone diluent. In the others oxygen was excluded by using nitrogen as the carrier gas for the ozone. The average showed that in the former case 0.997 gram atoms of oxygen were fixed in product per mole of ozone consumed. In the latter case, 1.02 gram atoms were fixed per mole of ozone. This result has been taken to indicate that one mole of ozone reacts with one mole of the hydrocarbon with the ultimate formation of oxygenated products plus one mole of molecular oxygen.

(7) E. W. Steacie and N. A. Parlee, *Can. J. Research*, B16, 203 (1938).

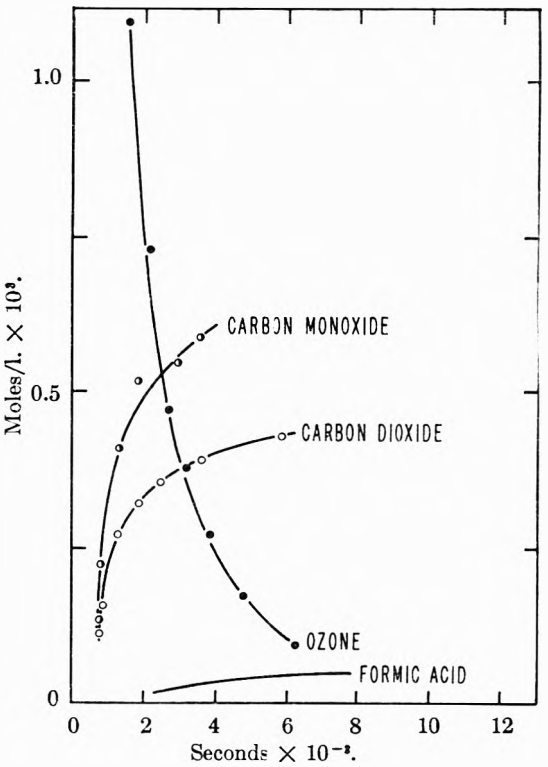

Fig. 1.—Methane plus ozone at 66.6°.

TABLE I

MOLES OF PRODUCT PER MOLE OF OZONE CONSUMED

Run no.	Temp., °C.	CO_2	CO	H_2O	Gram atoms oxygen fixed
		Oxygen diluent			
209	35	0.16	0.24	0.81	1.37
162	43.9	.130	.360	.49	1.11
225	48.3	.09	.22	.63	1.03
164	64.4	.019	.308	.653	1.10
		Nitrogen diluent			
167	35.4	0.080	0.184	0.53	0.874
163	44.4	.122	.227	.70	1.17
185	48.4	.107	.223	.66	1.09
166	64.4	.062	.231	.587	0.943

(b) **Effect of Surface.**—Since the reaction cell was composed of Pyrex glass and fitted with rock salt windows, it was felt desirable to investigate the effects of added Pyrex and salt surfaces on the course of the reaction independently. The former was accomplished by placing five lengths of 8 mm. diameter Pyrex tubing lengthwise into the cell, changing the Pyrex surface to volume ratio from 2.02 to 5.79 cm.$^{-1}$. Although the optical balance

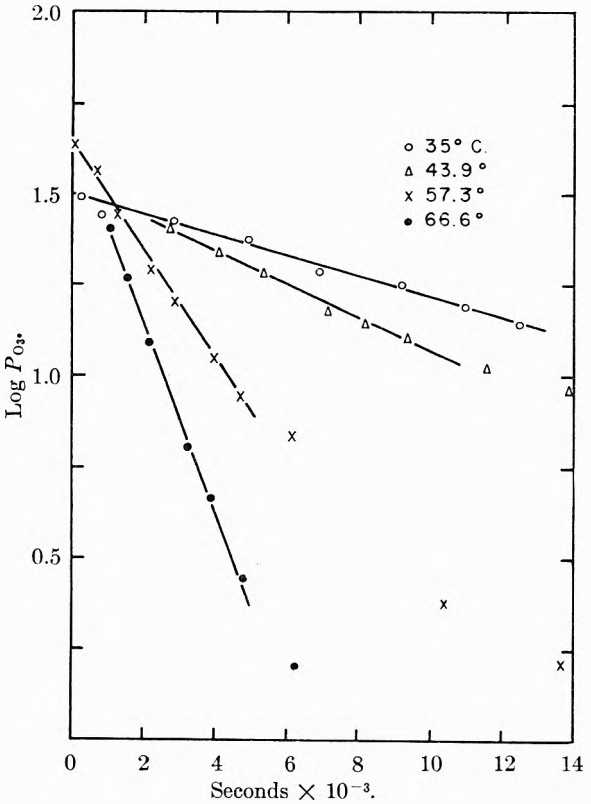

Fig. 2.—Methane plus ozonized oxygen.

of the spectrophotometer had to be modified somewhat to compensate for the interference offered by the tubing to the passage of the infrared radiation, the greater percentage of the radiation was unhindered in its travel through the cell. The insertion of a number of regular sodium chloride crystals into the body of the cell changed the salt surface to volume ratio from 0.209 to 0.891 cm.$^{-1}$. It was found that in neither case were the kinetics of the reaction changed, nor did the use of nitrogen rather than oxygen as the ozone diluent cause any significant differences in this series of experiments.

(c) **Kinetics.**—In Fig. 2 the logarithm of ozone partial pressure is plotted against time. From the linear plots obtained for the reaction of ozone with methane at four temperatures, it was inferred that the reaction is first order with respect to ozone. Points corresponding to an ozone partial pressure of less than 4 mm. were unreliable because product absorptions interfered with the fundamental ozone band at 1055 cm.$^{-1}$. In general, marked deviations from linearity were observed at low ozone concentrations.

From previous work[4,8,9] on the ozonolysis of hydrocarbons, it was felt that the reaction could be taken as second order, and the rate expression be given as

$$-d[O_3]/dt = k[O_3][CH_4]$$

where k, in this case, has the units cc. mole^{-1} sec.$^{-1}$. Data were taken from plots such as those of Figs. 1 and 2. Since, in each series of experiments, the concentration of methane was far in excess of that of ozone, the hydrocarbon concentration was taken as effectively constant during the course of each run.

The activation energy for the reaction was determined from Arrhenius' plots, both for the case when oxygen was used as the ozone diluent and when nitrogen was so employed. These values are given in Table II, together with the rate constants calculated for 25° and the pre-exponential term A determined from the equation

$$k = A \exp(-E^*/RT) \text{ cc. mole}^{-1} \text{ sec.}^{-1}$$

TABLE II

E^* (cal./mole)	A (cc. mole^{-1} sec.$^{-1}$)	k_{25} (calcd.) (cc. mole^{-1} sec.$^{-1}$)
	Oxygen added	
15,350	1.63×10^{11}	0.82
	Oxygen excluded	
13,900	1.43×10^{10}	0.84

The variation in the activation energy and the pre-exponential term when oxygen was excluded from the reaction mixture, is not regarded as significant.

Discussion

In all the experiments there was, on the average, an approximate equivalence between the number of gram atoms of oxygen fixed in products and the moles of ozone disappearing. On the basis of this finding, a chain mechanism involving oxygen molecules has been excluded. Were a molecular oxygen chain reaction important in the low temperature reaction of ozone with methane, there would be expected a significantly greater amount of oxygenated products.

The results of this work show that the reaction of ozone and methane, both with and without added oxygen, proceeds with an activation energy of approx. 14–15 kcal./mole. The thermal decomposition of ozone, on the other hand, occurs, according to recent investigations,[10,11] with an activation energy of 24.2 ± 0.2 kcal./mole. It might be questioned, therefore, in the light of this divergence of activation energy values, whether a mechanism which invokes oxygen atoms and not the ozone molecule itself as the initial attacking species, adequately fits the observed data. Consequently, it is not immediately obvious how the conclusions drawn by Kleimenov,[5] who postulates the prior decomposition of the ozone molecule and a subsequent reaction between methane and an oxygen atom, can be reconciled with the results of this work.

With respect to the reaction rate constants, activation energy and the pre-exponential term for the reaction of methane with ozone, we are impressed by the fact that, for all practical purposes, they are the same both in the presence and in the absence of added oxygen, and, at least in the tempera-

(8) R. D. Cadle, "Chemical Reactions in Los Angeles Smog," Proceedings of the Second National Air Pollution symposium, Stanford, Calif., Stanford Research Institute, 1952, p. 31.

(9) R. R. Sawyer and F. W. Behnke, Abstracts of the 135th Meeting of the American Chemical Society, Boston, Mass., April, 1959, p. 28-B.

(10) S. W. Benson and A. E. Axworthy, Jr., *J. Chem. Phys.*, **26**, 1718 (1957).

(11) J. A. Zaslowsky, H. B. Urbach, F. Leighton and R. J. Wnuk, Abstracts of the 135th Meeting of the American Chemical Society, Boston, Mass., p. 23-R.

ture range employed, independent of surface. The reaction is believed, therefore, to proceed by a similar mechanism in all the above cases.

Acknowledgment.—This research was supported by a grant from the Petroleum Research Fund, administered by the American Chemical Society. Grateful acknowledgment is hereby made to the donors of said fund. The authors are also indebted to Dr. Raymond R. Sawyer, Mr. Fred Behnke and the Perkin-Elmer Corporation of Norwalk, Connecticut for the generous loan of long path infrared cells used in the course of this work.

THE EFFECT OF STRUCTURE ON THE OSMOTIC AND ACTIVITY COEFFICIENTS OF SOME SULFONIC ACIDS AND THEIR SALTS

BY O. D. BONNER[1] AND O. C. ROGERS

Department of Chemistry, University of South Carolina, Columbia, South Carolina

Received April 15, 1960

Osmotic and activity coefficients are reported for benzenesulfonic and mesitylenesulfonic acids and the lithium and sodium salts of benzenesulfonic, *p*-ethylbenzenesulfonic, 2,5-dimethylbenzenesulfonic and mesitylenesulfonic acids at 25°. These measurements were made by isopiestic comparison of solutions of the sulfonates with sodium chloride solutions as reference standards. The osmotic and activity coefficients of the acids and salts are observed to decrease with increasing molecular weight. The magnitude of the values of these coefficients have the order Li > Na > H for the higher molecular weight sulfonates, thus indicating that these sulfonic acids are probably only moderately strong acids.

Since the introduction of sulfonic acid type of cation-exchange resins which consist of sulfonate exchange sites on polystyrene–divinylbenzene matrices, there have been many attempts to interpret the equilibrium data obtained for exchange reactions involving various pairs of ions. At least two[2] of these attempts have involved the use of model compounds similar in structure to the ion exchanges. This work has been handicapped by the scarcity of data for the various aromatic sulfonic acids and their salts. Robinson and Stokes[3] have reported osmotic and activity coefficients for the lithium, sodium and potassium salts of *p*-toluenesulfonic acid while Bonner[2b,4] and coworkers have reported data for *p*-toluenesulfonic, *p*-ethylbenzenesulfonic, 2,5-dimethylbenzenesulfonic, 4,4′-bibenzyldisulfonic and *m*-benzenedisulfonic acids. The only compound for which osmotic and activity coefficient data are available for both the parent acid and some of its salts is therefore *p*-toluenesulfonic acid.

Experimental

The various sulfonic acids with the exception of benzenesulfonic acid were prepared by sulfonation of the corresponding purified hydrocarbons. Benzenesulfonic acid was prepared by the hydrolysis of benzenesulfonyl chloride. The sulfonates were recovered from the sulfuric acid solution by neutralization with potassium hydroxide in the case of benzenesulfonic acid and sodium hydroxide for the other solutions. The salts were then recrystallized at least three times from water or water–methanol solutions and dried to constant weight. No structural isomers are possible for any of the sulfonates except the ethylbenzenesulfonates. The purity of the various salts was checked by passing solutions of weighed quantities of each salt through an ion-exchange column in the acid (hydrogen) form and titrating the liberated acid with standard alkali. In all instances the experimental and theoretical molecular weights of each salt agreed within the experimental error of the titration. Solutions of the acids for isopiestic comparison were obtained by ion exchange and standardized with standard alkali. Solutions of the various salts were then obtained by neutralization of the acid solutions with the appropriate base. It was not possible to reclaim the crystalline acids and weigh them accurately because of their hygroscopic nature.

Activity and osmotic coefficients of the acids and salts were determined by isopiestic comparison of solutions of these electrolytes with solutions of sodium chloride which were used as standards. Values of the osmotic and activity coefficients of sodium chloride are tabulated by Robinson and Stokes.[5] Osmotic coefficients were calculated from the equation

$$\nu\varphi = \nu_{ref}\frac{m_{ref}}{m}\varphi_{ref} \qquad (1)$$

Activity coefficients were calculated from the equation

$$\log\gamma = \log\gamma_{ref} + \log\frac{m_{ref}}{m} + \frac{2}{2.303}\int_0^{(m\gamma)^{1/2}_{ref}}\frac{\frac{m_{ref}}{m}-1}{(m\gamma)_{ref}^{1/2}}\,d\,(m\gamma)^{1/2}_{ref} \qquad (2)$$

Results and Discussion

The osmotic and activity coefficients of the various sulfonic acids and the corresponding lithium and sodium sulfonates are presented in Tables I and II. The values of these coefficients decrease as the organic content of the molecule increases (Fig. 1). The activity and osmotic coefficients of the acids are thus in the order benzenesulfonic> toluenesulfonic > dimethylbenzenesulfonic > mesitylenesulfonic. The activity and osmotic coefficients of the lithium and sodium salts of these acids follow the same pattern. These sulfonate activity and osmotic coefficient values are also smaller than those of the common uni-univalent type compounds such as the alkali metal salts. If one considers the sulfonate anion and the counter cation as the electrolyte, the organic part of the molecule with water can then be considered as a

(1) The data reported in this paper are from a project supported by the United States Atomic Energy Commission.

(2) (a) G. E. Myers and G. E. Boyd, THIS JOURNAL, **60**, 521 (1956); (b) O. D. Bonner, V. F. Holland and Linda Lou Smith, *ibid.*, **60**, 1102 (1956).

(3) R. A. Robinson and R. H. Stokes, *Trans. Faraday Soc.*, **45**, 612 (1949).

(4) O. D. Bonner, G. D. Easterling, D. L. West and V. F. Holland, *J. Am. Chem. Soc.*, **77**, 242 (1955).

(5) R. A. Robinson and R. H. Stokes, *Trans. Faraday Soc.*, **45**, 612 (1949).

TABLE I

TABLE OF OSMOTIC COEFFICIENTS AT 25°[a]

m	(1)	(2)	(3)	(4)	(5)	(6)	(7)	(8)	(9)	(10)
0.1	0.936	0.941	0.936	0.925	0.924	0.910	0.929	0.924	0.930	0.927
.2	.931	.945	.932	.912	.908	.880	.917	.908	.921	.912
.3	.929	.950	.930	.903	.890	.847	.904	.890	.914	.897
.4	.929	.955	.929	.895	.870	.820	.890	.867	.909	.881
.5	.930	.960	.929	.889	.857	.788	.872	.843	.904	.862
.6	.932	.967	.930	.884	.850	.758	.854	.818	.897	.845
.7	.934	.974	.933	.879	.843	.732	.834	.795	.884	.825
.8	.936	.980	.934	.875	.838	.706	.817	.772	.865	.805
.9	.938	.986	.935	.871	.834	.683	.800	.747	.843	.784
1.0	.941	.992	.936	.867	.831	.661	.782	.724	.824	.760
1.2	.945	1.003	.937	.860		.628	.750		.793	.713
1.4	.949	1.014	.937	.852		.604	.723		.770	.670
1.6	.954	1.025	.936	.843		.588	.705		.752	.637
1.8	.959	1.036	.934	.836		.577	.694		.737	.610
2.0	.965	1.047	.931	.830		.570	.685		.725	.590
2.5	.986	1.071	.921	.822		.573	.680		.714	.558
3.0	1.009	1.093		.818		.587	.697		.724	
3.5	1.039	1.115		.819		.606	.726		.744	
4.0	1.072	1.136				.634	.763		.772	
4.5	1.106	1.156				.671	.804			
5.0	1.141					.707				
5.5						.746				

[a] (1) Benzenesulfonic acid; (2) Li benzenesulfonate; (3) Na benzenesulfonate; (4) Li 2,5-dimethylbenzenesulfonate; (5) Na 2,5-dimethylbenzenesulfonate; (6) mesitylenesulfonic acid (1,3,5-trimethylbenzenesulfonic acid); (7) Li mesitylenesulfonate; (8) Na mesitylenesulfonate; (9) Li *p*-ethylbenzenesulfonate; (10) Na *p*-ethylbenzenesulfonate.

TABLE II

TABLE OF ACTIVITY COEFFICIENTS AT 25°[a]

m	(1)	(2)	(3)	(4)	(5)	(6)	(7)	(8)	(9)	(10)
0.1	0.784	0.794	0.781	0.768	0.768	0.743	0.773	0.768	0.775	0.770
.2	.745	.764	.742	.716	.711	.670	.724	.711	.729	.717
.3	.722	.753	.719	.682	.669	.614	.689	.668	.699	.679
.4	.708	.745	.706	.658	.635	.569	.660	.630	.679	.649
.5	.697	.743	.694	.639	.609	.530	.632	.598	.662	.618
.6	.690	.743	.687	.623	.589	.494	.605	.567	.646	.593
.7	.685	.745	.681	.609	.571	.461	.580	.539	.627	.566
.8	.680	.747	.675	.597	.556	.433	.556	.511	.604	.541
.9	.676	.750	.671	.586	.542	.408	.534	.484	.582	.517
1.0	.673	.754	.666	.575	.531	.386	.514	.459	.561	.493
1.2	.669	.761	.659	.557		.350	.477		.525	.448
1.4	.668	.771	.652	.540		.322	.445		.496	.410
1.6	.667	.782	.646	.525		.299	.421		.472	.378
1.8	.667	.794	.640	.512		.282	.402		.451	.352
2.0	.668	.806	.634	.500		.268	.386		.433	.331
2.5	.677	.836	.618	.477		.244	.358		.403	.291
3.0	.694	.868		.461		.230	.344		.386	
3.5	.717	.902		.448		.220	.339		.378	
4.0	.746	.936				.215	.339		.382	
4.5	.779	.971				.214	.345			
5.0	.818					.215				
5.5						.218				

[a] (1) Benzenesulfonic acid; (2) Li benzenesulfonate; (3) Na benzenesulfonate; (4) Li 2,5-dimethylbenzenesulfonate; (5) Na 2,5-dimethylbenzenesulfonate; (6) mesitylenesulfonic acid (1,3,5-trimethylbenzenesulfonic acid); (7) Li mesitylenesulfonate; (8) Na mesitylenesulfonate; (9) Li *p*-ethylbenzenesulfonate; (10) Na *p*-ethylbenzenesulfonate.

sort of mixed solvent. In a 5 m solution of toluenesulfonic acid, for example, there would be 5 moles of toluene having a molar volume of approximately 105 cc. per 1000 cc. of water. This would be equivalent to a mixed solvent containing nearly 35% hydrocarbon by volume with a resultant dielectric constant considerably lower than that of water. If one similarly considers a 5 m solution of mesitylenesulfonic acid, the molar volume of mesitylene being approximately 140, the solution would contain about 42% hydrocarbon by volume. The cause of the decrease in the values of the osmotic and activity coefficients with an increase in molecular weight of the sulfonate salts is then explainable as an increase in the degree of ion pairing as the effective dielectric constant in the neighborhood of the ions is decreased.

It is also noted that as the hydrocarbon content is increased, the activity and osmotic coefficients of the acids drop more rapidly than those of the corresponding lithium or sodium salts. This results in the osmotic coefficient of benzenesulfonic acid being larger than that of sodium benzenesulfonate, while the osmotic coefficient of sodium toluenesulfonate is larger than that of toluenesulfonic acid up to a concentration of 1.4 *m*, and the sodium salts of dimethylbenzenesulfonic acid and mesitylenesulfonic acid having larger osmotic coefficients than the parent acids up to the limit of their solubility. The change in the order of the activity and osmotic coefficients for the higher molecular weight sulfonates, placing hydrogen below lithium and sodium, is a further indication that sulfonic acids are only moderately strong acids with ionization constants of the higher molecular weight acids being probably the same order of magnitude but lower than that of nitric acid.[6,7] These ionization constants probably decrease as the molecular weight of the sulfonic acid increases because of the lower effective dielectric constant in the vicinity of the sulfonate group in a manner analogous to that of acetic acid in dioxane–water mixtures.[8]

The sulfonic acid type ion-exchange resin is known to be inhomogeneous in that all sulfonate sites do not exist in the same environment. There are probably concentration differences due to the statistical variation in the crosslinking. It is also recognized that commercial resins are not completely sulfonated in that the exchange capacity does not correspond to one sulfonate group for each aromatic ring which is present. Some of the exchange sites are therefore in the vicinity of several other sulfonate groups, while other exchange sites (probably those in the center of the beads where difficulty of diffusion causes incomplete sulfonation) are almost completely surrounded by the organic matrix. This probably explains the inability of Myers and Boyd[2a] to duplicate exactly ion-exchange equilibria using as a model a weakly crosslinked resin, containing essentially only one type of exchange site, and Bonner's difficulty when mixed solutions containing only two sulfonates were used as a model. The importance of the environment of a sulfonate group, as demonstrated by these osmotic and activity coefficient data, would indicate that a complex mixture of sulfonates would be necessary to serve as a model for an ion exchanger.

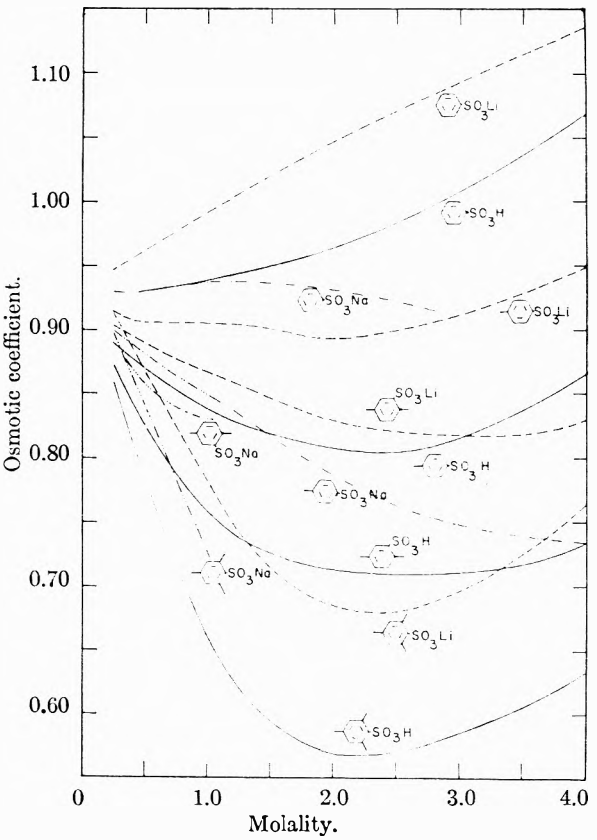

Fig. 1.—Osmotic coefficients of some sulfonic acids and lithium and sodium sulfonates.

(6) O. D. Bonner and Robert R. Pruett, THIS JOURNAL, **63**, 1417 (1959).

(7) Preliminary data indicate the ionization constant of mesitylenesulfonic acid to be about 0.2. These results will be published upon the completion of the investigation.

(8) H. S. Harned and B. B. Owen, "The Physical Chemistry of Electrolytic Solutions," Reinhold Publ. Corp., New York, N. Y., 756 (1958).

STUDIES OF THE TRANSPORT PROPERTIES OF THE SYSTEM Tl_2SO_4–H_2O. I. DIFFUSION COEFFICIENTS AT 25°[1]

BY J. M. CREETH[2] AND BETH E. PETER

Department of Physical and Inorganic Chemistry of the University of Adelaide, Adelaide, South Australia

Received April 16, 1960

Differential diffusion coefficients D for the system Tl_2SO_4–H_2O have been measured over the concentration range 0.16 to 4.83 g. dl.$^{-1}$ by the Rayleigh interference optical method. Previously reported thermodynamic measurements on the system have been used to obtain the factor $(1 + d \ln y_\pm/d \ln c)$; the ratio $D/(1 + d \ln y_\pm/d \ln c)$, which is a measure of the diffusional mobility of the electrolyte, has thus been obtained. The mobility shows unusual behavior in that it increases by about 25% over the concentration range cited: this effect is interpreted on the basis of ion association, the ion $TlSO_4^-$ being formed to an increasing extent as the concentration rises. An expression relating the mobility of the electrolyte to the mobilities of the three ions and the degree of dissociation α has been used to predict the mobility as a function of concentration; for this purpose the limiting ion conductances have been used to approximate the ion mobilities of Tl^+ and $SO_4^=$, while α values have been estimated from the thermodynamic measurements. Satisfactory agreement between the observed and the predicted mobility behavior has been found, on the basis of plausible values for the mobility of the ion $TlSO_4^-$.

The application of the thermodynamics of irreversible processes to binary diffusion in liquids enables a simple relation to be derived between the experimentally accessible diffusion coefficient and activity coefficient and the experimentally inaccessible frictional coefficient (or its reciprocal, the mobility). For the special case of electrolytes the relation[3,4] may be written as

$$D = U\nu RT(1 + d \ln y_\pm/d \ln c_1) \qquad (1)$$

where ν is the number of ions produced by one formula weight of electrolyte (component 1), c_1 and $y_\pm$ are, respectively, the concentration and stoichiometric mean ionic activity coefficient, on any scale based on mass per unit volume, and U represents the mobility of the electrolyte.[5]

Measurements of D and $y_\pm$ as a function of c therefore allow the mobility to be determined and a comparison to be made with the Onsager–Fuoss theory[3]: many electrolytes have been examined (at low concentrations) in this way by Harned, *et al.*[6] For unsymmetrical electrolytes, even when completely dissociated, good agreement is not to be expected, however, due to the limitations of the theory.[7] When extensive ion association occurs, the difficulties in the way of adequate theoretical representation become very great: it is recognized,[8–11] however, that in this case much of the observed concentration-dependence may be due to the variation of the *proportions* of the different ionic constituents, rather than to variation of the individual mobilities. Thus diffusion and activity data may make possible an *approximate* correlation with information on the degree of dissociation, and it is the purpose of this paper to report diffusion data on the system Tl_2SO_4–H_2O which, when combined with the thermodynamic results obtained earlier,[12] allow such a comparison to be made.

Experimental

Materials and Solutions.—The thallous sulfate used was the same twice-recrystallized sample as previously described[12]; solutions were prepared by weight using the appropriate air buoyancy corrections and density data. All concentrations are given in terms of g. dl.$^{-1}$ (of solution) and denoted c.

Diffusion Measurements.—All diffusion experiments were performed in the Spinco Model H Electrophoresis–Diffusion Apparatus, which had a slightly modified optical system.[13] Rayleigh interference optics[14–17] were employed throughout, and previously validated procedures[18] for the conduct of experiments followed as closely as possible. The terminology previously defined[18,19] will be used here without further comment. For experiments at mean concentrations of 2.5 g. dl.$^{-1}$ and higher, ethylene glycol was added to the thermostat bath to compensate approximately for the increased refractive index.[20] Although this procedure resulted in much better-defined interference fringes, it had the disadvantage that refocusing the camera lens was necessary and hence slightly varying magnification factors were employed for different experiments. Furthermore, evaporation of water from the bath during a run produced an appreciable shift of the interferogram relative to the reference fringes, and allowance for this had to be made by a slight modification of the measuring procedure.

In some experiments in the low concentration regions the "upper solution" consisted of water alone: the resulting

(1) In part from a dissertation submitted by Beth E. Peter to the University of Adelaide in fulfillment of the requirements of the B.Sc Honors degree, December, 1957.

(2) Lister Institute of Preventive Medicine, London, S.W. 1, England.

(3) L. Onsager and R. M. Fuoss, THIS JOURNAL, **36**, 2689 (1932) (equation 4·12·5).

(4) H. S. Harned and B. B. Owen, "The Physical Chemistry of Electrolytic Solutions," 3rd Ed., Reinhold Publ. Corp., New York, N. Y., 1958, pp. 118–122. For simplicity, the symbol U will be used in this paper to replace 1000 M_1/C_1.

(5) The mobility U in equation 1 is defined in terms of diffusion coefficients which are based on the "solvent-fixed" frame of reference; should other frames of reference be chosen, correction factors must be included on the right-hand side, or an alternative definition of the mobility adopted. *Cf.* L. J. Gosting, *Advances in Protein Chem.*, **11**, 429 (1956).

(6) References are collected in a review by H. S. Harned, *Disc. Faraday Soc.*, **24**, 9 (1957).

(7) R. H. Stokes, *J. Am. Chem. Soc.*, **75**, 4563 (1953).

(8) H. S. Harned and R. M. Hudson, *ibid.*, **73**, 5781, 5880 (1951).

(9) B. F. Wishaw and R. H. Stokes, *ibid.*, **76**, 2065 (1954).

(10) G. T. A. Müller and R. H. Stokes, *Trans. Faraday Soc.*, **53**, 642 (1957).

(11) J. M. Creeth and R. H. Stokes, THIS JOURNAL, **64**, 946 (1960).

(12) J. M. Creeth, *ibid.*, **64**, 920 (1960).

(13) J. M. Creeth, L. W. Nichol and D. J. Winzor, *ibid.*, **62**, 1546 (1958).

(14) J. St. L. Philpot and G. H. Cook, *Research*, **1**, 234 (1948).

(15) H. Svensson, *Acta Chem. Scand.*, **3**, 1170 (1949); **5**, 72 (1951).

(16) L. G. Longsworth, *Rev. Sci. Instr.*, **21**, 524 (1950).

(17) L. G. Longsworth, *J. Am. Chem. Soc.*, **74**, 4155 (1952).

(18) J. M. Creeth, *ibid.*, **77**, 6428 (1955). These procedures were shown to lead to the determination of the differential diffusion coefficient at the mean concentration, c, of the experiment, and the symbol D_c was used for this quantity. In the present paper the subscript will be dropped, for simplicity, and "D" will be taken to imply (except where the context makes an alternative meaning obvious) the differential value at the concentration cited.

(19) J. M. Creeth, THIS JOURNAL, **62**, 66 (1958).

(20) *Cf.* the procedure used by L. G. Longsworth, *ibid.*, **61**, 244 (1957), to surmount this problem.

Rayleigh patterns then showed evidence of pronounced second-order skewness,[18] and therefore could not be treated by the simple procedure for obtaining differential diffusion coefficients. The origin of this phenomenon lies in the fact that the theory[21] of concentration-dependence effects expresses the deviations in fringe position[18] in terms of derivatives $(\partial r_D/\partial c^r)_{c=\bar{c}}$, where $\bar{c} = (c_A + c_B)/2$, c_A and c_B being the initial concentrations of the upper and lower solutions, respectively, used in the diffusion experiment. For non-electrolytes, these derivatives are either finite or zero as c approaches zero, and consequently second-order effects (which are *also* proportional to $(\Delta c/2)^2$, where $\Delta c = c_B - c_A$) may be eliminated by making Δc sufficiently small. For electrolytes, however, we have $(\partial r_D/\partial c^r)_{c \to 0} = \infty$, due to the dependence of D upon $\sqrt{c}$. Accordingly, finite second-order deviations may persist even for very small values of Δc.

This situation presents interesting problems in the interpretation of fringe deviations, which are the subject of current study; however for the purpose of calculating differential diffusion coefficients from these interferograms, a complete analysis is unnecessary. It is sufficient to note that, since the functions[18] $S(z)$ and $T(z)$ both pass through zero at $z \sim 0.6$, a modification of the procedure applicable to mixed solute systems[19] (by interpolating in the graph of $(Y_t/\sqrt{t})$ *vs.* $(z^*)^2$ at the point defined by $z^* = 0.6$, and equating this value to $2M'\sqrt{D}$, where M' is the magnification, enables D to be calculated to a good approximation. However, effects due to second-order concentration-dependence of refraction increment are not eliminated in this procedure.

Experiments performed between solutions both of finite concentration gave satisfactorily constant Y_t values over the whole interferogram, the figures being quite comparable with those previously reported for sucrose[18] and glycine[19]: it is thus concluded that impurities in the sample were sensibly absent.

TABLE I

SOLUTION DATA AND DIFFUSION COEFFICIENTS FOR Tl_2SO_4 AT 25.00°

1	2	3	4	5	6	7	8
Δc[a]	$\bar{c}$[a]	J[b]	$\Delta n/\Delta c$[c]	Δt[d]	D[e]	$1 + \frac{d \ln y_\pm}{d \ln c}$	D^*[f]
0.2603	0.1644	25.80	9.717	13	1.40_5	0.891	1.57_5
.5093	.2547	44.96	9.656	58	1.37_1	.866	1.58_3
.7546	.3773	66.27	9.607	7	1.34_5	.840	1.60_2
1.0519	.5260	92.30	9.598	40	1.32_0	$.814_2$	1.62_2
1.2375	.6188	108.35	9.578	10	1.31_0	$.800_4$	1.637
1.0935	1.0561	95.02	9.506	51	1.267	$.749_7$	1.69_0
1.0031	1.5214	85.99	9.379	35	1.239	$.710_0$	1.745
0.9982	1.9828	85.38	9.357	18	1.215	$.679_1$	1.790
.9684	2.2853	82.63	9.333	22	1.201	$.661_8$	1.814
.9987	2.9689	84.70	9.277	13	1.176	$.629_7$	1.867
1.0264	3.4944	87.08	9.280	23	1.159	$.609_4$	1.901
0.9220	3.8574	77.73	9.222	20	1.149	$.597_3$	1.923
1.0770	4.8329	89.94	9.135	26	1.123	$.570_4$	1.969

[a] All concentrations expressed in g.dl.$^{-1}$. [b] Total number of fringes: in the cell used, of internal dimension along the optic axis 2.496_0 cm., Δn (the refraction increment for light of wave length 5461 Å.) $= 1.093_9 \times 10^{-5} \times J$. [c] Units of dl. g.$^{-1} \times 10^{-4}$. [d] Zero-time correction, sec. [e] Differential diffusion coefficient at mean concentration, in units of cm.^{2} sec.$^{-1} \times 10^{-5}$ [f] $D^* = D/(1 + d \ln y_\pm/d \ln c)_{c=\bar{c}}$.

Results

(a) **Refraction Increment Data.**—A by-product of this research is the accumulation of moderately precise data for the refractive index, n, of Tl_2SO_4 solutions, for light of wave length 5461 Å. The relevant figures are given in Table I, columns 1 and 3, where the concentration differences between the two solutions used in each diffusion experiment are listed, together with the corresponding value of J, the total number of fringes. The value of the refraction increment $\Delta n/\Delta c$ is directly obtainable from these figures, and is given in column 4. It is evident that this quantity is appreciably concentration-dependent, and on the assumption that n follows an equation of the form

$$n = n_0 + Rc + ac^{3/2} + bc^2 + \ldots \quad (2)$$

the refraction increment data were fitted, by the method of least squares, to a curve of the form

$$\Delta n/\Delta c = R + a'(c_B^{3/2} - c_A^{3/2})/\Delta c + b'(c_B^{3/2} - c_A^{3/2})^2/(\Delta c)^2;\ 0 < c < 5.0 \quad (3)$$

This analysis gave the following values for the coefficients: $R = 9.823 \times 10^{-4}$, $a' = -2.380 \times 10^{-5}$ and $b' = 1.16 \times 10^{-6}$ when $\Delta n/\Delta c$ is expressed in dl.g.$^{-1}$. As $\Delta c \to 0$, the coefficients a and a' become identical, while $b' = 8b/9$.

(b) **Diffusion Coefficient Data.**—The mean concentration of each experiment and the corresponding differential diffusion coefficient are shown in columns 2 and 6 of Table I, while the observed starting time corrections[22] are given in column 5. The D values lie on a smooth curve when plotted *vs.* $\sqrt{c}$, but it is not possible to express D as a power series in $\sqrt{c}$ without employing cubic terms. No analytical expression, therefore, has been derived from the data.

(c) **The Thermodynamic Factor.**—This can be computed directly from the activity coefficient data reported earlier,[12] but the following procedure, which is independent of the particular value of the standard potential E^0, makes more direct use of the primary data.[23] The e.m.f. E of the cell $Tl(Hg)/Tl_2SO_4(m,c)/Hg_2SO_4,Hg$ may be written

$$E = E_m^0 - 3k \ln 4^{1/3}m - 3k \ln \gamma_\pm = E_c^0 - 3k \ln 4^{1/3}10c/M - 3k \ln y_\pm \quad (4)$$

where m and $\gamma_\pm$ are, respectively, the molality and activity coefficient on the molal scale, $k = RT/2F$ and M is the formula weight of the electrolyte. The standard potentials, although unequal, are not functions of m or c. It then follows that

$$(1 + d \ln y_\pm/d \ln c) = -(1/3k)(dE/d \ln m)(d \ln m/d \ln c) \quad (5)$$

and analysis of the curve of E *vs.* $\ln m$ would therefore give the most important term directly: in order to ensure the correct limiting value at $m = 0$, however, advantage may be taken of the finding[12] that the following linear relationship exists[24]

$$E^{0\prime} = E + 0.058538 \ln m - 0.15623 m^{1/2} = \beta m + B \quad (6)$$

where B is a constant. Differentiating, we obtain

$$(dE/d \ln m) = [-3.8538 + 7.812m^{1/2} - 8.09_6 m] \times 10^{-2} \quad (7)$$

where the coefficient of m has been obtained (by the method of least squares) from the regression of $E^{0\prime}$ upon m.

The other derivative required is obtained as

(21) L. J. Gosting and H. Fujita, *J. Am. Chem. Soc.*, **79**, 1359 (1957).

(22) L. G. Longsworth, *ibid.*, **69**, 2510 (1947).

(23) With the exception noted, this procedure resembles that suggested by H. S. Harned and B. B. Owen, ref. 4, p. 243.

(24) The numerical coefficients represent, respectively, $3RT/2F$ and $(2.3026 \times 3RT/2F)2A\sqrt{3\rho_0}$ where A is the fundamental constant of the Debye–Hückel limiting law and ρ_0 the density of water at 25°. Values of the constants were taken from ref. 25, pp. 468, 469.

(25) R. A. Robinson and R. H. Stokes, "Electrolyte Solutions," 2nd Ed., Academic Press, Inc., New York, N. Y., 1959.

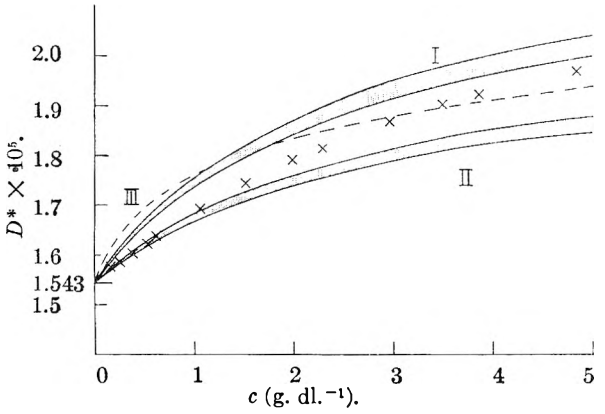

Fig. 1.—Predicted and observed variation of D^* with concentration for Tl_2SO_4. Curves I and II were calculated from equation 11, using, respectively, the values 4.83 and 4.14 × 10^{-9} cm.^{2} sec.$^{-1}$ mole joule^{-1} for the mobility of the $TlSO_4^-$ ion. (The median of the shaded area corresponds to the u_i and α values cited.) Curve III was calculated from the conductivity results of Righellato and Davies. Experimentally observed values of D^* are shown as ×.

follows. Expressing the molality in terms of c and the solution density, ρ

$$m = \frac{10^3 c}{M(100\rho - c)} \quad (8)$$

and differentiating, we find

$$(\mathrm{d} \ln m/\mathrm{d} \ln c) = 1 - \mathrm{d} \ln [1 + (\rho - \rho_0 - 0.01c)/\rho_0]/\mathrm{d} \ln c \quad (9)$$

Since the fraction is small compared with unity, this can be written

$$(\mathrm{d} \ln m/\mathrm{d} \ln c) = 1 - (1/\rho_0)[\mathrm{d}(\delta - \delta^2/2\rho_0)/\mathrm{d} \ln c] + \ldots \quad (10)$$

(where $\delta \equiv \rho - \rho_0 - 0.01c$) which is a form suitable for calculation. The solution density[26] and composition data were used to plot $(\delta - \delta^2/2\rho_0)$ *vs.* ln c and the slopes obtained graphically with ample accuracy.

Values of $(1 + \mathrm{d} \ln y_\pm/\mathrm{d} \ln c)$ were calculated for the particular concentrations corresponding to the $\bar{c}$ for each diffusion experiment, and are shown in column 7 of Table I. It is evident that over the concentration range covered, the thermodynamic factor varies markedly. Finally column 8 lists the value of D^*, defined as $D/(1 + \mathrm{d} \ln y_\pm/\mathrm{d} \ln c)$; from equation 1 it is clear that D^* is a direct measure of the mobility of the electrolyte.

Discussion

The diffusion coefficients obtained in this investigation differ quite markedly from the earlier values reported by Oholm[27] (after correction for the 5° temperature difference), particularly at the lower concentrations. Thus at $c = 2.52$ g. dl.$^{-1}$ Oholm found $D = 1.092$ while interpolation from Table I gives $D = 1.192 \times 10^{-5}$ cm.^{2} sec.$^{-1}$; at $c = 0.631$, the respective figures are 1.164 and 1.309 × 10^{-5} cm.^{2} sec.$^{-1}$. Since the values obtained in this work show a trend (at the lower concentrations) which appears to be quite compatible with the theoretical limiting value of 1.543 × 10^{-5} cm.^{2} sec.$^{-1}$ (*cf.* Fig. 1), it appears that Oholm's values are in error. The limiting value is obtained by applying the Nernst equation[28] to the limiting ion conductance data of Robinson and Davies[29] for Tl^+ and Jenkins and Monk[30] for $SO_4^=$.

The concentration-dependence of the mobility, revealed by the data of column 8, Table I (which are plotted as crosses in Fig. 1), is quite pronounced, and is in marked contrast with the behavior, for example, of barium chloride: the latter substance is one of the very few for which adequate data exist for comparison. Thus the data (for $BaCl_2$) of Harned and Polestra[31] (at 0.00542 M) and of Vitagliano and Lyons[32] (at 0.1066 M) for D, combined with thermodynamic factors derived from Robinson's[33] isopiestic data, give $D^* = 1.411$ and 1.421 × 10^{-5} cm.^{2} sec.$^{-1}$, respectively, while D^0, the limiting value, is 1.387 × 10^{-5} cm.^{2} sec.$^{-1}$; that is, the mobility varies only about 2% over a concentration range similar to that of the present results on Tl_2SO_4.

It is reasonable to seek an explanation for the large concentration-dependence in terms of incomplete dissociation, as was done by Harned and Hudson[8] for the case of $ZnSO_4$. In the latter case the observed D was about 10% greater (at 0.005 M) than that calculated from the Onsager–Fuoss theory (assuming complete dissociation): by employing independent estimates of the degree of dissociation, Harned and Hudson accounted satisfactorily for the discrepancy, and obtained reasonably constant values for the mobility of the neutral ion-pair. Since the product of association in the present instance is the *ion*, $TlSO_4^-$, and the concentration range is some twenty times greater, the situation is more complicated and only an approximate analysis will be attempted.

The necessary relation between the mobility of the electrolyte as a whole and the proportions and mobilities, u_i, of the three ions present was obtained by Creeth and Stokes,[11] and may be written[34]

$$U = \frac{u_1u_2\,\alpha(1 + \alpha) + u_2u_3\,\alpha(1 - \alpha) + u_1u_3\,(1 - \alpha^2)}{u_1(1 + \alpha) + 4u_2\alpha + u_3(1 - \alpha)} \quad (11)$$

where α is the degree of dissociation of the ion $TlSO_4^-$ (it is assumed that the first dissociation of Tl_2SO_4 is complete) and the subscripts 1,2,3 denote the ions Tl^+, $SO_4^=$ and $TlSO_4^-$, Selection of appropriate values of u_i and α presents, however, some difficulties (which are likely to be encountered in other systems of this type), and the reasons for various choices adopted are summarized below.

(a) The mobilities u_i required are, strictly, those corresponding to the "real" ionic strength,

(26) "International Critical Tables," Vol. 3, McGraw-Hill Book Co. New York, N. Y., 1928, p. 64; these values were supplemented by independent measurements, to be reported in a further communication.

(27) L. W. Oholm, *Finska Kemistsamfundets Medd.*, **45**, 122 (1936).

(28) *E. g.*, ref. 25, p. 288.

(29) R. A. Robinson and C. W. Davies, *J. Chem. Soc.*, 574 (1937).

(30) I. L. Jenkins and C. B. Monk, *J. Am. Chem. Soc.*, **72**, 2695 (1950).

(31) H. S. Harned and F. M. Polestra, *ibid.*, **76**, 2064 (1954).

(32) V. Vitagliano and P. A. Lyons, *ibid.*, **78**, 1549 (1956).

(33) R. A. Robinson, *Trans. Faraday Soc.*, **36**, 737 (1940).

(34) In the derivation of (11) it was assumed that no flow interaction terms enter into the expressions for the ionic velocities (equation 3 of ref. 11). If such interaction is not negligible, equation 11 will be a first approximation only.

Due to a change in definition, the u_i in (11) differ by a factor of the Avogadro number from those in the corresponding equation in ref. 11.

which is also a function of α. Since the diffusional mobility varies less with concentration than the mobility in conductance, the limiting values at zero concentration, u_i^0, are a good first approximation. In principle, it is possible to obtain a better approximation, for if α is known as a function of the concentration, the properly-weighted Onsager–Fuoss electrophoretic corrections may be made, at least for Tl^+ and $SO_4^=$. In the present application, since α is only known approximately, this course has not been followed, and the numerical values for u_1^0 and u_2^0 have been used. These were obtained directly from the limiting ion conductances, λ_i^0, by the equation

$$u_i^0 = \lambda_i^0/|z_i|F^2 \qquad (12)$$

where F is Faraday's constant and z is the valence. It seems unlikely that this procedure will introduce errors exceeding 2–3%, on the basis of the figures for $BaCl_2$.

(b) The mobility u_3, for $TlSO_4^-$, presents difficulties additional to those considered in (a), for it is not an operationally defined quantity: we have therefore solved (11) for two values of u_3, these being derived from the ion-conductance values $\lambda^0 = 45$ and 38.5 cm.^{2} ohm^{-1} equiv.$^{-1}$. The value 45 is that suggested by Righellato and Davies[35] as being applicable to all species MSO_4^-, but on the basis of Harned and Hudson's[8] finding that the mobilities of the *neutral* ion-pairs $ZnSO_4$ and $MgSO_4$ are equivalent to $\lambda = 44$ and 46, respectively, it is believed that it will represent an upper bound for the ion $TlSO_4^-$. (However, λ^0 for HSO_4^- is 51.[36]) The lower value was derived from λ^0 for $SO_4^=$ (= 80) on the assumption that the conductance is inversely proportional to the ionic radius, this quantity being taken, for the ion $TlSO_4^-$, as that of a sphere of volume equal to the sum of the volumes of Tl^+ and $SO_4^=$.[37] Since this reasoning ignores the secondary effect of the diminished charge, it is believed that the λ^0 will represent a lower bound. Applying equation 12 one finds $u_1 = 8.02$, $u_2 = 4.30$, $(u_3)_1 = 4.83$ and $(u_3)_2 = 4.14 \times 10^{-9}$ cm.^{2}sec.$^{-1}$mole joule^{-1}, the outer subscripts on the values for u_3 representing the two choices described above.

(c) The degree of dissociation of $TlSO_4^-$, α, is also not uniquely defined operationally; it is believed, however, that approximately correct values of α were obtained by an analysis of the stoichiometric activity coefficient data[12,38] in terms of a "model" activity coefficient equation based on the Bjerrum theory. The following figures suffice to show the general behavior: for m = 0.003, 0.01, 0.02, 0.04, 0.06, 0.08 and 0.10, α = 0.93, 0.85, 0.75, 0.61, 0.50, 0.43 and 0.38, respectively. These values were substituted in (11) and by virtue of the use of the two values of u_3, define two curves of D^* *vs.* c.[39] In order to illustrate the effects of errors in α, a limit of $\pm 2.5\%$ in $(1 - \alpha)$ was assigned to each α value, and from these figures four curves were constructed, two for each of the u_3 values. These curves are shown in Fig. 1, where the shaded area between the solid lines therefore represents the effect of a 5% uncertainty in $(1 - \alpha)$.

Because it is believed that uncertainties in the α values are the chief source of error in this analysis, it is of interest to construct a curve of D^* *vs.* c based on independent measurements of α. The conductivity studies of Righellato and Davies[35] on Tl_2SO_4 were interpreted, on contemporary theory, in terms of incomplete dissociation, and thus provide approximate values of α which extend over the whole concentration range studied here. (This set of α values agrees quite closely with those we have calculated from the value of K quoted by Bell and George,[40] using the *same assumptions* about the activity coefficients as these authors made; the α values are lower at the lower concentrations, and higher at the higher concentrations than those quoted earlier.) This set of α values and the *first* choice for u_3 were used to define the curve shown as III in Fig. 1. No other choice for u_3 is allowable here, on the grounds of self-consistency.[35]

It is clear from Fig. 1 that all the theoretical curves predict a rather large increase in D^* with c, in general agreement with the observed behavior. (The experimental points are, of course, obtained by rigorously defined procedures, and do not depend on any assumptions concerning α or u_i.) The general shape of curve III, however (obtained from the independent data cited), is in somewhat poorer agreement with the experimental points than either of the curves I and II. The discrepancies are largest at the low c values (where the effect of different choices of u_3 is minimal), and are indicative of a lower degree of dissociation than is compatible with the diffusion data. It is also evident that had u_3 been chosen to correspond to $\lambda^0 \sim 42$, and using the same α values, the resultant curve would have duplicated the experimental findings with a maximum error of about 2–3%.

(35) L. C. Righellato and C. W. Davies, *Trans. Faraday Soc.*, **26**, 592 (1930).

(36) M. Kerker, *J. Am. Chem. Soc.*, **79**, 3664 (1957); see also C. W. Davies, H. W. Jones and C. B. Monk, *Trans. Faraday Soc.*, **48**, 921 (1952).

(37) L. Pauling, "Nature of the Chemical Bond," Cornell University Press, Ithaca, N. Y., 1939.

(38) This analysis had the purpose of obtaining the dissociation constant K for $TlSO_4^-$, which is represented as

$$K = \frac{m\alpha(1 + \alpha)\gamma_{12}^2}{(1 - \alpha)\gamma_{11}^2}$$

(the subscripts indicate the valences of the appropriate pairs of ions). The procedure for obtaining α depends on the validity of the model equation for γ_{11} while the constancy of the result in terms of K depends *also* on the validity of the equation for γ_{11}. Thus the fact that the K values varied somewhat with m is insufficient grounds for believing the α values themselves to be in error. We have preferred to assume that the α values are correct, and assign the lack of constancy in K to the inadequacy of the equation for γ_{11} (for which some evidence exists); it should be emphasized, however, that if *all* the variation in K is assigned to errors in α, the effect is not large and is roughly comparable with the indicated spread shown in curves I and II.

(39) To be consistent with equation 1, the diffusion coefficient used to calculate D^* should have been corrected from the "volume-fixed" reference frame (applicable to the values quoted in column 8 of Table I; in these experiments the "volume-fixed" and "cell-fixed" reference frames are identical) to the "solvent-fixed" reference frame. Since (a) the correction amounts only to 1/2% for the highest concentration, and (b) limiting values of the mobilities have been substituted in (11), this correction has been ignored: should better values of α become available, so that u_i's could be computed at finite concentrations, the correction might be necessary and could readily be made.

(40) R. P. Bell and J. H. B. George, *Trans. Faraday Soc.*, **49**, 619 (1953).

Viscosity effects[25] are probably negligible in the concentration range considered.

Because of the assumptions involved in this comparison of theory and experiment, the rather close agreement noted cannot be taken as evidence that the state of the Tl_2SO_4–H_2O system (in respect of the properties considered) has been unequivocally defined; nevertheless, all the assumptions are plausible, and there is little doubt that the principle of incomplete dissociation provides a rational interpretation of these properties.

It may be noted that an alternative use of the procedures described is to combine stoichiometric activity coefficient and diffusion coefficient data to provide knowledge of the degree of dissociation independent of a model activity coefficient equation[41]: the comparable assumption now lies in the field of transport properties and is, of course, the value of the mobility of the complex ion.

Acknowledgments.—The authors are grateful to Professor D. O. Jordan for his interest in, and encouragement of, this work; they also wish to thank Professor R. H. Stokes, of the University of New England, Armidale, Australia, and Professors L. J. Gosting and J. W. Williams, of the University of Wisconsin, for stimulating and valuable discussions.

(41) The procedure suggested is essentially the reverse of that used[10,32,42] to determine mobilities of neutral ion-pairs when α is known.

(42) O. W. Edwards and E. O. Huffman, THIS JOURNAL, **63**, 1830 (1959).

THE EQUILIBRIUM: 2/3 Bi(l) + 1/3 $BiBr_3$(g) = BiBr(g) AND THE THERMODYNAMIC PROPERTIES OF $BiBr_3$[1]

BY DANIEL CUBICCIOTTI

Stanford Research Institute, Menlo Park, California

Received April 19, 1960

The reaction: 2/3 Bi(l) + 1/3 $BiBr_3$(g) = BiBr(g) was studied by a transpiration technique in the range 600 to 700°. The enthalpy change for the reaction was found to be 21.3 kcal. This was used to derive a standard enthalpy of formation of solid $BiBr_3$ of −63 kcal./mole at 298°K. The measured entropy of the reaction of 17 e.u. agreed well with a calculated value.

Introduction

Recently the equilibrium of liquid Bi with gaseous $BiCl_3$ and BiCl was studied and the thermodynamic properties of BiCl gas determined. The present paper reports a similar study of the bromide system; however, since the properties of BiBr have been well characterized from spectroscopic measurements, the results obtained were used to derive information about $BiBr_3$, both gaseous and solid.

Experimental

The method was the same as that used in the chloride work,[2] except that the condensed Bi–Br sample was analyzed by evaporating it to dryness twice with concentrated HNO_3 and then igniting to Bi_2O_3 in air at 600°. The $BiBr_3$ was made from Bi_2O_3 and HBr, dried and doubly distilled in an N_2 stream.

Results

Equilibrium Constants.—The experimental quantities from which the equilibrium constants can be derived are the moles of N_2 passed, the weight of the Bi–Br sample transported through the gas by the N_2, the weight of Bi_2O_3 produced from the Bi–Br, and a diffusion correction.[2] These quantities are given in Table I.

As in the chloride case[2] the results were fitted to the general equilibrium

$$2x/3\ \mathrm{Bi(l)} + x/3\ \mathrm{BiBr_3(g)} = \mathrm{Bi}_x\mathrm{Br}_x\mathrm{(g)}$$

A plot of logarithm of $BiBr_3$ pressure *vs.* logarithm of BiBr pressure can be used (a) to show that only one gaseous subhalide species is important in the equilibrium, and (b) to derive x since the slope of the line equals $3/x$. The data of Table I were plotted in that fashion. It was found that at each temperature the points followed a straight line with no systematic deviation; therefore, over the range of pressures studied only one gaseous subhalide is important in the equilibrium. The slope of the lines ranged from 2.9 to 3.1; consequently, x is 1.0 ± 0.03. Thus, we identify the gaseous subhalide species to be BiBr.

The equilibrium studied was, therefore

$$2/3\ \mathrm{Bi(l)} + 1/3\ \mathrm{BiBr_3(g)} = \mathrm{BiBr(g)} \qquad (1)$$

If one assumes that the fugacities of the gaseous species are equal to their pressures, the equilibrium constant becomes

$$K = \frac{p_{\mathrm{BiBr}}}{(p_{\mathrm{BiBr_3}})^{1/2}\,(a_{\mathrm{Bi}})^{2/3}}$$

The equilibrium constants, calculated for pressures expressed in atmospheres (so that the standard state of the gases is one atm.) and assuming the activity of liquid Bi to be unity, are given in Table I.

Enthalpies.—The enthalpy change for reaction 1 can be derived from the equilibrium constant and its change with temperature. To do so, the logarithm of the equilibrium constant was plotted *vs.* $1/T$. The slope of that line gave an enthalpy change of 21.3 ± 0.5 kcal. This may be taken as the enthalpy change for reaction 1 in the region of 925°K.

From this value the enthalpy change at 298°K. for the reaction

$$2/3\ \mathrm{Bi(s)} + 1/3\ \mathrm{BiBr_3(s)} = \mathrm{BiBr(g)}$$

(1) This work was made possible by the financial support of the Research Division of the United States Atomic Energy Commission.

(2) D. Cubicciotti, THIS JOURNAL, **64**, 791 (1960).

TABLE I

EXPERIMENTAL RESULTS AND EQUILIBRIUM CONSTANTS

Bi temp., °C.	Duration of expt., min.	Moles N_2, passed	Sample wt., g.	Bi_2O_3 wt., g.	Amount diffused, g.	p_{BiBr_3} mm.	p_{BiBr} mm.	$K \times 10^2$
606	1110	0.463	0.0942	0.0728	0.0020	0.040	0.46	1.63
607	1155	.462	.1117	.0842	.0025	.074	.51	1.46
607	972	.425	.1404	.1040	.0028	.125	.66	1.58
607	1050	.335	.1180	.0872	.0032	.136	.69	1.61
608	1262	.172	.1105	.0769	.0068	.393	.98	1.60
608	360	.113	.0960	.0645	.0025	.65	1.15	1.60
606	1097	.309	.2902	.1936	.0080	.74	1.23	1.63
607	396	.124	.1238	.0820	.0031	.828	1.28	1.63
608	1020	.125	.1872	.1196	.0114	1.40	1.55	1.67
633	1137	.326	.1643	.1226	.0051	0.176	1.01	2.17
632	1025	.306	.1952	.1428	.0058	.275	1.20	2.22
632	950	.272	.2852	.1990	.0085	.65	1.65	2.29
633	945	.167	.2728	.1806	.0126	1.32	2.04	2.23
633	970	.125	.2618	.1695	.0158	1.85	2.30	2.26
664	1028	.0618	.0789	.0576	.0115	0.407	2.10	3.41
663	1040	.299	.3894	.2822	.0122	0.61	2.38	3.37
664	978	.0450	.0928	.0647	.0175	1.07	2.74	3.22
662	1015	.106	.2122	.1471	.0174	1.24	2.95	3.34
661	300	.0363	.0776	.0531	.0055	1.43	3.03	3.24
662	900	.0399	.1165	.0789	.0219	1.80	3.42	3.37
661	324	.0398	.0997	.0667	.0068	1.92	3.22	3.11
663	990	.0371	.1154	.0773	.0256	1.94	3.35	3.04
662	995	.104	.2808	.1890	.0223	1.94	3.49	3.43
661	945	.0729	.2280	.1507	.0244	2.40	3.65	3.27
703	967	.0802	.1192	.0905	.0153	0.374	2.84	4.74
699	1058	.0553	.1228	.0917	.0240	.632	3.76	5.36
701	990	.0368	.1022	.0748	.0275	.891	3.95	4.94
699	950	.0514	.1300	.0952	.0243	.89	4.02	5.01
700	810	.0961	.2190	.1605	.0187	.91	4.10	5.08
704	938	.0404	.1121	.0820	.0260	.94	4.17	5.12
700	337	.0364	.1054	.0753	.0096	1.44	4.74	5.02
700	900	.0375	.1395	.0988	.0325	1.67	4.97	5.04
699	1010	.0346	.1455	.1028	.0415	1.78	5.17	5.12
699	292	.0392	.1873	.1268	.0130	3.42	6.45	5.13
710	1006	.0505	.1150	.0865	.0241	0.59	3.85	5.52
710	960	.0269	.0875	.0657	.0322	0.68	4.37	5.97
709	1035	.0417	.1121	.0834	.0287	0.75	4.13	5.48

was found to be 33.6 ± 1 kcal. The data used to derive that value were obtained from the following sources. For Bi the heat capacity of the solid and the liquid and the heat of fusion are given by Kubaschewski and Evans.[3] The heat capacity of BiBr gas was estimated to be 9 cal./mole degree, based on the rules for such estimation given by Kubaschewski and Evans.[3] For $BiBr_3$ gas the heat capacity was estimated to be 20 cal./mole degree based on the value 19 for $BiCl_3$ gas.[4] The heat of evaporation of $BiBr_3$ was taken from vapor pressure measurements.[5] The heat of fusion plus the heat of the transition of solid $BiBr_3$ at 155° were assumed to be 5.5 kcal. This was derived from the entropy of fusion of $BiCl_3$.[6] The heat capacities of the solid and liquid were estimated by the rules of Kubaschewski and Evans.[3] The value for the solid was taken to be 26 cal./mole degree up to the transition temperature, and above that temperature the solid and liquid values were taken to be 29.

The dissociation energy of gaseous BiBr is accurately known from spectroscopic data[7] and its enthalpy of formation at 298°K. derived from that value is 12.7 ± 0.3 kcal./mole.[4] This can be used to derive the enthalpy of formation of $BiBr_3$, which has not been previously determined. With the use of these data the enthalpy of formation of solid $BiBr_3$ at 298°K. is −63 ± 3 kcal./mole.

Entropies.—The standard free energy change for reaction 1 is calculated from the equilibrium constants to be 7.4 ± 0.1 kcal. at 600° and 5.7 ± 0.1 at 700°. These lead to a value of 17 ± 2 e.u. for

(3) O. Kubaschewski and E. C. Evans, "Metallurgical Thermochemistry," 2nd Ed., John Wiley and Sons, New York, N. Y., 1956.

(4) F. D. Rossini, D. D. Wagman, W. H. Evans, L. Levine and I. Jaffe, National Bureau of Standards, Circular 500, 1952.

(5) D. Cubicciotti and F. J. Keneshea, Jr., THIS JOURNAL, **62**, 999 (1958).

(6) S. W. Mayer, S. J. Yosim and L. E. Topol, *ibid.*, **64**, 238 (1960).

(7) T. L. Cottrell, "Strengths of Chemical Bonds," 2nd Ed., Butterworths, London, 1958.

the entropy change of reaction 1 at 650°, measured by this study.

The absolute entropies of the two gaseous species can be calculated from estimated molecular constant data. For BiBr the internuclear distance has been estimated[8] to be 2.48 Å., and the fundamental vibration frequency has been measured.[9] It was assumed that there was no electronic contribution to the entropy. These lead to a calculated absolute standard entropy of 73.6 e.u. for BiBr gas at 650°.

For $BiBr_3$ the internuclear distances have been measured.[10] The fundamental vibration frequencies can be estimated from the force constants of $BiCl_3$ with Badger's rule. The frequencies estimated in that way are 210(1), 91(1), 155(2) and 65(2) $cm.^{-1}$. (Numbers in parentheses are the degeneracies of the vibrational mode.) The absolute standard entropy of $BiBr_3$ gas calculated from those molecular constants is 116 e.u. at 650°.

When combined with the experimental values[3] for Bi, these entropies for BiBr and $BiBr_3$ lead to a calculated entropy change at 650° for reaction 1 of 17 e.u. This is in good agreement with the experimental value and provides additional evidence that reaction 1 was indeed the equilibrium studied, and BiBr was the only important subhalide species.

Acknowledgment.—The author is grateful to Mr. William E. Robbins who performed the experimental work.

(8) D. P. Stevenson, *J. Chem. Phys.*, **8**, 898 (1940).

(9) G. Herzberg, "Molecular Spectra and Molecular Structure," Vol. I, 2nd Ed., D. Van Nostrand Co., New York, N. Y., 1950.

(10) H. A. Skinner and L. E. Sutton, *Trans. Faraday Soc.*, **36**, 681 (1940).

PARTICLE SIZE DISTRIBUTION IN MONODISPERSE SULFUR HYDROSOLS[1]

BY ANTHONY J. PETRO

Chemicals Research Division, Esso Research and Engineering Company

Received April 22, 1960

The particle size distribution in monodisperse sulfur hydrosols has been investigated by a new instrument, the Coulter Counter. The hydrosols were prepared by the acid decomposition of dilute thiosulfate solutions and the particle sizes were measured independently by the Higher Order Tyndall Scattering method. Distribution curves were constructed from Counter data obtained at increments of 0.02 μ diameter. The results indicate that the distribution of particle sizes in these systems is relatively broad but single-peaked. Higher Order Tyndall Scattering was found to exist for mixtures of two monodisperse sols and it is concluded that this method is a measure only of the most populated particle size.

Introduction

Monodisperse sulfur hydrosols, or colloidal suspensions of sulfur with a very narrow distribution of particle sizes, were first prepared by Barnes and LaMer in 1946.[2] Further work by LaMer and his associates established the light scattering,[3,4] and electrokinetic[5] properties of these systems, and the mechanism[6-9] and kinetics[10] of their production. The bulk of the data indicates a very sharp distribution of particle sizes.

Until recently there has been no method available which could be used to determine successfully the particle size distribution of these sulfur sols. The electron microscope is inapplicable because osmotic effects cause the particles, in the form of supercooled liquid λ-sulfur droplets, to rupture during preparation of specimens.[11] In the past several years a novel method has been developed for measuring particle size. The method is referred to as the Coulter Method, the instrument used being the Coulter Counter.[12,13] This method was used in the present work to determine the actual distribution of particle sizes in these preparations.

Experimental

Preparation of Sols.—Sols were prepared by adding to 480 ml. of distilled water, 10 ml. of 0.1 *M* HCl and 10 ml. of 0.1 *M* $Na_2S_2O_3$, thus making the concentration of each reagent 0.002 *M*. The flask was thoroughly shaken and placed in a water-bath thermostated at 25 ± 0.1° for the desired length of time, usually 8–12 hours. After the sol had developed, a sample was removed and the particle size was determined by the Higher Order Tyndall Scattering (HOTS) Method according to Johnson and LaMer.[4] Another sample was treated as described below for measurement of particle size distribution by the Coulter Counter.

Particle Size by Light Scattering.—Monodisperse sols were observed[3] to scatter white light into its component colors, the number and positions of the red hues being a function of the particle size of the suspended sulfur.[4] By referring the angular positions of the scattered red "orders" to a set of standard curves, measurement of particle size by this method can be accomplished in less than one minute to within 0.01 μ in diameter. The scattering curves used in the present work were those of Petro and Smellie.[14] This set of curves is somewhat different from that published by Johnson and LaMer,[4] but it was found to be completely reproducible

(1) Portions of this paper were read before the American Chemical Society, Division of Colloid Science, Boston, Massachusetts, April, 1959.

(2) V. K. LaMer and M. D. Barnes, *J. Colloid Sci.*, **1**, 71, 79 (1946).

(3) M. D. Barnes, A. S. Kenyon, E. M. Zaiser and V. K. LaMer, *ibid.*, **2**, 349 (1947).

(4) I. Johnson and V. K. LaMer, *J. Am. Chem. Soc.*, **69**, 1184 (1947).

(5) R. H. Smellie, Jr., and V. K. LaMer, THIS JOURNAL, **58**, 583 (1954).

(6) V. K. LaMer and A. S. Kenyon, *J. Colloid Sci.*, **2**, 257 (1947).

(7) E. M. Zaiser and V. K. LaMer, *ibid.*, **3**, 571 (1948).

(8) V. K. LaMer and R. H. Dinegar, *J. Am. Chem. Soc.*, **72**, 4847 (1950).

(9) H. Reiss and V. K. LaMer, *J. Chem. Phys.*, **18**, 1 (1950).

(10) R. H. Dinegar, R. H. Smellie, Jr., and V. K. LaMer, *J. Am. Chem. Soc.*, **73**, 2050 (1951).

(11) V. K. LaMer, private communication.

(12) W. C. Coulter, "High Speed Automatic Blood Cell Counter and Cell Size Analyzer," paper presented at the National Electronics Conference, Chicago, Illinois, 1956. Also, R. H. Berg, ASTM Special Tech. Publ. No. 234,245 (1959).

(13) "Theory of the Coulter Counter," Coulter Industrial Sales Co., Elmhurst, Illinois, 1957.

(14) A. J. Petro and R. H. Smellie, Jr., to be published.

as long as two precautions were taken in preparing sols: namely, stock solutions of thiosulfate more than 5 days old could not be used, and the stock solutions must be prepared with freshly boiled distilled water. Otherwise, completely non-reproducible particle sizes are obtained, the scattering data corresponding to two different sizes. This scattering data has been verified independently[15] by measuring light transmission as a function of wave length.

Particle Size by Coulter Counter.—The main feature of the Coulter Counter is the tiny aperture drilled through a sapphire wafer which is cemented into the wall of a glass tube. This aperture allows completion of the electrical path between an inner and an outer electrode through an electrolyte solution. In the present work, an aperture 30 μ in diameter was used.

As a particle passes through the aperture it displaces its own volume of conducting electrolyte solution, causing a momentary change in conductivity of the circuit. The pulse is amplified and counted if its magnitude is above a preselected threshold value. The particles are made to pass through the aperture by establishing a pressure differential across the orifice as a result of displacing the mercury in a manometer connected in series. As liquid (and particles) flows through the aperture, the mercury returns to equilibrium and in so doing interrupts the start–stop connections in the manometer. In this way a reproducible sample volume is counted and each count is automatic. A typical count, at a given threshold setting, taken with the 30 μ aperture and on a 50 μl. sample volume, requires *ca.* 15 sec. for completion and may register as many as 100,000 counts.

The Counter was calibrated with a sample of monodisperse polystyrene latex obtained from the Dow Chemical Company. The particle diameter was reported to be 1.171 μ with a standard deviation of 0.0133 μ. However, upon comparing the HOTS of this material with the data of Plesner and LaMer[16] the diameter appeared to be 0.94 μ. This apparent discrepancy was resolved when it was realized that the scattering angles of Plesner and LaMer were the supplements of the angles read on the apparatus used in the present work and in previous work on sulfur sold.[4,14] The present instrument defines 180° as complete transmission and 0° as complete reflection.

The number of particles counted at a given threshold setting was the average of at least four trials, the electrode polarity being reversed after each count. The particle size corresponding to the threshold setting was calculated by the relationship[13]

$$d = kt^{1/3}$$

where d is the diameter, t is the threshold value in dial units, and k is a proportionality constant which was found to be 1.30. Differential particle size distribution curves were constructed by plotting $\bar{t}\,\Delta n/\Delta d$ *vs.* $\bar{d}$.

For the present work, a sample of sulfur sol was diluted with three times its own volume of 0.9% NaCl solution. This dilution ratio was chosen in order to obtain optimum values of conductivity and particle concentration. Counts were taken on the solution at intervals of *ca.* 0.02 μ diameter.

Two types of sols were produced for study. One had a "poor" scattering spectrum, *i.e.*, there was no correspondence to a set of angles for a single particle size, and the second type had a "good" spectrum. The former was prepared merely by not boiling the distilled water prior to preparing the stock thiosulfate solution.

Discussion

In order to interpret the results of this work it is desirable to review briefly some of the pertinent aspects of monodisperse sulfur hydrosols. Immediately upon mixing the reagents, elemental sulfur begins to be produced. This sulfur, however, remains in solution until a critical, reproducible, supersaturation level (*ca.* 3.1×10^{-6} g. at./l.)[10] is attained. At this stage, spontaneous nucleation occurs, producing *ca.* 4×10^{6} particles/ml. Continued formation of sulfur is so slow, because of the low concentrations of reagents, that further nucleation does not take place. The particles already formed grow uniformly by diffusion of newly-produced sulfur onto the particle surfaces. The key to monodispersity, then, is the control of the rate of reaction so that nucleation occurs once, or only over a very brief span of time.

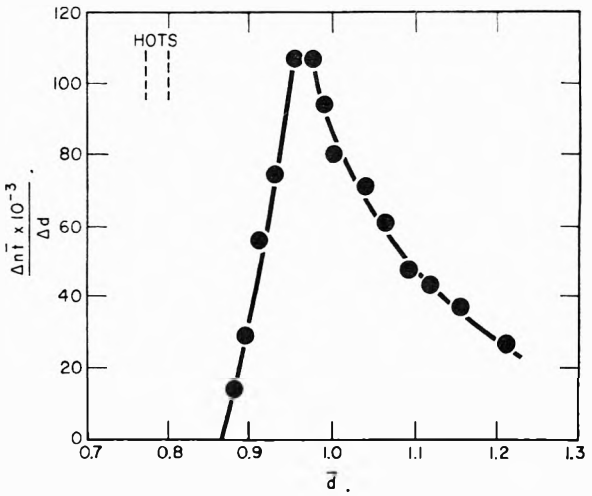

Fig. 1.—Particle size distribution curve for "poor" sol. —, HOTS results; —, Coulter Counter results. $\bar{d}$ is in microns.

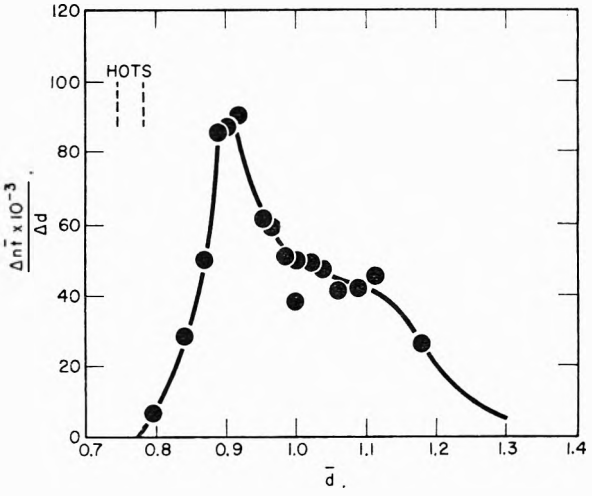

Fig. 2.—Particle size distribution curve for "poor" sol. —, HOTS results; —, Coulter Counter results. $\bar{d}$ is in microns.

One experimental problem had to be resolved before completely accepting the results obtained in this work. The Counter requires a conducting medium for operation. The effect of salts on the electrokinetic properties[5] and the kinetics of the reaction[5,17] would lead one to suspect that dilution of the sol with NaCl solution may significantly alter the system. To answer this question, a sample of counting solution was rechecked by the HOTS two hours after preparation and was found to show exactly the same spectrum as did the original undiluted sol. That is, not only was agglomeration undetectable as was any particle size increase due to salting-out dissolved sulfur, but the *p*H

(15) R. Toggenburger, M.S. Thesis, Trinity College, 1956.

(16) I. W. Plesner and V. K. LaMer, *J. Polymer Sci.*, **24**, 147 (1957).

(17) R. H. Dinegar and R. H. Smellie, Jr., *J. Colloid Sci.*, **7**, 370 (1952).

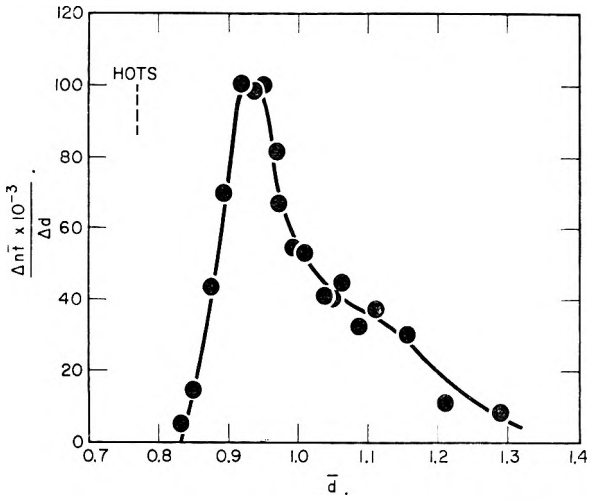

Fig. 3.—Particle size distribution curve for "good" sol. —, HOTS results; —, Coulter Counter results. $\bar{d}$ is in microns.

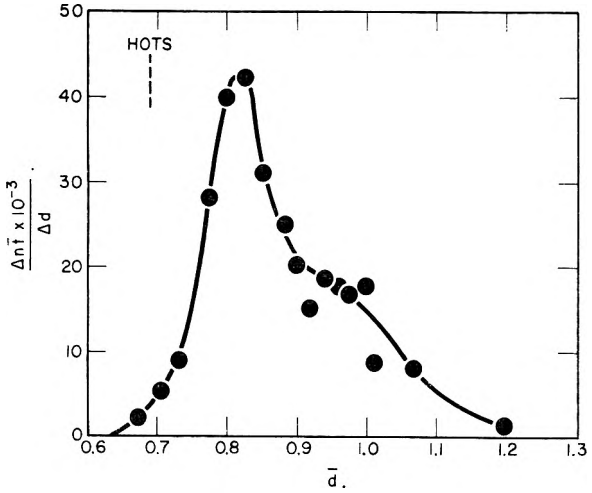

Fig. 4.—Particle size distribution curve for sol grown while stirred slowly. ---, HOTS results; —, Coulter Counter results. $\bar{d}$ is in microns.

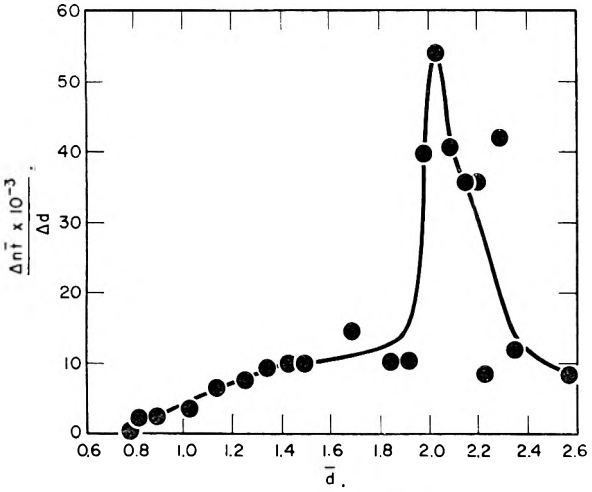

Fig. 5.—Particle size distribution curve for sol grown in the presence of 0.15 M (0.9%) NaCl. $\bar{d}$ is in microns.

increase (2.8 to 3.4) resulting from dilution by the salt solution effectively stopped the formation of further sulfur and, hence, stopped further growth of the particles.[17] Therefore, the length of time taken for the complete counting of the sample was immaterial.

Figures 1 and 2 show typical distributions obtained for "poor" sols. The diameter values measured by the HOTS are indicated by the dotted lines, the smaller values corresponding to obtuse ($90 < \Theta < 180°$) angle scattering and the larger values to acute ($\theta < 90°$) angle scattering. Although the peaks are single and well-defined, the distributions extend over a range of *ca.* 0.5 μ in diameter with a possible second peak appearing in Fig. 2.

Figure 3 shows a distribution for a "good" sol as indicated by the single diameter value obtained by the HOTS. This distribution is seen to be narrower than those of Figs. 1 and 2 by comparing the (height)/(width at mid-height) ratios which are 2.8, *ca.* 2.5, and 4.0 for Figs. 2, 3 and 4, respectively.

The discrepancy between the HOTS values and the Counter peak diameter is rather large considering the fact that both methods have apparently been calibrated to give the absolute size. However, since the calibration of the Counter was accomplished with polystyrene spheres, it is possible that the instrument reacts differently to sulfur, consistently yielding a diameter that is apparently *ca.* 0.15 μ greater than the HOTS value. It is also possible that the stated particle size of the polystyrene is too large by *ca.* 20%. There is no evidence to support either of these possibilities.

Figure 4 shows a distribution for a sol grown while being slowly (*ca.* 75 r.p.m.) stirred. This method was used in order to attempt to prepare a sol with a sharper distribution by preventing settling, with consequent alteration of local particle concentrations and concomittant widening of the distribution, but without affecting the diffusion gradients. It can be seen, however, that this experiment leads to a sol with a distribution almost identical to that of Fig. 3, the h/w ratio being 4.0.

Figure 5 shows the distribution of a sol prepared with 0.002 M HCl, 0.002 M $Na_2S_2O_3$ and 0.15 M (0.9%) NaCl and allowed to develop for 27 hours. The peak size is well beyond the range of the HOTS (0.4–1.2 μ) but the total distribution is quite wide. The peak size at *ca.* 2.0 μ is larger than the 1.3–1.4 μ value expected for a 27-hour sol. This result is consistent with observations of Zaiser and LaMer[7] who found the appearance of colloidal sulfur to occur earlier in 0.2 M KCl. Further, according to their results,[18] the particles grow faster in the presence of this high concentration of salt, giving a larger particle size in a given time, as was found. Apparently, initial condensation of sulfur is promoted by a salting-out effect. Since this condensation occurs earlier than in the absence of salt, when the rate of production of sulfur is still high, diffusion of newly-produced sulfur to the already-formed particles is not sufficiently rapid to prevent reattainment of the critical supersaturation level. Later nucleation might, therefore, be expected, giving rise to an abnormally wide distribution curve. Also consistent with this explanation is the fact that the total number of particles in this sol was

(18) Ref. 6, p. 573, Fig. 2, curve C.

found to be only 10% of the number formed in the absence of salt.

Each of the sols in Figs. 1–4 is seen to contain a tail of larger particles which may arise from three sources. Coalescence during early stages of growth, nucleation on minute dust particles, dissolved gases, etc., or non-uniform diffusion gradients around each particle can result in such distributions. Regardless of the mechanism by which the relatively wide distribution results, the fact that it exists is unexpected in view of the experiments of Johnson and LaMer.[4] These workers mixed, in varying proportions, two sols differing by only 0.02 μ in particle diameter as determined by the HOTS. The spectra of the individual sols were such that where one had a red band, the other had a green one. A mixture of equal volumes of the sols had no higher order scattering whereas intermediate mixtures showed broadening and dilution of the red orders. Johnson and LaMer concluded that if 10% of the particles were 2% larger or smaller than the mean size, they would be noticeable by the resultant HOTS and, hence, these preparations were highly monodisperse. The half-width of each of curves 3 and 4, however, is 0.12 μ, six times the difference in particle diameter of the sols used by Johnson and LaMer.

In order to investigate this abnormal result further, two sols whose particle diameters differed by more than 0.02 μ were mixed. The experiment of Johnson and LaMer[4] must have produced a resultant broad but nearly single-peaked distribution since the size difference was so small. Two mixtures were prepared. The first was a 50/50 mixture of sols whose diameters were 0.62 and 0.77 μ. The respective sets of HOTS angles were: 54, 77.5, 114, 146; and 40, 60.5, 81, 104, 130.5, 161. The HOTS data for the mixture was: 58–70 (vague), 79 (strong), 107.5 (strong), 135 (vague). The latter set of angles corresponds closely with that expected for a sol of diameter 0.79 μ, *viz.*, 38, 59, 79.5, 107.5, 135, 162, despite the fact that two orders have been lost in the mixing of the component sols.

The second was a 50/50 mixture of sols whose diameters were 0.63 and 0.73 μ. The respective sets of HOTS angles were: 52, 77, 111, 146; and 42, 64.5, 93, 128, 157. The HOTS data for the mixture was: 43.5 (strong), 76.5 (strong), 108 (vague), 151.5 (vague). In this case, mixing results in resolution and cancellation into a set of orders which

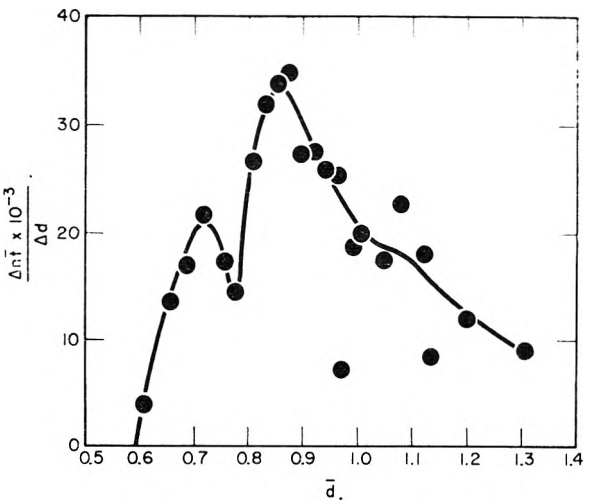

Fig. 6.—Particle size distribution curve for mixture 2, equal volumes of sols of 0.63 and 0.73 μ diameter particles.

does not correspond to a single particle size. This is apparently due to the smaller separation of particle sizes compared to the first mixture. In each of these two cases the combination of red orders is such that where their positions are very close they will reinforce but where farther apart they will cancel, with an intermediate region of dilution of intensity and broadening of the orders. The distribution of particle sizes in the second mixture, shown in Fig. 6, is that which would be expected by overlapping two similar but separated curves.

The systems just described are obviously not monodisperse, yet the very important result is noted that there is some scattering although it is less than for a "monodisperse" system. It may be concluded, therefore, that the HOTS is not completely indicative of a sharp distribution of particle sizes but is due to an unbalance in the number of particles scattering a given color at a given angle. If this unbalance exceeds a critical value, which is as yet undetermined, HOTS results and the corresponding particle size is a measure of the most populated size value.

Acknowledgment.—The author wishes to thank Professors R. H. Smellie, Jr., and V. K. LaMer for several very interesting and helpful discussions concerned with this study and for the loan of the apparatus for the HOTS measurements.

THE KINETICS OF THE OXALATE CATALYSIS OF THE IRON(II)–IRON(III) ELECTRON-EXCHANGE REACTION IN AQUEOUS SOLUTION[1]

BY R. A. HORNE[2]

Chemistry Departments, Brookhaven National Laboratory and Columbia University, Upton, N. Y., and New York City

Received April 22, 1960

The kinetics of the electron-exchange reaction between the two oxidation states of iron is first order in both iron(II) and iron(III) and oxalate-catalyzed in aqueous perchloric–oxalic acid media of 0.55 ionic strength. The specific reaction rate constants for the reaction path involving ferrous ion and $FeC_2O_4^+$ are 700, 1100 and 2140 sec.$^{-1}f^{-1}$ at 0, 10 and 20°, respectively, corresponding to an activation energy of 9.2 kcal. mole^{-1} and an entropy of activation of −14.1 cal. mole^{-1} deg.$^{-1}$. The specific reaction rate constants for the path involving ferrous ion and $Fe(C_2O_4)_3^-$ are in the range 2500–4500 sec.$^{-1}f^{-1}$. The exchange is also catalyzed by silver foil and by acetate, succinate and phenolate anions.

Introduction

Since the classical work of Hevesy and Zechmeister[3] on the electron-exchange between lead(II) and lead(IV) a great deal of effort had been devoted to studies of oxidation–reduction processes in aqueous solution, especially to those involving electron-exchange between two valence states of the same element.[4] In particular, the kinetics of the iron(II)–iron(III) electron-exchange and the catalysis of this reaction by complexing anions have received considerable attention.

Attempts to interpret the kinetics and establish the mechanism of the iron(II)–iron(III) exchange have tended to fall into two principal categories—anion bridging theories[5–10] and water bridging theories.[11–17] If the electron is transferred across an anion bridge, one might reasonably expect that the activation energy of the exchange process should change as the complexing anion is changed. In the case of the exchange involving Cr^{++} and $(NH_3)_5CrA^{++}$, Ogard and Taube[18] have observed such a correlation with the size of the complexing anion, the activation energies being 13.4, 11.1 and 8.5 kcal. mole^{-1} for fluoride, chloride and bromide ions, respectively. However, if the exchange involves a water bridge a marked heavy water isotope effect, even for the anion catalyzed processes,[17] and little dependence on the nature of the complexing anion is anticipated. In the case of the iron(II)–iron(III) exchange both anticipations have been vindicated.[6,19] The activation energies for the exchanges involving Fe^{++}, $FeClO_4^{++}$, $FeOH^{++}$, FeF^{++}, $FeCl^{++}$, $FeSCN^{++}$, FeF_2^+, $FeCl_2^+$ and $Fe(SCN)_2^+$ are 9.9, 9.5, 7.4, 9.1, 8.8, 7.9, 9.5, 9.7 and 8.6 kcal./mole respectively (see ref. 5, 20, 5, 12, 5, 21, 12, 5 and 21, respectively)—a range of values not outside the range of experimental error. The exchange involving FeN_3^{++} appears to be an exception.[22] But, it can be argued, fluoride, chloride, bromide, and even thiocyanate ion are similar. Any differences in the activation energies of their catalyses might be less than experimental error and hence escape detection. For this reason the catalysis of the iron(II)–iron(III) electron exchange reaction by a larger, non-halide, more structurally complex complexing anion, such as oxalate, is of interest.

Experimental Procedures

The iron(II) and iron(III) perchlorate stock solutions, the tracer Fe^{55} solution, and the solutions of perchloric acid, sodium perchlorate and buffered 2,2′-dipyridyl were prepared from the same quality materials and purified and analyzed in the same manner as described previously by Silverman and Dodson.[5] The oxalic acid solutions (Baker and Adamson, A.C.S., reagent) were analyzed by (a) titration with standard sodium hydroxide and (b) titration with standard potassium permanganate.[23] In the present experiments the increases in the hydrogen ion concentration and in the ionic strength due to the added oxalic acid were negligible.

The details of the experimental procedure have been described previously by Silverman and Dodson.[5] This procedure involves removing aliquots from the reaction mixture at regular time intervals; quenching the reaction by adding each aliquot to a buffered 2,2′-dipyridyl solution, thus removing the iron(II) as a complex; and precipitating, mounting and counting the iron(III) as the hydroxide.

Results and Discussion

The experimental results for the oxalate catalysis of the iron(II)–iron(III) electron-exchange reaction in aqueous solution are shown in Table I and Fig. 1.

In aqueous oxalate media, as in perchlorate,[5,20] fluoride,[12] chloride,[5] bromide[16] and thiocyanate[16,21]

(1) Research performed under the auspices of the U. S. Atomic Energy Commission.

(2) Joseph Kaye and Co., Inc., 49 Hampshire St., Cambridge Massachusetts.

(3) G. Hevesy and L. Zechmeister, *Ber.*, **53**, 410 (1920).

(4) (a) Notre Dame Symposium on Electron Transfer, THIS JOURNAL, **56**, 801ff (1952); (b) C. B. Amphlett, *Quart. Rev., London Chem. Soc.*, **8**, 219 (1954); (c) F. Basolo and R. G. Pearson, "Mechanisms of Inorganic Reactions," John Wiley and Sons, Inc., New York, N. Y., 1958, ch. 7; (d) University of Toronto Symposium on Charge Transfer Processes, *Canad. J. Chem.*, **37**, 120ff (1959).

(5) J. Silverman and R. W. Dodson, THIS JOURNAL, **56**, 846 (1952).

(6) J. Hudis and R. W. Dodson, *J. Am. Chem. Soc.*, **78**, 911 (1956).

(7) W. F. Libby, THIS JOURNAL, **56**, 863 (1952).

(8) M. Haissinsky, Discussion of "Electron Transfer in Solution and at Electrodes," French Soc. Phys. Chem., Paris, May 8, 1951, ONR, London, Tech. Rept. ONRL-73-51 (Aug. 20, 1951), pp. 1–2.

(9) H. Taube, *et al.*, *J. Am. Chem. Soc.*, **75**, 4118 (1953); **76**, 2103, 4053 (1954); **77**, 4481 (1955).

(10) D. L. Ball and E. L. King, *ibid.*, **80**, 1091 (1958).

(11) W. L. Reynolds and R. W. Lumry, *J. Chem. Phys.*, **23**, 2460 (1955).

(12) J. Hudis and A. C. Wahl, *J. Am. Chem. Soc.*, **75**, 4153 (1953).

(13) J. Weiss, *J. Chem. Phys.*, **19**, 1066 (1951).

(14) R. Platzman and J. Frank, *Z. Physik*, **138**, 411 (1954).

(15) R. W. Dodson and N. Davidson, in the discussion of ref. 7.

(16) R. A. Horne, Ph.D. Thesis, Columbia University, 1955.

(17) R. A. Horne, Paper presented at the 135th Natl. Meeting of the Am. Chem. Soc., Boston, 1959.

(18) A. E. Ogard and H. Taube, *J. Am. Chem. Soc.*, **80**, 1084 (1958).

(19) N. Sutin and R. W. Dodson, Paper presented at the 136th Natl. Meeting of the Am. Chem. Soc., Atlantic City, 1959.

(20) R. A. Horne, *Nature*, **181**, 410 (1958).

(21) G. S. Laurence, *Trans. Faraday Soc.*, **53**, 1326 (1957).

(22) D. Bunn, F. S. Dainton and S. Duckworth, *Trans. Faraday Soc.* **55**, 1267 (1959).

(23) L. F. Hamilton and S. C. Simpson, "Talbot's Quantitative Chemical Analysis," The Macmillan Co., New York, N. Y., 1946, pp. 129f, 160f.

TABLE I

THE IRON(II)-IRON(III) ELECTRON-EXCHANGE REACTION IN AQUEOUS PERCHLORIC-OXALIC ACID MEDIA

Ionic strength = 0.55, $(H^+) = 0.548$ as $HClO_4$, $(Fe(II)) = 1.02 \times 10^{-4} f$, and $(Fe(III)) = 0.650 \times 10^{-4} f$

Added oxalic acid $\times 10^5$, f	Half-life $t_{1/2}$, min.	Specific reaction rate constant, k, sec.$^{-1}$ f^{-1}
Temp. = 0.02 ± 0.01°		
0.000	....	1.31 ± 0.08 (av.)
2.00	17.7	3.89 ± 0.83
4.00	8.21	8.46 ± 1.16
6.00	5.48	12.6 ± 2.1
8.00	4.55	15.2 ± 1.6
10.0	3.70	20.3 ± 9.7
100	(0.88)	(79)
9000	(0.5)	(137)
Temp. = 9.88 ± 0.05°		
0.000	....	3.44 ± 0.13 (av.)
2.00	6.50	10.6 ± 0.5
4.00	4.85	14.2 ± 3.3
6.00	3.55	19.5 ± 1.6
8.00	2.67	26.0 ± 3.5
10.0	2.16	32.0 ± 11.0
Temp. = 20.57 ± 0.04°		
0.000	....	8.22 ± 1.43 (av.)
2.00	3.54	19.6 ± 3.0
6.00	1.45	47.5 ± 2.3
8.00	1.05	65.7 ± 0.0

media, the exchange is first order with respect to both of the iron valence states

$$R = k(\mathrm{Fe(II)})(\mathrm{Fe(III)}) \qquad (1)$$

where R is the rate of the reaction, k the over-all specific reaction rate constant, and (Fe(II)) and (Fe(III)) are the total concentrations of the iron(II) and iron(III) species. The over-all specific reaction rate constant was evaluated, corrections being made for induced exchange when indicated, by using a McKay plot[24] and the expression

$$k = 0.693\{[(\mathrm{Fe(II)}) + (\mathrm{Fe(III)})]t_{1/2}\}^{-1} \qquad (2)$$

where $t_{1/2}$ is the half-life of the exchange.

The formation of iron(II) and iron(III) complex ions can be represented by

$$Fe^{+++} + nA^{-a} \rightleftharpoons FeA_n^{3-na}, \quad \beta_{FeA_n} = (FeA_n^{3-na})/(Fe^{+++})(A^{-a})^n \qquad (3)$$

and

$$Fe^{++} + mA^{-a} \rightleftharpoons FeA_m^{2-ma}, \quad \gamma_{FeA_m} = (FeA_m^{2-ma})/(Fe^{++})(A^{-a})^m \qquad (4)$$

where β and γ are the over-all complex ion formation constants, and the exchange processes by

$$Fe^*A_n^{3-na} + FeA_m^{2-ma} \rightleftharpoons Fe^*A_m^{2-ma} + FeA_n^{3-na} \qquad (5)$$

The rate of a process such as (5) is then given by

$$R_{FeA_n-FeA_m} = k_{FeA_n-FeA_m}(FeA_n^{3-na})(FeA_m^{2-ma}) \qquad (6)$$

The over-all rate of the electron-exchange reaction is given by

$$R = \sum_{A,m,n} R_{FeA_n-FeA_m} = \sum_{A,m,n} k_{FeA_n-FeA_m}(FeA_n^{3-na})(FeA_m^{2-ma}) \qquad (7)$$

(24) H. A. C. McKay, *Nature*, **142**, 997 (1938).

Terms for polynuclear species, when significant, are readily added to expression 7. Equation 7 is quite general, being valid for all complexing anions, A, that have been studied to date, and for $n = 0$, 1 and 2. The limits on the values of m are unknown. Fortunately for many complexing anions $\beta >> \gamma$, and hence it may be possible to make the assumption that $m \approx 0$. Iron(II), for example, forms oxalate complexes[25] but they are less stable than the corresponding iron(III) complexes by a factor of 10^{13} and make a negligible contribution.[26] When $m = 0$ equation 7 becomes simply

$$R = \sum_{A,n} k_{FeA_n}(FeA_n^{3-na})(Fe^{++}) \qquad (8)$$

Now under these circumstances

$$(Fe^{++}) \approx (\mathrm{Fe(II)}) \qquad (9)$$

$$(Fe^{+++}) = (\mathrm{Fe(III)}) - \sum_{A,n}(FeA_n^{3-na}) = (\mathrm{Fe(III)}) - \sum_{A,n}\beta_{FeA_n}(Fe^{+++})(A^{-a})^n \qquad (10)$$

$$(Fe^{+++}) = (\mathrm{Fe(III)})/\left[1 + \sum_{A,n}\beta_{FeA_n}(A^{-a})^n\right] \qquad (11)$$

hence

$$R = \left[\frac{\sum_{A,n} k_{FeA_n}\beta_{FeA_n}(A^{-a})^n}{1 + \sum_{A,n}\beta_{FeA_n}(A^{-a})^n}\right](\mathrm{Fe(III)})(\mathrm{Fe(II)}) \qquad (12)$$

By comparison of equations 1 and 12 we see that the term in brackets in the latter is k.

For the case of the oxalate catalysis of the iron(II)-iron(III) electron-exchange reaction in perchlorate media the important terms in equation 8 are

$$R = k_{Fe}(Fe^{+++})(Fe^{++}) + k_{FeClO_4}(FeClO_4^{++})(Fe^{++}) + k_{FeOH}(FeOH^{++})(Fe^{++}) + k_{FeC_2O_4}(FeC_2O_4^{+})(Fe^{++}) + k_{Fe(C_2O_4)_2}(Fe(C_2O_4)_2^{-})(Fe^{++}) + \ldots \qquad (13)$$

The first two terms of equation 13 involve a controversial choice among the alternatives

(a) $\beta_{FeClO_4} \neq 0$, $k_{FeClO_4} \neq 0$, and $k_{Fe} \neq 0$
(b) $\beta_{FeClO_4} \neq 0$, $k_{FeClO_4} \neq 0$, and $k_{Fe} \approx 0$
(c) $\beta_{FeClO_4} \approx 0$, and $k_{Fe} \neq 0$

Hitherto alternative (c) has been preferred,[5,12,21] although there now appears to be evidence for (a) or (b).[20,27-29] Fortunately, for purposes of analyzing the oxalate catalysis, the first three terms in equation 13 can be combined into a single term

$$R = R_0' + k_{FeC_2O_4}(FeC_2O_4^{+})(Fe^{++}) + k_{Fe(C_2O_4)_2}(Fe(C_2O_4)_2^{-})(Fe^{++}) + \ldots \qquad (14)$$

where, since the ratic of the concentration of uncomplexed to complexed iron(III) is large (*e.g.*, about 40 at 10° with $10 \times 10^{-5} f$ total added oxalic acid), R_0' may be approximated by R_0

(25) M. Boltelsky, D. Chasson and S. F. Klein, *Anal. chim. Acta*, **8**, 460 (1953).

(26) H. von Stackelburg and H. von Freyhold, *Z. Elektrochem.*, **46**, 120 (1940).

(27) J. Sutton, *Nature*, **169**, 71 (1952).

(28) K. W. Sykes, *et al.*, "The Kinetics and Mechanism of Inorganic Reactions in Solutions," Chem. Soc., London, 1954, pp. 64 *et seq.*

(29) *Cf.* H. Coll, R. V. Nauman and P. W. West, *J. Am. Chem. Soc.*, **81**, 1284 (1959).

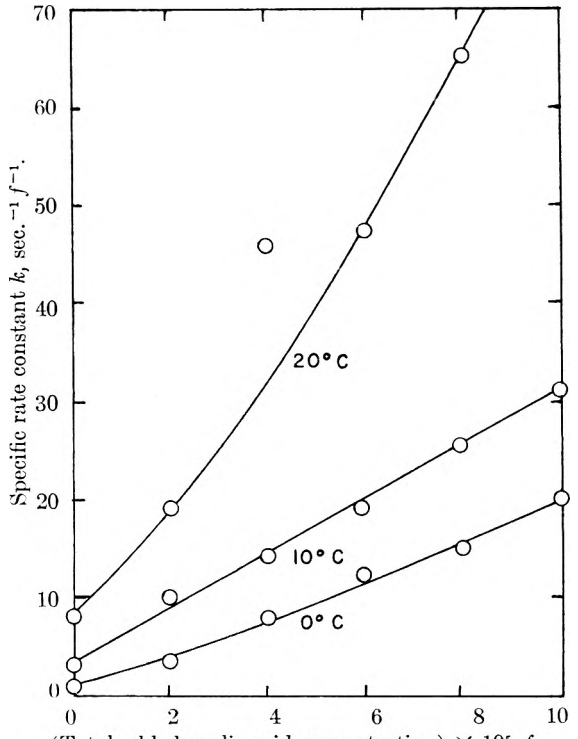

Fig. 1.—Oxalate catalysis of the iron(II)–iron(III) electron-exchange reaction.

$$R_0 = k_0(\mathrm{Fe(III)})(\mathrm{Fe(II)}) \qquad (15)$$

the rate of exchange under the same conditions of ionic strength and temperature but in the absence of oxalate ion, a term readily evaluated experimentally.

The method for analyzing the kinetic data for the anion-catalysis of the iron(II)–iron(III) electron-exchange reaction has been described by Silverman and Dodson.[5] However the analysis of the oxalate data is considerably complicated by the fact that oxalic is a weak acid, hence hydrogen ions compete with ferric ions for oxalates, and one can no longer make the simplifying assumption that the amount of complexing anion removed by complex-formation is negligible. The analysis is made even more difficult by the paucity of quantitative data concerning the formation constants of the ferric oxalate complexes.

At 25° and zero ionic strength[30]

$$H_2C_2O_4 \rightleftharpoons H^+ + HC_2O_4^-$$

$$K_1^0 = \frac{[H^+][HC_2O_4^-]}{[H_2C_2O_4]} = 5.36 \times 10^{-2} \qquad (16)$$

and

$$HC_2O_4^- \rightleftharpoons H^+ + C_2O_4^=$$

$$K_2^0 = \frac{[H^+][C_2O_4^=]}{[HC_2O_4^-]} = 5.3 \times 10^{-5} \qquad (17)$$

The corresponding values of K_1 and K_2 at an ionic strength of 0.55, calculated from an extended Debye–Hückel equation, estimating ionic radii on the basis of values cited by Pauling,[31] are 2.38 × 10^{-1} f and 7.80 × 10^{-4} f, respectively. The heat of the first ionization of oxalic acid can be estimated from the relation

$$\Delta F^0 = \Delta H^0 - T\Delta S^0 \qquad (18)$$

since the free energy can be calculated from K_1^0 and the entropy estimated by Pitzer's rule.[32] The value so obtained is −4.85 kcal./mole. The value of the heat of the second ionization of oxalic acid is readily calculated to be +0.73 kcal./mole from the empirical expression given by Pinching and Bates.[33] With the foregoing information values of K_1 and K_2 at 0, 10 and 20° and an ionic strength of 0.55 can be calculated. The results are summarized in Table II.

TABLE II

IONIZATION CONSTANTS OF OXALIC ACID AND THE FORMATION CONSTANTS OF IRON(III) OXALATE COMPLEXES AT 0.55 IONIC STRENGTH

Temp., °C.	K_1 for $H_2C_2O_4$ × 10, f	K_2 for $H_2C_2O_4$ × 10^4, f	$K_{FeC_2O_4^+}$ × 10^{-5}, f^{-1}	$K_{Fe(C_2O_4)_2^-}$ × 10^{-5}, f^{-1}	$K_{Fe(C_2O_4)_3^=}$ × 10^{-6}, f^{-1}
0	5.93	6.99	4.35	7.46	3.34
10	4.30	7.33	3.99	6.86	3.07
20	3.22	7.64	3.65	6.27	2.81

Lambling[34] has found the following values for the formation constants[35] of the iron(III) oxalate complexes

$$K^0_{FeC_2O_4} = [FeC_2O_4^+]/[Fe^{+++}][C_2O_4^=] = 2.14 \times 10^9 \qquad (19)$$

$$K^0_{Fe(C_2O_4)_2} = [FeC_2O_4)_2^-]/[FeC_2O_4^+][C_2O_4^=] = 7.93 \times 10^6 \qquad (20)$$

and

$$K^0_{Fe(C_2O_4)_3} = [Fe(C_2O_4)_3^=]/[Fe(C_2O_4)_2^-][C_2O_4^=] = 9.87 \times 10^5 \qquad (21)$$

Bobtelsky, Chasson and Klein[25] found only $FeC_2O_4^+$ and $Fe(C_2O_4)_3^=$ present in ferric oxalate solutions, but more recent work by Babko and Dubovenko[36] appears to substantiate the results of Lambling. The values of the formation constants of the iron(III) oxalate complexes can be estimated at an ionic strength of 0.55 by the method described above, but again, the heats of formation of these species are unknown and must be estimated. The heats of formation of iron(III) complexes tend to fall into two classes depending on whether the complexes are weak or strong. The oxalate complexes are comparatively strong. The two other strong complexes for which values of the heats of formation have been reported are $FeOH^{++}$ and $FeSCN^{++}$, both with a value of −1.6 kcal./mole.[37,38] The value for $FeSO_4^+$, which is expected to be comparable to that for $FeC_2O_4^+$, can be estimated from the data of Sykes[28] and Whitaker and

(30) L. S. Darken, *ibid.*, **63**, 1007 (1941).

(31) L. Pauling, "The Nature of the Chemical Bond," Cornell Univ. Press, Ithaca, N. Y., 1948.

(32) K. S. Pitzer, *J. Am. Chem. Soc.*, **59**, 2365 (1937).

(33) G. D. Pinching and R. G. Bates, *J. Research Natl. Bur. Standards*, **40**, 405 (1948).

(34) J. Lambling, *Bull. soc. chim. France*, 495 (1949).

(35) Remember that $\beta_{FeA_n} = \prod_{n=1}^{n=n} K_{FeA_n}$.

(36) A. K. Babko and L. I. Dubovenko, *Zhur. Obshchei Khim.*, **26**, 996 (1956); *J. Gen. Chem. U.S.S.R.*, **26**, 1133 (1956).

(37) E. Rabinowitch and W. H. Stockmayer, *J. Am. Chem. Soc.*, **64**, 335 (1942).

(38) R. H. Betts and F. S. Dainton, *ibid.*, **75**, 5721 (1953).

Davidson[39] to be about −1 kcal./mole. On the basis of these values, then, one might anticipate a value in the neighborhood of −1 to −1.6 kcal./mole for the heat of formation of $FeC_2O_4^+$. This quantity can also be estimated from equation 18, remembering that ΔF^0 is zero at equilibrium and evaluating ΔS^0 on the basis of Bureau of Standards values[40] and Cobble's[41] empirical formula correlating the hydration-corrected entropies of complex ions with their charge-to-radius ratios. The value so obtained, −1.4 kcal./mole, falls in the anticipated region. The foregoing considerations together with the assumption that the relative concentrations of the iron(III) oxalate complexes remain fairly constant over the temperature range involved enable one to calculate the formation constants of these complexes. The results are listed in Table II. Neither Lambling[34] nor Bobtelsky, Chasson and Klein[25] make any mention of acid ferric oxalate complexes.

Let the total amount of oxalate uncomplexed by iron be A, then

$$A = (H_2C_2O_4) + (HC_2O_4^-) + (C_2O_4^=)$$
$$= (H_2C_2O_4)/[1 + K_1/(H^+) + K_1K_2/(H^+)^2] \quad (22)$$

Hence

$$\frac{(C_2O_4^=)}{A} = \frac{K_1K_2/(H^+)^2}{[1 + K_1/(H^+) + K_1K_2/(H^+)^2]} \equiv \alpha \quad (23)$$

where α is a constant at a given temperature and hydrogen ion concentration. Now

$$(FeC_2O_4^+)/(Fe(C_2O_4)_2^-) = \frac{1}{\alpha A K_{Fe(C_2O_4)_2}} > 20 \quad (24)$$

and

$$(Fe(C_2O_4)_2^-)/(Fe(C_2O_4)_3^{\equiv}) = \frac{1}{\alpha A K_{Fe(C_2O_4)_3}} > 4.5 \quad (25)$$

thus we can use as our working hypothesis the assumption that with respect to the diminishment of the oxalate concentration (but not with respect to the rate contribution) the only complex present in significant amounts is $FeC_2O_4^+$. This makes it possible to derive an explicit expression for the concentration of oxalate ion. Because of its cumbersome nature, however, it is more convenient to use this expression only as a check and to analyze the bulk of the data by a graphical method.

Assume a series of values for the concentration of $FeC_2O_4^+$ ranging from the total iron(III) concentration down to zero. The concentration of $FeOH^{++}$ is next calculated from the relations

$$(FeOH^{++}) = K(Fe^{+++})/(H^+)$$
$$= K[(Fe(III)) - (FeC_2O_4^+) - (FeOH^{++})]/(H^+) \quad (26)$$
$$= K[(Fe(III)) - (FeC_2O_4^+)]/[K + (H^+)]$$

where (Fe(III)) is the total iron(III) concentration and K is the equilibrium constant (values quoted by Silverman and Dodson[5]) for the reaction

$$Fe^{+++} + H_2O \rightleftharpoons FeOH^{++} + H^+ \quad (27)$$

The ferric ion concentration is given by

$$(Fe^{+++}) = (Fe(III)) - (FeOH^{++}) - (FeC_2O_4^+) \quad (28)$$

(39) R. A. Whitaker and N. Davidson, *J. Am. Chem. Soc.*, **75**, 3081 (1953).

(40) F. D. Rossini, *et al.*, "Selected Values of Chemical Thermodynamic Properties," Natl. Bur. Standards, Washington, D. C., 1952.

(41) J. W. Cobble, *J. Chem. Phys.*, **21**, 1496 (1953).

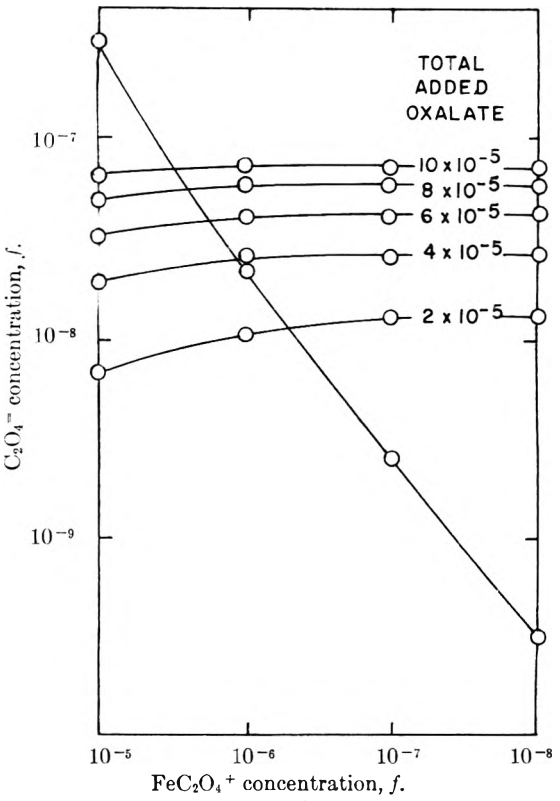

Fig. 2.—Graphical evaluation of the oxalate ion concentration at 0°.

the oxalate ion concentration by

$$(C_2O_4^=) = (FeC_2O_4^+)/(Fe^{+++})K_{FeC_2O_4} \quad (29)$$

The quantity $(C_2O_4^=)$ is now plotted *vs.* $(FeC_2O_4^+)$. But it is also true that

$$A = (\text{total oxalate initially added}) - (FeC_2O_4^+) \quad (30)$$

Since

$$(C_2O_4^=) = \alpha A \quad (31)$$

by substituting the arbitrary values of $(FeC_2O_4^+)$ into (30) and substituting the values of A thus obtained into (31) one can calculate a second series of values of $(C_2O_4^=)$ corresponding to various values of $(FeC_2O_4^+)$. Again plot $(C_2O_4^=)$ *vs.* $(FeC_2O_4^+)$. The value of the oxalate ion concentration for a given temperature and added amount of oxalic acid can now be read directly from the superimposed plots; the intersection of the two plots represents the desired oxalate ion concentration. A typical solution is shown in Fig. 2. Values of the oxalate ion concentrations evaluated in the foregoing manner are listed in Table III.

TABLE III

OXALATE ION CONCENTRATIONS AT 0.55 IONIC STRENGTH, $(H^+) = 0.548f$, AND $(Fe(III)) = 6.5 \times 10^{-5}f$

Total added oxalic acid $\times 10^5$, f	Concn. of oxalate ion $\times 10^8$, f 0°	10°	20°
0.00	0.00	0.00	0.00
2.00	1.32	1.16	1.04
4.00	2.60	2.35	2.05
6.00	3.90	3.50	3.10
8.00	5.20	4.50	4.00
10.00	6.50	5.70	5.02

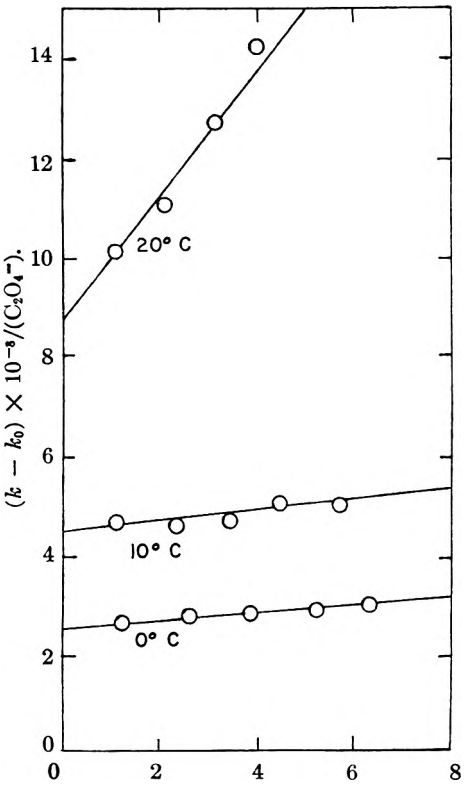

Fig. 3.—Analysis of the oxalate catalysis data.

The data for the oxalate catalysis of the iron(II)–iron(III) electron-exchange reaction now can be analyzed in the usual manner[5]

$$\frac{k(1 + K_{FeC_2O_4}(C_2O_4^-) + K_{FeC_2O_4}K_{Fe(C_2O_4)_2}(C_2O_4^-)^2 - k_0}{(C_2O_4^-)} = k_{FeC_2O_4}K_{FeC_2O_4} + k_{Fe(C_2O_4)_2}K_{FeC_2O_4}K_{Fe(C_2O_4)_2}(C_2O_4^-) \quad (32)$$

Because $(C_2O_4^-)$ is very small, eq. 32 reduces to

$$\frac{(k - k_0)}{(C_2O_4^-)} = k_{FeC_2O_4}K_{FeC_2O_4} + k_{Fe(C_2O_4)_2}K_{FeC_2O_4}K_{Fe(C_2O_4)_2}(C_2O_4^-) \quad (33)$$

where k is the over-all observed specific reaction rate constant. Figure 3 shows the data analysis curves and Table IV lists the results. The assumption has been made that the rate contributions

TABLE IV

SPECIFIC REACTION RATE CONSTANTS FOR THE OXALATE CATALYSIS OF THE IRON(II)–IRON(III) ELECTRON-EXCHANGE REACTION

Temp., °C.	$k_{FeC_2O_4}$, sec.$^{-1}$ f^{-1}	$k_{Fe(C_2O_4)_2}$, sec.$^{-1}$ f^{-1}
0	700	3560
10	1100	2550
20	2140	4520

of $Fe(C_4O_4)_3^{-3}$ and higher complexes are negligible. The linearity of the curves in Fig. 3 supports this assumption. A plot of $k_{FeC_2O_4}$ on a logarithmic scale *vs.* $1/T$, is linear, and its slope corresponds to an activation energy of 9.2 kcal./mole. The entropy of activation is −14.0 cal./mole-deg. The values of $k_{Fe(C_2O_4)_2}$ do not appear to warrant an attempt to calculate the corresponding thermodynamic properties of the exchange process involving $Fe(C_2O_4)_2^-$.

An activation energy of 9.2 kcal./mole for the electron-exchange process

$$Fe^*C_2O_4^+ + Fe^{++} \rightleftharpoons Fe^{*+++} + FeC_2O_4^+ \quad (34)$$

lies well within the range of values reported for the catalyses by halide and thiocyanate ions, thus providing further circumstantial evidence in favor of water-bridging rather than anion-bridging in the iron(II)–iron(III) electron-exchange reaction.

The mechanism of water-bridging may be described briefly as follows[16,17]: the ferric complex ion and ferrous ion rapidly form an activated complex

$$(H_2O)_{4 \text{ or } 5}Fe^*C_2O_4^+ + Fe(H_2O)_6^{++} \rightleftharpoons [(H_2O)_{4 \text{ or } 5}Fe^*C_2O_4Fe(H_2O)_6]^{+++} \quad (35)$$

The function of the centrally located complexing anion is to overcome coulombic repulsion, form a stabilized activated complex,[7] and draw the reactants into sufficient proximity so that their solvation spheres overlap. The actual effective electron transfer then proceeds *via* waters of solvation adjacent to the complexing anion

$$[(H_2O)_{3 \text{ or } 4}Fe^*\ldots C_2O_4\ldots Fe(H_2O)_6]^{+++} \quad (36)$$

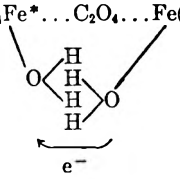

and the final step is the dissolution of the activated complex and any necessary rearrangements of the waters of solvation

$$[(H_2O)_{4 \text{ or } 5}Fe^*C_2O_4Fe(H_2O)_6]^{+++} \rightleftharpoons Fe^*(H_2O)_6^{++} + (H_2O)_{4 \text{ or } 5}FeC_2O_4^+ \quad (37)$$

Water rearrangement in the case of the oxalate catalysis is not rate determining when n in equation 7 is 0, 1 or 2.

The effect of a metal surface on the rate of the iron(II)–iron(III) electron-exchange reaction in aqueous perchloric acid media was investigated. At 0°, in 0.548 f $HClO_4$, and in the presence of silver foil with 100 cm.^{2} of surface area the over-all observed specific reaction rate of the exchange was 5.80 ± 0.63 sec.$^{-1}$ f^{-1}, 4 to 5 times greater than the rate in the absence of metal foil. Prestwood and Wahl[42] have observed catalysis of the thallium(I)–thallium(III) exchange by platinum black and Meier and Garner[43] catalysis of the europium(II)–europium(III) exchange by platinum wire. The iron(II)–iron(III) exchange is not accelerated by the presence of glass wool.

The rate of the iron(II)–iron(III) electron-exchange reaction was also studied in aqueous perchloric acid media in the presence of acetic, benzoic, fumaric, *o*-phthalic, succinic and carbolic acids. The results are summarized in Table V. Acetate,[44] succinate and phenolate anions all catalyze the exchange, the latter rather erratically. Contrary to expectation[45,46] iron(III) hydroxide

(42) R. J. Prestwood and A. C. Wahl, *J. Am. Chem. Soc.*, **70**, 880 (1948).

(43) D. J. Meier and C. S. Garner, THIS JOURNAL, **56**, 853 (1952).

(44) For studies of electron exchange in anhydrous acetic acid see L. H. Sutcliffe and F. Walkley, *Nature*, **178**, 199 (1956).

(45) M. Quintin, *Compt. rend.*, **232**, 1303 (1951).

(46) R. E. Hamm, C. M. Shull and D. M. Grant, *J. Am. Chem. Soc.*, **76**, 2111 (1954).

could not be precipitated in the presence of citrate ions, consequently the separation procedure failed in that instance. Benzoic, fumaric and *o*-phthalic acids are so slightly ionized in water that, at the acidities used, concentration of their anions large enough to give detectable catalysis are not formed. The acidity could not be reduced because increased hydroxide catalysis of the exchange[5] would make the rate too fast to be measured by the present techniques.

TABLE V

THE RATE OF THE IRON(II)–IRON(III) ELECTRON-EXCHANGE REACTION IN AQUEOUS SOLUTIONS OF SOME ORGANIC ACIDS

$(H^+) = 0.548 f$ (as $HClO_4$), $\mu = 0.55$

Temp., °C.	Fe(III) $\times 10^4$, f	Fe(II) $\times 10^4$, f	Added acid, f	k, sec.$^{-1}$ f^{-1}
0.08 ± 0.01	6.06	1.05	None	1.35 ± 0.46
0.08 ± .01	6.06	1.05	0.10 acetic	1.62 ± 0.30
20.35 ± .04	2.12	1.05	None	8.22 ± 1.43
20.35 ± .04	2.12	1.05	0.10 acetic	9.56 ± 0.46
20.35 ± .04	2.12	1.05	2.0×10^{-4} benzoic	8.87 ± .95
20.35 ± .04	2.12	1.05	4.0×10^{-4} fumaric	7.90 ± .50
20.35 ± .04	2.12	1.05	6.0×10^{-3} *o*-phthalic	8.24 ± .37
20.35 ± .04	2.12	1.05	0.10 succinic	15.3 ± 1.8
0.08 ± .01	2.12	1.05	.02 to 0.10 carbolic	1.5 to 3.3
9.82 ± .05	2.12	1.05	.02 to .10 carbolic	3.5 to 9.0
20.31 ± .03	2.12	1.05	.02 to .10 carbolic	8.1 to 9.3

The original intents[16] of the above studies with various organic anions were (a) to establish the position of the catalyzing anion in the activated complex and (b) to investigate the electron-transporting efficacy of conjugated systems.[47]

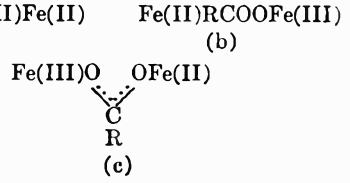

Although evidence for a central (b) rather than a terminal (a) position of the complexing anion appears strong[7,16] it is at best circumstantial. Both of these intents were frustrated by the realization that, aside from its position, the organic anion might be so oriented (c) (detailed application of the principle of maximum charge separation is made ambiguous by the electrostatic screening effect of the complexing anion) that only one carboxyl group (or hydroxyl group in a phenol) need be involved in electron transfer, thus making the structure of the remainder of the organic acid of secondary significance.

Acknowledgment.—The author is indebted to the United States Atomic Energy Commission for facilities and funds and to Doctors R. W. Dodson, L. G. Carpenter, J. Hudis and N. Sutin for many helpful discussions.

(47) *Cf.* D. R. Sebera and H. Taube, unpublished work discussed in H. Taube, *Canad. J. Chem.*, **37**, 129 (1959).

THE PREPARATION, CRYSTAL STRUCTURES AND SOME PROPERTIES OF ZIRCONIUM AND HAFNIUM DIRHENIDE[1]

BY N. H. KRIKORIAN, W. G. WITTEMAN AND M. G. BOWMAN

University of California, Los Alamos Scientific Laboratory, Los Alamos, New Mexico

Received April 25, 1960

The preparation of near stoichiometric zirconium dirhenide, $ZrRe_2$, and hafnium dirhenide, $HfRe_2$, by direct combination of the elements is described. The melting temperature for $ZrRe_2$ was found to be 2750 ± 50° and for $HfRe_2$, 2935 ± 75°. Both compounds have a hexagonal C-14 Laves Structure: $ZrRe_{2.01}$ $a_0 = 5.2701 \pm 0.0004$, $c_0 = 8.6349 \pm 0.0008$; $HfRe_{2.02}$ $a_0 = 5.2478 \pm 0.0002$, $c_0 = 8.5934 \pm 0.0006$. These dirhenides are extremely hard, with a DPH of 1400 for each. Both dirhenides were found to convert to the monocarbides of hafnium and zirconium in the presence of graphite at about 2150°.

Introduction

Alloys of rhenium show promise as materials which can under certain conditions withstand high temperatures. Due to their high melting points, intermetallic compounds of rhenium formed with the other transition metals are of particular interest, and these compounds are being investigated to an increasing extent. Two such compounds are $ZrRe_2$ and $HfRe_2$. The phase diagram of the zirconium–rhenium system has been reported by Savitskii, Tylkina and Tsyganova.[2] The phase diagram of hafnium–rhenium is unknown.

In addition, crystallographic data on $ZrRe_2$($a_0 = 5.262$, $c_0 = 8.593$) have been reported by Wallbaum[3] and on $HfRe_2$ ($a_0 = 5.239 \pm 0.002$, $c_0 = 8.584 \pm 0.002$) by Compton and Matthias.[4] In both instances no analytical data are given for the compounds. Savitskii and co-workers[2] also give a broad range of lattice constants for the three zirconium compounds observed: Zr_2Re ($a_0 = 10.12$, $c_0 = 5.42$); $ZrRe_2$ ($a_0 = 5.21$–5.25, $c_0 = 8.5$–8.6); Zr_5Re_{24}($a_0 = 9.60$–9.70).

This paper reports a method of preparing the pure dirhenide of zirconium and hafnium, their melting temperatures, lattice constants, microhardnesses and reactions with graphite.

The Preparation of the Dirhenides.—High-purity rhenium metal powder from Varlacoid Corporation, reactor-grade zirconium sponge from Wah Chang Corporation, and high-purity hafnium powder from the U. S. Bureau of Mines were used.

Except for < 500 p.p.m. Fe in the hafnium, spectroscopic analysis showed no impurity greater than 100 p.p.m. for the

(1) This work was done under the auspices of the U. S. Atomic Energy Commission.

(2) Z. M. Savitskii, M. A. Tylkina and I. A. Tsyganova, *Atomnaya Energ.*, **7**, 231 (1959).

(3) H. J. Wallbaum, *Naturwissenschaften*, **30**, 149 (1942).

(4) V. B. Compton and B. T. Matthias, *Acta Cryst.*, **12**, 651 (1959)

starting materials. The compounds were prepared by reacting the elements using an arc melter, on a water-cooled copper hearth in an atmosphere of purified argon. In both preparations, the product was shiny, hard and extremely brittle. The rhenium seemed to swell to take up the zirconium and hafnium.

Experimental

The compounds were powdered using a "diamond" mortar and pestle to about 200 mesh, and solid cylinders $^3/_8$" dia. and $^5/_8$" long were pressed using hard steel dies at 50,000 p.s.i. Both cylinders were sintered at 1800–2100° *in vacuo*, and axial holes about 50 mils diameter and $^1/_4$" to $^3/_8$" deep were drilled (with carbide drills) in the cylinder for observing the temperature during the melting temperature determinations.

The heating was done in a high frequency induction field with a 5 kw. Westinghouse generator using an eddy-current concentrator. The sintered plug was placed on a copper block which was about an eighth of an inch below the induction field. The wall to which the block was attached was an integral part of the water-cooled eddy current concentrator and was also kept cool by the flow of water through the concentrator. Melting temperatures were determined by heating the plugs until liquid appeared in the hole. Ordinarily, the appearance of liquid in the hole could be observed visually. However, a thermal arrest apparatus[5] was also used in order to facilitate the melting temperature measurements and to observe any phase change which might occur. Briefly, the method consists of taking light from the hole in the sample and focusing it on a photomultiplier tube connected to the y-axis of a time sweep oscilloscope. Abrupt changes in the smoothly changing slope of the display trace as the sample cools indicate a heat effect which would normally be present during a phase change. With proper calibration, it is then possible to ascertain the temperature at which the transition took place.

The temperature measurements were made with a Pyro optical pyrometer which was compared with a standard pyrometer. The standard pyrometer had been calibrated at both the National Bureau of Standards and Argonne National Laboratory.

The melting temperature measurements were made with 5 in. of helium present to diminish loss of zirconium and hafnium by vaporization. These losses will be discussed later.

Both compounds were analyzed after preparation and after determining the melting temperatures. The zirconium and hafnium were gravimetrically determined by precipitation with p-bromomandelic acid. The rhenium was determined gravimetrically by precipitating with tetraphenylarsonium chloride.

X-Ray powder patterns were made in a 114.6 mm. Debye–Scherrer camera using iron filtered cobalt radiation both after preparation of the compounds and also after determination of the melting temperature. The lattice constants were obtained from the back reflection lines by applying the least-squares extrapolation of Cohen[6] as modified by Hess[7] using an IBM-704. A standard deviation was calculated from each film. Similar patterns obtained from NaCl gave lattice constants agreeing with accepted values within the calculated error.

Results and Discussion

Chemical analysis indicated a shift of the composition of the zirconium dirhenide from $ZrRe_{2.01}$ to $ZrRe_{2.25}$ during the heating. For hafnium dirhenide, the change was minute, from $HfRe_{2.02}$ to $HfRe_{2.04}$. The X-ray diffraction patterns confirmed the hexagonal C-14 Laves Structure previously reported.[3,4] $ZrRe_{2.01}$ gave lattice constants, in angstroms, of $a_0 = 5.2701 \pm 0.0004$ and $c_0 = 8.6349 \pm 0.0008$; for $ZrRe_{2.25}$, $a_0 = 5.268 \pm 0.002$ and $c_0 = 8.628 \pm 0.005$. The cell dimensions for $HfRe_{2.02}$ are: $a_0 = 5.2478 \pm 0.0002$ and $c_0 = 8.5934 \pm 0.0006$; for $HfRe_{2.04}$, $a_0 = 5.2477 \pm 0.0007$ and $c_0 = 8.5917 \pm 0.0008$. Using the above cell dimensions for the near stoichiometric material, the calculated density of $HfRe_2$ is 17.85 g./cc. and for $ZrRe_2$, 14.82 g./cc. The pycnometric density of $HfRe_2$ was found to be 17.75 g./cc. and for $ZrRe_2$, 14.63 g./cc.

The change in lattice constant with composition, as measured on the rapidly cooled compounds, and the presence only of a single phase in the X-ray diffraction patterns indicates a range of homogeneity for the compounds. Previous work[2] has also indicated a range of homogeneity for compositions in the neighborhood of zirconium dirhenide. These authors, as well as Wallbaum[3] and Compton and Matthias[4] do not relate compositions with lattice constants. Accordingly, previously published lattice constants cannot be compared directly with those reported here.

Metallographic inspection of the near stoichiometric compounds showed the $ZrRe_2$ to be single phased. The $HfRe_2$ showed a lower melting, unidentified second phase in the grain boundaries in a small area of the specimen. Both the $ZrRe_2$ and $HfRe_2$ gave identical Vickers microhardness, DPH = 1400.

Since there is a shift in composition during heating, the melting temperatures should be identified with the composition richer in rhenium. The melting temperature of $ZrRe_{2.25}$ was observed to be 2750 ± 50° with a small break in the cooling curve indicative of a transition at 2710°. The $HfRe_{2.04}$ was observed to melt at 2935 ± 75° with an almost imperceptible break about 50° lower. The work of Savitskii[2] and co-workers reports the formation of $ZrRe_2$ by a peritectic reaction at 2450°. No effort was made to confirm this finding. However, our preparation of essentially stoichiometric $ZrRe_2$ by arc-melting gave no indication of a peritectic reaction.

Both compounds were found to be fairly stable at 2500° *in vacuo*. However at about 2500°, the sight window of the apparatus was coated by vapor from $ZrRe_2$. The condensate on the water-cooled walls of the eddy-current concentrator was examined by X-ray diffraction and found to be primarily zirconium metal and a small amount of rhenium. Appreciable vaporization was not observed for $HfRe_2$, even at somewhat higher temperatures.

The dirhenides are both less stable than the carbides of these metals (at least at high temperature), as evidenced by a visibly exothermic reaction between the dirhenides and carbon at 2150° to form the monocarbides of zirconium and hafnium. The stability of the dirhenides in the presence of graphite was observed by mixing outgassed powder with the compounds and heating in a crucible previously outgassed at 2200°. These crucibles did not satisfy black body conditions. At about 2150° both of the dirhenides reacted with the graphite. Heating was continued for 30 minutes after the reaction occurred. X-Ray diffraction patterns disclosed both a face-centered cubic pattern—presumably that of carbon-deficient ZrC

(5) G. N. Rupert, Los Alamos Scientific Laboratory, "An Apparatus for Observing Phase Transitions of Incandescent Material," to be published.

(6) M. U. Cohen, *Rev. Sci. Instr.*, **6**, 68 (1935); *Z. Krist.*, **94A**, 288, 306 (1936).

(7) J. B. Hess, *Acta Cryst.*, **4**, 209 (1951).

and HfC and the pattern of rhenium metal. However, it is possible that the product of the reaction could alternatively be a solution of rhenium in the ZrC and HfC. The lattice constant calculated for the cubic phase was $a_0 = 4.668$ Å. for the product of the $ZrRe_2$–C reaction and $a_0 = 4.616$ Å. for the product of the $HfRe_2$–C reaction.[8]

Acknowledgments.—The authors wish to acknowledge the preparation of the compounds by Patrick L. Stone and the reading of the many X-rays by Mary Jane Jorgensen. The valuable assistance of C. G. Hoffman for metallographic analysis; Joe A. Mariner, M. H. Corker and O. R. Simi for the spectroscopic data; and O. H. Kriege for chemical analyses is also gratefully acknowledged. Helpful discussions were held with C. P. Kempter and R. L. Petty concerning the treatment of the crystallographic data.

(8) Material supplementary to this article has been deposited as Document Number 6323 with the ADI Auxiliary Publications Project Photoduplication Service, Library of Congress, Washington 25, D. C. A copy may be secured by citing the document number and by remitting $2.50 for photoprints, or $1.75 for 35 mm. microfilm. Advance payment is required. Make checks or money orders payable to: Chief, Photoduplication Service, Library of Congress.

INFRARED AND ULTRAVIOLET ABSORPTION SPECTRA OF SOME SALTS AND METAL CHELATES OF ANTHRANILIC ACID

BY ANN GERTRUDE HILL[1] AND COLUMBA CURRAN

Nieuwland Laboratories, University of Notre Dame, Notre Dame, Indiana

Received April 25, 1960

Absorption maxima in the 3000 and 1550 cm.$^{-1}$ regions in potassium bromide disks, and in the 300 mμ region in potassium bromide disks and in ethanol solutions are reported for anthranilic acid, its sodium, potassium, calcium, stontium and barium salts and its chelates with magnesium, zinc, cadmium, nickel and copper. Chelation shifts the 320 mμ band of the anthranilate ion to shorter wave lengths, decreases the frequencies of the N—H stretching vibrations, causes an inversion of the relative intensities of the 1615 and 1580 cm.$^{-1}$ peaks and effects small shifts to higher frequencies of the band attributed to the antisymmetric COO^- stretching vibration. The spectra indicate a *trans* planar square configuration for all complexes. The chelates are appreciably dissociated in ethanol.

The usual effect of chelation of organic ligands with metals is to shift the ultraviolet absorption maxima of the ligands to longer wave lengths. Sone[2] has reported an extensive study of this effect and has concluded that for some complexes the extent of this shift is related to the strength of the ligand–to–metal bonds. It appeared to the authors that the direction of this shift might be reversed in metal chelates having as one of the donor centers an aryl amino group, as the formation of the fourth bond by the nitrogen atom results in a blocking of resonance between the amino group and the benzene ring. Hypsochromic shifts in the long wave length absorption maximum of N,N-dimethylaniline have been observed on coördination of this amine with sulfur trioxide[3] and with boron trichloride.[4]

The anthranilate (*o*-aminobenzoate) ion was selected for this investigation. The complexes studied were those of magnesium, zinc, cadmium, nickel and copper. As the cations of the first three metals do not absorb in the near ultraviolet, any changes in the absorption pattern of the anthranilate ion on chelation are most probably associated with changes in the absorption characteristics of the ligand itself. The spectra of sodium, potassium, calcium, strontium and barium anthranilates were obtained for comparison with those of the chelates.

The infrared spectra of these compounds were also determined in an effort to obtain information regarding the type of bonding between the ligand and the metal ions, as well as the configuration of the complexes. The spectra of the 2:1 complexes of aliphatic amino acids with copper and nickel[5] reveal decreases in the frequencies of the N–H stretching vibrations, indicating covalent N–M bonds, and a relatively small perturbation of the antisymmetric 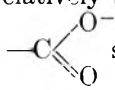 stretching vibration, suggesting essentially electrostatic COO^----M^{++} bonds. These data, together with the X-ray evidence for a *trans* coplanar square configuration of nickel and copper complexes of amino acids[6] and the magnitudes of their magnetic moments, were interpreted[5] as indicating the use of sp linear bond orbitals by copper and nickel in forming nitrogen-to-metal bonds. This interpretation was also applied to the spectrum of bis-(glycino)-zinc monohydrate[7] and recent X-ray evidence[8] has revealed a *trans* coplanar square arrangement of the nitrogen atom and an oxygen atom of each carboxylate group about the metal in the monohydrates of bis-(glycino)-zinc and bis-(glycino)-cadmium, with the metal atoms bound also by apparently longer

(1) Sister Ann Gertrude Hill, O.S.U., Ursuline College, Cleveland, Ohio. Supported under AEC Contract AT(11-1)-38, Radiation Project of the University of Notre Dame.

(2) K. Sone, *J. Am. Chem. Soc.*, **75**, 5207 (1953).

(3) J. A. Moede and C. Curran, *ibid.*, **71**, 852 (1949).

(4) H. A. Szymanski, Ph.D. thesis, University of Notre Dame, 1952.

(5) D. N. Sen, S. Mizushima, C. Curran and J. V. Quagliano, *J. Am. Chem. Soc.*, **77**, 211 (1955).

(6) A. J. Stosick, *ibid.*, **67**, 362, 365 (1945).

(7) D. M. Sweeny, C. Curran and J. V. Quagliano, *ibid.*, **77**, 5508 (1955).

(8) B. W. Low, F. L. Hirshfeld and F. M. Richards, *ibid.*, **81**, 4412 (1959).

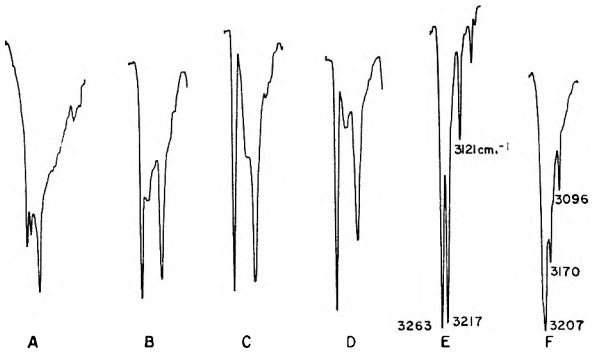

Fig. 1.—Absorption patterns in the 3000 cm.$^{-1}$ region in KBr disks: A, sodium anthranilate; B, bis-(anthranilato)-copper(II); C, bis-(anthranilato)-magnesium; D, bis-(anthranilato)-zinc; E, bis-(aniline)-dichlorozinc; F, *o*-phenylenediaminedichlorozinc.

bonds to carboxylate oxygen atoms directly above and below the metal atoms.

It is of interest to determine whether the structures characteristics of the aliphatic amino acids extend also to the metal chelates of aromatic amino acids, for which no X-ray data are available. Of particular interest are the zinc and cadmium chelates, as the great majority of compounds of these metals have a tetrahedral configuration due to the use of sp^3 bond orbitals.

Experimental

Anthranilic acid, Eastman material, was purified by vacuum sublimation or by recrystallization from hot water using a small amount of decolorizing charcoal.

Sodium and potassium anthranilates were prepared by mixing ethanol solutions of sodium or potassium hydroxide and anthranilic acid.

Sodium anthranilate solution was prepared by dissolving anthranilic acid in an equivalent amount of aqueous 1 *N* sodium hydroxide. After filtration, small quantities of the acid were added until the solution was very weakly acid. A freshly prepared solution was used for each preparation.

Bis-(anthranilato) complexes of magnesium, zinc, cadmium, nickel and copper were prepared by addition of aqueous solutions of the metal chlorides to a solution of sodium anthranilate. The precipitates were washed with several portions of distilled water and ethanol and vacuum dried at 130°.

Anal. Calcd. for $Mg(C_7H_6O_2N_2)$: $C_7H_6O_2N$, 92.48. Found: $C_7H_6O_2N$, 92.4. Calcd. for $Zn(A)_2$: C, 49.80; H, 3.58; N, 8.28; Zn, 19.36. Found: C, 50.1; H, 3.78; N, 8.9; Zn, 19.3. Calcd. for $Cd(A)_2$: Cd, 29.22. Found: Cd, 29.35. Calcd for $Ni(A)_2$: C, 50.84; H, 3.65; N, 8.47. Found: C, 50.42; H, 3.91; N, 8.93. Calcd. for $Cu(A)_2$: Cu, 18.82. Found: Cu, 18.8.

Calcium, strontium and barium anthranilates were prepared by heating solutions of the chlorides of these metals in distilled water to 80° and adding with stirring to a sodium anthranilate solution. The white crystalline products were washed with a dilute solution of sodium anthranilate and finally with ethanol. The compounds were vacuum dried at 120°.

Anal. Calcd. for $Ca(C_7H_6O_2N)_2$: $C_7H_7O_2N$, 87.88. Found: $C_7H_7O_2N$, 88.2. Calcd. for SrA_2: $C_7H_7O_2N$, 76.26. Found: $C_7H_7O_2N$, 77.1. Calcd. for BaA_2: $C_7H_7O_2N$, 66.95. Found: $C_7H_7O_2N$, 66.3.

Absorption measurements in the ultraviolet region were obtained with a Beckman DU spectrophotometer equipped with a Warren Spectracord attachment. Infrared spectra were obtained with a Perkin–Elmer Model 21 instrument, using a sodium chloride or calcium fluoride prism. The concentration of the KBr disks used for infrared measurements was about 0.5 mg. of sample in 300 mg. of KBr. In preparing the disk of anthranilic acid hydrochloride the die was not evacuated.

Results and Discussion

It has been demonstrated previously[9] that the coördination of amino groups with metals (the formation of nitrogen-to-metal dative bonds) results in appreciable decreases in the frequencies of the N–H stretching vibrations. The absorption maxima in the 3000 cm.$^{-1}$ region listed in Table I reveal that the compounds studied fall into two classes: sodium, potassium, calcium, strontium and barium salts, and magnesium, zinc cadmium, nickel and copper complexes. The high frequency peaks in the spectra of the former compounds are close to the value for anthranilic acid, whereas the spectra of the latter compounds reveal shifts of 149–187 cm.$^{-1}$ to lower frequencies. The cupric ion is expected to form the strongest N–M bond and the greatest shift is observed in the spectrum of the copper complex. The shifts are greater than those observed in this Laboratory in the spectra of metal complexes of aliphatic amino acids.

The absorption profiles in the 3000 cm.$^{-1}$ region are determined by the strength of coupling between the amino groups, their relative conformations and the extent of hydrogen bonding. The similarities between the absorption patterns in this region for the magnesium, zinc, cadmium, nickel and copper complexes suggest to the authors that they all have similar configurations. A comparison, Fig. 1, of these patterns with those of bis-(aniline)-dichlorozinc and *o*-phenylenediaminedichlorozinc, patterns typical of tetrahedral zinc complexes, suggests that the anthranilate complexes have a *trans* square planar arrangement of the four coördinating atoms about the metal atom. This is expected for the copper and nickel complexes and is not surprising for the others in view of the X-ray evidence for the glycino chelates. All the complexes except that of copper have almost identical spectral in the 2–15 μ region, and the spectrum of the copper complex differs significantly from the others only in the 1050 cm.$^{-1}$ region. The nickel chelate is paramagnetic, having a moment of 3.2 magnetons.[10] This is a typical value for an outer orbital complex of nickel(II) having an octahedral or tetragonal configuration. Tetrahedral complexes of nickel(II) are expected to have a larger orbital contribution to the magnetic moment; values of 3.6–4.0 have been reported recently for such complexes.[11]

The spectra of the anthranilates in the 1625–1520 cm.$^{-1}$ region reveal three absorption peaks that are not changed appreciably on deuteration of the amino group. The two high frequency peaks at 1615 and 1582 cm.$^{-1}$ in the salts are attributed to C=C ring vibrations and the third, the strongest in the spectra of all but the magnesium complex, is attributed to the antisymmetric COO^- stretching vibration (with perhaps some contribution from a third ring vibration). Stimson[12] has also assigned this peak in the spectra of the sodium and potassium salt to the COO^- vibration, and a similar as-

(9) G. F. Svatos, C. Curran and J. V. Quagliano, *J. Am. Chem. Soc.*, **77**, 6159 (1955).

(10) S. E. Livingstone, *J. Chem. Soc.*, 1042 (1956).

(11) N. S. Gill and R. S. Nyholm, *ibid.*, 3997 (1959).

(12) M. M. Stimson, *J. Chem. Phys.*, **22**, 1942 (1954).

TABLE I

ABSORPTION MAXIMA OF ANTHRANILIC ACID, ITS HYDROCHLORIDE, SALTS AND CHELATES IN KBr DISKS

	Ultra-violet, mμ	3500–3100 cm.$^{-1}$ cm.$^{-1}$ (%T)			1625–1500 cm.$^{-1}$ cm.$^{-1}$ (%T)		
Acid	335	3460(26)	3367(29)				1670(6)
Acid·HCl	282						1695(9)
Salts							
Na	312	3436(44)	3400(47)	3330(35)	1615(18)	1580(30)	1521(9)
K	318	3420(39)	3280(37)		1614(7)	1583(11)	1520(6)
Ca	323	3472(59)	3424(59)	3344(49)	1615(11)	1580(20)	1521(9)
Sr	320	3428(44)	3367(51)	3303(51)	1615(9)	1585(16)	1520(5)
Ba	319	3436(27)	3389(34)	3311(37)	1617(36)	1583(41)	1519(11)
Chelates							
Mg	294	3311(29)	3202(57)	3145(38)	1623(10)	1605(6)	1564(8)
Zn	296	3294(30)	3222(59)	3130(35)	1620(20)	1596(10)	1545(5)
Cd	298	3289(40)	3257(55)	3140(53)	1619(20)	1590(7)	1534(4)
Ni	289	3303(53)	3215(74)	3120(65)	1623(27)	1609(18)	1550(7)
Cu	284	3273(35)	3230(53)	3125(38)	1616(18)	1594(6)	1540(4)

signment of the peak at 1554 cm.$^{-1}$ in the spectrum of sodium benzoate has been made by Davies and Jones.[13]

The data in Table I reveal an inversion of the relative strengths of the absorption peaks at 1615 and 1582 cm.$^{-1}$ on chelation; the higher frequency peak is stronger in the salts and weaker in the chelates. The peak at 1582 cm.$^{-1}$ in the salts is shifted an average of 17 cm.$^{-1}$ to higher frequency on chelation. The shifts in the 1520 cm.$^{-1}$ peak on chelation are 14, 20, 25, 30 and 44 cm.$^{-1}$ for the cadmium, copper, zinc, nickel and magnesium complexes, respectively. In the spectra of the acid, acid chloride and methyl ester the carbonyl peaks occur at 1670, 1695 and 1697 cm.$^{-1}$, respectively. A comparison of the small shifts observed on chelation to the very large shifts on acid and ester formation suggests to the authors that in the anthranilato complexes the COO^{-}---M^{++} bonds are essentially electrostatic.

If the chelates have a *trans* planar configuration, as interpreted from the spectra, it may well be that the complexes in adjacent planes in the crystal lattice are so arranged as to permit octahedral coordination by carboxylate oxygen atoms directly above and below the metal atoms, as observed[8] in the monohydrates of bis-(glycino)-zinc and bis-(glycino)-cadmium. This arrangement is expected particularly for bis-(anthranilato)-nickel. If this octahedral coördination prevails, the bonds may have some sp^3d^2 character, but it appears to the authors that they are essentially sp N–M bonds and electrostatic O---M bonds. Intermolecular O—H–N hydrogen bonds are expected for these complexes in the solid state. For such interaction the N–H stretching peaks are surprisingly sharp, as they are in the spectrum of *trans*-bis-(glycino)-platinum(II),[14] for which a similar configuration and somewhat similar hydrogen bonding are probable.

The long wave length absorption maxima in the ultraviolet region for anthranilic acid, its hydrochloride, salts and metal chelates in potassium bromide disks are listed in the first column of Table I. The decrease in λ_{max} from the acid to the salts is associated with the weaker electron withdrawing character of the COO^{-} group compared to that of the COOH group. The further decrease on chelation is attributed to the blocking of resonance between the amino group and the ring by the formation of N–M bonds. The hydrochloride spectrum shows the greatest shift, followed by that of the copper chelate; with the exception of the magnesium chelate, the shifts are in the accepted order of nitrogen-to-metal bond strengths. These hypsochromic shifts are, of course, not so large as those observed on the chelation with metals of such highly conjugated ligands as Eriochromeschwarz T[15] and the purpurate anion,[16] in which chelation constrains the flow of π-electrons.

The spectra of anthranilic acid in potassium bromide and ethanol differ in that the 247 mμ peak in ethanol is a shoulder in the disk. A point of inflection occurs at 243 mμ in KBr and it is not shifted appreciably on salt formation or in the cadmium and zinc chelates. Ultraviolet spectra were also obtained in absolute ethanol and 95% ethanol for the compounds listed in Table I. The low solubilities of the zinc, cadmium, nickel and copper chelates necessitated the use of 10 cm. cells for the spectra of these complexes. The spectrum of the magnesium complex in absolute ethanol resembles very closely the curves for the calcium, strontium and barium salts, indicating that practically all the nitrogen-to-magnesium bonds are broken in solution; the ligand is probably displaced by alcohol molecules, an indication of the preference of magnesium for O–M bonds. This solvation of the magnesium cation is further evidenced by the greater solubility of the magnesium complex in ethanol compared to the other chelates. The spectra reveal that a portion of the bonds joining nitrogen to zinc, cadmium and copper are broken in absolute ethanol, and that in 95% ethanol the

(13) M. Davies and R. L. Jones, *J. Chem. Soc.*, 121 (1954).

(14) A. J. Saraceno, I. Nakagawa, S. Mizushima, C. Curran and J. V. Quagliano, *J. Am. Chem. Soc.*, **80**, 5018 (1958).

(15) G. Schwarzenbach and W. Biedermann, *Helv. Chim. Acta*, **31**, 678 (1948).

(16) G. Schwarzenbach, W. Biedermann and F. Bangerter, *ibid.*, **29**, 811 (1946).

nickel chelate is completely dissociated and the copper, zinc and cadmium chelates are appreciably hydrolyzed.

The dissociation of these chelates in solutions of high dielectric constant is attributed to the electrostatic character of the COO^-—M^{++} bonds and to the gain in resonance stabilization on the rupture of the nitrogen-to-metal bonds. It is evident that the study of the effect of chelation on weak ligands such as the anthranilate ion necessitates the determination of the spectra of the chelates in the solid state.

THE REACTION BETWEEN OXYGEN ATOMS AND DIBORANE[1,2]

BY FRANCIS P. FEHLNER AND ROBERT L. STRONG

Department of Chemistry, Rensselaer Polytechnic Institute, Troy, N. Y.

Received April 27, 1960

The gas-phase reaction between diborane and oxygen atoms, produced by the mercury photosensitized decomposition of nitrous oxide, has been studied at 25 and 100°. The only products formed initially are N_2 (internal actinometer), H_2, B_4H_{10}, B_5H_9 and a white solid with the empirical formula BHO. Observed initial rates compare favorably with those predicted from mechanism 2–7. A steady-state tetraborane concentration is reached at low diborane decomposition, due to the faster competitive reaction $O + B_4H_{10} \rightarrow BH_3O + B_3H_7$.

Introduction

The reaction between molecular oxygen and diborane has been studied at the explosion limits by several investigators.[3-5] Roth and Bauer[5] have proposed the following mechanism at the second explosion limit

$$B_2H_6 \rightleftarrows 2BH_3$$
$$BH_3 + O_2 \longrightarrow BH_2OH + O$$
$$O + B_2H_6 \longrightarrow BH_2OH + BH_3$$
$$BH_2OH + B_2H_6 \longrightarrow BH_3 + B_2H_5OH$$
$$BH_3 + O_2 + M \longrightarrow HBO_2 + H_2 + M$$
$$BH_3 + B_2H_6 \longrightarrow B_3H_7 + H_2$$
$$B_3H_7 \longrightarrow \text{higher hydrides}$$

(B_2H_5OH disproportionates to $B(OH)_3 + B_2H_6$)

In addition to the explosion limit results, this mechanism has been supported by work with various diluent gases, such as N_2, He, Ar, H_2, NO, NO_2 and $Fe(CO)_5$.[6,7]

An earlier investigation[8] of the oxygen atom–diborane reaction, using oxygen atoms from a silent glow discharge in molecular oxygen, gave an activation energy of equal to, or less than, 4 kcal./mole, but the kinetic scheme was obscured by the presence of molecular oxygen and ozone.

To eliminate these competing reactions, the technique developed by Cvetanovic[9] to study the interaction of oxygen atoms with hydrocarbons was used in this work. By this method, atomic oxygen is obtained from the mercury photosensitized (using 2537 Å. light) decomposition of nitrous oxide

$$Hg(6^1S_0) + h\nu \xrightarrow{2537\ \text{Å.}} Hg(6^3P_1)$$
$$Hg(6^3P_1) + N_2O \longrightarrow N_2 + O + Hg(6^1S_0)$$

Cvetanovic found that if only nitrous oxide and mercury were present in the mixture, molecular oxygen and oxides of mercury were formed.[9] If a hydrocarbon was added, however, the sole fate of the atomic oxygen was reaction with the hydrocarbon.[10] Direct mercury photosensitized decomposition of the hydrocarbon was kept to a minimum by the use of a large excess of nitrous oxide.

Experimental

Reaction System.—The glass reaction system (total volume = 350 ml.) consisted of a closed loop for circulation of the reactants through the quartz photolysis cell. The cell was 100 mm. long and 50 mm. o.d., and was completely enclosed by an air furnace. Both the inlet and outlet of the cell were attached to traps to thermostat the excess liquid mercury. Circulation of the reaction mixture through the cell at a rate of approximately 60 ml./min. (with a pressure of 215 mm.) was achieved by means of an all-glass pump similar to that described by Dodd and Robinson.[11] The primary modification of this pump was the use of nitrous oxide (dried by passage through a $Mg(ClO_4)_2$ drying tube), rather than air, bubbling through the mercury to produce the pumping action. The relatively small amount of mechanical carryover of N_2O to the reaction system had negligible effect on the total pressure, whereas preliminary results with air or undried N_2O led to very irreproducible results in nitrogen production and diborane decomposition.

The low-pressure mercury arc was constructed of 8 mm. o.d. Vycor tubing close-wound in the form of a flat spiral three inches in diameter. It was filled with neon (12 mm.) and a drop of mercury to saturate the gas with mercury vapor. A Corning No. 7910 Vycor filter was used to eliminate light of 1849 Å. wave length from the reaction cell. The effective intensity of the 2537 Å. radiation was determined with a propane actinometer,[12] and the light was monitored with an RCA 935 photocell.

Reagents.—Diborane was prepared and purified *in vacuo* from lithium aluminum hydride and boron trifluoride etherate by the method of Shapiro, *et al.*,[13] and stored at room

(1) From the thesis by F. P. Fehlner, submitted in partial fulfillment of the requirements for the Ph.D. degree to the Graduate School, Rensselaer Polytechnic Institute, 1959. Available from University Microfilms, Ann Arbor, Michigan.

(2) Presented at the 137th meeting of the American Chemical Society, Cleveland, April, 1960.

(3) F. P. Price, *J. Am. Chem. Soc.*, **72**, 5361 (1950).

(4) A. T. Whatley and R. N. Pease, *ibid.*, **76**, 1997 (1954).

(5) W. Roth and W. H. Bauer, "Fifth Symposium on Combustion," Reinhold Publ. Corp., New York, N. Y., 1955, p. 710.

(6) W. Roth and W. H. Bauer, THIS JOURNAL, **60**, 639 (1956).

(7) W. H. Bauer and S. E. Wiberley, Abstracts of Papers of the 133rd Meeting, American Chemical Society, San Francisco, April, 1958, p. 13-L.

(8) A. Alberto, Jr., Dissertation, Rensselaer Polytechnic Institute, Troy, N. Y., 1953.

(9) R. J. Cvetanovic, *J. Chem. Phys.*, **23**, 1203 (1955).

(10) R. J. Cvetanovic, *J. Chem. Phys.*, **23**, 1375 (1955); *Can. J. Chem.*, **34**, 775 (1956); *J. Chem. Phys.*, **25**, 376 (1956); *Can. J. Chem.* **36**, 623 (1958); *J. Chem. Phys.*, **30**, 19 (1959).

(11) R. E. Dodd and P. L. Robinson, "Experimental Inorganic Chemistry," Elsevier Press, Inc., Houston, Texas, 1954, p. 118.

(12) S. Bywater and E. W. R. Steacie, *J. Chem. Phys.*, **19**, 319 (1951).

(13) I. Shapiro, H. G. Weiss, M. Schmich, S. Skolnik and G. B. L. Smith, *J. Am. Chem. Soc.*, **74**, 901 (1952).

temperature behind a mercury cutoff. Just before use, it was frozen out at −196° and the hydrogen (from the thermal decomposition) removed. The required amount of diborane was then removed at a temperature low enough to prevent contamination by higher hydrides. Matheson Company nitrous oxide (98.0%) and propane (99.9%) were dried by trap-to-trap distillation. No impurities were detected by mass spectrometry.

Product Analysis.—The condensable products of a photolysis were trapped at −196° in a Le Roy still.[14] The noncondensables (hydrogen and nitrogen, but no oxygen, as shown by mass spectrometry and reaction with white phosphorus in preliminary determinations) were measured in a gas buret and transferred to a Cu–CuO furnace at about 300°, after which the unreacted nitrogen (which served as an internal actinometer) was measured with the gas buret and the amount of hydrogen in the original mixture was obtained by difference. Reproducibility was approximately ±5%.

Three fractions were recovered from the Le Roy still. The first, which was removed at −175°, contained all of the unreacted diborane, plus a small amount of nitrous oxide. It was measured with the gas buret and analyzed mass spectrometrically. The second fraction (−145°) was made up of most of the remaining nitrous oxide, and was discarded. The third fraction, recovered at room temperature, contained tetraborane, pentaborane, trace amounts of higher boron hydrides, and some nitrous oxide. It also was measured with the gas buret and analyzed with the mass spectrometer. Results of these analyses were reproducible to within ±10%.

Erratic and (as subsequently shown) low results of tetraborane analysis were experienced when all of the N_2O was removed from the Le Roy still at −145°. That all of the tetraborane and pentaborane were recovered by not removing all of the N_2O was demonstrated in a separate run wherein methanol (plus water) was added to the combined N_2O, B_4H_{10} and B_5H_9 fractions. The amount of hydrogen recovered, based on the reactions

$$B_4H_{10} + 12CH_3OH \longrightarrow 4B(OCH_3)_3 + 11H_2$$
$$B_5H_9 + 15CH_3OH \longrightarrow 5B(OCH_3)_3 + 12H_2$$

agreed within ± 1% with that calculated from mass spectrometric analyses of tetraborane and pentaborane in samples from similar runs.

In addition to the above products, a white solid was produced in the reaction cell. By infrared analysis, it appeared to be the same as that obtained from the slow oxidation of diborane[15] and pentaborane-9.[16] It spontaneously evolved hydrogen, most of it easily underwent methanolysis, and it could be hydrolyzed slowly, the latter reactions also producing hydrogen. Boron analysis was carried out by converting the solid to boric acid and titrating in the presence of mannitol with sodium hydroxide. In order to obtain enough boron to analyze quantitatively by this method, it was necessary to accumulate samples over several runs. A mass balance, from the diborane consumption and amounts of gaseous products formed, gave an empirical formula of $(BHO)_x$ for the solid; however, only about 60% of the boron and hydrogen was recovered by the above methods of analysis.

Except for trace amounts of hexaborane, no other products, particularly the "intermediate" that has been identified as a partial oxidation product in the slow oxidation of diborane[15] and pentaborane,[7,17] were found. Analytical methods used in an attempt to detect this intermediate were gas–liquid chromatography, mass spectrometry, infrared and total mass balance. Presumably molecular oxygen is necessary for the formation of this partial oxidation product.

Results

The general behavior of photolyses involving diborane, nitrous oxide and mercury was similar to that obtained with various hydrocarbons by Cvetanovic.[10] A slight increase in the nitrogen quantum yield with increasing light intensity was observed (Table I) which may have been due to the reaction of nitrous oxide with molecular fragments from the direct mercury photosensitized decomposition of diborane

$$R + N_2O \longrightarrow N_2 + RO$$

However, the rate of R production must depend on the light intensity to a power greater than unity. Similar reactions involving hydrocarbon free radicals and nitrous oxide have been suggested in other mechanisms,[18] although Cvetanovic[19] has detected no evidence for reactions of this type in his work with hydrocarbons. If the results of this work are extrapolated to zero diborane pressure *and* zero light intensity, a value of 0.75 for Φ_{N_2} is obtained, which is within experimental error of the constant value obtained by Cvetanovic.[9] The interaction of metastable Hg (6^3P_0) atoms may also be involved through a reactivation step leading to the 6^3P_1 state.

TABLE I

EFFECT OF LIGHT INTENSITY ON NITROGEN QUANTUM YIELD AT 25°

$[B_2H_6]/[N_2O] = 0.07$; $P_{N_2O} = 200$ mm.

$I_a \times 10^8$, einsteins/min.	R_{N_2}, μmoles/min.	Φ_{N_2}
13.1	0.085	0.65
70	.46	.66
108	.89	.82
167	1.31	.79
264	2.31	.88

In order to obtain kinetic information the amounts of diborane used and products formed were determined at room temperature and 100° as a function of time at several light intensities (2×10^{-8} to 3.3×10^{-6} einsteins/minute) and at diborane-to-nitrous oxide ratios of 0.07, 0.14 and 0.21. Typical results are shown in Fig. 1 ($I_a = 1.67 \times 10^{-6}$ einsteins/minute, $[B_2H_6]/[N_2O] = 0.07$) where amounts of products formed are plotted *vs.* nitrogen produced. (The amount of nitrogen produced, rather than time, was used as a measure of the extent of reaction in order to minimize drifts resulting from the decrease in light intensity with time due to clouding of the cell windows by the solid product. Rates of reaction were obtained by combining a plot of nitrogen production *vs.* time with the above data.) Under all conditions, a decrease in the rate of tetraborane production was observed at low percentage diborane decomposition. The steady-state concentration of tetraborane which was eventually reached (Fig. 1) was inversely proportional to $(I_a)^{1/2}$, and appeared to vary with $[B_2H_6]^{3/2}$. The region of tetraborane steady state was characterized by a decrease in the rate of diborane decomposition and pentaborane-9 production (Fig. 1), although this latter result is uncertain because of the relatively small amount of pentaborane produced.

At 100°, the tetraborane concentration reached a steady state at a very low diborane conversion, while the rate of pentaborane production decreased markedly with time. However, due to the thermal

(14) D. J. Le Roy, *Can. J. Research*, **28B**, 492 (1950).

(15) M. S. Goldstein, Ph.D. dissertation, Rensselaer Polytechnic Institute, Troy, N. Y., 1960.

(16) J. A. Hammond, Ph.D. dissertation, Rensselaer Polytechnic Institute, Troy, N. Y., 1958.

(17) J. F. Ditter and I. Shapiro, *J. Am. Chem. Soc.*, **81**, 1022 (1959).

(18) E. W. R. Steacie, "Atomic and Free Radical Reactions," Second Edition Reinhold Publ. Corp., New York, N. Y., 1954, Vol. 2, pp. 647, 652.

(19) R. J. Cvetanovic, private communication.

TABLE II

RATES OF PRODUCT FORMATION AND DIBORANE DECOMPOSITION

Reaction system volume = 350 ml.; P_{N_2O} = 200 mm. (Blank spaces indicate values not determined)

$I_a \times 10^8$, einsteins/min.	$[B_2H_6]/[N_2O]$	Temp., °C.	Initial rates, μmoles/min. N_2	H_2	B_2H_6 used	B_4H_{10}	B_5H_9	Solid[b] (boron)	Rates at B_4H_{10} steady state, μmoles/min. B_2H_6 used	B_5H_9	Steady-state concn., μmoles B_4H_{10}	B_5H_9
2[a]	0.07	25	0.013	0.020	0.014	0.0036	0.00024	...	..	....	..	..
13.1	.07	25	0.085	0.121	0.084	.0205	.0041	0.081	..	0.0024	9.6	..
167	.07	25	1.31	1.55	1.01	.163	.0435	1.14	0.41	.011	6.5	..
264	.07	25	2.31	2.78	1.84	.236	.0764	2.34	1.13	.046	5.3	..
330[a]	.07	25	2.99	3.34	..	..	....	..	..	...	5.0	3.2
150[a]	.14	25	1.05	1.49	..	.2	.052	..	..	...	18.5	..
167	.21	25	1.05	1.54	1.28	.46	.070	..	0.60	...	29.1	..
90[a]	.07	100	0.65	1.01	1.13	...	.110	..	0.28	...	2.1	10.5

[a] Estimated from nitrogen yields. [b] Calculated by difference.

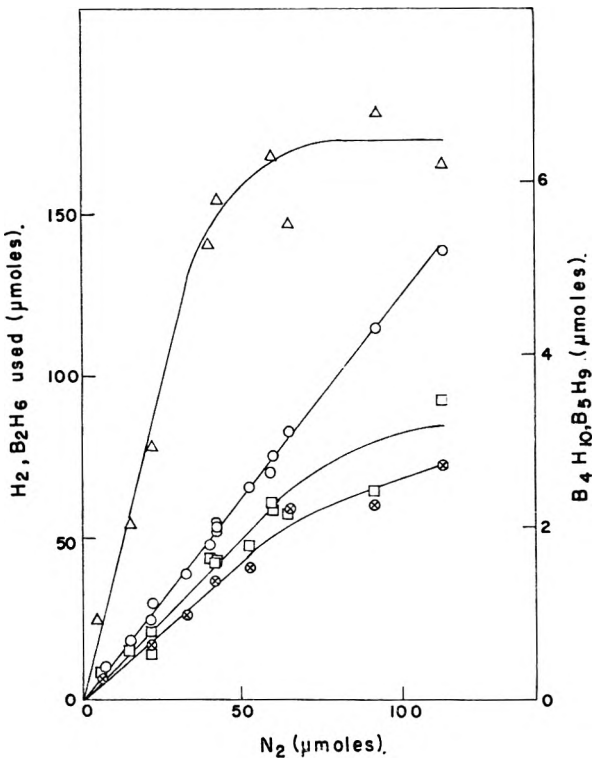

Fig. 1.—Uncorrected yields of products and disappearance of diborane. Conditions: temp. = 25°; $I_a = 1.67 \times 10^{-8}$ einsteins/min.; $[B_2H_6]/[N_2O] = 0.07$; P_{N_2O} = 200 mm. Key: ○, H_2; △, B_4H_{10}; □, B_5H_9; ⊗, B_2H_6 used.

instability of diborane[20] and tetraborane[21] at this temperature, these results are subject to considerable uncertainty. Thus, at 100° the tetraborane steady-state concentration was the same in the dark run, in the photolysis of diborane alone, and in the photolysis of the mixture.

Although the nitrous oxide was present in much larger amounts than the diborane, some diborane was destroyed by direct mercury photosensitization. A correction for this reaction required a knowledge of the diborane quenching cross section of Hg (6^3P_1) atoms, which was determined by the method of Cvetanovic.[22] The cross section relative to a substance of known quenching cross section (*i.e.*, *n*-butane) is obtained from the slope and *y*-intercept of a plot of $1/\Phi_{N_2}$ *vs.* $[B_2H_6]/[N_2O]$. The value for diborane thus calculated was 23.6 Å.^{2}.

In order to apply this correction, it was necessary to extend the work of Hirata and Gunning[23] on the direct mercury photosensitized decomposition of diborane to the lower pressures used in this work. A correction for the hydrogen produced by the thermal decomposition of diborane was small at room temperature, but appreciable at the higher temperature. No thermal reaction was observed between N_2O and B_2H_6, either at 25 or 100°.

TABLE III

INITIAL YIELD PER OXYGEN ATOM[a]

$I_a \times 10^8$, einsteins/min.	$[B_2H_6]/[N_2O]$	Temp., °C.	H_2	B_2H_6 used	B_4H_{10}	B_5H_9	Solid
2	0.07	25	1.54	1.08	0.28	0.018	..
13.1	.07	25	1.42	0.99	.24	.048	0.95
167	.07	25	1.18	.77	.13	.033	0.87
264	.07	25	1.20	.80	.10	.033	1.01
330	.07	25	1.12	..	..	...	..
150	.14	25	1.42	..	.2	.050	..
167	.21	25	1.47	1.22	.44	.067	..
90	.07	100	1.55	1.74	..	.169	..

[a] P_{N_2O} = 200 mm.

Results are given in Table II. Included are initial rates and rates measured at the tetraborane steady state. Since no higher oxides of nitrogen or molecular oxygen were produced, the rates relative to that of nitrogen production represent the rates of product formation per oxygen atom produced. These are given in Table III for the initial rates.

Discussion

The data may be interpreted in terms of a chain-reaction type of mechanism. The initial action is the production of oxygen atoms by the mercury photosensitized decomposition of nitrous oxide

$$Hg(6^1S_0) + h\nu \longrightarrow Hg(6^3P_1)$$
$$Hg(6^3P_1) + N_2O \longrightarrow N_2 + O + Hg(6^1S_0) \quad (1)$$

Initial Rates.—The reaction between oxygen atoms and diborane, under conditions of low prod-

(20) R. P. Clarke and R. N. Pease, *J. Am. Chem. Soc.*, **73**, 2132 (1951); J. K. Bragg, L. V. McCarty and F. J. Norton, *ibid.*, **73**, 2134 (1951).

(21) R. K. Pearson and L. J. Edwards, Abstracts of Papers of the 132nd Meeting, American Chemical Society, New York, September, 1957, p. 15-N.

(22) R. J. Cvetanovic, *J. Chem. Phys.*, **23**, 1208 (1955).

(23) T. Hirata and H. E. Gunning, *ibid.*, **27**, 477 (1957).

uct concentrations, is postulated to proceed by the mechanism

$$O + B_2H_6 \longrightarrow BH_2O + BH_3 \quad (2)$$
$$BH_3O \longrightarrow H_2 + (\text{solid}) \quad (3)$$
$$2BH_3 \longrightarrow B_2H_6 \quad (4)$$
$$BH_3 + B_2H_6 \longrightarrow B_3H_7 + H_2 \quad (5)$$
$$B_3H_7 + B_2H_6 \longrightarrow B_4H_{10} + BH_3 \quad (6)$$
$$\longrightarrow B_5H_9 + 2H_2 \quad (7)$$

Although there is a rapid depletion of Hg atoms in the photosensitized decomposition of N_2O alone[9] (indicating oxide formation), in the presence of diborane there is no mercury depletion or molecular oxygen produced, and reaction 2 appears to be the only reaction involving oxygen atoms, even at the lowest B_2H_6 pressure used. The reaction of oxygen atoms with diborane is therefore comparable to the effect found by Cvetanovic in the reaction of oxygen atoms with various olefins,[10] whereby considerable splitting of the C–C bond occurred with the smaller molecules, such as ethylene.

The white solid from reaction 3, which was shown to contain boron, hydrogen and oxygen, was found primarily on the window facing the mercury light source. Its properties have been discussed above.

Borine, BH_3, produced by reaction 2, can combine to form B_2H_6 or can react with the substrate diborane to produce B_3H_7 and H_2 (reaction 5). Reaction 5 has been proposed in the mechanism at the second explosion limit of the diborane–oxygen system,[5] as well as other reactions of the boranes.[24,25]

Expressions for the rate of disappearance of diborane and rates of formation of hydrogen, tetraborane, pentaborane-9 and solid can be derived from this mechanism assuming the usual steady states for the reactive intermediates O, BH_2O and B_3H_7. Thus

$$-R_{B_2H_6} = {}^1/_2R_{N_2} + 2R_{B_4H_{10}} + ({}^5/_2)R_{B_5H_9}$$
$$R_{H_2} = R_{N_2} + R_{B_4H_{10}} + 3R_{B_5H_9}$$
$$R_{solid} = R_{N_2}$$
$$\frac{R_{B_4H_{10}}}{R_{B_5H_9}} = \frac{k_6}{k_7}$$

Initial rates calculated from these expressions are compared in Table IV with the observed rates. Although the mechanism is undoubtedly oversimplified, it is in good agreement with the experimental data at all intensities and at low diborane pressures. It is possible that the discrepancies at higher diborane concentrations are due to the uncorrected interference of radicals from the mercury photosensitized decomposition of diborane.

The thermal decomposition of diborane and reaction products at 100° precludes any valid interpretation at the higher temperature. Salient observations were: the hydrogen yield per oxygen atom (*i.e.*, the rate of hydrogen production divided by the rate of nitrogen production) was constant and the same at 100° as at room temperature; the tetraborane concentration rapidly reached a steady state, which was presumably thermal; the rate of pentaborane-9 production decreased at low diborane decomposition, and the pentaborane concentration may even have reached a steady state. Part of the solid product formed was not removed by methanol, and probably was a boron hydride polymer.

Another possibility for the initial step (reaction 2) is the abstraction of a hydrogen atom

$$O + B_2H_6 \longrightarrow OH + B_2H_5$$

The formation of OH has been postulated as the initial step in the reaction of oxygen atoms with hydrocarbons.[26] However, calculated rates using this reaction were inconsistent with the experimental data. The symmetrical cleavage of the double bridge bond is also consistent with most known reactions of diborane.[27]

Tetraborane Steady State.—A steady-state tetraborane concentration was reached at relatively low diborane decomposition (Fig. 1). This is assumed to be due to a competitive reaction between oxygen atoms and tetraborane

$$O + B_4H_{10} \longrightarrow BH_2O + B_3H_7 \quad (8)$$

which leads to the observed decrease in the rate of diborane consumption. The intermediate products, BH_2O and B_3H_7, eventually lead to hydrogen (reactions 3 and 7), so that the rate of hydrogen production remains approximately constant throughout the course of the photolysis.

Again assuming the steady state for the intermediates O, BH_3, BH_2O and B_3H_7, as well as for the tetraborane, the expressions are obtained

TABLE IV

COMPARISON OF PREDICTED AND OBSERVED INITIAL RATES AT 25°[a]

$I_a \times 10^8$, einsteins/min.	$[B_2H_6]/[N_2O]$	Rates (μmoles/min.) Predicted R_{H_2}	Predicted $-R_{B_2H_6}$	Predicted R_{solid}	Predicted k_6/k_7	Observed R_{H_2}	Observed $-R_{B_2H_6}$	Observed R_{solid}
2	0.07	0.017	0.014	...	15.0	0.020	0.014	..
13.1	.07	0.118	0.094	0.085	5.0	0.121	0.084	0.081
167	.07	1.60	1.09	1.31	3.7	1.55	1.01	1.14
264	.07	2.78	1.82	2.31	3.1	2.78	1.84	2.34
150	.14	1.40	..	..	4	1.49	..	..
167	.21	1.72	1.62	..	6.6	1.54	1.28	..

[a] P_{N_2O} = 200 mm.

TABLE V

COMPARISON OF PREDICTED AND OBSERVED RATES AT 25° AT THE TETRABORANE STEADY STATE[a]

$I_a \times 10$ einsteins/min.	$[B_2H_6]/[N_2O]$	Rates (μmoles/min.) Predicted R_{H_2}	Predicted $-R_{B_2H_6}$	Obsd. R_{H_2}	Obsd. $-R_{B_2H_6}$
2	0.07	0.014	..	0.020	..
13.1	.07	0.097	..	0.121	..
167	.07	1.44	0.76	1.55	0.41
264	.07	2.54	1.35	2.78	1.13
150	.14	1.21	..	1.49	..
167	.21	1.26	0.70	1.54	0.60

[a] P_{N_2O} = 200 mm.

(24) W. C. Kreye and R. A. Marcus, Abstracts of Papers of the 134th Meeting, American Chemical Society, Chicago, September, 1958, p. 6-S.

(25) H. J. Emeleus and A. G. Sharpe, "Advances in Inorganic Chemistry and Radiochemistry," Vol. 1, Academic Press, Inc., New York, N. Y., 1959, p. 149.

(26) E. W. R. Steacie, "Atomic and Free Radical Reactions," Second Edition, Vol. 2, Reinhold Publ. Corp., New York, N. Y., 1954, p. 602.

(27) R. W. Parry and L. J. Edwards, *J. Am. Chem. Soc.*, 81, 3554 (1959).

$$-R_{B_2H_6} = {}^1/_2R_{N_2} + {}^5/_2R_{B_5H_9}$$
$$R_{H_2} = R_{N_2} + 3R_{B_5H_9}$$
$$R_{solid} = R_{N_2}$$

Predicted rates are compared in Table V with the observed rates at the intensities at which the pentaborane-9 rate of production appeared to have reached again a constant value. The lack of complete agreement indicates an incomplete mechanism. Neglected is the further competitive reaction

$$O + B_5H_9 \longrightarrow \text{products}$$

which could account for the observed decrease in the rate of pentaborane production.

Acknowledgment.—The authors gratefully acknowledge support in part by National Science Foundation grant NSF-G7383.

SURFACE HYDROXYL GROUPS ON γ-ALUMINA[1]

BY J. B. PERI AND R. B. HANNAN

Research and Development Department, Standard Oil Company, Whiting, Indiana

Received April 29, 1960

Even after drying at 1000° γ-alumina continues to evolve traces of water on further heating. This water appears to be bound to the surface of alumina and is known to affect its catalytic properties. To investigate the nature of bound water present in less than monolayer amounts, infrared study was made of transparent sheets of alumina aerogel. Hydroxyl groups, as well as water molecules, are initially held on the alumina surface. Heating at 400° removes all water molecules, but leaves many of the hydroxyl groups. Alumina dried above 650° gives absorption bands at 3698, 3737 and 3795 cm.$^{-1}$, assignable to "isolated" hydroxyl groups. These three bands can be eliminated from the spectrum either by further heating or by deuterium exchange, but they are not all removed at the same rate. Spectral changes ranging from perturbations to removal or creation of hydroxyl bands are observed as a result of interactions of the hydroxyl groups with adsorbed molecules other than water. Independent variations observed in the intensities of the three hydroxyl bands indicate that these bands represent chemically distinct groups on at least three different types of surface sites. Such groups may play different roles in catalytic reactions on alumina.

Introduction

The catalytic properties of γ-alumina depend largely upon the extent to which it has been dried.[2-4] Even after drying at 1000°, it continues to evolve traces of water, which is generally assumed to be bound as hydroxyl groups and is widely believed to exist on the surface of alumina crystallites. Hydroxyl groups have been assumed to supply protons, either directly[5] or indirectly,[6] in certain catalytic reactions on alumina. Removal of hydroxyl groups has been postulated as creating on the surface strained sites that are catalytically active.[4,7] Little direct evidence is available, however, concerning the nature of either the adsorbed water or the hydroxyl groups.

Direct study of hydroxyl groups on alumina has been handicapped by the lack of good experimental techniques. Infrared spectroscopy has shown much promise in studies of surface groups and adsorbed molecules on solid adsorbents.[8] However, it has given little detailed information about hydroxyl groups or adsorbed water on alumina,[9-11] because the aluminas used have caused high scattering losses.

The recent development of transparent plates of highly porous γ-alumina aerogel[12] has greatly reduced the problem of scattering losses. Through increased sensitivity and convenience, they permit infrared study of surface hydroxyl groups at low coverages. Spectral changes resulting from exchange of surface hydroxyl groups with deuterium, or from reaction with or perturbation by various adsorbed molecules, have also been studied to obtain further information.

Experimental

Sol containing 5 to 7 weight % alumina was prepared from high-purity aluminum and acetic acid with a mercuric oxide catalyst. Floating layers of the sol were converted[12] to transparent plates of aerogel. After calcination in air at 600° to remove impurities, plates had specific surface areas of 300 to 350 m.^{2}/g., as measured by nitrogen adsorption, and were shown by X-ray analysis to be γ-alumina. The surface areas decreased by 10 to 20% after prolonged use involving repeated evacuation at temperatures up to 950° and subsequent rehydration, but X-ray analysis showed no conversion to α- or θ-alumina. After vacuum drying at 600° plates up to 5 mm. thick (~80 mg./cm.^{2}) transmitted 90% or more of the incident radiation at 2.5 μ.

Reagents used were high-grade commercial materials further purified in the laboratory. Deuterium gas (Stewart Oxygen Co.; purity > 99.5%) was passed through a trap containing activated charcoal cooled with liquid nitrogen. Deuterium oxide (Stewart Oxygen Co.) was used without further treatment. All other chemicals were dried and then freed of permanent gases by vacuum distillation. These chemicals and the drying agents used were: reagent grade carbon tetrachloride, P_2O_5; ammonia (Matheson-anhydrous), freshly ignited CaO; 1-butene (Matheson C.P.), magnesium perchlorate; HCl (Matheson anhydrous), P_2O_5.

A Model 112 Perkin-Elmer spectrometer equipped with calcium fluoride optics was used. Spectrometer housings were flushed with dry air passed over Ascarite to remove carbon dioxide. Spectral band width in the hydroxyl-stretching region was about 10 cm.$^{-1}$.

(1) Presented at 136th Meeting, American Chemical Society, Atlantic City, September, 1959.

(2) J. C. F. Holm and R. W. Blue, *Ind. Eng. Chem.*, **43**, 501 (1951).

(3) W. S. Brey, Jr., and K. A. Krieger, *J. Am. Chem. Soc.*, **71**, 3637 (1949).

(4) S. G. Hindin and S. W. Weller, *Advances in Catalysis*, **IX**, 70 (1957).

(5) A. G. Oblad, J. U. Messenger and H. T. Brown, *Ind. Eng. Chem.* **39**, 1462 (1947).

(6) D. A. Dowden, *J. Chem. Soc.*, 242 (1950).

(7) E. B. Cornelius, T. H. Milliken, G. A. Mills and A. G. Oblad, THIS JOURNAL, **59**, 809 (1955).

(8) R. P. Eischens and W. A. Pliskin, *Advances in Catalysis*, **X**, 1 (1958).

(9) W. A. Pliskin and R. P. Eischens, THIS JOURNAL, **59**, 1156 (1955).

(10) A. C. Yang and C. W. Garland, *ibid.*, **61**, 1504 (1957).

(11) R. H. Lindquist and D. G. Rea, Presented at 132nd Meeting, American Chemical Society, New York, September, 1957.

(12) J. B. Peri and R. B. Hannan, *Spectrochim. Acta*, **16**, 237 (1960).

The infrared cell, shown in Fig. 1, was constructed of Vycor and quartz and permanently mounted in normal position in the spectrometer. Calcium fluoride windows were sealed with silver chloride to thin silver flanges, which were similarly sealed to the Vycor cell. Glyptal was used to seal any pinholes found in the window seals, and silver chloride or sealing wax was used to seal the ground joint. The aerogel plate could be moved between the furnace section and the infrared beam by an external magnet. Reproducible positioning of the plate in the beam was assured by the design of the cell and sliding armature. Either the alumina and the surrounding gas or the gas phase alone could be studied before evacuation. Temperature of the furnace section was controlled within 5°.

The vacuum system was of conventional design. A mercury diffusion pump permitted evacuation of the cell to less than 10^{-5} mm. of mercury. Provision was made for introduction of known amounts of various gases and vapors and for subsequent recovery of gases for analysis. Pressures were measured with mercury manometers and McLeod gauges.

Aerogel plates were usually evacuated for 1 to 2 hours at a given temperature and subsequently cooled to room temperature before spectra were recorded. Longer periods of evacuation were not considered necessary, because removal of water from alumina occurs slowly after the first half hour and the extent of drying could be estimated from the spectra.

Adsorption of various compounds was carried out at low pressures, and an appreciable fraction of the added material was usually adsorbed. At appropriate intervals, the alumina was calcined *in situ* at 600° in oxygen to remove possible organic contaminants. It was then rehydrated by admitting water vapor to the cell to about 1 cm. pressure and heating at 100 to 500° for periods of 15 minutes to 16 hours. Deuterium oxide was used to rehydrate the alumina in certain cases to produce a "deuterated" plate. Alternatively, the alumina was deuterated by exchange with deuterium oxide or deuterium gas.

Results and Discussion

Undried γ-alumina aerogel shows strong broad adsorption bands near 3300 and 1650 cm.$^{-1}$, corresponding to stretching and bending frequencies found in the spectrum of liquid water. These bands disappear after evacuation at 400°. A group of poorly resolved bands remains near 3700 cm.$^{-1}$ with a broad "tail" at lower frequencies. As the alumina is dried at higher temperatures, the "tail" disappears and the remaining bands decrease in number and intensity but become more sharply defined.

After evacuation at 650 to 700°, γ-alumina has well-defined absorption maxima at 3698, 3737 and 3795 cm.$^{-1}$.[13] These frequencies are within or above the range expected for the stretching vibrations of hydroxyl groups that are not hydrogen-bonded.[14] Such groups will be referred to as "isolated." Exposure of the alumina to deuterium oxide vapor and re-evacuation at 700° removed these three bands and produced three new ones at 2733, 2759 and 2803 cm.$^{-1}$. These frequencies are in the deuteroxyl-stretching range, and each is related to the original frequency by the factor 0.738. All three of the original frequencies must therefore have been due to hydroxyl-stretching vibrations. Because isotopic substitution shifted each band by the same factor, the multiplicity of bands cannot be due to combinations of a single hydroxyl frequency with alumina-lattice vibrations.

(13) Rea and Lindquist reported at the 136th Meeting of the American Chemical Society (Atlantic City, September, 1959) their finding of three hydroxyl bands similar in frequency to those reported here. Their study was made on pressed disks of γ-alumina powder prepared from aluminum isopropoxide and dried at 600°.

(14) L. J. Bellamy, "The Infrared Spectra of Complex Molecules," 2nd Edition, John Wiley and Sons, Inc., New York, N. Y., 1958.

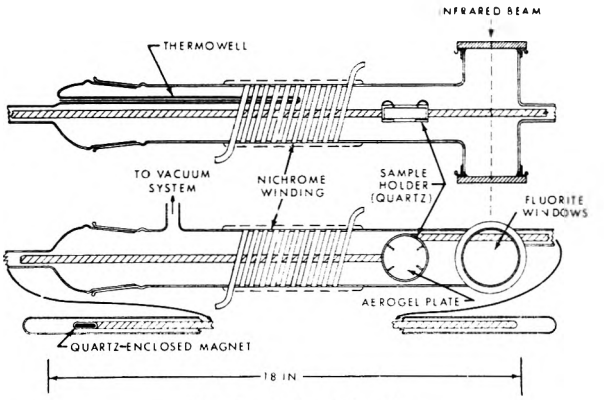

Fig. 1.—Infrared cell.

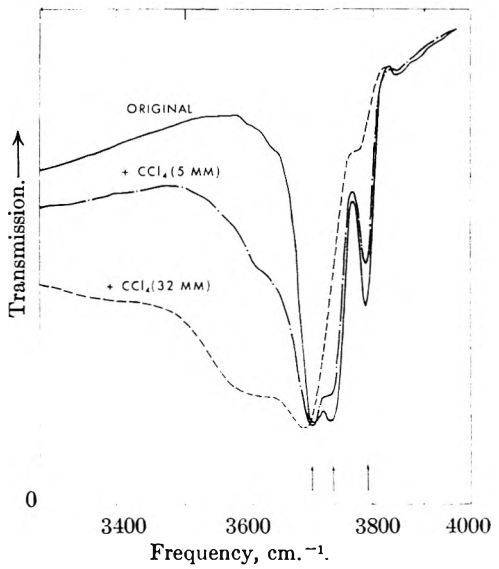

Fig. 2.—Effect of adsorbed CCl_4 on hydroxyl bands.

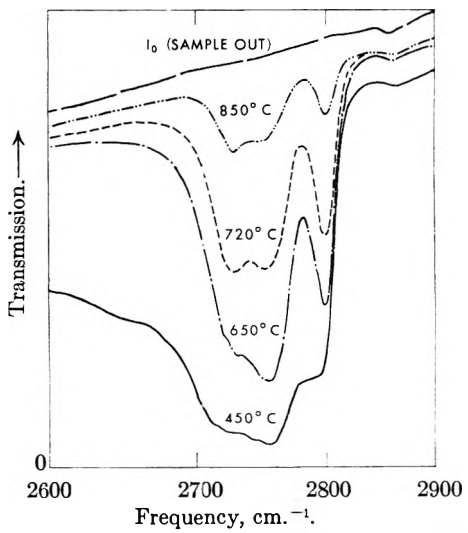

Fig. 3.—Removal of deuteroxyl groups by evacuation.

Adsorption of large molecules generally reduces the peak intensity of the surface-hydroxyl bands and broadens and shifts them to lower frequencies. The effects observed when carbon tetrachloride is adsorbed on alumina predried at 800° are shown

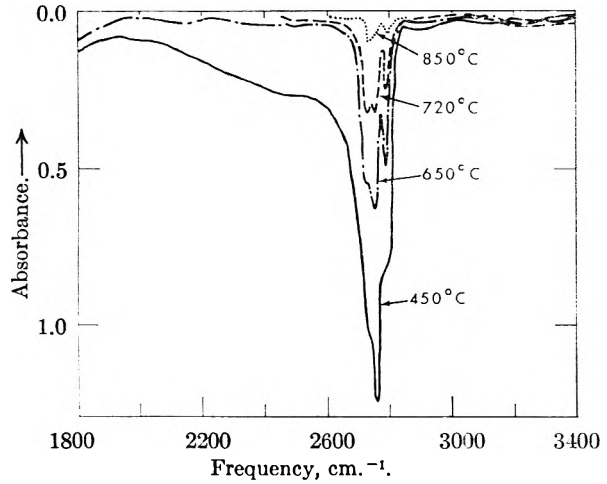

Fig. 4.—Removal of deuteroxyl groups by evacuation (replotted spectra).

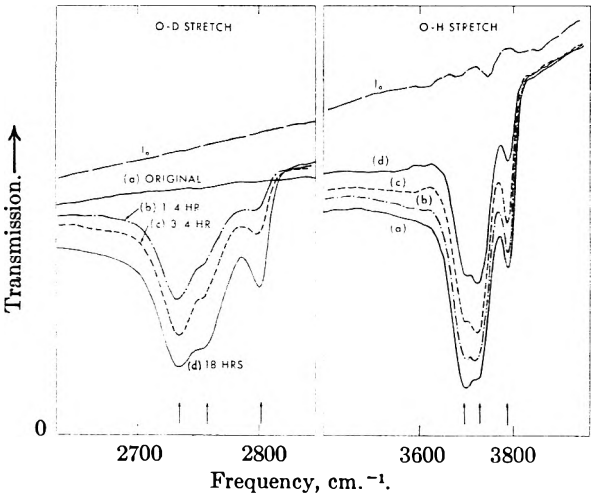

Fig. 5.—Exchange between D_2 and hydroxyl groups at 250°.

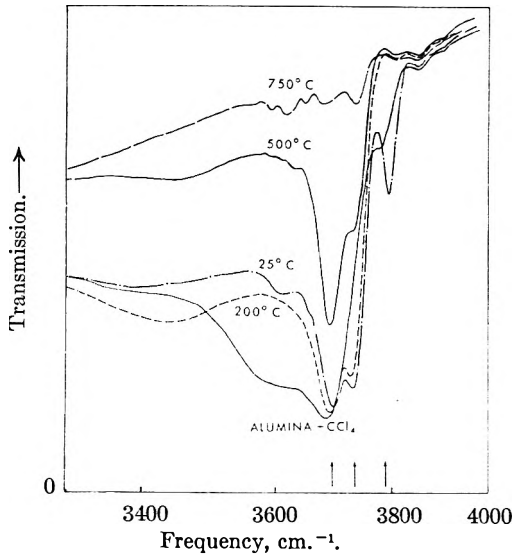

Fig. 6.—Removal of hydroxyl bands by desorption of carbon tetrachloride at indicated temperatures.

in Fig. 2.[15] The spectra were obtained with the indicated pressures of carbon tetrachloride in the cell. These effects demonstrate that the hydroxyl bands correspond to groups capable of directly interacting with adsorbed large molecules. The hydroxyl groups must therefore be on the surface, rather than within the alumina lattice.

Changes in deuteroxyl bands were produced by evacuating "deuterated" alumina at progressively higher temperatures. Almost all hydroxyl groups on the alumina had previously been converted to deuteroxyl groups by exchange with deuterium oxide. The observed results, shown in Fig. 3, are analogous to those for the hydroxyl bands. The deuteroxyl spectra are shown rather than the hydroxyl spectra because of the better resolution of the fluorite prism in this region. The central band decreased in intensity more rapidly than the other two, but all three clearly remained after drying at 850°. A better comparison of relative intensities is shown in Fig. 4, where the spectra are replotted on a linear absorbance scale over a wider frequency range. The "tail" at lower frequencies is evident for the alumina dried at 450°.

Hydroxyl groups can also be exchanged with deuterium gas. Between 250 and 500° exchange occurs at a convenient rate, depending on the degree of hydration of the alumina and the pressure of the deuterium gas. During such exchange, as shown in Fig. 5, the central band in both regions generally changed in intensity more slowly than the other bands. The lowest frequency band frequently changed faster than either of the others. At 250° complete equilibrium between deuteroxyl and hydroxyl bands was not reached even after 18 hours. Above 500°, however, equilibration occurred rapidly between all hydroxyl and deuteroxyl bands.

Further evidence of independent behavior of the three deuteroxyl bands was obtained during experiments involving butene and deuterated alumina predried at 800°. At 200°, only the band at 2733 cm.$^{-1}$ showed exchange of hydrogen with butene, the other two bands remaining unchanged. After this band had been completely converted to the corresponding hydroxyl band at 3698 cm.$^{-1}$, the cell was evacuated and the alumina heated to 400°. At this temperature, the bands at 2759 and 3698 cm.$^{-1}$ appeared to exchange or inter-convert to yield bands at 2733, 2759, 3698 and 3737 cm.$^{-1}$ in isotopic equilibrium. The band at 2803 cm.$^{-1}$ remained essentially unchanged.

Independent behavior of the individual hydroxyl or deuteroxyl bands was also observed in other experiments. An example of such behavior during removal of adsorbed carbon tetrachloride from alumina predried at 800° is shown in Fig. 6. The alumina originally held adsorbed carbon tetrachloride in equilibrium with the vapor at 32 mm. pressure. Evacuation at room temperature removed most of the adsorbed carbon tetrachloride and largely restored the three isolated hydroxyl bands. Evacuation at progressively higher temperatures, however, eliminated these bands in order from highest to lowest frequency, apparently as a result of reaction of hydroxyl groups with

(15) The spectra shown in the figures are, unless otherwise noted, smoothed tracings of the original spectra. The noise level in the original spectra was typically 1 to 2%.

residual carbon tetrachloride. After evacuation at 750°, all hydroxyl bands have disappeared from the alumina spectrum, the weak bands remaining being caused principally by residual water vapor in the spectrometer. A black deposit—apparently carbon—was left on the alumina.

Changes observed in hydroxyl and N–H stretching bands on alumina during adsorption and desorption of ammonia are shown in Fig. 7. When the surface held a large amount of adsorbed ammonia, the hydroxyl bands at highest and lowest frequency were greatly reduced in intensity and apparently shifted to lower frequencies. The central band, however, although somewhat shifted in frequency was reduced in intensity much less than the other two. When the alumina was subsequently heated *in vacuo* at 400° to desorb most of the ammonia, the lowest-frequency hydroxyl band increased beyond its original intensity. Concurrent changes in the N–H stretching spectra showed that the "ammonia" retained at 400° differed in character from the ammonia originally adsorbed at room temperature; hence transfer of a proton from the ammonia to an oxide ion may have occurred on heating ($NH_3 + O^- \rightarrow NH_2^- + OH^-$).

The independent variations in intensity of the hydroxyl and deuteroxyl bands are difficult to explain except on the basis that these three bands correspond to three chemically distinct types of hydroxyl groups on the alumina surface. The same data also show that groups of a single type cannot be readily converted to other types, and that the various types do not rapidly interchange hydrogen at temperatures up to at least 250°.

The number of hydroxyl groups on the alumina was obtained in several experiments by measuring the number of hydrogen atoms that could be exchanged with deuterium gas. Measured amounts of deuterium were exchanged with the alumina at 600° until the hydroxyl and deuteroxyl bands showed similar configurations and no longer changed with time. Mass-spectrometer analyses were made on the resulting mixtures of H_2, HD and D_2. Upon the assumption that each hydroxyl group occupies 8 Å.^{2} on a completely covered surface, typical results ranged from 40% coverage after drying at 400° to about 2% after drying at 800°. Although coverage depends primarily on drying temperature, it is also affected by the duration and rate of evacuation, as well as the number and distribution of hydroxyl groups initially present.

From spectra obtained during exchange with deuterium, the average infrared absorptivity of isolated hydroxyl groups was calculated to be about 8×10^4 cm.^{2}/mole. Beer's law can probably be used in comparing relative amounts of hydroxyl at coverages below 15%, where no hydrogen bonding appears to exist. Coverages after drying above 900° were estimated from absorbance to be 1% or less. The three hydroxyl bands were nevertheless still evident on such very dry alumina.

All three isolated hydroxyl bands could be restored in the spectrum of highly dried alumina by rehydrating the alumina with water vapor and subsequently evacuating above 600°. To investigate rehydration, enough water vapor to yield a final

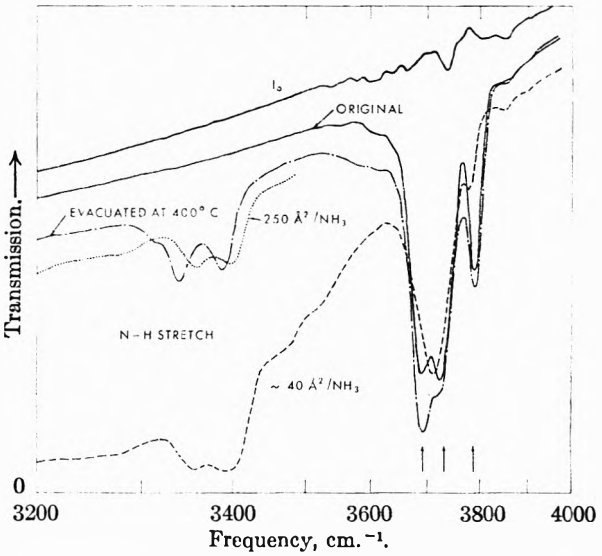

Fig. 7.—Adsorption of NH_3 on alumina predried at 800°

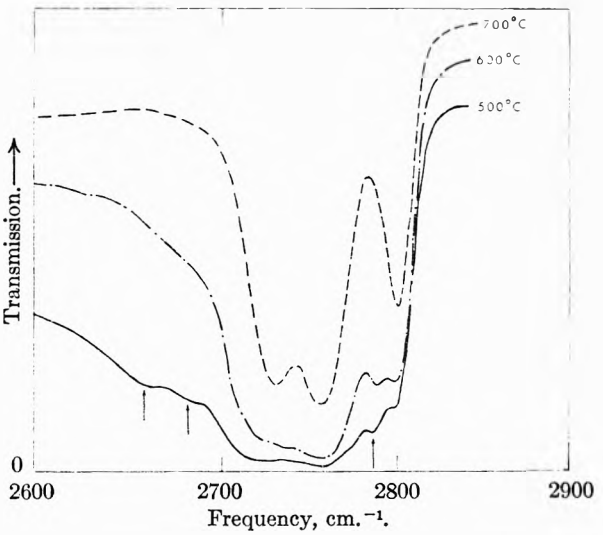

Fig. 8.—Detailed changes in O–D stretching bands on evacuation.

coverage of 40% was adsorbed at room temperature on alumina previously dried at 800°. Absorption bands produced were similar to those of the stretching and bending vibrations of liquid water. The hydroxyl band at 3795 cm.$^{-1}$ was replaced by a band near 3500 cm.$^{-1}$, but most of the isolated hydroxyl groups apparently were not perturbed by the adsorbed water. After standing at room temperature for one week, the alumina showed no significant spectral changes. Subsequent heating for half an hour in the closed system at 300° greatly reduced the "liquid" water bands, increased the isolated hydroxyl bands, and restored the band at 3795 cm.$^{-1}$. These results show that most of the added water did not react to form hydroxyl groups at room temperature but remained as molecular water. If some hydroxyl groups were produced, they became isolated groups only after heating. Water molecules did react with alumina at 300° to form hydroxyl groups and many of these were isolated. The greatest increase was observed at 3698 cm.$^{-1}$.

The spectral changes observed on drying alumina can be accounted for logically. After calcination at 600° and exposure to moist air, the alumina surface at room temperature holds both molecular water and surface hydroxyl groups. As it is heated during drying, water molecules not desorbed and removed from the system react to form hydroxyl groups. At higher temperatures, the reverse reaction causes surface hydroxyl groups to form water molecules, which are desorbed and removed. Ultimately, three types of hydroxyl groups remain, which represent isolated groups on different types of surface sites. Figure 8 shows detailed changes in the spectrum of a fairly thick plate of "deuterated" alumina as it is dried above 500°. The spectra recorded after drying at 500 and 600° have more than three absorption maxima. Several bands disappear between 500 and 700°. Some of these bands are probably caused by hydrogen-bonding between closely spaced hydroxyl groups. The broad tail at frequencies below those of the isolated hydroxyl bands is also believed to be caused by vibrations of hydrogen-bonded hydroxyl groups.

(16) M. Atoji and D. E. Williams, *J. Chem. Phys.*, **31**, 329 (1959).

Conclusion

The high frequencies of the bands remaining after drying at high temperatures suggest—but do not prove—that the attachment of hydroxyl groups to the surface is largely ionic in character. The observed frequencies lie above those normally found for metallic hydroxides which are not hydrogen bonded,[16] probably as a result of the location of the hydroxyl groups on the surface. The largely ionic character of alumina[17] appears to support this interpretation.

The groups corresponding to the band at 3698 cm.$^{-1}$ are apparently the most "acidic" of the three types of hydroxyl groups, as shown by the greater ease with which they exchange hydrogen. This behavior appears consistent with their lower vibrational frequency.

The different types of hydroxyl groups may well play different roles in catalytic reactions on alumina. Variations in the relative abundance of these types may be more important than the total amount of chemically bound water. Further work is in progress to elucidate the nature of these groups and the sites to which they are bound.

(17) R. Bersohn, *ibid.*, **29**, 326 (1958).

HEATS OF COMBUSTION AND FORMATION OF THE HIGHER NORMAL ALKYL CYCLOPENTANES, CYCLOHEXANES, BENZENES AND 1-ALKENES IN THE LIQUID STATE AT 25°[1]

BY SISTER M. CONSTANCE LOEFFLER, R.S.M., AND FREDERICK D. ROSSINI[2]

Chemical and Petroleum Research Laboratory, Carnegie Institute of Technology, Pittsburgh 13, Pennsylvania

Received April 29, 1960

Measurements were made of the heats of combustion, relative to that of *n*-hexadecane, of *n*-decylcyclopentane, *n*-decylcyclohexane, 1-hexadecene and *n*-decylbenzene, in the liquid state at 25°. The data confirm the work of Fraser and Prosen that, within the limits of present-day measurements, the increment per CH_2 group, in the heat of combustion or formation, is constant for the higher members of these normal alkyl series of hydrocarbons in the liquid state at 25°. Recommended values are given for the heats of combustion and formation, for the liquid state at 25°, for the members of these normal alkyl series of hydrocarbons having more than three carbon atoms in the normal alkyl chain. Values for the corresponding heats of vaporization at 25° are also given.

I. Introduction

It has been shown by Prosen and Rossini,[3] from measurements on 8 liquid normal paraffins in the range C_5 to C_{16}, that the increment per CH_2 group in the heat of formation of the higher normal paraffin hydrocarbons in the liquid state at 25° is a constant within the limits of present-day measurements. Later, Fraser and Prosen[4] reported data on one higher member of each of four other normal alkyl series of hydrocarbons and concluded that the increment per CH_2 group in the heat of formation of the higher members of these other normal alkyl series of hydrocarbons in the liquid state at 25° is also a constant of substantially the same value as for the series of normal paraffins.

In the assembly of the extensive set of precise and internally consistent tables of thermodynamic properties of hydrocarbons and related compounds, prepared by the American Petroleum Institute Research Project 44, the values for the normal paraffins assume a great importance in providing a base-line framework from which values for many compounds of other classes are calculated without experimental measurement.[5] Where possible, it is desirable to use the increments per CH_2 group derived from extensive measurements on the paraffin hydrocarbons in calculating values of appropriate thermodynamic properties for the members of other series of normal alkyl hydrocarbons.

Accordingly, because of the great importance of

(1) This investigation was supported in part by a grant from the National Science Foundation. Submitted in partial fulfillment of the requirements for the degree of Doctor of Philosophy in Chemistry at the Carnegie Institute of Technology.

(2) University of Notre Dame, Notre Dame, Indiana.

(3) E. J. Prosen and F. D. Rossini, *J. Research Natl. Bur. Standards*, **34**, 263 (1945).

(4) F. M. Fraser and E. J. Prosen, *ibid.*, **55**, 329 (1955).

(5) F. D. Rossini, K. S. Pitzer, R. L. Arnett, R. M. Braun and G. C. Pimentel, "Selected values of physical and thermodynamic properties of hydrocarbons and related compounds," API Research Project 44, Carnegie Press, Pittsburgh, Pennsylvania, 1953.

establishing the fact that the increment per CH_2 group in the heat of formation of the higher members of other normal alkyl series may be taken the same as for the normal paraffins, an investigation was carried out in this Laboratory to provide independent experimental evidence on this point. The present investigation reports experimental data on the heats of combustion, relative to that of *n*-hexadecane, of *n*-decylcyclopentane, *n*-decylcyclohexane, 1-hexadecene and *n*-decylbenzene, with presentation of the conclusions resulting therefrom.

II. Apparatus and Experimental Procedures

The experimental values of this investigation are based on the absolute joule as the unit of energy. Conversion to the defined thermochemical calorie is made using the relation 1 calorie = 4.184 (exactly) joules. In order to be consistent in the comparison of these values with those previously reported from this Laboratory, the molecular weight of carbon dioxide was taken as 44.010 g./mole.

In this investigation, the chemical and calorimetric apparatus and procedures were the same as described by Browne and Rossini.[6]

The compounds measured in the present investigation were API Research hydrocarbons, made available through the API Research Project 44 from materials purified by the API Research Project 6. The samples had the following values of purity, in mole per cent.: *n*-hexadecane, 99.96 ± 0.04; *n*-decylcyclopentane, 99.80 ± 0.18; *n*-decylclohexane, 99.88 ± 0.11; 1-hexadecene, 99.93 ± 0.06; *n*-decylbenzene, 99.88 ± 0.10. Description of the purification and determination of the purity of these samples already has been given.[7] The impurities in these samples would most likely be isomeric and would have an insignificant effect on the measurements.

The ampoules employed to contain the liquid hydrocarbon material were made of soft glass, and had a single capillary opening of such length as to permit the tip of a No. 27 hypodermic needle to extend a short distance into the body of the bulb. The hydrocarbon was first drawn into a 2-ml. glass syringe fitted with the hypodermic needle and then transferred directly to the weighed ampoule of the proper size. To minimize expansion of the liquid, the ampoule was handled as little as possible with the fingers during the filling process. The ampoule, filled to the tip of the capillary, was cooled with ice to draw the liquid far enough down into the neck to permit sealing of the tip with a hot flame.

The rise of temperature in each calorimetric experiment was near 2°, with the final temperature being near 30°, the temperature of the jacket of the calorimeter. The pressure of oxygen in the bomb before combustion was 30 atm., calculated for 25°. One ml. of water was placed in the bomb prior to each combustion experiment. The internal volume of the bomb was 380 ml.

The amount of reaction in each experiment was based on the mass of carbon dioxide formed in the combustion reaction in the bomb. One mole of carbon dioxide, 44.010 g., was taken as $1/n$ mole of hydrocarbon, where n is the number of carbon atoms per mole of the given hydrocarbon. The true mass of carbon dioxide was obtained as previously described.[6]

The energy supplied to the calorimeter system by the melting and burning of the iron fuse wire was determined in a series of blank experiments in which the starting temperature was close to the jacket temperature. The bomb contained the fuse (5 cm. wire, No. 36 AWG, Parr No. 45C10), purified oxygen, etc., as in a regular experiment, but without the hydrocarbon. The increase in the resistance of the platinum resistance thermometer was determined after the fuse was fired. Any unburned wire was weighed. The heat of combustion of the iron wire in oxygen in the bomb was taken as 6.63 kj./g. The electrical energy added to the calorimeter system in the firing of the fuse was thus determined to be 35.70 ± 0.46 j. (This portion of the work was performed in collaboration with D. M. Speros.)

III. Data of the Present Investigation

The results of the calorimetric combustion experiments are given in Table I for *n*-hexadecane, *n*-decylcyclopentane, *n*-decylcyclohexane, 1-hexadecene and *n*-decylbenzene, respectively. The symbols are as defined previously.[6] The quantity B, expressed in ohms per gram of carbon dioxide, represents the corrected increase in temperature of the standard calorimeter system caused by the formation of one gram of carbon dioxide formed in the combustion of the given hydrocarbon.

From the values of B given in Table I, values may be calculated for the standard heat of combustion, ΔHc^0 at 25°, according to the reaction

$$C_aH_b(\text{liq}) + \left(a + \frac{b}{4}\right) O_2(g) = a CO_2(g) + \frac{b}{2} H_2O(\text{liq}) \quad (1)$$

Because for *n*-hexadecane the value of the heat of combustion in the liquid state has been previously measured accurately,[8] and because it is similar to the other four compounds measured, *n*-hexadecane was used as the reference substance for the present measurements. For *n*-hexadecane, the standard heat of combustion at 25°, ΔHc^0, was taken as −2557.64 ± 0.48 kcal./mole,[3,8] for the reaction

$$C_{16}H_{34}(\text{liq}) + 24\frac{1}{2} O_2(g) = 16CO_2(g) + 17H_2O(\text{liq}) \quad (2)$$

From the value of ΔHc^0 at 25°, with appropriate values of heat capacities, the value of ΔHc^0 at 30° was calculated. Subtraction of $\Delta(PV)^0$ at 30° yields the value of ΔEc^0 at 30°, in accordance with the relation $\Delta H^0 = \Delta E^0 + \Delta(PV)^0$. Application of the Washburn[9] correction in the reverse direction, for the conditions of the bomb process in the present measurements, yields the value of ΔE_B at 30° for *n*-hexadecane in the present investigation.

With the value of ΔE_B for *n*-hexadecane, and the appropriate values of B, one may calculate values of ΔE_B for the other four compounds in accordance with the equation

$$(-\Delta E_B)_i/(-\Delta E_B)_n = B_i/B_n \quad (3)$$

To reduce the heat evolved in the bomb process, $-\Delta E_B$, to the change in internal energy, $-\Delta Ec^0$, for all the reactants and products in their standard states, the complete Washburn correction[9] was applied. The improved values of some constants[10] to be used in making the Washburn correction to 30° were incorporated in these calculations. The percentage correction to the bomb process at 30° was calculated to be −0.030 for *n*-hexadecane, −0.033 for *n*-decylcyclopentane, *n*-decylcyclohexane and 1-hexadecene, and −0.040 for *n*-decylbenzene.

The heat evolved in the combustion at constant pressure at 30°, $-\Delta Hc^0$, was obtained from

(6) C. C. Browne and F. D. Rossini, THIS JOURNAL, **64**, 927 (1960).

(7) A. J. Streiff, A. R. Hulme, P. A. Cowie, N. C. Krouskop and F. D. Rossini, *Anal. Chem.*, **27**, 411 (1955).

(8) E. J. Prosen and F. D. Rossini, *J. Research Natl. Bur. Standards*, **33**, 255 (1944).

(9) E. W. Washburn, *ibid.*, **10**, 525 (1933).

(10) W. N. Hubbard, D. W. Scott and G. Waddington, THIS JOURNAL, **58**, 152 (1954).

TABLE I

RESULTS OF THE COMBUSTION EXPERIMENTS

No. of expt.	Range of mass of CO_2 formed, g.	Range of k, $min.^{-1}$	Range of K, ohm	Range of U, ohm	Range of ΔR_e, ohm	Range of Δr_i, ohm	Range of Δr_n, ohm	Range of B, ohm/g. CO_2	Mean value and stand. dev. of the mean, ohm/g. CO_2
					n-Hexadecane				
9	2.64642	0.001505	0.000717	−0.000026	0.195655	0.000395	0.000009	0.0735714	0.0736056
	to	to	to	to	to	to	to		±0.0000080
	2.73772	0.001615	0.000968	0.000266	0.201870	0.000433	0.000027	0.0736523	
					n-Decylcyclopentane				
6	2.51289	0.001573	0.000778	0.000069	0.181516	0.000401	0.000021	0.0720653	0.0720854
	to	to	to	to	to	to	to	to	±0.0000065
	2.78635	0.001599	0.001268	0.000234	0.201242	0.000440	0.000027	0.0721109	
					n-Decylcyclohexane				
6	2.70543	0.001577	0.000694	0.000056	0.194859	0.000372	0.000014	0.0718737	0.0718928
	to	to	to	to	to	to	to	to	
	2.84374	0.001591	0.000995	0.000181	0.204857	0.000435	0.000024	0.0719296	±0.0000085
					1-Hexadecene				
5	2.73697	0.001580	0.000737	0.000022	0.198980	0.000382	0.000024	0.0725250	0.0725483
	to	to	to	to	to	to	to	to	±0.0000073
	2.77923	0.001598	0.000825	0.000165	0.202064	0.000435	0.000027	0.0725656	
					n-Decylbenzene				
6	2.76565	0.001582	0.000787	0.000069	0.186875	0.000388	0.000012	0.0673834	0.0674143
	to	to	to	to	to	to	to	to	±0.0000107
	3.01009	0.001612	0.001287	0.000238	0.203242	0.000412	0.000023	0.0674440	

TABLE II

VALUES[a] OF THE STANDARD HEATS OF COMBUSTION OF *n*-DECYLCYCLOPENTANE, *n*-DECYLCYCLOHEXANE, 1-HEXADECENE AND *n*-DECYLBENZENE

Compound Name	Formula	State	B at 30°, ohm/g. CO_2	$-\Delta E_B$, at 30°, kj./mole	$-\Delta E^0$ at 30°, kj./mole	$-\Delta H^0$ at 30°, kj./mole	$-\Delta H^0$, at 25°, kj./mole	$-\Delta H^0$, at 25°, kcal./mole
n-Decylcyclopentane	$C_{15}H_{30}$	liq	0.0720854 ±0.0000130	9805.41 ± 2.74	9802.18 ± 2.74	9821.08 ± 2.74	9824.08 ± 2.74	2348.01 ± 0.06
n-Decylcyclohexane	$C_{16}H_{32}$	liq	0.0718928 ±0.0000170	10431.17 ± 3.33	10427.72 ± 3.33	10447.89 ± 3.33	10451.10 ± 3.33	2497.87 ± 0.80
1-Hexadecene	$C_{16}H_{32}$	liq	0.0725483 ±0.0000146	10526.27 ± 3.05	10522.80 ± 3.05	10542.96 ± 3.05	10546.01 ± 3.05	2520.56 ± 0.73
n-Decylbenzene	$C_{16}H_{26}$	liq	0.0674143 ±0.0000214	9781.37 ± 3.70	9777.45 ± 3.70	9793.84 ± 3.70	9796.29 ± 3.70	2341.37 ± 0.88

[a] The uncertainties in this table are twice the standard deviation.

ΔEc^0. The term, $\Delta(PV)^0$ was determined to be partially cancelled and insignificant for the liquid substances, and becomes equal to RT times the increase in moles of gaseous products over reactants. The values of the heat capacities at constant pressure of CO_2(g), O_2(g) and liquid water, which were employed in the evaluation of the temperature coefficient of the heat content, in order to calculate $-\Delta Hc^0$ at 25°, have been reported.[5] The heat capacities of the hydrocarbons were obtained from unpublished data.[11]

The uncertainties assigned to the various quantities dealt with in this investigation were derived by the method previously described.[6]

The final values for the standard heats of combustion at 25° for *n*-decylcyclopentane, *n*-decylcyclohexane, 1-hexadecene and *n*-decylbenzene, in the liquid state, are given in Table II.

IV. Data of Other Investigations

The only previous measurements on the heats of combustion of these compounds so far reported in the literature appear to be those of Fraser and Prosen.[4] The most direct way of comparing their results with those of the present investigation is to compare the ratio of the heat of combustion of each of the compounds to that of *n*-hexadecane, measured in the same investigation in the same apparatus with the same procedure. This comparison is shown in Table II. It is seen that the two sets of measurements are, within the respective limits of uncertainty, in excellent agreement, with the values from the National Bureau of Standards having smaller uncertainties.

V. Increment Per CH_2 Group for Normal Alkyl Series of Hydrocarbons in the Liquid State at 25°

Using the values given in the tables of the API Research Project 44[5] for the *n*-butylcyclopentane, *n*-butylcyclohexane, *n*-butylbenzene and 1-hexene, with the latter value adjusted slightly on the basis of measurements made on 1-heptene and 1-octene in this Laboratory,[12] in conjunction with the values re-

(11) J. P. McCullough, *et al.*, U. S. Bureau of Mines, Bartlesville, Oklahoma.

(12) J. D. Rockenfeller and F. D. Rossini, Chemical and Petroleum Research Laboratory, Carnegie Institute of Technology. Unpublished data.

ported in this investigation for the one higher member of these four series, one obtains the following values of the increments per CH_2 group in the heat of combustion, $-\Delta Hc^0$, for the liquid at 25° in kcal./mole: normal alkyl cyclopentanes, 156.32 ± 0.12; normal alkyl cyclohexanes, 156.18 ± 0.14; normal alkyl monoölefins, 1-alkenes, 156.35 ± 0.10; normal alkylbenzenes, 156.32 ± 0.15. The mean of these values is 156.29 ± 0.07 kcal./mole. From the data of Fraser and Prosen,[4] the corresponding values, for the same series, respectively, are, in kcal./mole: 156.26 ± 0.07; 156.19 ± 0.08; 156.36 ± 0.09; 156.19 ± 0.07. The mean of these values is 156.25 ± 0.04 kcal./mole. Utilizing all the available experimental data from the National Bureau of Standards, Fraser and Prosen[5] reported a mean value of 156.24 kcal./mole. The value found by Prosen and Rossini[3] for the series of normal paraffins was 156.26 ± 0.05 kcal./mole.

TABLE III

COMPARISON OF PREVIOUS RESULTS WITH THOSE OF THE PRESENT INVESTIGATION

Compound	Ratio of the standard heat of combustion, $-\Delta Hc^0$, for the liq. state at 25°, of the given compd. to that of *n*-hexadecane[a] From Fraser and Prosen[4]	From the present investigation
n-Decylcyclopentane	0.91803 ± 0.00024	0.91804 ± 0.00031
n-Decylcyclohexane	.97683 ± .00023	.97663 ± .00036
1-Hexadecene	.98515 ± .00024	.98550 ± .00034
n-Decylbenzene	.91531 ± .00022	.91544 ± .00038

[a] The uncertainties given in this table are equivalent to twice the standard deviation of the mean.

On the basis of all the foregoing data, it appears that, within the limits of present-day measurements, the increment per CH_2 group in the heat of formation of the higher (more than three carbon atoms in the normal alkyl chain) members of any normal alkyl series of hydrocarbons in the liquid state at 25° is constant.

Since the values of the increment per CH_2 group from Fraser and Prosen[4] and from the present investigation are in good over-all accord with the value from the work of Prosen and Rossini on their extensive investigation of the normal paraffins, and because extensive tables of thermodynamic properties based upon the values for the normal paraffins have been created, it appears desirable to use for the higher members of other normal alkyl series of compounds the values of the increment per CH_2 group as for the series of normal paraffins.

VI. Values of the Standard Heats of Combustion and Formation for the Liquid State at 25°

On the foregoing basis, the values of the standard heats of combustion and formation for the members of the normal alkyl series of hydrocarbons, $Y-(CH_2)_m-H$, for values of m greater than 3, will be as follows for the liquid state at 25°

Normal alkyl cyclopentanes

$$(m + 5)\,C\,(c, \text{graphite}) + (m + 5)\,H_2\,(g) = C_5H_9—(CH_2)_m—H(liq) \quad (4)$$

$$-\Delta Hc^0 = 785.05 + 156.263m \text{ kcal./mole.} \quad (m > 3) \quad (5)$$

$$\Delta Hf^0 = -26.80 - 6.106\,m \text{ kcal./mole.} \quad (m > 3) \quad (6)$$

Normal alkyl cyclohexanes

$$(m + 6)\,C\,(c, \text{graphite}) + (m + 6)\,H_2\,(g) = C_6H_{11}—(CH_2)_m—H(liq) \quad (7)$$

$$-\Delta Hc^0 = 935.73 + 156.263\,m \text{ kcal./mole.} \quad (m > 3) \quad (8)$$

$$\Delta Hf^0 = -38.49 - 6.106\,m \text{ kcal./mole.} \quad (m > 3) \quad (9)$$

Normal alkyl monoölefins, 1-alkenes

$$(m + 2)\,C\,(c, \text{graphite}) + (m + 2)\,H_2\,(g) = C_2H_3—(CH_2)_m—H(liq) \quad (10)$$

$$-\Delta Hc^0 = 331.87 + 156.263m \text{ kcal./mole.} \quad (m > 3) \quad (11)$$

$$\Delta Hf^0 = 7.12 - 6.106m \text{ kcal./mole.} \quad (m > 3) \quad (12)$$

Normal alkyl benzenes

$$(m + 6)\,C\,(c, \text{graphite}) + (m + 3)\,H_2\,(g) = C_6H_5—(CH_2)_m—H(liq) \quad (13)$$

$$-\Delta Hc^0 = 778.41 + 156.263m \text{ kcal./mole.} \quad (m > 3) \quad (14)$$

$$\Delta Hf^0 = 9.14 - 6.106m \text{ kcal./mole.} \quad (m > 3) \quad (15)$$

In equations 4, 7, 10 and 13, the end group Y is cyclopentyl, cyclohexyl, vinyl and phenyl, respectively, with m being the number of carbon atoms in the normal alkyl radical. The values of the standard heats of formation ΔHf^0, for liquid water and for gaseous carbon dioxide, at 25°, appropriate to the foregoing calculations are as follows, in kcal./mole, respectively[5] −68.3174 and −94.0518.

VII. Values of Standard Heats of Vaporization

Utilizing the foregoing values for the standard heat of formation and the corresponding values for the standard heat of formation for the gaseous state, as given in the tables of the API Research Project 44,[5] one obtains the following equations giving the values for the standard heat of vaporization of the higher members of these normal alkyl series at 25°

Normal alkyl cyclopentanes:

$$\Delta Hv^0 = 6.28 + 1.18m \text{ kcal./mole.} \quad (m > 3) \quad (16)$$

Normal alkyl cyclohexanes:

$$\Delta Hv^0 = 7.24 + 1.18m \text{ kcal./mole.} \quad (m > 3) \quad (17)$$

Normal monoölefins (1-alkenes):

$$\Delta Hv^0 = 2.62 + 1.18m \text{ kcal./mole.} \quad (m > 3) \quad (18)$$

Normal alkyl benzenes:

$$\Delta Hv^0 = 7.26 + 1.18m \text{ kcal./mole.} \quad (m > 3) \quad (19)$$

In the foregoing equations 4 to 19, inclusive, m is the number of carbon atoms in the normal alkyl radical.

SULFOXIDES AS LIGANDS. II. THE INFRARED SPECTRA OF SOME DIMETHYL SULFOXIDE COMPLEXES

BY F. A. COTTON, R. FRANCIS AND W. D. HORROCKS, JR.

Department of Chemistry, Massachusetts Institute of Technology, Cambridge, Mass.

Received April 29, 1960

The infrared spectra of dimethyl sulfoxide, dimethyl sulfoxide-d_6, $[(CH_3)_3SO]I$, $[(CH_3)_3SO]NO_3$, $[(CD_3)_3SO]I$, $[(CH_3)_2SOCH_3]NO_3$ numerous complexes of dimethyl sulfoxide with metal salts and a few complexes of dimethyl sulfoxide-d_6 with metal salts are reported and discussed. Assignments are proposed for the bands observed in the region 650–4000 cm.$^{-1}$. The effects of complex formation and sulfoxonium ion formation by dimethyl sulfoxide upon its S–O stretching frequency are given particular attention and it is shown that the observed shifts may be correlated with the occurrence of S- or O-bonding in the adducts by considering the electronic nature of the S–O linkage.

Introduction

We have prepared a large number of compounds containing dimethyl sulfoxide (DMSO) as a ligand.[1] In many cases the structures of the compounds have been inferred from magnetic data and electronic spectra. Realizing at the outset that the infrared spectra could also be of value in deducing the structures of many of the compounds, a thorough vibrational study of $(CH_3)SO$ and $(CD_3)_2SO$[2] along with the thionyl halides[3] was undertaken in order that we might have at our disposal the most definite possible knowledge of the assignments for DMSO before attempting to assign the observed spectra of the complexes containing DMSO. Our analysis of the DMSO spectrum is now virtually complete and will be published separately. In this paper we shall use the information obtained from that study to analyze the spectra of a representative group of the DMSO complexes we have prepared.

Results and Discussion

The results of the thorough study of DMSO and DMSO-d_6 are the basis for analyzing the spectra of the complexes, and therefore they must be summarized first. The observed infrared bands are listed in Table I, together with assignments based upon our analysis of the entire body of infrared and Raman data which will be published separately.

In considering the spectra of the complexes, our chief interest will be in the behavior of the SO stretching frequency, since this should be most informative with respect to the nature of the metal-ligand bonding. The reason for this follows from the bond structure of the sulfoxide group. A considerable body of data on bond lengths and dipole moments of sulfoxides leads to the conclusion that the SO bond has an order around two.[4–8] This can be considered to be the result of resonance between the structures

TABLE I

INFRARED SPECTRA OF $(CH_3)_2SO$ AND $(CD_3)_2SO$ IN THE 600–4000 CM.$^{-1}$ REGION

Absorption bands,[a] cm.$^{-1}$				
$(CH_3)_2SO$		$(CD_3)_2SO$		
Solution[b]	Vapor	Solution[b]	Vapor	Assignments[c]
3000m	2973m	2250m	2250m	Asym. C–H str.
2918m	2908m	2133w	2133w	Sym. C–H str.
....	2183w	....	2185w	2 × (S–O str)
....	1455m			
1436s	1440ms	....[d]	1084s,sh	Asym. $CH_3(CD_3)$
1416m	1419m	....[d]	1043m	Def.
1404m	1405m			
1325w,sh	1319w,sh	1034s	1025m	Sym. $CH_3(CD_3)$
1306m	1304m	1005m	1015m	Def.
1291w,sh	1287m			
....	1111s,sh	....	1109s,sh	
1055vs,bd	1102vs	1064vs	1096vs	S–O str.
	1094s,sh			
1012s	1016m		824m,sh	
	1006m	811m	815m	
946s	829w		803m,sh	$CH_3(CD_3)$ rocks
921m	915w		756m,sh	
887w	898w	748m	750m	
690s	689m	....[e]	619	Asym. C–S str.
661m	672m	....[e]	611	Sym. C–S str.

[a] s = strong; m = medium; w = weak; v = very; sh = shoulder; bd = broad. [b] Chloroform and carbon disulfide solvents. [c] str = stretch; def. = deformation; sym. = symmetric; asym. = asymmetric. [d] Obscured by the strong broad S–O stretching band at 1064 cm.$^{-1}$. [e] The spectrum of $(CD_3)_2SO$ in solution was not recorded below 650 cm.$^{-1}$.

$$R_2\overset{+}{S}-\overset{-}{O} \longleftrightarrow R_2S=O \longleftrightarrow R_2\overset{+}{S}\equiv\overset{-}{O}$$
$$\text{I} \qquad\qquad \text{II} \qquad\qquad \text{III}$$

with II probably dominant. Similar considerations apply to the PO bond in phosphine oxides.[8] On this premise, it would be expected that coordination of the oxygen atom in R_2SO or R_3PO would result in a lowering of the SO and PO bond orders by decreasing the contributions of II and III. This will then operate to lower SO and PO stretching frequencies. It must also be noted, however, that coördination will also tend to raise the SO and PO stretching frequencies because of the usual kinematic effect of coupling two oscillators.[8] Experimental results on phosphine oxide complexes[8,9] have shown, however, that the bond order lowering dominates so that the net effect is a lowering of PO stretching frequencies by ~50 cm.$^{-1}$ in phosphine oxide complexes. We therefore except to find a similar effect in sulfoxide complexes.

With sulfoxides, however, there exists a pos-

(1) F. A. Cotton and R. Francis, *J. Am. Chem. Soc.*, **82**, 2986 (1960).

(2) F. A. Cotton, J. H. Fassnacht, W. D. Horrocks, Jr., and N. A. Nelson, *J. Chem. Soc.*, 4138 (1959).

(3) F. A. Cotton and W. D. Horrocks, Jr., *Spectrochem.* **16**, 358 (1960).

(4) C. W. N. Crumper and S. Walker, *Trans. Faraday Soc.*, **52**, 193 (1956).

(5) M. Lister and L. E. Sutton, *ibid.*, **35**, 497 (1939).

(6) S. C. Abrahams, *Acta Cryst.*, **10**, 417 (1957).

(7) P. W. Allen and L. E. Sutton, *ibid.*, **3**, 46 (1950).

(8) F. A. Cotton, R. D. Barnes and E. Bannister, *J. Chem. Soc.*, 2199 (1960).

(9) J. C. Sheldon and S. Y. Tyree, *J. Am. Chem. Soc.*, **80**, 4775 (1958).

sibility which has no parallel with phosphine oxides. It is possible for a sulfoxide to coördinate *via* the sulfur atom, which has a lone pair. In this case, the contribution of structures II and III will be enhanced and the bond order raised. Again, there will be the kinematic effect tending to raise the SO frequency, so that we may confidently expect the overall effect of coördination of a sulfoxide *via* sulfur to be a marked exaltation of the SO stretching frequency.

Before applying these principles to the analysis of the spectra of complexes of DMSO with metal ions and Lewis acids, we may demonstrate their validity by considering the infrared spectra of some S-alkyl and O-alkyl sulfoxonium salts.[10,11] An S-alkyl sulfoxonium salt was first reported by Kuhn and Trischman, but it was Smith and Winstein who showed that the metastable O-alkyl isomers usually exist, and they isolated a number of representative S-alkyl and O-alkyl sulfoxonium salts of DMSO.

As a typical S-alkyl salt we have chosen $[(CH_3)_3SO]^+I^-$. Its infrared spectrum was reported by Kuhn and Trischman,[10] but in order to be quite certain of correctly identifying the SO stretch we have also recorded the spectrum of $[(CH_3)_3SO]^+I^-$. The results are presented in Table II. There can be no doubt that the SO stretch is at 1233 cm.$^{-1}$, which represents a frequency increase of ~135 cm.$^{-1}$ over the figure for gaseous DMSO, and ~178 cm.$^{-1}$ over that for the solution, in agreement with the theory advanced above. Similarly $[(CH_3)_3SO]NO_3$ has a very strong, sharp absorption band at 1210 cm.$^{-1}$ assignable to SO stretching.

TABLE II

INFRARED SPECTRA OF $[(CH_3)_3SO]I$ AND $[(CD_3)_3SO]I$

Compound[a] $[(CH_3)_3SO]I$	Compound[a] $[(CD_3)_3SO]I$	Assignments
2965s	2240s	Asym. C–H(C–D) stretches
2892m	2120m	Sym. C–H(C–D) stretches
1418ms	1215m	Asym. $CH_3(CD_3)$ deformations
1408s	1192m	
1377w	1021m	Sym. $CH_3(CD_3)$ deformations
1341w	1006vw,sh	
1315m		
1233vs	1240vs	S–O stretch
1222m,sh	858s	CH_3 rocks
1039vs	840w,sh	
954s	764w	
757m		S–C stretch

[a] s = strong; m = medium; w = weak; v = very; sh = shoulder.

The O-methyl sulfoxonium salt studied was the nitrate since the O-methyl iodide is not known and more easily synthesized tosylates and brosylates described by Smith and Winstein[11] contain sulfonate groups which would confuse the spectral region of interest. The infrared spectrum of the O-methyl sulfoxonium nitrate has no bands between 1075 and 1300 cm.$^{-1}$. There are several broad bands in the 1050–925 cm.$^{-1}$ region among which must be the SO stretch, in agreement with expectation of a downward shift. Because of the difficulties attending the synthesis and handling of this compound, no effort was made to prepare a deuterated analog.

We now turn to the assignment of the spectra of the complexes. The spectra are all in general fairly similar, there being no pronounced dependence upon the number of coördinated molecules of DMSO or on the particular metal atom. Of course, compounds containing complex anions such as nitrate and perchlorate show bands characteristic of these species; these bands will not be considered in the following discussions. We shall show, however, that there are certain features of the spectra which can be used to infer that in most complexes the sulfoxide is attached through the oxygen atom, while in a few others, it is bound through sulfur.

We discuss the O-bonded complexes first. In Table III the complete spectra of two chemically rather different but representative compounds of this class are given, including in each case data for the analogous DMSO-d_6 compounds. From these data, it can be seen that the SO stretching band has moved down to 950 cm.$^{-1}$ in the $[Co(DMSO)_6]^{+2}$ ion and even further, to 915 cm.$^{-1}$, in $SnCl_4$·2DMSO. In the undeuterated $[Co(DMSO)_6]^{+2}$ there are strong bands both at ~1000 and at ~950 cm.$^{-1}$, and, without the data for the deuterated analog, there would be no way to be certain which of these bands should be assigned to SO stretching. The other assignments in Table III follow straightforwardly from the data and assignments in Table I. The spectra of a number of other O-bonded, complexes have been recorded. All of these spectra are quite similar to those given in Table III and no purpose would be served by tabulating them in full. Instead, we list in Table IV only the frequencies of the SO stretching bands.

TABLE III

INFRARED SPECTRA OF $[Co(DMSO)_6][CoCl_4]$, $[Co(DMSO\text{-}d_6)_6][CoCl_4]$, $SnCl_4$·2DMSO AND $SnCl_4$·2(DMSO-d_6)

Absorption bands $[Co(DMSO)_6][CoCl_4]$	Absorption bands $[Co(DMSO\text{-}d_6)_6][CoCl_4]$	Assignment	Absorption bands $SnCl_4$·2DMSO	Absorption bands $SnCl_4$·2(DMSO-d_6)
3002m	2240m	Asymmetrical C–H (C–D) stretch	3030m	2250m
2906m	2120w	Symmetrical C–H (C–D) stretch	2940m	2130m
1416m bd	1015s	Asym. $CH_3(CD_3)$ deformations	1432s 1419s 1406m	1019m 1012m sh
1314w 1292w	1039m	Sym. $CH_3(CD_3)$ def.	1330m 1310w	1040w
1009s sh 999s	819m 775w sh 760w	$CH(CD_3)$ rocks	1037s 991s 948s sh	830m 789w 768m
950vs	970vs	S=O stretch	915 vs bd	929s 914s
714w		Asym. C–S stretch Sym. C–S stretch	730m 685w	

We turn now to the second general class of complexes, those in which, we believe, the sulfoxide is coördinated through the sulfur atom. The compounds $PdCl_2$·2DMSO and $PtCl_2$·2DMSO appear to be of this type.[12] Their spectra are similar to the

(10) R. Kuhn and H. Trischman, *Ann.*, **611**, 117 (1958).

(11) S. Smith and S. Winstein, *Tetrahedron*, **3**, 317 (1958).

(12) It should be noted, however, that we have as yet no independent evidence on the structures of these compounds.

TABLE IV

FREQUENCIES OF S–O STRETCHING BANDS IN VARIOUS DIMETHYL SULFOXIDE COMPLEXES

Compound	Frequency, cm.$^{-1}$
Sulfur bonded	
$PdCl_2 \cdot 2DMSO$	1116
$PtCl_2 \cdot 2DMSO$	1157, 1134
Oxygen bonded	
$SnCl_4 \cdot 2DMSO$	915
$[Cr(DMSO)_6](ClO_4)_3$	928
$CrCl_3 \cdot 4DMSO$	935
$[Mn(DMSO)_6](ClO_4)_2$	955
$Mn(ClO_4)_2 \cdot 3DMSO \cdot 4H_2O$	954
$MnCl_2 \cdot 3DMSO$	950
$MnBr_2 \cdot 3DMSO \cdot 6H_2O$	952
$[Fe(DMSO)_6](ClO_4)_3 \cdot DMSO$	940
$FeCl_3 \cdot 2DMSO$	933
$FeI_3 \cdot 4DMSO$	937
$[Co(DMSO)_6](ClO_4)_2$	956
$CoCl_2 \cdot 3DMSO$	950
$CoBr_2 \cdot 3DMSO$	951
$CoI_2 \cdot 6DMSO$	948
$CoI_2 \cdot 3DMSO$	951
$Co(SCN)_2 \cdot 4DMSO$	953
$Co(SCN)_2 \cdot 3DMSO$	950
$[Ni(DMSO)_6](ClO_4)_2$	955
$NiCl_2 \cdot 3DMSO$	940
$NiBr_2 \cdot 6DMSO$	957
$NiBr_2 \cdot 4DMSO$	956
$NiBr_2 \cdot 3DMSO$	951
$NiI_2 \cdot 4DMSO$	930
$Cu(DMSO)_4(ClO_4)_2$	940 v bd
$CuCl_2 \cdot 2DMSO$	923
$CuBr_2 \cdot 2DMSO$	911
$[Zn(DMSO)_6](ClO_4)_2$	956
$ZnCl_2 \cdot 2DMSO$	952
$ZnBr_2 \cdot 2DMSO$	942
$CdCl_2 \cdot DMSO$	950

spectra of O-bonded compounds in the C–H stretching and deformation regions, *i.e.*, down to the ~1300 cm.$^{-1}$ bands. However, as may be seen from the data in Table V for $PdCl_2 \cdot 2DMSO$ and $PdCl_2 \cdot 2(DMSO\text{-}d_6)$, the SO stretching frequency is higher (1116 cm.$^{-1}$) in the complex than in the free ligand. In the platinum compound there are strong bands at 1157 and 1134 cm.$^{-1}$ one or both of which must be assigned to S–O stretching. In both the platinum and palladium compounds the four strong to medium intensity bands found between ~1025 and ~920 cm.$^{-1}$ may be assigned to CH_3 rocking modes. The bands at 730 and 683 cm.$^{-1}$ in the palladium compound and at 736 and 689 cm.$^{-1}$ in the platinum compound may presumably be assigned to C–S stretching frequencies. The behavior of these bands in these S-bonded compounds is in marked contrast to their behavior in the O-bonded compounds. In the latter the C–S stretching bands are generally much weaker (often the symmetric stretch is not observed) and at lower frequencies, *viz.*, at ~715 cm.$^{-1}$ and, if observable, at ~675 cm.$^{-1}$.

TABLE V

INFRARED SPECTRA OF $PdCl_2 \cdot 2DMSO$ AND $PdCl_2 \cdot 2(DMSO\text{-}d_6)$

Absorption bands $PdCl_2 \cdot 2$-DMSO	Assignment	Absorption bands $PdCl_2 \cdot 2$-(DMSO-d_6)
3010m	Asym. C–H(C–D) stretch	2250s
2920m	Symmetrical C–H(C–D) stretch	2120m
1423m, 1411m	Asym. $CH_3(CD_3)$ def.	1043w
1313m, 1298m	Sym. $CH_3(CD_3)$ def.	1029s, 1010s
1116vs	S–O stretch	1113s
1022s, 983m, 975w sh, 945m, 923m	$CH_3(CD_3)$ rocks	880w, 822vs, 787m, 778vs
730m	Asym. C–S stretch	709m
683m	Sym. C–S stretch	642m

Experimental

Preparation of Compounds.—The preparations of trimethylsulfoxonium iodide, $[(CH_3)_3SO]^+I^-$, and tri-(methyl-d_3)-sulfoxonium iodide have been described previously.[1] The O-methylsulfoxonium nitrate was prepared by the method of Smith and Winstein.[11,13] 3.41 g. (20.2 mmoles) of $AgNO_3$ was dissolved in 10 ml. (116.0 mmoles) of DMSO dried by passing through a column of molecular sieve pellets (type 4A $^1/_{16}$ inch pellets, Linde Aire Products) and distilled at reduced pressure from powdered molecular sieves. To this mixture, cooled in an ice-bath, were added dropwise 2.84 g. (20.0 mmoles) of CH_3I over a period of about ten minutes. A yellow-white precipitate of AgI was immediately observed. As soon as reaction was complete, the solution was filtered rapidly and the filtrate treated with 100 ml. of anhydrous ether; the mixture formed two layers and the ether layer was decanted. This process was repeated until the oil crystallized to a white solid. This was recrystallized once from chloroform–ether and dried in a vacuum desiccator. The product is extremely hygroscopic and isomerizes in the presence of moisture. The yield was very low. The $[(CH_3)_3SO]^+NO_3^-$ was prepared by treating an aqueous solution of $[(CH_3)_3SO]^+I^-$ with $AgNO_3$, filtering off the AgI formed and evaporating the resulting solution to dryness.

The complexes of DMSO were prepared by methods described elsewhere.[1] All samples used in the present work were thoroughly analyzed, authentic specimens.

Infrared Spectra.—The infrared spectra were taken on solid samples dispersed in the potassium halide corresponding to the anion present in the complex, pressed into translucent pellets in the usual manner. The complexes containing nitrate or perchlorate ions were studied in potassium bromide and chloride pellets and in hexachlorobutadiene and Nujol mulls. The spectra were taken on a Perkin–Elmer Model 21 recording infrared spectrometer employing a sodium chloride prism. The spectral region between 4000 and 650 cm.$^{-1}$ was investigated.

Acknowledgment.—We are grateful for generous financial support by the United States Atomic Energy Commission under Contract AT(30-1)-1965 and by the Monsanto Chemical Company through a fellowship to W. D. H., Jr.

(13) S. Smith and S. Winstein, private communication.

THE DIFFUSION COEFFICIENT OF FORMAMIDE IN DILUTE AQUEOUS SOLUTIONS AT 25° AS MEASURED WITH THE GOUY DIFFUSIOMETER

BY JOHN G. ALBRIGHT AND LOUIS J. GOSTING

Department of Chemistry, University of Wisconsin, Madison 6, Wisconsin

Received April 30, 1960

The isothermal diffusion coefficient for the system formamide–water was measured with a Gouy diffusiometer over the concentration range 0 to 51 g. of formamide per liter of solution. Each diffusion experiment also provided data for the difference in index of refraction between the two initial solutions used for that experiment. The densities of most of the solutions prepared for these experiments were measured at 25°. Relations are given which express the diffusion coefficient, the index of refraction and the density of the system as functions of concentration at 25°.

Formamide was chosen as the solute for this study because it was expected to have a high diffusion coefficient as a consequence of its low molecular weight. Such a non-electrolyte may be an interesting solute to use in future diffusion experiments with ternary systems. Furthermore, it is useful to have data for diffusion in more binary systems. Formamide has the interesting property that its dielectric constant is higher than that of water, and it has found application in some studies of proteins and other biological materials. The data reported in this paper confirm that formamide has a high diffusion coefficient; its value in dilute aqueous solution lies between those for urea and heavy water.

Experimental

Purification.—Doubly distilled water, which had been saturated with air, was used as solvent for all of the solutions. During the course of this experimental work, three different samples of formamide were purified by methods similar to those of earlier researchers.[1,2] In each case Matheson, Coleman and Bell 99% pure formamide was distilled at least twice at 1–2 mm. pressure at temperatures between 70 and 80°; only the middle $^2/_3$ fraction was retained from each distillation. The product of the last distillation was then fractionally crystallized at least six times; each time about 85% of the formamide was allowed to freeze and the remainder was discarded. Because of the hygroscopic nature of formamide, care was always taken to avoid exposing it to moist air.

The freezing point of the first purified sample was measured with a Beckmann thermometer which had been calibrated at the freezing point of water; a freezing point of $2.55 = 0.05°$ was found for this sample, which was in agreement with values reported in the literature.[1,3,4] This sample of formamide was used for experiments 1–5 (see Table I); these experiments were performed over a period of approximately a year. Because it has been observed that formamide is slightly unstable,[2] the possibility that significant errors might result from this decomposition was tested by comparing results from the first five experiments with those from three more experiments which were performed using two samples of freshly purified formamide. Experiments 6 and 7 were performed with the second purified sample and experiment 8 with the third purified sample. As noted under "Results" the data obtained with these three samples were consistent. For another test of decomposition, the rate of increase of specific conductance of formamide was measured at room temperature (25°) and found to be less than 10^{-7} mhos cm.$^{-1}$ hour^{-1}. If 20 (cm.^{2} ohm^{-1} equiv.$^{-1}$) is taken as the minimum estimated value for the equivalent conductance of a representative salt in formamide,[2,5] it may be concluded that over a period of a year the decomposition to ionizable products contributes less than 0.05 equivalent per liter (or less than 0.3% by weight if computed as ammonium formate). These tests indicate that no significant difficulty was encountered from decomposition.

The purity of the freshly prepared third sample was tested by conductance and freezing point measurements; the specific conductance (at about 25°) and the freezing point were found to be 6.5×10^{-6} mhos cm.$^{-1}$ and 2.40°, respectively. A new platinum resistance thermometer which had been calibrated by the Bureau of Standards was used for the latter measurements. It is of interest that if 2.55° is the correct freezing point of pure formamide (which has a cryoscopic constant of 3.50 degrees per mole, per kilogram of formamide),[6] the freezing point 2.40° corresponds to about 0.04 molal (non-electrolyte) impurity, or less than 0.1% by weight if the impurity is water.

Apparatus.—The diffusion apparatus used has been described in previous articles.[7] A new Tiselius electrophoresis cell was used for these experiments. The optical quality and precision of construction of the cell were first checked by a telescope with a Gauss eyepiece and were judged to be satisfactory. Then the cell was mounted in a new cell holder and aligned so that the cell windows were parallel to the bath windows. A Gaertner M2001RS toolmakers' microscope was used to measure the cell dimension a, the interior width of the cell along the optic axis. The optical distance[10] b, between the center of the cell and the emulsion of the photographic plate, was measured by using a combination of stainless steel rods and micrometers which had been calibrated against gage blocks. Distances a and b were found to be 2.5092 and 306.670 cm., respectively.

Method.—The general experimental methods used for the Gouy diffusion experiments are essentially those described in a previous paper.[11] All solutions were prepared by gravimetric methods with an accuracy of about one part per ten thousand. From the weight *in vacuo* of each component, and the density which was measured at 25° with a set of three single-stemmed 25-ml. Pyrex pycnometers, the concentration of each solution was calculated and tabulated as grams of solute per liter of solution.

In each experiment the cell was allowed to stand in the constant temperature bath for at least 45 min. to reach temperature equilibrium before taking photographs for determining the reference corrections,[11] δ and δ'. The initial boundary was formed by lowering a single stainless steel capillary to the optic axis and siphoning out about 75 ml. of liquid at a rate of 2–3 ml. per minute. From 7 to 10 pictures of the Gouy fringes were taken during the first 2 to 7.5 hours

(1) G. F. Smith, *J. Chem. Soc.*, 3257 (1931).

(2) F. H. Verhoek, *J. Am. Chem. Soc.*, **58**, 2577 (1936).

(3) J. Timmermans, "Physico-Chemical Constants of Pure Organic Compounds," Elsevier Publishing Co., Inc., New York, N. Y., 1950, p. 582.

(4) W. W. Bates and M. E. Hobbs, *J. Am. Chem. Soc.*, **73**, 2151 (1951).

(5) P. B. Davis, W. S. Putnam and H. C. Jones, *J. Franklin Inst.*, **180**, 567 (1915).

(6) F. H. Getman, *Rec. trav. chim.*, **55**, 231 (1936).

(7) Some modifications of the original equipment have been described in ref. 8 and 9. Those articles provide references to earlier descriptions of the apparatus.

(8) P. J. Dunlop and L. J. Gosting, *J. Am. Chem. Soc.*, **75**, 5073 (1953).

(9) P. J. Dunlop and L. J. Gosting, *ibid.*, **77**, 5238 (1955).

(10) The optical distance is equal to $\sum_i l_i/n_i$, where l_i is the distance along the optic axis in medium i of refractive index n_i; here n_i is the ratio of the velocity of light in medium i to the velocity of light in air at standard conditions (for example, see ref. 18 for the refractive index of water).

(11) L. J. Gosting, *J. Am. Chem. Soc.*, **72**, 4418 (1950).

of each diffusion experiment at approximately even intervals of $1/t'$, where t' is the time measured from the moment that siphoning was stopped.

By previously described methods of calculation,[12] the reduced height-area ratio,[9,13] $\mathfrak{D}_A$, was evaluated; for these experiments $\mathfrak{D}_A$ may be equated[14] to the diffusion coefficient D. Because the values of $Y_j/c^{-5/2}$ did not depend appreciably on fringe number, the average value of this quantity for fringe minima 1 through 6 was used for calculating the preliminary value, D', of the diffusion coefficient corresponding to each t'. To correct for the fact that the initial boundary for each experiment was slightly diffuse, the method of least squares was used to fit a linear function to the data for D' *vs.* $1/t'$; the value of D was obtained as the limiting value of this function[15,16] as $1/t' \rightarrow 0$. The average difference between the experimental D' and the corresponding values from the function determined by least squares in each experiment was calculated, and for the experiments performed these values ranged from 0.02 to 0.05%. Values of Δt, the starting time correction,[15] ranged from 6 to 16 sec.

The temperature of the bath was measured with a mercury-in-glass thermometer which was calibrated by the platinum-resistance thermometer at the completion of the series of experiments. During each experiment the temperature was between 24.995 and 25.010°; it was maintained constant to within ±0.002° in each experiment. The diffusion coefficients were converted to 25.000° by using the following series form of the Stokes–Einstein relation for dilute aqueous solutions

$$(D)_{25°} = (D)_T[1 + 0.0264(25 - T) + \ldots]$$

Here T is the temperature of the experiment.

Results

In Table I are presented the data from the diffusion experiments. The experiment numbers shown in column one indicate the order in which experiments were performed. Columns two and three list the mean concentration, $\bar{c} = (c_A + c_B)/2$, and the concentration increment, $\Delta c = c_B - c_A$, for each experiment; here c_A and c_B are the initial concentrations of formamide in the solutions above and below the starting boundary. Column four gives J, the total number of fringes for each experiment. The corresponding refractive index difference (relative to air), Δn, between the initial solutions A and B was obtained by substituting the value of J into the equation $\Delta n = J\lambda/a$; here λ is the wave length in air of the green line of mercury, 5460.7 Å., and as before a is the interior width of the diffusion cell. Division by the corresponding value of Δc yielded the value of the specific refractive increment, $\Delta n/\Delta c$, which is shown in the fifth column. Finally the main results of this experimental work, the diffusion coefficients corresponding to the concentrations shown in column two, are reported in column six. Examination of a graph of the experimental data for D *vs.* c for this concentration range showed that within experimental error a linear function expresses adequately the dependence of D on c.[17] Therefore the method of least squares was used to determine the constants in the relation

$$D \times 10^5 = 1.608_2 - 8.6_0 \times 10^{-4}c \quad (0 \leq c \leq 51) \quad (1)$$

which fits the experimental data from Table I for the diffusion of formamide in water at 25° with an average deviation of 0.03%.

TABLE I

DATA FOR FORMAMIDE IN WATER AT 25°

Exp. no.	$\bar{c}$, g./l.	Δc, g./l.	J	$(\Delta n/\Delta c) \times 10^4$, l./g.	$D^a \times 10^5$, cm.²/sec.
4	8.282	16.563	82.56	1.0848	1.6009
6	10.016	20.032	99.92	1.0855	1.5990
1	11.437	22.875	113.55	1.0803	1.5982
7	19.762	19.574	97.05	1.0791	1.5928
5	30.282	20.614	102.29	1.0799	1.5821
2	35.076	12.100	59.81	1.0758	1.5779
8	39.193	18.935	93.94	1.0769	1.5736
3	50.756	20.308	100.20	1.0738	1.5649

[a] These diffusion coefficients, D, are defined by Fick's first law in the form $J_1 = -D(\partial\rho_1/\partial x)$, where $\partial\rho_1/\partial x$ is the gradient of the solute concentration, ρ_1, expressed as grams per cc. of solution, and J_1 is the grams of solute crossing a square cm. per sec. for a volume-fixed frame of reference. Hence the values reported for D correspond to a volume-fixed reference frame.

Similarly a graph of the data for $\Delta n/\Delta c$ *vs.* $\bar{c}$ (at 25° and 5460.7 Å.) was found to be linear within experimental error, so the method of least squares was used to determine the two constants in the equation

$$(\Delta n/\Delta c) \times 10^4 = 1.086 - 2.33 \times 10^{-4}\bar{c} \quad (0 \leq \bar{c} \leq 51) \quad (2)$$

where the average deviation from the data is less than 0.2%. From equation 2 and the value[18] of the index of refraction of water for these conditions, the following equation was obtained for the refractive index of dilute aqueous solutions of formamide at 25° for λ = 5460.7 Å.

$$n = 1.3339771 + 1.086 \times 10^{-4}c - 1.19 \times 10^{-8}c^2 \quad (0 \leq c \leq 51) \quad (3)$$

Measured values of the density (in g./ml.) at 25° for most of the solutions which had been prepared for the diffusion experiments were used to obtain the following quadratic expression for the density, d, as a function of the formamide concentration.

$$d = 0.997075 + 1.464 \times 10^{-4}c - 1.97 \times 10^{-8}c^2 \quad (0 \leq c \leq 61) \quad (4)$$

Here 0.997075 is the density of pure water at 25°.[19] The other coefficients were determined by a method of least squares,[20] and the average deviation of the experimental densities from this function is 0.0013%.

A large graph of the data for D *vs.* c gave no evidence of correlation between sample number,

(12) L. J. Gosting and M. S. Morris, *ibid.*, **71**, 1998 (1949).

(13) L. J. Gosting and H. Fujita, *ibid.*, **79**, 1359 (1957).

(14) The relationship between the reduced height-area ratio, $\mathfrak{D}_A$, and the value of D, the actual diffusion coefficient corresponding to the mean concentration of the experiment, is considered in detail in ref. 13. From the experimental results reported in equations 1 and 3 of the present paper the value of K in equation 57 of ref. 13 is found to be 1×10^{-9} (g./l.)$^{-2}$. Therefore, for the relatively small concentration increments, Δc, used in the present studies, $\mathfrak{D}_A = D$ within experimental error.

(15) L. G. Longsworth, *J. Am. Chem. Soc.*, **69**, 2510 (1947).

(16) H. Fujita, *J. Phys. Soc. Japan*, **11**, 1018 (1956).

(17) Since $\mathfrak{D}_A = D$, $\bar{c}$ is replaced by c (see ref. 14).

(18) L. W. Tilton and J. K. Taylor, *J. Research Natl. Bur. Standards*, **20**, 419 (1938).

(19) N. E. Dorsey, "Properties of Ordinary Water-Substance," Reinhold Publishing Corporation, New York, N. Y., 1940, p. 201.

(20) The coefficients of c and c^2 (denoted here by β and γ) were evaluated by setting $\partial\xi/\partial\beta = \partial\xi/\partial\gamma = 0$, where $\xi = \sum_i [\beta c_i + \gamma c_i^2 - (d_i - 0.997075)]^2$. This differs from the normal method of fitting data to a quadratic by the method of least squares because the value of the coefficient of the zeroth power of c is preassigned.

or sample age (for the first sample of formamide), and the direction of deviation of each datum from equation 1. This provides good evidence that non-aqueous impurities were not present in the formamide in sufficient amounts to cause any significant error in these results. It should be noted that small amounts of water as impurity in the stock formamide would not cause appreciable error because the dependence of D on c is relatively small. Further evidence that no significant amounts of non-aqueous impurities were present was provided by the fringe deviation graphs[21]; at $f(\zeta_j) \simeq 0.5$, the average reduced fringe deviation, Ω_j, for each experiment was less than 2×10^{-4}, and for most experiments this quantity was about 1×10^{-4}. These observations, together with the evidence given under "Purification" for purity of the stock formamide, provide strong evidence that the diffusion coefficients reported in Table I are not significantly affected by impurities.

The data for $\Delta n/\Delta c$ *vs.* c show more scatter than has been encountered in studies of systems with solid solutes at this Laboratory. Because these data are sensitive to the presence of water as an impurity in the formamide (as contrasted to data for D), this scatter may be due to the difficulties of handling the hygroscopic liquid solute. From consideration of the concentration dependence of the density, the measured densities, even for the highest concentration of formamide studied, should not be significantly influenced by the small amounts of impurities indicated in the previous paragraph and under "Purification."

Acknowledgments.—This work was supported in part by the National Science Foundation, by a Rohm and Haas Grant-in-Aid to the Department of Chemistry, and by the Research Committee of the Graduate School from funds supplied by the Wisconsin Alumni Research Foundation.

(21) D. F. Akeley and L. J. Gosting, *J. Am. Chem. Soc.*, **75**, 5685 (1953).

THE DISSOCIATION PRESSURES AND THE HEATS OF FORMATION OF THE MOLYBDENUM SILICIDES[1]

BY ALAN W. SEARCY AND A. G. THARP[2]

Department of Mineral Technology, University of California, Berkeley, California, and Department of Chemistry, Purdue University, Lafayette, Indiana

Received April 30, 1960

Silicon partial pressures for dissociation of the three molybdenum silicides have been measured by the Knudsen effusion method. The heats of dissociation per gram atom of silicon vapor are calculated to be at 298°K. for Mo_3Si 131.9 ± 1.2 kcal., for Mo_5Si_3 131.1 ± 0.7 kcal., and for $MoSi_2$ 117.2 ± 0.6 kcal. The heats of dissociation of the molybdenum silicides when combined with the heat of sublimation of silicon yield the following heats of formation at 298°K.: Mo_3Si −23.5 ± 4 kcal.; $1/3Mo_5Si_3$ −22.6 ± 5 kcal.; $1/2MoSi_2$ −13.0 ± 5 kcal.

Of the many known transition metal silicides, the one of particular interest has been the disilicide of molybdenum. This silicide is used to fabricate resistance heating elements that are stable in oxidizing atmospheres up to 1750°. Such exceptional stability toward oxidation probably arises because the oxidation of molybdenum disilicide yields a thin adherent coating whose outermost layer is primarily silicon dioxide.[3,4] Availability of molybdenum disilicide as a practical material of commerce makes knowledge of its properties of exceptional value.

The phase diagram for the molybdenum–silicon system published by Ham and Herzig[5] shows the melting points of the three silicides of molybdenum to be above 2000°. The structures of the three phases have been determined.[6-8] The heat capacity of molybdenum disilicide has been determined by two groups of workers,[9,10] and the heat capacity and entropy of Mo_3Si have been measured by King and Christensen.[11] Robins and Jenkins[12] have determined the heats of formation for $MoSi_2$ and "Mo_3Si_2" by measuring the heat liberated when the elements were caused to combine.

In this paper are reported dissociation pressures, heats of dissociation, and the heats of formation for Mo_3Si, Mo_5Si_3 and $MoSi_2$. These data are calculated from Knudsen effusion measurements of the silicon dissociation pressures.

Experimental

Apparatus and procedures were similar to those described by Searcy and McNees.[13] All samples used for dissociation pressure measurements were made by direct synthesis from the elements. Spectroscopic analyses showed only trace impurities in either the molybdenum or silicon.

The dissociation pressure of Mo_3Si was measured in both molybdenum and tungsten vapor pressure cells. The molybdenum cells were 25 mm. high by 15 mm. in diameter with a 1.3 mm. wall thickness. These cells were placed inside a

(1) This work was supported by the Metallurgy and Materials Branch of the Office of Naval Research.

(2) Department of Chemistry, Long Beach State College, Long Beach, Calif.

(3) A. W. Searcy, *J. Am. Ceram. Soc.*, **40**, 431 (1957).

(4) E. Fitzer, Plansee Proc., 2nd Seminar, Ruette/Tyrol, 56 (1956).

(5) J. L. Ham and A. J. Herzig, NP-3396 Second Annual Report: "Arc-Cast Molybdenum Base Alloys," 1951.

(6) W. H. Zachariasen, *Z. physik. Chem.*, **128B**, 39 (1927).

(7) B. Aronsson, *Acta Chem. Scand.*, **9**, 137 (1955).

(8) D. H. Templeton and C. H. Dauben, *Acta Cryst.*, **3**, 261 (1950).

(9) T. B. Douglas and W. M. Logan, *J. Research Natl. Bur. Standards*, **53**, 91 (1954).

(10) B. E. Walker, J. A. Grand and R. R. Miller, THIS JOURNAL, **60**, 231 (1956).

(11) E. G. King and A. U. Christensen, Jr., *ibid.*, **62**, 499 (1958).

(12) D. A. Robins and I. Jenkins, *Acta Met.*, **3**, 598 (1955).

(13) A. W. Searcy and R. A. McNees, Jr., *J. Am. Chem. Soc.*, **75**, 1578 (1953).

graphite crucible which was contained in a concentric graphite crucible holder. The assembly was wrapped with 0.13 mm. tantalum metal radiation shields. Molybdenum lids for the vapor pressure cells were machined from molybdenum rod or cut from 0.13 mm. molybdenum sheets. The areas of the effusion orifices were determined from measurements of the diameter of the orifice with a traveling microscope. Readings were made to ±0.005 mm. The lengths of the orifices were measured with a micrometer. The machined lids were 1.3 ± 0.2 mm. thick with hole areas of 0.85 mm.². The holes were tapered to a knife edge at an angle of 27° upward from the horizontal. The 0.13 mm. thick lids were backed with an outside lid of molybdenum to bring the thickness of the lid to the wall thickness of the crucible. Effusion hole areas were varied by a factor of six. A graphite lid with a hole and taper sufficiently large to prevent interference with effusion of the vapor was used to cover the cell and crucible holder.

Tungsten vapor pressure cells were used for both $MoSi_2$ and Mo_3Si determinations. The assembly was similar to that described above except that the tungsten cells were 13 mm. high by 19 mm. in diameter with a wall thickness of 1.3 mm. The tungsten lids were weighed before and during a series of vapor pressure measurements to determine the extent of reaction between the silicon vapor and tungsten. For Mo_5Si_3 studies, this reaction was negligible; for $MoSi_2$, reaction was sometimes serious. This reaction problem is discussed in the next section of the paper.

A sample of $MoSi_2$ that had been used in several vapor pressure determinations was spectroscopically analyzed for tungsten. The amount of tungsten that was found in the silicide was negligible. Reaction of tungsten with the phases of lower silicon activity should be less than with $MoSi_2$.

The vapor pressure cell and the graphite crucible that held it were weighed before and after each heating to determine the amount of silicon that had effused through the cell orifice. An Ainsworth type FDI, semimicro balance with a set of weights that had been calibrated against a set of National Bureau of Standards weights was used for measurements to ±0.02 mg. All cells were heated to constant weight prior to the vapor pressure determinations. The molybdenum cells continued to lose some weight due to surface oxidation, but this loss became negligible after the inside surface was coated with a silicide. Analysis of the vapor condensate from an effusion run showed silicon to be the main detectable element with molybdenum present in only trace amounts.

Temperatures were measured with a Leeds and Northrup disappearing filament optical pyrometer which had been calibrated against a standard tungsten ribbon lamp. Observed temperatures were corrected for the light absorbed by the viewing window. The temperatures are believed to be accurate to ±7°.

All pressures were calculated from the Knudsen equation. Corrections were made for the length to radius ratio of the orifice, for thermal expansion, and for the time required to heat and cool the cell.

Results and Conclusions

Preliminary vapor pressure determinations for Mo_3Si–molybdenum mixtures revealed that the rate of escape of silicon from the cells decreased progressively after several hours at run temperatures.

The decrease of apparent pressures with time occurred because the layers of the molybdenum reaction product sintered and impeded escape of silicon. Essentially equilibrium pressures could be obtained, so long as the impedance caused by this sintered layer did not reduce the silicon pressure in the chamber of the effusion cell to a fraction of the equilibrium pressure that was less than the ratio of effusion hole area to sample surface area. Accordingly, to minimize the impedance the sample was reground to a fine powder after each pressure determination and degassed before the next determination.

Dissociation pressures were measured over the temperature range 2015 to 2288°K. The pressure of silicon vapor was so low at the lower temperatures that runs of six hours duration were necessary to obtain weight losses of a few tenths of a milligram. These small weight losses and the sintering of the sample combined to cause considerable scatter in the data. However, effusion hole areas were varied from 0.81 to 4.62 mm.². The resultant pressures showed no systematic change; furthermore, pressures obtained with a tungsten cell were in good agreement with those obtained with molybdenum cells.

Because of the considerable scatter of the data, a third law analysis was considered superior to a plot of log P *vs.* $1/T$ for determination of the heat of dissociation.[14] King and Christensen[11] have provided heat capacity and entropy data to a maximum temperature of 1500°K. The value of ΔC_p for the dissociation reaction $Mo_3Si(s) = 3Mo(s) + Si(g)$ was estimated to be -2.5 cal. deg.$^{-1}$ in the range 1500 to 2300°K. This estimate combined with data of Stull and Sinke[15] for the elements and the data of King and Christensen yielded for $-(\Delta F_T - \Delta H_{298})/T$: at 1900°K., 34.55;[16] at 2000°K., 34.49; at 2100°K., 34.44; at 2200°K., 34.39; and at 2300° K., 34.33 cal. deg.$^{-1}$.

Table I summarizes the calculations of ΔH_{298} for the reaction

$$Mo_3Si(s) = 3Mo(s) + Si(g) \qquad (1)$$

TABLE I

HEAT OF THE REACTION: $Mo_3Si(s) = 3Mo(s) + Si(g)$

T, °K.	Pressure of Si × 10^7, atm.	ΔH_{298}^0, kcal.	T, °K.	Pressure of Si × 10^7, atm.	ΔH_{298}^0, kcal.
2015[a]	5.44	127.2	2148[d]	13.00	131.8
2067[e]	4.74	131.0	2151[c]	10.40	132.9
2067[e]	4.98	130.8	2153[a]	15.60	131.3
2070[f]	5.77	130.4	2161[k]	12.70	132.7
2072[e]	3.94	132.1	2164[d]	11.30	133.3
2072[g]	6.55	130.0	2166[k]	12.90	132.9
2078[i]	3.62	132.8	2175[c]	10.50	134.3
2088[c]	7.09	130.7	2180[d]	10.30	134.7
2098[c]	7.44	131.1	2187[b]	27.20	130.9
2129[c]	12.80	130.7	2209[c]	36.20	130.9
2133[c]	14.30	130.5	2218[a]	28.80	132.5
2139[j]	12.30	131.5	2226[e]	40.60	131.4
2140[h]	12.40	131.5	2228[d]	22.80	134.1
2143[e]	10.10	132.6	2228[j]	27.10	133.3
2143[e]	13.00	131.5	2228[e]	36.10	132.1
2143[e]	17.80	130.1	2240[d]	21.30	135.1
2145[e]	14.40	131.1	2241[d]	31.00	133.5
2146[e]	9.80	132.9		Av.	131.9 ± 1.2

[a] Effusion hole area 4.62 mm.², Clausing correction 0.95. [b] Effusion hole area 3.22 mm.², Clausing correction 0.93. [c] Knife-edged tapered hole area 0.010 cm.², Clausing correction 1.0. [d] Effusion hole area 1.88 mm.², Clausing correction 0.723. [e] Effusion hole area 0.85 mm.², Clausing correction 0.846. [f] Effusion hole area 1.01 mm.², Clausing correction 0.837. [g] Effusion hole area 1.05 mm.², Clausing correction 0.840. [h] Effusion hole area 1.08 mm.², Clausing correction 0.843. [i] Effusion hole area 2.05 mm.², Clausing correction 0.890. [j] Effusion hole area 0.81 mm.², Clausing correction 0.835. [k] Tungsten effusion cell, effusion hole area 0.0178 cm.², Clausing correction 0.910.

(14) L. Brewer and A. W. Searcy, *J. Chem. Educ.*, **26**, 548 (1949).

(15) D. R. Stull and G. C. Sinke, "Thermodynamic Properties of the Elements," American Chemical Society, Washington, D. C., 1956.

(16) See J. L. Margrave, in "High Temperature—A Tool for the Future," Stanford Research Institute, Menlo Park, Calif., 1956, for use of these functions.

The heat of the reaction is 131.9 ± 1.2 kcal. at 298°K. A trend toward higher calculated heats of sublimation with increased temperature is apparent. This trend may arise because the escape of silicon at higher temperatures is impeded to a greater extent by the reaction product layer than is the escape of silicon at lower temperatures.

Calculated dissociation pressures for Mo_5Si_3 determined by use of effusion orifice areas from 0.96 to 2.69 mm.[2] and temperatures from 2050 to 2261° K. give sufficiently good agreement to show that equilibrium pressures were obtained within the effusion cells. Heat content and entropy data are not available for Mo_5Si_3. But for Mo_3Si and $MoSi_2$, the values of $H_T - H_{298}$ are nearly equal to additive values for the condensed elements: $H_{1500} - H_{298}$ for Mo_3Si is 31,190 cal. mole^{-1}, $3(H_{1500} - H_{298})$ for molybdenum plus $H_{1500} - H_{298}$ for silicon is 31,380 cal. mole^{-1}; $H_{1200} - H_{298}$ for $MoSi_2$ is 16,120 cal. mole^{-1}, $H_{1200} - H_{298}$ for molybdenum plus $2(H_{1200} - H_{298})$ for silicon is 16,530 cal. mole^{-1}. Furthermore, S_{1500} for Mo_3Si is 65.9 cal. deg.$^{-1}$ mole^{-1} *vs.* 65.7 cal. deg.$^{-1}$ for 3 molybdenum plus 1 silicon. These functions should be nearly additive for Mo_5Si_3 as well. Accordingly, for both Mo_5Si_3 and $MoSi_2$ the values of $-(\Delta F_T - \Delta H_{298})/T$ for

$$3/4Mo_5Si_3(s) = 5/4MoSi(s) + Si(g) \quad (2)$$

and for

$$5/7MoSi_2(s) = 1/7Mo_5Si_3(s) + Si(g) \quad (3)$$

can be estimated with confidence to be essentially identical with the values for reaction 1. Data for Mo_5Si_3 are summarized in Table II. The heat of reaction 2 is calculated to be at 298°K. 131.1 ± 0.7 kcal.

TABLE II

HEAT OF THE REACTION: $3/4Mo_5Si_3(s) = 5/4Mo_3Si(s) + Si(g)$

T, °K.	Pressure of Si × 10^7, atm.	$\Delta H_{298}°$, kcal.	T, °K.	Pressure of Si × 10^7, atm.	$\Delta H_{298}°$, kcal.
2050[a]	4.08	130.6	2187[a]	25.80	130.9
2054[b]	4.94	130.1	2189[b]	29.30	130.5
2069[b]	6.00	130.2	2206[c]	31.00	134.3
2084[a]	5.29	131.6	2227[a]	39.50	131.4
2091[a]	5.14	132.2	2228[b]	43.20	131.1
2126[a]	9.87	131.4	2234[c]	73.90	129.0
2136[a]	12.70	130.9	2235[c]	59.70	130.0
2136[b]	14.20	130.5	2239[c]	52.40	130.8
2150[c]	16.30	130.7	2239[c]	42.00	131.8
2155[a]	12.60	132.1	2252[c]	63.00	130.8
2184[a]	22.50	131.3	2261[c]	66.90	131.0
				Av.	131.1 ± 0.7

[a] Effusion hole are 2.69 mm.[2], Clausing correction 0.910. [b] Effusion hole area 0.96 mm.[2], Clausing correction 0.852. [c] Effusion hole area 1.48 mm.[2], Clausing correction 0.914.

Dissociation pressure measurements for $MoSi_2$ were made in the temperature range from 1926 to 2156°K. with effusion orifices of areas from 1.25 to 4.01 mm.[2]. Some variation in calculated pressure with effusion orifice area was observable, but the variation was not consistent with the variation to be expected from non-equilibrium effects within the cell. The smallest orifice yielded calculated pressures at lower temperatures that were lower than pressures calculated for larger orifices Examination of the tungsten vapor pressure cell revealed some reaction of the cell cover with silicon vapor. X-Ray examination of a portion of the cover obtained from the edge of the effusion orifice showed the presence of W_5Si_3. The anomaly in calculated pressures probably arose from the loss of silicon from the surface of the cell cover. To minimize such loss, lids were changed after use for relatively short periods or whenever reaction was observed to have occurred on the outer edge of the effusion orifice. The data summarized in Table III yield for reaction 3 $\Delta H_{298} = 117.2 \pm 0.6$ kcal.

TABLE III

HEAT OF THE REACTION: $5/7MoSi_2(s) = 1/7Mo_5Si_3(s) + Si(g)$

T, °K.	Pressure of Si × 10^6, atm.	$\Delta H_{298}°$, kcal.	T, °K.	Pressure of Si × 10^6, atm.	$\Delta H_{298}°$, kcal.
1926[a]	2.05	116.7	2073[c]	12.40	118.0
1958[b]	2.28	118.0	2082[a]	16.60	117.3
1970[a]	3.71	116.9	2082[b]	18.90	116.7
2003[c]	4.96	117.7	2129[c]	25.40	118.1
2004[b]	5.57	117.3	2139[a]	38.70	116.8
2011[c]	5.44	117.8	2139[b]	49.20	115.8
2017[a]	6.91	117.2	2156[a]	52.00	116.4
2022[b]	7.94	116.9		Av.	117.2 ± 0.6

[a] Effusion hole area 2.75 mm.[2], Clausing correction varied from 0.808 to 0.893 due to condensate around effusion orifice. The thickness and area of the hole were measured before and after each determination and the Clausing correction was taken as the average for the hole thickness during a run. [b] Effusion hole area 1.25 mm.[2], Clausing correction 0.744–0.830. Treated as in a above. [c] Effusion hole area 4.01 mm.[2], Clausing correction 0.892.

Dissociation pressure curves can best be derived for the silicide phases by use of equations of the form $\log P = a/T - 5.75 \log T + b$, in which a and b are constants and -5.75 is ΔC_p multiplied by the natural logarithm of 10. To obtain the values of a and b, the average values of ΔH_{298} for the dissociation reaction are used with the free energy functions to calculate values of $\log P$ at each extreme of the experimental temperature range. These two pressures at known temperatures are then used to evaporate the constants a and b. The silicon dissociation pressure equations are $\log P = 33{,}690/T - 5.75 \log T + 28.94$, $\log P = -32{,}940/T - 5.75 \log T + 28.67$, and $\log P = -29{,}800/T - 5.75 \log T + 28.62$ for reactions 1, 2 and 3, respectively, in the range 1900 to 2300°K.

The heat of formation of each molybdenum silicide phase at 298°K. can be obtained from the heat of dissociation data by use of these data with the heat of sublimation of silicon at 298°K., 108.4 ±3 kcal.[17] The calculated heats of formation are −23.4 ±4 kcal. for Mo_3Si, −22.6 ±5 kcal. for $1/3Mo_5Si_3$, and −13.0 ±5 kcal. for $1/2MoSi_2$. The quoted uncertainties are high enough so that the probability that the true values may lie outside these limits is believed to be almost zero. Direct calorimetric measurements of Robins and Jenkins[12] yielded −23.4 kcal. for $1/2$"Mo_3Si_2" and −15.7 kcal. for $1/2MoSi_2$. The "Mo_3Si_2" phase of Robins and Jenkins is presumably the phase identified here

(17) S. G. Davis, D. F. Anthrop and A. W. Searcy, *J. Chem. Phys.*, in press.

as Mo_5Si_3 to agree with results of recent structure studies.[7] Prior to the structure investigation the phase in question had been identified as $MoSi_{0.65}$ from composition *vs.* diffraction pattern studies.[18] The agreement in heats of formation obtained from the two investigations is satisfactory.

(18) L. Brewer, A. W. Searcy, D. H. Templeton and C. H. Dauben, *J. Am. Ceram. Soc.*, **33**, 291 (1950).

THE VOLUME CHANGE ON MIXING IN LIQUID METALLIC SOLUTIONS. I. ALLOYS OF CADMIUM WITH INDIUM, TIN, THALLIUM, LEAD AND BISMUTH

BY O. J. KLEPPA

Institute for the Study of Metals, University of Chicago, Chicago, Illinois

Received May 7, 1960

A method is described which permits direct determination of the volume change on mixing in liquid solutions at temperatures up to 500°. This method has been used for measurement of the excess volume in five binary alloy systems involving cadmium. The results are compared with available information on the excess entropy of mixing and on the heat of mixing. It is found that about 70% of the observed excess entropies at constant pressure can be attributed directly to the change in volume on mixing. The experimental heat-volume ratios compare in magnitude with the corresponding ratios derived for a temperature increment ($C_p/\alpha V$) and for the process of fusion of the pure components.

Introduction

In recent communications the author has demonstrated that in many liquid alloys involving zinc and cadmium, a semiquantitative correlation exists between the heat of mixing, the excess entropy of mixing and the difference in valence between the two components.[1,2]

In the present paper our study of these alloys is extended to an exploration of the volume change on mixing. In recent work on solution theory this *excess* volume usually is considered along with the excess free energy, the heat of mixing (*i.e.*, the excess heat) and the excess entropy.[3]

Unfortunately, the basic assumption on which these theories are usually based, namely the central force pair interaction approximation, is known not to hold for metallic systems. Therefore we shall in the present paper refrain from detailed comparison with the predictions of these theories. Instead we shall confine ourselves to a largely thermodynamic and phenomenological approach.

A survey of the earlier literature shows that information relating to the volume change on mixing in liquid alloys may be found in the works of many investigators. Among the more important contributors are Sauerwald and co-workers,[4] Arpi,[5] Matuyama,[6] Pelzel,[7] Knappwost and Restle[8] and Fisher and Phillips.[9] Much of this earlier information is summarized in the compilation of thermodynamic data authored by Kubaschewski and Catterall.[10]

In these earlier studies emphasis was placed on precise determination of the density of the pure metals and the alloys, and on the dependence of density on temperature and composition. From such data the excess volume, ΔV^M, at a given temperature, is readily calculated

$$\Delta V^M = (X_1M_1 + X_2M_2)/\rho - [X_1M_1/\rho_1 + X_2M_2/\rho_2] \quad (1)$$

Here ρ represents density, M_1 and M_2 are the molecular (atomic) weights of the two components, while X_1 and X_2 are the corresponding mole fractions in the mixture.

Where earlier data for the systems considered in the present study were available, it was found that the maximum value of ΔV^M should be of the order of 0.1–0.3 cc./g. atom, *i.e.*, the fractional volume change $\Delta V^M/V$ should be of the order of 2% or less. Thus it is apparent that density work of high quality is required in order to provide a basis for precise calculation of the excess volume.

In the present communication we describe a simple (although somewhat cumbersome) method which permits direct determination of the excess volume at temperatures up to about 500°. Using this method we have made measurements on five binary systems where cadmium is one of the two components. Most runs were performed at about 350°, while a few were carried out also at 450°. In a future communication similar data will be reported for liquid alloys of zinc, measured at 450°.

Experimental

The dilatometric "cell" used in the present research represents a development of a device previously used for the study of indium–mercury alloys at temperatures up to 150–160°.[11] The principal features of the method are readily recognized from the schematic diagram in Fig. 1.

The volume cell consists of a U-shaped Pyrex tube of about 15 mm. outside diameter. By means of narrow-bore

(1) O. J. Kleppa, *Acta Met.*, **6**, 225, 233 (1958).

(2) O. J. Kleppa and C. E. Thalmayer, THIS JOURNAL, **63**, 1953 (1959).

(3) I. Prigogine, "The Molecular Theory of Solutions," North Holland Publishing Co., Amsterdam, 1957.

(4) F. Sauerwald, *et al.*, *Z. Metallkunde*, **14**, 145, 254, 457 (1922); *Z. anorg. allgem. Chem.*, **135**, 327 (1924); **149**, 273 (1925); **153**, 319 (1926); **155**, 1 (1926); **181**, 347 (1929); **192**, 145 (1930); *Z. Metallkunde*, **35**, 105 (1943); *Z. anorg. allgem. Chem.*, **270**, 324 (1952).

(5) R. Arpi, *Z. Metallographie*, **5**, 142 (1914).

(6) Y. Matuyama, *Sci. Rep. Tôhoku Imp. Univ.*, **18**, 19, 737 (1929).

(7) E. Pelzel, *Z. Metallkunde*, **32**, 7 (1940); E. Pelzel and F. Sauerwald, *ibid.*, **33**, 229 (1941); E. Pelzel and H. Schneider, *ibid.*, **35**, 121 (1943).

(8) A. Knappwost and H. Restle, *Z. Elektrochem.*, **58**, 112 (1954).

(9) H. J. Fisher and A. Phillips, *J. Metals*, **6**, 1060 (1954).

(10) O. Kubaschewski and J. A. Catterall, "Thermochemical Data of Alloys," Pergamon Press, London and New York, 1956.

(11) O. J. Kleppa and M. Kaplan, THIS JOURNAL, **61**, 1120 (1957).

capillaries this is connected to a 0.1 cm.^{3} calibrated gas "buret." Through an S-shaped section (of arbitrary diameter) the "buret" is sealed to another capillary of the same diameter. During actual measurements this part of the assembly is filled with Octoil-S, in such a way that the two oil menisci are roughly at the same level. If under these circumstances, the volume of the gas contained in the cell assembly expands or contracts, this volume change will occur at constant pressure (provided the external pressure remains constant).

A determination of the volume change on mixing is carried out as follows: weighed samples of the two components are placed in the U-tube legs, which are then sealed off. The cell assembly, except for the oil-filled buret section, is then evacuated, checked for leaks, and filled with argon or nitrogen at about 1 atm. pressure. Now the U-tube is immersed in a large salt-bath "thermostat," at such an angle that the two liquid metals remain separated. The salt-bath used in the present work contained about 250 lb. of the eutectic mixture of lithium–sodium–potassium nitrate. The bath was constructed according to the description given by Beattie,[12] with a modified stirring arrangement as proposed by Collins.[13]

When the U-tube is first immersed into the bath, overpressure develops inside the cell assembly. This is released through stopcocks A and B. Stopcock A is then turned to connect the U-tube with the gas buret. If the salt bath temperature is constant, and if the temperature distribution along the capillary "lead" does not change with time, a constant oil level will be observed in the buret. In practice small fluctuations around a mean value usually are obtained.

After the oil level has remained essentially stationary to ± 0.001 cm.^{3} or better for not less than 0.5 hour, the two liquid metals are mixed by gently rocking the whole assembly around the axis C–C. Complete mixing usually is achieved in about 4 minutes, after which time the cell is returned to the original position. In successful experiments a new stationary oil level is observed, and additional mixing causes no further change in this level.

In introductory work the device was operated at atmospheric pressure, and it was assumed that this pressure remained constant during the 1–2 hours required to complete a typical experiment. However, it was soon recognized that even small changes in atmospheric pressure give rise to significant drifts in the apparent volume observed in the buret. These drifts were eliminated by connecting the external end of the buret assembly, by means of capillary rubber tubing, to a simple manostat, consisting of a 1.5 liter narrow neck Dewar vessel completely immersed in a room temperature thermostat.

Calibration and Evaluation Procedures; Errors

The capillary "buret" was calibrated by filling it with Octoil of known density, and weighing the oil drained from the tube. Calibration by two independent observers gave the same result within ± 0.0005 cm.^{3} (0.5%).

In order to evaluate the volume change on mixing from the observed buret readings it is necessary to assume that the temperature distribution along the "lead" capillary remains unchanged during the mixing experiment, and that the bath temperature and the pressure inside the cell remains constant. The net result of the mixing operation is then that a certain volume of gas at the bath temperature, ΔV_T, is "replaced" by a corresponding apparent volume change at room temperature, ΔV_{T_0}.

One has simply

$$\Delta V_T = (T/T_0)\Delta V_{T_0}$$

where T and T_0 are the absolute temperatures of bath and buret, respectively.

In the present work the bath temperature was measured by means of a chromel–alumel thermocouple, calibrated at the m.p. of lead (327°). The bath was controlled manually, and its temperature was readily kept constant to better than 0.05° for the period of the experiment. If the volume of "dead" gas contained in the immersed U-tube is 10 cm.^{3} (a typical value), this will give rise to an apparent volume change of the order of 0.001 cm.^{3} or less in the buret (at constant pressure and 600°K.).

The buret temperature was measured by means of a small "Anschutz" thermometer taped to the buret wall. During the period of a run this temperature remained constant to a few tenths of a degree.

In duplicate experiments involving a total of 0.6 to 0.8 g. atom of metal it was in most cases possible

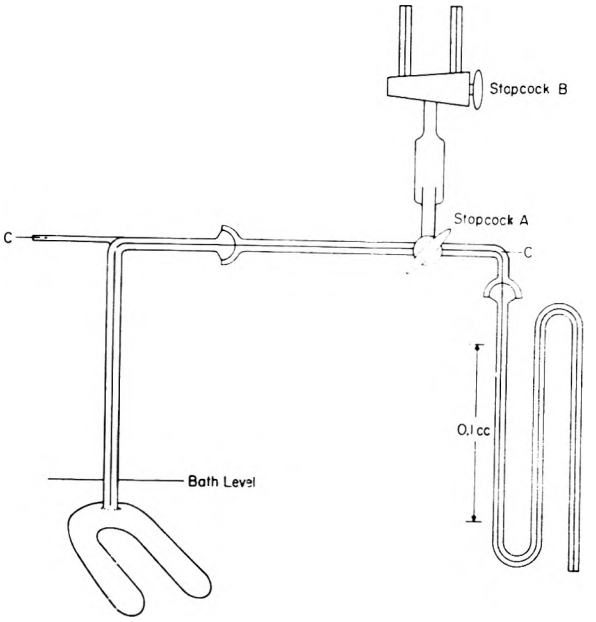

Fig. 1.—Schematic diagram of assembly used for volume change measurements.

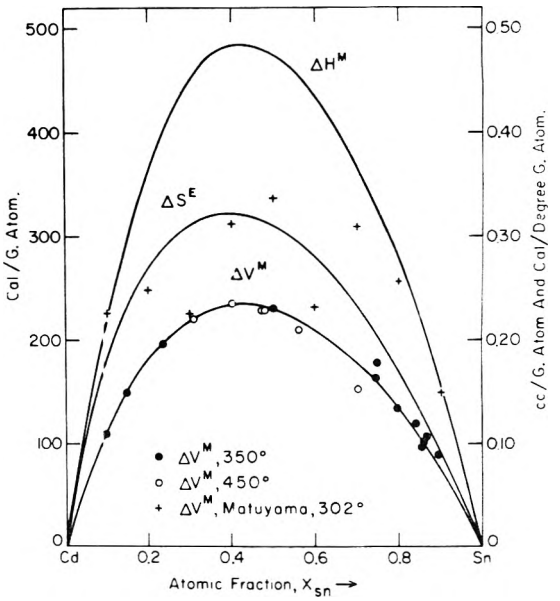

Fig. 2.—Molar integral volume change on mixing, heat of mixing and excess entropy of mixing in liquid cadmium–tin alloys. (Heat and entropy data from ref. 1).

(12) J. A. Beattie, *Rev. Sci. Instr.*, **2**, 458 (1931).
(13) S. C. Collins, *ibid.*, **7**, 502 (1936).

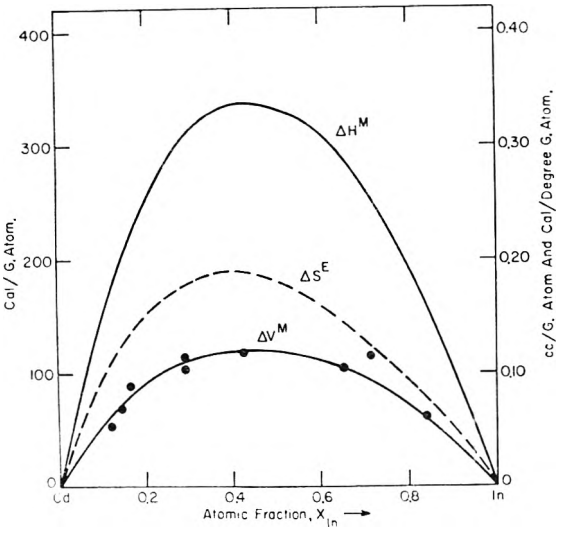

Fig. 3.—Volume change, heat and excess entropy of mixing in liquid cadmium–indium alloys (heat data and approximate entropy data from ref. 1).

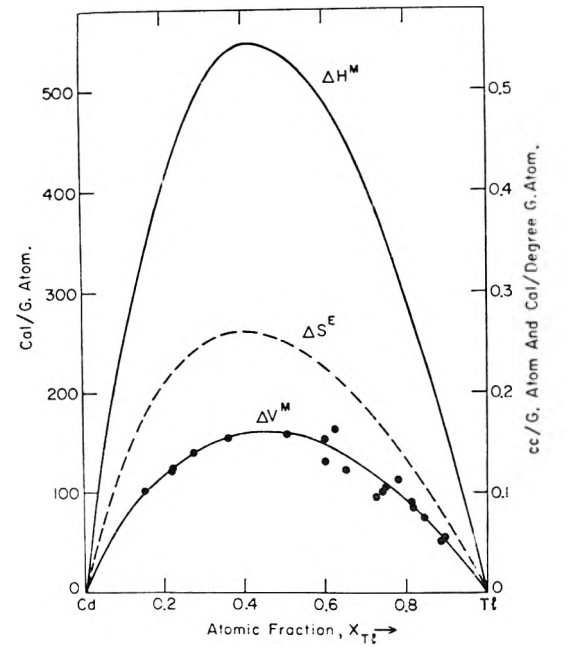

Fig. 4.—Volume change, heat and excess entropy of mixing in liquid cadmium–thallium alloys (heat data and approximate entropy data from ref. 1).

to achieve reproducible results to ± 0.003 cm.^{3} or better (for the apparent volume change as observed in the buret). The corresponding uncertainty in the molar volume change on mixing is of the order of ± 0.01 cm.^{3}/g. atom or less.

The metals used in the present research were all of 99.9+% purity, as checked by semi-quantitative spectrographic analysis.

Results

In the course of the present investigation about 90 different mixing experiments were initiated. Only about 65 of these were successful. Most of the failures were due to the development of leaks and/or to cracked cells. Nearly all runs were performed with the bath temperature near 350°, while a few measurements on cadmium–tin were carried out at 450°. The experimental results for cadmium–tin, which are presented graphically in Fig. 2, show that for this system the excess volume is essentially independent of temperature between 350 and 450°. In view of this observation no attempt was made to explore the possible temperature dependence of the excess volume for the other four binaries. The results for these systems are presented in Figs. 3–6. These figures give also corresponding curves for ΔH^M and ΔS^E, the heat of mixing and excess entropy of mixing. The significance of these curves will be considered in the discussion below.

For cadmium–tin, cadmium–lead and cadmium–bismuth the graphs also contain selected values of ΔV^M as calculated from the reported density data of Matuyama.[6] It will be recognized that for cadmium–tin and cadmium–bismuth Matuyama's data suffer from a lack of precision, and differ rather significantly from the present results. For cadmium–lead, on the other hand, Matuyama's values are less scattered, and agree quite well with our direct measurements. For cadmium–indium and cadmium–thallium no density or volume data were found in the published literature.

Summary of Volume Data

Smoothed curves representing the excess volumes for all five systems covered in the present work are given in Fig. 7. A comparison of the results for cadmium–indium and cadmium–tin is of particular interest, since these three metals are neighbors in the periodic system. It will be noted that for all compositions the volume change for cadmium–tin is essentially twice the corresponding change for cadmium–indium (ΔV^M_{max} for Cd–Sn is $+0.23_5$, for Cd–In $+0.12_0$ cm.^{3}/g. atom). This shows that for these systems there is a clear correlation between the magnitude of the volume change and the valence difference between the two partners. This is roughly analogous to the previously established correlations between excess entropy and valence difference, and between heat of mixing and valence difference.

Note, however, that the excess volume curves for the alloys of cadmium with thallium, lead and bismuth do not show a similar correlation. Thus we find that both cadmium–thallium and cadmium–lead have maximum values of ΔV^M of comparable magnitude (0.15–0.16 cm.^{3}/g. atom), while for cadmium–bismuth ΔV^M_{max} is about twice as large ($+0.31$ cm.^{3}). This confirms that liquid alloy systems where the two metals belong in different rows of the periodic system tend to be considerably more complex than where both partners come from the same row.[1,2]

Discussion

The first quantitative discussion of the relation between the volume change on mixing and the other thermodynamic excess functions was given by Scatchard.[14] He considered the mixing process as consisting of two consecutive steps: in the first step the mixing of the two components is performed at constant volume. This is followed by a second

(14) G. Scatchard, *Trans. Faraday Soc.*, **33**, 160 (1937).

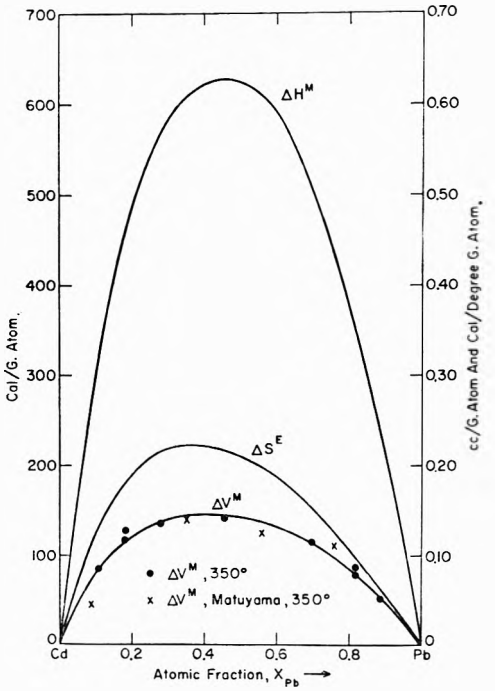

Fig. 5.—Volume change, heat and excess entropy of mixing in liquid cadmium–lead alloys (heat and entropy data from ref. 1).

step which involves a volume change of appropriate sign and magnitude, so that the initial pressure is recovered.

According to Scatchard's essentially thermodynamic reasoning a volume change on mixing should contribute quite significantly both to the entropy and to the heat of mixing, whereas the free energy should be relatively little affected. If, as in the cases considered in the present work, the fractional volume change ($\Delta V^M/V$) is small, we may neglect higher order terms in Scatchard's derivations, and write for the "volume contributions" to the three thermodynamic functions of principal interest

$$\Delta S_{vol} \cong \frac{\alpha}{\beta} \Delta V^M \qquad (2a)$$

$$\Delta H_{vol} \cong T \frac{\alpha}{\beta} \Delta V^M \qquad (2b)$$

$$\Delta F_{vol} = \Delta H_{vol} - T\Delta S_{vol} \cong 0 \qquad (2c)$$

In these expressions α denotes the thermal coefficient of expansion, while β is the isothermal compressibility. For all the pure liquid metals considered in the present study values of these parameters are available in the literature.[15]

In order to explore these volume–entropy–enthalpy correlations we have in Figs. 2–6 included curves which give the appropriate integral heats and excess entropies, along with the corresponding volume change. The thermal data were all taken from or calculated from values quoted in ref. 1.

These figures prove beyond doubt that there is indeed a large measure of analogy between the various excess functions. This is so both within each binary system, and if we go from one system to the other. This last point is well illustrated by Table I, which gives a summary of the correlation factors as derived from Figs. 2–6.

(15) O. J. Kleppa, *J. Chem. Phys.*, **18**, 1331 (1950).

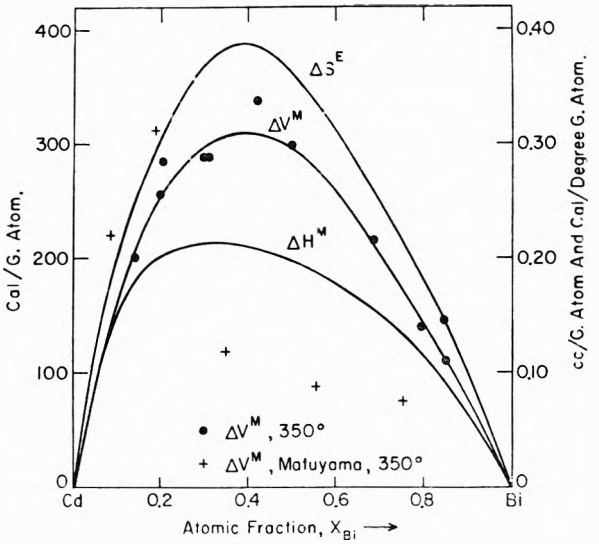

Fig. 6.—Volume change, heat and excess entropy of mixing in liquid cadmium–bismuth alloys (heat and entropy data from ref. 1).

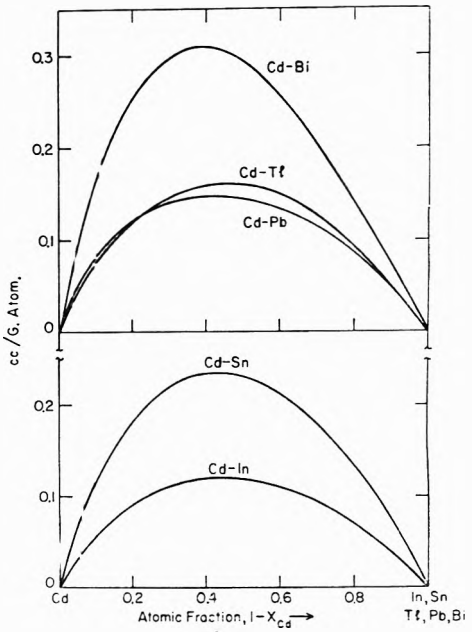

Fig. 7.—The volume change on mixing in the liquid alloys of cadmium with indium, tin, thallium, lead and bismuth at 350°.

From the two first columns in this table we find that our measured excess volumes "account" for roughly 70% of the experimental excess entropies. Thus, if the mixing process were carried out at 350° and constant volume (rather than at constant pressure) the excess entropies would be of the order of 30% of the constant pressure values. On the other hand, since $T(\alpha/\beta) \cong 0.6$ kcal./cm.^{3} at 600°K., we see that the enthalpy changes at constant volume will be of the order of 80% of those at constant pressure (except for Cd–Bi, see below).

In his original paper Scatchard considered the special case where the two solution partners are "normal" liquids, *i.e.*, are substances for which

$$(\partial E/\partial V)_T \cong \Delta E^v/V \qquad (3)$$

Here ΔE^v is the energy of vaporization, while V is the molar volume. For a system of this type we may with Scatchard expect to have

$$\Delta V^M \cong \beta \Delta F^E \qquad (4)$$

Now it is well known that relation 3 does not hold for metallic liquids. Therefore we are not surprised to find that there is no really quantitative support for relation 4 in the present volume data.

On the other hand, Grüneisen and others[16] have shown that a quantitative correlation exists between the volume expansion ΔV (resulting from a temperature increment), and the corresponding energy or enthalpy change. By use of a simple thermodynamic argument we derive the relation

$$\Delta H/\Delta V = C_P/\alpha V = 1/\gamma\beta_S$$

where ΔH and ΔV are connected increments in enthalpy and volume, while γ is Grüneisen's "constant" and β_S the adiabatic compressibility. For the pure liquid metals considered in the present work $C_P \sim 7$ cal./degree, $\alpha \sim 10^{-4}$ deg.$^{-1}$ while $V \sim 15$ cm.^{3}. Thus we have values of $\Delta H/\Delta V \sim 5$ kcal./cm.^{3}. This is of the same order of magnitude as the corresponding correlation ratios derived from the mixing data. More precise values of $C_P/\alpha V$ are given in the fourth column of Table I.

TABLE I

CORRELATION FACTORS FOR EXCESS ENTROPY AND VOLUME CHANGE AND FOR HEAT AND VOLUME CHANGE IN LIQUID ALLOYS OF CADMIUM AT 350°

System	$\Delta S^E/\Delta V^M$, cal./deg. cm.^{3}	α/β_s,[a] cal./deg. cm.^{3}	$\Delta H^M/\Delta V^M$, kcal./cm.^{3}	$C_P/\alpha V$,[a] kcal./cm.^{3}	$\Delta H^f/\Delta V^f$,[b] kcl./cm.^{3}
CdIn	(1.6–1.3)	1.1–0.9	2.8	3.6	2.3–2.0
CdSn	1.5–1.25	1.1– .8	1.9–2.1	3.6–3.9	2.3–3.5
CdTl	(1.7–1.4)	1.1– .8	3.3	3.6–2.7	2.3–1.8
CdPb	1.6–1.25	1.1– .8	3.8–4.4	3.6–2.9	2.3–1.8
CdBi	1.25	1.1– .7	1.0–0.7	3.6–2.9	2.3–(−3.7)

[a] Figures calculated from data in ref. 15. [b] Figures calculated from data quoted by Kubaschewski, *Trans. Faraday. Soc.*, **45**, 931 (1949).

Another estimate of the enthalpy–volume ratio characteristic of the considered metals may be obtained from the changes in enthalpy and volume on fusion. Appropriate values of $\Delta H^f/\Delta V^f$ are presented in the fifth column of Table I. (Note that this ratio for bismuth is meaningless in the present context, since bismuth contracts on fusion).

A comparison of our values of $\Delta H^M/\Delta V^M$ with these other ratios shows that our experimental values on the whole fall somewhere between $C_P/\alpha V$ and $\Delta H^f/\Delta V^f$. The only important exception among the studied systems is cadmium–bismuth, which in this and other respects is anomalous. It is believed that the special character of this system arises from a marked tendency toward chemical bonding between cadmium and bismuth. While this tendency is not strong enough to change the sign of ΔH^M from positive to negative, it nevertheless results in quite low values of ΔH^M compared to the "neighboring" systems cadmium–thallium and cadmium–lead. It is interesting to note that this bonding tendency in no way is reflected in the volume change data.

The correlation between heat of mixing and excess volume demonstrated in the present paper has parallels and possible applications outside the more limited field of liquid solutions. Reference is made here to some recent work on lattice defects in solids. It was demonstrated by Keyes[17] that in cases where self-diffusion has been studied both as a function of temperature and of pressure, a correlation exists between the enthalpy of activation and the corresponding "activation volume." Keyes showed that for a wide range of different substances, both solid and liquid, one finds

$$\Delta H_{act}/\Delta V_{act} = 1/k\beta$$

where k is a numerical factor of order unity. For many systems the best correlation was obtained with $k \sim 4$.

Very recently Lawson, *et al.*,[18] by means of the Mie–Grüneisen theory, derived a similar relation between the molar enthalpy of formation of a lattice vacancy, ΔH^*, and the corresponding volume change, ΔV^*. With a Grüneisen γ of about 2, the Keyes–Lawson heat–volume ratio is smaller than our thermodynamically derived ratio by a factor of the order of 2. This discrepancy probably arises from the breakdown of the approximately linear relation between the connected values of ΔH and ΔV at high fractional changes in volume. Note that the fractional volume change associated with a temperature rise of 1° is of the order of 10^{-4}. The equivalent fractional change for the mixing process $(\Delta V^M/V)$ is as much as two orders of magnitude larger, *i.e.*, comparable to $\Delta V^f/V$ which for typical metals is about 4×10^{-2}. However, $\Delta V^*/V$ is significantly larger, of the order of 0.5.

Acknowledgments.—Many of the measurements reported above were performed with the assistance of Mr. R. Petzold. The spectrochemical analyses were carried out by Miss M. C. Batchelder. This work was supported by the Office of Naval Research under Contract No. Nonr-2121(11) with the University of Chicago.

(16) See *e.g.*, G. Borelius, "Solid State Physics," Vol. 6, Academic Press, Inc., New York and London, 1958.

(17) R. W. Keyes, *J. Chem. Phys.*, **29**, 467 (1958).

(18) A. W. Lawson, S. A. Rice, R. D. Corneliussen and N. H. Nachtrieb, *ibid.*, **32**, 447 (1960).

HEAT CAPACITIES AND THERMODYNAMIC PROPERTIES OF GLOBULAR MOLECULES. I. ADAMANTANE AND HEXAMETHYLENETETRAMINE[1]

BY SHU-SING CHANG AND EDGAR F. WESTRUM, JR.

Department of Chemistry, University of Michigan, Ann Arbor, Michigan

Received May 9, 1960

Heat capacities of adamantane and hexamethylenetetramine have been determined from 5 to 350°K. by adiabatic calorimetry, and derived thermodynamic functions have been calculated at selected temperatures from these data. A transition, which is associated with a slight modification of crystal lattice and molecular freedom, occurs in adamantane at 208.62°K. The heat of transition of adamantane is 807 cal./mole, and the entropy of transition is 3.87 e.u. No thermal anomaly has been found for hexamethylenetetramine from 5 to 350°K. by calorimetry nor from room temperature up to 240° by thermal analysis, suggesting that stronger intermolecular forces inhibit molecular freedom. The molal values of C_p, S^0, $H^0 - H_0^0$ and $-(F_0 - H_0^0)/T$ at 298.15° *K.* for adamantane and for hexamethylenetetramine are 45.350, 36.397 cal./(deg. mole); 46.805, 39.048 cal./(deg. mole); 7270.0, 5452.2 cal./mole; and 22.422, 20.761 cal./(deg. mole); respectively.

Introduction

The study of the thermophysical properties of a series of highly symmetrical, globular molecules is highly desirable for a more detailed understanding of the thermodynamics and interpretation of the findings of other techniques concerning plastic crystals. Adamantane, tricyclo[3,3,1,$1^{3,7}$]decane (*cf.* Fig. 1), is the simplest saturated polycyclic hydrocarbon ($C_{10}H_{16}$) with its carbon atoms arranged in a cage-like skeleton resembling that of a so-called "characteristic cell" of a diamond crystal lattice. Moreover, adamantane is the prototype of a large family of diamondoid compounds with similar molecular structure obtained by replacing some of the cage-forming carbon atoms by other suitable atoms. Silicon, nitrogen and phosphorus may replace the tertiary or the bridge carbon atoms, while oxygen and sulfur may assume the role of one or more methylene groups in adamantane. For example, replacement of the four bridge carbon atoms with nitrogen atoms yields the hexamethylenetetramine molecule. A number of such diamondoid compounds have already been described.[2] Their highly symmetrical shape—or globularity—yields unusual and interesting properties.[3] For example, adamantane melts at 270° (in a sealed tube)—an exceptionally high melting point in comparison with chain or cyclic hydrocarbons of approximately the same molecular weight.

Hexamethylenetetramine (1,3,5,7-tetraazatricyclo[3,3,1,$1^{3,7}$]decane) has long been known as a condensation product from formaldehyde and ammonia and used medicinally under the name of urotropine. Adamantane, however, was first isolated by Landa and Macháček[4] as a minute constituent in naphtha from Hodonin, Czechoslovakia, in 1933. Since then a number of synthetic methods[5] have been devised with long tedious procedures and low over-all yields. Not until recently did Schleyer[6] point out that adamantane could be prepared as the by-product of a rearrangement reaction. Although the yield of this preparation is only about 15%, this simple two-step method using a readily available raw material is nevertheless the most efficient way to prepare a calorimetric sample of this compound.

Experimental

Preparation of Adamantane.—Adamantane was prepared by the method of Schleyer.[6] α-Dicyclopentadiene was purified both by fractional distillation under reduced pressure and by fractional crystallization. It was then hydrogenated to endotetrahydrodicyclopentadiene with quantitative yield by using finely divided platinum as a catalyst and cyclohexane as the solvent. After being washed with concentrated sulfuric acid, then with water, and dried with anhydrous sodium sulfate, the mixture (after concentration) yielded the endo-isomer which was purified by recrystallization from absolute ethanol. The rearrangement reaction was effected over a three-day period by stirring the endo-isomer in the presence of 20% by weight of powdered aluminum chloride at 180–190°. Adamantane is the by-product of that reaction and was separated from the reaction mixture through steam distillation. The yield of adamantane was about 15% and that of the exo-isomer about 55%. Most of the adamantane was separated by filtration from the distillate. By cooling the organic layer of the filtrate, another portion of product was obtained. Adamantane was purified by recrystallization three times from absolute methanol and yielded crystals of tetrahedral habit with average dimensions greater than one mm. The X-ray powder pattern of this sample showed a face-centered cubic lattice with $a = 9.52$ Å. in accord with the value 9.54 Å. reported by Giacomello and Illuminati.[7] Microchemical carbon and hydrogen determination gave the following results: 88.35% C and 11.65% H; (theoretical: 88.16% C and 11.84% H). Gas chromatographic analysis indicated only one peak. Within the precision of the analyses the material was pure adamantane.

Hexamethylenetetramine Sample.—Hexamethylenetetramine made by Eastman Kodak Company was purified by subliming it twice in a specially designed vacuum sublimation apparatus. The final product was composed largely of crystals of rhombic-dodecahedral habit about 3 mm. in diameter from the slow sublimation process. Microchemical analysis showed a composition of: 51.52% C, 8.48%H, and 40.00% N; (theoretical: 51.40% C, 8.63% H, and 39.97% N), all in accord within the precision of the analytical data.

Cryogenic Technique.—The Mark I cryostat employed for this low temperature adiabatic calorimetric measurement is similar in most respects to another one already depicted in the literature[8] and is being described elsewhere.[9] Gold-plated copper calorimeters (laboratory designations W-9[10] and W-10 for the hexamethylenetetramine and the adamantane, respectively) of approximately 100 ml. in volume were used. W-10 is of similar design to W-9 but differs in that

(1) This work was supported in part by the Division of Research of the U. S. Atomic Energy Commission.

(2) For review, *cf.* H. Stetter, *Angew. Chem.*, **66**, 217 (1954).

(3) J. Timmermans, *Ind. chim. belge*, **16**, 178 (1951).

(4) S. Landa and V. Macháček, *Collection Czech. Chem. Communications*, **5**, 1 (1933); S. Landa, V. Macháček and J. Mžourek, *Chem. Listy*, **27**, 415 (1933); **27**, 443 (1933); *Petroleum Z.*, **30**, 1 (1934).

(5) V. Prelog and R. Seiwerth, *Ber.*, **74B**, 1644 (1941); **74B**, 1769 (1941); H. Stetter, O. E. Bänder and W. Neumann, *Chem. Ber.*, **89**, 1922 (1956).

(6) P. v. R. Schleyer, *J. Am. Chem. Soc.*, **79**, 3292 (1957).

(7) G. Giacomello and G. Illuminati, *Gazz. chim. ital.*, **75**, 246 (1945); *Ricerca Sci.*, **15**, 559 (1945).

(8) E. F. Westrum, Jr., J. B. Hatcher and D. W. Osborne, *J. Chem. Phys.*, **21**, 419 (1953).

(9) E. F. Westrum, Jr., and A. F. Beale, Jr., to be published.

(10) E. Greenberg and E. F. Westrum, Jr., *J. Am. Chem. Soc.*, **78**, 4526 (1956).

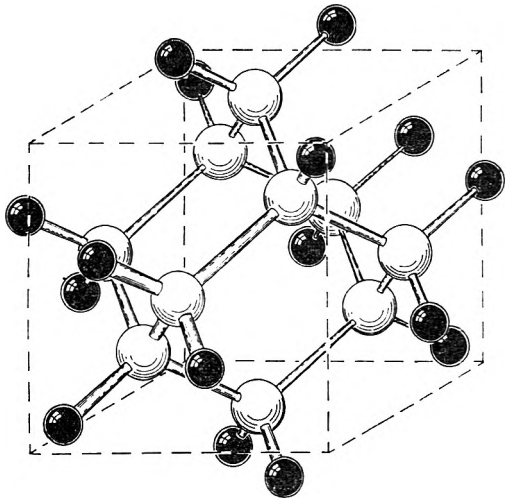

Fig. 1.—The molecular structure of adamantane.

there are no internal vanes and that the entire top of the calorimeter is of copper and removable. After the calorimeters were loaded with samples and evacuated, 6 cm. pressure of helium gas was added at 25° to improve heat conduction between the calorimeters and their contents. Samples massing (*in vacuo*) 42.8305 g. of admantane and 76.2870 g. of hexamethylenetetramine were used. Densities of 1.07 and 1.345 g./cm.^{3} were employed for the corrections to vacuo for adamantane and hexamethylenetetramine, respectively. Separate series of measurements were carried out to determine the heat capacity of the empty calorimeters with the same thermometer and heater and exactly the same amount of indium–tin solder (Cerroseal 50–50) for sealing and Apiezon-T grease for thermal contact with the thermometer and heater. Small corrections were applied for the slight differences in the quantities of helium in the calorimeters when run empty and with samples. The heat capacity of the empty calorimeter–thermometer–heater assembly represented a contribution increasing from 10% at 10°K. to 50% at 100°K., and thence gradually decreasing to 30% at 350°K.

Temperatures were measured with a capsule-type platinum resistance thermometer (laboratory designation A-3) inserted in the entrant, axial well in the calorimeter. The thermometer has been calibrated by the National Bureau of Standards against the International Temperature Scale above 90°K., and by comparison at 19 temperatures with the Bureau's platinum thermometer[11] over the range 10 to 90°K. Below 10°K. a provisional temperature scale was obtained by fitting the constants in the equation[11] $R = A + BT^2 + CT^5$ to the observed resistances at the boiling point of helium and at 10°K., and to dR/dT at 10°K. The temperature scale thus defined is considered to agree with the thermodynamic scale to 0.1° below 10°K., 0.03° from 10 to 90°K., and 0.04° from 90 to 400°K. Precision is considerably better, and the temperature increments are probably correct to a millidegree after corrections for quasi-adiabatic drift.

A 150-ohm fiber-glass insulated constantan heater was bifilarly wound in a conforming double thread on a cylindrical copper heater-sleeve surrounding the resistance thermometer. Measurements of temperature and of electrical energy were made with an autocalibrated White double potentiometer and calibrated standard cells and resistors. An electric timer operated by a calibrated tuning fork and amplifier were used to record the exact duration of energy input. The timer was frequently tested against signals from station WWV operated by the National Bureau of Standards.

Results

The actual heat capacity determinations are listed in Table I in chronological order in terms of the thermochemical calorie defined as 4.1840 absolute joules, the ice point of 273.15°K., and gram mole weights of adamantane and hexamethylenetetramine taken as 136.238 and 140.194, respectively. An analytically determined curvature correction was applied to the observed values of $\Delta H/\Delta T$. The approximate temperature increments usually can be inferred from the adjacent mean temperatures in Table I. The heat capacity data are also shown in Fig. 2.

A sharp (apparently first order) transition was discovered at 208.62°K. in adamantane. Thermal equilibrium was achieved quite rapidly (within an hour) in the transition region and apparent heat capacities as high as 4500 cal./(deg. mole) were observed. If an attempt is made to resolve the transitional contributions from the lattice (as shown by the dotted curve in Fig. 2), a transitional enthalpy increment of 807 cal./mole and a corresponding entropy increment of 3.87 e.u. are obtained. These probably represent minimal values.

TABLE I

THE HEAT CAPACITIES OF ADAMANTANE AND HEXAMETHYLENETETRAMINE [IN CAL./(DEG. MOLE)]

T, °K.	C_p	T, °K.	C_p	T, °K.	C_p
Adamantane; ($C_{10}H_{16}$, 1 mole = 136.238 g.)					
Series I		186.93	26.41	151.75	20.43
		194.32	28.29	154.28	20.78
5.09	0.040	202.35	31.12	156.76	21.13
5.69	.055	207.64	285.27	158.88	21.47
6.76	.088	212.37	52.33	160.97	21.75
8.06	.170	221.29	32.52	163.76	22.21
9.11	.278	231.48	34.04	167.25	22.72
10.06	.405	240.92	35.55	171.89	23.43
11.07	.562	249.94	36.97		
12.24	.783	258.71	38.45	Series IV	
13.54	1.083	256.55	38.05		
15.05	1.482	265.30	39.48	201.89	31.03
16.81	1.996	274.05	41.00	204.90	32.46
18.80	2.617	282.76	42.57	207.05	34.50
20.97	3.311	291.46	44.13	208.09	65.20
23.28	4.039	300.15	45.85		
25.81	4.803	308.83	47.41	Series V	
28.66	5.584	317.54	48.72		
31.81	6.369	326.25	50.15	208.62	2688.94
35.32	7.138	335.20	51.76	208.75	535.22
39.38	7.887	344.25	53.39	209.55	48.41
43.80	8.577			211.77	31.74
48.40	9.185	Series II			
53.20	9.730			Series VI	
58.23	10.24	193.23	27.98		
59.60	10.39	198.49	29.69	269.14	40.21
64.78	10.91	201.61	30.87	277.61	41.72
70.44	11.39	204.08	32.07	278.44	41.75
76.62	11.95	206.48	34.04	287.47	43.48
83.29	12.60	208.10	125.48	296.45	45.05
90.64	13.32	208.57	2470.76	305.10	46.81
98.73	14.14	208.61	3513.07	313.33	48.18
106.56	14.96	208.64	3864.16	321.79	49.41
114.49	15.81	208.66	4389.12	331.19	51.10
122.91	16.75	208.74	1583.61	341.03	52.91
131.08	17.77	210.00	44.73		
139.61	18.83	212.10	31.41	Series VII	
148.44	20.08	213.92	31.47		
157.32	21.38			208.64	3150.43
166.07	22.54	Series III		208.70	2402.83
174.72	23.83				
183.32	25.57	149.09	20.07		

(11) H. J. Hoge and F. G. Brickwedde, *J. Research Natl. Bur. Standards*, **22**, 351 (1939).

Hexamethylenetetramine; ($C_6H_{12}N_4$, 1 mole = 140.188 g.)

Series I

		208.24	23.89	50.28	9.790
		218.07	25.16	55.46	10.19
51.54	9.894	227.43	26.37		
55.54	10.19	236.29	27.56		
61.85	10.62	245.15	28.79		
68.74	11.01	254.10	30.03		
75.72	11.39	263.21	31.31		
82.61	11.81	272.39	32.57		
89.74	12.25	281.55	33.96		
97.37	12.72	290.59	35.28		
105.56	13.29	299.71	36.63		
113.61	13.91	308.93	38.00		
121.25	14.54	317.90	39.32		
114.72	14.00	327.18	40.69		
123.58	14.74	336.90	42.14		
131.97	15.50	346.36	43.54		
140.09	16.28				
148.29	17.08				
156.88	17.96				
165.80	18.92				
174.79	19.92				
183.92	20.96				
193.03	22.04				
201.84	23.10				
210.50	24.18				

Series II

31.87	7.301	22.16	4.691
34.20	7.764	24.60	5.461
37.40	8.309	27.49	6.269
41.26	8.845	30.68	7.041
45.65	9.349	34.00	7.728

Series III

5.04	0.027		
6.25	.069		
6.98	.110		
7.50	.167		
8.04	.220		
8.67	.326		
9.63	.490		
10.85	.780		
12.16	1.155		
13.55	1.610		
15.05	2.134		
16.64	2.728		
18.32	3.338		
20.11	3.982		
22.16	4.691		
24.60	5.461		
27.49	6.269		
30.68	7.041		
34.00	7.728		

No thermal anomaly has been found for hexamethylenetetramine from 5 to 350°K. by heat capacity measurements. Thermal analysis has been performed from room temperature up to 240°. This also did not indicate abnormal thermal behavior.

The molal values of C_p, S^0, $H^0 - H_0^0$, and $(F^0 - H_0^0)/T$ for adamantane and hexamethylenetetramine are listed at selected temperatures in Table II. These values were obtained by digital computer integration of a least squares fit polynomial through the experimental data points. The smooth heat capacities obtained in this manner were identical to those obtained from a large scale plot. The data were extrapolated below 5°K. with a Debye T^3 relationship. The entropies and free energy functions do not include contributions from nuclear spin

TABLE II

THERMODYNAMIC PROPERTIES OF ADAMANTANE AND HEXAMETHYLENETRAMINE

T, °K.	C_p, cal./(deg. mole)	S^0, cal./(deg. mole)	$H^0 - H_0^0$, cal./mole	$-(F^0 - H_0^0)/T$, cal./(deg. mole)
Adamantane ($C_{10}H_{16}$, 1 mole = 136.238 g.)				
5	0.040	0.013	0.0501	0.003
10	0.391	.111	0.8550	.026
15	1.468	.450	5.217	.102
20	3.000	1.076	16.29	.262
25	4.559	1.915	35.25	.505
30	5.937	2.872	61.59	.819
35	7.070	3.875	94.21	1.183
40	7.988	4.881	131.93	1.583
45	8.740	5.867	173.81	2.004
50	9.375	6.821	219.14	2.439
60	10.43	8.627	318.35	3.322
70	11.36	10.306	427.35	4.201
80	12.28	11.882	545.50	5.063
90	13.25	13.384	673.07	5.905
100	14.27	14.832	810.63	6.726
110	15.33	16.242	958.63	7.527
120	16.43	17.628	1117.4	8.311
130	17.61	18.984	1287.5	9.080
140	18.88	20.334	1469.9	9.835
150	20.24	21.683	1665.4	10.580
160	21.64	23.033	1874.8	11.316
170	23.12	24.389	2098.4	12.045
180	24.87	25.758	2338.0	12.769
190	27.24	27.161	2597.6	13.489
200	30.08	28.625	2883.1	14.209
210	(41.55)			
220	32.33	35.168	4252.2	15.840
230	33.81	36.658	4583.0	16.712
240	35.36	38.110	4928.8	17.573
250	36.98	39.586	5290.4	18.424
260	38.65	41.068	5668.6	19.266
270	40.37	42.559	6063.7	20.101
280	42.13	44.059	6476.2	20.930
290	43 90	45.568	6906.3	21.754
300	45.68	47.087	7354.2	22.573
350	54.31	54.787	9857.3	26.623
273.15	40.92	43.031	6191.7	20.363
298.15	45.35	46.805	7270.0	22.422
Hexamethylenetetramine ($C_6H_{12}N_4$, 1 mole = 140.188 g.)				
5	0.025	0.008	0.0313	0.002
10	0.572	.134	1.081	.026
15	2.118	.635	7.525	.133
20	3.941	1.496	22.72	.360
25	5.581	2.558	46.66	.691
30	6.885	3.695	77.96	1.097
35	7.902	4.836	115.03	1.550
40	8.688	5.945	156.59	2.030
45	9.294	7 005	201.61	2.525
50	9.772	8.010	249.32	3.023
60	10.49	9.859	350.84	4.011
70	11.08	11.521	458.77	4.967
80	11.65	13.038	572.41	5 883
90	12.25	14.444	691.89	6.757
100	12.91	15.769	817.66	7.592
110	13.64	17.033	950.35	8.394
120	14.44	18.253	1090.6	9.165
130	15.31	19.443	1239.3	9.910
140	16.25	20.611	1397.1	10.632
150	17.25	21.766	1564.5	11.336
160	18.30	22.913	1742.2	12.024
170	19.39	24.055	1930.6	12.698
180	20.52	25.195	2130.1	13.361
190	21.68	26.335	2341.1	14.014
200	22.87	27.477	2563.8	14.658
210	24.11	28.623	2798.7	15.296
220	25.39	29.774	3046.2	15.928
230	26.72	30.932	3306.7	16.555
240	28.08	32.098	3580.6	17.178
250	29.46	33.272	3868.3	17.798
260	30.87	34.454	4169.9	18.416
270	32.29	35.646	4485.7	19.032
280	33.73	36.846	4815.8	19.647
290	35.19	38.056	5160.4	20.261
300	36.67	39.274	5519.7	20.874
350	44.08	45.483	7538.4	23.944
273.15	32.74	36.023	4588.1	19.226
298.15	36.40	39.048	5452.2	20.761

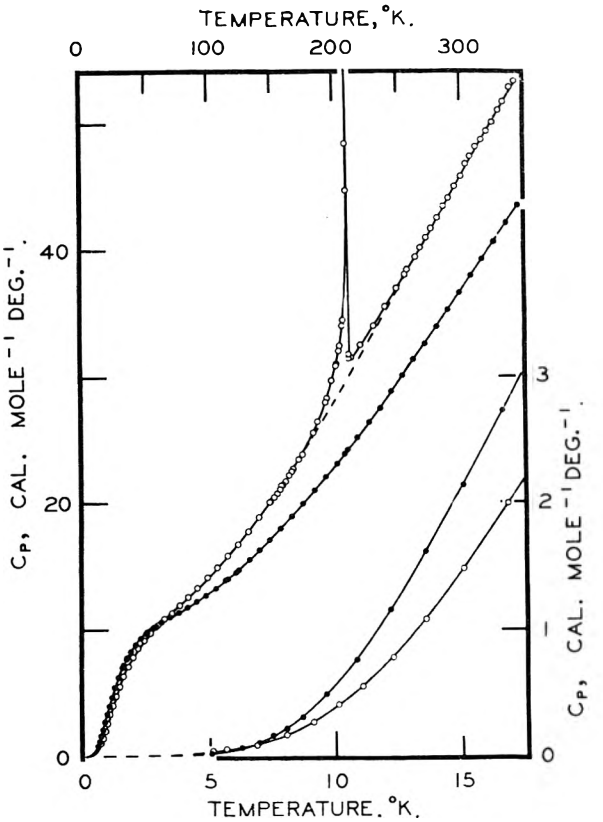

Fig. 2.—Heat capacities of adamantane (○) and of hexamethylenetetramine (●).

or isotope mixing and are hence "practical" values for chemical thermodynamic purposes.

The over-all accuracy of the calorimetric technique was ascertained by measuring the heat capacity of a standard sample of benzoic acid. As a further test of the precision of the calorimetry and heat capacity type runs in the transition region, several enthalpy increments, each covering the entire anomalous region, were made and compared with heat capacity determinations in Table III. Excellent confirmation was obtained. The normal heat capacity values are considered to have a probable error of 0.1% above 25°K., 1% at 10°K., and about 5% at 5°K. The estimated probable error in the thermodynamic functions is 0.1% above 100°K. In order to make the tables internally consistent and to permit interpolation, the tabulated values occasionally include more digits than are justified by the probable error.

The heat of combustion reported by Landa and Macháček[4] on adamantane was converted to an enthalpy increment. The heat of formation of hexamethylenetetramine of Delépine and Badoche[12] was corrected to graphite as the standard state for carbon and to modern heats of formation[13] of CO_2 and H_2O. Combining these results with practical entropies and the data of the present investigation yields the following increments for the formation reactions (with graphite as standard state) at 298.15°K.

(12) M. Delépine and M. Badoche, *Compt. rend.*, **214**, 777 (1942).

(13) "Selected Values of Chemical Thermodynamic Properties," Circular 500, National Bureau of Standards, Washington, D. C., 1952.

TABLE III

ENTHALPY AND ENTROPY INCREMENTS OVER THE TRANSITION REGION IN ADAMANTANE

Energy increments	T_{final}, °K.	$T_{initial}$, °K.	$H_{225°K.} - H_{195°K.}$, cal./mole	$S_{225°K.} - S_{195°K.}$, cal./(deg. mole)
7	211.20	205.30	1679.6	8.029
7	213.29	206.43	1678.4	8.017
1	212.17	205.02	1679.0	8.019
1	211.94	205.27	1679.4	8.023
		Av.	1679.2 ± 0.1	8.020

Substance	ΔH_f^0, kcal./mole	ΔS_f^0, e.u.	ΔF_f^0, kcal./mole
Adamantane	−31.6	−216.484	32.9
Hexamethylenetetramine	28.8	−247.911	102.7

Discussion

Although adamantane and hexamethylenetetramine have the same basic molecular structure, they differ in crystallographic aspects. At 25° adamantane molecules form a (close packed) face-centered cubic lattice of the space group T^2_d-F$\bar{4}$3m with a = 9.43 Å. according to Nowacki.[14] This cell dimension is at variance with the value 9.54 Å. reported by Giacomello and Illuminati.[7] From the X-ray work done on an adamantane single crystal at temperatures below the transition point, it has been shown that the crystal lattice at low temperatures is slightly different from that of the high temperature form.[15] At temperatures lower than the transition point adamantane crystal exists in a body-centered tetragonal lattice with the unit cell dimensions a = 6.641 Å. and c = 8.875 Å. Apparently, during the transition one of the cubic axes of the high temperature form shrinks about 6% and becomes the c axis of the low temperature form, while the molecular positions on the plane perpendicular to it remain almost unchanged.

The transition is probably of the pseudo-rotational–reorientation type. The adamantane molecules are presumably able to rotate more freely or to assume different and hence random orientation on the lattice sites of the high temperature form. Consequently, the molecules approximate sphericity, and since only intermolecular van der Waals forces are involved, a close packed structure results. At low temperatures the rotation may be sufficiently restricted to allow the adamantane molecules to form a more compact structure permitted by the actual molecular shape, which deviates somewhat from sphericity. Further X-ray diffractional analysis on the low temperature modifications of adamantane is essential for the determination of the exact mechanism of the transition.

Hexamethylenetetramine exists in a body-centered cubic lattice of the space group T^3_d-I$\bar{4}$3m with a = 7.02 Å. throughout the temperature range investigated.[16,17] X-Ray oscillation photographs

(14) W. Nowacki, *Helv. Chim. Acta*, **28**, 1233 (1945).

(15) C. E. Nordman, unpublished data.

(16) R. G. Dickinson and A. L. Raymond, *J. Am. Chem. Soc.*, **45**, 22 (1923); H. W. Gonell and H. Mark, *Z. physik. Chem.*, **107**, 181 (1923); H. Mark, *Ber.*, **57B**, 1820 (1923); R. W. G. Wyckoff and R. B. Corey, *Z. Krist.*, **89**, 462 (1934); R. Brill, H. G. Grimm, C. Hermann and C. Peters, *Ann. Physik*, **34**, 383 (1939).

(17) P. A. Shaffer, Jr., *J. Am. Chem. Soc.*, **69**, 1557 (1947).

taken by Shaffer[17] indicate the existence of torsional thermal vibrations. He considers that the hydrogen bonding does not appear to interfere greatly with the rotational vibration of the molecules, but it apparently precludes them from taking part in a transition similar to that in adamantane below 500°K. The molecular symmetry and the intermolecular hydrogen bonds determine the specific orientation of the molecules and thus the lattice type of the hexamethylenetetramine crystal.

NOTE ADDED IN PROOF.—Proton magnetic resonance studies of solid adamantane by D. W. McCall and D. C. Douglass [*J. Chem. Phys.*, **33**, 777 (1960)] reveal an abrupt diminution in the second moment at −130° which is interpreted as involving a rotational transition with an activation energy of about 5 kcal./mole. These authors however appear to confuse the onset of rotation with the cooperative phenomenon leading to the transition to a plastic crystalline phase which occurs 65° higher in temperature, as shown by the data of the present work.

Acknowledgment.—The authors thank Elfreda Chang and H. Gary Carlson for assistance with the calorimetry and evaluation of the data.

HEAT CAPACITIES AND THERMODYNAMIC PROPERTIES OF GLOBULAR MOLECULES. II. TRIETHYLENEDIAMINE[1]

BY SHU-SING CHANG AND EDGAR F. WESTRUM, JR.

Department of Chemistry, University of Michigan, Ann Arbor, Michigan

Received May 13, 1960

The heat capacity of 1,4-diazabicyclo[2,2,2]octane has been determined from 5°K. to within several degrees of the phase transition occurring at 353°K. by adiabatic calorimetry and found to be normal over this region. The derived thermodynamic functions were evaluated from these data. The molal values of the heat capacity at constant pressure, the entropy, the enthalpy increment and the free energy function at 298.15°K. are: 36.56 and 37.67 cal./(deg. mole), 5525 cal./mole, and −19.14 cal./(deg. mole), respectively.

Introduction

In the previous paper of this series[2] low temperature heat capacity studies were reported on two globular diamondoid molecules (adamantane and hexamethylenetetramine) because of interest in their molecular freedom in the solid state and in the thermodynamics of plastic crystals. Another family of globular molecules, which are rather more symmetrical tops than spherical rotators, have the basic skeleton of bicyclo[2,2,2]octane. Members of this family such as the prototype molecule itself, quinuclidine(1-azabicyclo[2,2,2]-octane), and triethylenediamine (1,4-diazabicyclo-[2,2,2]octane), as well as the 1,4-derivatives of these molecules, provide another very interesting series for the study of molecular freedom in plastic crystals. Because of the availability of a sample, triethylenediamine was the first compound of this series to be investigated.

Experimental

Preparation of Sample.—A specially purified triethylenediamine sample, furnished by the Houdry Process Corporation under the trade name of Dabco, was sublimed twice in high vacuum. Large tabular, transparent crystals were obtained. These crystals appear to be stable in dry air but in contact with ambient atmospheric air they at once become translucent. The effect is probably caused by a strong tendency of these hygroscopic crystals to adsorb water molecules onto their surface. In order to assure the purity of the calorimetric sample it was twice more sublimed at relatively low temperatures in high vacuum with the sublimation apparatus contained in an anhydrous nitrogen atmosphere. Handling of the crystals was minimized, and the calorimeter was loaded in the anhydrous nitrogen atmosphere. The crystals used for the calorimetry were in the form of transparent, hexagonal platelets of approximately a centimeter in diameter and with a waxy appearance. They are quite soft and can be readily bent. The melting point of the sample was found to be 158.5°. Microchemical analysis has indicated the composition to be: 64.39% carbon, 10.81% hydrogen and 24.75% nitrogen (theoretical: 64.24% C, 10.78% H and 24.96% N).

Cryogenic Technique.—The Mark I low temperature adiabatic cryostat, a gold-plated copper calorimeter (laboratory designation W-9), and a calibrated platinum resistance thermometer (laboratory designation A-3) were used in measuring the heat capacity of this sample.[1] The calorimeter was loaded with 54.043 g. (*in vacuo*) of triethylenediamine, evacuated, and filled with helium at 8 cm. pressure at 300°K. to provide thermal contact between the calorimeter and the sample. The heat capacity of the empty calorimeter–heater–thermometer assembly was determined by a separate series of measurements and represented from 25 to 45% of the total observed heat capacity.

Results

The experimental heat capacity determinations are listed in Table I in chronological order in terms of the thermochemical calorie defined as 4.1840 absolute joules. The ice point is taken as 273.15° K. and the atomic weights of carbon, nitrogen and hydrogen as 12.010, 14.008 and 1.008, respectively. The molecular weight of triethylenediamine was taken as 112.172 g. An analytically determined curvature correction was applied to the observed values of $\Delta H/\Delta T$. The approximate temperature increments usually can be inferred from the adjacent mean temperatures in Table I. Molal values of the heat capacity at constant pressure, the entropy, the enthalpy increment and the free energy function are listed at selected temperatures in Table II. These values were all obtained from a smooth curve (fit by least squares to the experimental data) generated by a digital computer or by appropriate integration based on this curve. The reported values of the heat capacity are believed to have probable errors less than 0.1%-

(1) This work was supported in part by the Division of Research of the U. S. Atomic Energy Commission.

(2) S. S. Chang and E. F. Westrum, Jr., THIS JOURNAL, **64**, 1547 (1960).

at temperatures above 25°K., about 1% at 10°K. and 5% at 5°K. The probable errors of the thermodynamic functions are considered to be less than 0.1% above 100°K.

TABLE I

HEAT CAPACITY OF TRIETHYLENEDIAMINE, CAL./(DEG. MOLE)

T, °K.	Cp	T, °K.	Cp	T, °K.	Cp
Series I		43.59	8.015	31.87	5.330
		48.17	8.836	34.90	6.119
103.00	14.39	53.39	9.638		
111.02	15.04	59.07	10.38	Series V	
119.16	15.71	65.38	11.12		
127.95	16.44	72.38	11.80	198.65	23.17
137.06	17.23	79.81	12.48	207.55	24.14
145.92	18.01			216.80	25.20
154.21	18.75	Series IV		226.24	26.33
162.56	19.53			235.33	27.45
171.47	20.38	4.91	0.014	244.16	28.59
180.58	21.28	5.91	.027	252.95	29.76
189.58	22.21	7.15	.055		
198.72	23.18	8.28	.099	Series VI	
		9.34	.161		
Series II		10.36	.238	251.68	29.55
		11.46	.340	260.51	30.81
77.10	12.25	12.65	.481	269.38	31.99
83.34	12.81	13.86	.657	278.77	33.44
90.25	13.39	15.11	.871	288.25	34.93
97.71	13.97	16.48	1.144	297.29	36.43
105.36	14.58	18.05	1.500	306.48	37.99
		19.84	1.947	315.85	39.73
Series III		21.86	2.495	325.24	41.66
		24.12	3.136	334.60	43.91
35.72	6.307	26.76	3.895	343.87	46.66
39.50	7.184	29.25	4.604		

Discussion

The occurrence of a transition at 74° occasioned by a change in crystal structure has been reported by Farkas, *et al.*[3,4] Although this temperature lies within the range of the present investigation, no transition has been observed in the calorimetric measurements. Thermal analysis, however, indicates the transition to take place in our sample at about 353°K. Indeed, the heat capacity curve approaching this temperature does show an increase in slope consistent with the occurrence of a transition within a few degrees. Since the calorimetric sample has been very carefully purified and handled in the anhydrous nitrogen atmosphere of the drybox to prevent contamination by moisture and carbon dioxide, it is probable that higher purity of the sample may have occasioned the apparent higher transition temperature. Debye-Scherrer X-ray powder diffraction data[4] on the phase stable at 300°K. have been presented. The space group[5] of the phase studied was C_{6h}^2-$P6_{3/m}$. The structure of the presumably more symmetric higher temperature phase has not been reported.

(3) A. Farkas, G. A. Mills, W. E. Erner and H. B. Maerker, *Ind. Eng. Chem.*, **51**, 1299 (1959).

(4) A. Farkas, G. A. Mills, W. E. Erner and J. B. Maerker, *J. Chem. Eng. Data*, **4**, 334 (1959).

(5) S. Seki, unpublished data.

TABLE II

THERMODYNAMIC FUNCTIONS OF TRIETHYLENEDIAMINE ($C_6H_{12}N_2$, 1 mole = 112.172 g.)

T, °K.	Cp, cal./deg. mole	S^0, cal./deg. mole	$H^0 - H_0^0$, cal./mole	$-(F^0 - H_0^0)/T$, cal./deg. mole
5	0.014	0.005	0.017	0.002
10	.209	.055	0.430	.012
15	.851	.242	2.854	.052
20	1.987	.633	9.782	.144
25	3.391	1.225	23.17	.298
30	4.816	1.970	43.72	.513
35	6.132	2.813	71.14	.780
40	7.290	3.709	104.77	1.090
45	8.285	4.627	143.77	1.432
50	9.135	5.545	187.37	1.797
60	10.50	7.337	285.87	2.572
70	11.58	9.040	396.47	3.376
80	12.51	10.648	517.0	4.185
90	13.35	12.171	646.4	4.989
100	14.16	13.620	784.0	5.780
110	14.96	15.007	929.6	6.556
120	15.77	16.344	1083.3	7.316
130	16.61	17.640	1245.2	8.061
140	17.48	18.902	1415.7	8.790
150	18.38	20.139	1594.9	9.506
160	19.30	21.354	1783.3	10.208
170	20.25	22.552	1981.0	10.899
180	21.23	23.737	2188.4	11.580
190	22.25	24.912	2405.7	12.251
200	23.31	26.080	2633.5	12.913
210	24.42	27.244	2872.1	13.568
220	25.58	28.407	3122.0	14.216
230	26.80	29.571	3383.9	14.858
240	28.06	30.738	3658.1	15.495
250	29.36	31.909	3945.2	16.128
260	30.72	33.087	4245.5	16.758
270	32.14	34.272	4559.7	17.385
280	33.63	35.468	4888.5	18.009
290	35.21	36.676	5232.6	18.632
300	36.88	37.897	5593.0	19.254
350	(48.70)	(44.350)	(7693.4)	(22.369)
273.15	32.60	34.65	4662	17.58
298.15	36.56	37.67	5525	19.14

The study of the pseudo-rotation and fusion transitions are of great interest in elucidating the nature of this material, which is believed to be a plastic crystal above the 353°K. transition. These thermophysical properties of triethylenediamine are currently under study in a high temperature calorimeter and are expected to provide additional information on the nature of this interesting material.

Acknowledgment.—The authors thank Dr. G. A. Mills and Dr. A. Farkas of the Houdry Process Corporation for their provision of a sample of purified triethylenediamine and for helpful suggestions. We acknowledge the coöperation of Bruce H. Justice in the calorimetry.

THE HEAT CAPACITY AND THERMODYNAMIC PROPERTIES OF SODIUM FORMATE FROM 5 TO 350°K.

BY EDGAR F. WESTRUM, JR., SHU-SING CHANG AND NORMAN E. LEVITIN

Department of Chemistry, University of Michigan, Ann Arbor, Michigan

Received May 9, 1960

The heat capacity of anhydrous sodium formate has been determined at low temperatures by adiabatic calorimetry, and found to be normal. Thermodynamic functions were evaluated from these data. The heat capacity at constant pressure, entropy, enthalpy increment ($H^0 - H_0^0$), and free energy function $[(F^0 - H_0^0)/T]$ at 298.15°K. are 19.76 ± 0.01 cal./(deg. mole), 24.80 cal./(deg. mole), 3766.9 cal./mole, and −12.16 cal./(deg. mole), respectively.

Thermophysical properties of relatively few salts of organic acids have been reported at low temperatures. In the present investigation the heat capacity of sodium formate has been investigated and its thermodynamic properties evaluated.

Experimental

Sodium Formate Sample.—Two crystalline sodium formate hydrates exist in equilibrium with the aqueous solution[1,2]; the dihydrate is the stable form between 15.3 and 27.9°, while the trihydrate is stable only at temperatures below 15.3° and the anhydrous salt above 27.9°. An aqueous solution of reagent sodium formate (HCO_2Na) saturated at 90° was filtered and allowed to cool very slowly by gradually decreasing the temperature of the water-bath surrounding it. However, the temperature was maintained above 30° to prevent the formation of hydrate. After two recrystallizations from distilled water the crystals of the anhydrous salt were separated and baked in an oven at 130° and finally dried in high vacuum.

Microchemical analysis indicated the following percentages by weight: 66.32 ± 0.12 formate, 33.86 ± 0.05 sodium, 17.76 ± 0.02 carbon, and 1.51 ± 0.3 hydrogen (theoretical: 66.19, 33.81, 17.76 and 1.48, respectively). The formate content was determined by oxidation with alkaline permanganate solution, and sodium was determined by the triple acetate method.

Cryogenic Technique.—The Mark I cryostat employed for low temperature adiabatic calorimetry was similar to the one used by Westrum, Hatcher and Osborne,[3] and will be described elsewhere.[4] A gold-plated copper calorimeter (laboratory designation W-10) was used in these measurements, which is similar to W-6 previously described[5] except that it is gold-plated overall, has no vanes for thermal conduction, and the entire cover is removable for admission of sample. The calorimeter was loaded in an anhydrous nitrogen atmosphere with 77.0217 g. (*vacuo*) of sample, evacuated and filled with helium at 8.0 cm. pressure at 300°K. in order to provide thermal contact between the calorimeter and sample. Buoyancy corrections were made on the basis of a pycnometric density of 1.967.[6] The specific heat of the calorimeter was determined separately with the same thermometer–heater assembly and the same amounts of indium–tin (Cerroseal) solder for sealing, of Apiezon-T grease (for thermal contact with the thermometer and heater) and of helium gas in the sample space. The empty calorimeter–heater-thermometer assembly represented from 25 to 40% of the total heat capacity observed.

A capsule-type platinum resistance thermometer (laboratory designation A-3) was used to measure temperatures. This was calibrated by the National Bureau of Standards against the International Temperature Scale above 90°K. and by comparison at 19 temperatures with the Bureau's platinum thermometers over the range from 10 to 90°K.[7] Below 10°K. the temperature scale was obtained by fitting the equation $R = A + BT^2 + CT^5$ to the observed resistance of the thermometer at 10°K., at the boiling point of helium, and dR/dT at 10°K. The temperature scale thus defined is considered to agree with the thermodynamic scale within 0.1° below 10°K., 0.03° from 10 to 90°K. and 0.04° from 90 to 400°K.

A Fiberglas insulated constantan wire (150-ohms) was bifilarly wound on a double threaded copper sleeve and served as heater. Measurements of temperature and of electrical energy were made with a calibrated White double potentiometer, calibrated resistors and a calibrated standard cell. Time duration of the energy input was measured by an electric timer checked against standard time signals.

Results

The experimental heat capacity determinations are presented in Table I in chronological sequence to permit the estimation of the approximate temperature increments of the individual runs by differencing the adjacent mean temperatures. Corrections for curvature (amounting to less than 0.1%) occasioned by the finite temperature increments employed have been made in these values. The data are presented in terms of the defined thermochemical calorie equal to 4.1840 absolute joules and the mole weight of 68.010 g. No anomalies

TABLE I

HEAT CAPACITY OF SODIUM FORMATE [IN CAL./(DEG. MOLE)]

T, °K.	C_p	T, °K.	C_p	T, °K.	C_p
Series I		290.46	19.59	13.55	0.146
		307.85	20.01	14.77	.193
99.69	11.468	317.34	20.28	16.12	.253
105.55	12.010	326.78	20.56	17.65	.333
113.22	12.661	336.11	20.88	19.27	.435
121.26	13.264	345.33	21.06	20.96	.556
129.48	13.808			22.80	.704
137.71	14.311	Series II		24.84	.903
146.21	14.765			27.13	1.139
152.68	15.10	294.47	19.65	29.68	1.441
161.27	15.50	298.72	19.76	32.42	1.797
170.28	15.87	302.09	19.87	35.37	2.216
179.68	16.25			38.62	2.707
189.01	16.57	Series III		42.41	3.311
198.36	16.89			46.77	4.042
208.09	17.20	4.84	0.006	51.37	4.822
217.17	17.48	5.65	.011	55.69	5.558
226.11	17.74	6.39	.014	60.31	6.325
234.95	18.00	7.03	.017	65.69	7.191
243.59	18.23	8.19	.026	67.93	7.536
252.95	18.49	9.21	.040	74.47	8.487
262.52	18.76	10.22	.060	81.12	9.403
271.95	19.02	11.27	.083	88.26	10.295
281.27	19.26	12.39	.110	95.95	11.106

(1) E. Groschuff, *Ber.*, **26**, 1790 (1903).

(2) E. Elöd and K. Tremmel, *Z. anorg. allgem. Chem.*, **165**, 161 (1927).

(3) E. F. Westrum, Jr., J. B. Hatcher and D. W. Osborne, *J. Chem. Phys.*, **21**, 419 (1953).

(4) E. F. Westrum, Jr., and A. F. Beale, Jr., to be published.

(5) E. Benjamins and E. F. Westrum, Jr., *J. Am. Chem. Soc.*, **79**, 287 (1957).

(6) H. Schröder, *Ber.*, **14**, 21 (1881).

(7) H. J. Hoge and F. G. Brickwedde, *J. Research Natl. Bur. Standards*, **22**, 351 (1939).

TABLE II

THERMODYNAMIC PROPERTIES OF SODIUM FORMATE

(HCO_2Na, 1 mole = 68.010 g.)

T, °K.	C_p, cal./deg. mole	S^0, cal./deg. mole	$H^0 - H_0^0$, cal./mole	$-(F^0 - H_0^0)/T$ cal./deg. mole
5	0.006	0.002	0.007	0.001
10	.054	.016	.124	.004
15	.202	.062	.718	.014
20	.485	.156	2.374	.037
25	.914	.307	5.812	.075
30	1.481	.522	11.75	.131
35	2.161	.800	20.81	.206
40	2.925	1.138	33.49	.300
45	3.743	1.529	50.15	.415
50	4.589	1.967	70.97	.548
60	6.273	2.954	125.33	.865
70	7.850	4.041	196.07	1.240
80	9.255	5.183	281.76	1.661
90	10.47	6.345	380.54	2.117
100	11.51	7.504	490.58	2.598
110	12.40	8.643	610.2	3.096
120	13.17	9.756	738.1	3.605
130	13.84	10.837	873.3	4.119
140	14.44	11.885	1014.7	4.637
150	14.97	12.899	1161.8	5.154
160	15.44	13.881	1313.9	5.669
170	15.87	14.830	1470.4	6.180
180	16.25	15.748	1631.0	6.686
190	16.61	16.636	1795.4	7.187
200	16.94	17.497	1963.1	7.681
210	17.26	18.331	2134.2	8.168
220	17.56	19.141	2308.3	8.649
230	17.85	19.928	2485.4	9.122
240	18.14	20.694	2665.4	9.588
250	18.41	21.440	2848.1	10.048
260	18.68	22.167	3033.6	10.500
270	18.96	22.878	3221.8	10.945
280	19.25	23.572	3412.9	11.384
290	19.53	24.253	3606.8	11.816
300	19.81	24.920	3803.5	12.241
350	21.09	28.078	4828.9	14.281
273.15	19.05	23.098	3281.7	11.084
298.15	19.76	24.797	3766.9	12.163

were observed at any temperature. It is considered that the probable error of the heat capacity data is less than 0.1% at temperatures above 25°K. Below this temperature the probable error increases gradually to about 1% at 10° and to 5% at 5°K.

The thermodynamic properties computed by quadrature of the heat capacity data on a digital computer are provided at selected temperatures in Table II. Nuclear spin and isotope mixing contributions have not been included in the entropy or in the free energy function. Extrapolation below 6°K. was made with the Debye limiting law. The estimated probable error in the thermodynamic functions is less than 0.1% above 100°K.

As a test of the accuracy of the heat capacity measurements and the enthalpy integration techniques, a continuous energy input from 98.31 to 148.25°K. was made in 21 minutes. The observed enthalpy increment agreed within 0.04% with that obtained by numerical quadrature over the same range of temperature.

Discussion

The mean specific heat of sodium formate has been reported as 0.312 cal./(deg. g.) between 21 and 57° by Pagliani[8] and 0.2916 cal./(deg. g.) between 10 and 93° by de Heen,[9] which correspond to the mean molal heat capacities of 21.22 and 19.83 cal./(deg. mole), respectively. Over the same ranges, the data of this investigation indicate mean molal heat capacities of 20.14 and 20.53 cal./(deg. mole), respectively.

By utilizing the enthalpy of solution for sodium formate,[10] the enthalpy of neutralization of aqueous formic acid,[10-12] the enthalpy of solution of formic acid,[13] the enthalpy of vaporization and correction for dimerization,[14] and the heat of combustion of formic acid,[11] the enthalpy of formation of sodium formate equal to −155.03 kcal./mole[15] is obtained at 298.15°K. This value, together with the entropies of the elements[15] and the entropy of sodium formate from this research, yields a Gibbs' free energy of formation of sodium formate of −139.12 kcal./mole.

Acknowledgment.—The authors appreciate the assistance of J. C. Trowbridge and Bruce H. Justice in the calculation of the data. The partial financial support of the Division of Research of the U. S. Atomic Energy Commission is gratefully acknowledged.

(8) S. Pagliani, *Atti Accad. Sci. Torino*, **17**, 106 (1881); *Ann. Phys. Beibl.*, **1882**, 369.

(9) P. de Heen, *Bull. Acad. Belg.*, [3] **5**, 760 (1883).

(10) M. Berthelot, *Ann. chim. et phys.*, [5] **4**, 74 (1875).

(11) J. Thomsen, "Thermochemische Untersuchungen," J. A. Barth, Leipzig, 1882–1886.

(12) M. Berthelot, *Ann. chim. et phys.*, [4] **30**, 456 (1873).

(13) W. A. Kaye and G. S. Parks, *J. Chem. Phys.*, **2**, 141 (1934); A. A. Glagoleva, *J. Gen. Chem. (U. S. S. R.)*, **6**, 1769 (1936).

(14) J. O. Halford, *J. Chem. Phys.*, **10**, 582 (1942).

(15) "Selected Values of Chemical Thermodynamic Properties," Circular 500, National Bureau of Standards, Washington 25, D. C.

NUCLEAR MAGNETIC RESONANCE SPECTRA OF THE TRIPHENYLCARBONIUM AND METHYLDIPHENYLCARBONIUM ION

BY D. E. O'REILLY AND H. P. LEFTIN

Mellon Institute and the Gulf Research & Development Co., Pittsburgh, Penna.

Received May 9, 1960

Proton magnetic resonance spectra of triphenylcarbonium and methyldiphenylcarbonium ions were measured in solutions of triphenylcarbinol and diphenylethylene in sulfuric acid. Chemical shifts for ring protons were obtained by the moment method and interpreted in terms of stereochemical and electronic structures of the ions. The calculated "mesomeric" contributions to the chemical shift are correlated with charge densities calculated by the LCAO and SCMO methods. Chemical shifts in the spectrum of triphenylcarbinol in sulfuric–acetic acid solvent are given and the J_0 acidity function for this solvent system is evaluated from the resonance data.

Introduction

The postulation of carbonium ion intermediates has been a useful device for the successful correlation of kinetic and product distribution data for diverse organic reactions. While in many instances the existence of such ions is mere conjecture, it has been known for some time that phenyl substituted carbonium ions (*e.g.*, triphenylcarbonium ion) are relatively stable and can be formed reversibly.[1] Major evidence establishing this fact has been provided by conductivity, cryoscopic and spectrophotometric measurements.[1] Little is known, however, about the internal structure of these ions. Nuclear magnetic resonance methods are ideally suited to such investigations. Thus, for example, chemical shift and spin coupling data can provide information concerning both electronic and stereochemical features. The present publication presents the results of an n.m.r. study of the triphenylcarbonium and methyldiphenylcarbonium ions.

Results and Discussion

It has been well established that triphenylcarbinol ionizes in sulfuric acid to give stable carbonium ions according to the reaction

$$(C_6H_5)_3COH + 2H_2SO_4 \longrightarrow (C_6H_5)_3C^+ + 2HSO_4^- + H_3O^+$$

The carbonium ion is stabilized by resonance distribution of charge. Many structures have been proposed for this ion; however, only two merit serious consideration. In the first of these, the ion is propellor shaped with all three rings equivalent in the resonance hybrid (Model A).[2] In the other (Model B) the positive charge is distributed over only one or two of the rings.[3] The proton magnetic resonance spectrum of triphenylcarbinol in concentrated sulfuric acid is consistent with Model A, wherein all rings are equivalent for times longer than of the order of 10^{-2} second, *i.e.*, of the order of the frequency separation between proton absorptions described below. The rings are probably equivalent for a time period shorter than 10^{-2} second, but evidence for this is not furnished by the n.m.r. spectra.

Figure 1a shows the proton n.m.r. spectrum at 40.00 mc./s. of triphenylcarbinol in concentrated sulfuric acid at a concentration of 5 mole %. The resonance signal consists of five resolved peaks. Triphenylcarbinol dissolved in CS_2 exhibits two resonance absorptions at −99 and 79 c./s. (relative to pure water at 25°), due to the aromatic ring protons and the alcoholic proton. The aromatic protons exhibit a chemical shift very close to that for benzene dissolved in CS_2, and are all magnetically equivalent. This effect is the result of cancellation of the inductive effects by the ring-current effects of the various groups as illustrated by the data of Table I.

TABLE I

CHEMICAL SHIFTS FOR TOLUENE AND DERIVATIVES IN CS_2 (RELATIVE TO BENZENE AT 40.00 MC./S.)

Compound	(δ, c./s.)[a]
$C_6H_5CH_3$	6.8
$(C_6H_5)_2CH_2$	5.2
$(C_6H_5)_3CH$	4.1
$(C_6H_5)CH_2OH$	4.0
$(C_6H_5)_3COH$	0.7
C_6H_6	0.0

[a] $\delta = [(H - H_0)/H_0] \cdot \nu_0$ where H_0 is the resonance field for the reference and ν_0 is the fixed resonance frequency.

Figure 1b shows the proton n.m.r. spectrum of 1,1-diphenylethylene (DPE) at 5 mole % in concentrated sulfuric acid. The aryl proton resonance consists of seven partially resolved peaks. The proton n.m.r. spectrum of DPE in CS_2 consists of two resonance absorptions due to the ring protons (−98 c./s.) and the ethylenic protons (−25 c./s.). The positions and approximate intensities of n.m.r. bands for triphenylcarbonium (TPC) and methyldiphenylcarbonium (MDPC) ions in concentrated sulfuric acid are given in Table II.

TABLE II

POSITIONS AND RELATIVE INTENSITIES OF THE PROTON N.M.R. ABSORPTION OF TPC AND MDPC IN CONCENTRATED SULFURIC ACID AT 40.00 MC./S. (RELATIVE TO BENZENE IN CS_2)[a]

TPC		MDPC	
−δ, c./s.	I	−δ, c./s.	I
		−164	21
		−6	1
7	2	6	2
13	8	14	8
20	4	20	45
27	2.5	26	10
38	1	33	5
		40	2

[a] With correction for the difference in bulk-susceptibility between CS_2 and H_2SO_4.

(1) J. E. Leffler, "The Reactive Intermediates of Organic Chemistry," Interscience Publishing, Inc., New York, N. Y., 1956, Chapter V.

(2) G. N. Lewis, T. T. Magel and D. Lipkin, *J. Am. Chem. Soc.*, **64**, 1774 (1942).

(3) M. S. Newman and N. C. Deno, *ibid.*, **73**, 3644 (1951).

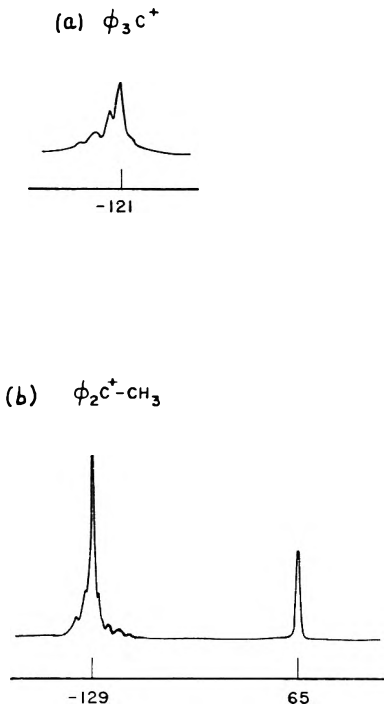

Fig. 1.—(a) Proton n.m.r. spectrum of triphenylcarbinol dissolved in concentrated sulfuric acid; (b) Proton n.m.r. spectrum of 1,1-diphenylethylene dissolved in concentrated sulfuric acid. Abscissas are labeled in c.p.s. at 40 Mc./sec., relative to pure water.

For theoretical purposes, the chemical shifts for the aryl protons of TPC and MDPC are referred to benzene in CS_2. A bulk-susceptibility correction[4] to account for the shift due to the difference between the susceptibilities of H_2SO_4 and CS_2 has been made. Spectra of triphenylcarbinol in liquid SO_2 and acetic acid were also obtained. The shift of the most intense peak of TPC from that of triphenylcarbinol in the above-mentioned solvents agrees within 1 c.p.s. with that obtained for CS_2 solvent after a bulk-susceptibility correction is made. indicative of the lack of influence of solvent on the chemical shift of the aromatic protons in triphenylcarbinol.

As a consequence of the formation of carbonium ions, the aromatic protons of TPC and MDPC undergo a chemical shift to lower field and become resolved into several lines. Chemical shifts to low field can result[4] from (a) a decrease in electron charge density at the carbon atom to which a proton is bonded, or (b) the magnetic field produced by the current induced in the pi electron loop of the rings upon application of a magnetic field.

In order to obtain the chemical shifts for the various ring protons of TPC and MDPC from the observed spectrum, the moment method of Anderson and McConnell[5] was employed; for this purpose, the first, second and third frequency moments of the observed spectra were determined. For reasons discussed below, the ring protons of TPC and MDPC were considered to consist of three equivalent groups; the *ortho*, *meta* and *para* position protons. In this case, the moment method allows the evaluation of the individual chemical shifts for these protons, since frequency moments up to and including the third do not involve spin-spin coupling parameters. Thus, evaluation of frequency moments up to the third does permit evaluation of chemical shifts but yields no information on spin-spin coupling constants. With the use of Fig. 4 of ref. 5, chemical shifts for the various protons of TPC and MDPC were evaluated and are given in Table III. The solution for δ_o, δ_m and δ_p for TCP from the calculated moments is unique. For MDPC, three solutions are possible. Of these, the one given in Table III corresponds continuously to that of TPC, and furthermore, is the only one which yields a value of δ_p larger than δ_m or δ_o, analogous to the result obtained for TPC. For both spectra the assignment of two of the shifts to *ortho* or *meta* protons was made on the basis that the *ortho* shift has a larger absolute value than the *meta* shift. This assumption is justified below. It must be noted that the error in the magnitude of the calculated shifts may be as large as $\pm 20\%$ due to errors in the intensities of resonance lines displaced most from the mean shift. However, the order of the calculated shifts is believed to be correct, *i.e.*, $|\delta_p| > |\delta_o| > |\delta_m|$.

Table III

ortho, *meta* and *para* Proton and Mean Chemical Shifts for TPC and MDPC as Evaluated by the Moment Method[a]

	TPC	MDPC
$\delta_o(\delta_m)$[b]	−17	−24
$\delta_m(\delta_o)$	−11	−14
δ_p	−32	−32
δmean	−17	−22

[a] Shifts relative to benzene in CS_2 at infinite dilution at 40.00 mc./s. [b] Alternative assignment.

The central carbon atom of TPC and MDPC was assumed to form three coplanar bonds so as to satisfy the requirements of the usual resonance structures that can be written for the molecule. In addition, free rotation of groups bonded to the central carbon does not occur due to the partial double bond character of these bonds. However, the phenyl rings of TPC or MDPC cannot be perfectly coplanar due to steric repulsions of ortho-hydrogens.

As already mentioned, inter-ring-current shifts will produce a significant contribution to the observed shifts of the ring protons of TPC and MDPC. For evaluation of this effect, the orientations of the phenyl rings relative to one another and the average time spent in each orientation must be known. This information is, however, not presently available. A model for TPC is proposed for evaluation of the ring-current shift. The central carbon bonds are assumed to be coplanar and the phenyl rings to be twisted, all in the same sense, out of the plane of the bonds to the central carbon atom. The magnetic field produced by an induced ring current may be represented by the field of a magnetic dipole; hence the chemical shift, $\Delta\sigma_{ij}$, of proton i produced by the ring current in ring j may be evaluated by the equation

(4) J. A. Pople, W. G. Schneider and H. J. Bernstein, "High Resolution Nuclear Magnetic Resonance," McGraw-Hill Book Co., Inc., New York, N. Y., 1959.

(5) W. Anderson and H. M. McConnell, *J. Chem. Phys.*, **26**, 1496 (1957).

$$\Delta\sigma_{ij} = \frac{e^2a^2}{2mc^2R^3_{ij}}(3\cos^2\phi_{ij} - 1) \qquad (1)$$

where a is the effective radius of the phenyl ring current loop, R_{ij} is the distance from the center of phenyl ring j to proton i, ϕ_{ij} is the angle between the perpendicular to ring j and radius vector R_{ij} and the remaining symbols have their conventional significance. The ring-current shifts for *ortho*, *meta* and *para* protons of the phenyl rings have been evaluated for several different angles of twist, θ, as well as the distance between adjacent *ortho* protons as a function of θ. Shifts were calculated relative to that for the protons of benzene. The results are shown in Fig. 2. At $\theta = 23°$, the distance between *ortho* protons is equal to twice the expected van der Waals radius of hydrogen (1.80 Å.). The corresponding ring-current shifts are employed in the following discussion.

A second contribution to the chemical shift for the protons of TPC and MDPC relative to benzene will result from the positive charge of the molecule. Moreover, a linear relationship is expected between proton chemical shift due to positive charge density on the carbon to which it is bonded and positive charge on the carbon, *i.e.*

$$\delta^+ = q\rho \qquad (2)$$

where δ^+ is the proton chemical shift due to positive charge, ρ is the positive charge density on the carbon atom to which the proton is attached and q is a constant. Some justification of equation 2 may be given by noting that the chemical shifts for hydrogen bonded to a carbon sp^2 orbital is expected to be proportional to the ionic character of the C–H bond. A positive charge density placed on the carbon due to a decrease in pi electron density may be expected to cause a proportionate increase in the ionic character and, hence, to increase the chemical shift of the hydrogen from that for neutral C–H bond.

The TPC ion has been treated by the conventional Hückel LCAO method by Streitweiser[6] and by the self consistent molecular orbital (SCMO) method by Brickstock and Pople.[7] The results of these two methods differ considerably as shown in Table IV.

TABLE IV

RING CURRENT AND POSITIVE CHARGE (MESOMERIC) CONTRIBUTIONS TO THE CHEMICAL SHIFT FOR TPC AND VALUES OF THE POSITIVE CHARGE DENSITY CALCULATED BY THE LCAO AND SCMO METHODS

	δ[a]			ρ[b]	
Position	Total obsd.	Ring-current, $\theta = 23°$	Mesomeric	LCAO	SCMO
ortho	−17	−11	− 6	0.074	0.05
meta	−11	− 4	− 7	.000	.06
para	−32	− 4	−28	.074	.19

[a] Relative to benzene in CS_2 at infinite dilution, corrected for bulk-susceptibility of solvents. [b] In units of electronic charge.

The "mesomeric" contribution to the chemical shift, δ^+, was calculated from the observed shifts by subtraction of the ring-current contribution calculated for $\theta = 23°$ from equation 1. As is apparent from the table, the mesomeric contribution to the shift is nearly directly proportional to the value of δ calculated by the SCMO method but not proportional to the values of ϵ calculated by the Hückel LCAO method; q (SCMO) is equal to -130 ± 10 c./s. per unit of positive charge.

Unfortunately, similar theoretical calculations do not appear to be available for the MDPC ion. SCMO calculations, however, have been made for the diphenylcarbonium (DPC) ion by Brickstock and Pople.[7] These results show that no two protons on a phenyl ring are equivalent with regard to positive charge density. However, it is quite possible that the observed spectrum corresponds to an averaged spectrum due to rotation of the phenyl rings in MDPC in a time which is short relative to the reciprocal of the chemical shift between pairs of *ortho* or *meta* protons. This assumption was implicitly made above in the evaluation of the chemical shifts by the moment method. In Table V are given chemical shifts and positive charge densities at various ring positions for MDPC. The ring-current contribution was evaluated from Fig. 2 with $\theta = 23°$.

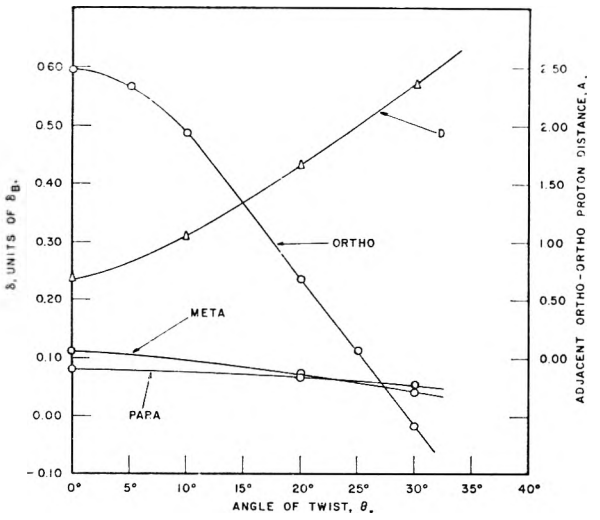

Fig. 2.—Chemical shift from *ortho*, *meta* and *para* protons of TPC *versus* angle of twist θ of phenyl rings from molecular plane. Distance D between adjacent *ortho* protons is also given as a function of θ.

TABLE V

RING CURRENT AND MESOMERIC CONTRIBUTIONS TO THE CHEMICAL SHIFT FOR MDPC

		δ[a]		ρ[b]	
Position	Total, obsd.	Ring-current	Mesomeric	Calcd. eq. 2	SCMO-DPC
ortho	−24	−5 (−13)	−19 (−11)	0.15 (0.08)	0.07
meta	−14	−2 (−3)	−12 (−11)	.09 (.08)	.05
para	−32	−2 (−3)	−30 (−29)	.23 (.22)	.23

[a] Relative to benzene in CS_2 at infinite dilution corrected for bulk-susceptibility of solvents. [b] In units of electronic charge.

Better agreement between the SCMO values of ρ for DPC and those calculated from the shifts for MDPC by equation 2 may be obtained if θ is somewhat less than 23°, as could occur if the angle between the two phenyl rings were to become larger than 120°. Values of the positive charge calcu-

(6) A. Streitweiser, Jr., *J. Am. Chem. Soc.*, **74**, 5288 (1952).

(7) A. Brickstock and J. A. Pople, *Trans. Faraday Soc.* **50**, 901 (1954).

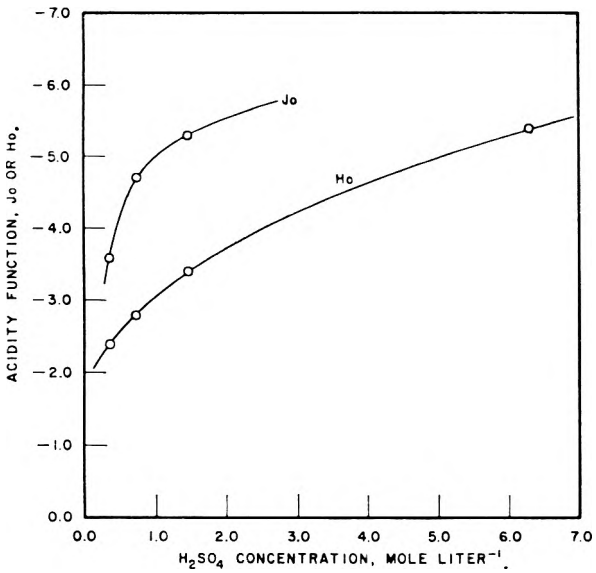

Fig. 3.—H_0 and J_0 functions *versus* sulfuric acid concentration in sulfuric acid–acetic acid mixtures. H_0 data are those of ref. *b*, Table VI; J_0 data are those of Table VI.

lated from equation 2 with $\theta = 15°$ are given in parentheses in Table V.

As was noted above and in Table III, there is an ambiguity in the assignment of the values of δ, since the assignment of the shift for the *ortho* and *meta* protons, as determined by the moment method, is not unequivocal. If the alternative assignment denoted in parenthesis in Table III is adopted, the chemical shifts continue to be in best agreement with the charge densities as computed by the SCMO method rather than the Hückel method, although the relationship given by equation 3 is not quantitatively obeyed.

The relative stability of triarylcarbonium ions is strongly determined by the electronic effects of ring substituents. Major evidence in support of this fact is based on spectral[5] and conductivity[9] data. This fact has been used in setting up an acidity scale for non-aqueous media analogous to that of Hammett.[10] Gold and Hawes[11] defined the J_0 acidity function by

$$J_0 = \left(pK_{R^+} - \log \frac{C_{R^+}}{C_{ROH}}\right) \qquad (3)$$

for the reaction

$$R^+ + H_2O \rightleftharpoons ROH + H^+ \qquad (4)$$

where clearly

$$pK_{R^+} = -\log \frac{a_{ROH}\, a_{H^+}}{a_{R^+}\, a_{H_2O}} \qquad (5)$$

When J_0 values for a solvent system are known, thermodynamic pK_{R^+} data can be obtained from a spectrophotometric examination according to equation 3, since the electronic spectra of carbonium ions differ markedly from those of their carbinol precursors. Conversely, once having established reliable pK_{R^+} data, the acidity function J_0 of many solvent systems can be established.

Nuclear magnetic resonance techniques have been successfully applied to studies of chemical equilibria.[4] In order to test this technique for equilibria involving carbonium ions, the n.m.r. spectrum of triphenylcarbinol was examined in a series of solvents composed of sulfuric–acetic acid mixtures covering the range 0 to 100 wt. % H_2SO_4. The proton resonance of the aromatic protons consisted of a single broadened line in the mixed solvents studied. The signal shifted to lower field with increasing acid strength as illustrated in Table VI. As before, a bulk-susceptibility correction was made for each sample. The diamagnetic susceptibility of a mixture was computed by the Wiedemann additivity law[4] from the known concentrations and susceptibilities of the components.

Table VI

Chemical Shift of Aromatic Protons (Triphenylcarbinol in Acetic–Sulfuric Acid Mixtures, 25°)

Solvent (wt. % H_2SO_4 in CH_3COOH)	Moles/l.	H_0[b]	Chemical shift (c./s. at 40 mc./s.)	Calcd. J_0
0	0.00		0	
3.5	0.36	−2.4	3.2	−3.6
7.0	0.72	−2.8	10.7	−4.7
11.7	1.44	−3.4	13.2	−5.3
46.6	6.3	−5.4	14.0	−6
100	..		14.2[a]	

[a] Average of two signals. [b] N. F. Hall and W. F. Spengeman, *J. Am. Chem. Soc.*, 62, 2487 (1940).

From the known $pK_{R^+} = 4.18$ for triphenylcarbinol (Deno, Jaruzelski and Schriesheim, ref. 8) the value of J_0 for any of these acid solutions can be calculated from the n.m.r. data. The ratio C_{R^+}/C_{ROH} was obtained from the observed shift according to

$$\frac{C_{R^+}}{C_{ROH}} = \frac{\delta - \delta_{ROH}}{\delta_{R^+} - \delta} \qquad (6)$$

where δ is the observed chemical shift and δ_{R^+}, δ_{ROH} are the chemical shifts for triphenylcarbonium ion and carbinol, respectively. The J_0 values calculated from the chemical shift data are given in Table VI where they are compared to available H_0 values for this system. As shown in Fig. 3, J_0 parallels the H_0 data although J_0 increases more rapidly. A similar feature has been found in the sulfuric acid–water system.[12,13]

Deuterium Exchange.—The triphenylcarbonium ion dissolved in 80% D_2SO_4 (99.5% deuterated) showed no evidence of isotope exchange in eight hours at 25°. The intensity of the n.m.r. signal obtained from the phenyl protons remained unchanged and no increase of the acid H resonance was detected. This result is in agreement with the work of Deno and Evans,[14] and may be taken to

(8) G. Branch and H. Walba, *J. Am. Chem. Soc.*, **76**, 1564 (1954); N. C. Deno, J. J. Jaruzelski and A. Schriesheim, *J. Org. Chem.*, **19**, 155 (1954).

(9) N. N. Lichtin and P. D. Bartlett, *J. Am. Chem. Soc.*, **73**, 5530 (1951); N. N. Lichtin and H. P. Leftin, This Journal, **60**, 164 (1956).

(10) L. P. Hammett, "Physical Organic Chemistry," McGraw-Hill Book Co., New York, N. Y., 1940, Chapter IX.

(11) V. Gold and B. W. V. Hawes, *J. Chem. Soc.*, 2102 (1951).

(12) N. C. Deno, J. J. Jaruzelski and A. Schriesheim, *J. Am. Chem. Soc.*, **77**, 3044 (1955).

(13) M. A. Paul and F. A. Long, *Chem. Revs.*, **57**, 1 (1957).

(14) N. C. Deno and Wm. L. Evans, *J. Am. Chem. Soc.*, **78**, 582 (1956).

indicate that hyperconjugation involving "no bond" structures such as

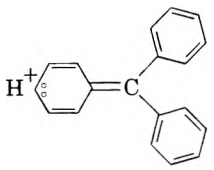

does not play an important role in stabilization of this ion.

Experimental

Reagents.—Triphenylcarbinol, m.p. 162–163°, was prepared by recrystallization of Eastman White Label material. Diphenylethylene (n_D 1.6093) was prepared by distillation of Aldrich Chemical Co. DPE. Deuteriosulfuric acid was prepared by deuteriolysis of anhydrous sulfur trioxide using D_2O (99.5%) from Stewart Oxygen Co.

Measurements.—N.m.r. measurements were made with a Varian Associates model V-4300A spectrometer and 12 inch electromagnet. Chemical shifts were measured by the audio sideband technique with the use of a frequency counter. The chemical shifts of Tables I, II and VI were measured by use of trimethylsilane in a capillary placed in the tube which contained the material under study.

Acknowledgment.—The portion of this work carried out at the Mellon Institute was sponsored by the Gulf Research & Development Company as a part of the research program of the Multiple Fellowship on Petroleum.

KINETICS OF METHYLCYCLOHEXANE DEHYDROGENATION OVER PT-Al_2O_3

BY J. H. SINFELT, H. HURWITZ AND R. A. SHULMAN

Esso Research and Engineering Company, Linden, N. J.

Received May 12, 1960

The kinetics of methylcyclohexane dehydrogenation over a platinum-on-alumina catalyst were investigated over the temperature range 315 to 372°, at methylcyclohexane partial pressures ranging from 0.07 to 2.2 atmospheres and hydrogen pressures ranging from 1.1 to 4.1 atmospheres. The reaction was found to be nearly zero order with respect to methylcyclohexane and hydrogen over the range of conditions studied. The activation energy for the reaction was found to be 33 kcal./mole. The near zero order behavior of the reaction suggests that the active catalyst sites are heavily covered with adsorbed molecules or radicals at reaction conditions. It is suggested that adsorption equilibria are not established at the conditions used in this study. A simple kinetic scheme, according to which the reaction rate corresponds to the rate of desorption of toluene, is proposed to account for the observed kinetics.

Introduction

The formation of aromatics by the catalytic dehydrogenation of saturated six-membered ring hydrocarbons is a well-known reaction. The transition metals and their oxides are active catalysts for such dehydrogenation reactions. Supported metal catalysts, such as platinum or palladium-on-alumina, are particularly active. It has been shown by hydrogen chemisorption measurements that freshly prepared platinum on alumina catalysts are characterized by extremely high dispersion of the platinum on the support.[1] The high dispersion of the platinum is an important factor contributing to the very high activity of these catalysts.

Although a number of investigations on the dehydrogenation of cyclohexanes over supported platinum catalysts have been reported[2–4] the kinetics of the reaction have not been extensively investigated. Therefore, it was decided to study the kinetics of methylcyclohexane dehydrogenation over a platinum-on-alumina catalyst to gain some insight into the nature of the surface phenomena involved in the reaction.

(1) L. Spenadel and M. Boudart, THIS JOURNAL, **64**, 204 (1960).

(2) V. Haensel and G. R. Donaldson, *Ind. Eng. Chem.*, **43**, 2102 (1951).

(3) W. P. Hettinger, C. D. Keith, J. L. Gring and J. W. Teter, *ibid.*, **47**, 719 (1955).

(4) A. I. M. Keulemans and H. H. Voge, THIS JOURNAL, **63**, 476 (1959).

Experimental

Procedure.—Reaction rates were measured in a flow system in the presence of added hydrogen using a 1/2 inch i.d. stainless steel reactor with a volume of about 20 cc. The reactor was surrounded by an electrically heated aluminum block to maintain isothermal operation. The runs were made with a catalyst charge of 6 g. diluted with inert ceramic beads to fill the reactor volume. Prior to introducing the methylcyclohexane feed, the catalyst was pretreated with flowing hydrogen for three hours at 527°. Reaction products were analyzed by a 1/4 inch i.d. chromatographic column coupled directly to the outlet of the reactor. The column was 4 meters long, packed with firebrick impregnated with polyethylene glycol, and operated at a temperature of 90°. This gave excellent resolution of the methylcyclohexane, toluene and other aromatics used in this study.

Reaction periods of 30 minutes were employed in all of the runs to ensure the attainment of steady-state conditions prior to sampling the reaction products. Several reaction temperatures were used in this work, ranging from 315 to 372°. Total pressure was varied from 1.4 to 6.3 atmospheres and hydrogen to methylcyclohexane mole ratio from 2 to 20. Molal space velocities ranged from 0.2 to 1.0 g. mole of methylcyclohexane per hour per g. of catalyst, depending on the reaction temperature.

Materials.—Phillips pure grade methylcyclohexane (> 99 mole % purity) was used in all the experiments. The methylcyclohexane was dried with Drierite ($CaSO_4$) to less than 5 p.p.m. by weight of water before using. The benzene and *meta*-xylene which were used in binary mixtures with methylcyclohexane in some of the experiments were also Phillips pure grade and were dried in the same way. The hydrogen was passed through a Deoxo cylinder containing palladium catalyst to convert trace amounts of oxygen to water, and then dried over Linde 5A molecular sieves. The catalyst used in this study contained 0.3 wt. % platinum

and was prepared by impregnation of alumina (surface area = 155 m.²/g.) with aqueous chloroplatinic acid.

Results

The methylcyclohexane dehydrogenation experiments were carried out at low conversion levels to obtain initial reaction rates. For sufficiently low conversions in a flow system the reaction rate is given by

$$r = \frac{F\Delta x}{W} \qquad (1)$$

where F is the feed rate in moles per unit time, W is the amount of catalyst, and Δx is the extent of conversion. The quantity F/W is the molal space velocity, and hence the rate at low conversions is simply the product of F/W and Δx.

The dehydrogenation of methylcyclohexane was found to be an extremely clean reaction, with toluene being the only observed product. Data showing the initial rate of reaction as a function of the partial pressures of methylcyclohexane and hydrogen are summarized in Table I. Rate data are presented for three different temperatures: 315, 344 and 372°. The data in Table I were all obtained over a single charge of catalyst. Catalyst activity was checked periodically throughout the run at a standard set of conditions. No loss in activity was observed.

TABLE I

SUMMARY OF RATE DATA FOR METHYLCYCLOHEXANE DEHYDROGENATION[a]

Temp., °C.	p_M, atm.	p_H, atm.	F/W	Δx	r
315	0.36	1.1	0.21	5.6	0.012
315	.36	3.0	.20	5.8	.012
315	.07	1.4	.21	4.1	.0086
315	.24	1.4	.21	5.2	.011
315	.72	1.4	.21	6.2	.013
344	.36	1.1	.53	5.7	.030
344	.36	3.1	.52	6.2	.032
344	.08	1.4	.52	3.9	.020
344	.24	1.4	.55	6.2	.034
344	.68	1.4	.52	6.5	.034
372	.36	1.1	1.02	7.4	.076
372	.36	4.1	1.02	7.8	.080
372	1.1	4.1	1.05	11.8	.124
372	2.2	4.1	1.05	12.5	.131

[a] p_M = methylcyclohexane partial pressure; p_H = hydrogen partial pressure; F/W = molar space velocity, g. moles of methylcyclohexane/hr./g. catalyst; Δx = mole % conversion to toluene; r = rate of dehydrogenation, g. moles toluene formed/hr./g. catalyst.

Thermodynamic calculations using free energy data from API Project 44[5] show better than 90% conversion of methylcyclohexane to toluene at equilibrium for all conditions studied except the one point at 315° and 3.0 atmospheres hydrogen partial pressure, at which equilibrium corresponds to about 50% conversion to toluene. Since the conversion levels were low (4–12%) in all these experiments, the effects of the reverse reaction can be neglected.

The rate of dehydrogenation was found to be nearly independent of the methylcyclohexane partial pressure; for example, a tenfold increase in the methylcyclohexane partial pressure increased the rate less than twofold. In addition, the rate was found to be essentially independent of hydrogen partial pressure. Thus, over the range of temperatures and pressures studied, the reaction is nearly zero order with respect to both methylcyclohexane and hydrogen.

Some measurements were made to determine how the presence of aromatics affects the rate of dehydrogenation of methylcyclohexane. This was done to determine if inhibition by the reaction product toluene was appreciable when determining rates at low conversions. In these experiments 1:1 molal mixtures of methylcyclohexane with either benzene or *meta*-xylene were passed over the catalyst in the presence of hydrogen, and the dehydrogenation rates compared with that of pure methylcyclohexane in the presence of hydrogen alone. The methylcyclohexane and hydrogen partial pressures were maintained constant in this comparison, so that we have a direct measure of the effects of the added components on the rate of dehydrogenation. The partial pressures of methylcyclohexane, hydrogen and the third component (benzene or *meta*-xylene) were 0.36, 1.4 and 0.36 atmospheres, respectively. The effects of the added aromatics on the rates at 315° are shown by the ratio r_1/r_2, in which r_1 and r_2 are the rates in the presence and absence of the aromatics, respectively. The rate of dehydrogenation of

Feed	r_1/r_2
Methylcyclohexane	1.0
Methylcyclohexane + benzene, 1:1	0.8
Methylcyclohexane + xylene, 1:1	0.8

methylcyclohexane in a 1:1 mixture with benzene or *meta*-xylene is thus 80% of the rate in the presence of hydrogen alone. In a 1:1 mixture with toluene the rate would undoubtedly be affected to the same extent. In any case, at the low toluene concentrations (4–12%) encountered in the experiments on methylcyclohexane, the inhibiting effect of the toluene would be small. The effect of toluene itself on the rate cannot be measured very accurately by our technique, since in the presence of a large amount of toluene the small conversion of methylcyclohexane to toluene would have to be obtained as the difference between two large numbers (toluene out minus toluene in). Some other technique, such as the use of radioactive tracers, would be better for this type of measurement.

Discussion

As already pointed out, the rate of dehydrogenation of methylcyclohexane is nearly zero order with respect to methylcyclohexane and is zero order with respect to hydrogen. The small effect of methylcyclohexane pressure which is observed can be accounted for by a rate expression of the form

$$r = \frac{k'bp_M}{1 + bp_M} \qquad (2)$$

where k' is a rate constant, p_M is the methylcyclo-

(5) "Selected Values of Physical and Thermodynamic Properties of Hydrocarbons and Related Compounds," API Research Project 44, Carnegie Press, Inc., New York, N. Y., 1953.

hexane partial pressure, and b is a parameter which is a function of temperature. The physical significance of k' and b will be discussed later. The value of k' can be determined from the intercept of a plot of $1/r$ *vs.* $1/p_M$, and b can then be evaluated from the slope. The values of k' and b at the temperatures investigated were found to be

Temp., °C.	k'	b
315	0.013	27
344	.043	11
372	.154	3

where k' is expressed in g. mole/hr./g. catalyst and b is expressed in reciprocal atmospheres. From an Arrhenius plot of ln k' *vs.* $1/T$, the activation energy for the reaction is found to be 33 kcal./mole. Since the effect of methylcyclohexane pressure on the rate is small, the intercept of a plot of $1/r$ *vs.* $1/p_M$ can be determined more accurately than the slope, so that the values of k' are defined more precisely than the corresponding values of b.

At sufficiently high methylcyclohexane partial pressures, the rate given by equation 2 approaches the value k', which represents the rate at conditions where the reaction is truly zero order. At the pressures used in the present work, the measured rates are only slightly lower than the values of k', since the kinetics are close to zero order.

The near zero-order behavior of the reaction suggests that the active platinum sites are almost completely covered with adsorbed hydrocarbon molecules or radicals formed from the methylcyclohexane. According to the transition state theory of reaction rates, the rate of a zero order surface reaction is given by

$$r = C_a \frac{kT}{h} \exp(-E/RT) \qquad (3)$$

where C_a represents the number of adsorbed molecules or radicals per cm.^{2} of active surface, kT/h is a frequency factor of the order of 10^{13}, and E is the activation energy.[6] Assuming 1.1×10^{15} sites per cm.^{2} of platinum surface,[1] we can take $C_a = 1.1 \times 10^{15}$ for the number of hydrocarbon molecules or radicals per cm.^{2} on a fully covered surface, assuming that one molecule or radical is adsorbed on each site. Using the experimental rate data we can calculate the activation energy from equation 3 and compare it with the value determined from the observed temperature dependence of the rate constant. To make this calculation the experimental rate must be expressed in molecules/sec./cm.^{2} of platinum. Taking the platinum surface area as 276 m.^{2}/g.,[1] and recalling that the weight fraction of platinum on the catalyst is 0.003, the rate in g. mole/hr./cm.^{2} of platinum at 315° becomes

$$r = \frac{0.013}{0.003 \times 276 \times 10^4} = 1.57 \times 10^{-6}$$

Multiplying this by 6.02×10^{23} and dividing by 3600, the rate in molecules/sec./cm.^{2} of platinum is 2.6×10^{14}. Substituting this value into equation 3, the activation energy E is calculated to be 37 kcal./mole. The agreement with the experimental value of 33 kcal./mole is fair.

According to the Langmuir-Hinshelwood mechanism of surface reactions, the reactant molecules are considered to be in adsorptive equilibrium with the surface, so that the reaction rate is determined by the rate of transformation of the adsorbed molecules on the surface. Applying this to methylcyclohexane dehydrogenation, the near zero-order behavior with respect to methylcyclohexane would suggest that the active catalyst sites are quite heavily covered with adsorbed methylcyclohexane. The parameter b in equation 2 would then be an adsorption equilibrium constant for the adsorption of methylcyclohexane, and k' a specific rate constant for the conversion of adsorbed methylcyclohexane to toluene on the surface. From the temperature dependence of b, a value of the order of 30 kcal./mole for the heat of adsorption of methylcyclohexane would be indicated. However, it is highly unlikely that adsorption of methylcyclohexane as such would involve a heat of adsorption of this magnitude, particularly at high surface coverage. Interpreting the kinetic data on the basis of adsorption equilibria also leads to other difficulties. Since the adsorption of methylcyclohexane probably involves dissociation of hydrogen from the molecule, increasing hydrogen pressure should reduce the concentration of the adsorbed species in question, and hence decrease the rate of toluene formation. However, this was not found. Furthermore, the small inhibiting effects of benzene and *meta*-xylene on the rate are not readily explained in terms of adsorption equilibria. One would expect that aromatics, by virtue of their unsaturation, would be more strongly adsorbed than methylcyclohexane. There is evidence of this at a much lower temperature (−22.5°) based on kinetic studies of the reaction of benzene with deuterium over platinum films at benzene pressures of the order of 1 mm.[7] The rate of deuteration was zero order in benzene and uninhibited by the deuterocyclohexanes formed, indicating strong adsorption of benzene relative to cyclohexane. Extending this conclusion to the present study, benzene and *meta*-xylene would be expected to inhibit methylcyclohexane dehydrogenation substantially. Since this was not observed, it is suggested that adsorption equilibria are not established at the conditions used in this study. The small inhibiting effects of the benzene and *meta*-xylene are then interpreted to mean that their rates of adsorption are small compared to the rate of adsorption of methylcyclohexane, so that their coverage of the active surface is small.

In view of the above considerations, an alternative mechanism is proposed. It is suggested that the active catalyst sites are heavily covered with adsorbed toluene and that the reaction rate is the rate of desorption of toluene from the surface. To account for the observed kinetics, a simple kinetic scheme is proposed

(6) S. Glasstone, K. J. Laidler and H. Eyring, "The Theory of Rate Processes," McGraw-Hill Book Co., New York, N. Y., 1941, Chapter VII.

(7) J. R. Anderson and C. Kemball, "Advances in Catalysis," Academic Press, Inc., New York, N. Y., 1957, Vol. IX, p. 51.

$$M \xrightarrow{k_1} T_a \xrightarrow{k_2} T$$

in which M and T represent methylcyclohexane and toluene in the gas phase, and T_a represents adsorbed toluene. It is postulated that adsorption equilibria are not established, and that the individual steps are effectively irreversible. Step 1 represents the adsorption of methylcyclohexane with subsequent reaction to form toluene on the surface, while step 2 is the desorption of toluene from the surface. The first step is likely a combination of steps involving partially dehydrogenated hydrocarbon molecules or radicals. The present treatment is therefore a simplification, but is adequate for our purposes. The parameters k_1 and k_2 are rate constants for steps 1 and 2, respectively. Assuming that coverage of the active sites by components other than toluene is very small, we can write the following steady-state expression for the net rate of formation of adsorbed toluene

$$\frac{dT_a}{dt} = k_1 p_M(1 - \theta_T) - k_2\theta_T = 0 \qquad (4)$$

where θ_T represents the fraction of the active sites covered by toluene. The rate of formation of the product toluene is given by

$$r = k_2\theta_T \qquad (5)$$

Solving equation 4 for θ_T and substituting in equation 5, we obtain the rate expression

$$r = \frac{k_2\left(\frac{k_1}{k_2}\right)p_M}{1 + \left(\frac{k_1}{k_2}\right)p_M} \qquad (6)$$

which is of the same form as equation 2 with $k' = k_2$ and $b = k_1/k_2$. The experimental activation energy of 33 kcal./mole now corresponds to the activation energy E_2 for desorption of toluene from the surface. From the observed temperature dependence of b we can estimate the difference in activation energies (E_2 - E_1) of steps 1 and 2 to be about 30 kcal./mole. The value of E_1 is then about 3 kcal./mole, which may be interpreted as an activation energy for chemisorption of methylcyclohexane.

The above kinetic scheme leads to a rate expression which satisfactorily accounts for the observed rate data. At the conditions of the present study, it appears that methylcyclohexane dehydrogenation over a platinum on alumina catalyst is an example of a surface reaction in which the assumption of adsorption equilibria may not apply.

In the simple kinetic scheme just described, the exact nature of the surface reaction leading to the formation of adsorbed toluene (step 1) was not considered. The detailed mechanism of such a step has been the subject of considerable discussion. As a special case of his more general multiplet theory of catalysis, Balandin[8] originally suggested (in 1929) that cyclohexane is converted to benzene over metals like platinum, palladium, or nickel in a single step by the simultaneous removal of six hydrogen atoms. In order for this to occur it is necessary that the cyclohexane ring be adsorbed in a very definite manner such that a sextet of metal atoms is involved in the simultaneous rupture of six carbon–hydrogen bonds. According to this theory the active catalyst unit is thus an aggregate of metal atoms which must be spaced within certain definite limits consistent with the geometry of the cyclohexane ring. While there is a great deal of experimental evidence attesting to the importance of geometrical factors in the catalytic dehydrogenation of six-membered rings,[8] more recent findings indicate that chemisorption of the cyclohexane ring need not involve the simultaneous rupture of six carbon–hydrogen bonds. For example, in the exchange of deuterium with cyclohexane over platinum metal films,[9] the initial product is predominantly $C_6H_{11}D$ rather than $C_6H_6D_6$. The latter would have been the only primary product if chemisorption of cyclohexane occurred strictly by the sextet mechanism. Furthermore, for platinum-on-alumina catalysts similar to that used in the present study, the work of Spenadel and Boudart[1] showed that if any platinum crystallites are present, they must on the average consist of blocks containing less than two unit cells on a side. It is questionable whether crystallites such as these could accommodate the cyclohexane ring in the manner envisioned in the sextet mechanism.

Alternatively, it seems probable in methylcyclohexane dehydrogenation that the formation of toluene on the surface proceeds by a stepwise mechanism, involving intermediate surface species of varying degrees of dehydrogenation.

Acknowledgment.—The authors wish to express their appreciation to the Esso Research and Engineering Company for permission to publish the results of this work. They also wish to acknowledge helpful discussion with Professor M. Boudart of Princeton University.

(8) B. M. W. Trapnell, "Advances in Catalysis," Academic Press, Inc., New York, N. Y., 1951, Vol. III, p. 1.

(9) J. R. Anderson and C. Kemball, *Proc. Roy. Soc.* (*London*), **A226**, 472 (1954).

THE PERMEABILITY OF AN ACRYLAMIDE POLYMER GEL

BY MALCOLM L. WHITE

Central Research Division, American Cyanamid Company, Stamford, Connecticut

Received May 27, 1960

An apparatus was devised for measuring the water permeability of a semi-rigid, vibrating gel formed by the copolymerization of acrylamide with methylenebisacrylamide. The permeability of the gel was found to vary from 38×10^{-16} cm.^{2} for a gel containing 5% polymer to 2.1×10^{-16} cm.^{2} for a gel containing 35% polymer. The permeability was found to be independent of the amount of crosslinking, leading to the hypothesis of a "brush heap" type structure for the gel. The average pore radius of the gel was calculated to vary from 1.8 to 0.5 mμ in the 5 to 35% polymer concentration range, with the maximum pore radius in a 10% gel lying somewhere below 17 mμ (average pore radius = 1.3 mμ). The transport process occurring in the gels was found to be predominantly viscous flow in the more dilute gels, but in the most concentrated gels studied (25–35%) diffusion appeared to become important in the movement of water through the gel.

Introduction

Acrylamide, when copolymerized in an aqueous solution with methylenebisacrylamide, using an oxidation–reduction catalyst system, such as an amine with ammonium persulfate, forms a semi-rigid, water-insoluble gel which is thermally stable. This gel is practically transparent and is strong enough to support its own weight, although under heavy loads it will fracture. The gel can be formed with a minimum of 2.5% of the monomer mixture, with the maximum concentration of polymer in the gel being limited only by the solubility of the acrylamide and methylenebisacrylamide. The amount of the crosslinking agent (methylenebisacrylamide) can be varied from a minimum of 1% of the total monomer content to about 10% of the total monomer content, the maximum amount being limited by its solubility in water (3.1% at 20°). With increasing polymer concentration the gel becomes stronger and more rigid, retaining, however, its transparent nature. Increasing the crosslinking also increases the strength, at a given total polymer concentration, up to about 7% of methylenebisacrylamide in the monomer mixture, with larger amounts not affecting the strength. A solid mixture of 95% acrylamide and 5% methylenebisacrylamide is sold under the trademark Cyanogum 41 by the American Cyanamid Company.[1] It has been found that water-soluble material can diffuse into and out of the gel, so that it is possible, for example, to use it for electrophoretic measurements.[2] The purpose of the work reported here was to measure the permeability of the gel and from this data determine values for the average pore size.

A review of the literature revealed that very little has been published on the measurement of water permeability in gels. Pallman and Devel[3] measured the water permeability of agar and gelatin gels by measuring the flow of water, under a hydrostatic head, through a column of the gel. In agar gels they found the permeability coefficient decreased from 4.4×10^{-12} to 0.2×10^{-12} cm.^{2} as the % agar increased from 2 to 8%, and that an 8% gelatin gel had a permeability coefficient of 2.0×10^{-12} cm.^{2}. Signer and Egli,[4] using a similar experimental method, found somewhat lower values for gelatin gels, ranging from 0.18×10^{-12} to 0.014×10^{-12} cm.^{2} for approximately the same range. For silica gels they found the permeability to be about ten times greater than for gelatin gels.

Preliminary observations had indicated that the acrylamide polymer gel was less permeable than agar or gelatin gels so an apparatus was devised for measuring small flows of water through a thin section of gel at relatively high pressures.

Experimental

An apparatus similar to that used by Madras, *et al.*,[5] for measuring the permeability of cellophane was constructed in which the cell for holding the gel (see below) was clamped by means of threaded couplings between two chambers constructed of glass pipe. Both chambers were filled with boiled, distilled water and nitrogen pressure applied to one side, pressures from 6 to 30 p.s.i. being measured on an Ashcroft bronze tube laboratory test gauge and below 6 p.s.i. on a U-tube mercury manometer. Connected to the chamber on the other side was a 0.25 mm. capillary tube for measuring flow rates, fixed horizontally so that there was no hydrostatic pressure difference between the two halves of the apparatus. The capillary tube was calibrated with mercury to determine the volume per cm. of length, a value of 1.35×10^{-3} ml./cm. length being obtained. In operation the whole apparatus was immersed in a water-bath held at 25.00 ± 0.02°. Any greater variation in temperature caused changes in the volume of water which affected the flow rate as measured in the capillary tube.

Because of the limited strength of the gel, it was not possible to put a disk of the gel directly between the two halves of the apparatus, for the disk deformed and fractured when clamped. To overcome this difficulty a cell was designed (Fig. 1) for holding the gel so that it could be securely clamped in the apparatus with a minimum of leakage around it. A disk of gel $^1/_{32}$" thick and $^3/_4$" in diameter was formed by laying a neoprene washer of these dimensions on a lucite plate, filling the washer to near overflowing with a catalyzed but ungelled solution and then pressing another lucite disk down on top of the washer so that all air was excluded. After the solution had polymerized to form a gel the lucite disks were removed and the gel disk in the neoprene washer was put between the two halves of the cell which was then wrapped with tape to keep the two halves aligned and then clamped between the two compartments of the permeability apparatus. This procedure allowed the gel to be completely contained so that a tight leakproof seal could be made without fracturing or deforming the gel. Any air trapped in the porous stainless steel disks was removed by applying a vacuum to the porous disks in the apparatus. It was determined that the area of the porous disks blocking the surface of the gel disk was less than 5% of the total area of the gel disk, which is less than the error in the final measurements.

The gel solutions were made from stock solutions of acrylamide recrystallized from acetone and methylenebisacrylamide recrystallized from methanol, filtered to remove any suspended solid material. The catalyst system used was

(1) "Cyanogum 41 Gelling Agent," American Cyanamid Company, Market Development Department, 30 Rockefeller Plaza, New York 20, N. Y., 1958.

(2) S. Raymond and L. Weintraub, *Science*, **130**, 711 (1959).

(3) H. Pallman and H. Devel, *Experientia*, **1**, 325 (1945).

(4) R. Signer and H. Egli, *Rev. trav. chim.*, **69**, 45 (1950).

(5) S. Madras, R. L. McIntosh and S. G. Mason, *Can. J. Research*, **278**, 764 (1949).

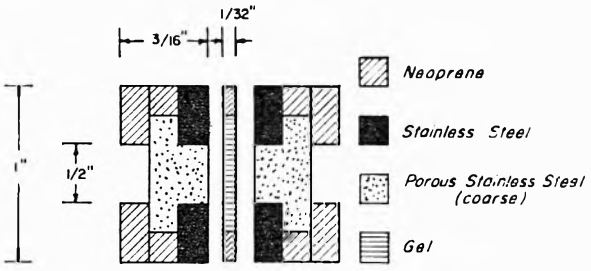

Fig. 1.—Cell for holding gel.

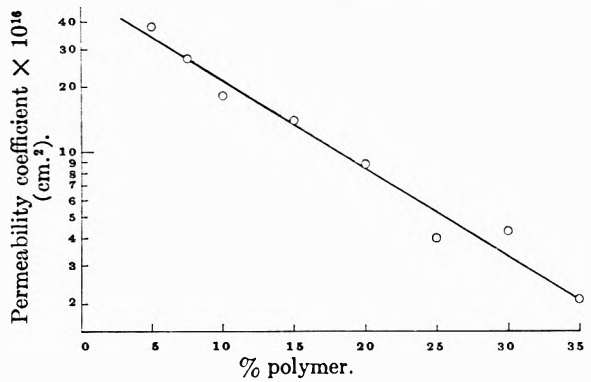

Fig. 2.—Permeability coefficients of gel as function of polymer concentration.

dimethylaminopropionitrile (redistilled at 30 mm.) at a final concentration of 0.4% (based on solution volume) and ammonium persulfate (J. T. Baker Analyzed) at 0.5% final concentration. The percentage of polymer in the gel is expressed in grams of polymer in 100 ml. of solution. The polymer concentrations in the gels studied varied from 5 to 35%. The ratio of acrylamide to methylenebisacrylamide is shown as a fraction, *e.g.*, 95/5 indicating that the monomer mixture contained 5% crosslinking agent. Gels having ratios of 99/1, 95/5 and 90/10 were studied. The catalyzed solution gelled in 1–2 minutes, which allowed ample time for forming the gel disks as previously described.

Results

The equation used for determining the permeability coefficient K_s of the gel was[5]

$$K_s = \frac{VL\eta}{tA\,\Delta P}$$

where V is the volume of liquid (in ml.), having a viscosity η (in poises) flowing through a sample of thickness L (in cm.) and area A (in cm.²), in a given time t (in sec.), under a pressure differential ΔP (in dynes/cm.²) resulting in a value for K_s in cm.².

In making a run, the volume of solution passing through the gel was measured by the rate of flow of water in the capillary tube at three or four different nitrogen pressures between 6 and 30 p.s.i. A plot was made of the flow rate in the capillary tube (as cm./min.) against the pressure. In all cases a straight line was obtained which extrapolated to near the origin, although it did not always go through it. The slope of this line was calculated and then combined with the constant terms, along with the appropriate conversion factors, in the above equation to determine K_s. The thickness of the sample, L, was taken as $^1/_{32}$" (0.0792 cm.), the area as 1.29 cm.² ($^1/_2$" diameter of disk exposed to flow), and the viscosity of water as 0.00895 poise.[6]

(6) National Research Council, "International Critical Tables," Vol. 5, McGraw-Hill Book Co., New York, N. Y., 1929.

Determinations of the permeability coefficients of several gel disks at each of three different polymer concentration levels showed that the reproducibility of the results was within 10% at each of the levels.

Figure 2 shows a plot of the log permeability coefficient *versus* % polymer in the gel for 95/5 crosslinking ratio. Below 2.5% polymer the permeability coefficient undoubtedly goes to a very high value, for no gel will form below 2.5% polymer. Above this concentration the permeability coefficient decreases logarithmically in a steady manner so that at the 35% level the permeability has dropped about twenty-fold.

The permeabilities of a 99/1 and a 90/10 gel at the 10% polymer level were determined, giving values of 20.4×10^{-16} cm.² and 19.0×10^{-16} cm.², respectively. This shows that the permeabilities are independent of the amount of crosslinking in the range studied.

Discussion

The dependence of the permeability coefficient on the per cent. polymer in the gel and its independence of the amount of cross-linking suggests that the gel has a "brush heap"[7] type structure consisting of a random intertwining of polyacrylamide chains that are occasionally crosslinked with the methylenebisacrylamide. In a 95/5 gel, for example, the crosslinking will occur, on the average, once every 40 monomer units, so that the formation of pores is controlled primarily by the number of polyacrylamide chains (concentration of polymer) and is relatively little affected by the amount of crosslinking (concentration of methylenebisacrylamide).

Several equations have been derived for relating the permeability coefficient to pore size. The one used for the present work is the one given by Ferry[8]

$$r = \sqrt{\frac{8K_s}{S}}$$

where r is the average pore radius (in cm.), K_s is the permeability coefficient (in cm.²) and S is the specific water content. This equation is valid for the case of parallel cylindrical pores of circular cross section, assuming the water flow to be governed by Poiseuillés law and also assuming that all the pores open onto the surface and that there is no significant amount of immobilized or "bound" water. Morton[9] has given equations for other types of pore structures, but the above relation was used, for it gave intermediate values of pore size and was used by Madras, *et al.*,[5] in calculating the pore size of cellophane, the permeability of a 10% (95/5) gel being essentially the same as that of uncoated cellophane swollen in water.

Figure 3 shows a plot of the average pore radius (in mμ) as a function of polymer concentration in the gel. The water content S was calculated from the known polymer concentrations in the gels. It appears that the average pore size becomes very large below about 2.5% polymer concentration,

(7) J. W. McBain, "Colloid Science," D. C. Heath & Co., Boston, Mass., 1950.

(8) J. D. Ferry, *Chem. Revs.*, **18**, 373 (1936).

(9) T. H. Morton, *Trans. Faraday Soc.*, **31**, 262 (1935).

which is the minimum concentration at which a gel will form, so that below this value the pores can be considered as infinitely large. As the polymer concentration increases the pore size decreases at a diminishing rate, so that above 35% polymer concentration the pore size is changed relatively little by increasing concentration. Elford and Ferry[10] have suggested that the error in the average pore size determination by this method is not more than 25% for membranes of pore size greater than 20 mμ. Since the pore size of the gels are considerably below 20 mμ the error in the pore size values may be greater in the direction that the calculated values are too small.[8]

An attempt was made to measure the distribution of pore sizes by the method described by Erbe[11] in which isobutyl alcohol is forced through a membrane wet with water, the rate of flow at different pressures being related to pore radius by the equation

$$r = 2\sigma/p$$

where p is the pressure required to force a liquid through a pore at radius r, when the interfacial tension between the liquids is σ. Under a pressure of 30 p.s.i. (the maximum possible in the apparatus used) no isobutyl alcohol would flow through a 10% (95/5) gel when the alcohol was put in the high pressure side of the apparatus and water in the low pressure side, so that it was not possible to calculate even a maximum pore size, but it was possible to calculate a value below which the maximum pore size must lie. Using a water–isobutyl alcohol interfacial tension of 1.73 dynes/cm. and a pressure of 30 p.s.i. this value was calculated to be 17mμ. Examination of the gel disk after contact with isobutyl alcohol showed no change in the appearance of the gel, although putting a portion of the gel into isobutyl alcohol will cause the gel to dehydrate, shrink and become opaque and brittle. Apparently having water in contact with the low pressure face of the disk prevented any dehydration of the gel, so the maximum pore size limit value may be considered as valid within the limits described above.

In considering liquid flow through membranes there is the possibility of transport not only by viscous flow, but by diffusion. Ticknor[12] in considering the flow of water through cellophane showed that some idea of whether the flow was viscous or diffusion could be obtained by calculating a "diffusion coefficient" from the permeability coefficient using the equation

$$D = \frac{RTK_s}{\epsilon V \eta}$$

where D is the diffusion coefficient (in cm.^{2}/sec.), R is the gas constant (in ergs/mole-deg.), T is the absolute temperature (in °K.), K_s is the permeability coefficient (in cm.^{2}), ϵ is the fractional void volume, V is the molar volume (in cc./mole) and η is the viscosity (in poise). For cellophane swollen in water,

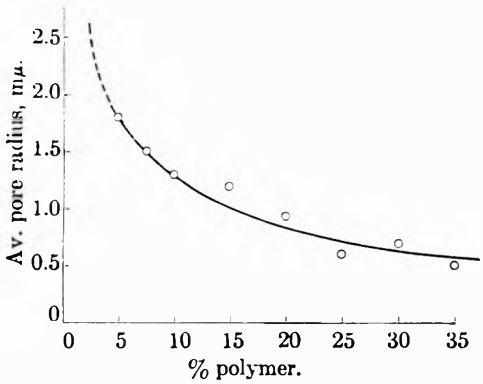

Fig. 3.—Average pore radius of gel as function of polymer concentration.

the D values calculated for water permeation were found to be about ten times the value for the self diffusion coefficient of water, indicting that viscous flow was the predominant transport process in this case.

D values were calculated from the permeability coefficients for the acrylamide gel, using the above equation, the results being shown in Table I. It is apparent that for the more dilute gels the calculated diffusion coefficients are very much larger than the self diffusion coefficient of 2.8 × 10^{-5} cm.^{2}/sec. (at 25°)[13] so that the transport phenomenon can be considered as being primarily viscous flow. For the gels containing 25 to 35% polymer, however, the calculated diffusion coefficient is of the same order of magnitude as the self diffusion coefficient, indicating that in these gels diffusion may be an important factor in the transport process.

TABLE I

CALCULATED "DIFFUSION COEFFICIENTS" FROM PERMEABILITY DATA

% Polymer	$K_s \times 10^{14}$, cm.^{2}	$D \times 10^6$, cm.^{2}/sec.	% Polymer	$K_s \times 10^{14}$, cm.^{2}	$D \times 10^6$ cm.^{2}/sec.
5	37 9	61.0	20	8.8	16 8
7.5	27.0	44.6	25	3.5	7.1
10	18.2	30.9	30	4.3	9.4
15	14.0	25.2	35	2.1	4.9

Ticknor[12] calculated that diffusion would become important when the capillary radius was less than approximately twice the radius of the permeating molecule, but that for capillaries larger than this, viscous flow would predominate. For the 25 to 35% polymer gels the average pore radius is seen to be about 5 Å. (Fig. 3) which is approaching twice the radius of the water molecule (1.5 Å.),[14] so that the transport would be expected to become diffusion dependent.

Acknowledgments.—The author wishes to thank Dr. D. J. Berets for suggesting this work and Dr. G. H. Dorion for many helpful discussions during its course. Professor A. S. Michaels of M.I.T. was most helpful in pointing out the importance of diffusion in this work.

(10) W. J. Elford and J. D. Ferry, *Brit. J. Exp. Pathol.*, **16**, 1 (1935).

(11) F. Erbe, *Kolloid-Z.*, **63**, 277 (1933).

(12) L. B. Ticknor, THIS JOURNAL, **62**, 1483 (1958).

(13) J. H. Wang, C. V. Robinson and I. S. Edelman, *J. Am. Chem. Soc.*, **75**, 466 (1953).

(14) R. A. Robinson and R. H. Stokes, "Electrolyte Solutions," Academic Press, Inc., New York, N. Y., 1955.

THERMAL ANALYSIS OF THE CHROMOUS CHLORIDE–SODIUM CHLORIDE SYSTEM

BY JEROME C. SHILOFF

Pigments Department, E. I. du Pont de Nemours Co., Inc., Wilmington, Delaware

Received May 31, 1960

The phase diagram of the system $CrCl_2$–NaCl was measured. One intermediate compound, Na_3CrCl_5, which melts incongruently at 458°, was found. $CrCl_2$ and Na_3CrCl_5 form a eutectic at 46.3 mole % $CrCl_2$ and 437°. The melting point of $CrCl_2$ was found to be 820°.

Introduction

An interest in solutions of $CrCl_2$ in NaCl by this investigator necessitated study of the condensed phase diagram of that binary system. A thermal analysis was carried out by means of cooling curves of a number of compositions throughout the entire concentration range. Concentrations of the melts were determined after cooling by standard quantitative analytical methods. This paper reports the results of the investigation.

Experimental Procedure

Reagents.—The $CrCl_2$ was prepared *in situ* by the direct chlorination of Electromet electrolytic grade chromium at 850°. The chlorine, which was dried with magnesium perchlorate, was a special oxygen free grade supplied by Mathieson. The sodium chloride was Mallinckrodt's analytical reagent grade. It was dried at 500° *in situ* by the passage of argon through it for one hour. The argon used throughout this study was dried with magnesium perchlorate, and oxygen and nitrogen were removed by passing it over hot titanium turnings.

Apparatus.—The melts were contained in a Vycor glass cell, shown in Fig. 1, placed in a resistance heated tube furnace three inches in diameter and 13 inches long. The temperature of the melt was measured by a calibrated Pt–Pt, 13% Rh thermocouple and continuously recorded on a Minneapolis-Honeywell Brown "Electronik" potentiometer recorder. Measured temperatures were accurate to ±3°. The thermocouple was contained in the agitator-thermocouple well which provided agitation of the melt by a vertically reciprocating motion. The cooling rate of the melt was about 4.5° per minute. It was continuously blanketed by a purge of argon entering through the horizontal side-arm and effusing through the glass wool plug in the top of the cell.

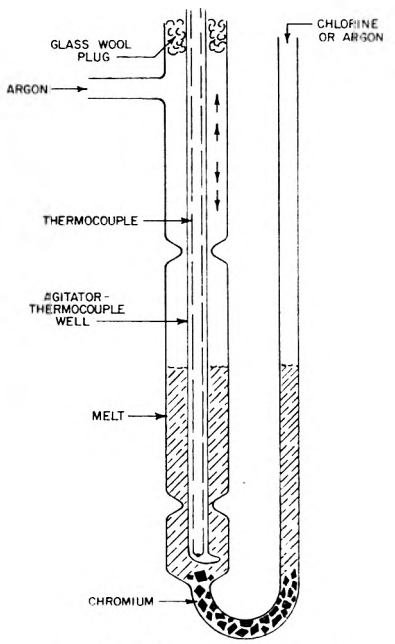

Fig. 1.—Thermal analysis cell.

Procedure.—To load the cell, a quantity of chromium (in pea-sized chunks) was placed in the bottom in the position shown in Fig. 1. NaCl was added to the large tube. The approximate amounts of chromium and NaCl used were determined by the melt concentration desired. Pure $CrCl_2$ was prepared by omitting the NaCl and using a larger amount of chromium.

The NaCl was then dried as described above, after which the cell temperature was increased to 850°, and the argon drying stream replaced by chlorine. The chromium was initially chlorinated to $CrCl_3$, but as the $CrCl_3$ vapor passed over the unreacted chromium downstream it was reduced to liquid $CrCl_2$ which then dissolved in the molten NaCl. Chlorination was terminated before all the chromium had reacted, and the melt was agitated by bubbling argon through it for one hour to make certain that any unreduced $CrCl_3$ would be reduced by the remaining chromium. That this reduction removes all $CrCl_3$ was demonstrated by chemical analysis.

The argon bubbling was then halted, the agitator-thermocouple well started, and cooling of the melt begun. The temperature of the melt, as a function of time, was continuously recorded with the Brown recorder. The various time–temperature inflections and plateaus were plotted as a function of concentration of the cooled melt to give the phase diagram.

Results

The complete phase diagram is shown in Fig. 2. One intermediate compound was found, Na_3CrCl_5.

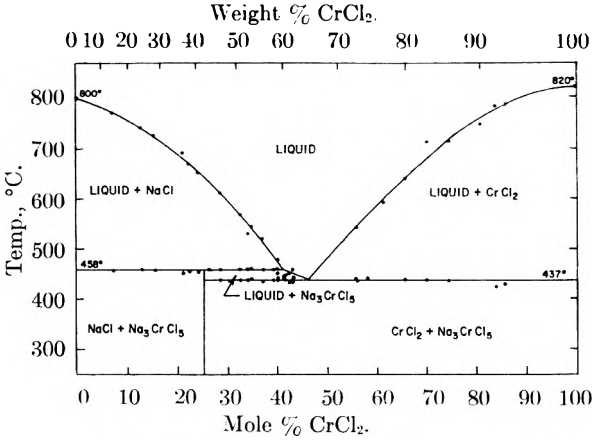

Fig. 2.—$CrCl_2$–NaCl phase diagram.

It melts incongruently at 458°. $CrCl_2$ and Na_3CrCl_5 form a eutectic at 46.3 mole % $CrCl_2$ which melts at 437°. The melting point of pure $CrCl_2$ was found to be 820°. This compares favorably with the literature values of 824°[1] and 815°.[2]

Acknowledgments.—The author wishes to acknowledge his appreciation to Mr. Willard M.

(1) W. Fischer and R. Gewehr, *Z. anorg. Chem.*, **222**, 303 (1935).
(2) H. A. Doerner, U. S. Bureau of Mines Bull. 577 (1937).

Johnston who performed the chemical analyses for this work, and to the Pigments Department of E. I. du Pont de Nemours Co., Inc. for permission to publish these data.

PHASE STUDIES IN THE PORTION OF THE SODA-ALUMINA-SILICA-WATER SYSTEM PRODUCING ZEOLITES

BY ANDREW J. REGIS,[a] L. B. SAND,[a] C. CALMON[b] AND M. E. GILWOOD[b]

Tem-Pres,[a] Inc., State College, Pa.; The Ionac Chemical Co.,[b] Birmingham, N. J.

Received June 8, 1960

Phase studies have been made in the system Na_2O–$NaAlO_2$–SiO_2–H_2O at 100° and atmospheric pressure. The following phases were synthesized: hydroxy-sodalite, hydroxy-cancrinite, faujasite, phillipsites and Linde's zeolite A. Composition triangles showing co-existing phases which crystallize over a range of starting compositions are given for 1, 7, 14, 21 and 30 day runs. These show the disappearance of metastable phases—hydroxy-cancrinite, faujasite and cubic phillipsite, to produce equilibrium or near-equilibrium assemblages in the 30 day runs. The phase relationships obtained after one day at 200 and 300° and saturated vapor pressure also are given. A plot of *n*-heptane adsorption is given for one set of runs. Analcime, albite and nepheline hydrate I appear as decomposition products of zeolite A (195°) and the phillipsites (about 260°). Limiting conditions of composition, temperature and time were determined for the hydrothermal synthesis of Barrer's Na-phillipsite types (cubic, orthorhombic and tetragonal).

Introduction

In this study we have been concerned with systematically synthesizing and determining the phase relationships and *n*-heptane adsorption of the crystals produced from preparations of colloidal silica and soluble salts of sodium and aluminum at a temperature of 100° and atmospheric pressure. The effect of time in determining the co-existing phases crystallizing from a given starting composition at this temperature and pressure was studied by making a series of runs of 1, 7, 14, 21 and 30 day duration. The co-existing phase produced in 1 day at 200 and 300° at saturated vapor pressure also were determined. Data not obtained in this synthetic study were possible variations in the amount of aluminum substitution for silicon in the various zeolite structures. Also not determined were the compositions of the liquid phases.

Syntheses were carried out using soluble salts and colloidal silica rather than glasses, dried co-precipitated gels, calcined gels formed by evaporation of soluble salts, mixtures of soluble oxides or other widely used methods of preparation. Although these latter preparations have been effective for hydrothermal phase studies at elevated temperatures, they are not suitable starting materials, with the possible exception of glasses, for studies below about 200°. These network hydrated aluminosilicates crystallize rapidly from preparations of colloidal silica and soluble salts and it is possible to study the *p–t–x* conditions necessary to produce the low temperature zeolites and co-existing phases. Previous phase studies which include the sodium zeolite analcime as a phase, are those of Friedman,[1] of Yoder[2] and of Sand, Roy and Osborn.[3] Syntheses of sodium zeolites without determining in detail the phase relationships are by Barrer[4] on mordenite, Barrer and White[5] on analcime and mordenite, Barrer and Grüter[6] on faujasite, and Ames and Sand[7] on mordenite.

Breck,[8] *et al.*, reported the synthesis of the sodium zeolites—mordenite and faujasite—and of their new synthetic zeolite A in addition to the syntheses of numerous other zeolites. This was a significant contribution to experimental phase chemistry in that it pointed the way toward the physical–chemical study of aluminosilicates formed by hydrothermal solutions at low temperatures. More recently Barrer, Baynham, Bultitude and Meier[9] have reported the syntheses of sodium zeolites in excess sodium hydroxide solutions from temperatures of 60 to 250°. These sodium zeolites include analcime, mordenite, zeolites of the harmontone, faujasite and chabazite groups, zeolite A, a zeolitic phase related to rhodesite, in addition to basic sodalite, basic nosean and a phase related to nepheline hydrate.

Abbreviations used in the figures and tables are: A = zeolite A; Ab = albite; Ac = analcime; Am = amorphous silica; C = hydroxy-cancrinite; F = faujasite; NH = nepheline hydrate I; P_c = cubic phillipsite; P_t = tetragonal phillipsite; P_0 = orthorhombic phillipsite; and S = hydroxy-sodalite.

Methods of Investigation

The objective of this study was to determine the phase relationships of the crystalline phases only, and as soluble components were involved, a constant solid: liquid weight ratio of 1:6 was selected. The diagrams only show, therefore, the co-existing phases produced from a given starting mixture with this proportion of specific solids. The experimental procedure used was: 1, a solid: liquid weight ratio of 1:6; 15 g. of solid in the 100° runs, 3 g. in the higher temperature runs; 2, the sequence of adding starting chemicals to distilled water: (a) NaOH, (b) $NaAlO_2$, and (c) Ludox—a commercial dispersed ammonia-stabilized colloidal silica; 3, blended in a high speed mixer for two minutes; 4, run in sealed glass jars or silver-lined pressure vessels; 5, on completion of runs—filtered, washed to *p*H 8 and dried at 100°; 6, the solids analyzed by optical and X-ray diffraction methods.

(1) I. Friedman, *J. Geol.*, **59**, 19 (1951).
(2) H. S. Yoder, *Am. J. Sci.*, **248**, 312 (1950).
(3) L. B. Sand, R. Roy and E. F. Osborn, *Ec. Geol.*, **52**, 169 (1957).
(4) R. M. Barrer, *J. Chem. Soc.*, 2158 (1948).
(5) R. M. Barrer and E. A. D. White, *ibid.*, 1561 (1952).
(6) R. M. Barrer and W. F. Grüter, *Helv. Chim. Acta*, **39**, 518 (1956).
(7) L. L. Ames and L. B. Sand, *Am. Mineralogist*, **43**, 476 (1958).
(8) D. W. Breck, W. G. Eversole, R. M. Milton, T. B. Reed and T. L. Thomas, *J. Am. Chem. Soc.*, **78**, 5963 (1956).
(9) R. M. Barrer, J. W. Baynham, F. W. Bultitude and W. M. Meier, *J. Chem. Soc.*, 195 (1959).

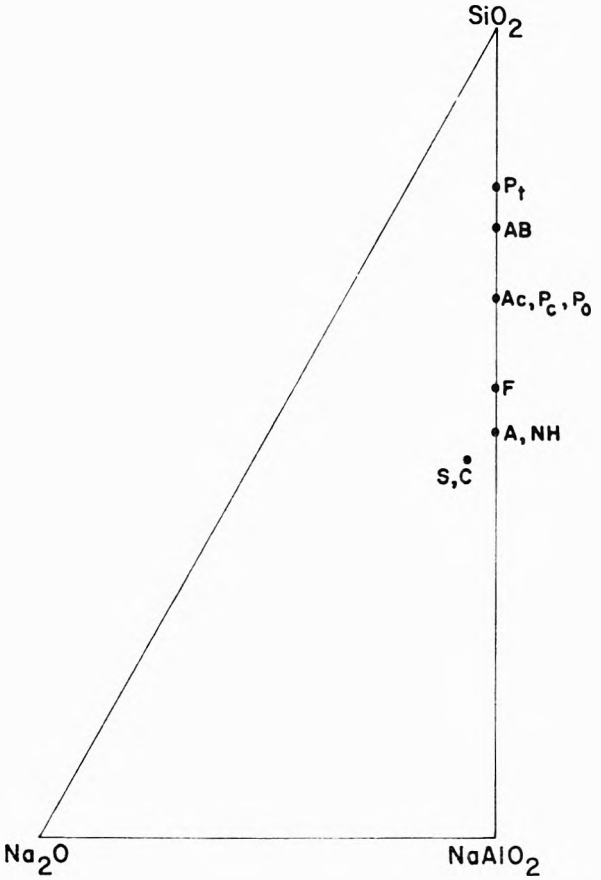

Fig. 1.—A plot of the anhydrous compositions, on a mole per cent. basis, of the crystalline phases.

Starting compositions were taken at the intersections of selected constant ratio lines of $Na_2O:Al_2O_3$ and $Al_2O_3:SiO_2$. The other variable, time, covered a reasonable range to show the disappearance of several metastable phases in the system.

A kinetic system of this type presents a problem in giving a graphical representation of the data. It was found that the standard representation for co-existing equilibrium phases in a hydrothermal system was applicable to the non-equilibrium assemblages produced. The phase relationships are represented by locating the components Na_2O, Al_2O_3 and SiO_2 at the base apexes of a tetrahedron and projecting all compositions to this base from the H_2O apex. On the resulting diagrams, the composition producing a single crystalline phase is represented by a point, two phases are produced along a join, and three phases co-exist within a triangle. Under the non-equilibrium conditions studied, where several components are soluble, and metastable phases are produced, the starting composition producing a single crystalline phase changes with time. The diagrams show clearly the interaction in the system between the crystals produced and the solution with time as equilibrium is approached.

The adsorption number given for a product expresses the relative reduction per unit weight of material in pressure of the system due to the adsorption of the volatile liquid by the solid. The apparatus used for determining this value is described below.

The unit consisted of a glass bulb (150 ml.), jacketed for steam heating, with a "T" at the bottom (one outlet leading to a vacuum pump and the other to a manometer), and at the top a removable funnel. The bottom of the funnel, resting in the center of the bulb, had a hook to which a glass cup could be suspended. The sample could be weighed out (0.15 g.) in the cup while resting in a weighing bottle. In the neck of the funnel a porous disc was built in and kept covered with mercury as a seal.

A known volume of volatile liquid (*n*-heptane) was introduced into the evacuated system with a calibrated dropper in contact with the porous disc under the mercury. The pressure in the manometer was noted. The heptane was swept out. The weighed sample in the cup was suspended into the interior and the system evacuated once more. The adsorbate was then introduced and the new pressure observed after the system came to equilibrium. The difference in pressure divided by the weight of the solid product gave the adsorption number. Checks on the system were run frequently with one product set as a control.

Results

Phase Relationships.—The co-existing solid phases formed at 100° in the system were faujasite, Barrer's phillipsite types, hydroxy-sodalite, hydroxy-cancrinite, zeolite A and amorphous silica with adsorbed sodium. A diagram plotting the anhydrous compositions on a mole per cent. basis of the crystalline phases is given in Fig. 1. The critical phase data from the 1, 7, 14, 21 and 30 day runs at 100° are given in Table I. The phase relationships are diagrammed in Figs. 2 and 3. The non-equilibrium phase relationships observed for runs of one day at 200 and 300° at saturated vapor pressure are given in Fig. 4 with an equilibrium diagram for comparison. Nepheline hydrate I ($Na_2O\cdot Al_2O_3\cdot 2SiO_2\cdot H_2O$) is a synthetic phase first reported by Barrer and White.[8] Starting compositions producing a single crystalline phase at 100° under the experimental conditions specified are given in Table II. In Fig. 5 are drawn adsorption contours for *n*-heptane on the crystalline products made at 100° atmospheric pressure, and one day duration. The contours drawn from calculated values were plotted on the phase diagram shown on the left in Fig. 1, taking the adsorption of zeolite A as 80, faujasite as 135, and cubic phillipsite as 20. The contours drawn from the observed adsorption values are in fairly good agreement except in the high silica region where reaction rates are slow.

Description of Crystalline Phases.—Faujasite occurred as a metastable phase, appearing in the one and seven day runs only. It formed as irregularly shaped crystals and aggregates less than 5 μ in size. The index of refraction was 1.465, and no birefringence was noted.

The synthetic zeolite A, not yet reported as a natural mineral, was synthesized as a co-existing phase over a wide range of starting compositions in runs from 1–30 days. As can be seen in the phase diagrams, in the composition triangle Na_2O–$NaAlO_2$–zeolite A, two of the phases are soluble and in this field of starting compositions, zeolite A is produced as the only crystalline phase.

It occurred as isotropic, very small cubic crystals and aggregates. The size increased from less than 5 μ in the short runs to 20 μ in the longer runs. The index of diffraction was 1.467. This phase is produced up to 195° saturated vapor pressure.

The three types of phillipsite made were the cubic, tetragonal and orthorhombic symmetry types first reported by Barrer, *et al.*,[10] and their nomenclature is followed. The three phases are similar and appear to fall into the phillipsite–harmotome group. Our X-ray diffraction data agreed essentially with their data.

The compositions of the cubic and orthorhombic types are very similar, having the approximated

(10) R. M. Barrer, J. W. Baynham, F. W. Bultitude and W. M. Meier, *ibid.*, 195 (1959).

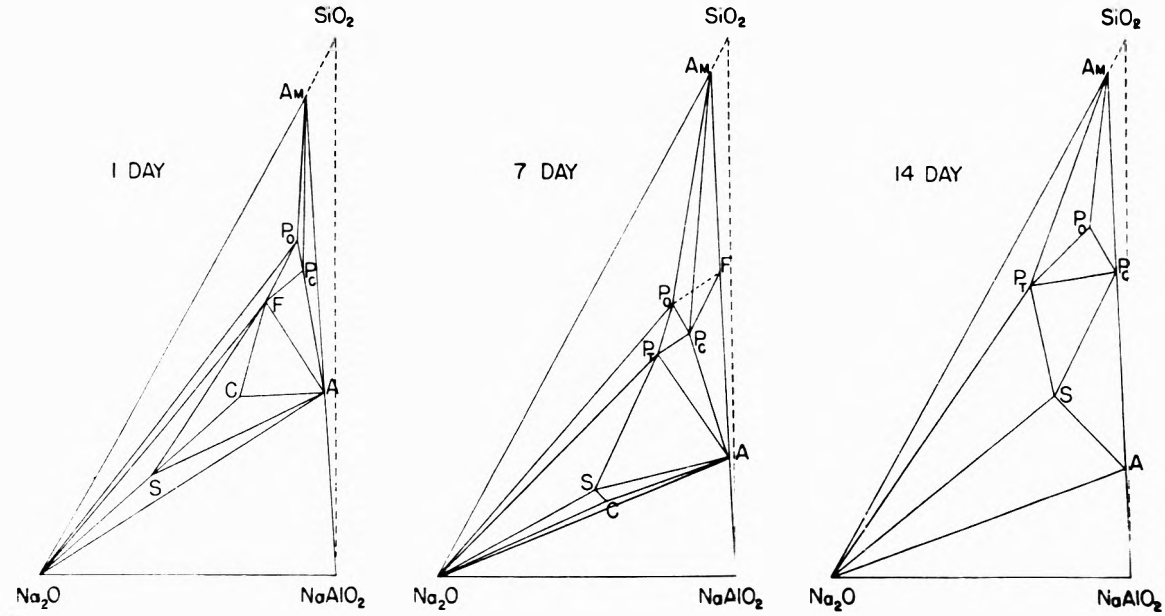

Fig. 2.—Phase relationships observed for crystals produced at 100° after 1, 7 and 14 day runs at atmospheric pressure.

TABLE I

CRITICAL PHASE DATA FROM 1, 7, 14, 21, AND 30 DAY RUNS AT 100° AND ATMOSPHERIC PRESSURE

Starting compositions given in molar ratios of $Na_2O:Al_2O_3:SiO_2$. Minor phases in parentheses.

Starting composition	Phases 1 Day	7 Day	14 Day	21 Day	30 Day
3:1:0.5	S + (C)	A + S + (C)	S + (A)	S + (A)	S + (A)
3:1:3	F + (S) + (A)	Pc + Am	S	S + (P)	Pt + (S)
2:1:0.5	A + (Am)	A + (Am)	S	S	S
2:1:3	F + (Am)	Pc + F + (Am)	P + (S)	Pt	Pt + (S)
1.5:1:1	A + (S)	A + S	S + (P)	S + (P)	S + (P)
1.5:1:2	A + (F)	Pt + A	Pt	Pt + (S)	Pt + S
1.25:1:0.5	A + (Am)	A + (Am)	A	S + (A)	S + (A)
1.25:1:1.5	A + (Am)	Pc + (A)	Pc + (S)	Pc + (S)	Pt + Po + (S)
1.25:1:3	F + (Pc)	Pc + F	Pt + Pc	Po + (A)	A + Po + Pt
2:1:6	Am	Am + Pc	Am	Pc + (A)	Pt + Pc + A
1.5:1:10	Am	Am + Pc	Am	Am	Am
2.5:1:4	F + (S)	Po + (Am)	Pt + S	Pt + (S)	Pt
10:1:1	S	S + (P)	S + (P)	S + (P)	S + (P)
10:1:4	S + (P)	S + Po	S	S + (P)	A + (S) + (P)
10:1:10	F + (Po)	Am + Pt	Pt + (S)	S + (P)	Pt + (A) + (S)
10:1:25	Am	Am	Am + A	Pt + (Am)	Pt + (A) + (S)
3:1:2	A	S + (P) + (A)	S	S	S + (A)
5:1:4	F + (Po)	S + (P) + (Am)	Pc + (A) + (S)	S + (P)	S
5:1:6	F + (Po)	Am	Pt + (S)	Pt	Pt
2.5:1:3	A + (F)	Pc + (Am)	S + (P)	Pt + (A) + (S)	Pt + (S)
2:1:1	A	Am + Pc	S	S	S
2:1:4	Am + (F)	Pc + Am	Pt + Pc	Pt + Po + (A)	Pt + Po + A

composition of $0.6Na_2O{\cdot}Al_2O_3{\cdot}4SiO_2{\cdot}7\text{–}8H_2O$. The tetragonal phillipsite type had an average composition of $Na_2O{\cdot}Al_2O_3{\cdot}8SiO_2{\cdot}16\text{–}20H_2O$.

Chemical analysis of the three phillipsite types are given in Table III.

Cubic Na-phillipsite crystallized from runs up to three weeks duration, but in the 30 day runs it was not observed. It occurred as irregular and lath-shaped crystals less than 10 μ in size. The index of refraction varied from 1.460 to 1.486 with 1.477 as the mean index. No birefringence was noted.

The orthorhombic Na-phillipsite was difficult to crystallize as a pure phase, and only two of the starting compositions used, in a 7 day and in a 21 day run, produced it as a single phase. In all the other runs, it occurred associated with the cubic and tetragonal types and with zeolite A and faujasite along with amorphous silica. It occurred as irregularly shaped crystals less than 5 μ in size and as spherulitic aggregates. They exhibited very low birefringence and were difficult to distinguish from the cubic type. The indices of refraction were n_α 1.474, n_β 1.477, and n_γ 1.482.

The tetragonal Na-phillipsite occurred only in runs longer than three days. Three distinct types of habit were noted. The most typical were first or second-order prisms and pyramids in very small, 5 to 10 μ size crystals. Also noted in many of the

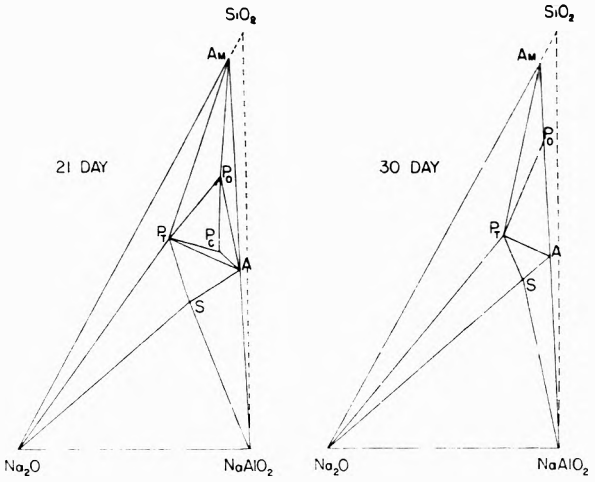

Fig. 3.—Phase relationships observed for crystals produced at 100° after 21 and 30 day runs at atmospheric pressure.

TABLE II

STARTING COMPOSITIONS, GIVEN IN MOLE RATIOS OF Na_2O:Al_2O_3:SiO_2, WHICH PRODUCE A SINGLE CRYSTALLINE PHASE AT 100°

The compositions along joins with soluble components are not given, nor in the area for zeolite A formed by joins with the two soluble components. These can be obtained by adding the soluble component(s) to the compositions listed.

Phase	Duration of run, days	Starting composition
A	1	1.1:1:1
	7	1.1:1:0.6
	14	1.1:1:0.5
	21	1.1:1:1.5
	30	1.2:1:1.8
S	1	7.0:1:2
	7	3.6:1:1
	14	2.0:1:1.6
	21	2.3:1:1.7
	30	1.6:1:1.8
C	1	3.0:1:2
	7	3.0:1:0.7
F	1	3.0:1:4
	7	1.2:1:3
P_c	1	1.7:1:3.5
	7	1.6:1:2
	14	1.2:1:2.3
	21	1.5:1:2.3
P_t	7	2.5:1:2.3
	14	6.0:1:8
	21	5.0:1:7
	30	3.0:1:4.5
P_0	1	2.0:1:5.5
	7	2.5:1:3.5
	14	2.0:1:5.5
	21	1.8:1:5.5
	30	1.5:1:7

preparations were spherulites, up to 85 μ, commonly showing undulatory extinction and very low birefringence. In the 30 day runs, the tetragonal phillipsite occurred as complex twins of first and second-order prisms. No differences in indices of refraction were noted for the three habits. They were n_ω 1.491 and n_ϵ 1.495.

TABLE III

CHEMICAL ANALYSIS—MOLAR RATIO OF COMPONENTS TO ALUMINA

	Alumina	Silica	Na_2O	H_2O
A Tetra	1.0	7.8 (7.6)[a]	0.7 (0.9)[a]	19.8 (16.0)[a]
B Ortho	1.0	4.2	.5	7.9
C Cubic	1.0	4.1 (4.2)[a]	.6 (0.6)[a]	6.8 (6.7)[a]

[a] Analysis on a new sample preparation.

In the short runs sodalite occurred as very small, irregularly shaped crystals less than 5 μ, and as spherulitic aggregates up to 35 μ in size. Both habits were isotropic and varied in index of refraction from 1.489 for the small crystals to 1.504 for the spherulites.

In the longer runs, the sodalite occurred as isotropic or very low birefringent spherulitic crystal aggregates with a prismatic or radiating texture. These were up to 90μ in size and the index of refraction varied from 1.500 to 1.514. The index of refraction for the very small crystals ranged from 1.489 for those crystallized in 7 day runs to 1.499 for those crystallized in 30 day runs.

Cancrinite occurred only as a minor metastable phase, usually associated with sodalite in the 1 and 7 day runs. It occurred as very small, irregularly shaped crystals, exhibiting moderate birefringence. Its mean index of refraction was 1.512.

Discussion

In addition to the commercial interest in the adsorptive properties of zeolites (Milton[11]), the phase chemistry data from studies in systems producing synthetic zeolites are also of interest in interpreting the paragenesis of this group of aluminosilicates. Due to the industrial desirability of hydroxy phases, and the fact that reactions occur most rapidly in the highly alkaline systems, practically all of the work has been done with the alkali added as a hydroxide. Although this has been the simplest place to initiate studies of the phase relationships in these systems, future studies of geological interest undoubtedly will include other anions such as $(CO_3)^{-2}$, Cl^- and $(SO_4)^{-2}$. The zeolite structures form rapidly and persist under the highly alkaline conditions, but there are no known natural occurrences where these extreme conditions occur. For example, hydroxy-cancrinite and hydroxy-sodalite are known only as synthetic phases. It is seen from the phase diagrams in the shorter runs in this system that the Linde zeolite A is formed from the widest range of starting compositions, yet it is the only crystal structure encountered that has not been found as yet in nature. Perhaps it has not been identified in samples prior to the publication of Breck's data on the synthetic material in 1956, or perhaps deposits in which it might occur have not been studied in sufficient detail using modern instrumental methods. The probability of this is illustrated by the recent work of Deffeyes,[12] who has found large quantities of the hitherto rare zeolite, erionite in altered volcanic ash in Nevada. It was found experimentally that calcium and carbonate ions do not prevent the formation of zeo-

(11) R. M. Milton, U. S. Patent 2,882,243 (1959).

(12) K. S. Deffeyes, *Am. Mineralogist*, **44**, 501 (1959).

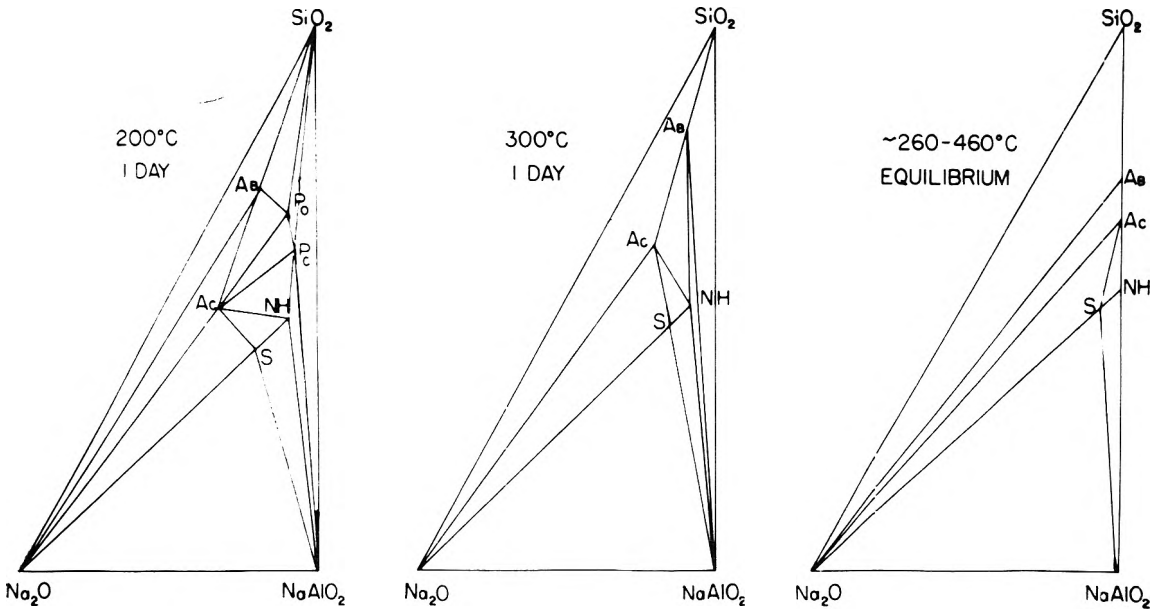

Fig. 4.—Phase relationships observed for crystals produced at 200 and 300° after one day at saturated vapor pressure. An equilibrium phase diagram is given for comparison.

lite A, and that zeolite A forms from volcanic glass. A hot spring alteration of volcanic ash in an alkali basin and perhaps an area where there is active trona disposition are likely localities to search for natural zeolite A. The presence of chloride appears to preclude the formation of zeolite A, so it is less likely that zeolite A would be found under normal evaporite conditions, although zeolite A crystallizes from solutions at 25°.

To evaluate the effects of the various anions, as well as varying the ratios of sodium, potassium and calcium, requires an extensive and long-range program. Barrer, *et al.*,[10] already have synthesized numerous zeolites using other cations and anions, but in order to interpret the genesis in nature of the zeolites and associated minerals, systematic determinations of both the nonequilibrium and equilibrium phase relationships would be needed. The non-equilibrium data are especially useful in studying the crystallization and subsequent reaction and disappearance of the metastable phases. Thermal and chemical stabilities on the natural zeolites give supplementary data, but usually on these only the upper limit of hydrothermal stability is determined. On many of the natural zeolites, it is difficult to isolate sufficient quantities of a phase to make a series of hydrothermal runs and to obtain even partial chemical analyses, particularly with respect to the exchangeable ions. Determination of the stabilities of these natural hydrated aluminosilicates containing large amounts of exchangeable ions also involves the problem of leaching of the soluble ions which occurs during the establishment of equilibrium between the solid and fluid phases.

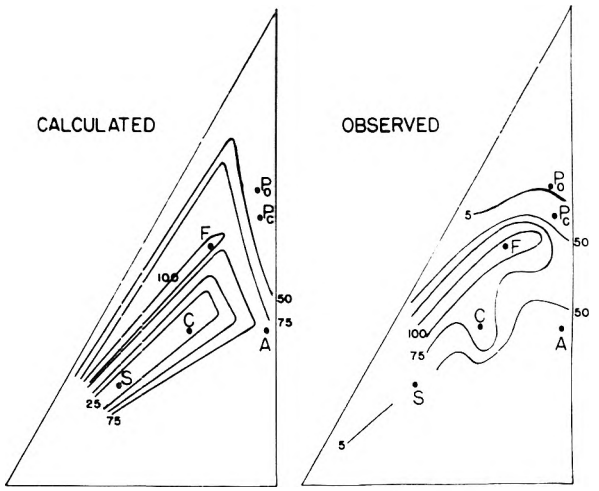

Fig. 5.—*n*-Heptane adsorption contours on calculated and observed values on crystalline products obtained at 100° and atmospheric pressure after one day.

One important conclusion reached in this study is that phase relationships at low temperatures of the hydrated alkali aluminosilicates can be determined by close control of the experimental procedure, especially of consistency in the reacting materials used and in maintaining a constant weight ratio of solids to liquid.

Acknowledgments.—We gratefully acknowledge the assistance of James Murray and James DiPiazza in the phase studies and C. Irons in the adsorption studies.

NOTES

NEAR ULTRAVIOLET ABSORPTION OF THE METHYLTHIOPHENES

BY JEAN SICÉ[1]

Department of Pharmacology, The Chicago Medical School, Chicago 12, Illinois

Received February 3, 1960

The physical[2] and chemical properties of thiophene have emphasized repeatedly the aromatic character of this heterocycle. Such a character also has been invoked to explain the near ultraviolet spectral absorption of the same molecule.[3] Differences nevertheless have been observed between the spectral absorptions of thiophene and of benzene or of their corresponding derivatives;[4,5] certain of these differences are discussed in the present communication.

Experimental

The ultraviolet spectral absorptions were determined in hexane solution with a Beckman DK-1 quartz recording spectrometer. All the substances had been immediately distilled under nitrogen through a 50-plate all-glass Podbielniak column until spectroscopically pure. The results are reported in Table I.

TABLE I

SPECTRAL ABSORPTION OF THE METHYLTHIOPHENES

Substance	Maximum, cm.$^{-1}$	f^k
Thiophene[a]	43,200	0.10
2-Methyl[b]	42,700	.20
2,5-Dimethyl[c]	42,400	.19
3-Methyl[d]	42,700	.14
3,4-Dimethyl[e]	42,000	.12
2,4-Dimethyl[f]	42,800	.17
2,3-Dimethyl[g]	42,800	.16
2,3,5-Trimethyl[h]	42,200	.17
2,3,4-Trimethyl[h]	42,000	.13
2-Methoxy[i]	41,400	.12
2-Methyl-5-methoxy[i]	40,200	.16

The spectral absorptions of these substances have been reported previously by: [a] American Petroleum Institute Research Project 44, Ultraviolet Data, Carnegie Institute of Technology, Pittsburgh, Pa., Spectrogram 208 (1948). [b] *Ibid.*, 541 (1953). [c] *Ibid.*, 312 (1949). [d] *Ibid.*, 463 (1952). [e] *Ibid.*, 313 (1949). [f] *Ibid.*, 311 (1949). [g] *Ibid.*, 310 (1949). [h] J. Sicé, *J. Org. Chem.*, 19, 70 (1954). [i] Reference 4. [k] The oscillator strength, $f = 4.32 \times 10^{-9} \int \epsilon d\nu$.

Discussion

The spectral absorption of the methylthiophenes was more intense than that of thiophene; the influence of the methyl group was greater in the 2- than in the 3-position. The symmetrical 2,5- or 3,4-dimethylthiophene absorbed slightly less than the corresponding monosubstituted thiophene; the intensities of the absorptions of the asymmetrical 2,3- and 2,4-dimethylthiophene were intermediate between those of the corresponding 2- and 3-methylthiophene. The comparable intensities of the two asymmetrical dimethylthiophenes indicated that the effect of each methyl group was exerted directly on the electronic structure of the ring, and that the interaction of the methyl groups was negligible. The different intensities of the two trimethylthiophenes confirmed these correlations.

The explanation of the different effects of the methyl group, when placed in the 2- or in the 3-position of the heterocycle, was found by a comparison of the spectral absorptions of different 2-substituted thiophenes. Their intensities varied inversely as the electrophilic character of the substituents, decreasing from the 2-iodo to the 2-bromo, to the 2-chloro,[6] and to the 2-methoxythiophene. This effect, which is diametrically different from that observed with the corresponding benzene derivatives,[7] could be related to the respective strengths of the electrophilic character of the sulfur atom and of the substituents. The normal effect of a strongly electrophilic group would be opposed by the similar character of the heteroatom; the migration of charge between the ring and the substituent would therefore be small,[8] and so was the intensity of the spectral absorption of 2-methoxythiophene. A weak electrophilic group, being nucleophilic with respect to the heteroatom, would become an appreciable electron donor to the ring; the migration of charge and the intensity of the absorption of 2-iodothiophene[6] were correspondingly large. The intensity of the spectral absorptions in the 3-substituted series followed a pattern opposite to that of the 2-substituted series; they varied directly as the electrophilic character of the substituents, increasing from the 3-methoxy to the 3-bromothiophene,[8,9] as in the corresponding benzene derivatives.[7]

The near ultraviolet absorption band of thiophene was uniformly displaced toward lower frequencies when methyl groups were present in either position of the ring. The shifts of the absorption bands of the 2,5- and 3,4-dimethylthiophene and of the trimethylthiophenes suggested that the displacement was greater with the substituent in the 3- than in the 2-position. The same effects were observed with different electron donating substituents. The absorption band of thiophene was displaced toward progressively lower frequencies from the 2-methyl to the 2-bromo[6]

(1) This investigation was supported by a Senior Research Fellowship (SF-283) and by a Research Grant (C-4114) from the U. S. Public Health Service.

(2) H. C. Longuet-Higgins, *Trans. Faraday Soc.*, **45**, 173 (1949); J. Metzger and F. Ruffler, *J. chim. phys.*, **51**, 52 (1954).

(3) G. Milazzo, *Gazz. chim. ital.*, **83**, 787 (1953).

(4) J. Sicé, *J. Am. Chem. Soc.*, **75**, 3697 (1953).

(5) O. Dann and H. Distler, *Chem. Ber.*, **87**, 365 (1954).

(6) F. S. Boig, G. W. Costa and I. Osver, *J. Org. Chem.*, **18**, 775 (1953).

(7) W. W. Robertson and F. A. Matsen, *J. Am. Chem. Soc.*, **72**, 5252 (1950).

(8) The changes in the intensities of the spectral absorptions of the alkyl and halogenothiophenes were directly proportional to the directions and to the magnitudes of their electric dipole moments; R. T. Charles and H. Freiser, *ibid.*, **72**, 2233 (1950); M. T. Rogers and T. W. Campbell, *ibid.*, **77**, 4527 (1955).

(9) S. Gronowitz, *Arkiv Kemi*, **13**, 239 (1958).

(42,400 cm.$^{-1}$), to the 2-methoxy, and to the 2-iodothiophene[6] (41,200 cm.$^{-1}$); or from the 3-methyl to the 3-bromo (41,500 cm.$^{-1}$) and to the 3-methoxythiophene[9] (39,500 cm.$^{-1}$). These results indicated that the decrease of the excitation energy of the near ultraviolet absorption of thiophene was related to the mesomeric effects of the substituent, whether it be in the 2- or in the 3-position. In this respect thiophene resembled benzene.[7] The difference between the excitation energies of the isomeric 2- and 3-isomers could not be attributed to an inductive effect of the substituent, since such an effect would have elicited the opposite result. This difference indicated furthermore a decrease of the mesomerism in the 2-position of the thiophene molecule.

NEAR ULTRAVIOLET ABSORPTION OF THE ORGANIC SULFIDES

By Jean Sicé[1]

Department of Pharmacology, The Chicago Medical School, Chicago 12, Illinois

Received February 3, 1960

The near ultraviolet spectral absorption of the saturated alkyl sulfides[2,3] showed two bands. The strongest absorption (f, *ca.* 0.03) occurred about 46,500 cm.$^{-1}$. This first band underwent a blue shift of approximately 1100 cm.$^{-1}$ when the spectral absorptions were determined successively in hexane and in ethanol solution. The blue shift indicated that the absorption was related to a n→B transition of the unpaired 3p electrons of the heteroatom.[4] The nucleophilic effect of the alkyl groups influenced the energy of these unpaired electrons because the intensity of the absorption of the 46,500 cm.$^{-1}$ band varied directly as the inductive power of the carbon chains, increasing from ethyl sulfide (f, 0.02) to *t*-butyl ethyl sulfide (f, 0.03) and to *t*-butyl sulfide (f, 0.04). The excitation energy of the n→B transition decreased simultaneously, the band of *t*-butyl sulfide occurring at a frequency 700 cm.$^{-1}$ lower than that of ethyl sulfide.

The second absorption band of the saturated alkyl sulfides was observed about 44,000 cm.$^{-1}$; this band did not undergo a blue shift, and it was not present in the spectral absorption of *t*-butyl sulfide.[2] The 44,000 cm.$^{-1}$ band, therefore, indicated a transition between delocalized molecular orbitals; these are occupied in the saturated sulfides by electrons that can be contributed only by the sulfur and by the adjacent carbon atoms.[5] The sulfur orbitals are occupied by the lone-pair 3pd electrons[6] of the heteroatom; the carbon orbitals are occupied by the virtual unshared electrons which result from the hyperconjugation[7] of the two methylene groups which are next to the sulfur atom. The 44,000 cm.$^{-1}$ band of the saturated sulfides then can be assigned tentatively to a N → V transition between the delocalized orbitals of the C–S–C group.

TABLE I

NEAR ULTRAVIOLET SPECTRAL ABSORPTION RELATED TO THE N → V TRANSITIONS OF THE ALIPHATIC SULFIDES

Substance	Max., cm.$^{-1}$	f[a]	Max., cm.$^{-1}$	f[a]
t-Butyl S	....	0	....	0
t-Butyl ethyl S	*ca.* 44,000	*ca.* .002	....	0
Ethyl S	*ca.* 44,000	*ca.* .002	....	0
t-Butyl vinyl S	43,600	.10	*ca.* 40,000	*ca.* .07
Ethyl vinyl S	42,700	.13	40,000	.05
Vinyl[b] S	41,400	.15	38,600	.13

[a] The oscillator strength, $f = 4.32 \times 10^{-9} \int \epsilon d\nu$. [b] The results of the present investigation [$\lambda_{max}^{hexane\ or\ ethanol}$ 242 mμ. (ϵ 8,500) and 259 mμ. (ϵ 7,400)] confirmed the data of H. Mohler and J. Sorge, *Helv. Chim. Acta.*, **23**, 1200 (1940). They differed from the values which have been reported by C. C. Price, *et al.*, *J. Am. Chem. Soc.*, **75**, 4747 (1953); **81**, 2672 (1959).

The substitution of one alkyl group of the saturated aliphatic sulfides by a vinyl group decreased slightly the excitation energy of the transition; the intensity of the absorption increased markedly. Both these changes were more pronounced with the hyperconjugated[7] ethyl vinyl sulfide than with the non-hyperconjugated *t*-butyl vinyl sulfide. The increase of the absorption must therefore be related to the extent of the delocalization of the carbon 2p orbitals in the C–S or C–S–C group. The substitution of the second saturated alkyl group by a vinyl group, as in vinyl sulfide, further decreased the excitation energy, and increased the intensity of the absorption of the C–S–C group. The 42,000–44,000 cm.$^{-1}$ transition appears, therefore, to be a constant feature of the C–S–C or C–S group, regardless of the π-electronic constitution of the rest of the molecule.

The vinyl sulfides had a second band of absorption which corresponded, in energy and in intensity, to a similar band of the iso-electronic polyenes.[8] The second band of the vinyl sulfides may be assigned, by analogy, to the N → V transition of the respective four (alkyl vinyl sulfides) or six (vinyl sulfide) molecular orbitals that are completely delocalized.

Thiophene[9] and thianaphthene[10] vapor have a number of electronic transitions which have been assigned to their aromatic systems. These substances also have at, respectively, 42,990 and 43,070 cm.,$^{-1}$ a transition which has remained unassigned. The excitation energy of this electronic transition is similar to that of the segregated transition of the aliphatic sulfides; such a similarity suggests that

(1) This investigation was supported by a Senior Research Fellowship (SF-283) and by a Research Grant (C-4114) from the U. S. Public Health Service.

(2) E. A. Fehnel and M. Carmack, *J. Am. Chem. Soc.*, **71**, 84 (1949).

(3) W. E. Haines, *et al.*, This Journal, **58**, 270 (1954).

(4) G. J. Brealey and M. Kasha, *J. Am. Chem. Soc.*, **77**, 4462 (1955).

(5) *Cf.* W. T. Simpson, *ibid.*, **73**, 5363 (1951); **78**, 3585 (1956).

(6) W. Moffitt, *Proc. Roy. Soc.* (*London*), **A200**, 409 (1949).

(7) The alkyl groups hyperconjugate with the electrophilic sulfur atom as they do with the benzene ring; *cf.* F. A. Matsen, W. W. Robertson and R. L. Chuoke, *Chem. Revs.*, **41**, 273 (1947). The intensity of the absorption and the strength of the hyperconjugating effect decreased concomitantly in both cases from ethyl to isopropyl to *t*-butyl. The wane of the electronic transition cannot be attributed to a steric effect since the three point group C–S–C has obligatorily a planar configuration.

(8) *s-cis*-Butadiene absorbs in the 42,000 cm.$^{-1}$ region of the spectrum; A. D. Walsh, *Quart. Revs.*, **2**, 73 (1948). Hexatriene has an intense band (f, 0.14) with a maximum at 38,800 cm.$^{-1}$; G. F. Woods and L. H. Schwartzman, *J. Am. Chem. Soc*, **70**, 3394 (1948).

(9) G. Milazzo, *Gazz. chim. ital.*, **78**, 835 (1948).

(10) R. C. Heckman and H. Sponer, *Phys. Rev.*, **91**, 242 (1953).

the transition of the cyclic sulfides could also be a segregated transition of their C–S–C group.

The segregated N → V transition is not exclusive with the C–S–C group; it also appeared in the oxygen analogs of the sulfides. The first absorption of vinyl ether[11] or of furan,[12] in the vapor phase, occurs around 49,200 cm.$^{-1}$. Such an excitation energy is too high for a *s-cis*-dienic structure;[8] it might therefore be related to a transition of the system of π-electrons of the C–O–C group which is common to both the open and the cyclic molecule. The delocalized orbitals of this quadruplet remain strictly localized within the C–O–C group; they never mix with the π-orbitals of the other ethylenic groups of the molecule, because neither vinyl ether nor furan has a transition that may be related to a sextet.

The segregation of the quadruplet of the C–X–C group[5] could depend on the intensity of the electrophilic character of the heteroatom, because the localization of the quadruplet is the rule with the highly electrophilic oxygen atom. The localization would occur with the sulfur atom only when the π-electrophilic character of the heteroatom is increased above its normal level. This increase could result from the excitation of the sulfur atom.

Experimental

All the substances were distilled under nitrogen through a 50-plate all-glass Podbielniak column until spectroscopically pure. The ultraviolet spectral absorptions were determined with a Beckman DK-1 quartz recording spectrometer; all the values were obtained in hexane solution, unless otherwise specified.

t-Butyl Vinyl Sulfide.—This substance was prepared in 45% yield by the dehydrohalogenation of *t*-butyl 2-chloroethyl sulfide[13] with a boiling solution of sodium hydroxide in 2-methoxyethanol, the product of the reaction being removed continuously: b. p. (cor.) 116.5° (760 mm.), n^{23}D 1.4610, d^{23}_4 0.832, λ_{max} 234 mμ (ϵ 4,500) and 250 mμ (ϵ 4,700).

Anal. Calcd. for $C_6H_{12}S$: C, 62.00; H, 10.41; S, 27.59. Found: C, 62.61; H, 10.45; S, 27.08.

(11) A. J. Harrison, *et al.*, *J. Chem. Phys.*, **18**, 221 (1950); **30**, 357 (1959).

(12) L. W. Pickett, N. J. Hoeflich and T. C. Liu, *J. Am. Chem. Soc.*, **73**, 4865 (1951).

(13) T. P. Dawson, *ibid.*, **69**, 1211 (1947).

STABILITY AND CATALYTIC ACTIVITY OF PLATINUM ETHYLENE CHLORIDE

BY A. S. GOW, JR., AND HEINZ HEINEMANN

The M. W. Kellogg Co. Research & Development Department, Jersey City 3, N. J.

Received February 25, 1960

Evidence for the low-temperature homogeneous, liquid phase hydrogenation of ethylene in acetone and toluene solutions of ethylene platinous chloride has been reported by Flynn and Hulburt.[1] This suggested that the ethylene in this complex might react in the same manner as ethylene adsorbed on platinum and other metals, and be capable of exchanging its hydrogens with tetradeuterioethylene, as in the heterogeneous exchange between C_2H_4 and C_2D_4 on nickel-kieselguhr, reported by Douglas and Rabinovitch.[2] We have, therefore, studied the homogeneous H–D exchange between ethylene platinous chloride and tetradeuterioethylene in several solvents at temperatures between −15 to 100°, under a range of partial pressures of ethylenes. Since it was necessary to determine the conditions under which the reactions would be homogeneous, we also have investigated the thermal decomposition of this complex, as well as the hydrolysis in 4% aqueous hydrochloric acid in the presence of ethylene.

(1) J. H. Flynn and H. M. Hulburt, *J. Am. Chem. Soc.*, **76**, 3393 (1954).

(2) J. E. Douglas and B. S. Rabinovitch, *ibid.*, **74**, 2486 (1952).

Experimental

The solvents used were chloroform, acetone, toluene and 4% aqueous hydrochloric acid. The first three were middle fractions obtained by fractional distillation of C.P. reagents. Anhydrous toluene was prepared by shaking with metallic sodium in an all-Pyrex vessel for 15–17 hours at 100°; after thorough removal of hydrogen, a known amount of the solvent was transferred by distillation to a reaction vessel containing a known amount of complex. The aqueous HCl was prepared by the addition of the required amount of the 38% acid to CO_2-free distilled water. Very pure ethylene platinous chloride, $[Pt(C_2H_4)Cl_2]_2$, was prepared by the method of Chatt and Searle,[3] as modified by Joy and Orchin.[4] The ethylene was Matheson C.P. grade. The tetradeuterioethylene was obtained from Tracerlab, and contained 95.1% C_2D_4, 3.5% C_2HD_3 and 1.4% C_2H_3D.

All reactions were carried out in Pyrex vessels provided with break-off seals and appropriate inlet tubes which were sealed with a torch after introduction of known amounts of reagents. All transfer operations were carried out in conventional Pyrex high-vacuum equipment. The vessels, containing known amounts of reagents were vigorously shaken in a constant temperature bath. Analyses of gaseous products were made with a model 21–103 Consolidated Electrodynamics Corp. mass spectrometer. Free platinum in the residues was detected by X-ray diffraction techniques.

The thermal decomposition of the complex was studied in constant volume systems and also at low pressure in all-Pyrex apparatus. In the experiment at low pressure, gaseous products were continually removed by freezing in liquid nitrogen. In one constant volume system, the reaction was studied in an apparatus similar to that described by Booth and Halbedel,[5] so that the rate of pressure rise with temperature could be observed.

Results and Discussion

A. Stability of Complex.—It was found that the solid complex is fairly stable below about 130°, but decomposes rapidly and irreversibly at temperatures above 160°. The estimated half-lives at 130 and 172° were 4.5 days and 1.7 hours, respectively. The gaseous products in experiments carried out at constant volume and nearly atmospheric pressure, contained 40–50% ethylene and a mixture of chlorinated products, among which were CH_2=CHCl, 1,2-$C_2H_4Cl_2$, C_2H_5Cl, 1,1-$C_2H_4Cl_2$ and HCl, in decreasing order of concentration. The residues consisted of free platinum and platinous chloride. In the experiment carried out at low pressure at 180°, the gaseous product contained over 98% ethylene, and the residue consisted almost entirely of platinous chloride. These experiments clearly show that the primary thermal decomposition reaction results in the formation of ethylene and platinous chloride, and that subsequent reactions result in the formation of free platinum and chlorinated hydrocarbons.

Hydrolysis of this complex in 4% aqueous hydrochloric acid in the presence of ethylene was

(3) J. Chatt and M. L. Searle, "Inorganic Syntheses," Vol. V, McGraw-Hill Book Co., Inc., New York, N. Y., 1957, pp. 210–215.

(4) J. R. Joy and M. Orchin, private communication.

(5) H. S. Booth and H. S. Halbedel, *J. Am. Chem. Soc.*, **68**, 2652 (1946).

incipient after 1 hour at 100°, and led to the formation of appreciable quantities of free platinum, carbon dioxide and ethane and smaller amounts of methane. The dilute solutions used made analysis of the aqueous phase impractical, and it was not possible to determine the reactions which had occurred. Since the presence of carbon dioxide and saturated hydrocarbons among the products has not been reported in previous investigations[6,7] of the hydrolysis of this complex, it would be of interest to study the reaction in more concentrated solutions, so that an analysis of the aqueous phase could be made. With these data, the nature of these reactions could be better understood.

B. H–D Exchange.—No H–D exchange was observed under the conditions

Solvent	Reaction temp., °C.	Reaction time, hr.
Chloroform	24	0.25
4% HCl	27	17
4% HCl	100	1
Acetone	−15	1
Toluene	− 8	28
Toluene	20	36
Toluene	50	12

Solid phases were present in the experiment in acetone and that in toluene at 20°. In the former, we believe that the solid phase consisted of a mixture of $[Pt(C_2H_4)Cl_2]_2$ and *trans*-$Pt(C_2H_4)_2Cl_2$; in the latter, the white solid phase was believed to be the *cis*-form of $Pt(C_2H_4)_2Cl_2$, as described by Chatt and Wilkins.[8] The partial pressure of ethylene in the experiment in acetone at −8° was approximately 600 mm., while that in the experiment in toluene at 20° was approximately 900 mm. According to Chatt and Wilkins,[8] the dissociation pressure of the *trans*-form of the diolefin complex is approximately 1 atmosphere at −6°. These data make the presence of this species in both experiments probable. In addition, the bright canary yellow color of both solutions, characteristic of the *trans*-form of the diolefin complex, substantiates this belief.

In toluene at 100°, a suspended phase always appeared after 15 min., and H–D exchange was incipient at the end of 2 hours, and approximately 60% complete after 17 hours. This suspended phase was invisible to the naked eye and could only be detected by means of the Tyndall effect. X-Ray diffraction indicated the presence of free platinum in the residues obtained after all gases and solvents were removed at the end of these experiments. Since the initial C_2H_4/C_2D_4 ratio was nearly unity in these experiments, the greater proportion of C_2H_4 and C_2H_3D in the recovered ethylenes indicated that the solvent was involved in the H–D exchange, which apparently took place heterogeneously on the platinum. This observation is of considerable interest, as it would indicate that the homogeneous hydrogenation of ethylene reported by Flynn and Hulburt[1] was not accompanied by exchange and raises the question whether there is a major difference between the system as used in our experiments and in their work.

In all of the experiments, replacement of complexed ethylene by tetradeuterioethylene had essentially reached equilibrium within 15 minutes, indicating that mass transfer between phases was not rate-controlling.

We believe that studies of the H–D exchange between C_2H_4 and C_2D_4 on platinum at temperatures below 50° and the homogeneous deuteration of ethylene in solutions of ethylene platinous chloride may furnish the necessary data to enable one to draw conclusions concerning the similarity of the chemical behavior of ethylene complexed with platinum salts with that of ethylene adsorbed on platinum.

(6) J. S. Anderson, *J. Chem. Soc.*, 971 (1934).

(7) J. R. Joy and M. Orchin, Unpublished Thesis, University of Cincinnati, Cincinnati, Ohio.

(8) J. Chatt and R. G. Wilkins, *J. Chem. Soc.*, 2622 (1952).

DIFFUSION OF METHYL RADICALS IN THE GAS-PHASE PHOTOLYSIS OF AZOMETHANE[1]

BY SIDNEY TOBY

School of Chemistry, Rutgers, the State University, New Brunswick, N. J.

Received February 27, 1960

Some years ago Hill[2] performed some calculations on the difficult subject of radical diffusion. Taking acetone vapor as his model, he considered the effect of a photolyzing beam concentric with, but of smaller diameter than, a cylindrical photolysis cell. Attempts by Nicholson[3] to use Hill's results to explain the Arrhenius curvature encountered below about 80° in the gas-phase photolysis of acetone met with little success. The situation has been reviewed by Noyes.[4]

Arrhenius curvature also is encountered in the gas-phase photolysis of azomethane.[5] The system is simpler than the acetone photolysis because the CH_3N_2– radical is too shortlived to react (unlike the corresponding acetyl radical) and because the Arrhenius curvature occurs below −10°, when more than 99% of the methyl radicals dimerize rather than abstract from azomethane. Some experiments in which a reduced light beam was used[5] afforded the opportunity of testing Hill's expression for the mean radical diffusion distance.

The photolysis of azomethane (A) may be represented by

$$A + h\nu \longrightarrow 2CH_3 + N_2 \quad (0)$$

$$2CH_3 \longrightarrow C_2H_6 \quad (1)$$

$$CH_3 + A \longrightarrow CH_4 + -CH_2N_2CH_3 \quad (2)$$

$$CH_3 + \text{A-wall} \longrightarrow CH_4 + -CH_2N_2CH_3 \quad (3)$$

$$CH_3 + A \longrightarrow CH_3A- \quad (4)$$

together with reactions involving higher substituted hydrazines[6] which may be neglected for present purposes.

The mean square CH_3 diffusion distance, λ^2,

(1) This work was supported in part by a Cottrell Grant from the Research Corporation.

(2) T. L. Hill, *J. Chem. Phys.*, **17**, 1125 (1949).

(3) A. J. C. Nicholson, *J. Am. Chem. Soc.*, **73**, 3981 (1951).

(4) W. A. Noyes, Jr., THIS JOURNAL, **55**, 925 (1951).

(5) S. Toby, *J. Am. Chem. Soc.*, **82**, 3822 (1960).

(6) M. H. Jones and E. W. R. Steacie, *J. Chem. Phys.*, **21**, 1018 (1953).

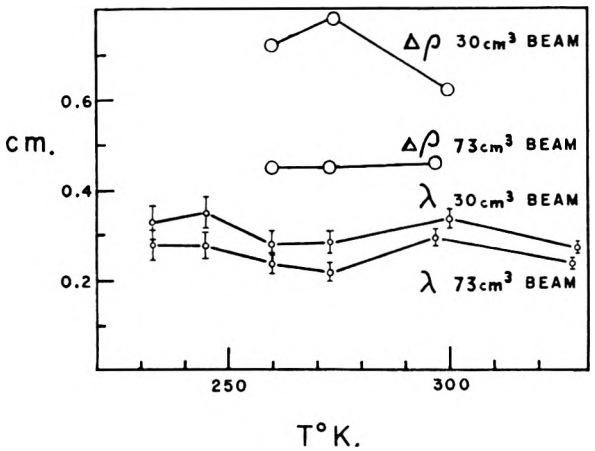

Fig. 1.—Variation of radical diffusion distances with temperature.

may be calculated by Hill's method[2] assuming the CH_3 radicals are diffusing through a uniform concentration of A. We obtain

$$\lambda^2 = \frac{4}{3\pi^{3/2}\sigma^2\, 6.02 \times 10^{20}[\mathrm{A}]}\left(\frac{RT}{M}\right)^{1/2} \bar{l}\ \mathrm{cm.}^2$$

where σ is the collision diameter of A, [A] is in moles liter^{-1}, M is the molecular weight of CH_3, and $\bar{l}$ is the mean radical lifetime where

$$1/\bar{l} = 2k_1[CH_3] + k_2[A] + (RT/2\pi M)^{1/2}[\text{A-wall}] + k_4[A][CH_3]$$

may be taken as the mean cell concentration $= (r_{C_2H_6}/V_0k_1)^{1/2}$ mole liter^{-1} where V_0 is the volume of the photolysis cell. The values for [A], $r_{C_2H_6}$ and V_0 are taken from reference 5. Rate data used are summarized in Table I. Since the work was not done in the "low-pressure" region of methyl radical recombination E_1 will not have an apparently negative value.[7]

E_1 is not known with any accuracy; however, Gomer and Kistiakowsky[8] found a maximum value of 0.7 kcal. mole^{-1} and we shall take the value 0.5 ± 0.5 kcal. mole^{-1}. The values of λ obtained are plotted against temperature in Fig. 1 for the two reduced light beam series. The uncertainties shown for the value of λ are due to the uncertain value of E_1.

TABLE I

RATE DATA USED

Data	Ref.
$\sigma = 5.5$Å.	5
$k_1 = 2.0 \times 10^{10}$ l. mole^{-1} sec.$^{-1}$ at 170°	9
$k_2/k_1^{1/2} = 160e^{-6860/RT}$ l.$^{1/2}$ mole$^{-1/2}$ sec.$^{-1/2}$	4
$(RT/2\pi M)^{1/2}[\text{A-wall}] = R_{CH_4}k_1^{1/2}/R_{C_2H_6}^{1/2} - [A]k_2$ sec.$^{-1}$	4
$k_4/k_2 = e^{1200/RT}$	5

The effective reaction volume can be calculated from the straight-line portion of the Arrhenius plot[5] and this gives the effective reaction radius ρ. If the radius of the light beam $= \rho_l$ effective diffusion distance $\Delta\rho = \rho - \rho_l$. Values of $\Delta\rho$ are shown in Fig. 1 (the values of $\Delta\rho$ at 55° have been omitted since the corresponding Arrhenius points were not collinear with the others and give erratic values).

Agreement of λ with $\Delta\rho$ within a factor of 2 may be taken as encouraging in view of the many experimental errors involved. The largest single source of error probably is ρ_l which is very difficult to measure accurately with the imperfectly focussed, high intensity beam typical of most photochemistry, as Nicholson[3] noted. It is interesting that the diffusion effects are independent of temperature over the range employed and that there is distinctly more diffusion from the smaller of the two beams. Although the average values of ρ (1.61 and 1.95 cm. for the two series) are considerably smaller than the cell radius (2.7 cm.), a sufficient number of radicals reach the wall so that there is still considerable Arrhenius curvature.[5] Much less curvature would be expected if the only heterogeneous reactions occurred at the cell windows. A puzzling feature is that the curvature does not appear to decrease with decreasing ρ_l. This implies that most of the heterogeneous reactions *do* occur at the cell window, for the ratio of the planar area of a cylinder to its volume is independent of the radius.

(7) (a) K. U. Ingold, I. H. Henderson and F. P. Lossing, *J. Chem. Phys.*, **21**, 2239 (1953); (b) A. D. Stepukhovich, *Zhur. Fiz. Khim.*, **32**, 2415 (1958); [*C. A.*, **53**, 10916b (1959)].

(8) R. Gomer and G. B. Kistiakowsky, *J. Chem. Phys.*, **19**, 85 (1951).

(9) A. Shepp, *ibid.*, **24**, 939 (1956).

THERMAL FREE RADICAL REACTIONS IN THE RADIOLYSIS OF LIQUID HYDROCARBONS

BY G. R. FREEMAN

Department of Chemistry, University of Alberta, Edmonton, Alberta

Received March 16, 1960

In a recent article, Wagner has clearly demonstrated that thermal radical–radical reactions are largely responsible for the formation of the C_6 to C_{10} products in the early stages of the radiolysis of liquid *n*-pentane.[1] He also concluded from kinetic analysis that, at the dose rates used (10^8 to 4×10^9 rad./hr.), hydrogen abstraction reactions by the alkyl radicals (reaction 1) could not compete effectively with radical combination (reaction 2).

$$R + HS \longrightarrow RH + S \qquad (1)$$

$$2R \longrightarrow R_2 \qquad (2)$$

where R and S are alkyl free radicals and HS is a hydrocarbon molecule. Thermal hydrogen atoms, however, appeared to react nearly completely *via* reaction 1 when their only alternative was to combine with other free radicals. It also appeared, from the results of Phibbs and Darwent[2] and of Dewhurst,[3] that disproportionation of the alkyl radicals (reaction 3) did not occur in the liquid phase.

$$2R \longrightarrow RH + R' \qquad (3)$$

where R′ is an olefin.

During recent experiments in this Laboratory, cyclohexane was found to be a major product of the liquid phase radiolysis of cyclohexene.[4] It was

(1) C. D. Wagner, THIS JOURNAL, **64**, 231 (1960).

(2) M. K. Phibbs and B. de B. Darwent, *J. Chem. Phys.*, **18**, 679 (1950).

(3) H. A. Dewhurst, THIS JOURNAL, **62**, 15 (1958).

(4) G. R. Freeman, *Can. J. Chem.*, **38**, 1043 (1960).

suggested that the cyclohexane was formed by the reaction

$$c\text{-}C_6H_{11} + c\text{-}C_6H_{10} \longrightarrow c\text{-}C_6H_{12} + c\text{-}C_6H_9 \quad (1a)$$

Bicyclohexyl was a product also, which indicates the occurrence of the reaction

$$2c\text{-}C_6H_{11} \longrightarrow (c\text{-}C_6H_{11})_2 \quad (2a)$$

The cyclohexyl radicals presumably were formed by the addition of hydrogen atoms to cyclohexene. Furthermore, during the radiolysis of cyclohexane–cyclohexene solutions, large yields of bicyclohexenyl were obtained even when the cyclohexene concentration was small.[4] It was proposed that cyclohexenyl radicals were generated by reaction 1a and that they combined according to reaction 2b.

$$2c\text{-}C_6H_9 \longrightarrow (c\text{-}C_6H_9)_2 \quad (2b)$$

However, the dose rates used in these experiments (about 10^4 rad./hr.) were several orders of magnitude smaller than those used by Wagner.

Using the dose rate and the yields of cyclohexane and bicyclohexyl in the pure cyclohexene system and the yields of bicyclohexyl and bicyclohexenyl in the cyclohexane–cyclohexene solutions, it may be calculated that $k_{1a}/k_{2a}^{1/2} \approx 10^{-4}$(l./mole sec.)$^{1/2}$. It is reasonable to assume that the diffusion controlled reaction 2a has a rate constant $k_{2a} \approx 10^{10}$ l./mole sec.[1,5] Thus $k_{1a} \approx 10$ l./mole sec. Although this value only indicates an order of magnitude, it is in approximate agreement with that used by Wagner for reaction 1 (12 l./mole sec.), which he derived from gas phase data. This might be taken as support for the suggestion that the cyclohexane in the cyclohexene system is produced by a free radical mechanism.

In the radiolysis of pure cyclohexane, the value of the ratio of the initial yields, G_i, of cyclohexene and bicyclohexyl is $G(\text{cyclohexene})_i/G(\text{bicyclohexyl})_i = 1.84$.[5] The yields of both cyclohexene and bicyclohexyl are greatly decreased by the addition of small amounts of benzene to the cyclohexane.[5] When the electron fraction of benzene was increased from zero to 0.027, ΔG(cyclohexene) $= -1.47$ and ΔG(bicyclohexyl) $= -0.79$. Thus the value of the ratio $\Delta G(\text{cyclohexene})/\Delta G(\text{bicyclohexyl}) = 1.86$ under these conditions is equal to the value of the ratio of the initial yields of these products in pure cyclohexane. Wagner pointed out that the ratio of the rate constants for disproportionation and combination, k_3/k_2, should have a value of 1.8 for straight chain *sec*-alkyl radicals in the gas phase.[1,6] It appears that this value holds equally well for liquid cyclohexane and that cyclohexyl radicals are precursors of a large portion of the cyclohexene formed during the radiolysis of liquid cyclohexane. This is contrary to the conclusions of Wagner[1] and of Dewhurst[3] concerning the liquid phase radiolysis of *n*-pentane and *n*-hexane, respectively. The above results favor a head-to-tail mechanism of disproportionation, not a mechanism involving combination of the radicals with subsequent decomposition involving the shift of a hydrogen atom.

(5) G. R. Freeman, *J. Chem. Phys.*, **33**, 71 (1960).

(6) J. W. Kraus and J. G. Calvert, *J. Am. Chem. Soc.*, **79**, 5921 (1957).

The values of the ratio G(pentene)/G(decane) calculated from Wagner's results are 1.75, 1.27 and about 1.45 for photon irradiations (3.8×10^7 rad.) at -115 and 25° and electron irradiations (10.5×10^7 rad.) at 20°, respectively. At these high doses the pentene yields had been appreciably reduced by secondary reactions.[1] The doses used in the above reported cyclohexane experiments were approximately 0.5×10^7 rad.[4,5] Thus the results of Wagner are consistent with a free radical disproportionation mechanism for the production of pentene during the radiolysis of liquid *n*-pentane.

EVIDENCE FOR HYDROGEN MIGRATION IN A NEGATIVE ION–MOLECULE REACTION

By C. E. Melton, G. A. Ropp and T. W. Martin[1]

Chemistry Division, Oak Ridge National Laboratory,[2] Oak Ridge, Tennessee

Received March 21, 1960

In the course of a previous investigation[3] it was found that the negative ion mass spectra of binary mixtures of the formic acids (HCOOH and DCOOH) showed a small concentration (0.1%) of polymeric negative ions of masses 91, 92 and 93 in the pressure range of 10^{-5} to 10^{-3} mm. and at a temperature of 200 ± 25° in the ionization chamber. A typical scan of these polymeric ions for a 51:49 mole % mixture of HCOOH:DCOOH at a total pressure of 10^{-4} mm. is displayed in Fig. 1, together with the reference ions at masses 45 and 46. In the previous investigation[3] it was shown using known gas mixtures that the 45 ($HCOO^-$) and 46 ($DCOO^-$) ion intensities, when isotopically corrected, give an accurate quantitative measure of the partial pressures of HCOOH and DCOOH, respectively.

The polymeric ions were first thought to arise from an ionization–dissociation reaction of the neutral formic acid dimers known to be in equilibrium with the monomers in this system. This mechanism of formation is felt to be most improbable because (1) a detailed calculation based on the excellent data of Coolidge[4] indicates that the dimer concentration is negligible, being only about 1 part to 10^6 parts of monomer at 100° and 10^{-4} mm. total pressure, and (2) extrapolating the Coolidge data to the actual experimental conditions of 10^{-4} mm. and 200°, we calculate that the dimer mole fraction should be decreased almost two more orders of magnitude in sharp contrast to the experimental observation that the absolute polymeric ion intensity is not noticeably affected in the temperature range of 100–200°. (3) A plot of the relative abundance of the polymeric ions *vs.* pressure, Fig. 2, shows a linear relationship extrapolating through zero. This pressure dependence would be expected for products re-

(1) Summer research participant from Vanderbilt University.

(2) Operated for the U. S. Atomic Energy Commission by the Union Carbide Corporation.

(3) G. A. Ropp and C. E. Melton, *J. Am. Chem. Soc.*, **80**, 3509 (1958).

(4) A. S. Coolidge, *ibid.*, **50**, 2166 (1928).

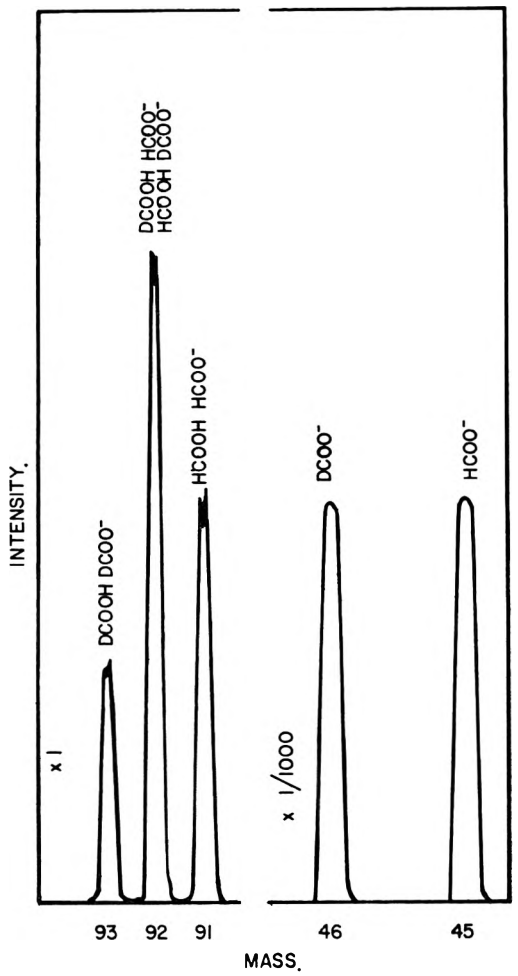

Fig. 1.—Isotope effect in a negative ion–molecule reaction. Secondary ions at masses 91, 92 and 93 were formed by passing $DCOO^-$ and $HCOO^-$ through a 51:49 mole % mixture of HCOOH:DCOOH.

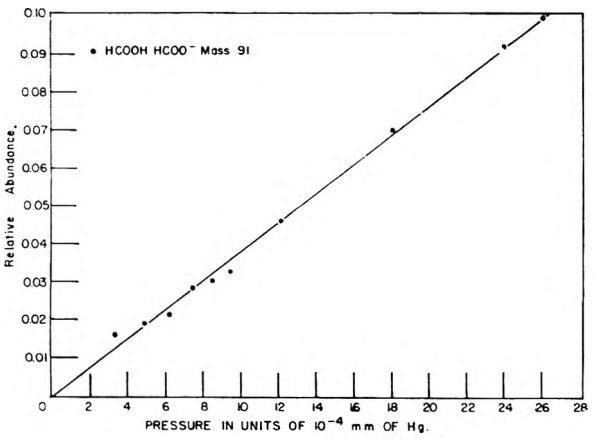

Fig. 2.—Relative abundance of $H_3C_2O_4^-$ *vs.* HCOOH pressure.

sulting from an ion–molecule reaction[5] and (4) the only ions observed at low (2–5 e.v.) electron energy were $DCOO^-$, $HCOO^-$ and the polymeric ions. This observation is suggestive that $DCOO^-$ and $HCOO^-$ are precursors for the polymeric ions. Therefore, we conclude that the polymeric ions are formed by the bimolecular negative ion–molecule reactions

$$HCOO^- + HCOOH \xrightarrow{k_1} HCOOHCOOH^- \quad (91) \quad (1)$$

$$HCOO^- + DCOOH \xrightarrow{k_2} HCOODCOOH^- \quad (92) \quad (2)$$

$$DCOO^- + HCOOH \xrightarrow{k_3} DCOOHCOOH^- \quad (92) \quad (3)$$

$$DCOO^- + DCOOH \xrightarrow{k_4} DCOODCOOH^- \quad (93) \quad (4)$$

If we define [HCOOH] = a, [DCOOH] = b, and assume $k_1 = k_2 = k_3 = k_4$, then on a statistical basis the rates of formation of the 91, 92 and 93 product ions would be proportional to a^2, $2ab$ and b^2, respectively. Applying this statistical calculation to the data shown in Fig. 1, we expect the ratios 91:92:93 to be approximately 1:2:1, but we observe 1:1.6:0.6. It follows from this marked departure from statistical behavior that the k's for the four reactions are not equal because of an "isotope effect."

In order to explain this isotope effect, we searched for a structure of the collision complex which would show a mass discrimination. The simplest structure to consider would be that of a single attachment of the negative ion to the neutral molecule, *e.g.*

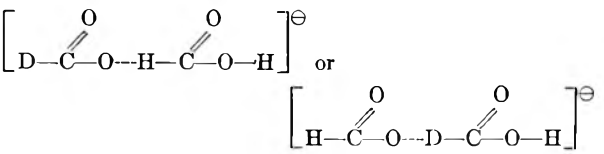

This type of structure is discounted because the O---H---C bond is considered improbable for this system. A more conventional type of hydrogen bonding involving single attachment, *e.g.*

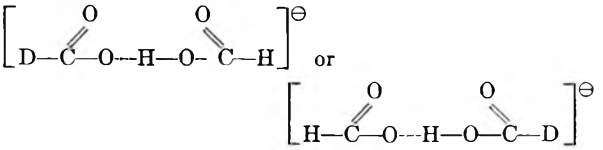

will not explain the experimental results.

Therefore, a double attachment mechanism appears necessary to explain the observed isotopic effect. The first case of double attachment of ion to neutral molecule considered also involves the O---H---C bond, *e.g.*

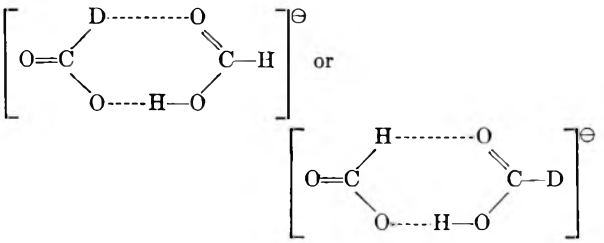

This structure is likewise discarded for the same reason as for the single attachment structure, and, in addition, it represents a completely unsymmetrical and unfavorable resonance structure.

The remaining double attachment structure is analogous to that of the neutral formic acid dimer, *e.g.*

(5) (a) H. M. Rosenstock and C. E. Melton, *J. Chem. Phys.*, **26**, 314 (1957); (b) C. E. Melton and G. F. Wells, *ibid.*, **27**, 1132 (1957).

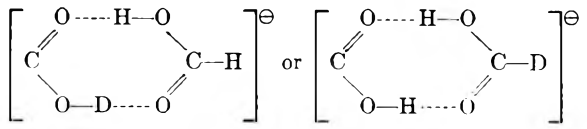

Having chosen this structure, the isotope effect then can be explained on the basis of the simple mechanism

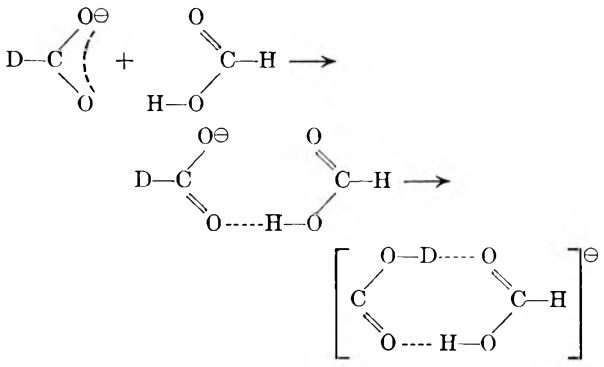

which assumes that each of the polymeric ions is formed by the rearrangement of the initial collision complex. The rearrangement always involves the migration or tunnel effect of the hydrogen or deuterium nucleus originally attached to the negative reactant ion to form the more stable and symmetrical double hydrogen-bonded resonance structure. Since the deuterium would migrate more slowly than hydrogen, the collision complex for reactions 3 and 4 would dissociate on the average more often than that for reactions 1 and 2; hence, $k_3 = k_4 < k_1 = k_2$. On the basis of this hydrogen rearrangement mechanism, the relative abundances of the various polymeric ions for any given mixture become

$$91:92:93 = a^2:(2 - y)ab:(1 - y)b^2$$

where $(1 - y)$ is the isotope discrimination factor, k_3/k_1.

Strong experimental confirmation of this postulated mechanism is presented in Table I where the calculated results were obtained taking $y = 0.65$, which gives a minimum error for all the mixtures studied. These considerations are equally applicable for a rearrangement of the formate ion prior to formation of the collision complex.

TABLE I

PER CENT. ABUNDANCE OF NEGATIVE IONS FROM HCOOH–DCOOH MIXTURES (all data taken at ~200°)

Mixture		Mass 91		Mass 92		Mass 93	
Mass 45 $HCOO^-$ obsd.	Mass 46 $DCOO^-$ obsd.	$HCOO^-$ $HCOOH^-$ obsd.	calcd.	$HCOO^-$ $DCOO^-$ $HCOOH^-$ obsd.	calcd.	$DCOO^-$ $DCOOH^-$ obsd.	calcd.
67	33	52	56	40	38	7	6
60	40	45	48	46	44	9	8
54	46	42	41	47	48	11	11
47	53	32	33	52	52	16	15
32	68	18	18	55	52	27	30

Structural rearrangements of positive ions are well known[6] but similar processes of negative ions have not been reported previously. It is also interesting that the "even" negative ion $HCOO^-$ appears to react with smaller bimolecular rate constants than are observed for most "even and odd" positive ions.[7] For example, by methods previously described,[7] we find for these reactions from this study and a previous study[8]

$$HCOO^- + HCOOH \xrightarrow{k_1} HCOOHCOOH^-$$

$$HCOO^- + N_2 \xrightarrow{k^*} CN^- + [NO_2H]$$

(where $[NO_2H]$ represents all of the neutrals necessary for a material balance) that $k_1 = 2.9 \times 10^{-11}$ and $k^* = 7.6 \times 10^{-11}$ in units of cc. molecule^{-1} sec.$^{-1}$. The smaller rate constants of these negative ion reactions represent smaller probabilities or steric factors of reaction. This is consistent with the greater structural changes associated with these reactions.

(6) (a) P. N. Rylander and S. Meyerson, *J. Am. Chem. Soc.*, **78**, 5799 (1956); (b) V. Hanus, *Nature*, **184**, 1796 (1959).

(7) T. W. Martin and C. E. Melton, *J. Chem. Phys.*, **32**, 700 (1960).

(8) C. E. Melton and G. A. Ropp, *J. Am. Chem. Soc.*, **80**, 5573 (1958).

CHEMISORPTION AS A PREREQUISITE TO HETEROGENEOUS CATALYSIS

BY W. M. H. SACHTLER AND N. H. DE BOER

Koninklijke/Shell-Laboratorium, Amsterdam (Shell Internationale Research Maatschappij N.V.)

Received March 28, 1960

To understand mechanisms in heterogeneous catalysis it must be known whether stable chemisorption of all reactants is necessary or whether reactions occur between loosely adsorbed complexes. For the simple reaction

$$H_2 + D_2 = 2HD$$

Bonhoeffer, *et al.*,[1] and Farkas[2] assumed a dissociative chemisorption of both gases, followed by random desorption of atom pairs. A different mechanism was advocated by Rideal[3] and Eley,[4] who considered the reaction between a chemisorbed atom and an impinging molecule. We have approached the problem in a new way, using gold as a catalyst.

Gaseous hydrogen molecules are not measurably chemisorbed on gold below 200°. On the other hand, when formic acid decomposes on a gold catalyst the gold surface becomes partly covered by hydrogen atoms during the steady state of the decomposition reaction.[5] Consequently, when a mixture of HCOOH + D_2 is in contact with a gold catalyst, only the light hydrogen isotope passes through the stage of atomic chemisorption, whereas the heavy isotope is not chemisorbed.

We have taken advantage of this particular situation to carry out a number of experiments, the results of which are given below. The gold was

(1) K. F. Bonhoeffer and A. Farkas, *Z. physik. Chem.*, **B12**, 231 (1931); K. F. Bonhoeffer, F. Bach and E. Fagans, *ibid.*, **A168**, 313 (1934).

(2) A. Farkas, "Orthohydrogen, Parahydrogen and Heavy Hydrogen," Cambridge Univ. Press, 1935.

(3) E. K. Rideal, *Proc. Cambridge Phil. Soc.*, **35**, 130 (1939).

(4) D. D. Eley and E. K. Rideal, *Proc. Roy. Soc. (London)*, **A178**, 429 (1941).

(5) J. Fahrenfort, L. L. van Reijen and W. M. H. Sachtler, "The Mechanism of Heterogeneous Catalysis," 1960, in press; *Z. Elektrochem.*, **64**, 216 (1960).

used either in powder form or dispersed on a carrier.

I. Hydrogen exchange at 150°.

(A) $H_2 + D_2$ ⟶ no formation of HD
(B) $HCOOH + D_2$ ⟶ only H_2 and CO_2 are formed; no formation of HD
(C) $HCOOH + DCOOD$ ⟶ H_2, D_2 and HD are formed in equilibrium distribution
(D) $HCOOD$ ⟶ H_2, D_2 and HD are formed in equilibrium distribution

The rates of reactions C and D are those of formic acid decomposition, *e. g.*, 6.4×10^{-3} molec. site^{-1} sec.$^{-1}$ for COOH. For the constant k, given by: $k = [HD]^2/[H_2][D_2]$, a value of 3.50 ± 0.1 was found in all experiments where mixtures of HCOOH + HCOOD + DCOOD were decomposed. The theoretical figure for equilibrium, as given by Farkas,[2] is $k_{th} = 3.52$.

II. Hydrogen oxidation at 120°.

(E) $2H_2 + O_2$ ⟶ very slow formation of H_2O
(F) $2HCOOH + O_2$ ⟶ fast formation of H_2O
(G) $2HCOOH + O_2 +$ excess D_2 ⟶ fast formation of H_2O, containing no DOH or D_2O, except traces; no H_2 present in the gas phase

From these results it is concluded that under the conditions used dissociative chemisorption of hydrogen is essential for the catalytic mechanism of both reactions studied. Moreover, result G shows that oxygen quantitatively consumes chemisorbed hydrogen atoms, whereas the gaseous D_2 molecules remain untouched.

ON THE OXIDATION OF GOLD

By N. A. Shishakov

Institute for Physical Chemistry, Academy of Science, Moscow, U.S.S.R.

Received April 1, 1960

It has been shown in two recent papers of Carpenter and Clark with co-workers[1] that different oxides arise on the surface of gold as a result of its interaction with oxygen at low pressures. The authors concluded that these oxides belong to the spinel type with iron, copper and lead cations, which were arisen from contamination of gold. However, the proofs for this statement are quite insufficient. For instance, the authors attribute one of their electron diffraction diagrams to $FeO \cdot Fe_2O_3$ with the length of unit cell $a = 8.34$ Å., but they do not indicate the degree of agreement between observed and theoretical spacings and intensities.

The following fact will show that the neglecting of such requirements may lead to quite erroneous results. It was shown in our previous communication[2] that the surface of gold heated at 500° in oxygen under normal pressure gives excellent electron diffraction diagrams with a number of rings, listed in this communication. The structure remained unknown, but it may be noted that the diagram is very like to that which was attributed to the spinel in the paper.[1] It was found, however, that such a likeness exists only in first approximation. Among the 27 observed rings only 24 fitted to the theory, giving $a = 8.97$ Å. $\pm$ 0.5%, the others three rings (220, 331, 664) give the discrepancy more than 1%. It follows therefrom that the crystal lattice is not really that of spinel type. Just for this reason I have used above 27 reflections to build the radial distribution curve, according to Mackle and Sutton[3] and obtained from it among others a maximum at $r = 1.4$ Å., which shows that there are oxygen molecular ions in the structure. Hence it appears that the surface structure is of peroxide type, probably due to the gold, but not of spinal type.

An additional proof of existence of surface gold peroxide was obtained by the study of particular texture-diagram from the surface of gold heated at 500°, or nearly so, in oxygen at normal pressure. It has been found[4] that the structure belongs to hexagonal type with $a = 5.28$ and $c = 6.75$ (Trillat[5] obtained from a thin leaf, but otherwise in similar conditions, the same period $a = 5.28$ Å.).

Of course it was possible to determine the positions only of heavy gold atoms, but at the same time the interstices between them were found to be large enough to locate the molecules of oxygen with their large axes parallel to the sixfold axis of lattice.

It may be pointed out also that various electron diffraction diagrams arise when condensed gold is heated in oxygen at other temperatures from 100 to 900°. Many examples are given in a recent book.[6] However, in no case were indications obtained on the spinel or other structures of unnoble metals.

It is seen from these considerations that gold is capable of giving surface peroxides after heating and that the existence of unnoble oxides is improbable.

(1) L. D. Carpenter, D. Clark, W. H. Mair and T. Dickinson, *Trans. Faraday Soc.*, **55**, 1924 (1959).
(2) N. A. Shishakov, *J. Phys. Chem.* (*Russ.*), **31**, 33 (1957).
(3) H. Mackle and L. Sutton, *Trans Faraday Soc.*, **7**, 691, 951 (1937).
(4) N. A. Shishakov, *Kristallographie* (*Russ.*), **2**, 686 (1957).
(5) J. J. Trillat, *Sh. Oketani, J. de phys. et rad.*, **8**, 59, 93 (1937).
(6) N. A. Shishakov and V. V. Andreewa, "Oxide Films on Metals," *Acad. Sci. URSS, Moscow*, 1959.

DIFFUSION MEASUREMENTS WITH A DIAPHRAGM CELL

By H. L. Toor

Chemical Engineering Department, Carnegie Institute of Technology, Pittsburgh 13, Pennsylvania

Received April 11, 1960

In the measurement of diffusion coefficients by the diaphragm cell method, quasi steady-state diffusion is allowed to take place through the pores of a diaphragm. The differential diffusion coefficient to be measured is defined by Fick's first law

$$j = -D(C)\nabla C \qquad (1)$$

where j is the flux vector and C the concentration of diffusing substance.

The integral diffusion equation for a diaphragm in which the concentrations at the parallel $x = 0$ and $x = L$ faces[1] are C_1 and C_2, respectively, is normally obtained as follows: It is assumed that (1) the

(1) The diaphragm faces are defined by two y-z planes in a rectangular coördinate system whose x coördinates are 0 and L. Diffusion takes place only through these faces.

net velocity of the fluid medium is zero so that there is no convection within the diaphragm, (2) steady-state is obtained (the above assumptions are usually valid and are assumed valid in this note) and, (3) the diffusion within the diaphragm is unidirectional.

With the unidirectional assumption eq. 1 reduces to

$$j_x = -D(C)\frac{dC}{dx} \tag{2}$$

where x is the distance normal to the two parallel faces of the diaphragm. By continuity, j_x must now be independent of x so eq. 2 may be immediately integrated

$$N = j_x A_e = \bar{D}(C_1 - C_2)\frac{A_e}{L_e} \tag{3}$$

where

$$\bar{D} = \frac{1}{C_2 - C_1}\int_{C_1}^{C_2} D(C)dC \tag{4}$$

and N is the total rate of diffusion across either face of the diaphragm. The quantities A_e and L_e are somewhat ambiguous, but normally are considered to be the effective length and total open cross-sectional area of the diaphragm.[3]

In practice A_e/L_e is obtained by calibration of the diaphragm with a known system and eq. 3 and 4 are then used to determine $\bar{D}$ in an unknown system. The differential coefficient is obtained from the measured integral value by standard methods.[2]

The above procedure is open to criticism for even though there is no *net* flux over the entire diaphragm in a direction other than x, a little consideration shows that the diffusion within the tortuous paths of a diaphragm can by no means be unidirectional. Therefore dC/dx in eq. 2 must be replaced by $\partial C/\partial x$ and both j_x and $\partial C/\partial x$ must vary with y and z at any x. Thus, without assumption 3 eq. 2 cannot be integrated, so eq. 3 and 4 are unproven, and at this point must be considered to be merely intuitive. The equations do not appear to be at all obvious, especially when the diffusion coefficient is not independent of concentration.

The object of this note is to show that assumption 3 is unnecessary, for eq. 3 and 4 will be shown to be valid in the sense that A_e/L_e depends only upon the internal diffusion path of the diaphragm, no matter what that path may be.

Since the three dimensional nature of the diffusion cannot now be ignored, the starting point is eq. 1 rather than eq. 2. If the former equation is combined with a differential material balance and assumptions 1 and 2 are used one obtains

$$\nabla\cdot(D(C)\nabla C) = 0 \tag{5}$$

and this equation holds at all points in the fluid within the diaphragm. The boundary conditions are

$$C(0, y, z) = C_1$$
$$C(L, y, z) = C_2$$

and at every point along the walls of the pores.

$$\partial C/\partial n = 0$$

where n is distance in the direction normal to the pore wall. The diffusion within the pores is now completely defined by the above boundary value problem. Although it is not amenable to solution because of the geometrical complexities,[4] the form of the solution can be deduced as follows: with the transformations

$$C' = \frac{C_1 - C}{C_1 - C_2} \tag{6}$$

$$\epsilon = \int_0^{C'} \frac{D(C_1 - C_1C' + C_2C')}{\bar{D}}\,dC' \tag{7}$$

$$r' = \frac{r}{L} \tag{8}$$

eq. 5 is reduced to Laplace's Equation

$$\nabla'^2\epsilon = 0 \tag{9}$$

and the boundary conditions now are

$$\epsilon(0, y', z') = 0$$
$$\epsilon(1, y', z') = 1$$
$$\frac{\partial\epsilon}{\partial n'} = 0 \text{ at the pore walls}$$

The ∇' operator is based on the reduce length coördinate given by eq. 8 and r is the position vector.

Since there are no quantities in eq. 9 and the boundary conditions besides numerical constants, the dependent variable ϵ and the independent space variable r', ϵ must be a function of r' alone. Thus the solution may be written as

$$\epsilon = f(r') \tag{10}$$

where the function f depends only upon the internal geometry of the diaphragm, is continuous and is defined at all points within the pores of the diaphragm.

The x direction component of the vector flux j at any point is given by

$$j_x = -D(C)\frac{\partial C}{\partial x} \tag{11}$$

and with eq. 6 to 8 and 10 it becomes

$$j_x = \frac{\bar{D}}{L}(C_1 - C)\frac{\partial\epsilon}{\partial x'} = \frac{\bar{D}}{L}(C_1 - C_2)\frac{\partial f(x', y', z')}{\partial x'} \tag{12}$$

By assumption 2 the total rate of diffusion across any y-z plane must be independent of x, since the only net diffusional flow through the diaphragm is in the x direction. Furthermore since the rate of diffusion across any y-z surface is the integral of j_x over that surface, integration of eq. 12 over all the surfaces formed by the intersection of any y-z plane with the fluid inside the pores gives the total rate of diffusion *through* the diaphragm. Choosing the $x = 0$ plane for convenience, calling A_0 the total area of all the surfaces formed by the intersection of this y-z plane with the pores (this is the total open area of the diaphragm at the $x = 0$ face) and using eq. 12

$$N = \int_0^{A_0} j_x\Big|_{x=0} dA = \bar{D}(C_1 - C_2)\left[\frac{1}{L}\int_0^{A_0}\frac{\partial f}{\partial x'}\Big|_{x'=0} dA\right] \tag{13}$$

where $\bar{D}$ is given by eq. 4 and L is the diaphragm thickness.

But the term in brackets depends only upon the diaphragm geometry and by comparison with eq. 3 is equal to A_e/L_e. Consequently, the use of eq. 3 and 4 for diffusion measurements does not depend at all upon the assumption of unidirectional dif-

(2) A. R. Gordon, *Ann. N. Y. Acad. Sci.*, **46**, 285 (1945).

(3) The open area of the diaphragm may vary with x.

(4) These complexities are in the third boundary condition.

fusion. Put in another manner, as far as diffusion is concerned the diaphragm does effectively behave as if it were made up of a series of parallel capillaries.

Acknowledgment.—The author is grateful to the National Science Foundation for their support of this work.

A MODIFICATION OF FUJITA'S METHOD FOR THE CALCULATION OF DIFFUSION COEFFICIENTS FROM BOUNDARY SPREADING IN THE ULTRACENTRIFUGE

BY K. E. VAN HOLDE

Department of Chemistry and Chemical Engineering, University of Illinois, Urbana, Illinois

Received April 13, 1960

Fujita[1] has shown theoretically that the boundary spreading during the ultracentrifugation of a homogeneous solute is quite strongly influenced by a concentration dependence of the sedimentation coefficient. For this reason, calculation of diffusion coefficients from the sedimenting boundary by use of equations which neglect the concentration effects can lead to considerable error. This has been demonstrated experimentally by Baldwin,[2] and the superiority of Fujita's approach shown.

The approximate equation obtained by Fujita[1,3] for the height–area ratio (H/A) of the sedimenting boundary may be written

$$\frac{H}{A}\sinh\frac{\tau}{2} = \frac{G(\xi_m)}{2kC_0r_0} \qquad (1a)$$

or, to a good approximation in most cases of interest

$$\frac{H}{A}\tau = \frac{G(\xi_m)}{kC_0r_0} \qquad (1b)$$

where

$$\tau = 2S(0)\omega^2 t \qquad (2a)$$

$$\xi_m = \frac{r_0\omega^2S(0)kC_0}{2D^{1/2}}\left(1 - \frac{1}{2}(1 - kC_0)\omega^2S(0)t\right)t^{1/2} \qquad (2b)$$

Here t is time, ω the angular velocity of the ultracentrifuge rotor, r_0 the meniscus position, D the diffusion coefficient, and C_0 the initial solute concentration. The dependence of the sedimentation coefficient S upon the concentration is assumed to be of the form

$$S = S(0)(1 - kC) \qquad (3)$$

where k is the constant appearing in equations 1 and 2, and $S(0)$ is the sedimentation coefficient at zero solute concentration. The diffusion coefficient is assumed to be independent of C. The function $G(\xi_m)$ is

$$G(\xi_m) = 2\xi_m\left[\xi_m + \frac{e^{-\xi_m^2}}{\pi^{1/2}[1 + \Phi(\xi_m)]}\right] \qquad (4a)$$

where

$$\Phi(\xi_m) = \frac{2}{\pi^{1/2}}\int_0^{\xi_m} e^{-q^2}dq \qquad (4b)$$

Because of the unwieldy form of the function G, Fujita[3] has proposed use of a tabulated inverse function, $G^{-1}\ (kC_0r_0\ (H/A)\tau)$, which may be used in a graphical method for the evaluation of D. However, this suffers from the disadvantage that $S(0)$ and the constant k, which measures the dependence of S upon C, must be known in advance. Thus, a series of experiments must be carried out, to evaluate the concentration dependence of S, before D can be evaluated from any experiment.

While Fujita has shown that excellent results can be obtained in this way, the method is clearly unsuited to the case where one wishes to obtain a fair estimate of D from a single sedimentation experiment. For this reason, it is desirable to attempt to cast equation 1b into a form which involves as variables only quantities which can be evaluated during a single experiment. This can be done fairly easily for the case where ξ_m is small. This will be true in many experiments with globular proteins, where k is generally small. In this event $G(\xi_m)$ can be usefully expanded in a Maclaurin series

$$G(\xi_m) = G(0) + \xi_mG'(0) + \frac{\xi_m^2}{2}G''(0) + \frac{\xi_m^3}{6}G'''(0) \qquad (5)$$

Evaluation of the coefficients in this series leads to the expression

$$G(\xi_m) = \frac{2}{\pi^{1/2}}\xi_m + 2\left(1 - \frac{2}{\pi}\right)\xi_m^2 + \frac{2}{\pi^{1/2}}\left(\frac{4}{\pi} - 1\right)\xi_m^3 + \ldots \qquad (6)$$

if $\xi_m \leqslant 0.4$, the first two terms of this series will give a satisfactory approximation for most cases. Insertion of (6) into (1b), noting that

$$(1 - kC_0)S(0) = S \qquad (7)$$

where S is the sedimentation coefficient at concentration C_0, we obtain, after rearrangement

$$\left(\frac{H}{A}\right)t^{1/2}\left(1 - \frac{1}{2}\omega^2St\right)^{-1} = \frac{1}{(4\pi D)^{1/2}} + \left(1 - \frac{2}{\pi}\right)\frac{r_0\omega^2S}{4D}\left[\frac{kC_0}{1 - kC_0}\right]\left(1 - \frac{1}{2}\omega^2St\right)t^{1/2} + (0)t + \ldots \qquad (8)$$

The variable on the left may be plotted *vs.* the quantity $(1 - {}^1/_2\ \omega^2St)t^{1/2}$ for the various photographs, to yield a straight line, with an intercept at $t = 0$ given by

$$\text{intercept} = \frac{1}{(4\pi D)^{1/2}} \qquad (9a)$$

The slope of the line will be

$$\text{slope} = \left(1 - \frac{2}{\pi}\right)\frac{r_0\omega^2S}{4D}\left[\frac{kC_0}{1 - kC_0}\right] \qquad (9b)$$

and the ratio

$$\frac{(\text{slope})}{(\text{intercept})^2} = (\pi - 2)r_0\omega^2S\left[\frac{kC_0}{1 - kC_0}\right] \qquad (9c)$$

will allow evaluation of k. Thus estimates of the diffusion coefficient, the sedimentation coefficient and the concentration dependence of S are obtained from a single experiment. The left side and first term on the right in equation 8 are similar to the limiting equation obtained by Fujita[4] for the sedimentation of a differential boundary between two solutions, with the assumption of negligible concentration dependence.

(1) H. Fujita, *J. Chem. Phys.*, **24**, 1084 (1956).
(2) R. L. Baldwin, *Biochem. J.*, **65**, 503 (1957).
(3) H. Fujita, THIS JOURNAL, **63**, 1092 (1959).
(4) H. Fujita, *J. Chem. Phys.*, **31**, 5 (1959).

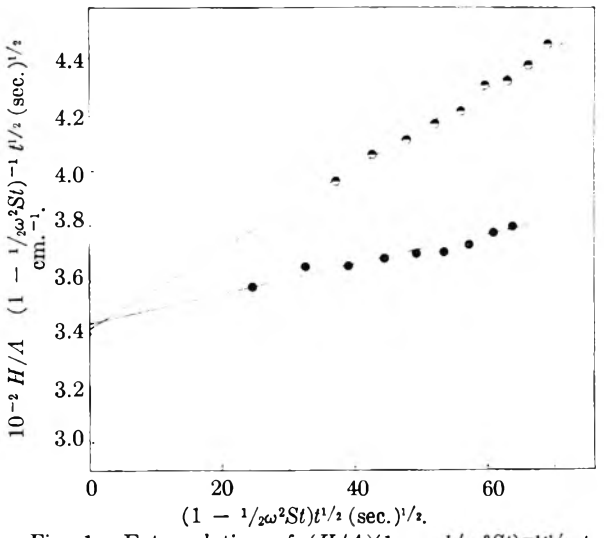

Fig. 1.—Extrapolation of $(H/A)(1 - {}^1/_2\omega^2St)^{-1}t^{1/2}$ to $t = 0$ for bovine serum albumin. Data of Baldwin[2] at $C_0 = 0.67$ g./100 ml. (filled circles) and at $C_0 = 1.35$ g./100 ml. (half-filled circles).

As a test, the method has been applied to the same data of Baldwin[2] which were used by Fujita.[3] The protein is bovine serum albumin, sedimenting in buffer, at protein concentrations of 0.67 g./100 ml. and 1.35 g./100 ml. Graphs according to equation 8 are shown in Fig. 1. Within experimental error, the data seem to lie on straight lines. The constants evaluated from the intercept and slope are recorded in Table I.

TABLE I

COMPARISON OF D AND k VALUES

C_0 (g./100 ml.)	$D^a \times 10^7$	$D^b \times 10^7$	$D^c \times 10^7$	k^a	k^d
0.67	6.72	6.79	6.85	0.055	0.057
1.35	6.85	6.93	6.94	0.073	0.059

[a] From equation 8. Units of D are cm.^{2}/sec., units of k (g./100 ml.)$^{-1}$. [b] By Fujita's method, ref. 3. [c] Evaluated by Baldwin from free diffusion data of Gosting.[5] [d] From S *vs.* C_0 graph; Baldwin.[2]

It is felt that in the region of small ξ_m and τ, the method outlined here yields results for D which compare favorably with those of Fujita's method. The value obtained for k is presumably more sensitive to assumptions in the theory.

In conclusion, it should be noted that pronounced heterogeneity should lead to marked deviations from the simple straight line extrapolation.

This investigation was supported in part by a PHS research grant No. A3096, from the National Advisory Council on Arthritis and Metabolic Diseases, Public Health Service.

(5) Values quoted by Fujita, ref. 3.

B^{11} N.M.R. SPECTRA OF ALKYLDIBORANES, TRIALKYLBORANES AND $NaBHEt_3$

BY ROBERT E. WILLIAMS,[1] H. DWIGHT FISHER[2] AND CHARLES O. WILSON[1]

Olin Mathieson Research Laboratory,[1] Pasadena, California

Received April 18, 1960

Boron-11 chemical shift values of a large number of compounds[3,4] have been compiled. The spectrum of triethylborane is found at lowest field by a considerable margin and consists of a broad singlet suggesting perhaps unresolved proton–boron coupling. (The boron–boron coupling of the single bond in tetraborane[5] had been found to be about 23 c./s.). The possibility of detecting boron–boron coupling in diborane and its derivatives had long been considered to be of interest. These questions led to a B^{11} n.m.r. survey of the various methyldiboranes, B-deuteriomethyldiboranes, some ethyldiboranes, the trimethyl- and triethylboranes, as well as trimethylborane-d_9. The system triethylborane–sodium hydride also was investigated.

The various samples were prepared by mixing the isotopically appropriate trialkylborane with the isotopically appropriate diborane[6] and placed in 5 mm. o.d. tubes for B^{11} n.m.r. study at 12.8 mc. The chemical shifts were measured in parts per million from BF_3 etherate as zero. Compounds were isolated by vapor–liquid partition chromatography. The column consisted of 20 ft. of 10 mm. i.d. Pyrex tubing, coiled to fit into a large dewar, packed with a 30% Kel-F 90 on 30 mesh firebrick. Separations were carried out at −15° to 5° with a helium flow rate of 60 cc. per minute.

Trialkylboranes.—The chemical shift of trimethylborane has a value of −84 compared to −85 for triethylborane and tripropylborane.[3] The half-width of the resonance of triethylborane-d_{15} and of the isotopically normal triethylborane are found to be identical (70 c./s.). Since deuterium–boron coupling would spread the B^{11} n.m.r. spectrum only one third of the equivalent proton–boron coupling the width of the B^{11} n.m.r. spectrum of triethylborane must, therefore, result from factors other than proton–boron coupling (possibly quadrupole relaxation).

Alkyldiboranes.—The spectra of the various isotopically normal methyldiboranes are shown in Fig. 1; the chemical shift values (δ) are represented as dots, the spin coupling constants between boron and terminal protons (J_t) and between boron and bridge protons (J_b) are recorded along the right. The methyldiboranes prepared from deuteriodiborane showed essentially identical chemical shift values (in parentheses) at 12.8 mc. No deuterium–boron coupling was resolved. The chemical shifts of the few ethyldiboranes studied did not differ detectably from their methyl analogs.

All of the above spectra were obtained in the liquid phase. Those of the mono- and trialkyldiboranes were obtained at reduced temperature because of rapid disproportionation. In Fig. 1 it is shown that 1,2-dimethyldiborane (Y) rapidly appears in the methyldiborane by disproportionation. In the trimethyldiborane spectrum an impurity arising during the synthesis of trialkylborane is represented by (Z). Satisfactory spectra of tetra-

(1) Now affiliated with National Engineering Science Co. Pasadena, California.

(2) Hughes Tool Co., Culver City, California.

(3) T. P. Onak, H. Landesman, R. E. Williams and I. Shapiro, THIS JOURNAL, **63**, 1533 (1959).

(4) W. D. Phillips, H. C. Miller and E. L. Muetterties, *J. Am. Chem. Soc.*, **81**, 4496 (1959).

(5) R. E. Williams, S. G. Gibbins and I. Shapiro, *ibid.*, **81**, 6164 (1959).

(6) C. O. Wilson and I. Shapiro, *Anal. Chem.*, **32**, No. 1, 78 (1960).

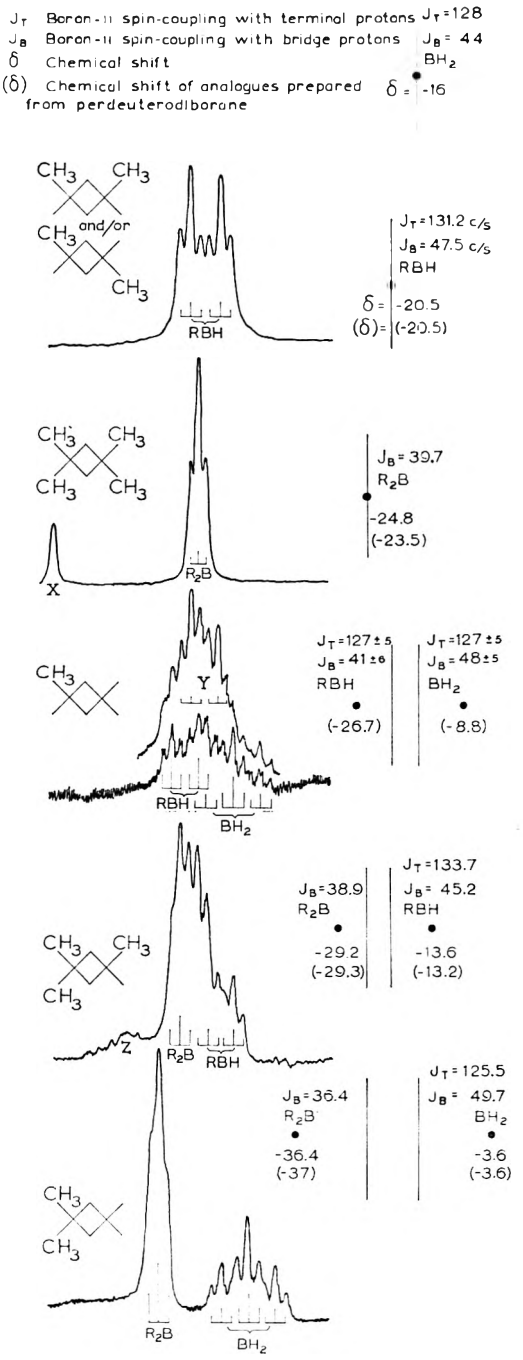

Fig. 1—B^{11} nuclear magnetic resonance data of methyldiborane.

methyldiborane could only be obtained in the presence of a significant excess of trimethylborane. The excess of trimethylborane (X in Fig. 1) maintains the concentration of tetramethyldiborane. Without the influence of trimethylborane upon the various alkyldiborane equilibria the tetramethyldiborane rapidly disproportionates to produce trimethylborane and the lesser alkylated diboranes.

The spectra of the methyldiboranes may best be interpreted by pointing out two effects that apparently determine the resulting B^{11} chemical shifts. First, alkyl groups tend to shift the associated boron nuclei to lower field. In the symmetrical series diborane, 1,2-dimethyldiborane and tetramethyldiborane, the trend is to lower field with alkylation; these molecules are made up of two identical "halves." Second, unsymmetrical substitution promotes an even greater divergence of chemical shift values. When two "halves" of the molecule differ by one alkyl group the shifts to lower and higher field are enhanced; when the "halves" differ by two alkyl groups, the divergent shifts are even greater; *i.e.*, the chemical shifts of 1,1-dimethyldiborane, where the divergence of BH_2 and BR_2 groups is about doubled. Certain cyclic alkyldiboranes (1,2-tetramethylenediborane and 1C-methyltrimethylenediborane)[7] have chemical shift values similar to those of 1,2-dimethyldiborane.

Similar chemical shift behavior upon alkylation was also observed in 2,4-dimethylenetetraborane.[8,9] No resolution of boron–boron coupling could be detected in the spectra of any of the diboranes and certainly cannot exceed a few cycles (Fig. 1).

$NaBHEt_3$–BEt_3 Exchange.—Sodium hydride reacts with triethylborane and is known to form a liquid which is immiscible with additional triethylborane. This liquid, saturated with triethylborane, produced a broad peak in the B^{11} spectrum; as the excess triethylborane was removed the peak shifted to higher field. Addition of diethyl ether reduced the viscosity and narrowed the peak. When excess sodium hydride was introduced into the sample, the spectrum remained unchanged. However, upon re-examination, several months later, the singlet had changed into a doublet centered at the chemical shift position of the previous singlet. Apparently rapid intermolecular exchange of the protons takes place at room temperature in the presence of even a trace of BEt_3; thus, the boron nuclei spend a portion of their time as BEt_3 and a portion of the time as $NaBHEt_3$. Exchange evidently cannot take place in the absence of a trace of triethylborane as removed by several months' contact with NaH.

(7) H. G. Weiss, W. J. Lehmann and I. Shapiro, *J. Am. Chem. Soc.*

(8) B. C. Harrison, I. J. Solomon, R. D. Hites and M. J. Klein, Abstracts of the 135th ACS Meeting, Boston, Mass., also (*Inorganic and Nuclear Chem.*, 1960).

(9) S. G. Gibbins, I. Shapiro and R. E. Williams, *J. Phys. Chem.*

KINETICS OF THE REACTION OF HYDROGEN IODIDE AND DI-*t*-BUTYL PEROXIDE IN CARBON TETRACHLORIDE[1]

BY GEORGE A. LO AND WENDELL M. GRAVEN

Chemistry Department, University of Oregon, Eugene, Oregon

Received April 18, 1960

Analysis for dialkyl peroxides by chemical methods is difficult,[2] as a result of their unreactive behavior toward the usual oxidation–reduction reagents.

In contrast to the behavior of hydroperoxides, such as *t*-butyl hydroperoxide, or diacyl peroxides, such as dibenzoyl peroxide, di-*t*-butyl peroxide is not reduced readily by alkali iodide in the presence

(1) Taken from the M.A. thesis of G. A. Lo, University of Oregon, 1960.

(2) G. J. Minkoff, *Proc. Roy. Soc. (London)*, **A224**, 176 (1954).

of acetic acid,[3] nor by concentrated aqueous solutions of hydriodic acid.[4]

The relatively sluggish nature of the reaction between hydriodic acid and dialkyl peroxides permits investigation of the kinetics of one type of reduction reaction of organic peroxides.

Experimental

Materials.—Di-*t*-butyl peroxide, the minimum purity of which was stated by Wallace and Tiernan Co. to be 97%, was further purified by fractional distillation under reduced pressure in an all-glass system. The fraction boiling at 52.5 ± 0.5° under 98.5 mm.,[5] and exhibiting a refractive index, $n^{20}D$, of 1.3878, was used in this investigation.

Production of hydrogen iodide usually was accomplished by dropping 50% hydriodic acid on phosphorus pentoxide. In several runs hydrogen iodide, produced by heating 80% phosphoric acid with sodium iodide, was substituted without any apparent effect on the results. Nitrogen was used to sweep the hydrogen iodide through a calcium chloride drying tube cooled with ice and a trap cooled with Dry Ice–acetone into the reaction vessel. A fresh preparation under an atmosphere of Matheson's "prepurified" nitrogen, was made for each individual run.

Reagent grade carbon tetrachloride was used directly or dried over magnesium perchlorate without observing any significant change in the results.

Methods.—For quantitative analysis of the organic reaction product, as well as the unreacted peroxide, an Infracord Model 137 spectrophotometer was employed. Reference to calibration curves prepared from absorbancies of standard solutions at wave lengths corresponding to characteristic absorption bands of peroxide, 11.4 μ, and alkyl iodide, 8.8 μ, made possible the quantitative analyses which were necessary for determining the stoichiometry of the reaction.

A colorimetric method, which was used for determination of iodine and hydrogen iodide concentrations, involved the use of a Klett–Summerson photoelectric colorimeter.

Concentrations of iodine solutions in carbon tetrachloride within the range of 10^{-5}–$10^{-3}M$ were determined with a precision of ±2% from an empirical equation obtained by a least squares fitting of the absorbancies of standard iodine solutions to a Beer's law expression.

Colorimetric determinations of hydrogen iodide concentrations were carried out in the same manner as the iodine analyses after oxidation with dibenzoyl peroxide. A volumetric precipitation method using standard silver nitrate with eosin as an adsorption indicator was used to check the accuracy of the colorimetric method. Agreement between the two methods approximated the previously cited average deviation of the colorimetric determinations.

Kinetic studies of the reaction were carried out in a three-neck flask which was equipped with an inlet tube for introduction of hydrogen iodide into the carbon tetrachloride solution, an opening for introduction of the peroxide solution, a gas-tight stirrer and a stopcock arrangement for withdrawing aliquots of the reaction mixture while maintaining a nitrogen atmosphere within the vessel. The exterior of the vessel was covered to shield the contents from light before it was immersed in a Lo-temp constant temperature bath. A mercurial thermoregulator facilitated maintenance of a bath temperature constant to within ±0.02° for indefinite periods. The temperature of the bath was measured with a thermometer which had been calibrated against a platinum resistance thermometer certified by the National Bureau of Standards.

Prior to the production of hydrogen iodide the gas-generation vessel and the reaction vessel, together with the carbon tetrachloride which it contained, were deaerated with a stream of nitrogen. The duration of flow of hydrogen iodide to the reaction vessel determined the initial concentration of the hydrogen iodide solution which was determined by colorimetric analysis of an aliquot prior to the addition of peroxide. While the hydrogen iodide solution was being produced in the reaction vessel a di-*t*-butyl peroxide solution of known concentration was prepared by quantitative dilution of a measured volume of peroxide with carbon tetrachloride. This solution also was deaerated and brought to the temperature of the bath.

Addition of the peroxide solution to the reaction vessel initiated the reaction. Although "zero" time was chosen as the completion of the addition of peroxide solution it should be apparent that the origin of the time scale which is shown in each of the figures is not absolute. The stirrer was operated for several minutes to ensure thorough mixing of the solutions.

Progress of the reaction was followed by colorimetric measurement of the concentration of liberated iodine in aliquots withdrawn from the reaction mixture at periodic intervals. The concentration of hydrogen iodide in the reaction mixture was also monitored by adding excess dibenzoyl peroxide to the aliquot after the colorimetric measurement and repeating the iodine analysis after a suitable time interval.

In a few runs a constant concentration of hydrogen iodide was maintained by stirring the reaction mixture while keeping an atmosphere of hydrogen iodide gas in contact with it.

The presence in the reaction mixture of iodine was identified by the characteristic violet color of its solution in carbon tetrachloride. The presence of water was shown by the formation of a separate phase in certain runs and confirmed by tests with anhydrous copper sulfate. The only organic reaction product which was identified from the infrared absorption spectrum of the reaction mixture was *t*-butyl iodide. However, in order to obtain reasonably conclusive evidence from infrared spectrophotometric measurements the concentrations of reactants ranged from 10^{-2}–$10^{-1}M$, although the kinetic measurements were made at much lower concentrations.

Results

Six runs were made with relatively high initial concentrations of reactants, the peroxide being in substantial excess, in order to obtain quantitative information regarding the stoichiometric relations among reactants and products. From the known initial concentrations of reactants and subsequent analyses after the reaction had removed nearly all of the hydrogen iodide the consumption of reactants and formation of products shown in Table I were obtained.

With the additional knowledge that water is one of the reaction products the data of Table I are consistent with the stoichiometric equation

$$(CH_3)_2COOC(CH_3)_3 + 4HI = 2(CH_3)_3CI + 2H_2O + I_2 \quad (1)$$

TABLE I

STOICHIOMETRIC RELATIONSHIPS WITH HIGH REACTANT CONCENTRATIONS

Reactants consumed (moles/l. × 10^3)		Products formed (moles/l. × 10^3)	
HI	*t*-Bu_2O_2	*t*-BuI	I_2
..	2.0	3.4	1.8
5.2	..	2.4	1.1
..	3.7	7.1	3.0
4.3	1.5	2.3	1.1
4.1	1.1	..	1.0
2.4	..	1.1	0.57

In more than half of the kinetic runs the peroxide concentrations were 10 to 100 times as large as the 10^{-4}–$10^{-3}M$ initial hydrogen iodide concentrations. Under these conditions the reaction was sufficiently rapid so that the final iodine concentrations corresponded to the completion of the reaction. Without exception the final iodine concentrations were equal to one-half the initial hydrogen iodide concentrations, thus eliminating *t*-butyl iodide as a

(3) F. H. Dickey, J. H. Raley, F. F. Rust, R. S. Treseder and W. E. Vaughan, *Ind. Eng. Chem.*, **41**, 1673 (1949).

(4) N. A. Milas and D. M. Surgenor, *J. Am. Chem. Soc.*, **68**, 205 (1946).

(5) W. Lobunez, J. R. Rittenhouse and J. G. Miller, *ibid.*, **80**, 3505 (1958).

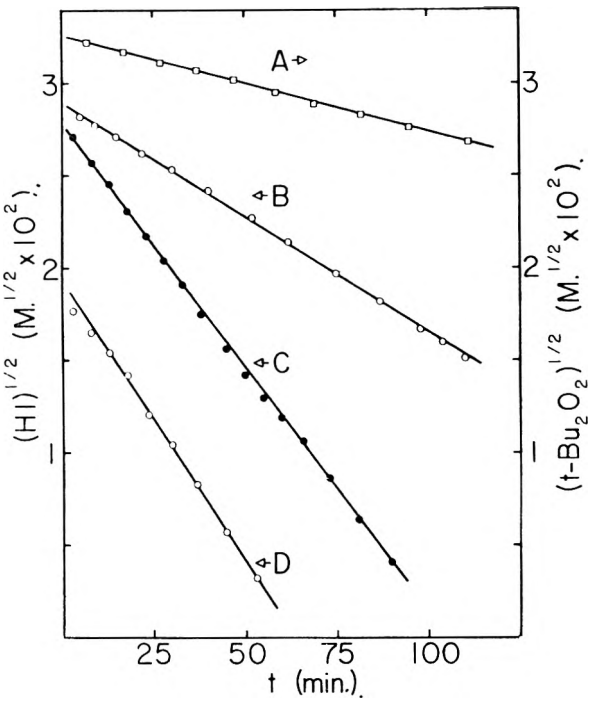

Fig. 1.—Dependence of reaction rate on reactant concentrations. A: $(t\text{-Bu}_2\text{O}_2)_i = 1.06 \times 10^{-3}$ *M*, $(\text{HI}) = 1.0 \times 10^{-2}$ *M*, $T = 24.80°$; B: $(t\text{-Bu}_2\text{O}_2)_i = 5.26 \times 10^{-3}$ *M*, $(\text{HI})_i = 8.53 \times 10^{-4}$ *M*, $T = 24.80°$; C: $(t\text{-Bu}_2\text{O}_2)_i = 2.17 \times 10^{-2}$ *M*, $(\text{HI})_i = 7.82 \times 10^{-4}$ *M*, $(t\text{-BuOH})_i = 2.94 \times 10^{-4}$ *M*, $T = 24.80°$; D: $(t\text{-Bu}_2\text{O}_2)_i = 2.21 \times 10^{-2}$ *M*, $(\text{HI})_i = 3.60 \times 10^{-4}$ *M*, $T = 24.80°$.

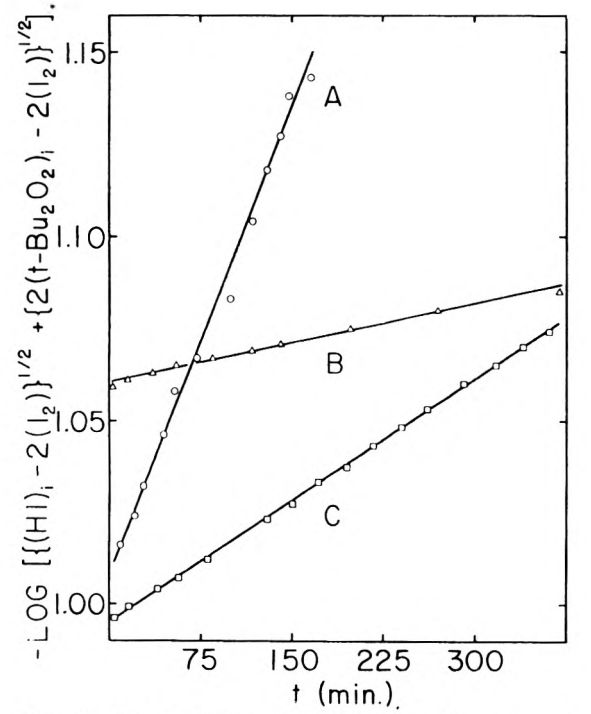

Fig. 2.—Effect of temperature on reaction rate. A: $(t\text{-Bu}_2\text{O}_2)_i = 1.08 \times 10^{-3}$ *M*, $(\text{HI})_i = 2.66 \times 10^{-3}$ *M*, $T = 34.90°$; B: $(t\text{-Bu}_2\text{O}_2)_i = 1.08 \times 10^{-3}$ *M*, $(\text{HI})_i = 1.70 \times 10^{-3}$ *M*, $T = 14.70°$; C: $(t\text{-Bu}_2\text{O}_2)_i = 2.17 \times 10^{-3}$ *M*, $(\text{HI})_i = 1.25 \times 10^{-3}$ *M*, $T = 24.80°$.

possible reaction product. In this range of concentrations infrared absorption measurements could not be used to identify the organic reaction product.

It was demonstrated that within the higher concentration range *t*-butyl alcohol in carbon tetrachloride was converted rapidly to *t*-butyl iodide by hydrogen iodide at room temperature. Therefore, stoichiometric equation (2) is considered to represent the reaction under conditions of low hydrogen iodide concentration.

$$(\text{CH}_3)_3\text{COOC}(\text{CH}_3)_3 + 2\text{HI} = 2(\text{CH}_3)_3\text{COH} + \text{I}_2 \quad (2)$$

For determining the order of the reaction with respect to hydrogen iodide runs were made with a 10 to 100-fold excess of peroxide whose concentration could be treated as constant throughout the reaction. The initial concentration of hydrogen iodide was determined colorimetrically and its decreasing concentration was computed from the iodine concentrations measured at successive time intervals. Straight lines were obtained when the square root of the hydrogen iodide concentration was plotted against time, thus indicating a half order rate dependence on hydrogen iodide concentration. Typical examples of such plots are shown by curves B, C and D of Fig. 1.

For determining the order of the reaction with respect to di-*t*-butyl peroxide runs were carried out with constant hydrogen iodide concentration by keeping the solution saturated. The amount of peroxide consumed at successive time intervals was calculated from the amount of liberated iodine. Straight lines were obtained when the square root of the peroxide concentration was plotted against time, also indicating a half-order rate dependence on peroxide concentration. Curve A of Fig. 1 shows an example of these plots.

Addition of *t*-butyl alcohol in moderate concentration to the initial reaction mixture had no effect on the results as shown by curve C of Fig. 1.

The rate law (3) is suggested by the data which have been presented.

$$\text{d}(\text{I}_2)/\text{d}t = k(t\text{-Bu}_2\text{O}_2)^{1/2}(\text{HI})^{1/2} \quad (3)$$

Confirmation of this rather unusual reaction rate expression was obtained from runs in which the reactant concentrations were comparable.

Using the stoichiometry of equation 2 the rate law can be rewritten with the concentration of iodine as the dependent variable to facilitate integration, which yields the expression

$$-\log [\{(\text{HI})_i - 2(\text{I}_2)\}^{1/2} + \{2(t\text{-Bu}_2\text{O}_2)_i - 2(\text{I}_2)\}^{1/2}] = kt/3.26 + \text{constant} \quad (4)$$

where the i subscripts indicate initial concentrations. Data at three temperatures resulted in linear plots of the logarithmic term of equation 4 *vs.* time as shown in Fig. 2. An Arrhenius-type plot of the slopes of curves A, B and C, which span a 20° temperature range, yields a straight line, the slope of which corresponds to an activation energy of 22 kcal.

A reaction rate constant k can be computed from the slope of each of the three types of plots. Values of k obtained from 18 runs at 24.80° ranged from 1.1–3.6 $\times 10^{-5}$ sec.$^{-1}$, with a mean value of 2.0 $\pm$ 0.7 $\times 10^{-5}$ sec.$^{-1}$. Although the precision of measurement of k is unsatisfactory it should be noted that in these runs the initial concentrations of hydrogen iodide and di-*t*-butyl peroxide were

varied over 65-fold and 25-fold ranges, respectively, without observing evidence of a trend indicative of deviation from the rate law

$$d(I_2)/dt = 2.6 \times 10^{11} \exp(-22000/RT)(t\text{-}Bu_2O_2)^{1/2}(HI)^{1/2}$$

ULTRAFILTRATION OF SALT SOLUTIONS AT HIGH PRESSURES[1]

By C. E. Reid and H. G. Spencer

Department of Chemistry, University of Florida, Gainesville, Florida

Received April 14, 1960

Desalting by ultrafiltration recently has been investigated at pressures less than 100 atm.[2-4] This work is a study of the effect of higher pressures on the desalting properties of three membranes: polyvinyl alcohol, cellulose acetate and cellophane.

The bound water and ion-selective theories[2,3] for the function of the membranes in the desalting process indicate that convective and diffusive flows are involved, and that the convective flow of solution can be reduced by diminishing the pore size through the use of high pressure. Ticknor's proposal[5] that diffusive and convective flows of pure liquids occur in cellophane, and that pore size determines the type of flow, is essentially equivalent to the bound water theory. The bound water theory also emphasizes that ions which do not fit into the bound water network do not participate in the diffusive flow. If this is essentially correct, these relationships apply

$$Q_d = fQ \qquad (1)$$

and

$$Q_c = (1 - f)Q \qquad (2)$$

where Q is the flow rate, f the fraction of the ions rejected, Q_d the diffusive flow rate, or the flow of pure water, and Q_c the convective flow rate, or the flow of solution.

Experimental

Apparatus.—The desalting apparatus differs from the one reported previously[3] in that the pressure is applied by means of a piston-type pressure intensifier instead of by compressed air, and the porous disc which supports the membrane was made of stainless steel (Micro Metallic Inc.) instead of porcelain. Pressures were read directly from Bourdon pressure gauges.

The backstrokes of the intensifier piston, which occurred at intervals of 10 to 30 minutes, resulted in momentary pressure drops of as much as 20 atm. Flow rates, compared at 70 atm., were lower on this apparatus than those normally obtained on apparatuses with porcelain backing discs, which are more porous than the steel. However, the salt rejection values did not differ significantly. Comparisons of flow rates obtained with this apparatus should be significant, although different from those obtained with porcelain backing disks.

Materials.—Uncoated cellophane (du Pont PT-300) and cellulose acetate (du Pont CA-43), both approximately 0.88 mil (22 μ) thick, were tested without further treatment. Polyvinyl alcohol membranes, 0.6 mil (15 μ) thick, were prepared by casting aqueous solutions of du Pont Elvanol, Grade 72–60, and baking the resulting membranes to render them insoluble. Polyvinyl alcohol membranes also were modified by forcing a dilute (less than 5%) solution of hydrogen peroxide through them. Hydrogen peroxide solutions of higher concentration dissolved the membranes. Polyvinyl acetate membranes were prepared and tested, but were too flimsy to be evaluated at these high pressures.

Procedure.—All tests were made at room temperatures using 0.1 M NaCl solutions. The concentration in the apparatus was maintained constant during the run. Flow rates are reported as microliters per hour per cm.^{2} of membrane surface. Values were limited to an accuracy of ± 5 μl./hr./cm.^{2}. Salt rejection was determined by Mohr titration of the effluent and the solution in the apparatus. Frequent comparison of this method to analysis by conductivity measurements showed agreement within 2% rejection. Successive determinations of the salt rejection, in fractional reduction of chloride concentration, were within ± 0.01.

For cellophane, a different membrane was used in each run, which was duplicated at each pressure except 340 atm., where only a single run was carried out. Flow rates for the duplicate runs were reproducible within ± 5 μl./hr./cm.^{2}, and the salt rejection values did not differ more than 0.02. All the membranes were cut from the same 12 inch square of cellophane so that they might be as uniform as possible. For the other membranes, the various pressures were applied in succession to a single membrane.

Results

The results of the ultrafiltration measurements are presented in Table I. Essentially, salt rejection increased smoothly with pressure in all cases except

Table I

Results of Ultrafiltration Measurements

Membrane	P	Q	f	Q_d/P	Q_c/P
Cellophane	70	80	0.09	0.10	1.04
	135	110	.11	.09	0.73
	205	130	.14	.09	.55
	270	120	.22	.10	.35
	340	110	.37	.12	.20
Cellulose acetate	270	17	0.99	0.06	0.0006
	205	14	.99	.07	.0007
	135	7	.97	.05	.0015
Polyvinyl alcohol	70	60	0.06	0.06	0.80
	135	80	.10	.06	.53
	205	90	.16	.07	.37
	270	140	.20	.10	.41
	305	210	.16	.11	.58
(Failed at higher pressure—very rapid flow)					
Polyvinyl alcohol	70	50	0.09	0.07	0.64
	170	80	.13	.06	.41
(Failed at higher pressure—very rapid flow)					
Polyvinyl alcohol	100	110	0.13	0.13	0.96
(treated with H_2O_2)	170	120	.24	.17	.54
(Failed at higher pressure—very rapid flow)					

at the high pressures for one polyvinyl alcohol membrane, which could have resulted from the development of a minute leak before the large scale failure at higher pressures. Flow rates increased with pressure, with the exception that a maximum occurred at about 200 atm. for cellophane. Convective permeability, Q_c/P, decreased smoothly with pressure, except for the above mentioned polyvinyl alcohol membrane, while the diffusive permeability, Q_d/P, remained nearly constant or perhaps increased slightly. In the definition of diffusive permeability, P might better be replaced by the applied pressure dif-

(1) Based on the M.S. thesis of H. G. Spencer, February, 1958.

(2) C. E. Reid and E. J. Breton, *J. Appl. Polymer Sci.*, **1**, 133 (1959).

(3) J. G. McKelvey, K. S. Spiegler and M. R. J. Wyllie, This Journal, **61**, 174 (1957).

(4) Proceedings of a symposium, "Saline Water Conversion," National Academy of Sciences and National Research Council, Publication 568, Washington, D. C., 1957.

(5) L. B. Ticknor, This Journal, **62**, 1483 (1958).

ference minus the osmotic pressure; in this work, however, the effect of this correction would be only 1 to 4%, which is less than the uncertainty in other measurements.

The values reported in Table I are averages of the readings occurring after an induction period of 50 to 80 hours. At pressures of 205 atm. and above the induction period was characterized by an increase in salt rejection and a decrease in flow rate, while only the change in flow rate was significant below 205 atm. Several experiments with cellophane demonstrate the reversibility of the induction: (a) Salt rejection of 0.22 at 270 atm. decreased to 0.12 when the pressure was reduced to 135 atm. (b) The induction period was reproduced when the applied pressure was reduced to zero for 12 hours and then reapplied.

Discussion

The salt rejection of the membrane is increased by increasing the applied pressure, and this change is reversible. The behavior of the convective and diffusive permeabilities suggests that this change is a continuous reduction of the pore size. The reduction in convective permeability is large enough in cellophane to produce the maximum in its flow rate curve. These results support the theory of two mechanisms of flow and the role of pore size in determining the type of flow.

The increased salt rejection of polyvinyl alcohol when treated with hydrogen peroxide may be the result of degradation of the chain lengths which would allow greater deformation by pressure. However, infrared spectra of the treated membranes showed increased absorption at the frequency associated with the carbonyl group. Thus, the effect of introducing carbonyl groups into the membrane, and so changing its hydrogen bonding properties, should not be neglected in accounting for the change in salt rejection.

Acknowledgments.—The authors gratefully acknowledge the financial support of the Office of Saline Water, United States Department of the Interior.

THE THERMAL ISOMERIZATION OF *trans*-1,2-DICHLOROETHYLENE

BY COLIN STEEL

Chemistry Department, College of Forestry, State University of New York Syracuse, N. Y.

Received April 19, 1960

When Rabinovitch and Hulatt[1] reinvestigated the thermal isomerization of *trans*-1,2-dichloroethylene they obtained rate constants which were 1/50 to 1/150 the size of the commonly accepted values of Jones and Taylor.[2] Work carried out both in this Laboratory and at Edinburgh confirms the findings of Rabinovitch and Hulatt and indicates that the reaction proceeds by a free radical chain, so it can no longer be considered an example of a unimolecular reaction.

(1) B. S. Rabinovitch and M. J. Hulatt, *J. Chem. Phys.*, **27**, 592 (1957).

(2) J. L. Jones and R. L. Taylor, *J. Am. Chem. Soc.*, **62**, 3480 (1940).

Experimental

1. **Apparatus and Procedure.**—Both B.D.H. (England) and Eastman Kodak *trans*-1,2-dichlorocthylene were used. The samples were fractionally distilled until less than 0.2% of the *cis* isomer, as detected by gas chromatography, was present and then were kept in the dark at 3° until required. Two cylindrical Pyrex reaction vessels provided with axial thermocouple wells were used. Vessel I was 22 cm. long and had a diameter of 5 cm. Vessel II was 14 cm. long and had a diameter of 3.2 cm. These were contained within an electric furnace.

In the experiments with dichloroethylene alone the material was degassed thoroughly and then vaporized to the desired pressure in the storage bulb before the latter was momentarily opened to the reaction vessel. At the end of the run the products were frozen into an evacuated bulb held at liquid nitrogen temperature and then analyzed by gas chromatography. To eliminate complications due to back reaction, *viz.*, *cis*-$C_2H_2Cl_2 \rightarrow$ *trans*-$C_2H_2Cl_2$, the reaction was terminated when less than 10% of the *cis* isomer had been formed. Under these conditions the experimental first-order rate constant is given by $k(\text{sec.}^{-1}) = (\ln T_0 - \ln T_t)/t$, where t is the time of reaction and T_0 and T_t are the percentages of the *trans* isomer at times 0 and t. In the experiments with added gas (toluene or propylene) the procedure was similar, samples of the degassed hydrocarbon and dichloroethylene being frozen into a common mixing bulb. The percentage of added gas relative to the dichloroethylene was checked by analyzing a sample of the prereaction mixture by gas chromatography.

2. **The Effect of Mercury Vapor on the Reaction.**—If the reaction proceeds by a chain mechanism there is always the possibility that it may be inhibited by mercury vapor. The dichloroethylene pressure was read by means of a mercury manometer which was joined to the reaction vessel *via* a stopcock. After the initial pressure had been read the manometer was closed to the reaction vessel during the run. Since the reaction vessel was pumped down to 10^{-6} mm. before each run and was separated from the diffusion pump by a liquid air trap, the amount of Hg vapor in the vessel must have been very small. The dichloroethylene pressure was always 10 mm. or more so that unless the chains are very long any inhibition should be slight. To check this point a system was built which contained no mercury manometer, the pressure in the reaction vessel being estimated from the known total yield in products. No change in the rate constant was observed.

Results

1. **Surface Effects.**—Seasoning the reaction vessel with dichloroethylene for 20 hours at 500° resulted in a 30-fold reduction in the rate from that found with a clean vessel. However all attempts to obtain a reproducibly seasoned surface failed; not only were the rates sensitive to the temperature and duration of seasoning but the surface so obtained was not stable. Thus if air was admitted to the vessel for even a few minutes the vessel became deconditioned, that is, the rates increased, and even if no air was admitted the vessel slowly became deconditioned with the passage of time. This sensitivity of the rate to the nature of the surface probably is the reason for the erratic results obtained by Rabinovitch and Hulatt. When a vessel which had been seasoned repeatedly by the above procedure was opened to the atmosphere while hot the surface became coated with a lustrous layer of carbon. Although this surface proved to be stable, since subsequent opening to the air caused no further increase in the rate (runs 45–50), the best reproducibility was obtained by using a "clean" reaction vessel, which was opened to the air after every run to oxidize any material deposited on the surface. The following discussion refers to work in which a "clean" reaction vessel was used.

When the surface to volume ratio of reaction vessel II was increased fourfold by packing it with small pieces of 3 mm. Pyrex tubing the rate of isomerization decreased by somewhat more than threefold (Table I).

TABLE I

THE EFFECT OF SURFACE ON THE RATE OF ISOMERIZATION

Run	Press., cm.	Temp., °C.	$k \times 10^5$, sec.$^{-1}$	Vessel	Surface	Packing
54	10	295	69	II	Clean	Unpacked
59	10	379	2630	II	Clean	Unpacked
134	10	342	670	II	Clean	Unpacked
98–124[a]	10	342	200	II	Clean	Packed
132	2.9	342	187	II	Clean	Unpacked
133	2.9	342	55	II	Clean	Packed
45	7	391	460	I	Carbonized	Unpacked
46	7	391	440	I	Carbonized	Unpacked
47	7	325	36	I	Carbonized	Unpacked
48	7	388	510	I	Carbonized	Unpacked
49	7	310	13	I	Carbonized	Unpacked
50	7	347	80	I	Carbonized	Unpacked

[a] Interpolation from data given in Fig. 1.

2. Variation in the Rate with Substrate Pressure.—For the work reported in this section the packed reaction vessel II was used. Figure 1 shows a set of experimental results obtained at 342°. The experimental first-order rate constants are seen to be proportional to the pressure of dichloroethylene, so the reaction is kinetically second order. The open circles represent the extrapolation back to zero reaction time of several runs at each of the three pressures. Even after one run the reaction vessel became slightly seasoned so the experimental rate constant k decreased with increasing time. That the effect was due to seasoning was shown by performing a run of short duration (no. 114, 116) immediately after one of long duration (no. 113, 115) without opening the vessel to the air between the runs. The rate constants for runs 114 and 116 are significantly lower than those in which a completely unseasoned vessel was employed (no. 112, 117, 118). It should be noted that this seasoning is slight compared to the seasoning effect mentioned in the previous section.

3. Inhibition by Toluene and Propylene.—If the isomerization proceeds by a chain mechanism then hydrocarbons should exhibit an inhibiting effect by virtue of the reaction RH + X → R + HX where X is the chain-carrying radical and RH is the hydrocarbon. Toluene was chosen because of its proven ability to stop chains. Furthermore it introduces no complications since the benzyl radical, R, which is formed is very stable and is simply removed by dimerization. Table II shows the results with dichloroethylene–toluene mixtures at 342, and the decrease in rate with the increase in the percentage of toluene is evident. Propylene also was found to be an effective inhibitor (Table III) but in this case the reactions undoubtedly are more complex since the radical X not only can abstract hydrogen from the propylene but also can add on to the double bond.

Discussion

The results show that the reaction cannot be regarded as a unimolecular isomerization but are consistent with a chain mechanism in which the chain-carrying radicals are terminated either on the walls or by the reaction X + RH → R + HX. When the vessel is seasoned the surface is coated with a layer of polymeric hydrocarbon which provides a better radical trap, by virtue of the above reaction, than does the clean surface.

It is tempting to postulate a scheme in which chlorine atoms act as the chain-carrying radicals in a manner similar to iodine atoms in the iodine catalyzed isomerization of *cis*- and *trans*-dichloroethylene[3]

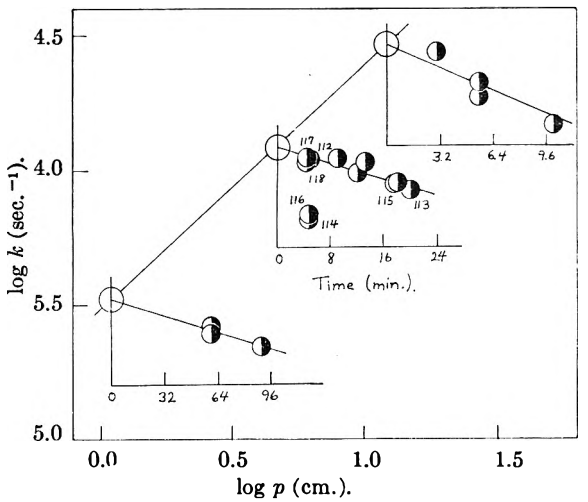

Fig. 1.—Variation in the first-order rate constant of isomerization at 342° with *trans*-dichloroethylene pressure. Insets show variation in rate constant with time of reaction.

TABLE II

INHIBITION BY TOLUENE[a]

$C_2H_2Cl_2 \times 10^7$, moles cc.$^{-1}$	Toluene $\times 10^7$, moles cc.$^{-1}$	$k \times 10^5$, sec.$^{-1}$
2.60	0	30[b]
26.0	0	312[b]
10.4	0 51	19.0
26.1	1 29	18.1
5.89	0 29	14.6
10.4	51	0.51
5.89	.29	15.7
6.08	1.32	3.1
3.68	1.14	2.4
7.25	2.23	3.7
2.05	0.76	1.6
4.37	1.79	1.7
2.71	1.12	1.8

[a] Reaction in packed vessel II at 342°. [b] Interpolation from data given in Fig. 1.

TABLE III

INHIBITION BY PROPYLENE[a]

$C_2H_2Cl_2 \times 10^7$, moles cc.$^{-1}$	Propylene $\times 10^7$, moles cc.$^{-1}$	$k \times 10^5$, sec.$^{-1}$
23.5	0	190
17.5	14.1	1.8
14.4	11.6	1.1
27.0	28.2	0.65
17.4	72.2	0.22

[a] Reaction in unpacked vessel II at 379°.

(3) R. E. Wood and R. G. Dickinson, *J. Am. Chem. Soc.*, **61**, 3259 (1939).

$$\text{Initiation} \longrightarrow \text{Cl}\cdot \quad (1)$$
$$\text{Cl}\cdot + \textit{trans}\text{-}C_2H_2Cl_2 \longrightarrow C_2H_2Cl_3\cdot \quad (2)$$
$$C_2H_2Cl_3\cdot \longrightarrow \text{Cl}\cdot + \textit{trans}\text{-}C_2H_2Cl_2 \quad (3)$$
$$C_2H_2Cl_3\cdot \longrightarrow \text{Cl}\cdot + \textit{cis}\text{-}C_2H_2Cl_2 \quad (4)$$
$$\text{Cl}\cdot \longrightarrow \text{termination} \quad (5)$$

That most of the $C_2H_2Cl_3$·radicals react by (3) and (4) rather than being lost by dimerization or by a metathetical reaction with dichloroethylene is not surprising when we consider that the activation energies for reactions 3 and 4 probably are only about 30 kcal. Indeed the experimental data fit such a scheme well, but a difficulty arises when we consider the nature of the initiation reaction. If chlorine atoms arise from the unimolecular decomposition of *trans*-dichloroethylene the experimental activation energy will be close to E_1, the activation energy of reaction 1. The latter should be equal to the C–Cl bond dissociation energy which is probably at least 70 kcal. mole^{-1}.[4] However the experimental activation energy was found to be only 32 ± 2 kcal. mole^{-1} (Table I, runs 45–50). Rabinovitch and Hulatt obtained the same value.[5] If the chain-carrying radicals arise from a reaction which is second order with respect to dichloroethylene and if the termination is second order with respect to chlorine atoms similar over-all kinetics are obtained but the experimental activation energy is only half the activation energy for the initiation reaction. Thus although an initiation of the type

$$2CHCl{=}CHCl \longrightarrow \cdot CHCl{-}CHCl{-}CHCl{-}CHCl\cdot \quad (1')$$
$$\cdot CHCl{-}CHCl{-}CHCl{-}CHCl\cdot \longrightarrow CHCl{=}CH{-}CHCl{-}CHCl\cdot + \text{Cl}\cdot$$

is possible, there is no direct experimental justification for it.

The data for the inhibited reaction do not throw more light on the problem. If we assume that in the presence of toluene (or propylene) the main termination reactions are

$$C_2H_2Cl_3\cdot + RH \longrightarrow C_2H_3Cl_3 + R\cdot \quad (6)$$

and

$$\text{Cl}\cdot + RH \longrightarrow HCl + R\cdot \quad (7)$$

then the steady-state expressions for first-order and second-order initiation are, respectively

$$\frac{k}{[C_2H_2Cl_2]} = \frac{k_1k_2k_4}{(k_3k_7 + k_4k_7)[RH] + (k_6k_7)[RH] + (k_2k_6)[RH][C_2H_2Cl_2]} \quad (8)$$

and

$$\frac{k}{[C_2H_2Cl_2]^2} = \frac{k_1'k_2k_4}{(k_3k_7 + k_4k_7)[RH] + (k_6k_7)[RH]^2 + (k_2k_6)[RH][C_2H_2Cl_2]} \quad (9)$$

Unfortunately few of the individual rate constants are known precisely. Linear plots for both $k/[C_2H_2Cl_2]$ and $k/[C_2H_2Cl_2]^2$ *vs.* the denominator of the right-hand side in (8) and (9) can be obtained by choosing reasonable values for k_2, k_3, k_4, k_6 and k_7.

(4) T. L. Cottrell, "The Strengths of Chemical Bonds," Butterworth's Publications, London, 1958.

(5) B. S. Rabinovitch, private communication, 1958.

In one case when an old sample of dichloroethylene which had been standing in the laboratory for some time was used high rates comparable to those of Jones and Taylor were obtained. It would therefore appear that the high rates obtained by those workers were due to the presence of impurities which can act as chain initiators and we cannot overlook the possibility that despite the care exercised in purification trace impurities are still present which would account for the low activation energy.

Acknowledgments.—My thanks are due to Dr. J. H. Knox and Dr. M. Szwarc for helpful advice and to the National Science Foundation for financial support.

POLAROGRAPHY OF NIOBIUM AND TANTALUM PEROXIDE COMPLEXES

BY JOHN H. KENNEDY

Explosives Department, E. I. du Pont de Nemours & Company, Wilmington, Delaware

Received April 22, 1960

The polarography of peroxide complexes of vanadium, tungsten and molybdenum has been studied by Kolthoff and Parry.[1] They observed kinetic waves or peaks in acid solution which were very sensitive to the metal ion concentration. Niobium and tantalum form stable peroxide complexes[2,3] and, because of their similarity to vanadium, tungsten and molybdenum, it was hoped that they, too, would give kinetic waves.

Experimental

A Sargent Model XXI Polarograph was used for the polarographic measurements. All runs were made at 25° with a drop time of 3.5 seconds and a drop weight of 11.0 mg./drop. The solutions were not de-aerated because bubbling in nitrogen promoted decomposition of the peroxide (catalyzed by niobium and tantalum), and non-reproducible results were obtained. Oxygen reduction does not occur until −0.1 v. *vs.* S.C.E., and thus did not interfere.

Solutions were prepared by adding a sodium niobate or tantalate solution to a hydrogen peroxide solution buffered to the desired *p*H with a phosphate buffer.

Sodium niobate and tantalate were prepared by fusing the oxides in potassium hydroxide, dissolving in water, and adding sodium hydroxide to precipitate the sodium salts. Washed free of excess sodium hydroxide, these salts were water-soluble.

Baker and Adamson 30% hydrogen peroxide was used, and all other chemicals were reagent grade.

Blank runs were made, *i.e.*, containing no niobium or tantalum. The blank current was measured at the potential corresponding to the niobium (or tantalum) peak and was subtracted from the peak current observed in the presence of Nb and Ta at the same potential to yield the catalytic peak current, i_p. These are the values reported in Table I.

Results and Discussions

Figure 1 shows the polarographic wave which was observed for peroxide reduction at *p*H 5 in the presence of 4×10^{-5} *M* niobium. About 50 mv. before the peak the current started to rise slowly, but dropped off sharply when the peak was reached. The current following this peak was also enhanced by the presence of niobium but this effect

(1) I. M. Kolthoff and E. P. Parry, *J. Am. Chem. Soc.*, **73**, 5315 (1951).

(2) N. Adler and C. F. Hiskey, *ibid.*, **79**, 1827 (1957).

(3) H. Schafer and F. Schulte, *Z. anal. Chem.*, **149**, 73 (1956).

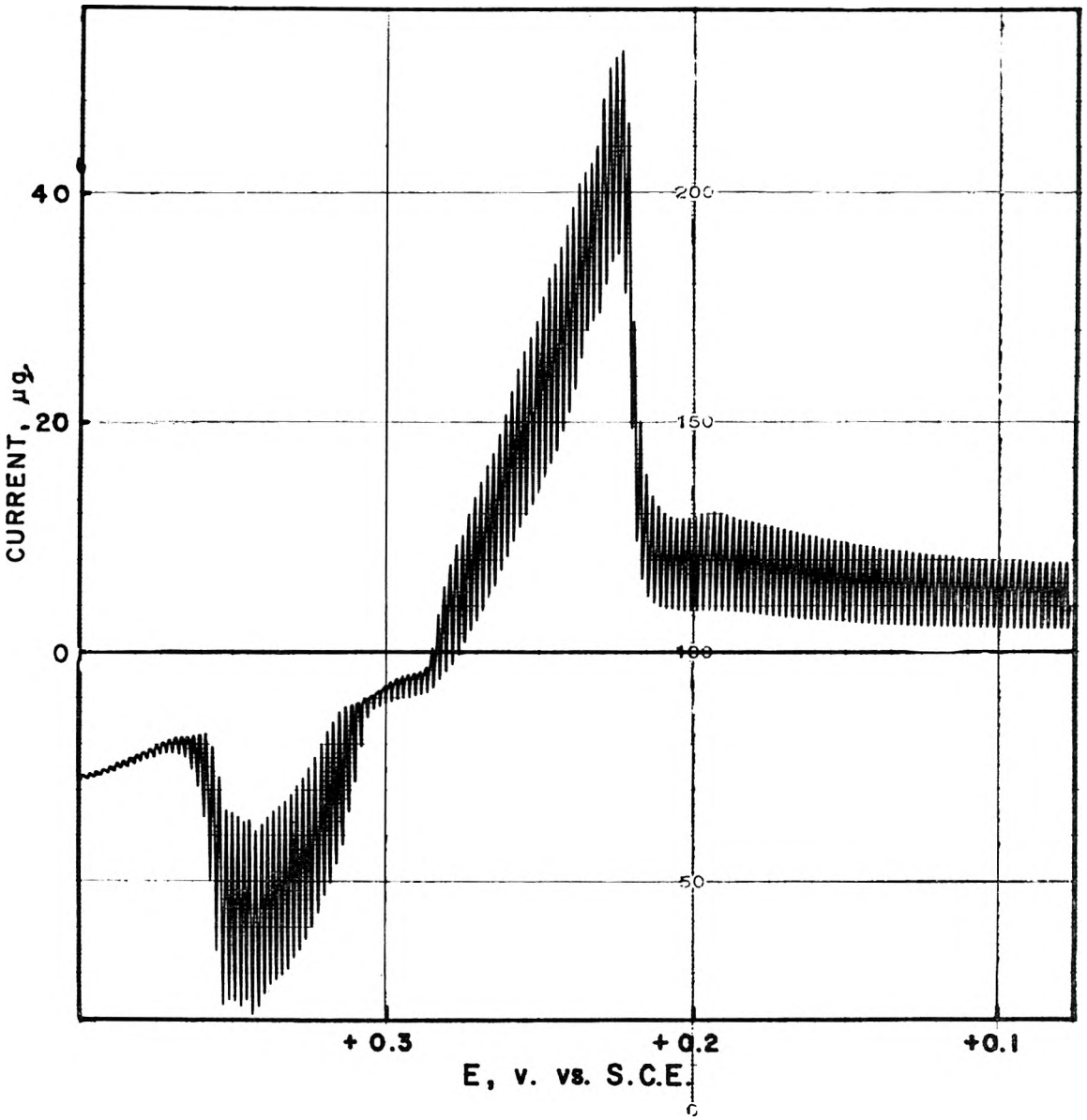

Fig. 1.—Polarography of Nb in H_2O_2 *p*H 5, 4×10^{-5} *M* Nb. 0.05 *M* H_2O_2.

TABLE I

PEAK CURRENT DEPENDENCE ON *p*H (0.05 *M* H_2O_2)

*p*H	Nb i_p, μa/μ*M*	Nb E_p, v.	Ta i_p, μa./μ*M*	Ta E_p, v.
2	..	....	0.05	+0.38
3	0.04	+0.32	.06	+ .33
4	0.10	+ .25	.09	+ .28
5	1.0	+ .237	.23	+ .23
6	0.8	+ .19	.87	+ .15
7	0.02	+ .18	.26	+ .12

was much smaller than the peak current. The peak current was proportional to the concentration of niobium in the range 10^{-6} to 10^{-4} *M*. This same general behavior was found for all solutions of niobium and tantalum in the *p*H range 2–7, but the peak heights increased to a maximum at *p*H 5 for niobium and *p*H 6 for tantalum. Table I shows the catalytic peak current, i_p, for niobium and tantalum at various *p*H.

The peak current was constant when the height of mercury was varied from 30.8 to 66.2 cm. indicating that this was a kinetic current.

The effect of changing the peroxide concentration was studied (in the range 0.01–1 *M*), and it was found that the current varied approximately with the one-half power of the peroxide concentration.

If the solution was allowed to stand for several hours in the polarographic cell, the observed current decreased. This effect was associated more with the blank than with the samples since the difference between sample peak height and the blank peak height was nearly constant for over an hour, and then decreased slowly. The reagents must have contained a trace impurity which gave a peak current similar to niobium, and either decomposed or volatilized to cause the decrease in blank peak current. Kolthoff and Parry ascribed this blank current to vanadium in the sodium phosphate, but the potassium dihydrogen phosphate used in this study was checked by emission spectrograph, and

no vanadium was detected. However, the sensitivity of this method was 1 p.p.m. while the catalytic peroxide peak was sensitive to even smaller concentrations of vanadium.

The decrease in sample peak current after hours of standing was due to hydrogen peroxide decomposition catalyzed by the niobium or tantalum. In fact, if large concentrations of niobium (0.1 *M*) were added to hydrogen peroxide an evolution of bubbles was observed.

Addition of a maximum suppressor, Triton X-100, had no effect on the peak current, except that when it was present in excess of 0.01%, a small decrease was observed. This would seem to indicate that the peak was not an adsorption phenomenon. However, electrocapillary curves were obtained by measuring the drop time as a function of potential for potassium chloride solutions containing Triton X-100, and these showed that although the Triton X-100 shifted the maximum drop time to about −0.2 v. *vs.* S.C.E., there was no change in drop time at potentials more positive than 0.0 v. *vs.* S.C.E. Thus, even if this was an adsorption phenomenon it is not surprising that Triton X-100 did not decrease the peak height. Electrocapillary curves could not be obtained with peroxide solutions containing 0.01 *M* niobium because bubbles of oxygen formed causing erratic drop times.

The shift of potential with *p*H was close to 50 mv. per *p*H unit toward easier reduction in acid solution. The peak potential was not a theoretically interpretable half-wave potential, but its shift with *p*H does show that hydrogen ions were involved in the electrode reaction. Since the peak current also varied with the *p*H, one may also say that hydrogen ions were involved in the kinetic reaction.

Kolthoff and Parry gave the following explanation for the catalytic wave due to vanadium, molybdenum or tungsten. The high current was caused by the chain reaction

$$MoO_4^{--} + H_2O_2 \longrightarrow MoO_5^{--} + H_2O \quad (1)$$

$$MoO_5^{--} + 2H^+ + 2e^- \longrightarrow MoO_4^{--} + H_2O \quad (2)$$

The rate of reaction 1 was so fast that the current was not a function of diffusion of the metal peroxide complex to the electrode, but of the rate of formation of the complex. Thus, the current depended on the metal ion concentration, hydrogen peroxide concentration and *p*H. The sharp peak current indicated that the rate of reaction 1 was affected by the potential of the electrode which may indicate that adsorption effects were causing this dependence.

Because of the shift in potential with *p*H, a type of reaction 2 seems plausible for the niobium and tantalum cases. However, niobium and tantalum exist as polynuclear species in aqueous solution (as well as molybdenum in weakly acid solutions) so that reaction 1 must be more complicated for these elements. Since the predominant species changes with *p*H this could explain why the current varied so markedly with *p*H. Adler and Hiskey showed the existence of four niobium peroxide complexes in different *p*H regions; in weakly acid solutions such as gave the high peak currents, a 1:1 complex was the most stable. In more acid solutions a 2:1 complex was found while in basic solution, the predominant species was a 4:1 complex.

The peak current constitutes a sensitive test for niobium and tantalum, capable of detecting 10^{-7} *M* concentrations of these two elements. This method was used to determine the small amounts of niobium formed by beta decay in a Zr^{95}–Nb^{95} solution. Zirconium was found to have some catalytic effect on the hydrogen peroxide reduction, but gave no peak at +0.23 v. in a solution at *p*H 5.

Thus, niobium and tantalum have been found to belong to the group of metals whose peroxide complexes catalyze the reduction of hydrogen peroxide at the dropping mercury electrode.

Acknowledgment.—The author thanks Dr. E. A. Tomic of our laboratories for furnishing a sample of Zr^{95} oxalate and calculating the amount of Nb^{95} present from the age of the sample. The author also expresses his appreciation to V. L. Altemus, Jr., for performing much of the experimental work presented here, and to H. M. Hubbard for his helpful suggestions and reviewing of the manuscript.

CALORIMETRIC HEATS OF ADSORPTION FOR HYDROGEN ON NICKEL, COPPER AND SOME OF THEIR ALLOYS

BY LOIS S. SHIELD AND W. WALKER RUSSELL

Department of Chemistry, Brown University

Received April 27, 1960

In a recent study[1] of the activity of nickel, copper and some of their alloys as catalysts for the ortho-parahydrogen interconversion at −196° and at near room temperature, it was found that catalytic activity changed little in the alloy composition range from 5 to over 90% copper. However, outside of this range alloying a few per cent. of copper or nickel with nickel or copper sharply decreased and increased catalyst activity, respectively. It was thought that a better understanding of the foregoing phenomena might be obtained if differential heats of hydrogen adsorption were made on the same type of catalysts.

Experimental

The all-glass gas handling system followed in principle that earlier described[2] but incorporated a McLeod gauge, a mercury diffusion pump and calorimeter. Gas purification, B.E.T. measurements and catalyst preparation followed an earlier disclosure.[1] However, catalyst shrinkage during reduction made a preliminary reduction necessary, after which cooling and adsorption of carbon dioxide allowed the no longer pyrophoric catalyst to be packed into the calorimeter. After sealing in place final reduction was carried out also at 350°. Outgassing was carried out at 300°, a little helium added to hasten thermal equilibrium in the calorimeter at room temperature, at which measurements were made, and the helium outgassed to 10^{-5} mm. prior to a run.

The calorimeters were in principle like that described by Beebe and Camplin[3]; however, the catalyst sample was placed in a perforated cylindrical copper basket between narrow layers of small, thin copper discs. The single junction of a copper–constantan thermocouple was attached to the middle of the basket exterior. The basket was completely surrounded by a thin polished silver radiation shield. The basket and concentric shield were suspended from a narrow central spindle tube which also served as a gas exit tube dur-

(1) P. B. Shallcross and W. W. Russell, *J. Am. Chem. Soc.*, **81**, 4132 (1959).

(2) W. W. Russell and L. G. Ghering, *ibid.*, **55**, 4468 (1933).

(3) R. A. Beebe and E. R. Camplin, THIS JOURNAL, **63**, 480 (1959).

ing catalyst reduction. A heavy copper shield into which was inserted the cold junction of the thermocouple fitted snugly around the outside of the vacuum jacket of the calorimeter. Around this and also submerged in the water-bath was a glass tube spiral to equilibrate thermally gases entering the calorimeter. The thermocouple wires left the calorimeter either through pressed glass seals, or by short tungsten–glass seals. As no calibration heater element was built into the calorimeter, the heat capacity was calculated from specific heat data at 20° for Pyrex glass, pure copper and pure nickel, with linear interpolation in the case of the alloy catalysts. The thermocouple circuit and galvanometer, and also the method of determining circuit sensitivity followed the work of Garner and Veal.[4] The galvanometer had a sensitivity of 0.046 μv./mm., and a period of 5.8 sec. The circuit sensitivity was always at least 40 cm./deg. Galvanometer scale readings *vs.* time plots were analyzed by the method of Cork.[5] The fraction θ of catalyst surface covered by adsorbed hydrogen was calculated on the assumption that each hydrogen atom occupied one metal site and that 100, 110 and 111 surface planes were equally probable.

Results and Discussion

The differential heats of hydrogen adsorption were measured over the greatest range of monolayer coverage, for the pure nickel catalyst, and fell off nearly linearly from 24 (extrapolated) to 8 kcal./mole as θ increased from zero to 0.6. Heats of hydrogen adsorption on the 5 and 62 atom % copper alloy catalysts also decreased approximately linearly from about 15 (extrapolated) to about 7 kcal./mole as θ increased from zero to 0.3. As measurements on the pure copper catalyst were limited to θ values near 0.15 no trend was ascertainable. The heavy curve in Fig. 1 shows the dependence of the heat of hydrogen adsorption upon the atom % copper in the catalyst at $\theta = 0.15$, a monolayer coverage in the range actually measured for each catalyst. Alloying 5% or less of copper with nickel has caused the heat of hydrogen adsorption to drop over 40%, while further increasing the copper content to over 60% causes a drop of less than one kcal./mole, then to pure copper the additional drop is a little over one kcal./mole. This dependence of the heat of hydrogen adsorption upon alloy catalyst composition is strikingly similar to the dependence found for the catalytic activity of these alloy catalysts in the ortho–parahydrogen interconversion both at −196° (lower dotted curve) and at −20° (upper dotted curve). The detailed shapes of the curves at high percentages of copper are less certain, and especially so close to 100% copper since the presence of very small traces of nickel in "pure" copper is known greatly to affect catalytic activity,[6] and also probably heats of adsorption.

Although the effect of alloying 5% copper with nickel was to drop sharply both the catalytic activity and the heats of hydrogen adsorption at all surface coverages studied, it does not necessarily follow that high heats of hydrogen adsorption mean high catalytic hydrogenating activity. On the contrary for the hydrogenation of ethylene on the transition metals[7] Beeck found catalytic activity to decrease as the heat of hydrogen adsorption at zero coverage increased. As in the present work, Beeck's heats of hydrogen adsorption[7] decreased at various rates with increasing surface coverage, and it appears clear that any direct relation between heats of hydrogen adsorption and hydrogenating activity may depend strongly upon employing heats obtained with the type and extent of surface coverage which is appropriate for the chemical reaction occurring upon the catalyst surface. In the aforementioned study[1] of the ortho–parahydrogen interconversion on these catalysts the importance of fixed hydrogen was suspected and was stressed. Such hydrogen was assumed not to participate directly in the interconversion but rather to exert an activating and/or a deactivating effect upon the more loosely adsorbed, reactive hydrogen. The present work appears to support this view. Such fixed hydrogen is believed to adsorb under reaction conditions, or may be preadsorbed on the catalyst. Catalysts exhibiting high heats of hydrogen adsorption at low surface coverages would be expected to be most effective in fixing hydrogen and thus modifying the catalytic properties of their surfaces. When hydrogen was adsorbed and fixed on the catalyst surfaces at an interconversion temperature of −20°, the catalytic activity dependence shown in the upper dotted curve in Fig. 1 was obtained. However, when hydrogen was fixed by preadsorption at 325°, the pure nickel catalyst was partially poisoned while the activities of the nickel–copper alloy catalysts were enhanced for reaction at −20°, the 62 atom % copper catalyst showing maximum enhancement. In the present work similarly preadsorbing hydrogen on this latter catalyst has decreased the initial heat of subsequent hydrogen adsorption to 4 kcal./mole at an equilibrium pressure of 0.28 mm., and to 2.6 kcal./mole when the equilibrium pressure had risen to 7.2 mm. These smaller heats of adsorption are believed to be much more characteristic of hydrogen adsorbed in a reactive condition than zero coverage heats.

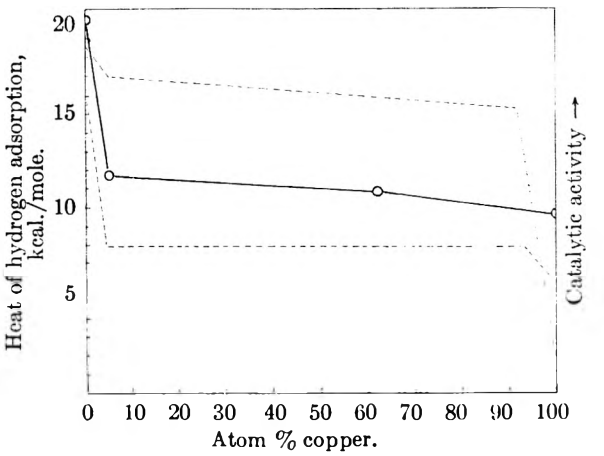

Fig. 1.—The effect of catalyst composition upon: (a) the heats of hydrogen adsorption, heavy curve; (b) catalytic activity, at −196°, lower dotted curve; at −20°, upper dotted curve.

The lack of sensitivity to alloy composition, over a wide alloy composition range, shown by the interconversion reactions (no deliberately preadsorbed hydrogen) and by the heats of adsorption at $\theta = 0.15$ represent a case in which fixed hydrogen induced promoting and poisoning effects appear nearly to balance out. An explanation appears

(4) W. E. Garner and F. J. Veal, *J. Chem. Soc.*, 1436 (1935).

(5) J. M. Cork, "Heat," John Wiley and Sons, Inc., New York, N. Y., 1942, p. 56.

(6) B. B. Corson and V. N. Ipatieff, THIS JOURNAL, **45**, 431 (1941).

(7) O. Beeck, *Disc. Faraday Soc.*, **8**, 118 (1950).

possible in terms of the following model. Except near the ends of the alloy composition range, both nickel and copper atoms are present in large numbers and supposedly randomly dispersed in the catalyst surfaces which because of the mode of catalyst preparation must be far from ideal single f.c.c. crystals. Such surface heterogeneity should lead to the co-existence of surface areas of various types capable of adsorbing hydrogen with a certain spectrum of heats of adsorption to yield fixed hydrogen and adjacent adsorbed hydrogen some of which may be highly activated and some of which may be less or little activated. The integrated effect of such surface heterogeneity, as well as of induced heterogeneity, appears to be that the over-all rates of the ortho–parahydrogen interconversion and, over a limited range of surface coverage, the heats of hydrogen adsorption appear nearly constant on the alloy surface of highly imperfect crystals when the nickel–copper alloy contains more than a few per cent. of both components.

HAMMETT ACIDITIES OF CHROMIA CATALYSTS

BY S. E. VOLTZ, A. E. HIRSCHLER AND A. SMITH

Sun Oil Company, Marcus Hook, Pennsylvania

Received April 27, 1960

During the past decade, significant progress has been made in the determination of the properties of solid acid catalysts. Acid distributions have been determined by titration in non-aqueous medium with amines in the presence of Hammett indicators. The results have clearly shown the importance of the acid strengths to the catalytic properties of both cracking and re-forming catalysts.[1-4]

The extents of surface oxidation of transition metal oxides, such as chromia, have been shown to be intimately related to their surface chemistry and catalytic properties.[5-19] Chromia catalysts are more active for many hydrocarbon reactions in the reduced state than in the oxidized state. The extents of surface oxidation of these catalysts have been determined by gas adsorptions and iodometric titrations. The correspondence between the two methods has also been established. The electronic properties of chromia catalysts are very dependent on the extent of oxidation of the surface. The electrical conductivity is much higher in the oxidized state than in the reduced state. In many respects, chromia exhibits some of the properties of a p-type semiconductor in the oxidized state and of an n-type semiconductor in the reduced state.

Attempts have been made to measure the acidities of chromia catalysts by the vapor phase adsorptions of amines and aqueous titrations. None of these measurements have given any indication of the distributions of acid sites on these catalysts.

The work reported in this paper shows the types of distributions of acid sites that are found on chromia catalysts and an attempt has been made to correlate these results with the extents of surface oxidation and catalytic properties.

Experimental

Unsupported chromia was prepared from dilute solutions of chromic nitrate and ammonium hydroxide. The gel was dried at 110° and then cycled several times in oxygen and hydrogen at 500°. Chromia–alumina (Series A, Grade 100) was obtained from the Houdry Process Corporation. A sample of this latter catalyst was impregnated with aqueous potassium hydroxide solution to give the equivalent of 1% K_2O. The impregnated catalyst was dried at 110° and calcined at 500°. Oxidized and reduced samples of these catalysts were prepared by treating ground portions of each catalyst with oxygen or hydrogen, respectively, at 500° for four hours.

F-10 alumina (Alcoa) and S-34 silica–alumina (Houdry Process Corp.) were used as indicator catalysts in the acidity determinations. These catalysts were dried at 500°.

The extents of surface oxidation of the chromia catalysts were determined by an iodometric method.[7-9,12]

For the acidity measurements, freshly activated catalysts were placed in weighed vials in a dry box under nitrogen. A weighed amount of 100–120 mesh indicator catalyst was mixed with a weighed amount of −200 mesh chromia catalyst in each vial. Various amounts of a standardized solution of *n*-butylamine in benzene were added to different vials. The vials were thoroughly shaken and equilibrated overnight. The proper Hammett indicator was added and the color of the alumina (or silica–alumina) particles of the mixture was determined under a microscope. In this way, the equivalence point of each mixture was measured and the acidity of the chromia catalyst was then calculated readily. Butter Yellow, dicinnamalacetone and anthraquinone were used to measure the acidity at pK_a values of +3, −3 and −8, respectively.

Ethylenediamine was purified by repeated distillations over sodium and standardized by titration with perchloric acid in glacial acetic acid.

Results

The acidity of a dark chromia catalyst cannot be determined by titrating it directly with an organic base. The color changes of the Hammett indicator are too difficult to observe on such a dark solid. It is necessary, therefore, to mix the chromia catalyst with a white indicator catalyst and titrate the mixture. The acidity of the chromia catalyst then can be calculated readily.

The Hammett acidities of the F-10 alumina were 0.29, 0.29 and 0.27 milliequivalent *n*-butylamine/g. catalyst at pK_a values of +3, −3, and −8, respectively. The corresponding values for S-34 silica–alumina were 0.16, 0.16 and 0.11 milliequivalent *n*-butylamine/g. catalyst. F-10 alumina contains practically all strong acid sites; S-34

(1) O. Johnson, THIS JOURNAL, **59**, 827 (1955).
(2) H. A. Benesi, *J. Am. Chem. Soc.*, **78**, 5490 (1956).
(3) H. A. Benesi, THIS JOURNAL, **61**, 970 (1957).
(4) A. E. Hirschler and A. Schneider, Paper No. 56, Division of Colloid Chemistry, National A.C.S. Meeting, Atlantic City, N. J., Sept. 1959.
(5) S. E. Voltz and S. Weller, *J. Am. Chem. Soc.*, **75**, 5227 (1953).
(6) S. E. Voltz and S. W. Weller, *ibid.*, **75**, 5231 (1953).
(7) S. E. Voltz and S. W. Weller, *ibid.*, **76**, 1586 (1954).
(8) S. W. Weller and S. E. Voltz, *ibid.*, **76**, 4695 (1954).
(9) S. E. Voltz and S. W. Weller, *ibid.*, **76**, 4701 (1954).
(10) S. W. Weller and S. E. Voltz, *Z. physik. Chem., N.F.*, **5**, 100 (1955).
(11) S. E. Voltz and S. W. Weller, THIS JOURNAL, **59**, 566 (1955).
(12) S. E. Voltz and S. W. Weller, *ibid.*, **59**, 569 (1955).
(13) S. W. Weller and S. E. Voltz, "Advances in Catalysis," Vol. IX, Academic Press, Inc., New York, N. Y., 1957, p. 215.
(14) R. Chaplin, P. R. Chapman and R. H. Griffith, *Proc. Roy. Soc. (London)*, **A224**, 412 (1954).
(15) P. R. Chapman, R. H. Griffith and J. D. F. Marsh, *ibid.*, **A224**, 419 (1954).
(16) R. H. Griffith, J. D. F. Marsh and M. J. Martin, *ibid.*, **A224**, 426 (1954).
(17) Y. Matsunaga, *Bull. Chem. Soc. (Japan)*, **30**, 868 (1957).
(18) Y. Matsunaga, *ibid.*, **30**, 984 (1957).
(19) C. D. Holland and P. G. Murdoch, *A.I.Ch.E. J.*, 386 (1957).

silica–alumina has a lower acidity and a lower proportion of strong acid sites. This is not surprising in view of the amount of chloride present in the alumina.

The acidities of oxidized chromia catalysts are identical when determined with either F-10 alumina or S-34 silica–alumina. Some minor difficulties were encountered in the determination of the acidities of certain reduced chromia catalysts with silica–alumina. All the data reported for chromia catalysts were determined with F-10 alumina.

The extents of surface oxidation and Hammett acidities of several chromia catalysts are summarized in Table I. The extent of surface oxidation of oxidized chromia (unsupported) is much larger than that of the reduced catalyst. The Hammett acidity in the oxidized state is about twice that in the reduced state. More than one-half of the total acid sites are strongly acidic. The specific surface area of this catalyst is 16 m.^{2}/g.

TABLE I

EXTENT OF SURFACE OXIDATION AND HAMMETT ACIDITY OF CHROMIA CATALYSTS

Catalyst	Oxidation state[a]	Extent of surface oxidation[b] (meq./g.)	Hammett acidity[c] (meq./g.) +3	−3	−8
Cr_2O_3[d]	Oxidized	0.46	0.09	0.09	0.05
Cr_2O_3[d]	Reduced	.15	.04	.04	.02
Cr_2O_3–Al_2O_3[e]	Oxidized	.68	.25	.25	.19
Cr_2O_3–Al_2O_3[e]	Reduced	.08	.16	.16	.10
Cr_2O_3–Al_2O_3–K_2O[f]	Oxidized	.86	.14	.14	.01
Cr_2O_3–Al_2O_3–K_2O[f]	Reduced	.04	.07	.07	.02

[a] Catalysts were pretreated with oxygen or hydrogen at 500° for 4 hours. [b] Milliequivalents KI/g. catalyst. [c] Milliequivalents *n*-butylamine/g. catalyst. [d] Unsupported chromic oxide. [e] Houdry chromia–alumina catalyst, Series A, Grade 100. [f] Houdry chromia–alumina catalyst impregnated with 1% K_2O(ex. KOH).

The properties of the commercial chromia–alumina catalyst are somewhat similar to those of unsupported chromia. The extent of surface oxidation and Hammett acidity are both greater in the oxidized state than in the reduced state. A greater proportion of the total acid sites are strongly acidic in chromia–alumina. This catalyst is primarily used in commercial dehydrogenation processes. Its specific surface area is about 70 m.^{2}/g.

Alkali increases the extent of surface oxidation of chromia–alumina. It reduces the acidity; the strong acid sites are preferentially neutralized. The Hammett acidity in the oxidized state is also about twice as great as that in the reduced state. The increased extent of surface oxidation is probably related to the formation of chromates or dichromates on the surface.[9]

Several catalysts were titrated with ethylenediamine in the presence of dicinnamalacetone (pK_a of −3). F-10 alumina, oxidized chromia–alumina, and reduced chromia–alumina, have acidities of 0.68, 0.45 and 0.32 milliequivalent ethylenediamine/g. catalyst, respectively. Comparison of these data with the corresponding titrations with *n*-butylamine indicate that about twice as many equivalents of ethylenediamine are required in each case.

Discussion

Reduced chromia catalysts are more active than the corresponding oxidized ones for hydrogen–deuterium exchange, ethylene hydrogenation, and isomerization (double bond) of pentene-1.[9] These reactions can be carried out under sufficiently mild conditions that the condition of the surface of the catalyst is not appreciably altered during the reaction. Reduced chromia catalysts are also extremely active for the dehydrogenations of cyclohexane and butanes.[9] Alkali reduces the activities of most of these catalysts for all the above hydrocarbon reactions.[9] In conclusion, it seems that the most active states of chromia catalysts for hydrocarbon reactions have relatively low extents of surface oxidation and Hammett acidities.

In contrast, both oxidized and reduced chromia catalysts have the same catalytic activities for the oxidation of carbon monoxide.[8] Alkali is a poison for either type of catalyst in this reaction.[9] For the aqueous decomposition of hydrogen peroxide, the oxidized catalysts are more active than the reduced ones and alkali acts as a promoter.[4,9] These results indicate that in non-hydrocarbon reactions the situation is very complicated and more work will be required before general conclusions can be made.

Within experimental error, the differences in acidities between the oxidized and reduced states of the chromia and chromia–alumina catalysts (in meq./g.) are one-half of the corresponding differences between the amounts of Cr^{+6} present on the surfaces. For example, the difference in the extents of surface oxidation of oxidized and reduced chromia is 0.31 meq./g. (from Table I, 0.46–0.15 = 0.31 meq./g.). The difference in the acidities is 0.05 meq./g. Assuming that the reduction of Cr^{+6} by potassium iodide is to Cr^{+3}, then the concentration of Cr^{+6} ions on the surface is 0.31/3 or 0.10 meq./g. Thus, one acid site corresponds to two Cr^{+6} ions.

The extent of surface oxidation of the oxidized chromia–alumina catalyst (Series A, Grade 100) listed in Table I is equivalent to 0.097 meq./m.^{2} It is interesting to compare this value with that of Houdry Type R chromia–alumina catalyst. Type R catalyst has a surface area of 50 m.^{2}/g. and the extent of surface oxidation in the oxidized state is 131 micromoles of O_2/g.[6] This corresponds to 0.10 meq./m.^{2}. The agreement between the two types of chromia–alumina catalysts is very good.

The addition of alkali decreases the quinoline chemisorptions of chromia–alumina catalysts.[9] The amounts of quinoline chemisorbed on these catalysts are less than the amounts of *n*-butylamine taken up from benzene solution. The differences probably are due to the large size of the quinoline molecule or the relatively low basicity of quinoline.

For reduced chromia–alumina, exactly twice as many equivalents of ethylenediamine are required to neutralize the acidity as with *n*-butylamine. This result can be interpreted that the acid sites are too far apart on the surface for a single diamine molecule to react with two sites. Alternatively, the reactivity of the second amino group of the

adsorbed diamine molecule may be too low to react with an acid site.

In the case of the oxidized chromia–alumina, the butylamine titer exceeds that of the reduced catalyst by 0.09 meq./g. while the ethylenediamine titer is 0.13 meq./g. higher. This result would indicate that for 64% of chromia acid sites an ethylenediamine molecule is able to neutralize two chromia acid sites (or one alumina site plus one chromia acid site). This might indicate that the distance between two chromia acid sites or between a chromia and an alumina acid site is less than the distance between two alumina sites.

The nature of the acid sites on oxidized chromia catalysts is not completely clear. It seems reasonable that the increased Hammett acidity in the oxidized state is associated to a large extent with higher valent chromium ions (Cr^{+6}) on the surface. The high electrical conductivity of oxidized chromia is thought to be associated with the presence of both Cr^{+3} and Cr^{+6} on the surface. It thus appears that the acid sites are related to the defects which are also responsible for the semiconductivity properties.

The Hammett acidity exhibited by reduced chromia (unsupported) is a property inherent with the reduced state of the surface. In contrast, it is not possible at this point to completely distinguish between chromia acid sites and alumina acid sites on reduced chromia–alumina. It does seem reasonable, however, that the large portion of the acidity is due to reduced chromia sites. The exact nature of the acid sites on reduced chromia and chromia–alumina catalysts is more obscure than that of the acid sites on the oxidized catalysts.

THE INTERACTION OF ARGON WITH HEXAGONAL BORON NITRIDE

By R. A. Pierotti[1] and J. C. Petricciani

Department of Chemistry, University of Nevada, Reno, Nevada

Received May 11, 1960

The interaction of the rare gases with graphite has been extensively investigated experimentally and theoretically by numerous authors. Barrer,[2] Crowell and Young[3] and Pace[4] have calculated the heat of adsorption of an isolated argon atom over various positions on the basal plane of graphite. The results of Crowell and Young and of Pace indicated that the graphite surface was energetically homogeneous with respect to the adsorption of argon and that the adsorbed argon film was mobile or non-localized. Their conclusions have been verified experimentally.[4,5] Barrer's results were inconsistent with the others.

X-Ray diffraction studies indicate that the hexagonal modification of boron nitride has a crystal structure which is remarkably similar to that of graphite.[6] The nearest neighbor distance in boron nitride is 1.44 Å.,[7] in graphite it is 1.42 Å.;[8] the interlaminar spacing in boron nitride is 3.33 Å.,[7] in graphite it is 3.35 Å.[8]

The aims of the present investigation were to calculate the heat of adsorption for the argon–boron nitride system, to compare these calculations with similar calculations for the argon–graphite system, and to compare the calculated results to the experimental data for the two systems.

Results

The interaction of an isolated argon atom with a covalent, non-polar solid can be calculated by assuming a Lennard-Jones (6–12) potential and summing over all pairwise interactions of the argon atom with the atoms of the solid. The total interaction energy ϕ of the atom with the solid then is given by

$$\phi = -C\left(\sum_i \frac{1}{r_i^6} - \frac{1}{2} r_0^6 \sum_i \frac{1}{r_i^{12}}\right),$$

where r_i is the distance of the argon atom from the ith atom of the solid, C is the dispersion force constant and is obtained from the Kirkwood–Muller formula,[9,10] r_0 is a repulsive constant which can be evaluated semi-empirically.

Barrer and Pace used the equilibrium distance of an argon atom above a graphite surface as the value of r_0. Crowell and Young justly criticized this choice of r_0 and instead evaluated it by calculating potential energy *versus* distance curves for several values of r_0 until a value was found which gave a minimum in the potential energy at the equilibrium distance (assumed to be the mean of the interlaminar distance in graphite and the internuclear separation of a pair of argon atoms in crystalline argon). In the present work, the r_0's for an argon atom interacting with either a boron atom or a nitrogen atom are assumed to be equal. The value of r_0 then was selected so that it yielded a minimum in the potential energy at the equilibrium distance. The equilibrium distance over a boron atom was chosen to be the mean of the interlaminar distance in boron nitride and the internuclear separation of two argon atoms in crystalline argon. It should be mentioned that Crowell and Young state that r_0 is the equilibrium distance between an argon atom and an isolated atom of the solid. This is not correct, since repulsive forces are not pairwise additive as are dispersion forces.

The summations were carried out over four different sites of the basal plane of boron nitride: (a) over the center of the hexagon, (b) over a boron atom, (c) over a nitrogen atom and (d) over a position midway between a boron and nitrogen atom. The nearest 300 atoms were included in both the attractive and repulsive summations. The additional attractive interactions were ob-

(1) School of Chemistry, Georgia Institute of Technology, Atlanta 13, Georgia.

(2) R. M. Barrer, *Proc. Roy. Soc.* (*London*), **A161**, 476 (1937).

(3) A. D. Crowell and D. M. Young, *Trans. Faraday Soc.*, **49**, 1080 (1953).

(4) E. L. Pace, *J. Chem. Phys.*, **27**, 1341 (1957).

(5) Sydney Ross and W. W. Pultz, *J. Colloid Sci.*, **13**, 397 (1958).

(6) W. Hückel, "Structural Chemistry of Inorganic Compounds," Elsevier Publishing Co., Amsterdam, 1951, Vol. II, p. 598..

(7) A. A. Giardini, U. S. Bur. Mines Info. Circular 7664, 1953.

(8) H. Lipson and A. R. Stokes, *Proc. Roy. Soc.* (*London*), **A181**, 101 (1942).

(9) A. Muller, *ibid.*, **A154**, 624 (1936).

(10) R. A. Pierotti and G. D. Halsey, This Journal, **63**, 680 (1959).

tained by integration and amounted to 6% of the total; the additional repulsive interactions were shown to be negligible.

The physical constants used in the calculations are shown in Table I. The results of the calculations for the argon–boron nitride system are listed in Table II. Included there are: ϕ, the interaction energy; r_e, the equilibrium distance over each site; e_0, the zero-point energy (calculated from the curvature of the potential energy curve in the region of the minimum); and ΔH_0, the heat of adsorption at 0°K. Table III contains the same quantities calculated by Crowell and Young for the argon–graphite system.

TABLE I

PHYSICAL PROPERTIES OF ATOMS

Atom	Density, g./cc.	Polarizability ($\times 10^{24}$)	Susceptibility ($\times -10^{29}$)
Argon	1.65[a]	1.63[b]	3.24[c]
Boron	2.33[d]	1.17[d,e]	1.24[f]
Nitrogen	...	0.867[b,g]	0.796[d]

[a] J. R. Partington, "An Advanced Treatise in Physical Chemistry," Vol. III, Longmans, Green and Co., Inc., New York, N.Y., 1952, p. 149. [b] H. Margenau, *Rev. Modern Phys.*, 11, 1 (1939). [c] K. E. Mann, *Z. Physik*, 98, 548 (1936). [d] "Handbook of Chemistry and Physics," Chemical Rubber Publishing Co., Cleveland, Ohio, 1950. [e] Calculated from index of refraction. [f] "International Critical Tables," Vol. VI, McGraw-Hill Book Co., Inc., New York, N.Y., 1926–28. [g] From Landolt's Rule—1/2 polarizability of N_2.

TABLE II

CALCULATED QUANTITIES FOR THE ARGON–BORON NITRIDE SYSTEM

	Description of site	r_e (Å.)	$\phi_{min} \times -10^{12}$, erg/molecule	$e_0 \times 10^{12}$, ergs/molecule	$-\Delta H_0$, cal./mole
a.	Over hexagon	3.54	0.1390	0.0033	1960
b.	Over boron atom	3.59	.1358	.0033[a]	1910
c.	Over nitrogen atom	3.58	.1368	.0033[a]	1920
d.	Over mid-point between a boron and a nitrogen atom	3.59	.1358	.0033[a]	1910

[a] Assumed to be the same as over the hexagon.

TABLE III

CALCULATED QUANTITIES FOR THE ARGON–GRAPHITE SYSTEM FROM CROWELL AND YOUNG

	Description of site	r_e, Å.	$\phi_{min} \times -10^{12}$, ergs/molecule	$e_0 \times 10^{12}$ ergs/molecule	$-\Delta H_0$ cal/mole
a.	Over hexagon	3.55	0.1253	0.0041	1750
b.	Over midpoint between two carbon atoms	3.60	.1233	.0045	1710
c.	Over a carbon atom	3.60	.1230	.0044	1710

Discussion

It is clear from Table II that there is very little difference between the energies over the various sites. The position over the center of the hexagon, as might be expected, is the lowest, but the heights of barriers between the different positions are small as compared to kT at the usual liquid nitrogen adsorption temperatures. It is concluded, therefore, that there is little hindrance to translation over the surface and that the adsorbed film is non-localized.

These calculations can be compared to the experimental data obtained by Ross and Pultz.[5] They measured isotherms of argon adsorbed on boron nitride at 78 and at 90°K. and determined the isosteric heat of adsorption and the entropy of the adsorbed film. The experimental heat of adsorption at low coverages is 2200 cal./mole at 84°K. The calculated heat at 0°K. plus the contribution due to the heat capacity of the film (about 100 cal./mole at 85°K.[11]) is 2060 cal./mole.

Ross and Pultz use their data to calculate an entropy term, ΔS^0, which has as a reference state either an ideal localized film or an ideal non-localized film. The values obtained then were compared with theoretical values for ideal models of localized and non-localized films. They conclude that argon adsorbed on boron nitride is of the non-localized type in agreement with the conclusions of this investigation.

If the calculated and experimental quantities for the argon–boron nitride system are compared with the same quantities for the argon–graphite system (Tables II–IV), it is seen that the two systems show marked similarities. These similarities exist in spite of the great differences in their electrical properties: graphite being a conductor and boron nitride an insulator. The fact that dispersion energy calculations and experimental results for the two systems are the same (or almost so) does imply that the non-conducting electrons in boron nitride do not appear greatly different from the conducting π-electrons in graphite, at least insofar as the physical adsorption of monatomic atoms is concerned. Attempts have been made to distinguish between metals as a class different from non-metals by means of physical adsorption (graphite is usually considered along with the metals).[12] The results of the present work agree with the conclusions of Pierotti and Halsey[10] from multilayer studies that this cannot be done, at least not using the present theories of gas–metal interactions.

TABLE IV

COMPARISON OF THE PREDICTED AND EXPERIMENTAL DATA FOR THE ARGON–BORON NITRIDE AND THE ARGON–GRAPHITE SYSTEMS

Solid	Calcd. r_0 (Å.)	Calcd. r_e (Å.)	Expt. r_e (Å.)	Calcd. $-\Delta H_{ss}$, cal./mole	Expt. $-\Delta H_{ss}$, cal./mole	Type of ads. Pred.	Type of ads. Obsd.
BN	4.04[a]	3.54[a]	...	2060[a]	2200[b]	Mobile[a]	Mobile[b]
C	4.05[c]	3.55[c]	3.35[d]	1850[c]	2300[b,d]	Mobile[c]	Mobile[b]

[a] The present work. [b] Ross and Pultz.[5] [c] Crowell and Young.[3] [d] Constabaris and Halsey, *J. Chem. Phys.*, 27, 1433 (1959). [e] Crowell and Youngs' data corrected for the heat capacity of the film.

This work was made possible by a Frederick Gardner Cottrell Grant from the Research Corporation.

(11) W. J. C. Orr, *Trans. Faraday Soc.*, **35**, 1247 (1939).

(12) J. H. de Boer, "Advances in Catalysis," Academic Press, New York, N. Y., 1956, Vol. VIII, p. 17.

THE G_{OH} IN THE Co-60 RADIOLYSIS OF AQUEOUS $NaNO_3$ SOLUTIONS

BY H. A. MAHLMAN

Oak Ridge National Laboratory,[1] Chemistry Division, Oak Ridge, Tennessee

Received July 11, 1960

In the radiation chemistry of aqueous solutions an initial decomposition of solvent into H atoms and OH radicals is assumed. The detected molecular products H_2 and H_2O_2 result from the reaction of like initial products while the reaction of unlike radicals regenerates water. The yields are calculated from the total energy absorbed by the solution relative to the ferrous dosimeter assuming the 100 e.v. yield of ferric ions to be 15.60. The reduction of Ce^{+4} in an 0.8 N H_2SO_4 solution has been determined to be equal to $2G(H_2O_2) + G_H - G_{OH} + [0.45 - G(H_2)]$. This yield is deduced from the reduction of ceric ion by H_2O_2 and H atoms, the oxidation of cerous ion by OH[2] and the lowering of the $G(H_2)$ by ceric ion.[3]

When thallous ion is present the cerous yield becomes $2G(H_2O_2) + G_H + G_{OH} + [0.45 - G(H_2)]$. The thallous ion effectively converts the oxidizing OH radical into a reductant[4]

$$Tl^+ + OH \longrightarrow Tl^{++} + OH^- \qquad (1)$$
$$Tl^{++} + Ce^{+4} \longrightarrow Ce^{+3} + Tl^{+3} \qquad (2)$$

and the difference in $G(Ce^{+3})$ from the solutions is equal to $2G_{OH}$. The "direct action effect"[5] upon $NaNO_3$ should manifest itself by increasing the $G(Ce^{+3})$ the same amount in both the Ce^{+4}–acid–$NaNO_3$ and Ce^{+4}–acid–$NaNO_3$–Tl^+ systems. Therefore, the difference between the two ceric systems should continue to monitor $2G_{OH}$.

The solutions irradiated were 0.8 N H_2SO_4, 0.004 M Ce^{+4} and contained the desired $NaNO_3$ concentration. The identical solutions also were irradiated with 10^{-3} M Tl^+ present. In Table I are presented the cerous yields obtained from Ce^{+4}–acid–$NaNO_3$ solutions and Ce^{+4}–acid–$NaNO_3$–Tl^+ solutions, as calculated from the total energy absorbed by the solution. This work confirms and extends previous work[5] 10-fold, from 0.5 to 5.0 M $NaNO_3$. The calculated G_{OH} is constant over the entire $NaNO_3$ concentration from 0.1 to 5.0 M and equal to 2.86. This average G_{OH} is exactly the same average observed[5] in the range 0.02 to 0.5 M $NaNO_3$.

TABLE I

THE G_{OH} OBSERVED IN CERIC SOLUTIONS 0.8 N IN H_2SO_4

$NaNO_3$ added, M	$G(Ce^{+3})^a$ Tl^+	$G(Ce^{+3})^b$	$\Delta G(Ce^{+3})^c$	G_{OH}
0.1	8.93	3.33	5.60	2.80
.3	10.15	4.37	5.78	2.89
.5	10.83	5.03	5.80	2.90
.7	11.18	5.51	5.67	2.84
1.0	11.75	5.90	5.85	2.92
2.0	12.24	6.58	5.66	2.83
3.0	12.49	6.86	5.63	2.82
4.0	12.89	7.09	5.80	2.90
5.0	13.05	7.37	5.68	2.84
			Av.	2.86

[a] Ce^{+4}–acid–$NaNO_3$–Tl^+. [b] Ce^{+4}–acid–$NaNO_3$. [c] $\Delta G(Ce^{+3}) = 2G$ OH.

A constant G_{OH} indicates that the total energy absorbed by the solution is effective in decomposing solvent. For example in a 5.0 M $NaNO_3$ solution the water absorbs only 78% of the total energy absorbed by the solution. If only this energy decomposed the water solvent, the expected OH radical yields would be 0.78 of that observed.

Possible reduction reactions of NO_3^- by OH radical in 1.0 M HNO_3 have been reported.[6] All of these reactions yield products that reduce Ce^{+4} (*i.e.*, HO_2, NO_2^- and H_2O_2) and would predict a decreasing G_{OH}. The constant G_{OH} observed indicates that the OH radical does not react with the nitrate ion.

(1) Operated for the U. S. Atomic Energy Commission by the Union Carbide Corporation.

(2) A. O. Allen, *Radiation Research*, **1**, 87 (1954).

(3) H. A. Mahlman, *J. Am. Chem. Soc.*, **81**, 3203 (1959).

(4) T. J. Sworski, *Radiation Research*, **4**, 483 (1956).

(5) T. J. Sworski, *J. Am. Chem. Soc.*, **77**, 4689 (1955).

(6) G. E. Challenger and B. J. Masters, *ibid.*, **77**, 1063 (1955).

COMMUNICATION TO THE EDITOR

CERTAIN TRANSPORT PROPERTIES OF BINARY ELECTROLYTE SOLUTIONS AND THEIR RELATION TO THE THERMODYNAMICS OF IRREVERSIBLE PROCESSES

Sir:

For a single binary electrolyte dissolved in an unionized solvent (like water), the vector transport properties, *i.e.*, diffusion, conductance, and transference, can be expressed in terms of the thermodynamics of irreversible processes by means of the Onsager coefficients. Thus using the defining equations for these properties together with the expression[1] (in one dimension)

$$J_i = -\sum_{j=1}^{2} L_{ij}\left(\frac{\partial \mu_j}{\partial x} + z_j \mathfrak{F}\frac{\partial \phi}{\partial x}\right) \qquad (1)$$

for the flows J_1 and J_2 of cation and anion based on solvent-fixed reference frame, it can be shown[2] that

$$t_i = \frac{\sum_j z_i z_j L_{ij}}{\sum_i \sum_j z_i z_j L_{ij}} \qquad i,j = 1,2 \qquad (2)$$

$$\lambda = \frac{r_i z_i \Lambda_c}{1000} = \mathfrak{F}^2 \sum_i \sum_j z_i z_j L_{ij} \qquad (3)$$

(1) S. R. DeGroot, "Thermodynamics of Irreversible Processes," Interscience Publishers, Inc., New York, N. Y., 1951.

(2) R. W. Laity, *J. Chem. Phys.*, **30**, 682 (1959), has given expression for t_i, λ, and M in terms of the inverse description of (1), i.e., $X_i = \Sigma R_{ij} J_j$.

$$M \equiv \frac{D^0 c}{1000\,RTr\left(1 + c\,\frac{\partial \ln y}{\partial c}\right)} = - \frac{z_1 z_2}{r_1 r_2}\left[\frac{L_{11}L_{22} - L_{12}L_{21}}{\sum_i \sum_j z_i z_j L_{ij}}\right] \quad (4)$$

where L_{ij} denote phenomenological coefficients with $L_{12} = L_{21}$, μ_i the chemical potential, z_i the signed valence, $\mathfrak{F}$ the faraday, ϕ the electrical potential, x the distance, t_i the transference number ($t_1 + t_2 = 1$), λ the specific conductance, Λ the equivalent conductance, c the molarity, D^0 the solvent fixed diffusion coefficient, R the gas constant, T the temperature, y the molarity activity coefficient, r_1 and r_2 the ion stoichiometric coefficient, and $r = r_1 + r_2$. M is defined by equation 4.

Conversely, it can be shown from equations 2–4 that

$$L_{ij} = \frac{r_i z_i t_i t_j \Lambda c}{z_i z_j\,(1000\mathfrak{F}^2)} + \frac{r_i r_j D^0 c}{1000\,RTr\left(1 + c\,\frac{\partial \ln y}{\partial c}\right)} \quad (5)$$

Some preliminary values of L_{12}/c and L_{12}/I, where I is the ionic strength, have been calculated from experimental data at 25° for 1–1, 2–1, and 3–1 electrolytes and are plotted in Fig. 1; L_{12}/I seems to show a common limiting slope.

Calculations are in progress for a number of other electrolytes. These results, comparisons with the Onsager–Fuoss expression,[3] and the derivations will be the subject of a subsequent paper. Ternary systems will also be considered.

The L_{12} directly represents the interionic interaction, and hence is extremely important. Thus the law of independent ion mobilities at infinite dilution results from L_{12} being zero there. However, as the concentration increases, L_{12} increases rapidly at first and then more slowly. As it is of opposite sign from L_{11} and L_{22}, it contributes heavily to the rapid decline of the conductance.

For a second example, the empirical extension of the Nernst–Hartley limiting diffusion law[4]

$$D^0 = \left(\frac{rRT}{r_1 z_1 \mathfrak{F}^2}\right) t_1 t_2 \Lambda \left(1 + c\,\frac{\partial \ln y}{\partial c}\right) \quad (6)$$

is known to be in serious error[5] even in solutions as dilute as 0.01 molar.[4] However consideration of equation 5 with $i = 1$, $j = 2$ readily shows that

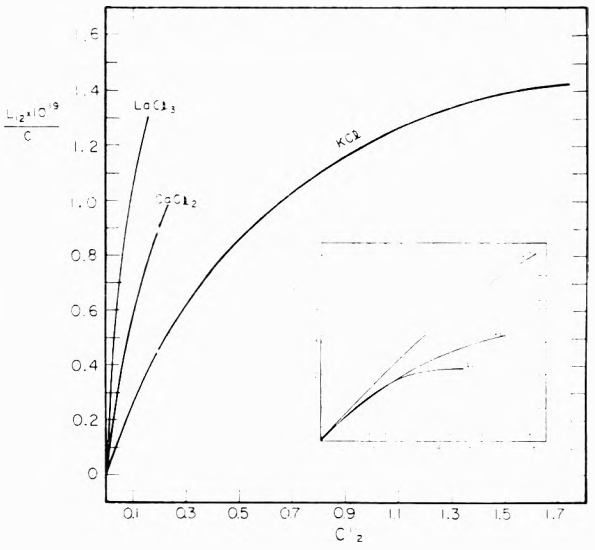

Fig. 1.

difference between the right- and left-hand sides of equation 6 is

$$\left[\frac{1000RTr\,(1 + c\,\partial \ln y/\partial c)}{r_1 r_2}\right]\frac{L_{12}}{c} \quad (7)$$

i.e., the failure of equation 5 is due precisely to the existence of a non-zero L_{12}.

It seems clear therefore that any serious theory of diffusion or conductance must focus its attention on the calculation of L_{12}.

The thermodynamics of irreversible processes also yields an interesting conclusion on the possible influence of viscosity on the above properties. In the general case there is an additional entropy production term involving viscous forces and flows[6] besides those involving the vector flows and forces of equation 1.

However according to Curie's theorem,[6] vector flows cannot result from tensor forces and similarly for tensor flows and vector forces. Since the forces of equation 1 are vectors (1st rank tensors) and the viscous force is a 2nd rank tensor, there can be no term involving viscosity in the linear laws (equation 1) for the vector J_i. Consequently since the vector properties are completely determined by equations 1, there cannot be the direct connection between diffusion, etc., and viscosity, as there was between D, t, and Λ. Thus it is not surprising to find the quantitative failure of Walden's rule and of other transport property "correction" factors involving the bulk viscosity.

UNIVERSITY OF CALIFORNIA
LAWRENCE RADIATION LABORATORY DONALD G. MILLER
LIVERMORE, CALIFORNIA

RECEIVED JULY 25, 1960

(3) L. Onsager and R. M. Fuoss, *J. Phys. Chem.*, **36**, 2689 (1932).

(4) R. A. Robinson and R. H. Stokes, "Electrolyte Solutions," 2nd Ed., Academic Press, Inc., New York, N. Y., 1959, p. 288–290.

(5) We also note that since D^0 is the *solvent-fixed* diffusion coefficient, care must be taken in calculations of $D/(1 + c\partial \ln y/\partial c)$ not to use the usually reported coefficients D^v, as they are measured on a volume-fixed reference frame. Although the same at infinite dilution, D^0 and D^v diverge rapidly in concentrated solutions (*e.g.*, see R. P. Wendt and L. J. Gosting, *J. Phys. Chem.*, **63**, 1287 (1959)). The calculation of D^0 from D^v requires knowledge of partial molal volumes, but lack of these data is not serious as it can be shown that $D^0/(1 + c\partial \ln y/\partial c) = D^v/(1 + m\partial \ln \gamma/\partial m)$, where m is the molality and γ the molality activity coefficient.

(6) Reference 1, pp. 120–122.

NO. 21 EPR AT WORK SERIES

HYPERFINE STRUCTURE IN ORGANIC FREE RADICALS BY EPR

(ELECTRON PARAMAGNETIC RESONANCE)

Interaction in organic free radicals of the unpaired electron with the magnetic moments of the protons frequently gives rise to well defined hyperfine structure. Often this structure permits identification of an unknown radical. One may also extract detailed information on electron wave functions from this observed hyperfine splitting.

EXAMPLE

Tetracene positive ion free radical.

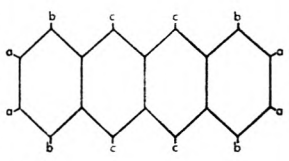

FIG. A TETRACENE

Tetracene, Figure A, when dissolved in concentrated H_2SO_4 forms a positive ion free radical, which has been investigated with EPR by Weissman and others[1]. We recently reëxamined this radical[2] using the high sensitivity Varian 100 kc EPR spectrometer. Figure B shows the total spectrum and Figure C, the seven central lines obtained with a slower scan of the DC magnetic field. The temperature was 65°C and the concentration, 10^{-4} molar.

The resonance saturates easily, and the V-4500-41A low-high power bridge was therefore necessary to permit observation at 30 db attenuation of the klystron power (0.20 mw at the sample). All lines are 60 milligauss peak-to-peak, and the line width is independent of temperature. When using 100 kc field modulation one expects resonance sidebands to occur at ± 30 milligauss from the line center, and it is felt that these sidebands determine the observed line width. Work of this type requires good magnetic field homogeneity and magnet power supply stability. A Varian 12" rotating magnet and regulated power supply were used.

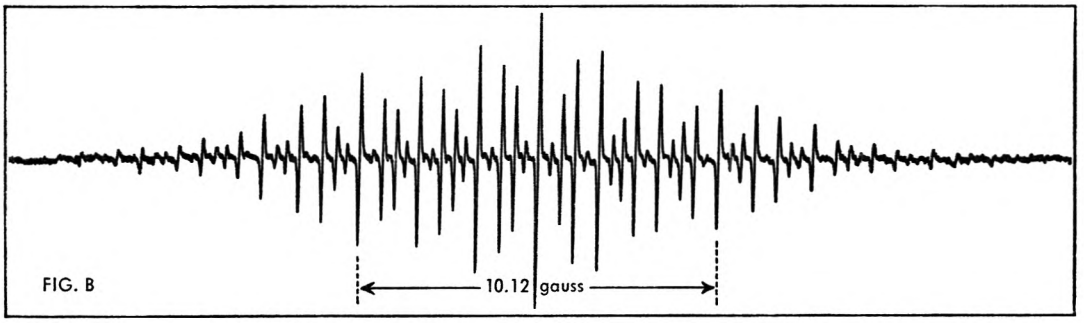

FIG. B

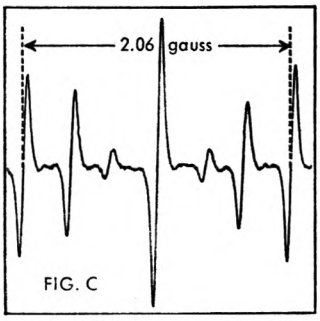

FIG. C

The spectrum may readily be reconstructed. From Figure A it can be seen that there are three classes of protons, a, b and c, with four protons in each class. Four identical protons give rise to five energy levels with degeneracies of 1, 4, 6, 4, 1, and three such groups of 4 give rise to 5^3, or 125 lines with easily determined relative intensities. In fact, we find one of the splittings is within 1% of being three times another, which results in 85 lines, 81 of which can be seen in the figure. The three splittings are 1.03 gauss, 1.69 gauss, and 5.06 gauss. Calculated intensities agree closely with experimental values.

[1] *S. I. Weissman, E. DeBoer and J. J. Conradi, J. Chem. Phys. 26, 963 (1957); E. DeBoer and S. I. Weissman, J. Am. Chem. Soc. 80, 4549 (1958); A. Carrington, F. Dravnieks and M. C. R. Symons, J. Chem. Soc. 947, (1959).*

[2] *H. W. Brown and J. S. Hyde, (to be published).*

For literature which fully explains the 100 kc EPR Spectrometer and its application to basic and applied research in physics, chemistry, biology and medicine, write the Instrument Division.

402C